THE FLOW OF LIQUID POLYMERS THROUGH

FIBROUS REINFORCEMENTS

by

PATRICK ROBERT GRIFFIN

A thesis submitted to the University of Plymouth in partial fulfilment for the

degree of

DOCTOR OF PHILOSOPHY

School of Manufacturing, Materials and Mechanical Engineering

Faculty of Technology

September 1995

Declaration

The contents of the final permanently bound thesis are identical to the version submitted for examination (except where amendments have been made to meet the requirements of the examiners)

THE FLOW OF LIQUID POLMERS THROUGH FIBROUS REINFORCEMENTS

Patrick R. Griffin

Abstract

Resin Transfer Moulding (RTM), at present, is a semi-automated, low volume production process for fibre reinforced plastics with much work being undertaken to achieve full automation and medium volume production. The efficient and consistent impregnation of thermosetting resin into a reinforcement pack are key requirements in the development of RTM.

For mass production and automation accurate predictions of mould fill times are critical in order to plan production. At present, the fill times are predicted by assuming Darcy's law and using experimentally determined permeability value. Permeability measurements display a large amount of scatter which affects the accuracy of simulations of mould filling.

Commercial fabrics such as 'Injectex' are now available which achieve high permeability to resin flow through a modified microstructural architecture of fibre tows.

This thesis seeks to examine the relationship between microstructure and permeability in these fabrics in the context of possible decreases in mechanical properties which may result from non-uniform fibre distribution. An image analysis technique is used to characterise and quantify the regions of flow within the fabric architecture which are then correlated with a series of permeability measurements determined experimentally. This then leads onto a mathematical model for the prediction of the permeability of the fibre pack.

Contents

References

APPENDICES

- - - - - - - - - -

List of Figures

Chapter 3

<u>List of Figures</u> (continued)

List of Tables

List of Tables (continued)

List of Plates

Chapter 5

Glossary of Terms

A

Accelerator - a material which when mixed with a catalyst or resin, will speed up the chemical reaction between the catalyst and the resin.

Anisotropic - properties which differ in different load directions i.e. in fibre reinforcements the properties vary with respect to the orientation of the fibres.

Anisotropy Index - the ratio of properties in the major flow direction to the minor flow direction

Areal Weight - The weight per unit area of a fabric or tape reinforcement usually measured in g/m^2.

B

Balanced Laminate - a composite laminate in which all laminae angles other than 0° and 90° occur only in pairs and are symmetrical about the centre line of the laminate.

Bundle - the name given to a collection of fibres which are essentially parallel. Also referred to as a tow of fibres.

C

Carbon Fibre - Fibre produced by the pyrolysis of organic precursor fibres such as rayon, polyacrylonitrile (PAN) and pitch in an inert environment.

Catalyst - A substance which changes the rate of chemical reaction without itself undergoing permanent change in composition. A substance which speeds up the cure of a resin markedly.

Cavity - the space inside a mould into which a resin is injected.

Crimp - the waviness of a fibre or fabric produced by the weaving process.

Cure - to irreversibly change the properties of a thermosetting resin by chemical reaction. This may be accomplished with or without heat and pressure

D

Drape - the ability of a fabric to conform to a contoured shape.

E

'E' Glass - A family of glass with an aluminosilicate composition and maximum alkali content of 2%. The most commonly used reinforcement glass which is used in electrical laminates due to its high resistivity. Also called electric glass.

Exotherm - the evolution of heat during the curing reaction of thermosetting resin

F

Filament - the smallest part of fibrous reinforcement. They are usually very long and have a small diameter (high aspect ratio)

Fill - yarn oriented at right angles to the warp in a woven fabric. Also known as the weft yarn

G

Gel - the jellylike formation that develops when a thermosetting resin is curing. The resin will not flow when it has reached the gel point

H

Hand Lay-up - the process of working resin into successive layers of plies on a mould face by hand.

Hardener - a substance which when mixed with the base resin, promotes the curing action of the resin

Heterogeneous - a material or flow consisting of dissimilar components, i.e. a flow of resin which exhibits different flow properties in arbitrary directions

Homogeneous - a material which exhibits uniform composition in all directions

Hygroscopic - capable of absorbing and retaining atmospheric moisture

I

Impregnate - to saturate the reinforcement with resin so there are no spaces left unfilled

Inter-Tow Flow - fluid flow between the fibre tows (bundles)

Intra-Tow Flow - fluid flow into the fibre tows (bundles)

Isotropic - exhibiting uniform properties in all directions

L

Lamina - a single ply or layer within a laminate

Laminate - the result of bonding laminae together with resin, usually with the aid of pressure or heat

Lay-up - the positioning of the dry reinforcement into the mould cavity

M

Macro - considering the properties of a material from an overall rather than specific viewpoint

Matrix - the homogeneous resin phase which impregnates the dry reinforcement

Micro - consideration of the reinforcement, laminate or rein flow from a fibre scale viewpoint

N

Nesting - the placing of plies of fabric so that the tows lie in the valleys of the adjacent layer

Needlepunched mat - a mat reinforcement formed of short strands felted together in a needle loom.

O

Orientation - the alignment of the fibres with respect to a datum direction. Dictates the direction of flow of resin in high volume fraction composites

Orthotropic - possessing three mutually perpendicular planes of elastic symmetry

P

Permeability - the rate of diffusion of a gas or liquid through a porous medium without affecting its chemical composition

Pick Count - number of filling yarns per centimetre in a woven fabric

Ply - a layer of reinforcement within a lay-up

Porosity - the trapping of air in a material or the space in a laminate for the resin to fill i.e. 1- the fraction of the mould volume taken up by fibres.

Preform - a preshaped fibrous reinforcement contoured to the desired thickness of the finished part.

Q

Quasi-Isotropic - a property which approximates isotropy. Applies to random mat for example

R

Reinforcement - a material of high strength bonded into a rein to increase its mechanical properties. Reinforcements may be fibrous or particulate

Resin - usually associated with polymers and is used to bond reinforcements together.

Resin System - a mixture of resin and ingredients such as catalyst, hardener and accelerator.

Resin-Rich Area - a localised area with a low fibre content.

S

Size - a material which is deposited onto the reinforcement to improve the bonding characteristics of the fibres

Starved Area - a localised area where the resin content is low due to insufficient wetting or improper porting arrangements.

Symmetrical laminate - a laminate in which there is symmetry of layers in terms of orientation with respect to the centre line

T

Textile fibres - ones which are produced by a variety of methods as in the clothing industry such as weaving, knitting and braiding.

Thermosetting plastic - a plastic, which when formed may not be reformed by melting unlike thermoplastics which may be remoulded.

Tow - an untwisted bundle of continuous filaments. Tows are designated using K to describe how many individual filaments are present i.e. 3K = 3000

U

Unidirectional laminate - a laminate in which the vast majority of the fibres are oriented in one direction

V

Viscosity - the property of resistance to flow offered by a material expressed as the relationship between applied shear stress and the resultant strain rate

Voids - air or gas which is trapped in a laminate which are incapable of transmitting loads

Volume Fraction - the fraction of the volume of a mould cavity occupied by fibre reinforcement

W

Warp - the lengthways yarn in a woven fabric, also referred to as the machine direction

Weft - the transverse yarns in a woven fabric

Wet-out - the condition reached when the voids in the reinforcement have substantially been filled with resin.

X

X-axis - the axis with which is used as the 0° reference axis in the design of lay-ups

Y

Y-axis - at right angles to the x-axis in the plane of the laminate

Yarn - an assemblage of twisted filaments, fibres or strands to form a continuous length suitable for weaving

Z

Z-axis - the axis normal to the plane of the laminate i.e. the thickness direction

Acknowledgements

Author's Declaration

At no time during the registration for the degree of Doctor of Philosophy has the author been registered for any other university award

This study was financed by the School of Manufacturing, Materials and Mechanical Engineering Pump Priming Fund

A programme of advanced study was undertaken, which included attendance at Advanced Composites Manufacturing Centre (ACMC) short courses in composite manufacturing and Resin Transfer Moulding (RTM) and attendance at the RTM short course at the University of Nottingham.

Relevant Scientific seminars and conferences were regularly attended at which work was presented; external institutions were visited for consultation purposes and a number of papers prepared for publication.

Presentations and Conferences Attended:

Microscopy of Materials II, University Museum, Oxford 11-13th April 1994

15th International European Chapter of the Society for the Advancement of Materials and Process Engineering, Toulouse,France, June 8-10th 1994

Flow Processes in Composite Materials '94, Galway, Eire, July 7-9th 1994

External Contacts:

Eric Taylor (Carr Reinforcements)
Nick Clarke (Polymer Engineering Ltd)
Fiona Scott (British Aerospace)

Signed...

Date.......6TH SEPT 1995.

CHAPTER 1

INTRODUCTION

This chapter provides the background to the research programme undertaken.

After discussing the construction and merits of composite materials,

manufacturing methods are then assessed. This assessment deals with the

subjects of production quality, efficiency and health and safety. Attention is

then switched to the complex resin flow and fibre impregnation in each

method. Particular attention is paid to the prediction of the mould filling

processes by the use of an empirically determined permeability value.

1:1 Composite Materials

Although composite materials appear to be relatively new in the area of

materials science, the principles of their construction are not. The idea of a

composite is to use the properties of two dissimilar materials to create a new

material whose properties are unique, sometimes superior and are often not

present in the constituent materials. The idea of this is based upon the so-called

'natural' composites which include some flexible tissues in the body and,

probably the most well known, wood. Wood is a composite of cellulose tubes,

which acts as the reinforcement and lignin, which bonds the cellulose tubes

together. A schematic diagram of the structure of wood is shown in Figure 1.1

from Higgins [1] and owing to the orientation of the cellulose fibres,

directional mechanical properties are produced. These directional properties

1

are an important factor in composite manufacturing, particularly with regard to resin flow and will be dealt with in greater detail as the thesis progresses.
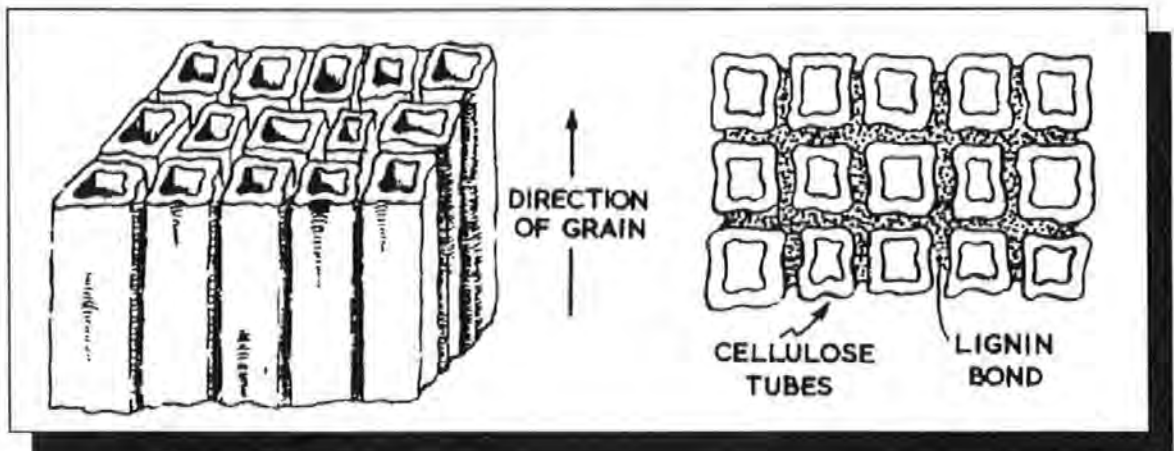
Figure 1:1 The Composite Nature of Wood [1]

1:2 Properties of Composite Materials

The polymer / fibre composite industry has grown steadily since its inception and already boasts an impressive array of components which have been manufactured from various combinations of reinforcement (fibre) and matrix (resin). Components ranging from pipes, pressure vessels and storage tanks up to aircraft components [2], helicopter rotor blades and aircraft wings [3] are all in extensive use owing to a number of attractive properties obtainable from composite materials. Most applications rely on various permutations of the following properties offered by composite materials

• i) light weight

• ii) corrosion resistance

• iii) non-magnetic

• iv) high stiffness and strength per unit mass (specific stiffness and strength)

• v) low thermal conductivity and expansion

• vi) ease of manufacture

• vii) improved fatigue resistance

There now follows a description of the roles of the constituent materials together with examples and a comparison with more traditional materials.

1:2:1 Matrix and Interfacial Bonding

The task of the matrix is to restrian the fibre reinforement in position whilst providing protection from damage and most importantly to transfer loads to the fibres. The loads are transferred through shear to the reinforcement. The nature of the interfacial bonding between fibres and matrix has a major influence on the load transfer capacity between matrix and fibres. Adhesion at the interface may be achieved by one of the following methods

i) Mechanical Bonding - which involves a high enough coefficient of friction acting between the surfaces

ii) Physical Bonding - depending upon the van der Waals forces acting between surface molecules

iii) Chemical Bonding at the interface.

Thermosetting polymer matrices are available in several categories such as polyesters, epoxies, vinylesters and phenolics depending upon the requirement of the component. ' Thermosets' are used because their low viscosities (generally < 2000cP) aid the impregnation of the fibre tows which maximise the mechanical properties of the composite. Table 1.1 shows properties of commonly used thermosetting resin matrices together with their composition. It is observed that the use of these matrices is limited by the component service temperature.

Resin Type	Composition	Relative Density	Tensile Strength (MN/m²)	Elongation (%)	Impact (J)	Typical Max. Service Temperature (°C)
Epoxides	Polymers generally cross-linked by amines	1.15	35-80	5-10	0.5-1.5	200
Polyester (unsaturated)	Unsaturated linear polymers, cross-linked by various vinyl monomers	1.12	55	2	0.7	220
Polyester (Alkyd Resins)	Condensation products of glycol, phthalic anhydride	2	25	-	0.25	150
Phenolic (Phenol Formaldehyde)	Condensation product of either phenol or cresol with formaldehyde	1.35	35-55	1	0.3-1.5	75

Table 1.1 Composition and Properties of Typical Thermosetting Resins [1]

The matrix selection is important because the matrix will be in contact with the environment for which the component is designed, therefore a component which requires a fire resistant property may require a phenolic matrix whereas a component where strength is required may require an epoxy resin. Manufacturing implications are introduced when using certain resins (usually certain epoxies) owing to the requirement of heat to aid the cross linking process and cure and maximise the mechanical properties.

1:2:2 Fibre Sizing

Improved interfacial adhesion is achieved by the use of a size or primer material which coats the fibres. This material is chemically compatable with both the fibre and the matrix and is discussed in detail by Bascom [4]. Common sizes are vinylsilane coated on glass fibres for processing with polyester resins and aminosilane for epoxy resins. The silane promotes adhesion between the size and the glass while the vinyl or amino groups

4

promote adhesion to the particular resin. Sizes also provide resistance to physical damage and moisture absorption and can improve the processability of the reinforcements by providing a uniform surface for the matrix to flow over and impregnate. Applications of size are usually around 1% by weight of the reinforcement. This may vary according to the level of protection required with woven fabrics being more vulnerable to damage compared to pre-impregnated materials (prepregs).

1:2:3 Fibrous Reinforcements

Reinforcements are available in several materials such as glass (E, S, T, RH), carbon (High Modulus,High Tensile Strength) and aramids (Kevlar). These are obtainable in many geometric forms ranging from randomly oriented to woven, stitched, knittted and braided reinforcement used for tubes and pipes. A more detailed review of reinforcement configuration will be found in Chapter 2:7.

Reinforcements are classified into two distinct groups, depending on the fibre length,

i) *Continuous*-used where load transmission is required in specific directions

ii) *Discontinuous* - used where a general strength is required to reinforce the polymer matrix.

Due to the high aspect ratio (e.g. 10000:1 of length:diameter) of the fibres, they are only effective when they are loaded parallel to their axis. Owing to the length of continuous fibres, it is possible to apply substantial loads due to

the large contact area available to shear forces. Continuous fibre composites possess higher mechaical properties because

• i) they can be aligned in the direction of the load

• ii) higher volume fractions may be achieved . With discontinous shorter fibres, the contact area is much reduced and hence only small loads may be transmitted before the shear forces become too large and the fibres pull out. A minimum effective length is applied to the fibres which depends on he aspect ratio of the fibres (length/fibre diameter) and for many glass reinforced plastics, the critical length is only several hundred micrometres. Table 1.2 from Hull [5] shows a comparison of the properties of fibres made from a range of materials.

Material	Tensile Strength (GN/m^2)	Relative Density	Young's Modulus (GN/m^2)	Specific Strength (GN/m^2)	Specific Modulus (GN/m^2)
'S' Glass	4.5	2.5	88	1.8	35
Steel (drawn wire)	4.2	7.74	200	0.54	26
'E' Glass	1.4 - 2.5	2.55	76	1.4	29
Carbon (High Strength)	3	1.74	230	1.8	130
Carbon (High Modulus)	2.1	2	420	1.1	210
Boron	2.8	2.36	390	1.2	160

Table 1:2 Properties of Fibrous Materials [5]

It is important to realise that the composite material is manufactured by combining the two phases and therefore it is these properties which are compared with conventional materials. The figures in Table 1.1 are misleading in the fact that a composite contains only between 30 and 70% of fibres by volume. Properties of the composite can be predicted by various

6

rules of mixtures such as Equations 1a and 1b for Young's Modulus parallel and perpendicular to the fibres in a unidirectional, continuous fibre composite

$$E_{c(ll)} = E_f.V_f + E_m.(1 - V_f) \cdots \text{Equation 1a}$$

$$E_{c(\perp)} = \frac{E_m.E_f}{E_m.V_f + E_f(1 - V_f)} \cdots \text{Equation 1b}$$

where

E_c = *the Young's Modulus of the Composite*

E_f = *the Young's Modulus of the Fibre Reinforcement*

E_m = *the Young's Modulus of the Matrix resin*

V_f = *the Volume Fraction of the Fibre Reinforcement*

As the fibres provide the strength to the composite, it is important to realise that varying the volume fraction of the fibres affects the mechanical properties of the composite as a whole. When using rules of mixtures, it is important to remember that the orientation of the fibres affects the properties and that loads applied at any angle other than parallel to the axis of the fibre will reduce the effectiveness of the reinforcement. Also it important to remember that the presence of voids in the matrix will be detrimental to the overall properties of the composite. Judd et al. [6] concluded from tests that the interlaminar shear strength reduced by about 7% for every 1% of voids up to a void content of 4%.

1:3 Comparison of Composites with Traditional Materials

Comparing the properties of fibre reinforced plastics with those of more common materials, the potential of composites as competitive alternatives to conventional materials is observed. Table 1.2 from Higgins [1] shows a range

of properties associated with commonly used metallic alloys and plastic

materials and compares them to combinations of fibres and plastics. In terms

of mechanical properties, there does not appear to be to much to be gained

from the use of composites but a clear advantage is seen with density and

hence the weight of components may be drastically reduced. This is

obviously a major advantage where fuel economy is of paramount

importance such as in transport [7,8].

Material	Density (Mg/m^3)	Young's Modulus (GN/m^2)	Tensile Strength (MN/m^2)	Elongation to Fracture (%)	Coefficient of Thermal Expansion $(\times 10^{-6}/^{\circ}C)$	Heat Resistance $(^{\circ}C)$
High Strength Al-Zn-Mg Alloy	2.8	72	503	11	24	350
Quenched and Tempered Low Alloy Steel	7.85	207	2050-2600	12-28	11	800
Nimonic Steel (nickel-based alloy)	8.18	204	1200	26	16	1100
Nylon 6.6	1.14	2	70	60	90	150
Glass Filled Nylon (25% by Volume)	1.47	14	207	2.2	25	170
Carbon-Epoxy Unidirectional Laminate (parallel to fibres) V_f= 60%	1.62	220	1400	0.8	-0.2	260
As above (perpendicular to fibres)	1.62	7	38	0.6	30	260
Glass-Polyester Unidirectional Laminate (parallel to fibres) V_f= 50%	1.93	38	750	1.8	11	250
As above (perpendicular to fibres)	1.93	10	22	0.2	11	250
Glass-Polyester (Randomly orientated fibres) V_f= 20%	1.55	8.5	110	2	25	230

Table 1:3 Comparison of the Properties of Typical Engineering

Materials at Room Temperature [1]

The advantages gained from the reduced weight may be seen in Table 1.4 where the specific strength and specific modulii are quoted for the materials in Table 1.3. The strength to weight ratio of the unidirectional carbon/epoxy laminate is 5 times greater than the low alloy steel while the glass/polyester is almost twice as much. The carbon/epoxy laminate also offers a 5 times greater stiffness to weight ratio compared with its steel alloy counterpart. Hence, there are advantages of using composites in applications where weight savings would be beneficial, without reducing the mechanical properties, e.g. aircraft applications.

Material	Specific Young's Modulus Young's Modulus / Specific Gravity (GN/m^2)	Specific Tensile Strength Tensile Strength / Specific Gravity (MN/m^2)
High Strength Al-Zn-Mg Alloy	25.7	180
Quenched and Tempered Low Alloy Steel	26.4	261-276
Nimonic Steel (nickel-based alloy)	24.9	147
Nylon 6.6	1.8	61
Glass Filled Nylon (25% by Volume)	9.5	141
Carbon-Epoxy Unidirectional Laminate (parallel to fibres)V_f=60%	135	865
Glass-Polyester Unidirectional Laminate (parallel to fibres) V_f=50%	19.7	390
Glass-Polyester (Randomly orientated fibres)V_f=20%	5.5	71

Table 1:4. Specific Modulus and Strength of Common Materials

1:4 Manufacturing Routes

The combining of the two constituents to produce the final composite material component is achieved in a number of ways. The principal methods are:

♦Hand lay-up onto a single faced mould

♦Matched Tool Compression Moulding

♦Resin Injection or Resin Transfer Moulding (RTM)

♦Filament Winding (for circular, elliptical or similar shapes)

♦Pultrusion of symmetrical shaped members

♦ Vacuum Bagging / Autoclaving of components to ensure high fibre volume

fraction and quality.

1:4:1 Resin Flow Processes

The manufacturing techniques listed previously may be divided into two

categories for the purposes of this research:

i) Short range flow of resin (10-500 microns)

i.e. of the order of the thickness of a reinforcement ply

ii) Long range flow of resin (up to several metres)

i.e. of the order of a component length.

1:4:2 Short Range Flow Processes

This category includes processes such as autoclaving, compression moulding,

filament winding, pultrusion and vacuum bagging. In these processes, the

resin is only required to travel short distances to impregnate the fibre pack.

This is due to the fibre pack being partly impregnated either by the use of

pre-impregnated materials (prepregs) or by the laminator wet laying the

reinforcement before consolidation. Consolidation is the use of pressure and

sometimes heat to maximise the fibre volume fraction and mechanical

properties by squeezing the voids out of the fibre pack. The main advantage of processes involving short range flow is that air entrapment is reduced because the resin has already impregnated the fibre tows. Apart from hand lay-up techniques, the other processes in this category are all expensive to operate because of capital equipment costs and the increased cost of raw materials. Therefore, they only tend to be used in specialist applications such as the aerospace industry where high volume fractions (>55%) are used and the quality is of great importance.

1:4:3 Long Range Flow Processes

Long range flow processes include Resin Transfer Moulding (RTM) and Vacuum Assisted Resin Injection (VARI), where a thermosetting resin is required to impregnate a dry reinforcement to produce the component. Depending upon the porting arrangement, the resin may have to flow several metres to fully impregnate the reinforcement.

1:5 Resin Transfer Moulding

RTM involves the injection, at low pressure (typically <4 bar), of a precatalysed thermosetting resin into a pre-laid fibre pack in a preshaped closed mould. The resin may be introduced by a single port, array of ports and or a gallery depending upon the arrangement of the fibres within the mould. The resin impregnates the fibres by displacing the air, fills the mould and is allowed to cure, possibly with the aid of heat, before demoulding. Vacuum may be used in addition to the injection pressure to aid the

impregnation, but this requires good mould sealing and extra cost to the manufacturer.

Figure 1.2 shows schematically the main stages of RTM, from reinforcement loading and mould closure through to the resin injection and demoulding.
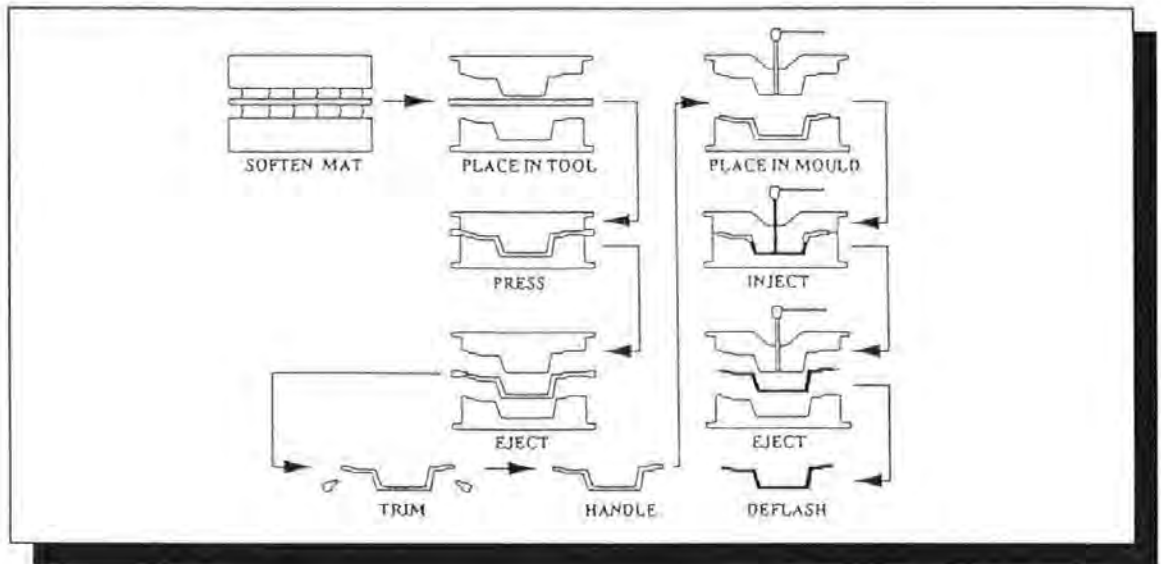
Figure 1.2 Schematic Diagram of the RTM Process

RTM was introduced in the mid 1940's to manufacture U.S. navy patrol boats [9], but actually lay dormant until the 1980's. Since being 're-discovered', the process has developed rapidly because of the

• i) intricate shapes may be produced accurately with two quality surfaces

• ii) low injection pressures allow the use of soft (composite) tooling option which reduces the capital cost

• iii) fibre volume fraction and hence properties are more controllable

• iv) parts for medium volume production are economic

• v) labour requirements are reduced compared to the hand lay-up method

• vi) improved health and safety is achieved due to the retention of volatiles (such as styrene), within the mould.

Table 1.5 from Gotch [10] shows some typical levels of styrene present in some processes with and without extraction. The levels of styrene permitted in the U.K. are 100 ppm until 1996 when it will be reduced to 50ppm.

Process	Without Extraction (ppm)	With Extraction (ppm)
Hand Lay-up	60-100	25-80
Spray Deposition	170-200	70
Resin Injection	25	/
Vacuum Impregnation	25	/
Cold Press Moulding	60	25

Table 1.5 Typical Styrene Levels evident in Processes (parts per million)

Several standard techniques are available for the measurement of harmful volatiles notably CEN/TC 137 N90 and N96 regarding workplace atmospheres. Being an enclosed process, RTM contains these volatiles and therefore poses less of a health and safety risk. Styrene levels are easily within the maximum allowable limit without expensive extraction.

1:6 Components manufactured by RTM

Components manufactured by RTM may be divided into two categories according to the volume fraction

i) Low Volume Fraction (<30%) - components manufactured from continuous and discontinuous random mats are found in this category. The 30% limit is approximately the maximum volume fraction obtainable with random mats because of the nature of the stacking of the fibres. Random mats, particularly Continuous Filament Mat (CFM) provide low cost structures with uniform strength characteristics.

Examples of components manufactured in this volume fraction category are Ford Transit van roofs [11], boat hulls [12], panels for freight containers, tanks for chemicals and gearbox housings. The low volume fraction of fibres in the components and the use of low viscosity polyester resins means that impregnation is fast and turn round time of the moulding is much reduced.

ii) High Volume Fraction (>40%) - the majority of the components in this category may be termed 'advanced composites' owing to the fact that the components require a specific volume fraction and orientation of fibres to cope with a particular type of load. The components manufactured take advantage of the increased properties offered by directional woven or stitched reinforcements to maximise their mechanical properties. The high fibre content presents problems in manufacture such as mould distortion. The increased fibre content also presents problems in the impregnation of the fibre pack as the nature of the resin flow becomes more dependent on the fibre orientation and distribution as the volume fraction is increased. Volume fractions up to 90% are possible in theory but in practice only 65-70% is possible due to imperfect packing and fibre misalignment. The investigation of resin impregnation and its relationship with reinforcement architecture forms the basis for much of the work in this thesis.

1:7 Simulation of the RTM Process

The potential of RTM to develop into an automated mass production process [13] has led to a great deal of research and development into modelling the

process. The vast majority of modelling has concentrated on the use of

Darcy's law to predict the passage of resin through reinforcements. Darcy's

law, derived to predict the losses in a water supply system, states that the

flow velocity of the fluid is directly proportional to the pressure gradient

driving the flow. The constant of proportionality, referred to as the

permeability, has been adopted as a method of classifying the reinforcements

used in RTM. Permeability describes the ease with which a fluid flows

through a porous medium, a high permeability implying a high flow rate.

However, Darcy's law was derived for particulate porous media which was

assumed to be homogeneous. In the case of fibre packs certain flow

complications are introduced. The flow of a fluid through a reinforcement is

influenced by a number of factors with respect to the reinforcement

i) the amount of fibres in the mould (volume fraction)

ii) the orientation of the fibres

iii) the distribution of the fibres

A fibre pack, particularly one consisting of a woven reinforcement, consists

of areas of differing fibre distribution (on a scale from a few microns up to a

few millimetres) and differing orientation. Consequently, there are several

different impregnation mechanisms involved in the total wetting out of the

reinforcement illustrated in Figure 1:1:

• **i) inter-tow flow** -. these gaps may be of the order of a few square

millimetres in size and dominate the overall flow.

• **ii) capillary flow** - these gaps are only a few square microns and contribute to the impregnation of the fibre tows in the axial direction.

• **iii) transverse flow** - these gaps are parallel slits perpendicular to the tows a few microns wide. This flow is drawn into the tows from the inter tow flow which progresses at a faster rate.
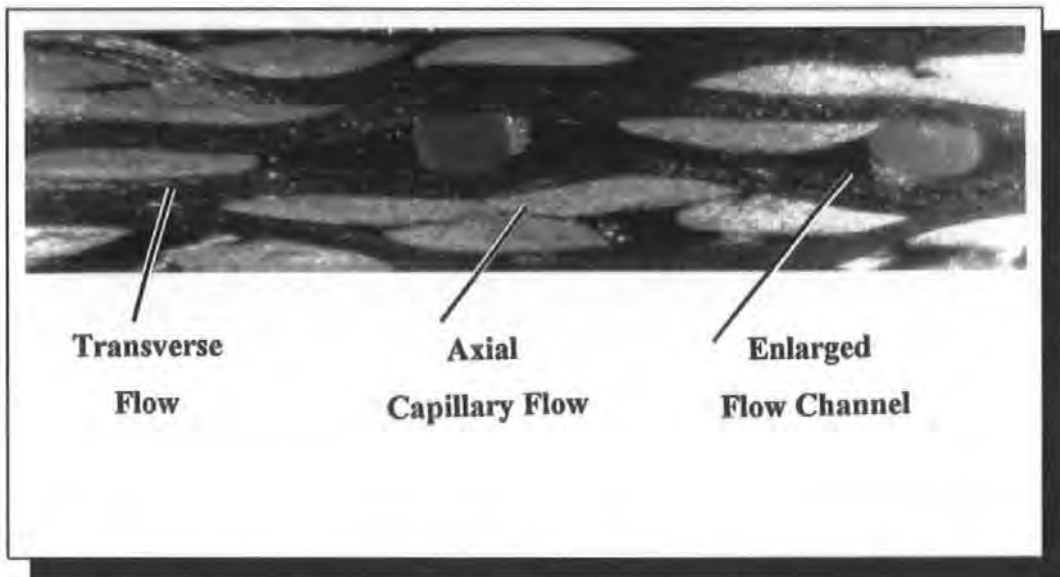
Figure 1:3 A Laminate Micrograph showing the Three Different Regimes of Flow

The permeability of a reinforcement pack is difficult to reproduce because Darcy's law does not account for the difference in pore structure between particulates and fibrous media.

1:8 Optimisation and Future Development of RTM

Process optimisation is a key point in the development of RTM. Much work has been undertaken with the aim of designing reinforcements which impregnate faster using lower viscosity resins, hence reducing the production cycle time. The control of fabric permeability is the key to process control. Several computer simulations exist which use experimentally determined

permeability values. The variation of permeability from pack to pack means that errors will occur in the simulation of the process. This thesis is dedicated to tackling the problems of permeability measurement and the governing flow phenomena of RTM. Fabrics designed to enhance fill-rates are investigated from a fill-rate versus mechanical properties viewpoint. The size and architecture of the flow channels in the fabrics is investigated with the use of an image analysis technique to enable a new prediction of mould fill to be produced based on the proportion of each type of flow present in the laminate.

CHAPTER 2

MODELLING THE PROCESS

2:1 Porous Media Theory

Porous media are an important part of everyday life and have a number of important applications. Therefore, it is important that we understand their characteristics of permitting the flow of fluids through them. The many differing geometries of media produce a variety of directional flow properties which need to be defined in order to predict the flow through them. The modelling of the flow of resin through fibres is based on work undertaken on particulates which have a different geometry. This research concentrates on the understanding of the flow mechanisms of a resin through a fibrous pack. In this chapter, there is a brief description of the two categories of medium together with a detailed development of the governing equations for fluid flow through fibrous beds developed from particulate theory.

2:1:1 Particulate Media

These materials, such as sandstone and limestone are found commonly in a number of important areas of industry, particularly oil exploration. The original use of the work was in monitoring the losses through aquifers which were used in the water supply system for the town of Dijon in France. Henri Darcy [14] was responsible for the design of the system and his work is still used extensively as the basic theory in solving problems involving both particulates

and fibrous media. The petroleum industry is an obvious application of his work in the extraction of oil, with various sea bed rocks being classified according to the ease with which oil flows through them. Exploration and reservoir engineers are interested in how easily the oil may be extracted through these rocks in order to determine production rates. Later fundamental work was carried out by Blake, Carman and Kozeny. This work was semi-empirical and involved the determination of flow path constants such as tortuosity (defined in 2:3:5) and geometry. Several methods have been developed to measure the permeability of rocks as described in Chapter 2:6.

2:1:2 Fibrous Media

The development of reinforced plastics has led to the requirement to produce a reliable model which would predict the flow of resin through a fibre pack. This fibre reinforcement is considered as a porous medium and initially, existing particulate theories were used to model the flow. Owing to the differing geometry of fibres, i.e. a long continuous phase rather than a small discontinuous phase, modifications were needed to the particulate equations. These are discussed later in this chapter. Fibrous reinforcements are available in a large number of different configurations produced by many techniques such as uniaxial, bi,tri and quadriaxial which may be woven, stitched or braided and continuous and discontinuous random mats which all give rise to differing flow patterns. With both forms of media, the classification regarding their flow properties is by use of permeability coefficients.

2:2 Permeability -Definition

Permeability is defined as the ease with which a fluid, vapour or gas passes through a porous medium. It appears in a number of applications which are evident in everyday life from petrol hoses to 'waterproof' clothing. There are several British Standards available which use permeability to assess the relative merits of a particular material in a particular application. Where explosive gases such as oxygen, acetylene or hydrogen are concerned it is obviously very important to know if there is any leakage through the tubes which transport them and BS 903 (A46) and BS 103.11 deal with methods of testing for leakage. In the packaging industry, it is important to know the permeability of water vapour through various different types of packaging, usually polymers. This relates to keeping food stuffs fresh and is dealt with in BS 3177. The materials are tested using a desiccant such as anhydrous calcium chloride which is weighed before the test and the amount of water vapour absorbed is recorded for a square metre of material in 24 hours. The units of permeability are thus g/m^2 day. Civil engineers use BS 1377(5 & 6) to test materials encountered in the building industry, such as sand, to determine their drainage characteristics. Permeability has been used extensively by the petroleum industry in the classification of types of porous rocks encountered on the sea bed. These permeability figures are used to estimate the time that it will take to recover the crude oil contained in the pores of the rocks. Permeability has also been adopted as a method for classifying the fluid flow

characteristics of fibre packs used in reinforced plastics processing. However, there is no standard method of measuring the permeability of fibre beds although there have been several methods developed from theory similar to those used in flow through particulate media. Darcy's law has been extensively used to explain the flow properties of porous media. Permeability appears in Darcy's law as the constant of proportionality between the flow velocity and the pressure gradient. Its magnitude is dependent upon the pore size and structure, the viscosity of the infiltrating fluid and the driving pressure behind the fluid. The units of permeability in the SI system are m^2 but are more commonly quoted in the cgs system as darcies. A medium has a permeability of 1 darcy if a fluid of viscosity 1cP flows with a velocity of 1 cm/s under a pressure gradient of 1 atm/cm. Therefore 1 darcy is the equivalent to the following:

$$1 \ darcy = 1(cm/s)(cP)/(atm/cm) = 9.869 \times 10^{-13} \ m^2 = 9.869 \times 10^{-9} \ cm^2$$

In particulate and fibre beds, transparent faced moulds have been used extensively to monitor the infusion of fluids, obtain permeability values and to gain a better understanding of the flow mechanisms. In particular, some agreement has been reached regarding the fact that more than one type of flow is apparent in the filling process due to the different configuration of the reinforcements and fibre distribution. This subject is investigated in greater detail in chapters 5,6 and 7.

2:3 Permeability in Particulates

2:3:1 Derivation of Permeability and Darcy's Law

The original definitions of permeability are found in work dealing with particulate media and this section describes the following porous media theories.

i) Darcy's Law

ii) Blake - Carman - Kozeny Theory

Darcy's law states that the flow velocity of the fluid is proportional to the pressure gradient causing the flow. Throughout research in this area, several symbols have been used to signify permeability and these will be consistent with the authors who derived them. If a volume Q flows in t seconds across a cross-sectional area A, then the direct linear flow rate is

$$u = \frac{Q}{A.t}$$ - - - - - - Equation 2:1

and Darcy's law states that

$$u = -B_1.\frac{\delta p}{\delta x} = B_1.\frac{\Delta p}{L}$$ - - - - - Equation 2:2

where:
   B_1 = the permeability coefficient
   Δp = the total pressure drop across a sample, length L
   where the flow is parallel to the x direction

This condition implies that

i) the fluid is assumed to be Newtonian

ii) the fluid is inert to the porous medium, i.e. chemical, adsorptive and capillary effects are absent.

Therefore the flow rate is inversely proportional to the viscosity, μ and the viscosity will be part of the permeability coefficient, with the coefficient B_o, becoming the specific permeability coefficient for viscous flow

$$u = -\frac{B_o}{\mu} \cdot \frac{\delta p}{\delta x} = \frac{B_o}{\mu} \cdot \frac{\Delta p}{L} \quad \text{- - - - - Equation 2:3}$$

Dupuit [15] realised that the linear velocity u of the fluid must be less than the actual velocity u_e in the pore space. This was due to the fact that the particles reduced the area to be filled by a proportion according to the porosity, ε as reported by Carman [16].The layer will therefore have a fractional pore volume equal to the fractional pore area. The following equation is known as the Dupuit relation.

$$u_e = \frac{u}{\varepsilon} \quad \text{- - - - Equation 2:4}$$

In petroleum technology, Muskat [17] employed mixed units which resulted in the permeability unit being a darcy. This corresponded to a flow of 1 cm^3/sec through a cm-cube with a pressure difference of 1 atm/cm between opposite faces using a fluid of 1 cP viscosity. The millidarcy has been used extensively in the measurement of permeability of particulates. If the porespace of the porous medium is uniform then it follows that the permeability will be similar in the principal directions (i.e. the directions parallel to the direction of the axis system used) and will have isotropic flow properties. In several substances such as sandstone and mica, the particles are not uniform and therefore the permeabilities will be different in the principal directions. Mica is a saucer shaped particle which when layed on top of one another produces highly anisotropic flow as can be seen in table 2:3 taken from tests by Johnson and Hughes [18].

23

2:3:2 Pore Structure or 'Texture'

This is the governing parameter which dictates the permeability of a medium. It is therefore important that a relationship is obtained between the pore structure and the permeability. In some cases such as filters or membranes, where the permeability is known, the pore size may be deduced. The problem with obtaining a relationship between pore structure and permeability is the modelling of the very complex network of inter-connecting pores. It has been common practice by a number of researchers [19-22] to consider the pores as an array of parallel capillaries. This does not allow for the inter connection of the capillaries and so the medium has zero permeability normal to the capillaries. The capillary model implies that the pore size needs to be related to an equivalent capillary size. As the pores have a wide distribution of sizes and there is only one permeability value associated with a given particulate medium, it is important that the correct mean pore size is selected and this is done by a statistical investigation of the particle sizes.

2:3:3 Porosity

The first attempt to derive a porosity function for a uniform bed of spheres was made by Slichter [23] in 1897. He assumed the mean cross-section of the capillary to be triangular and deduced expressions for the cross-sectional area and length of the capillaries. He then applied the equivalent of Poiseuille's law for capillary flow through a triangular cross section and obtained the following permeability relationship

$$u = \frac{d^2}{K(\varepsilon)\mu} \cdot \frac{\Delta p}{L} \quad \text{------ Equation 2:5}$$

where:

    $K(\varepsilon)$ = the permeability as a function of porosity varying from
    8100 darcies for $\varepsilon = 0.26$ to 1230 darcies for $\varepsilon = 0.46$.

A completely different method was adopted by Blake [24] in 1922, who

introduced the concept of the hydraulic radius. The work carried out by

Stanton [25] in 1914 involved the production of a single valued plot of the

Reynold's number $\frac{\rho.u_e.d_e}{\mu}$ against $\frac{R}{\rho.u_e^2}$ where u_e is the linear velocity in a

pipe of diameter d_e and R is the frictional force per unit area of the wetted

surface. For non-circular pipes, Schiller [26] produced good correlation for the

same non-dimensional group plotted against another non-dimensional group

$\frac{\rho.u_e.m}{\mu}$, where *m is the mean hydraulic radius* given by,

$$m = \frac{\text{cross-sectional area normal to the flow}}{\text{wetted perimeter}} \quad \text{- - - Equation 2:6}$$

For a pipe of uniform cross-section the hydraulic radius may be written as

$$m = \frac{\text{volume filled with fluid}}{\text{wetted surface area}} \quad \text{- - - Equation 2:7}$$

For a circular pipe, Dullien reported that $m = d_e/4$ and therefore $d_e = 4m$ may

be regarded as the mean pipe diameter. For a random packed bed of particles,

the fractional free cross-sectional area is equivalent to the porosity, ε and

therefore the bed may be regarded as a pipe with a complicated cross-section

which gives

$$m = \frac{\varepsilon}{S} \quad \text{------ Equation 2:8}$$

where: S = the particle surface area per unit volume of bed.

If this expression for m is used with Dupuit's equation, $u_e = u/\varepsilon$, then Stanton's dimensionless groups become $R.\varepsilon^2/\rho.u^2$ and $\rho.u/\mu.S$. If $R = \Delta p.\varepsilon/L.S$ then the first group becomes $\Delta p.\varepsilon^3/L.\rho.u^2.S$ which Blake recommended for turbulent flow through packed columns. In the viscous and streamline flow, these groups lead to a relationship analogous to Poiseuille's law for circular pipes as seen below,

$$\frac{\Delta p \varepsilon^3}{L.\rho.u^2.S} = k\frac{\mu.S}{\rho.u} \text{ or } u = \frac{\varepsilon^3}{k.\mu.S^2}.\frac{\Delta p}{L} \quad \text{---- Equation 2:9}$$

where

   k= the Kozeny constant (depends on shape of flow channel)

It then follows that the specific surface area of the particles S_o is given by,

$$S_o = S / (1 - \varepsilon) \quad \text{------ Equation 2:10}$$

where : $S_o = \dfrac{\Sigma \text{ perimeters of the particles}}{\Sigma \text{ cross-sectional area of the particles}}$ ----- Equation 2:11

and then rearranging equation 2:3,

$$B_o = \frac{\mu.u.L}{\Delta p} = \frac{\varepsilon.m^2}{k} = \frac{\varepsilon^3}{k.S^2} = \frac{1}{k.S_o^2}.\frac{\varepsilon^3}{(1-\varepsilon)^2} \quad \text{--- Equation 2:12}$$

The effect of porosity is accounted for by the function $\varepsilon^3/(1-\varepsilon)^2$ and the average particle size used when particles are non-spherical and non-uniform is accounted for by S_o. For uniform spheres $S_o = 6/d$ and it is therefore seen that the surface mean particle size is thus

$$d_m = 6 / S_o$$

where:

   d_m = *the diameter of a sphere with the same specific area per unit volume as the particles.*

Therefore the permeability with respect to viscous flow is written as follows

$$B_o = \frac{d_m^2}{36.k}.\frac{\varepsilon^3}{(1-\varepsilon)^2} \quad \text{--- Equation 2:13}$$

The practical effectiveness of this equation depends upon the constancy of k for particles of varying shapes and beds of differing porosities.

Kozeny [27] also applied the hydraulic radius concept but clarified the limitations of k. He assumed the pore space to be a bundle of capillaries with a common hydraulic radius and a cross-section representative of the average shape of a pore cross-section. He also assumed the path of a streamline through a pore space to be tortuous with an average length L_e greater than the length of the test piece L and suggested that the L_e term should be the average length of the capillaries. For viscous flow through a non-circular capillary of hydraulic radius m and length L_e ,the effective velocity may be written

$$u_e = \frac{m^2}{k_o.\mu}.\frac{\Delta p}{L_e} \quad \text{------- Equation 2:14}$$

where:
k_o = the shape factor. For a circular capillary $k_o = 2$ and equation 2:14 is equivalent to Poiseuille's Law.

2:3:4 Shape Factor

The shape factor k_o varies for different cross sections of capillary as shown in Table 2:1 . Common shapes are rectangular, elliptical and annular shapes and therefore k_o lies in the range 2 - 2.5 and is reasonably independent of shape. The shape factor k_o was determined experimentally by Sullivan [28] using equation 2:15 . The shape of the capillaries were produced by varying

the distance and stacking of various fibres such as goat wool and copper wire. The change in flow rate was then monitored for each capillary shape

$$Q = \left(\frac{\zeta.A}{k_o.\mu}\right).\left(\frac{\Delta p}{L}\right).\left(\frac{1}{(S_o)^2}\right).\left(\frac{\varepsilon^3}{(1-\varepsilon)^2}\right) \quad \text{- - - - - Equation 2:15}$$

where :

$\zeta = sin^2\phi$

$\phi = $ *angle between a normal to the interface and the direction of macroscopic flow i.e. normal to the fibre*

$Q = $ *the volumetric flow rate*

$A = $ *the cross sectional area of the medium*

$\varepsilon = $ *the porosity of the reinforcement pack*

If the fibres are aligned then the value of ζ is unity

SHAPE OF CAPILLARY	k_o
Circle	2
Ellipse, semi-axes a,b : a= 2b	2.13
a=10b	2.45
Square	1.78
Rectangles, sides a,b: a=2b	1.94
a=10b	2.65
Parallel sided Slit	3
Equilateral Triangle	1.67
Annuli in pipes with concentric cores	2.0-3.0

Table 2:1 Values of k_o for Viscous Flow in Various Cross-Sections [16]

Substitution of $u_e = u/\varepsilon$, $m = \varepsilon/S$ and L/L into equation 2:14 yields the following -

$$u = \frac{L}{L_e}.\frac{\varepsilon^3}{k_o.\mu.S^2}.\frac{\Delta p}{L} \quad \text{- - - - - - - Equation 2:16}$$

Comparison with equation 2:9 shows that $k = k_o(L_e/L)$. The ratio L_e/L is known as the tortuosity factor and is illustrated in Figure 2.1.

2:3:5 Tortuosity
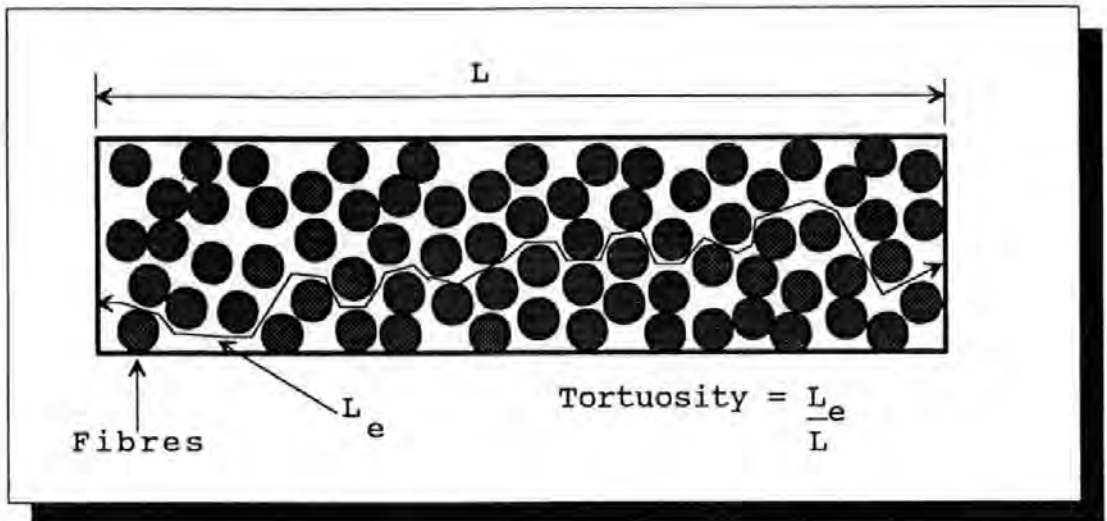
Figure 2:1. Explanation of the Tortuosity Factor

Several estimates of the tortuosity factor have been made. Published values include Bartell et al. [29] who used 0.5π, the ratio between the diameter and semi-circumference of a circle. Carman [30] who used $\sqrt{2}$ after an experiment with a coloured streamline suggested that the average angle of flow of the streamline was 45° to the actual angle of flow, hence $L_e/L=1/\cos45° = \sqrt{2}$.

The introduction of the tortuosity factor requires the Dupuit equation (equation 2:4) to be modified . The pore velocity parallel to the direction of flow is u/ε if the fraction of the area available is ε, but the actual path is tortuous and the true velocity is higher and therefore the Dupuit relationship is replaced by the following

$$u_e = \frac{u}{\varepsilon} \cdot \frac{L_e}{L} \quad - - - - - \text{Equation 2:17}$$

which when combined with equation 2:14, gives

$$u = \left(\frac{L}{L_e}\right)^2 \frac{\varepsilon^3}{k_o.\mu.S^2} \cdot \frac{\Delta p}{L} \quad - - - - - - - \text{Equation 2:18}$$

Comparison of equations 2:18 and 2:9 shows that

$$k = \left(\frac{L_e}{L}\right)^2 . k_o \quad \text{- - - - - -} \text{Equation 2:19}$$

where :

    k = the Kozeny constant

Typical values of the Kozeny constant for different porosities are shown in

Table 2:2

POROSITY (ε)	Kozeny Constant (k)
0.3	3.5
0.4	5
0.5	6.2
0.6	7.6
0.7	11

Table 2:2 Kozeny Constant for various Porosities reported by Rose [31]

2:4 Blake - Carman - Kozeny Relationship

The work done by Blake, Kozeny and Carman [16,24,27] led to the

expression for linear flow velocity in particulate media,

$$u = \frac{L}{L_e} . \frac{\varepsilon^3}{k_o . \mu . S^2} . \frac{\Delta p}{L} \quad \text{- - - - - -} \text{Equation 2:20}$$

This is known as the Kozeny-Carman equation . It was derived independently

of Blake. The equation describes laminar flow where the Reynolds Number is

less than 2000. The hydraulic radius concept has been shown to be a good

approximation under turbulent conditions. The previous section discussed the

derivation of the hydraulic radius equation and highlighted the number of

experimentally determined variables contained in it. Dullien [32] reported that

by combining the Hagen-Poiseuille equation with both Darcy's Law and the

pore velocity : effective velocity ratio (u/u_e), the following expression was

obtained for permeability.

$$K = \frac{\varepsilon.D_h^2}{16.k_o.\left(\frac{L_e}{L}\right)^2} \quad\text{-----}\ \text{Equation 2:21}$$

Dullien used the hydraulic diameter which is defined as 4 times the volume of voids in the medium divided by the surface area of the channels

$$D_h = 4.\left(\frac{\varepsilon}{1-\varepsilon}\right).\frac{1}{S} \quad\text{----}\ \text{Equation 2:22}$$

By substituting for D_h, the following is obtained, which is identical to equation 2:12

$$K = \frac{\varepsilon^3}{k_o.\left(\frac{L_e}{L}\right)^2.(1-\varepsilon)^2.S^2} \quad\text{----}\ \text{Equation 2:23}$$

The derivation of the equations thus far shows how dependent the permeability values are on experimentally determined constants for different arrangements of particles. In practice, there are a number of factors which provide inconsistencies to measurements of this nature. Specifically, the particles are not all the same size and shape and hence an error is induced by using a statistically determined average pore size for a specific material. However this is a standard method of dealing with this type of problem.

Following the derivation of particulate media permeability equations, the application of similar theory to fibre packs is now discussed.

2:5 Permeability in Fibrous Beds

There has been a great deal of work conducted in the area of modelling the flow of fluids in fibrous packs. Darcy's law, derived for use with particulate media is widely accepted as a good approximation of this flow. The flow may be either linear or radial depending upon the method perceived to produce the most efficient filling of the mould. These fluid inlet geometries will now be discussed in more detail and will take into account isotropic and anisotropic flow.

2:5:1 Linear, Isotropic, Darcy Flow

This type of flow is encountered when the fluid flows equally out in one direction from a line inlet or gallery source as shown in figure 2:2.
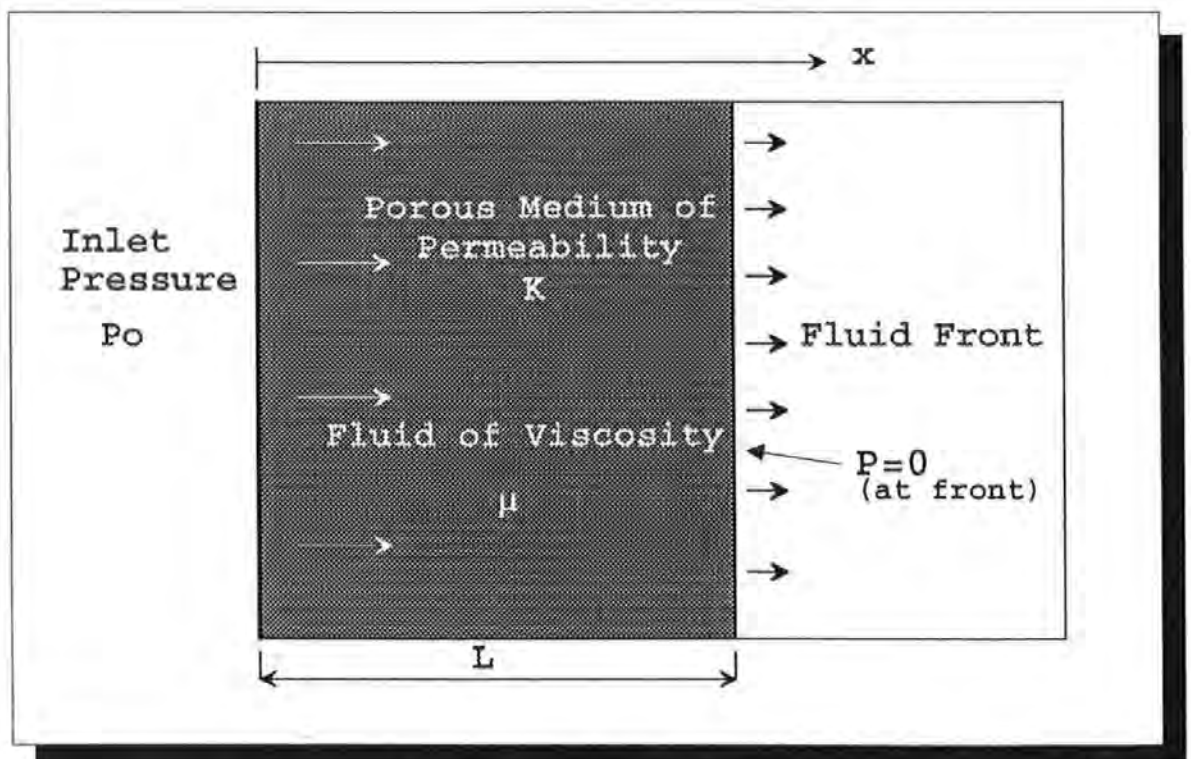
Figure 2:2. Linear One-Dimensional Darcy Flow

Darcy's law models this flow geometry with the following equation;

$$u_x = -\frac{K}{\mu}\cdot\frac{dP}{dx} = \frac{Q}{A} \text{ - - - - - Equation } 2:24$$

where
u_x *= the superficial velocity of the fluid in the x direction*
dP/dx *= the pressure gradient in the fluid*
μ *= the fluid dynamic viscosity*
K *= the permeability of the porous medium*
Q *= the volumetric flow rate of the fluid in the medium*
A *= the area available for flow - i.e. the cross-sectional area of the front*

This shows Darcy's law in its simplest form. For predicting fill- times,

Equation 2:24 is integrated over the flow distance to give the fill time

equation 2:25-

$$u = \frac{dx}{dt}\cdot\frac{K}{\mu}\cdot\frac{dP}{dx}$$

$$\int_0^{t_L} dt = \frac{\mu}{K.P_o}\cdot\int_0^{L} x.dx$$

The flow time is thus -

$$t_L = \frac{\mu.L^2}{2.K.P_o} \text{ - - - - - - Equation } 2:25$$

2:5:2 Radial, Isotropic Darcy Flow

The most commonly used inlets are point sources which produce radial

flow. The shape of the flow will be dependent upon the fibre orientation

and volume fraction of the fibre pack. For an isotropic radial flow, as

portrayed in Figure 2.3 overleaf, the Darcy equation is expressed in circular

co-ordinates
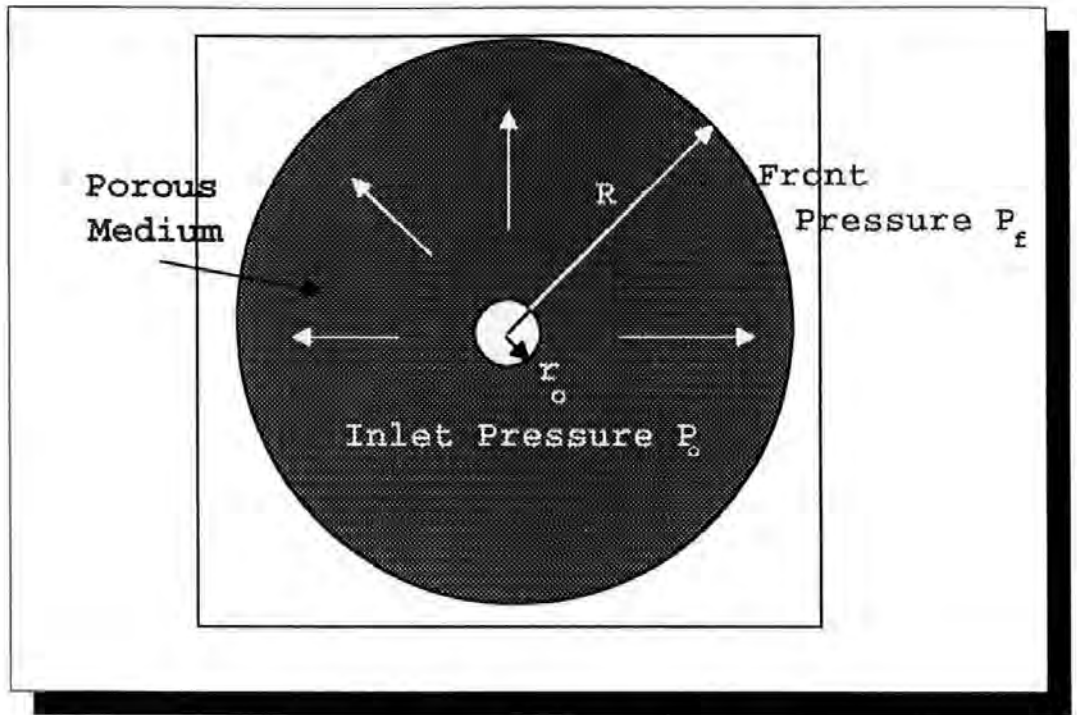
Figure 2:3. Radial, Isotropic Darcy Flow

$$-v_r = \frac{K}{\mu}.\frac{dP}{dr} \quad \text{------- Equation 2:26}$$

The mass continuity in this situation is as follows:

$$2\pi r_o.v_o = 2\pi.r.v_r \quad \text{----- Equation 2:27}$$

where
  v_o = *the superficial fluid velocity at the boundary of the inlet port*
  r_o = *the inlet port radius*
  r = *the radial distance flowed from the inlet port*
  v_r = *superficial fluid velocity at radius r*
  K = *the permeability of the fibre bed*
dP/dr = *the pressure gradient in the fluid*
  μ = *the fluid dynamic viscosity*

Combining equations 2.26 and 2.27 and integrating, equation 2:28 is

obtained

$$\frac{K}{\mu}.P_o = r.v_r.\ln\left(\frac{r}{r_o}\right) \quad \text{------- Equation 2:28}$$

A mass balance of the region behind the expanding flow front shows it to

be moving forward at the interstitial velocity of the fluid at the front, i.e.

$$v_r = \varepsilon.v_f \quad \text{-------- Equation 2:29}$$

If equation 2:29 (the Dupuit Relation) is substituted into equation 2:28 , then equation 2:30 is obtained

$$\frac{K.P_o}{\varepsilon.\mu}dt = r \ln\left(\frac{r}{r_o}\right) dr \quad \text{------ Equation 2:30}$$

Integrating

$$\int_{r=r_o}^{R} r \ln\left(\frac{r}{r_o}\right) dr = \frac{K.P_o}{\varepsilon.\mu} \int_{t=0}^{T} dt \quad \text{------ Equation 2:31}$$

where

T is the time to fill radial distance R.

Integrating equation 2:31:

$$\left[\frac{r^2}{2}\right]\left[\frac{r^2}{2}\ln\left(\frac{r}{r_o}\right)\right]_{r_o}^{R} - \int_{r_o}^{R}\frac{r^2}{2r} = \frac{K.P_o}{\varepsilon.\mu}T \quad \text{----- Equation 2:32}$$

By rearranging equation 2:32 we obtain the following

$$\frac{R^2}{4}\left(2\ln\left(\frac{R}{r_o}\right) - 1\right) + \frac{r_o^2}{4} = \frac{K.P_o}{\varepsilon.\mu}T \quad \text{------ Equation 2:33}$$

$$K = \frac{\varepsilon.\mu}{P_o.T}\left[\left(\frac{r_o^2}{4}\right) + \frac{R^2}{4}\left(2\ln\left(\frac{R}{r_o}\right) - 1\right)\right] \quad \text{---- Equation 2:34}$$

This equation may be rearranged according to the parameter being measured, usually either permeability K or fill time T.

2:5:3 Radial, Anisotropic Darcy Flow

For the case of an isotropic flow, the front is circular. For anisotropic flow as would be observed during a central injection of a unidirectional lay-up, the front is elliptical in shape. In this case, Darcy's law takes a different form:

35

$$-\overrightarrow{v} = \frac{\overline{K}}{\mu}.\text{grad } P \quad \text{------- Equation 2:35}$$

where
* grad P = the pressure gradient at some point in the flow*
* μ = the isotropic dynamic viscosity of the fluid*
* $\overrightarrow{v}$ = the superficial velocity vector at some point in the flow*
* $\overline{K}$ = the permeability tensor*
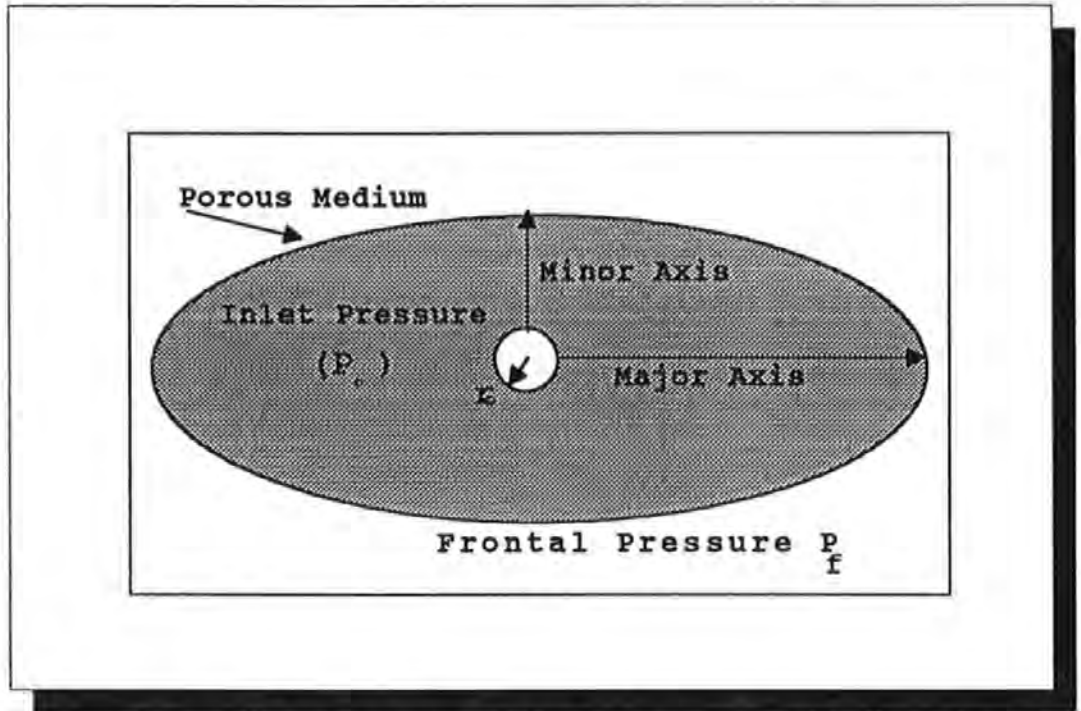
Figure 2:4 Radial, Anisotropic Darcy Flow

The mass flux continuity equation generalises as the following

$$\text{div}\,\overrightarrow{v} = 0 \quad \text{------- Equation 2:36}$$

The flow may be considered to be two dimensional in the plane of the mould. This is the same plane as that of the principal axes. Thus the permeability tensor becomes a 2x2 matrix and grad P and $\overrightarrow{v}$ become a 2x1 vector. The governing equation is then derived. The principal axes system, $\overline{K}$ reduces to the matrix

$$\begin{bmatrix} K_{11} & 0 \\ 0 & K_{22} \end{bmatrix} \quad \text{----- Equation 2:37}$$

36

The non-zero diagonal terms, K_{11} and K_{22} are the principal permeabilities in the direction of the first and second principal directions respectively. If the principal axes are x and y then from 2:35 and 2:36:

$$0 = \text{div}\left[\begin{pmatrix} K_{11} & 0 \\ 0 & K_{22} \end{pmatrix}\begin{pmatrix} \frac{\partial P}{\partial x} \\ \frac{\partial P}{\partial y} \end{pmatrix}\right] \qquad \text{---- Equation 2:38}$$

which produces

$$K_{11}\frac{\partial^2 P}{\partial x^2} + K_{22}\frac{\partial^2 P}{\partial y^2} = 0 \qquad \text{------ Equation 2:39}$$

The relative magnitude of the K_{11} and K_{22} determines the aspect ratio of the flow front. If:

$$\alpha = \frac{K_{11}}{K_{22}} \qquad \text{------- Equation 2:40}$$

The governing equation is then obtained as follows

$$\frac{\partial^2 P}{\partial x^2} + \alpha\frac{\partial^2 P}{\partial y^2} = 0 \qquad \text{------ Equation 2:41}$$

When $\alpha = 1$, then the bed is isotropic and the flow is governed by the Laplace equation. In general, the principal axes of the porous medium will be oriented at the same angle θ, as the axes in which the permeability is measured. A particularly clear and succinct derivation of the permeability tensors was developed by Carter [32] and these tensors are as follows;

$$K_{11} = \frac{K_x + K_y}{2} + \frac{K_x - K_y}{2}.\cos 2\theta \qquad \text{------- Equation 2:42}$$

$$K_{22} = \frac{K_x + K_y}{2} - \frac{K_x - K_y}{2}\cos 2\theta \qquad \text{------- Equation 2:43}$$

where

K_{22} and K_{11} are the experimental permeabilities

K_x and K_y are the principal permeabilities

θ = the angle between the two co-ordinate systems

2:5:4 Modification of Carman-Kozeny for Fibrous Beds

The Carman-Kozeny equation for particulates has been used to describe the flow of Newtonian Fluids through packed beds of spherical particles and this is now extended for packs of fibres. The equation which models this is;

$$K = \frac{r_f^2}{4.k_o.\left(\frac{L_e}{L}\right)^2} \cdot \frac{\varepsilon^3}{(1-\varepsilon)^2} \quad \text{----- Equation 2:44}$$

where r_f = the fibre radius

In this situation, there are two distinct types of flow

i) Axial (along the fibres)

ii) Transverse (across the fibres)

Therefore the Kozeny constant varies in each direction of flow due to the different resistance to flow. Modifications have been made to the Carman-Kozeny equation to take into account the possibility of flow in both transverse and axial directions. The packing arrangement of the fibres has also been dealt with by Gebart [34] and this is highlighted below. Two ordered arrangements have been selected and these are hexagonal and square packing. For flow perpendicular to the fibre lay-ups the permeabilities are as follows,

$$K_{\perp(\text{SQUARE})} = \frac{16}{9\pi.\sqrt{2}} \cdot \left(\sqrt{\frac{V_{f(max)}}{V_f}} - 1\right)^{\frac{5}{2}} .r \quad \text{----- Equation 2:45}$$

$$K_{\perp(\text{HEX})} = \frac{16}{9\pi.\sqrt{6}} \left(\sqrt{\frac{V_{f(max)}}{V_f}} - 1\right)^{\frac{5}{2}} .r \quad \text{------- Equation 2:46}$$

where $V_{f(max)}$ = the maximum volume fraction when the fibres touch.

$V_{f(max)}$ = $\pi/4$ *for square and* $\frac{\pi}{2\sqrt{3}}$ *for hexagonal arrangements*

For flow parallel to the fibres, Gebart concluded that the flow was dependent on an experimentally determined constant, and the general equation is

$$K_{//} = \frac{8 \cdot r^2}{k_o} \cdot \frac{(1 - V_f)^3}{V_f^2} \qquad \text{- - - - - Equation 2:47}$$

where $k_o = 32 \cdot k$

The shape factor in fibres is primarily a function of the volume fraction which can only be altered by moving the fibres together or apart, hence changing the flow geometry. Typical values for the shape factor were determined by Schlichting [35] and are 57 for square and 53 for hexagonal arrangments which gave Kozeny constants of 1.78 and 1.66 respectively. The Carman-Kozeny equation was modified further by Williams et al. [36] who combined the Darcy equation (equation 2:24) for linear isotropic flow with the Carman-Kozeny equation and introduced the mean hydraulic radius m. The mean hydraulic radius is given by,

$$m = \frac{r}{2} \cdot \frac{\varepsilon}{1 - \varepsilon} \qquad \text{- - - - Equation 2:48}$$

where

  r = fibre radius

The flow rate Q, from Darcy's law for linear one-dimensional flow may then be written as

$$Q = \frac{\varepsilon \cdot A \cdot m^2 \cdot \Delta p}{k \cdot \mu \cdot L} \qquad \text{- - - - - - - - Equation 2:49}$$

39

2:6 Measurement of Permeability

The purpose of this section is to review the development of permeability measurement from its origins in particulate media up to present day procedures for fibre beds.

2:6:1 Permeability of Particulates

The work of Darcy, Blake, Kozeny and Carman led to the experiments to verify their respective equations. The early experimental set-ups used particles of a predetermined size, determined by the Sauter mean diameter method which involved analysis with sieves of different sized meshes. Some work was also carried out by Latini [37] to determine the degree of anisotropy in specific rocks such as mica. Anisotropy in rocks is caused by particles which are, on average, asymmetric in shape and have a specific orientation. This is even more pronounced in fibre beds due to the vastly different flow areas in the axial and transverse directions. There has been a steady development of apparatus designed to measure the permeability of porous rocks, both consolidated and unconsolidated.

Figure 2:5 shows the first apparatus, designed by Fancher et al. [38] in 1933 which used a bored rubber holder for the sample into which fluid flowed from the base with pressure tappings to enable the pressure to be determined. Johnson et al. [39] then designed a radial flow experiment, the apparatus of which is shown in Figure 2:6.
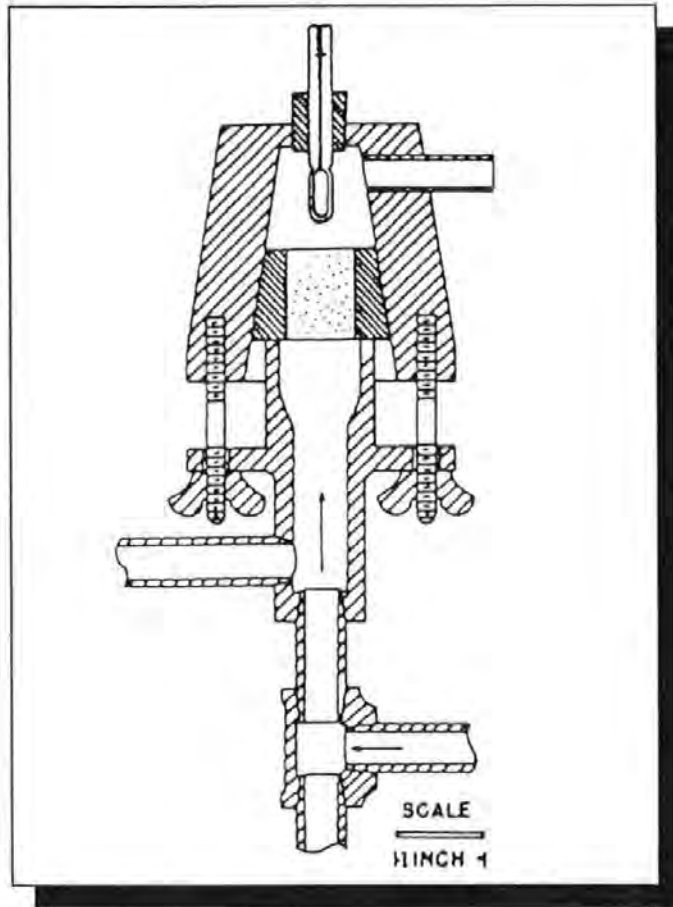
Figure 2:5 Fancher's Particulate Media Permeability Apparatus [38]
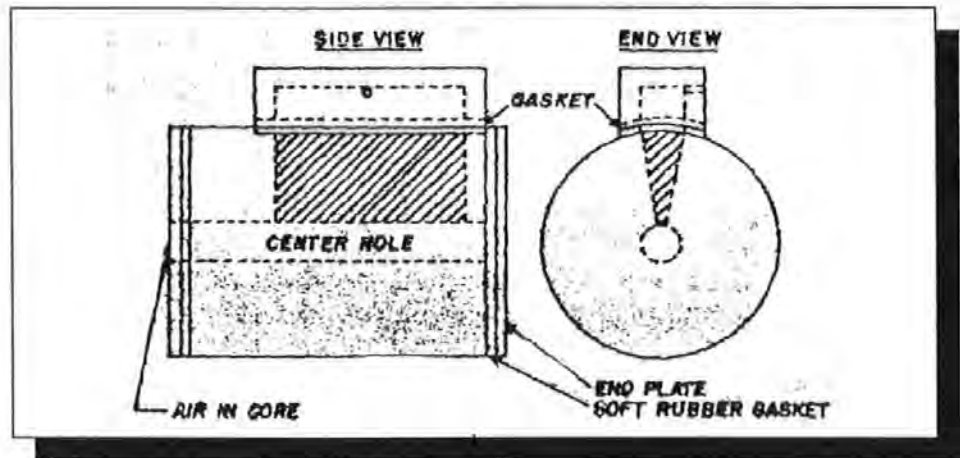
Figure 2:6 Johnson et al.'s Radial Permeability Apparatus [39]

Johnson et al.'s apparatus used a gas which was forced into the sample

through a bore in the centre. This allowed permeabilities to be measured

with respect to the angle of the bedding plane. These two methods used

41

consolidated media. For unconsolidated media, the permeability

measurements were taken 'in-situ' since samples of the bed cannot be taken

without altering its structure. Two types of permeability apparatus were

designed at Syracuse University, the first of which is shown in Figure 2:7.

This was built by Latini [37] in 1967 and allows flow in two orthogonal

directions to be measured simultaneously.
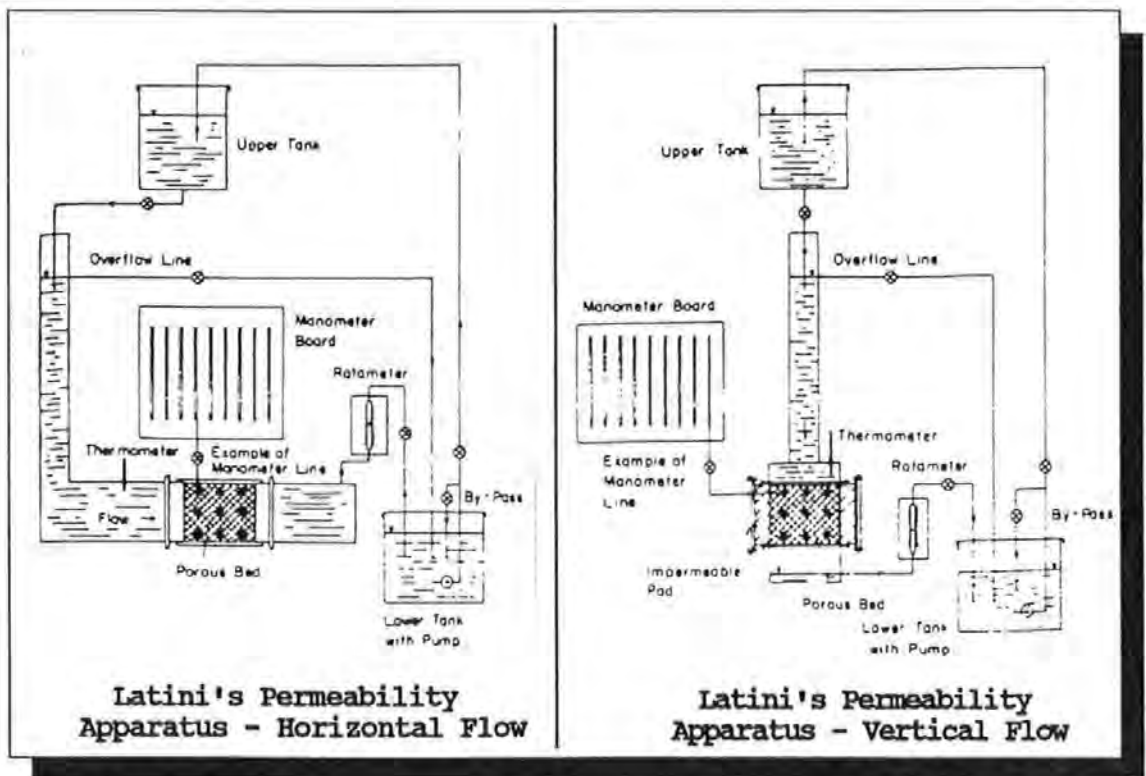
Figure 2:7 Latini's Horizontal and Vertical Permeability Apparatus [37]

The second apparatus, shown in Figure 2:8, was built by Fontugne [40] in

1969 and employs simultaneous two dimensional flow measurements.

The directional nature of these measurements simulates the directional nature

of sands, salts and clays apparent where oil recovery is required.

Measurements taken at Syracuse using the two methods are shown in Tables

2:3 and 2:4. Table 2:3 reproduces Latini's measurements and shows
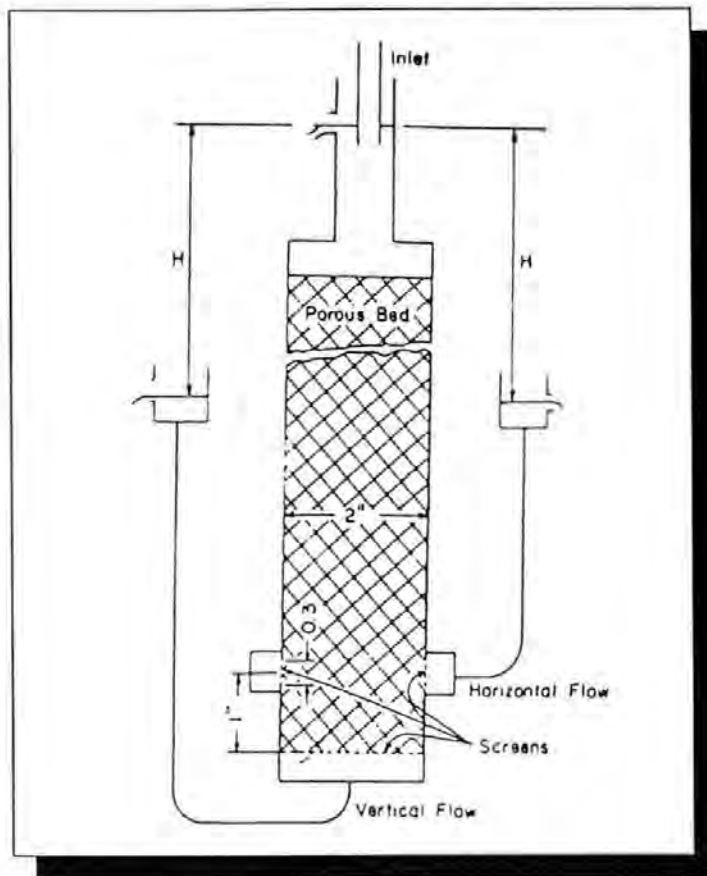
Figure 2:8. Fontugne's Simultaneous Horizontal/ Vertical Permeability Apparatus

significant anisotropy in beds of naturally settled sand particles; vertical

permeabilities were 20% less than horizontal permeabilities for naturally

settled limestone particles.

Fontugne's data (Table 2:4) also measured two dimensional permeability

simultaneously. He found that the horizontal permeability in a sand sample

with a small particle size was approximately 20% greater than the vertical

permeability, but for a larger grain size, the vertical permeability was 20%

larger. Mica and activated carbon particles were also measured, the mica

being highly anisotropic due to its flake-like geometry.

SAMPLE	POROSITY ε	VERTICAL PERMEABILITY B_v (cm^2 x 10^7)	HORIZONTAL PERMEABILITY B_h (cm^2 x 10^7)	PERMEABILITY RATIO B_h/B_v	EQUIVALENT DIAMETER
SAND SAMPLE 1	0.38	5.1	5.4	1.06	254
	0.44	9.6	10.1	1.05	254
SAND SAMPLE 2	0.38	0.76	0.79	1.04	100
LIMESTONE SAMPLE A	0.46	9.9	11	1.11	230
	0.51	14.4	17.4	1.21	220
LIMESTONE SAMPLE B	0.45	17.8	19.7	1.11	326
	0.5	30.5	36.5	1.2	334
LIMESTONE SAMPLE C	0.46	25.1	28.1	1.12	369
	0.5	41	50.5	1.23	383

Table 2:3 Directional Properties - Unidirectional Flow

SAMPLE	POROSITY ε	VERTICAL PERMEABILITY B_v (cm^2 x 10^7)	HORIZONTAL PERMEABILITY B_h (cm^2 x 10^7)	PERMEABILITY RATIO B_h/B_v	EQUIVALENT DIAMETER #
SAND SAMPLE 1	0.42	5.21	4.85	0.93	204
	0.48	7.8	8.54	1.1	220
SAND SAMPLE 2	0.42	1.98	2.43	1.23	126
	0.44	2.61	3.54	1.36	133
	0.45	3.15	4.01	1.28	136
LIMESTONE SAMPLE 1	0.49	9.26	11.3	1.22	191
	0.52	14.3	16.7	1.17	210
LIMESTONE SAMPLE 2	0.48	20	22.2	1.11	304
	0.52	32.4	32.5	1.01	315
LIMESTONE SAMPLE 3	0.5	50.7	40.8	0.81	424
	0.53	70.4	56.3	0.8	432
MICA	0.87	0.09	0.17	1.93	2
ACTIVATED CARBON	0.77	1.38	1.38	2.16	17
	0.76	0.97	0.97	2.46	15

Table 2:4. Directional Properties - Two Dimensional Flow

the equivalent diameter is the hydraulic radius of the bed multiplied by the fluid viscosity

2:6:2 Permeability Measurement of Fibre Beds

A significant amount of time has been spent by a number of institutions regarding the measurement of the permeability of fibre reinforcements. In most cases, the permeability has been used to show how the flow properties vary with changes in the parameters of the process. This section reviews the work undertaken in the area of fibre permeability measurement and shows the degree to which permeability is affected by the following parameters

- fibre volume fraction
- injection (driving) pressure
- injection fluid
- the stacking sequence of the layers
- the fluid viscosity
- fibre orientation
- reinforcement architecture
- fibre surface treatment

2:6:3 Fibre Reinforcement Permeability Measurement Apparatus

The methods used for measurement of permeability have been based around two theories

i) Darcy's Law

ii) Carman-Kozeny Theory

The vast majority of the tests carried out are based on two dimensional flow because most RTM type components are thin shell structures and therefore through thickness flow is relatively small. All the moulds used for permeability measurement have been of the visualisation type to enable accurate measurement of flow rates. A selection of moulds is now shown with varying degrees of complexity and instrumentation. In all the moulds, the same parameters are being measured but the flow directions may be linear or radial

from point and line sources. The first mould was used by Adams and Montgomery at Princeton University and is shown in Figure 2:9.
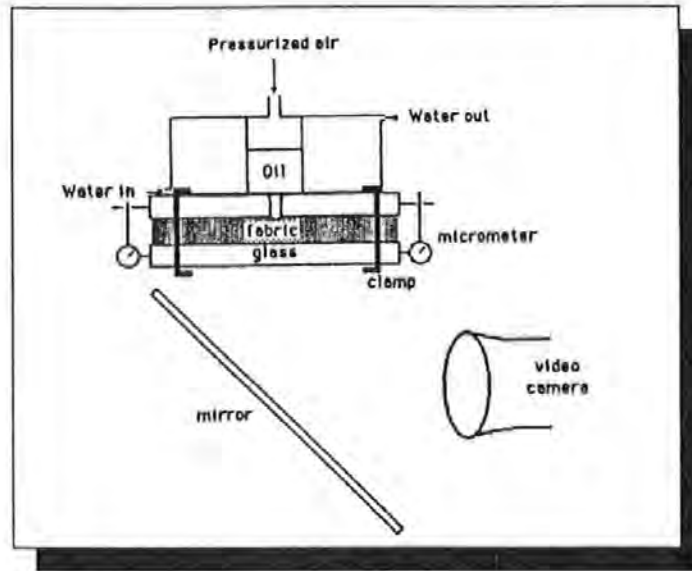
Figure 2:9 Adam's et al.'s Permeability Apparatus

In this set-up, the oil was kept at a constant temperature by a water bath and a driving pressure forced the oil into the reinforcement. The whole injection was recorded on a video camera and replayed to plot the progression.

Figure 2:10 shows two moulds developed by Kendall et al. [41] at Nottingham University for different modes of flow, linear and radial. The moulds use vacuum pressure and are therefore sealed around the perimeter.
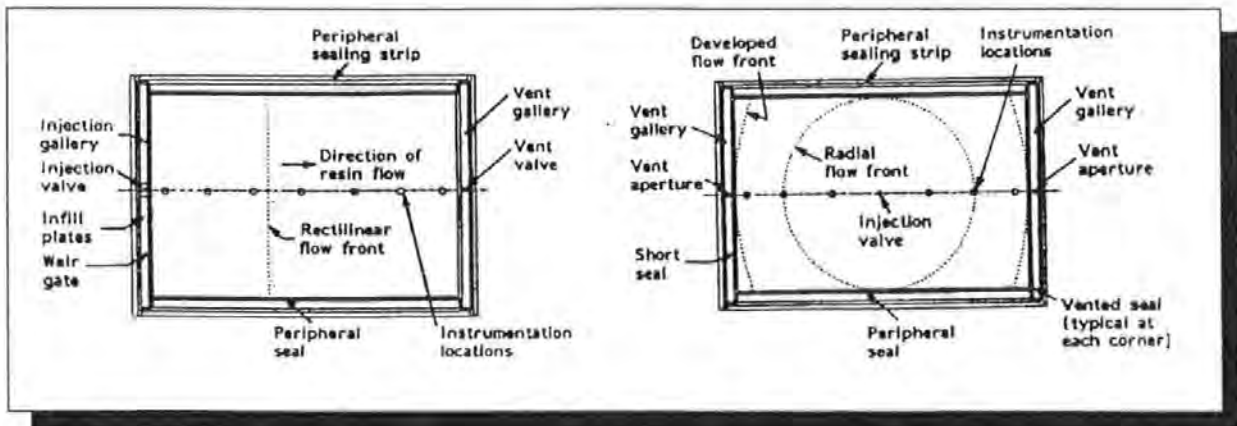
Figure 2:10. Linear and Radial Visualisation Moulds used by Kendall et al.

The majority of the permeability tests undertaken involve two-dimensional (in-plane) flow. Van Harten [42] has done extensive tests on woven reinforcements and fibre mats on the following mould shown in Figure 2:11.
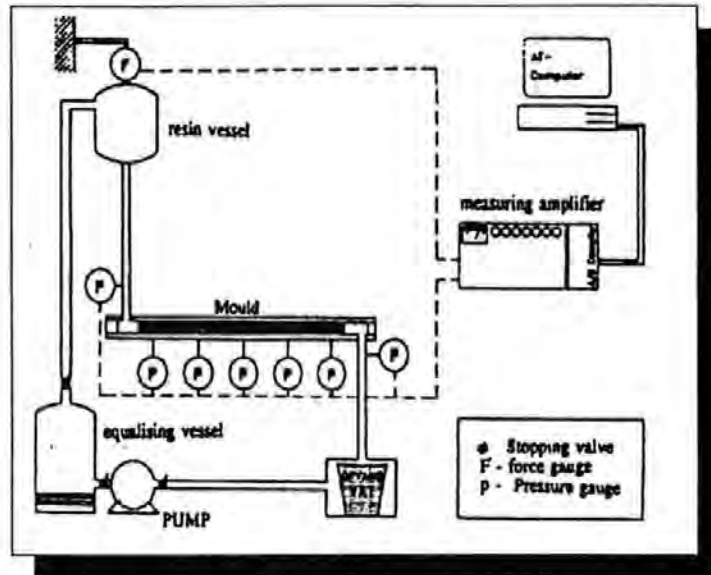
Figure 2:11 Van Harten's Permeability Apparatus

The set-up was used for both linear and radial flow and flow rates of the fluid into the mould were measured. Results are discussed later in this section. Gebart et al. [34] designed a sophisticated mould seen in Figure 2:12, which included mould deflection gauges, to measure the radial flow through anisotropic fabrics. The temperature and pressure of the injection were monitored for viscosity and pressure drop measurement. Two moulds were used for the tests, a rectangular one for linear flow and a square one for radial flow. The same parameters were measured for each with mould deflection more apparent in the radial flow experiments. Another permeability measurement rig was designed by Verheus et al [43]at TNO in Delft, Holland.

47
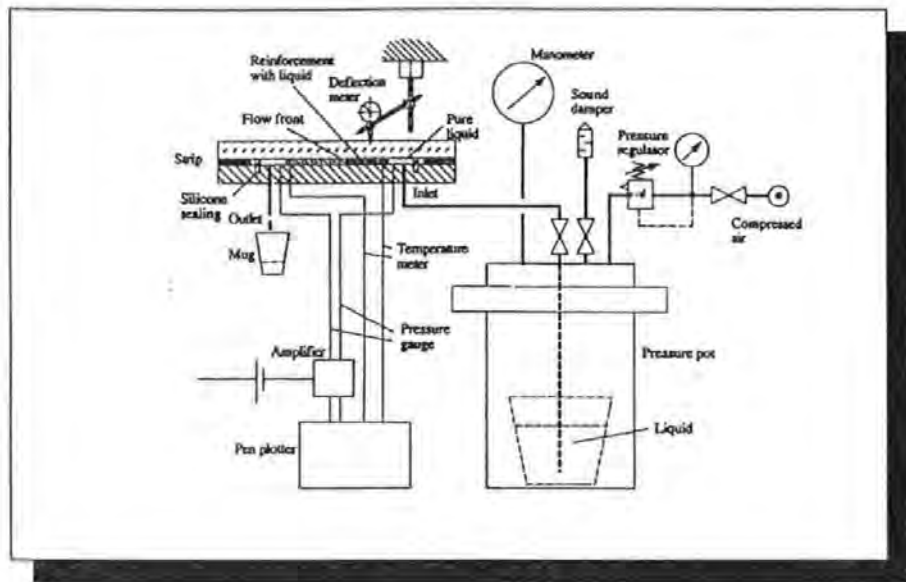
Figure 2:12. Gebart et al.'s Permeability Radial and Linear Flow Apparatus

This may be used for three dimensional flow but has been used in this case to measure in-plane permeabilities of random continuous mat and 'Injectex', a highly anisotropic flow enhancing weave. As will be noticed in Figure 2:13, the mould is very long and narrow which reduces mould deflection considerably. A variable cavity thickness is possible with the adjustable mould side.
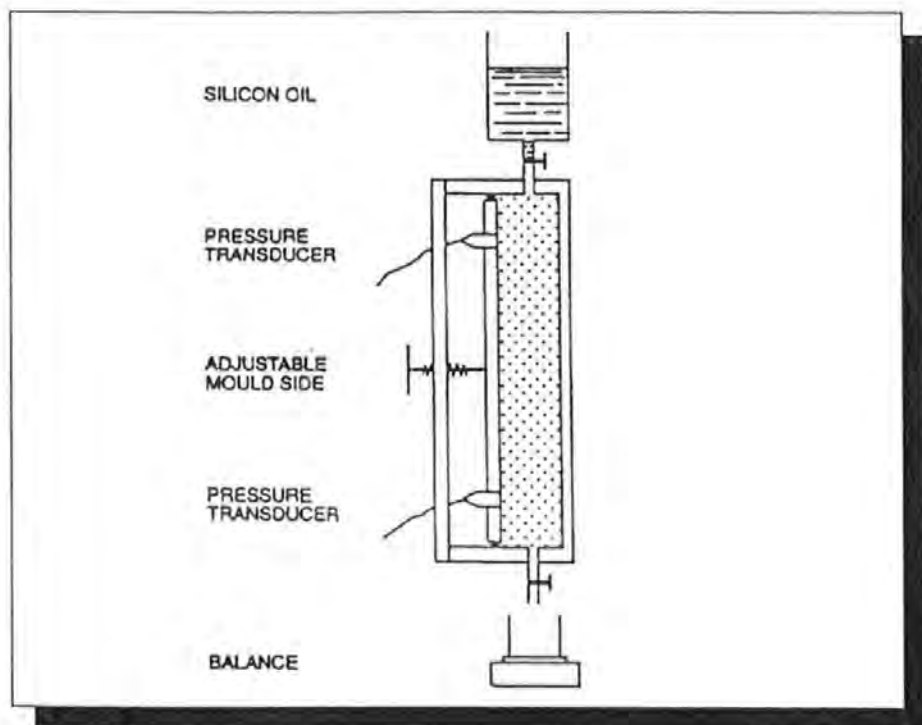
Figure 2:13 Verheus et al.'s Adjustable Permeameter [43]

Transverse and in-plane flow have been investigated by Trevino et al. [44] and the respective moulds are shown in Figures 2:14 and 2:14a.
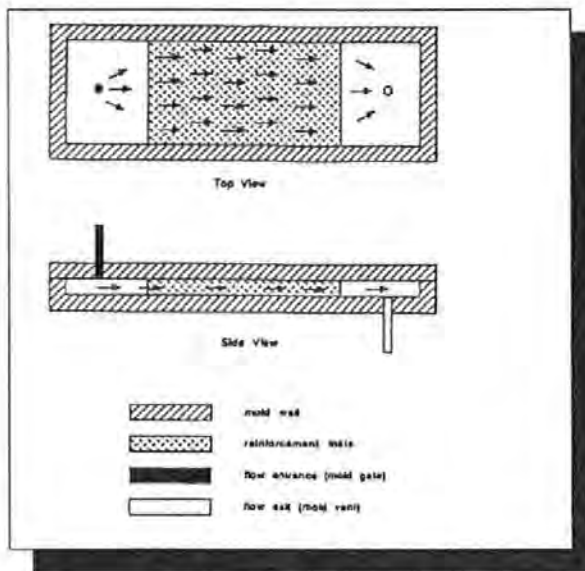
Figure 2:14 Trevino et al.'s In-plane Mould.
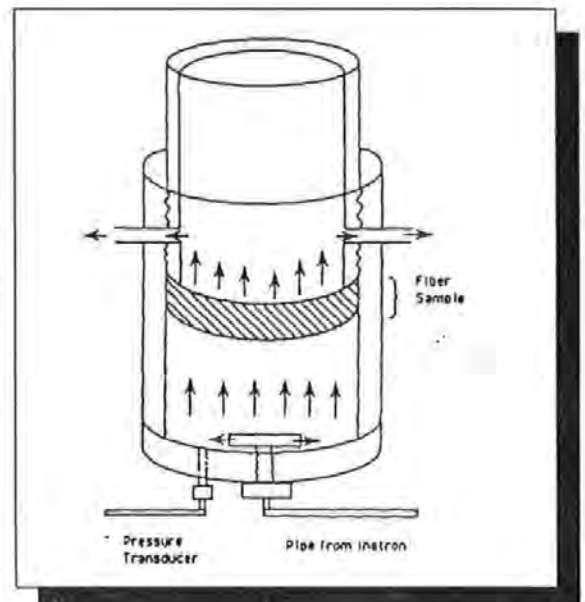
Figure 2:14a Trevino et al's Transverse Flow Mould

These two moulds were used to determine the three dimensional flow properties of the fibre samples tested, which in this case were random, stitched bi-directional and unidirectional glass mats. As expected the results showed that in the three directions, the flow increased with a reduction in volume fraction (increase in porosity). For the bidirectional fabric, the 'z' direction (through thickness) permeability was significantly less than the in-plane permeabilities. Perry et al. [45] at Ohio University designed a system to measure the three permeabilities in an 'all-in-one' set-up controlled from a single hydraulic cylinder. The system consisted of three moulds for in-plane, transverse and radial flow. The fabric tested was a 5-harness satin carbon and it was found that the transverse permeability was significantly larger than the in plane permeabilities even at 58% volume fraction.

The permeability of a fabric at such high volume fractions is small due to the maximum packing fraction being approached and in this case the permeability is in the region of 0.1 to 0.5 darcies (9.869×10^{-14} - $4.9345 \times 10^{-13} m^2$)
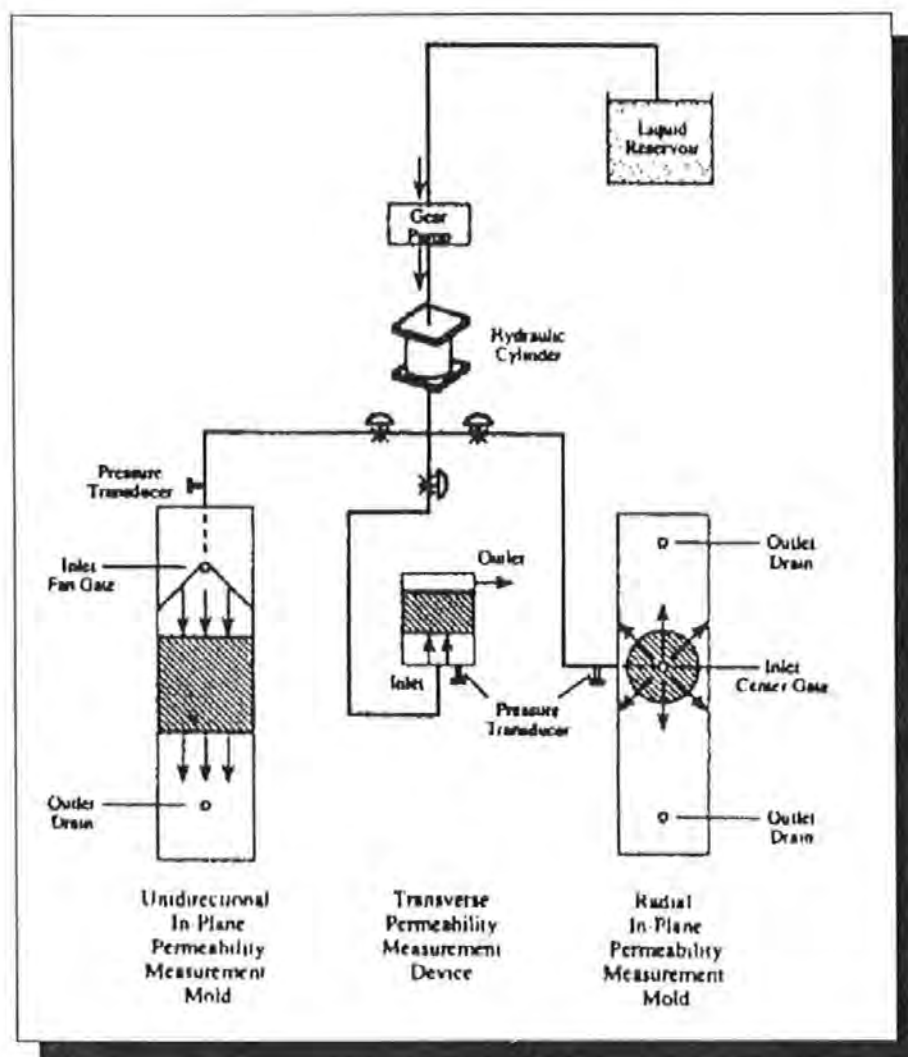
Figure 2:15 Perry et al.'s Experimental Set-up

Ahn et al. [46] designed an apparatus to enable them to measure the permeability and capillary pressure in tandem and this is shown diagramatically in Figure 2:16. The capillary pressure was determined by obtaining a form factor 'F' as seen in equation 2:50 from knowledge of the surface tension and the contact angle. Using the Carman-Kozeny equation, it was shown that the

permeability and the porosity function have a linear relationship. The fibre bed consisted of a plain-woven T-300 carbon fabric.

$$P_c = \frac{F}{D_f} \cdot \frac{(1-\varepsilon)}{\varepsilon} \cdot \sigma \cdot \cos\theta \ \text{----- Equation 2:50}$$

where
F = the form factor depending upon the fibre orientation
(F=4 for longitudinal and F=2 for transverse flow direction)
σ = the surface tension of the wetting fluid (Pa.m)
θ = the contact angle between liquid and solid
D_f = the fibre diameter
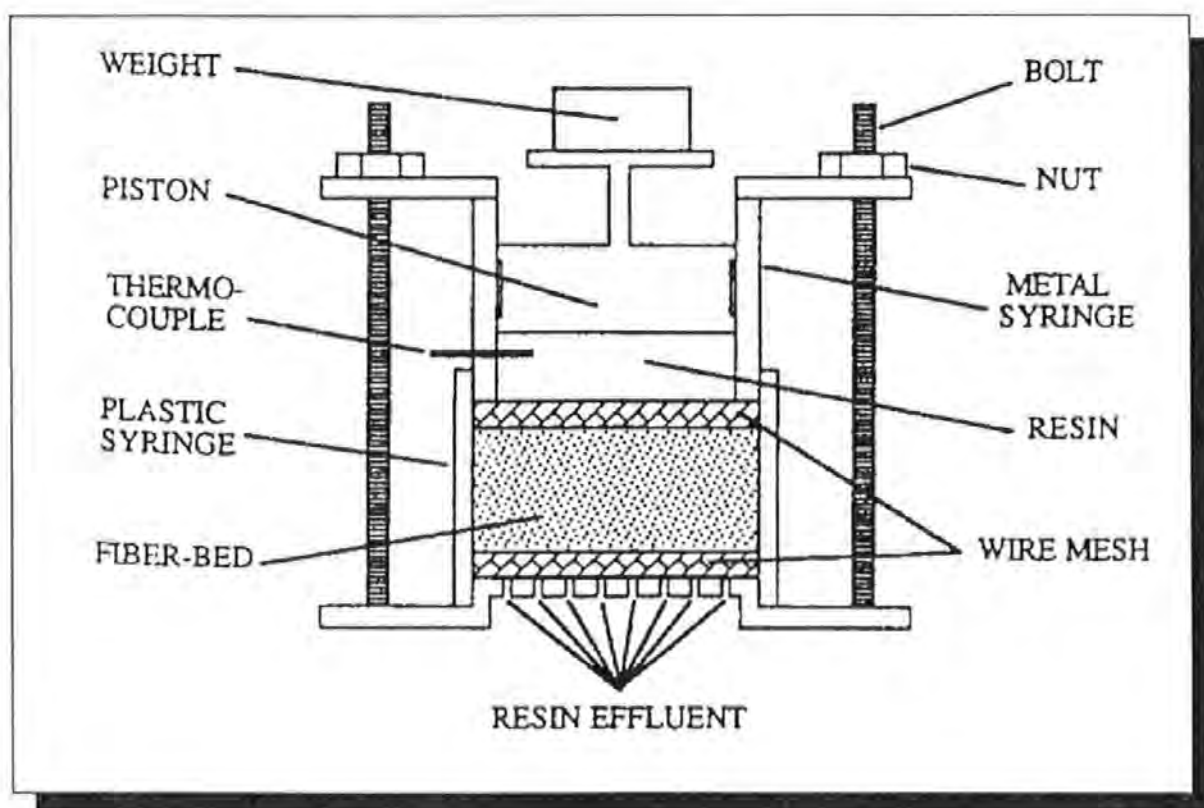
Figure 2:16. Ahn et al.'s Simultaneous Capillary Pressure and Permeability Measurement Rig

The permeability figures obtained from these apparatus are now discussed in more detail.

2:6:4 Permeability Measurement using Darcy's Law

The majority of permeability measurements taken have employed Darcy's Law and a selection of the experimental measurements is now reviewed. Figure 2:17 shows the results of tests undertaken by Adams et al. [47] using the mould shown in Figure 2:9.
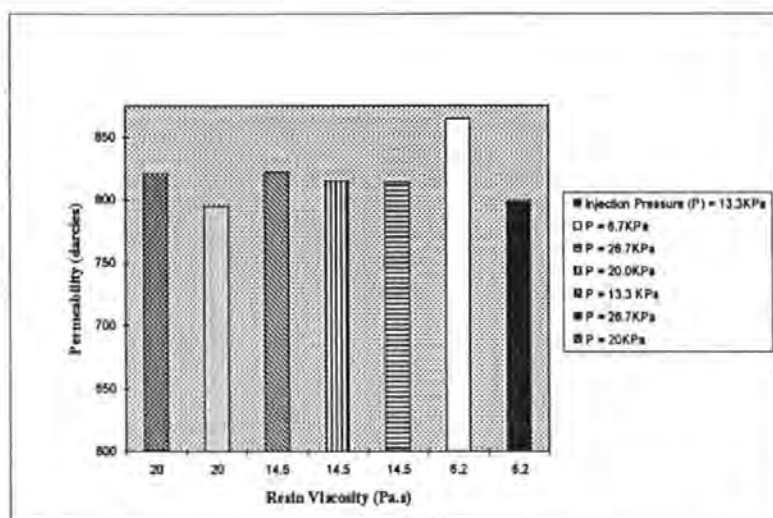
Figure 2:17 Permeability of Polypropylene (5-280) Plain Weave to Shell Epon 828 Epoxy Resin using Radial Flow

In these tests, the volume fraction was constant but the injection pressure was varied along with the resin viscosity. As will be observed, the permeability is greatest for the lowest resin viscosity (6.2Pa.s) at the lowest pressure which suggests that a driving pressure which is too large will have a detrimental effect on the permeability. This is due to the pressure causing the fibres to crush together, increasing the volume fraction locally and creating an obstruction to flow. Work on the same mould has been undertaken to determine the sensitivity of permeability to the stacking sequence of the layers. In this work, two fabrics of high and low permeability are stacked in different sequences and the results are shown in Figure 2:18.
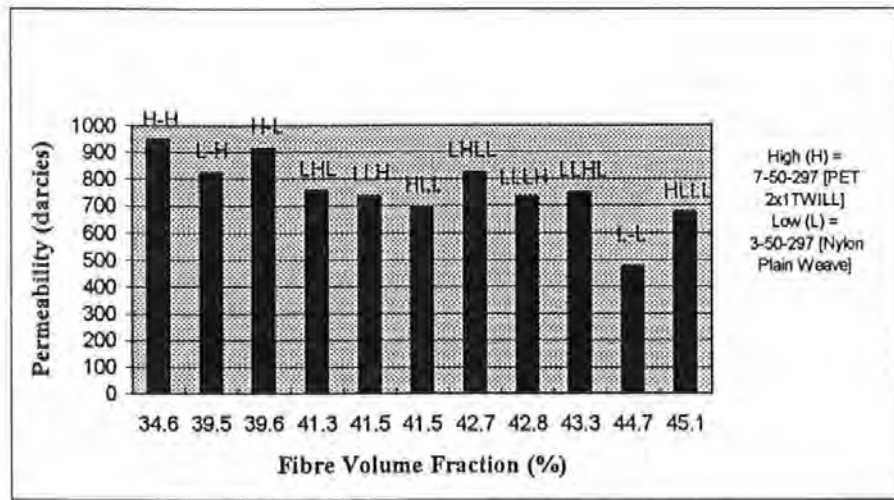
Figure 2:18 The Multilayer Effects of High and Low Permeability Fabrics

Initial results with 2 layers were as expected but later experiments are interesting in that laminates with the same proportion of each type of reinforcement have widely differing permeability values when stacked in a different order. This shows that the stacking sequence is another contributor to the variation of permeability values. Further work by Adams on the same mould involved a selection of bi and triaxially woven fabrics and non-woven fabrics. They were tested using Shell Epon 828 resin and the results are shown in Table 2:5. The volume fractions range from 14% to 58.5% and the difference in permeabilities is very marked. The PET fabric of three different tow sizes increases in permeability with an increase in tow size from 105 to 1000 filaments. This is due to the larger inter tow spaces which promote flow. Introduced in this work is the anisotropy index (γ) which is a ratio of the major and minor permeabilities of the two principal flow directions. As mentioned previously, permeability is used as a measurement to detect variations in flow properties due to subtle changes in the reinforcement.

REINFORCEMENT	LAY-UP ORIENTATION	VOLUME FRACTION (%)	PERMEABILITY (K_1) darcies	PERMEABILITY (K_2) darcies	ANISOTROPY INDEX (K_2/K_1)	FLOW DIRECTION (wrt the fibres)
MONOFILAMANT FABRICS						
PET105 (Plain)	2 x parallel	43.8	48	48	1	
PET 297 (2x1 Twill)	2 x parallel	33	702	702	1	
PET 1000 (Plain)	2 x parallel	44.2	3166	3166	1	
Nylon 297 (Plain)	2 x parallel	36	264	264	1	
PP 280 (Plain)	2 x parallel	33.5	381	267	0.7	90°
PP280	2 x perpendicular	32.5	360	360	1	
BI AND TRIAXIAL FABRICS						
PET 61 (Plain)	2 x parallel	58.5	40	25	0.63	90°
PET 61	2 x perpendicular	58.4	27	27	1	
PET41(60°-0°-60°)	2 x parallel	52.9	224	139	0.62	12°
PET 41	2 x perpendicular	53	145	145	1	
NON WOVEN FABRICS						
PET mat	2 x parallel	8.89	526	526	1	
TYPAR	2 x parallel	41.1	165	165	1	
REEMAY	2 x parallel	12.5	403	287	0.71	10°
REEMAY	2 x perpendicular	14.1	299	299	1	

Table 2:5. In-Plane Permeability Data for Selected Monofilamant, Bi and Triaxially Woven Fabrics and Nonwoven Fabrics (Using Shell Epon 828 of Viscosity 9.44 Pa.s at 25 °C).

Reinforcement	Permeability (K_1) darcies	Permeability (K_2) darcies	Anisotropy Index	Notes
3-50-297 (Nylon Plain Weave)	463	463	1	UNTREATED
3-50-297 (Nylon Plain Weave)	475	475	1	TREATED
HC-3-335 (Nylon Plain Weave)	541	541	1	UNTREATED
HC-3-335 (Nylon Plain Weave)	560	560	1	TREATED
5-280 Polypropylene Plain Weave	453	309	0.68	UNTREATED
5-280 Polypropylene Plain Weave	458	301	0.68	TREATED

Table 2:6. The Effect of Reinforcements Coated with MS-122 Release Agent on Surface Wettability.

Table 2:6 shows the result of coating a reinforcement in release agent (MS-122). The nylon plain weave increases in permeability marginally when treated, but with the polypropylene plain weave, the permeability alters to maintain the anisotropy index. Montgomery et al. [48], also from Princeton investigated a range of fabrics by increasing the injection pressure gradually over the range 0.67 to 4 bars. The gradual pressure increase was designed to avoid fibre wash in low volume fractions. Figure 2:19 shows the results of these tests and as observed, there is a fine balance between the volume fraction, areal weight and the configuration of the reinforcement.
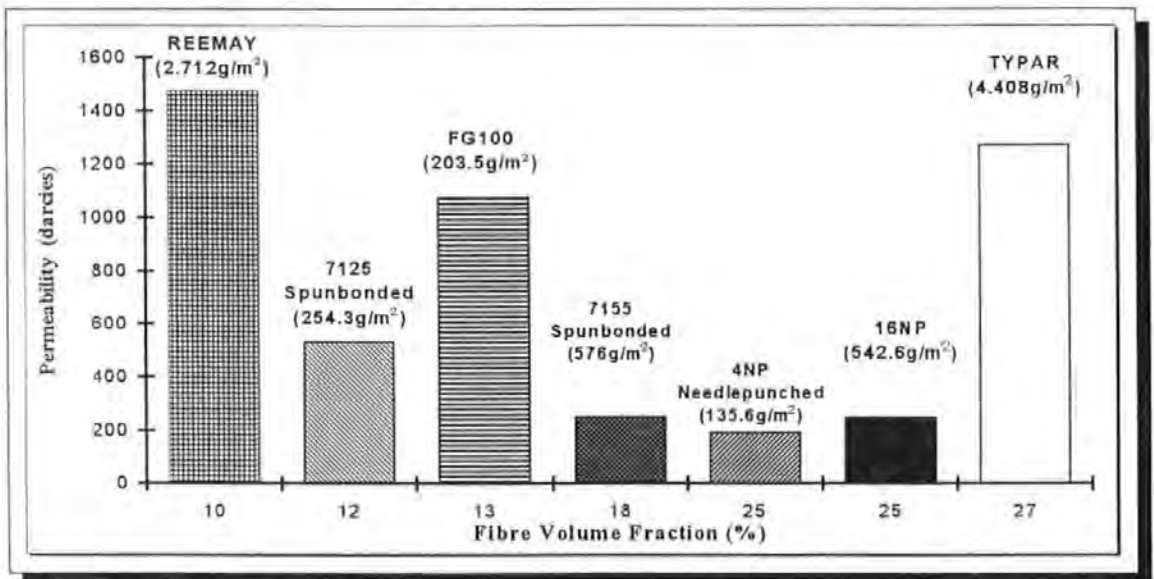
Figure 2:19 Radial Flow of Silicone Oil of Viscosity 1Pa.s through Various Reinforcements

Montgomery et al [49] continued the work with thermoplastic reinforcements with silicone oil used as the injection fluid. The permeability values were reported with error bands which were useful to fellow researchers to give ideas of what to expect in terms of the scatter of the values. The error bands do not appear to have a trend and to some extent are dependent on the handling of the reinforcement and also uncontrollable problems of stacking and local

changes in volume fraction. It was found in this work that by increasing the injection pressure on an anisotropic fabric meant that the anisotropy was increased.

REINFORCMENT MATERIAL	AREAL WEIGHT (g/m²)	VOLUME FRACTION (%)	VISCOSITY (Pa.s)	PRESSURE HEAD (KPa)	PERMEABILITY (K_1) darcies	PERMEABILITY (K_2) darcies
HOMOGENEOUS GEOTEXTILES						
POLYESTER	250	13	1	90.72	355 +/- 32	312 +/- 37
POLYESTER	250	13	5	362.89	380 +/-19	311 +/- 17
POLYESTER	250	13	10	362.89	360 +/- 39	307 +/- 33
HETEROGENEOUS GEOTEXTILES						
POLYESTER	550	15	1	90.72	218 +/- 6	208 +/- 1
POLYESTER	550	15	5	181.45	318 +/- 89	267 +/- 58
POLYESTER	550	15	5	272.17	240 +/- 10	229 +/- 20
POLYESTER	550	15	10	362.89	245 +/- 20	227 +/- 29
NON-WOVEN GEOTEXTILES						
POLYESTER	250	12	All textiles tested with the same viscosities and pressure heads as used with the above two sets of tests.		569 +/- 132	513 +/- 149
POLYESTER	590	18			261 +/- 26	261 +/- 26
POLYESTER	200	13			1175 +/- 160	1039 +/- 102
POLYPROPYLENE	140	25			210 +/- 19	174 +/- 5
POLYPROPYLENE	540	25			276 +/- 19	226 +/- 16

Table 2:7. Radial Flow of Silicone Oil through Fibre Packs
Reference : Montgomery et al. [49]

It is important to realise the effects of axial and transverse flow on the injection and Gebart [50] shows in Figure 2:20, the difference between the two directions in an aligned fibre bed. There is a convergence at higher volume fractions because the axial flow channel size tends toward the transverse size but at volume fractions between 30 and 40% there is a significant difference.

A very common type of reinforcement is continuous randomly oriented mat (Unifilo) [51]. Verheus [52] tested two random mats of slightly differing structure and the results are shown graphically in Figure 2:21. Fannucci et al. [53] compared the flow properties of woven and random reinforcements and

showed that woven mat has by far the better impregnation properties due to the inter-tow spacing and highlighted the limitations of random mat in terms the maximum volume fraction attainable.
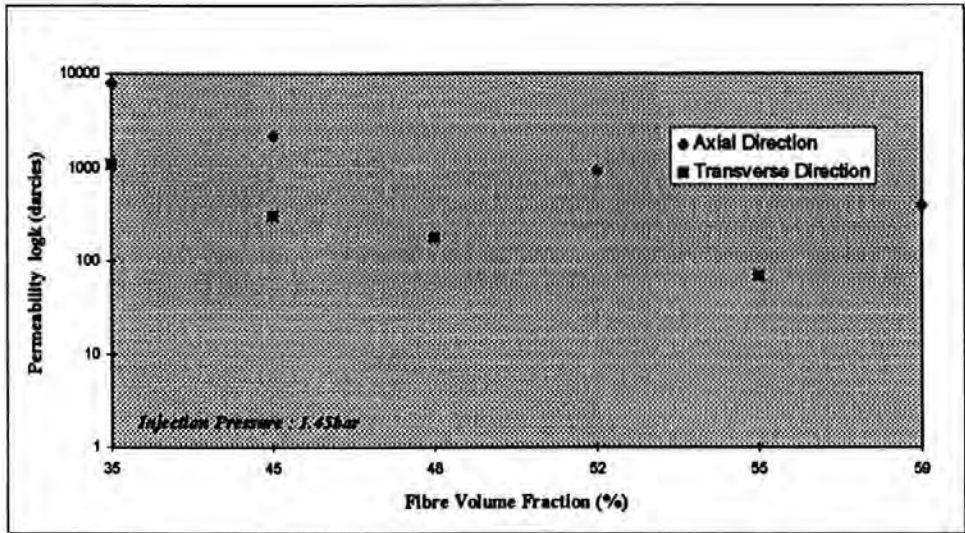
Figure 2:20 Axial / Transverse Flow of Jotun Norpol (PO-2454) of Viscosity 0.2 Pa.s through Aligned Fibres
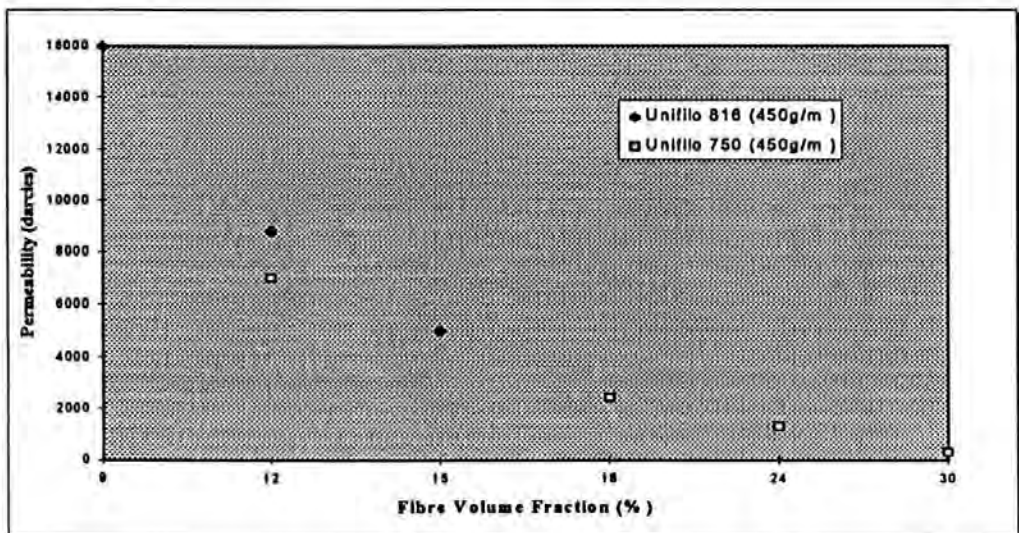
Figure 2:21 Permeability of Continuous Random Mat to Silicone Oil of Viscosity 0.2 Pa.s using 0.5 bar Vacuum Pressure

Van-Harten [54] has also carried out work on random and woven reinforcements at low volume fractions. As expected the volume fraction increase produced a decrease in permeability.
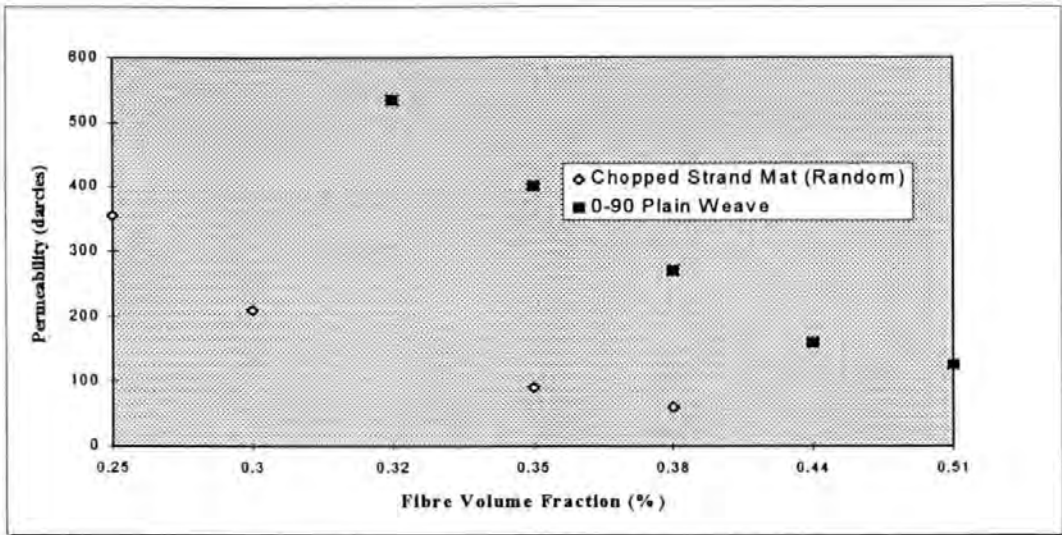
Figure 2:22 The Effect of Fibre Orientation on in-plane Permeability
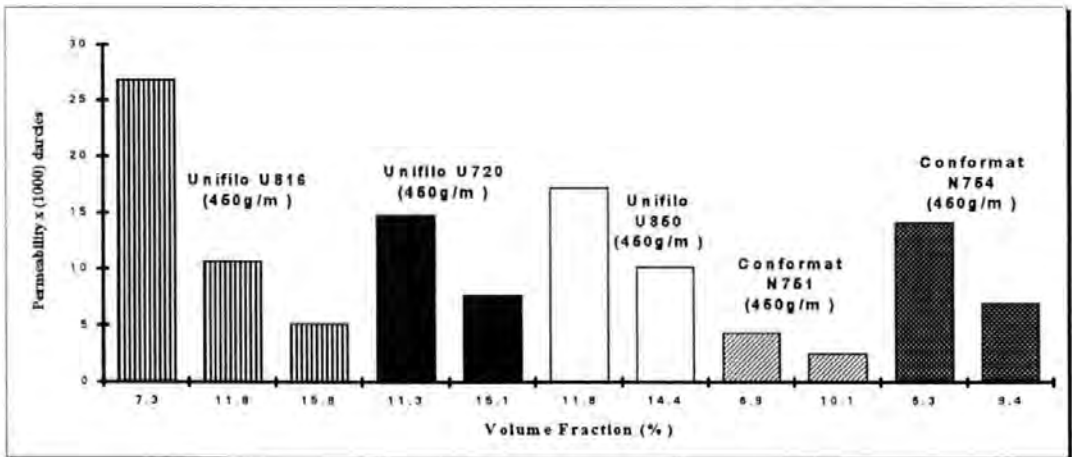
Figure 2:23 Radial Flow of Silicone Oil through Various Fibre Mats
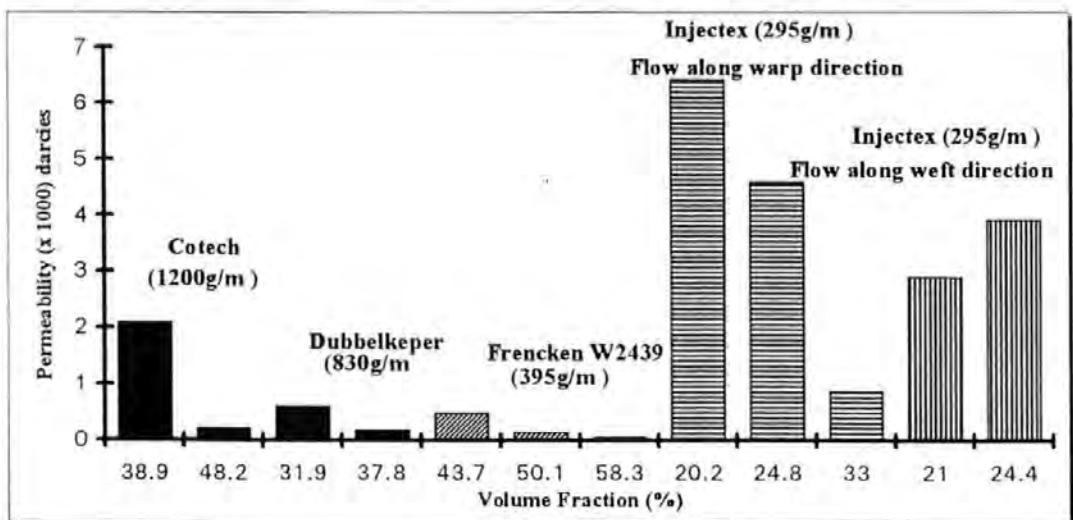
Figure 2:24 Radial Flow of Silicone Oil through Various Woven Fabrics

The effect of pressure drop on the permeability can be seen from work by Martin et al. [55] on continuous strand, random weave fabric.
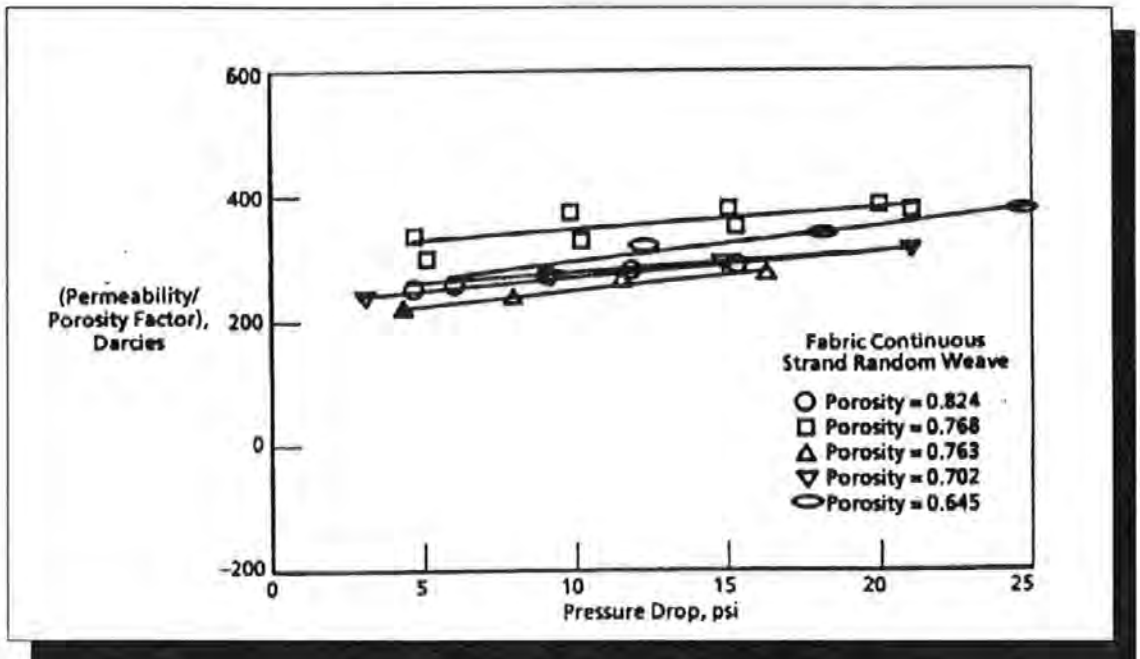
Figure 2:25 Martin et al.'s Permeability / Pressure Drop Relationship for Different Porosities [55]

Figure 2:25 shows that the permeability increases with an increase in pressure drop for volume fractions ranging from 18 to 36%. The pressure was once again increased gradually to reduce fibre wash.

Fabric development has produced new materials with the aim of impregnating the fibres more rapidly. 'Injectex' was the first commercial development fabric and consists of a 2x2 twill weave with twisted tows in the weft direction of the weave. The twisted tow maintains its rounder cross-section under compressive forces and induces larger flow channels in its vicinity, thus enhancing the flow. This flow enhancement was demonstrated by Thirion et al. [56] who introduced varying amounts of 'Injectex' into a laminate of 'Lyvertex G814'

taffeta woven carbon fabric. The results showed a very significant increase in permeability for increasing amounts of 'Injectex'. Extensive testing of Injectex has taken place by Van-Harten [42] and Verheus et al. [43] and the anisotropy produced by the twisted tow only being woven in the weft direction is very evident. Verheus mixed layers of 0 and 90 degrees orientation with a constant volume fraction in a similar way to Adams' work previously and once again the permeability is seen to be sensitive to the stacking arrangment as shown in Figure 2:26.
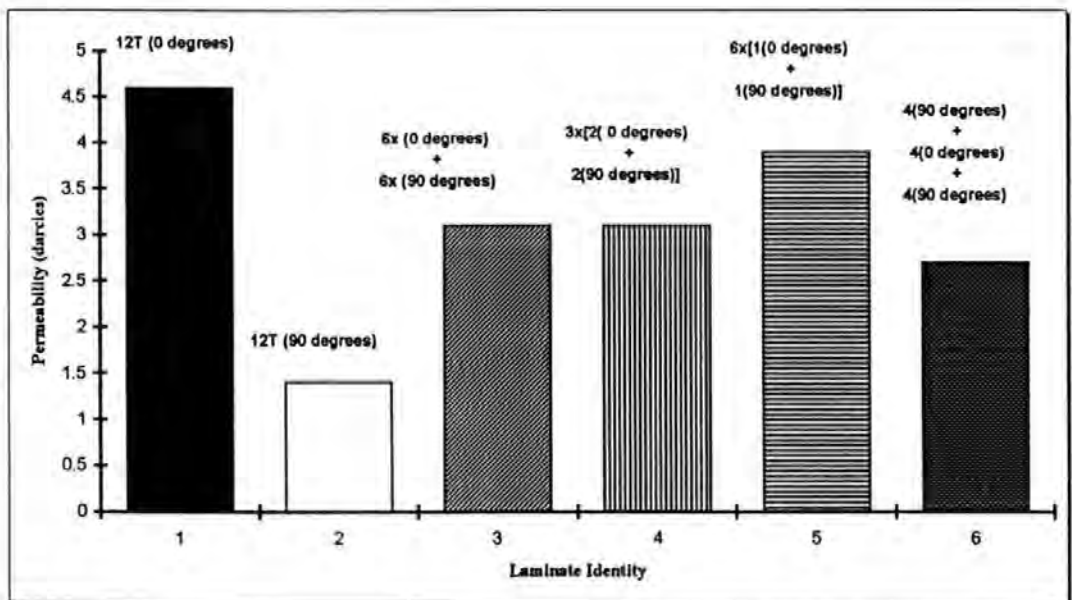
Figure 2:26 Permeability of an Anisotropic Fabric (Injectex 12091) using a Vacuum Pressure of 0.5 bar

A set of development fabrics similar to 'Injectex', are used extensively in this research program. They are designed to produce a varying degree of flow enhancement by varying the percentage of spiral bound weft tows. These will be dealt with in detail in Chapter 3.

2:6:5 Permeability Measurement using Carman-Kozeny

This is limited to aligned fibre beds and involves the measurement of axial and transverse permeability. All the tests undertaken have used a fluid of constant viscosity, either corn or silicone oil or water to remove the problem of the viscosity increase. A different Kozeny constant has been determined for different flow conditions. Lam et al. [57] used both silicone oil and water for transverse and axial flow experiments and the results are shown in Table 2:8.

VOLUME FRACTION (%)	FLOW MEDIA	KOZENY CONSTANT	PERMEABILITY (x 10^{-3} darcies)	NOTES
20 - 42	Water of Viscosity 1cP	11 - Transverse	10 -101	
20 - 42	Silicone Oil of Viscosity 5cP	11 - Transverse	10 -70	
20 - 42	Water of Viscosity 1cP	11 - Transverse	10 - 90	
22 - 50	Water of Viscosity 1cP	0.68 - Axial	152 - 1215	
22 - 50	Water of Viscosity 1cP	0.68 - Axial	152 - 1110	
22 - 50	Silicone Oil of Viscosity 5cP	0.35 - Axial	307 - 1421	
30 - 52	Water of Viscosity 1cP	0.68 - Axial	205 - 1317	
25 - 60	Water of Viscosity 1cP	1.24 - Axial	101 - 1258	Flow through 30° cross plies
24 - 59	Water of Viscosity 1cP	1.65 - Axial	89 - 1256	Flow through 45° cross plies
35 - 50	Water of Viscosity 1cP	2.70 - Axial	89 - 807	Flow through 90° cross plies

Table 2:8. Transverse and Axial Permeability Experiments based on the Carman-Kozeny Methodology

In all cases, the axial flow was larger than the transverse flow and the permeabilities were all of the order of 1 - 0.001 darcies which is supported by all the other reported values. Gutowski et al. [58] used corn oil and silicone oil to measure the permeability in aligned fibres. Table 2:9 shows that the silicone oil of high viscosity produced similar results to corn oil of low viscosity in

similar volume fractions. Table 2:10 shows the effect of small differences in volume fraction on transverse permeability. For transverse flow, the permeability reduced from 9.7 millidarcies at 69% volume fraction to 6.8 millidarcies at 72% volume fraction.

VOLUME FRACTION (%)	FLOW MEDIA	KOZENY CONSTANT	PERMEABILITY (darcies)	FLOW RATE inches/ mm (m/s)
45 - 70	Corn Oil of Viscosity 0.05 Pa.s	0.7	4 - 0.5	0.002 (8.47×10^{-7})
50 - 73	Corn Oil	0.7	4 - 0.5	0.005 (2.117×10^{-6})
41 - 65	Silicone Oil of Viscosity 9.62 Pa.s	0.7	6.2 - 0.5	0.002 (8.47×10^{-7})
40 - 67	Silicone Oil	0.7	7.8 - 0.4	0.01 (4.233×10^{-6})

Table 2:9. Axial Flow of Various Fluids through Hercules AS-4 Carbon Fibres (Aligned) using the Carman-Kozeny Methodology

VOLUME FRACTION (%)	KOZENY CONSTANT	PERMEABILITY ($\times 10^{-3}$ darcies)
69	17.9	9.7 - 11.8
69.5	17.9	9.3 - 9.4
70.5	17.9	7.6 - 8.1
71.5	17.9	6.9 - 8.0
72	17.9	6.8 - 7.8

Table 2:10. Transverse Flow of a Constant Viscosity Fluid through Hysol-Grafil XA-S Fibres using the Carman-Kozeny Methodology

Skartsis et al. [59] reported results showing the variation of permeability and Kozeny constant with respect to the pressure difference for water flowing transversely through aligned fibres. These results are shown graphically in Figure. 2:27 It was found that the Kozeny constant increased for a reduced pressure drop while the permeability increased for an increased pressure drop.

Skartsis also found this to be the case with water and silicone oil flowing axially through aligned fibres of 50% volume fraction as shown in Figure 2:28. The work associated with Carman-Kozeny methods is undertaken at high volume fractions which suggests that it would be useful to model the impregnation of fibre tows where the volume fractions are much higher than the overall volume fraction.
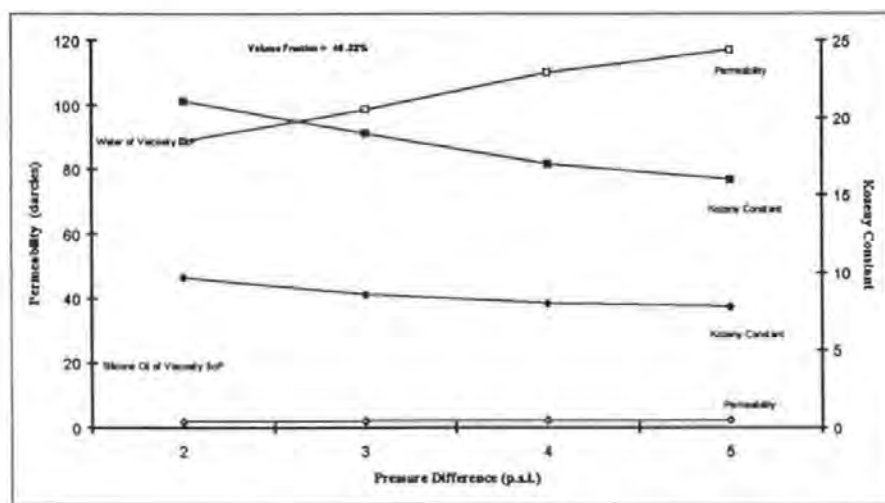
Figure 2:27 Transverse Flow of Two Fluids through Aligned Fibres by the Carman-Kozeny Method
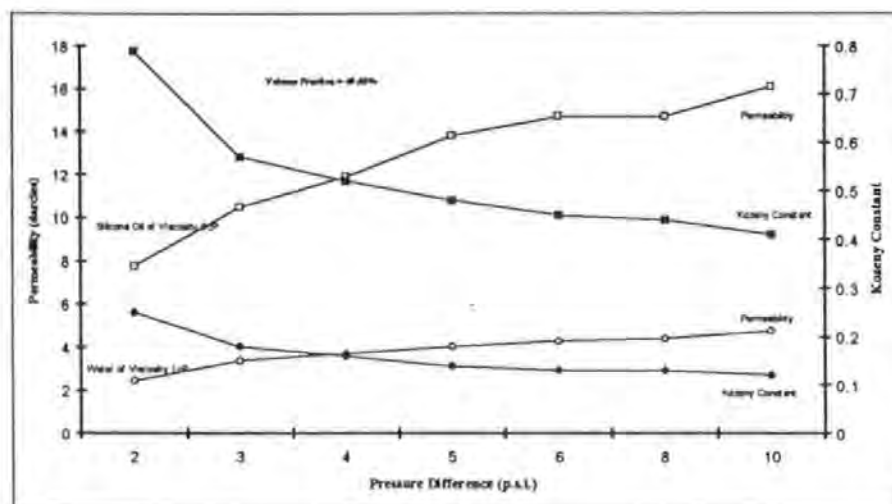
Figure 2:28 Axial Flow of Two Fluids through Aligned Fibres by the Carman- Kozeny Method

63

2:7 Flow Path Architecture

The progress of a fluid through a reinforcement is defined by its flow channel architecture. The architecture is a function of several variables:

- the volume fraction of the laminate.

- the stacking and nesting of the layers

- the configuration of the reinforcement i.e. woven, stitched

- the size of the tows (which affects the areal weight of the reinforcement)

- the shape of the fibre tows

- the fibre distribution within the tows

The architecture of the flow channels forms a major part of this research project and embodies a specially developed woven carbon reinforcement highlights a number of the points above

2:7:1 Categories of Reinforcement

Prior to any detailed analysis being undertaken, it is first important to gain an understanding of the categories of reinforcement available which are used in the Fibre Reinforced Plastics (FRP) industry. These include :

i) random orientation

ii) woven

iii) stitched

iv) knitted

v) braided

64

2:7:2 Randomly Orientated Reinforcement

Random reinforcement consists of fibres laid in a random, two-dimensional mat. The mat may consist of continuous or discontinuous fibres which are positioned on top of one another to produce a specific weight of mat and bound together with a binder. The most commonly used examples of random reinforcement are Unifilo (continuous) and Chopped Strand Mat [CSM] (discontinuous) which is shown in Figure 2:29.

Figure 2:29 Discontinuous (CSM) and Continuous (Unifilo) Random Mat

The random laying of the fibres on top of one another restricts the use of random reinforcement to relatively low volume fraction (<30%) components where no specific directional properties are required.

2:7:3 Woven Reinforcements

Where directional properties are required, a different fibre form is used and initially this was provided by woven reinforcements. Woven fibres have been used extensively because of their similarity with textile fabrics and hence the similar manufacturing (weaving) techniques. Woven fabrics are manufactured by x,y coordinate system interlacing. The x-axis is the weft or 'fill' direction

while the y-axis is the warp or machine direction. The warp yarns or 'ends' and weft yarns or 'picks' pass over and under each other in specific configurations. There are many textile weaves but only a few have been adopted by the reinforced plastics industry and they are now described in more detail.

i) Plain Weave or 'tabby' is the most common and the simplest weave and consists of warp yarns (machine direction) passing over and under every weft yarn in succession as shown in figure 2:30. The weight of the weave is altered by varying the size of the yarns or tows. Owing to the weave style, plain weave exhibits the highest crimp of all the woven fabrics. This is caused by the 'curvature' of the yarns in the weave and its effect is discussed later.
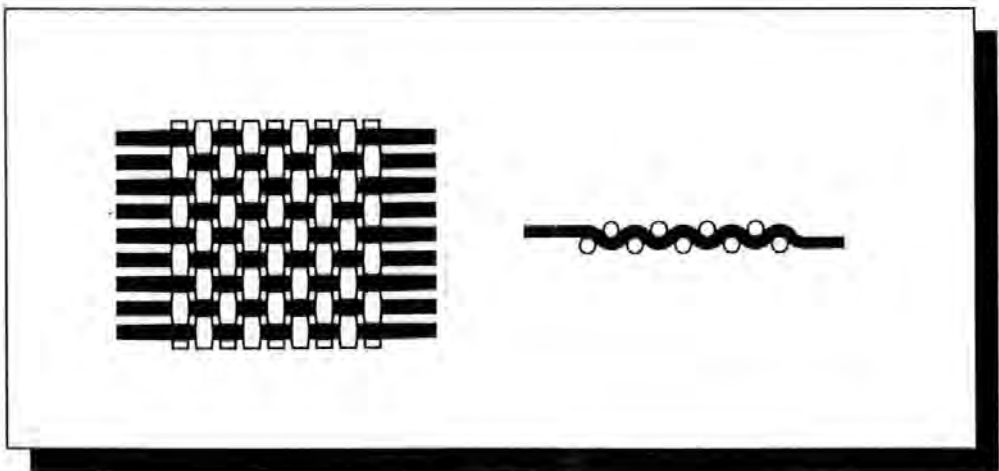
Figure 2:30 Plain Woven Reinforcement Architecture

ii) Twill Weave is available in a several versions for example, 1:2 and 2:2. This refers to the frequency with which the warp and weft tows interlace during the weaving operation. Twill consists of the warp yarn passing over and under the weft yarn in a diagonal pattern to the required frequency as shown in Figure 2:31.
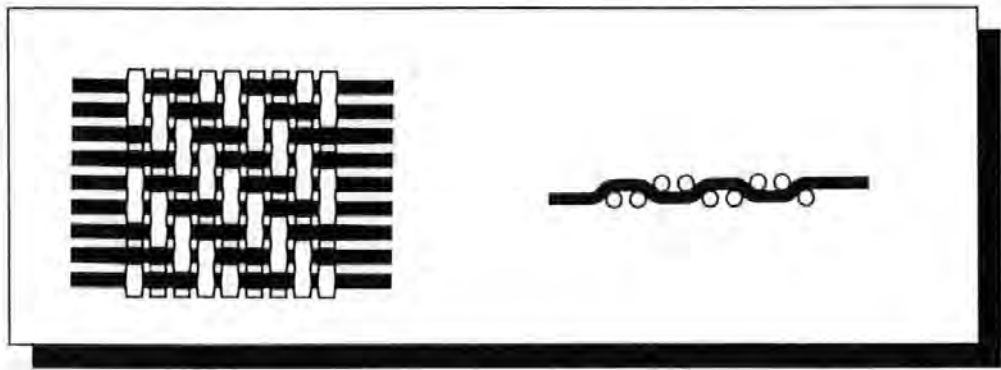
Figure 2:31 Twill (2x2) Woven Reinforcement Architecture

iii) Satin Weave is also available in several versions of which 5-Harness and 8-Harness are the most common. In satin weave, there may be either a floating warp or weft yarn where one yarn passes over a specified number of tows before interlacing. Figure 2:32 shows a 5-Harness satin weave with both warp and weft floats and shows the tows passing over four and under one in succession.
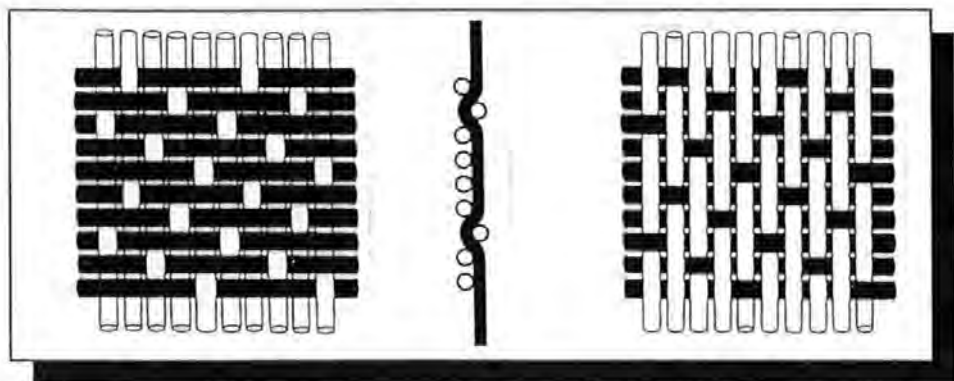
Figure 2:32 Satin (5 Harness) Woven Reinforcement Architecture

A comprehensive catalogue of the weaves used in the textile industry are shown to a greater degree by Hatch [60] and Ko [61]. The FRP industry has also experimented with different fibre types in the warp and weft directions to combine the properties of the individual materials.

Weaves, owing to their individual styles all have different properties regarding both mechanical performance and manufacturing. Weave properties important in reinforced plastics are

i) Crimp

ii) Drapability and Conformability

iii) Stability

Crimp is related to the weave style by how much the individual tow is distorted to interlace between warp / weft tows and is most pronounced in plain weave. With all weaves described previously, there are varying degrees of crimp and different proportions of the weave are straight with 8-Harness satin having the largest straight portion. Newton et al. [62] proposed a model to characterise the tensile strength of a 2 layer, 8-Harness satin weave laminate. Photomicrographs were used to determine yarn paths through the composites. This model was then extended to other fabric arrangements and demonstrated that different weaves produce different yarn curvatures and a wide range of mechanical properties. It will be appreciated that the crimp of a fabric will be affected if the space between the yarns or tows is altered. Shibata et al [63] considered the influence of yarn crimp on the flexural strength of epoxy matrix composites. By increasing the yarn density or diameter, or decreasing the warp yarn float i.e. the distance between crimps, the flexural strength of the epoxy composite is reduced as shown in Figure 2:33, as the

yarn ends or picks move closer, crimp is increased and the mechanical properties fall
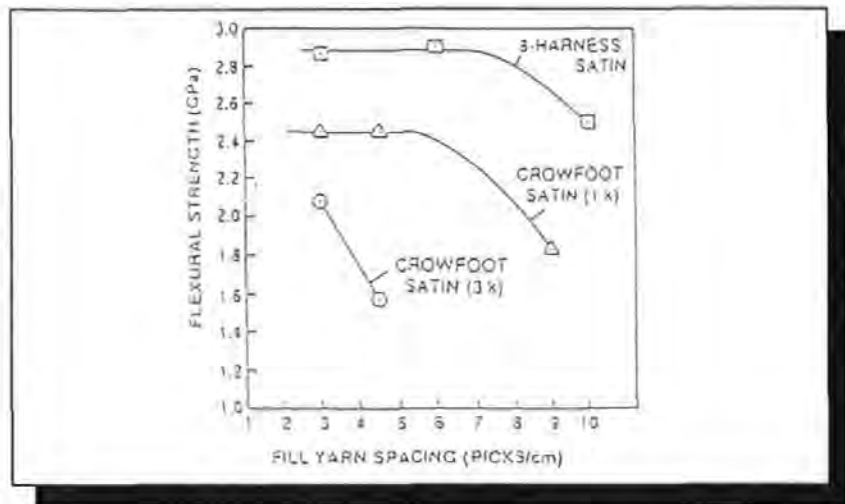
Figure 2:33 The Effect of Fill Yarn Spacing on the Flexural Strength of an Epoxy Composite

Drapability and Conformability are two similar characterisics of textiles which measure how easily a fibre weave conforms to a given shape, for example a sphere without cresasing or distortion. It has been suggested that the two terms require a discreet definition as they are currently used interchangeably. Drape is the natural ability of fabric a to follow a shape. Plain weave due to its many restraining points and corresponding small float, is a stable weave and does not drape well whereas satin weave is more drapable because it is looser than plain and has a larger float. **Conformability** is the ability of a fabric to conform to a shape with the aid of an operator or with mechanical assistance. Both drape and conformability are measured from a procedure known as the circular bend procedure which is found in the ASTM Standard D4032 [64]. British standard BS 3356 (1990) [65] measures the

bending length and flexural rigidity of fabrics while BS 5058 (1986) [66] assesses the drape of fabrics.

Stability is related to drapability because stable weaves which do not fray or shear easily such as plain are very stable. Satin weave is loose and frays easily which makes it more unstable. Satin weave is also more susceptible to handling damage which results in tow misalignment.

It can clearly be seen that there are many advantages and disadvantages related to each type of weave and therefore care should be exercised taken when designing components using woven reinforcements.

2:7:4 Stitched Reinforcements

To enable reinforcements to become more versatile, several new forms have been designed in order to increase the mechanical properties and to make the laying-up procedure more efficient. The first method of manufacture is stitching which can take a number of forms as shown in Table 2:11.

ORIENTATION	-45°/+45°	0°/-45°/+45°	-45°/90°/+45°	0°/-45°/90°/+45°	0°/90°	0°
Identity	Biaxial	Triaxial	Triaxial	Quadriaxial	Biaxial	U-D
Areal Weights g/m²	318-1002	885-1169	1027-1769	610-2336	300-850	425-567

Table 2:11 Configurations of 'E' Glass Stitched Reinforcements

The primary feature of stitched reinforcements is the absence of crimp, as the fibres are laid on top of each other in specified directions and stitched together. This implies that the fibres may be aligned in the direction of the load and hence the maximum mechanical properties may be obtained, assuming 100% wet-out. Stitched fabrics tend to have a more uniform distribution of fibres than

woven ones and this decreases the amount of inter-tow flow channels which aid through thickness flow. The more layers that are stitched together, the worse the through thickness flow properties becomes unless the tow structure is maintained. This problem is highlighted by 'Quadrax' which is a stitched reinforcement comprising of four layers of 0,45,90,-45° orientation as shown in Figure 2:34. The 0° layer has tows whereas the other layers are more evenly distributed
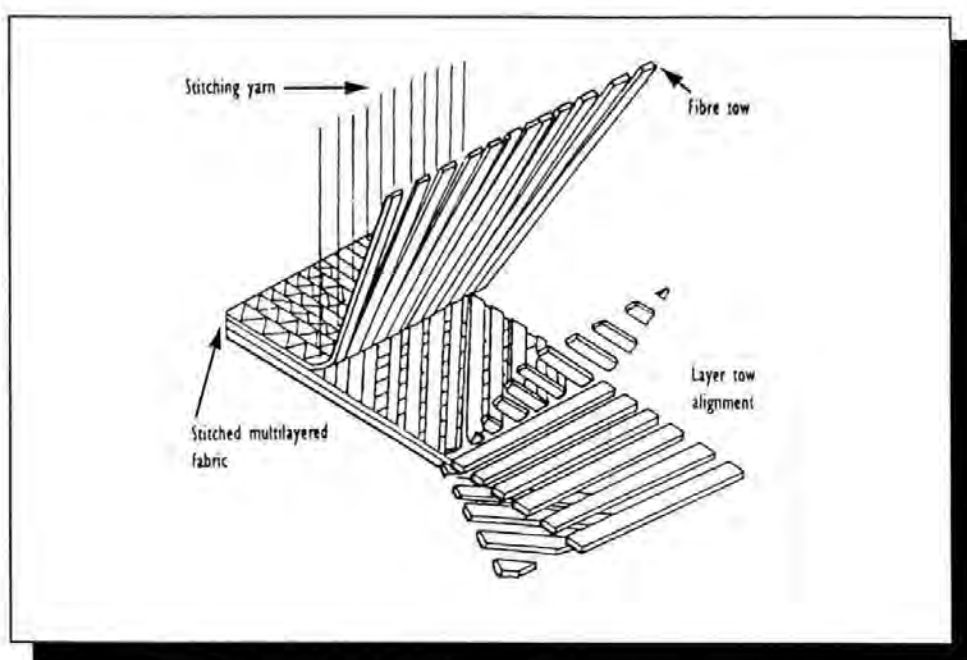
Figure 2:34 Quadriaxially Stitched Fabric

The through thickness flow of this fabric is poor because of the 45 degree layers covering the flow channels in the 0-90 layers. Problems have been encountered in trying to inject high volume fraction components of large cross section [67] because the layers do not fit snugly into the mould and relatively large preferential flow channels are produced around the periphery of the

reinforcement. This leads to premature witnessing of points in the mould before the mould has filled and subsequent dry areas.

Preforms are manufactured shapes of reinforcement which are placed in a cavity in one piece rather than several layers. The fibres are preplaced in the required direction and bound together in the same way as random mat by using heat and minimal pressure. Handling damage is reduced as there is no need to handle separate layers individually but the preforming process incurs extra cost which may be saved by reduced labour costs in cutting-up time of the fabric.

2:7:5 Knitted Reinforcements

Preforms may also be knitted from raw reinforcement which may be accomplished in a number of knitting styles. Knitting provides scope for the manufacture of intricate shapes of preforms. The knitting machinery and techniques are used extensively in the textile industry and have been adapted to fibre reinforcements. Knitted preforms are used in the manufacture of radomes. Common knitting styles are shown in Figure 2:35.

Knit stitch (Face loop)   Purl stitch (Back loop)   Float stitch (Miss stitch)   Tuck stitch with held loop
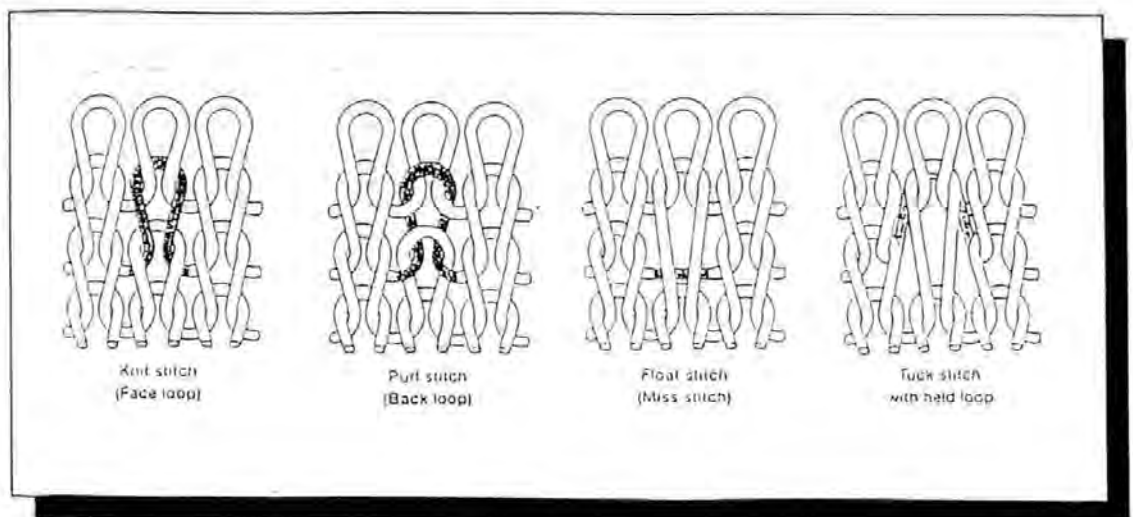
Figure 2:35 Examples of Different Knit Styles

72

2:7:6 Braided Reinforcements

Certain geometries of component have proven to be problematic when laying up, for example tubes and tapers. This is due to an unsightly seam being produced by wrapping layers of reinforcement around the component and wrinkles may be produced if there is a decrease in diameter as with a taper. To counter this problem, braided reinforcements have been introduced, the manufacture of which is shown in Figure 2:36. Braids are formed by each yarn intertwining with every other yarn at some point but not actually completely twisting around one another. They can be made by hand or by high speed equipment for the manufacture of tubes. Braids shear easily when stretched and can be made to fit varying diameters with fibres being oriented to counter torsional forces. Examples of components manufactured using braided reinforcements are golf clubs, drive shafts, fishing rods, artificial limbs, boat masts and radomes.
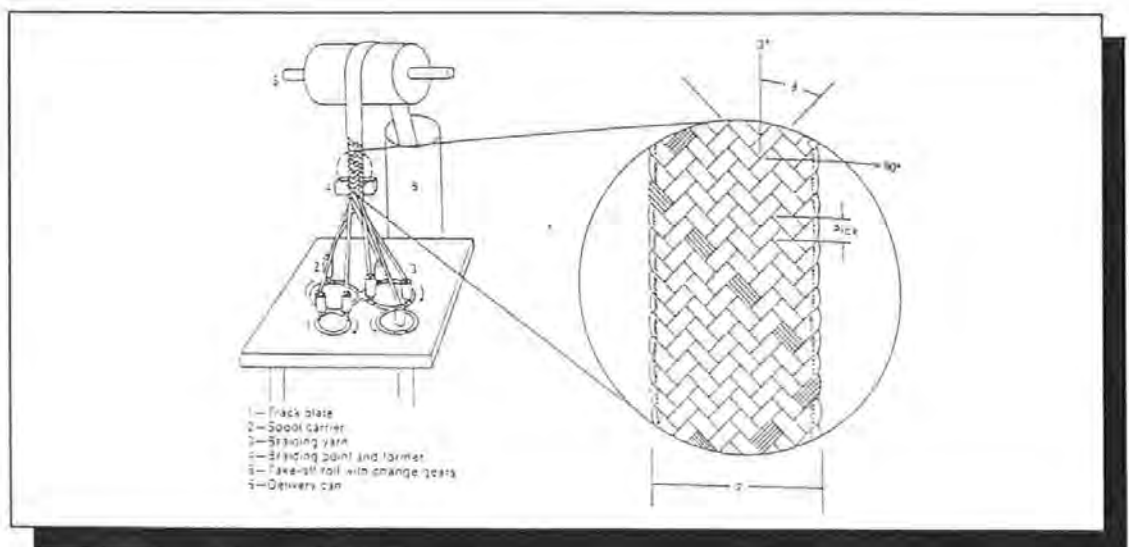
Figure 2:36 Manufacturing Flat Braids

2:8 Modelling of the Fibre Bed

The requirement for a model is brought about by the inherent complexity of the network of pores apparent in both particulate and fibrous media. The first such model was developed by Rose et al. [68] and reported by Dullien [69] for the oil extraction industry and is known as the pore doublet. This model is shown diagramatically in Figure 2:37 below.
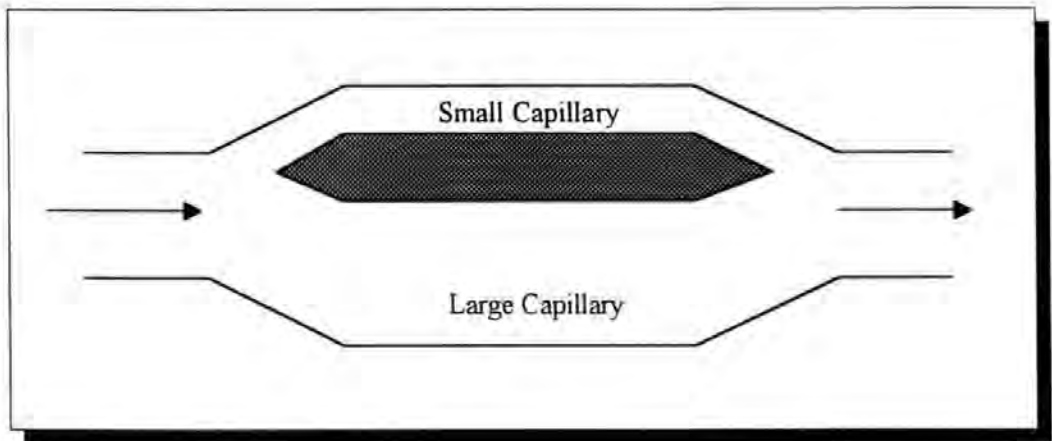
Figure 2:37 The Pore Doublet Model [69]

The purpose of the pore doublet model was to determine the oil displacement by water in strongly water-wet media. Models developed by Rose and Cleary [68], and independently by Moore and Slobod predicted the trapping of oil in either the larger or smaller capillary of the doublet, depending on the conditions of the displacement. This was used with the exploration and extraction of oils from the sea-bed and was used to determine the extraction rates. The accurate prediction of the flow of fluids through fibrous beds is fraught with problems as with the particulates. A typical fibre pack as shown in Figure 2:38 consists of thousands of fibres, which may be relatively ordered

as in a woven reinforcement or randomly distributed as shown in Figure 2:38. Upon closer, macroscopic inspection the fibres are not mutually parallel and appear to meander around one another in any given tow.

Figure 2:38. A Plan View of a Plain Weave and
Chopped Strand Mat (CSM) [5]

All modelling work regarding the fibre pack has grossly simplified this actual condition to an array of parallel cylinders with parallel capillaries. Another problem which is obvious from Figure 2:38 is that there are two distinct sizes of zones available for flow-

i) large inter-tow channels

ii) inter-fibre spaces within the tows (axial or transverse).

Parallel cylinder models are used in conjunction with the Carman-Kozeny equation to determine the permeability. The Carman-Kozeny equation may only be used for uni-directional fibre but permeabilities in both the axial and transverse directions may be determined by using two separately determined Kozeny constants for each direction.

It has been determined that the Kozeny constant in the axial direction is approximately 20 times greater than the transverse direction.

Wheeler in his thesis [70] discussed four fibre arrangments as shown in Figure 2:39, which show different fibre distributions, some ordered and some random.
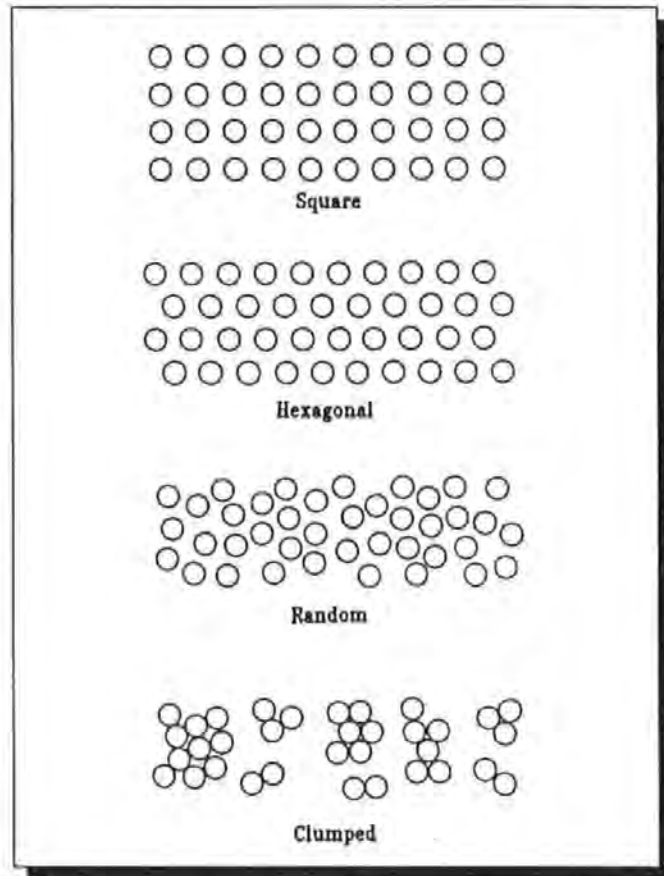
Figure 2:39. Wheeler's Fibre Arrangements [70]

He then derived a model for both axial and transverse flow and compared it to two previously derived models by Happel and Cogswell [71,72]. Wheeler's model is based on the unit cells shown in Figures 2:40 and 2:41, which are for axial and transverse flow conditions respectively.
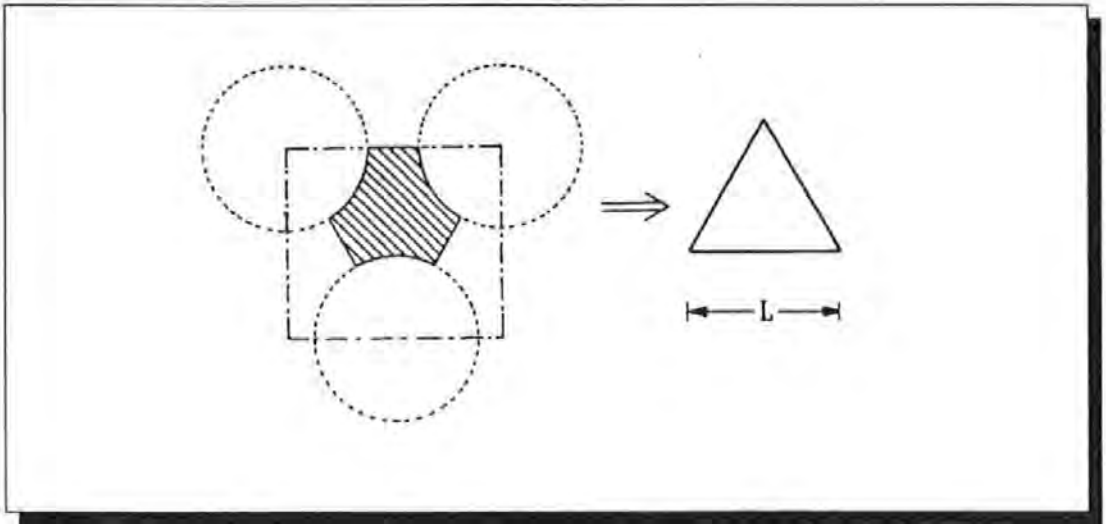
Figure 2:40 Wheeler's Model for Axial Flow in Fibres [70]
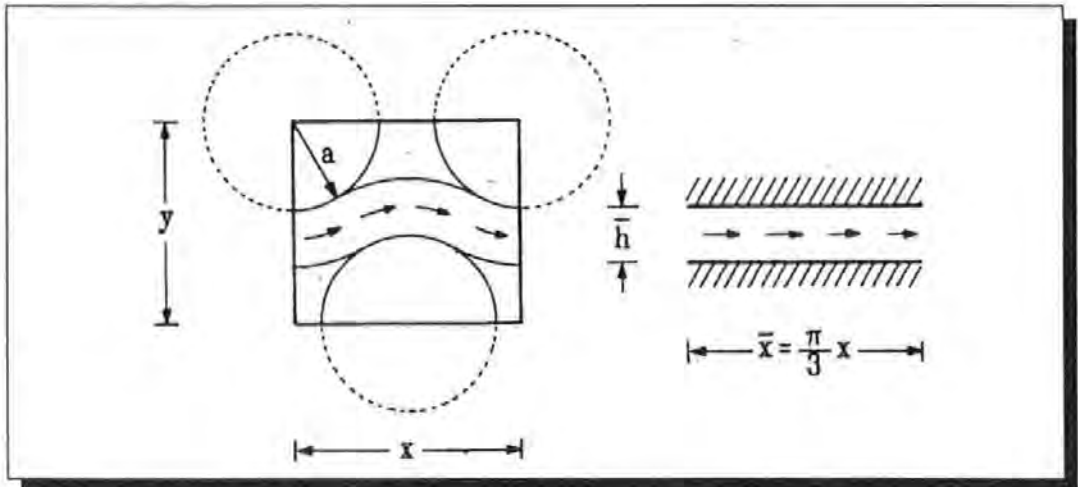
Figure 2:41 Wheeler's Model for Transverse Flow in Fibres [70]

By determining the maximum packing fractions for the square and hexagonal lay-ups (respectively 78.5% and 90.69%), the three models are discussed with respect to their axial and transverse permeabilities. These permeabilities depend upon the volume fraction and the transverse permeability should tend to zero as the packing tends to a maximum, in both methods of packing.

For axial flow, shown diagramatically in Figure 2:40, Wheeler considered a hexagonally arranged bed of fibres and assumed there to be Poiseuille flow down tubes of triangular cross-section. By determining the mean flow rate down the cell, the following equation was developed describing the axial permeability,

$$\frac{K_A}{D^2} = \frac{\pi\sqrt{3}}{480} \cdot \frac{(1-V_f)^2}{V_f}$$

------ Equation 2:51

The model for transverse flow shown diagramatically in Figure 2:41, considers the flow also as Poiseuille flow but between parallel plates of separation $\bar{h}$. Also by determining the flow rate across the cell, the transverse flow was developed in to the following equation,

$$\frac{K_T}{D^2} = \frac{\left[\left(\frac{2\pi}{V_f.\sqrt{3}}\right)^{\frac{1}{2}} - 2\right]}{48\left(\frac{\pi\sqrt{3}}{2.V_f}\right)^{\frac{1}{2}}}$$

------ Equation 2:52

The next model considered was due to Happel [71] which is shown in Figure 2:42. It consists of two cylinders, the inner of which consists of one rod and the outer is a fluid envelope with a free surface. The transverse permeability was found to be as follows

$$\frac{K_T}{D^2} = -\frac{1}{32.V_f} \cdot \left[\ln(V_f) + \left(\frac{1-V_f^2}{1+V_f^2}\right)\right]$$

------ Equation 2:53

78
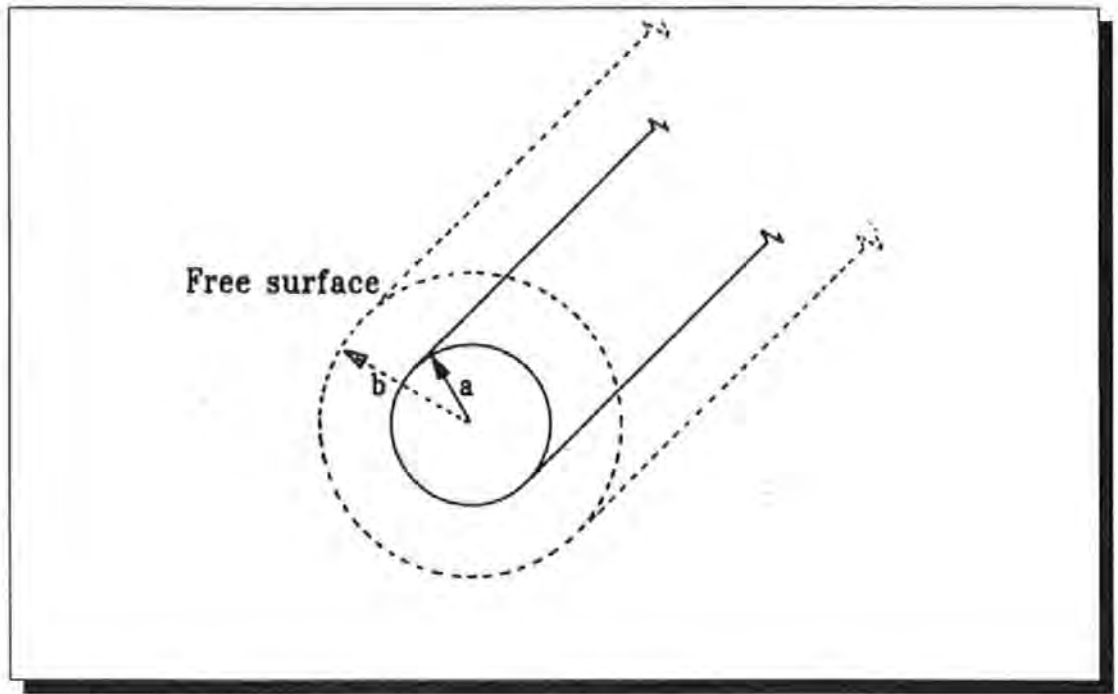
where $V_f = a^2/b^2$

Figure 2:42 Happel's Two Cylinder Model [71]

The axial permeability was found to be as follows,

$$\frac{K_A}{D^2} = \frac{1}{32}\left[4 - V_f - \frac{1}{V_f}(3 + 2\ln(V_f))\right] - - - - \text{Equation 2:54}$$

The final model considered was proposed by Cogswell [72] and consisted of an array of square packed octagonal rods as shown in Figure 2:43 overleaf. The transverse permeability was determined by taking the flow through a simple element as Newtonian flow through a slit with convergent and divergent entrance and exit flows. From his analysis he found that the transverse permeabiltiy was given by,

79

$$\frac{K_T}{D^2} = \frac{\left[\left(\frac{\pi}{V_f}\right)^{\frac{1}{2}} - \left(\frac{\pi(1+\sqrt{2})}{2}\right)^{\frac{1}{2}}\right]^3}{48\left[0.58\left(\left(\frac{\pi}{V_f}\right)^{\frac{1}{2}} - \left(\frac{\pi(1+\sqrt{2})}{2}\right)^{\frac{1}{2}}\right)\left(\frac{\pi}{2(1+\sqrt{2})}\right)^{\frac{1}{2}}\right]}$$

- Equation 2:55.
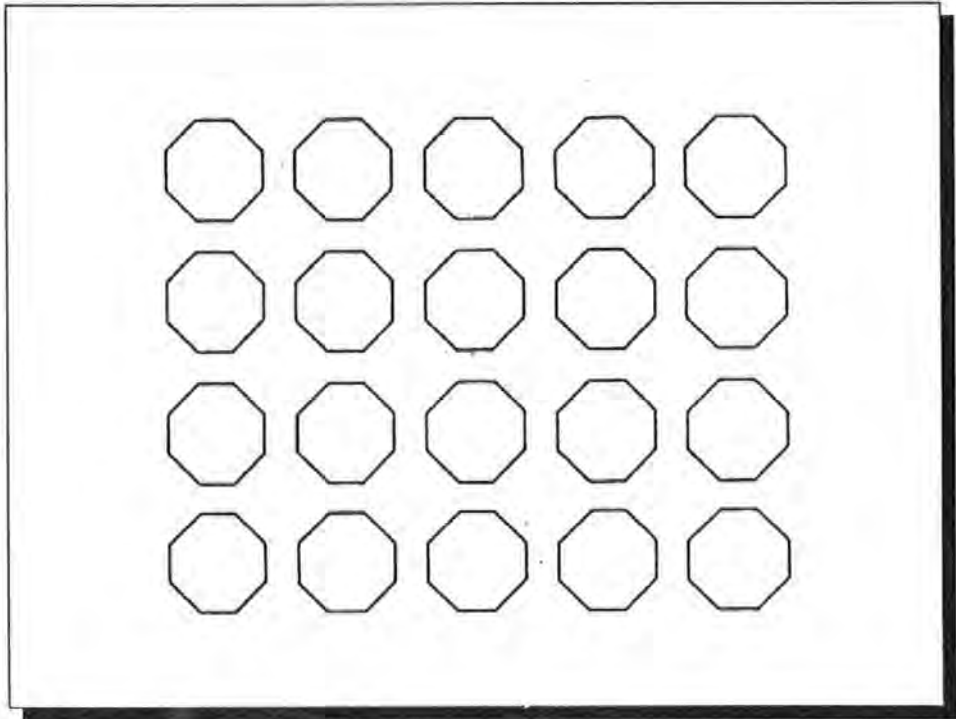
Figure 2:43 Cogswell's Model of Octagonal Rods [72]

For axial flow, the flow is assumed to be Poiseuille flow through a channel of square cross section and the following equation is produced.

$$\frac{K_A}{D^2} = \frac{V_f}{128\pi}\left[\left(\frac{2\pi}{V_f}\right)^{\frac{1}{2}} - \left(\frac{\pi(1+\sqrt{2})}{2}\right)^{\frac{1}{2}}\right]^4$$

- - - - Equation 2:56

The three models were then compared to each other at a given constant

volume fraction. The results showed that good agreement was observed for

transverse flow with Wheeler's and Cogswell's models. For axial flow all the models showed good agreement at volume fractions around 60% but at lower and higher volume fractions, there is disagreement.

The majority of the modelling of the fibres has assumed the fibre bed to be an array of cylinders and the consequent use of the hydraulic radius concept has resulted.

2:8:1 Simulating the Fibre Pack

Astrom et al. [73] has published a review of measurements of the Kozeny constant for axial flow along a number of different aligned materials using various fluids. This is summarised in Table 2:12.

Fibre	Fluid	Comment	Researcher and Reference
Goat and Glass Wool, Hair, Copper Wire	Air		Sullivan [74]
Steel Rod	Air	Ideally Packed Bed	
Wool	Air		Anderson et al [75]
Jute	Air		Roy et al. [76]
Nylon, Carbon Starch & Silane Glass	Nitrogen Oil, Epoxy, Glycerol		Williams et al. [36]
Carbon	Oil		Gutowski et al. [58]
Carbon	Oil, Water		Lam et al. [57]
Carbon Metal Rod	Oil, Water Oil	Ideally Packed Bed	Skartsis et al. [59]

Table 2:12 Summary of Axial Flow Experiments along Cylinders and Fibres [73]

Experiments have been conducted in a similar vane for flow transverse to the fibres with similar materials and fluids. The packing arrangements have been varied from square to hexagonal and comparing them to actual fibre beds it

seems that the discrepancies are caused by non-uniformities in packing arrangements, fibre alignment and fibre volume fraction.

Unfortunately, few composite components are manufactured from solely unidirectional reinforcements and usually use either random, stitched or woven reinforcement which introduce 'clumping' in tows providing uneven fibre distribution. Clustering of fibres has been discussed by Summerscales [77] in terms of variation of the hydraulic radius to reduce the wetted perimeter and hence increase the flow rate into a fibre pack. This agrees with Carman-Kozeny which indicates that the flow rate is inversely proportional to the square of the wetted perimeter. The clustering of fibres is a common occurrence in reinforced plastics and is usually the result of the fabric configuration. Therefore there are usually a number of different sized flow channels in evidence which require modelling. This is the main aim of the research described in this thesis, to determine the proportion of each of the flow modes present, be it axial capillary, transverse or large channel flow.

2:9 Capillary and Gravitational Effects

In a process such as RTM, the injection pressure is an important parameter in determining the rate of fill of a mould. Ahn el al. [46] discussed the constituents of the total pressure and formulated the following

$$P_T = P_M + P_G + P_V + P_C \quad ----- \text{Equation 2:57}$$

where P_T = the total pressure

P_M = the applied or mechanical pressure

P_G = the gravitational pressure

P_V = the vacuum pressure (if applicable)

P_C = the capillary pressure ($\approx$ 4 - 40 KPa from Gibson [78]

The applied or mechanical pressure is very large compared to the gravitational pressure and therefore the latter is neglected, but the vacuum and capillary pressures are comparable to the applied pressure and need to be taken account of. The capillary pressure has been estimated [78] from knowledge of fibre alignment. Using the Young-Laplace equation, the capillary pressure is expressed as:

$$P_c = \frac{4.\sigma.\cos\theta}{D_e} \quad ------ \text{Equation 2:58}$$

where σ = the surface tension of the wetting fluid

θ = the contact angle between liquid and the solid

D_e = the equivalent diameter of pores in a fibrous form.

83

The equivalent diameter is equal to the capillary diameter for a single pore. The fibre bed is usually anisotropic and as a consequence the pores of the preform are of different size and shape. The anisotropic / geometric configuration are combined in a dimensionless form factor F and for one dimensional resin flow, the capillary pressure is described previously by equation 2:50,

$$P_c = \frac{F}{D_f} \cdot \frac{(1-\varepsilon)}{\varepsilon} \cdot \sigma \cdot \cos\theta \quad \text{- - - - - - Equation 2:50}$$

where ε = the porosity of the preform

D_f = the diameter of a single fibre

For flow perpendicular to the fibres, the form factor F is equal to 2 and for flow in the axial direction is equal to 4. For complex fibre arrangements, the form factor may only be determined indirectly from the permeability measurement.

2:9:1 Surface Tension and Contact Angle Effects

The surface tension σ of a resin may be determined by several techniques. It is a thermodynamic property and for pure liquids depends only on temperature. The contact angle depends on the chemistry and topology of the surface of the fibre. The angle may be measured by several techniques but the most relevant is the wicking method which uses a fibre bundle. The measured contact angle is influenced by resin viscosity as well as surface tension. Table 2:13 shows the variation of surface tension with different temperatures on different liquids.

84

LIQUID	TEMPERATURE (°C)	SURFACE TENSION (dynes/cm)
Mineral Oil	50	32
	60	31
	70	31
Epikote 828	50	47
	60	46
	70	44
Aqueous Glycerol (96.5% Glycerol by Weight)	50	61
	60	61
	70	60
Silicone Oil	39	21
PPG 1025	39	33
Oxitex 40	55	39
Concentrated Aqueous Sucrose	39	75
Ethanol	20	23

Table 2:13 Surface Tension of Various Liquids [36]

Table 2:14 gives an idea of the minimal change of surface tension of two resin systems during a constant temperature curing cycle of 60 °C.

TIME (MINS)	SURFACE TENSION (dynes/cm)	
	Resin System 1 *	Resin System 2 #
20	47	43
40	47	43
60	47	43
80	48	43
100	48	43
120	48	/

* = Epikote 828, 100g : Diaminodiphenylmethane, 27g

\# = Epikote 828, 100g : Nadic Methyl Anhydride, 90g :

2,4,6-tris(dimethylaminomethyl)phenol (DMP 30) 2g.

Table 2:14 Surface Tension of Resin during Cure [36]

Williams et al. [36] concluded that the differing surface tensions affected the meniscus of the fluid front which affected the air entrapment and ultimately the quality of the composite.

Dave [79] reported an investigation by Melrose et al. [80] regarding the relationship of infiltration rate and capillary forces. The study concludes that if the fluid moves through the medium with a velocity greater than the free-infiltration rate i.e. the rate at which fluid spontaneously displaces some air, the larger capillaries will fill first and entrap air in the smaller capillaries. However, if the infiltration rate is lower than the free infiltration rate, the capillary forces will dominate and trap air in the larger pores. An equivalent method of expressing the effects of viscosity and surface tension on the measured contact angle has been described by a factor known as the Capillary Number as seen below-

$$Ca = \frac{\mu.v}{\sigma}$$ - - - - - - - Equation 2:59

where μ = the viscosity of the resin

v = the relative velocity of resin past dry fibres

The capillary number is the ratio of viscous to surface tension forces. Its critical value depends upon the infiltration rate, the fibre network configuration and the pore geometry. In general, for low values of Ca, the contact angle remains constant but as Ca increases so does the contact angle. A similar approach was adopted by Skartsis et al. [59] whereby the equivalent diameter in equation 2:58 was replaced by the hydraulic radius 'm', giving,

$$P_c = \frac{\sigma. \cos\theta}{m}$$ - - - - - - - Equation 2:60

where m = the hydraulic radius = $D_e/4$

The Blake Carman Kozeny equation expresses the true velocity v_t (i.e. the superficial velocity divided by the porosity) in the following terms

$$v_1 = \frac{m^2}{\mu.k.l}\left(\Delta P_a + \frac{\sigma.\cos\theta}{m}\right) \quad \text{------- Equation 2:61}$$

where ΔP_a = the applied pressure difference across the bed.

Williams et al.[36] used equation 2:61 to describe axial flow through aligned fibre beds.

From equation 2:60, it is seen that the capillary pressure is inversely proportional to the hydraulic radius and permeability is proportional to the square of the hydraulic radius. From this it should not be assumed that pore non-uniformities affect capillary pressure-induced flows in the same way that steady flow is affected. Skartsis focussed his attention on accounting for the non-uniformities of an actual fibre bed. He modified equation 2:60 to take account of the parallel-type non-uniformities and also to improve the estimation for the flow channel size, which culminated in equation 2:61:

$$v_1 = \frac{m^2}{\mu.k.l}\left(\Delta P_a + \sqrt{\frac{k}{k_{ideal}}}.\frac{2.\sigma.\cos\theta}{r_c}\right) \quad \text{---- Equation 2:62}$$

where

$$r_c = \frac{2r\sqrt{\left(\frac{\varepsilon}{\pi}\right)}}{(1-\sqrt{\varepsilon})}$$

k_{ideal} = Kozeny constant for an ideal bed.

From this work, Skartsis concluded that the overall contribution of the capillary forces to the permeation is significantly reduced when non-uniformities of the parallel type prevail.

More recent work has concentrated on the differing types of mechanisms of impregnation encountered in different manufacturing techniques. Connor et al [81] have investigated four different impregnation situations, two of which are relevant to long range flow in dry fibres and two of which are more relevant to filament winding and powder impregnation. The contact angles were measured between plates of materials (glass, brass and PTFE) and also at a microscopic level between fibres. For small contact angles, the fibres were pulled together by the wicking of the resin melt but for contact angles greater than $\pi/2$, an equilibrium distance was reached between the fibres. The conclusion from this work was that capillary pressures can have a significant influence on impregnation quality and rate in low pressure processes such as vacuum bagging because of the relative magnitudes of the pressures.

Van Harten [42] reported detailed investigations into capillary action within the fibre tows in terms of the contact angles on individual fibres. Figure 2:44 shows the possibilities which occur within the bundle. The fluid forms a contact angle between the two fibres and capillary forces draw the fluid between the fibres to encounter another fibre. If the fluid touches this new fibre the capillary action continues. If not then the fluid has to wait for the pressure rise in the fluid due to the front progression which causes the

meniscus of the capillary to become convex. Upon contact with the next fibre in the tow, the capillary action proceeds. If an air bubble is trapped in a capillary, the increasing of the fluid pressure after front passage increases the pressure around its periphery and as a consequence, the bubble reduces in size.

Schematic Cross Section of a fibre bundle enveloped by resin before impregnation

Changing fluid meniscus at a distance between fibres of 1/4 and 1/8 of a fibre diameter

Meniscus becoming convex due to fluid driving pressure

Meniscus after contact with new fibre in the bundle
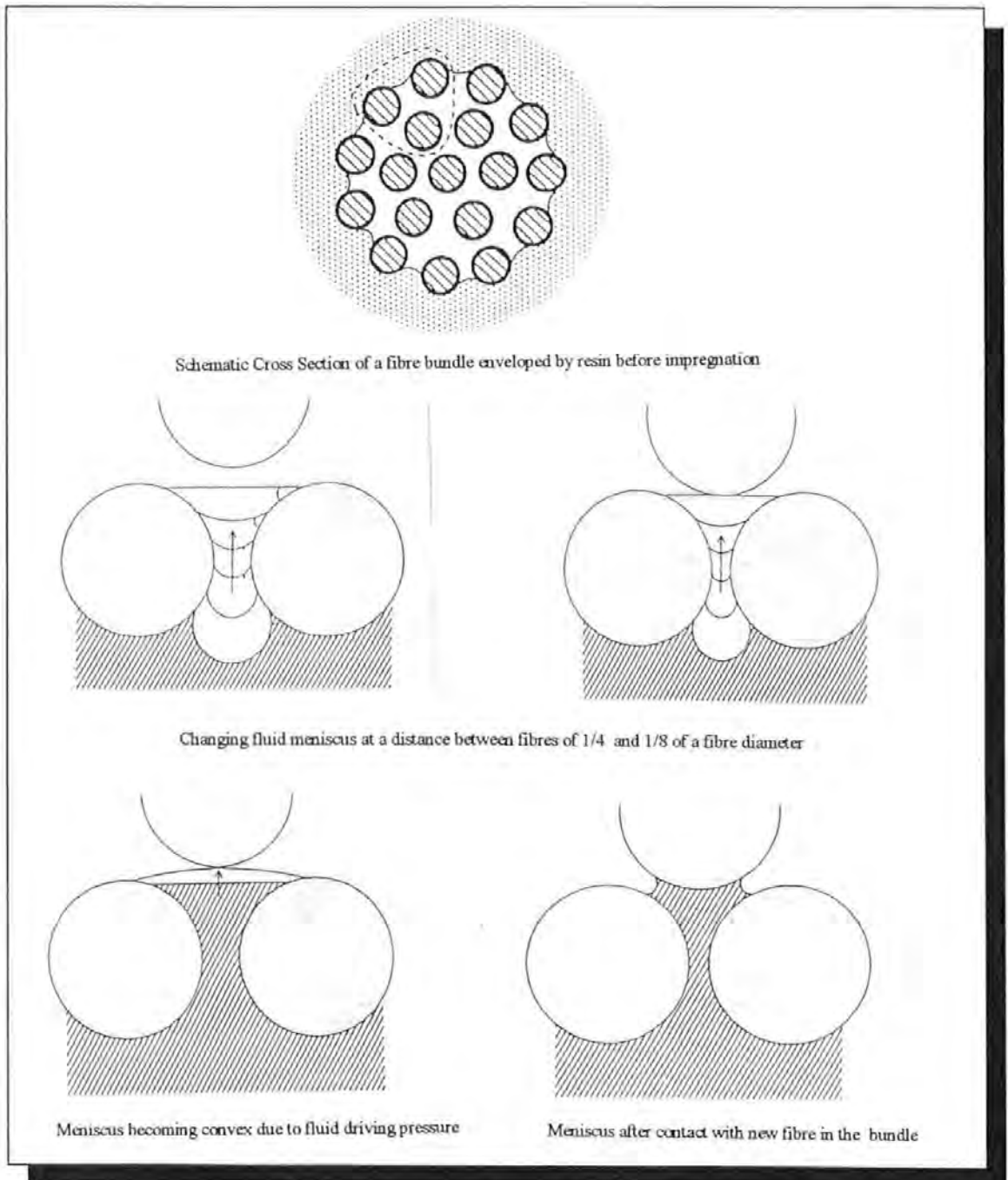
Figure 2:44 Resin Impregnation into a Fibre Tow

Parnas et al [82] developed a model which accounted for two types of flow

mechanism, the observable macroscopic flow and the impregnation of

individual fibre tows. Although strictly speaking this is transverse flow, the

subject of void formation is very important. In this model, a fluid flows

perpendicular to a simplified unidirectional fibre pack. As the advancing

front encounters a tow, it flows around it entrapping a pocket of air. After

surrounding of a tow, it acts as a sink and the fluid slowly impregnates. It is

suggested that there are two permeabilitiies associated with this type of flow,

the one associated with impregnation being less than the general

permeability of the fibre pack.

Gibson [78] has conducted a review of the impregnation mechanisms

involved with high viscosity thermoplastic resins as opposed to thermosets,

and also the technology available to produce good quality wet-out. The

surface energy effects were discussed for two configurations, resin in the

form of cylinders and also spheres to simulate both commingled fibres and

powder impregnation.

2:10 Injection Fluid Properties

There are a number of important considerations regarding the fluid which need to be taken into account during the flow process. These are listed below,

i) the viscosity

ii) the processing temperature

iii) the mixture ratio of the resin constituents

2:10:1 Fluid Viscosity

A very important consideration when undertaking fluid flow experiments through a porous media is the viscosity of the fluid. This becomes even more important when dealing with curing resins, as the viscosity changes with time, processing temperature, mixing methods (homogeneity) and constituent ratios. Fluids cannot resist shearing forces, therefore if a shear force is applied to a fluid which is in contact with a boundary, the particles in the fluid will move at the velocity of the boundary causing the shear force. Successive layers from the boundary will move at increasing velocities. Shear stresses are set up in the fluid to oppose the relative motion of these layers. For a Newtonian fluid, the shear stress is directly proportional to the velocity gradient in the fluid and is given by :

$$\tau = \mu.\frac{\delta v}{\delta y} \qquad \text{-------- Equation 2:63}$$

where

τ = the shear stress applied to the fluid
$\delta v/\delta y$ = the velocity gradient across the fluid thickness
μ = the coefficient of dynamic viscosity

91

As can be envisaged, the number of fibres present in a fibre mat imply that there are literally thousands of sites for shear forces. However, the difference is that the boundary layer is stationary and the fluid is in motion. The result is that the flow channels are assumed to be an array of tubes and the velocity profile across the tubes will be parabolic.

Several investigations into viscosity characteristics have been made to determine the type of fluid being investigated. Initially, with flow through particles, the fluid under investigation was a particular type of oil such as that encountered by Al-Fariss et al. [83] from the Peace River area of Canada. Tests showed that the behaviour characteristics of the oil were modelled well by the Herschel-Bulkey Model:.

$$\tau = H.\gamma^n + \tau_0 \quad \text{- - - - - Equation 2:64}$$

where :
> H = *the consistency index*
> γ = *the shear rate*
> n = *the flow behaviour index*
> τ_o = *the yield stress*

Wissler [84] investigated the flow of visco-inelastic, power-law fluids through porous beds which alters the Darcy equation to the following,

$$Q = k'\left(\frac{\Delta P}{K.L}\right)^{\frac{1}{n}} \quad \text{- - - - Equation 2:65}$$

where :

> k' = *a parameter that depends upon the power law exponent 'n'.*
> n = *a power law parameter*

Roller [85] reported work using the empirical model shown in equation 2:66 for isothermal processes which assumes no control over chemical

conversion-time relationships. This model was extended by Roller [86] to

include non-isothermal systems, the model of which is shown in equation 2:67.

$$\ln \mu(t) = \ln \eta_\infty + \Delta E_\mu/R.T + t.k_\infty. \exp(\Delta.E_k/R.T) \qquad \text{- - - Equation 2:66}$$

$$\ln \mu(t, T) = \ln \eta_\infty + \Delta E_\mu/R.T + \int_0^t k_\infty. \exp(\Delta E_k/R.T) \qquad \text{- - - - - - Equation 2:67}$$

where
$\mu(t)$ = viscosity as a function of time at temperature T
n_∞ = calculated viscosity at $T = \infty$
ΔE_μ = Arrhenius activation energy for viscosity
$R =$ the Universal Gas Constant
T = Absolute Temperature
t = time
k_∞ = kinetic analog of μ_∞
ΔE_x = kinetic analog of ΔE_μ

There has however, been a general agreement from authors [87,88,89] that

thermosetting resins used in composites manufacturing, display Newtonian

characteristics during the early part of their viscosity-time characteristics. It is

important to remember that during the manufacture of composites by long

range flow processes such as RTM, it is critical that the injection is complete

before the viscosity reaches the gel point. At this point, the resin ceases to flow

and the cure reaction rate increases up to peak exotherm

Groleau et al [90] investigated an empirical method of modelling iso- and

non-isothermal viscosity for resins used in RTM. An expression similar to

equation 2:67 was obtained, although a slightly different expression for

temperature dependent viscosity was obtained. To determine the suitability of a

resin for RTM, the viscosity and pot-life are investigated. The ideal resin

would be low in viscosity, regardless of temperature and have a long pot-life which could be controlled by changing the processing temperature.

A typical viscosity-time cure profile of a polyester resin is shown in Figure 2:45 and as already indicated, there are two distinct regions of interest,
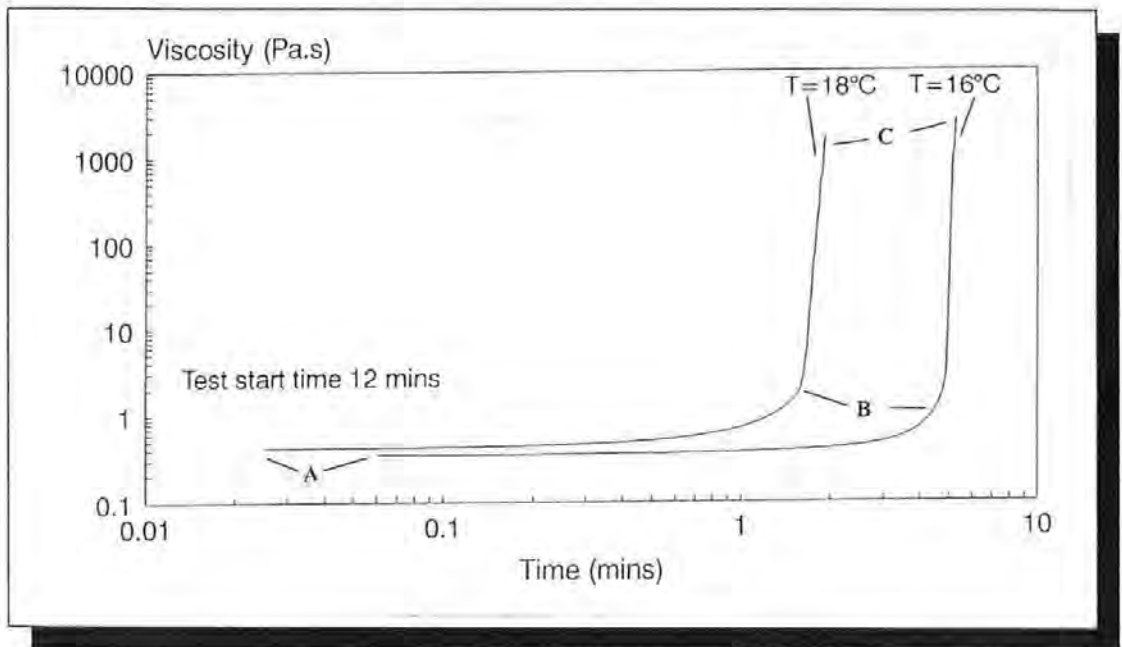
Figure 2:45 Viscosity Time Profile for Jotun Norpol 42-10 Polyester Resin

i) the initial part of the curve (A-B) shows a gradual increase in viscosity due to the cross-linking reaction. This appears to show inconsistency in that the 16°C line exhibits a lower viscosity than the 18°C. This is due to a cross-over point where the relative rates of change of viscosity differ due to the differing temperatures.

ii) the second section (B-C) of the curve shows the viscosity increasing rapidly after the gel point (i.e. the point at which the resin ceases to flow).

To enable efficient impregnation of the reinforcements, it is important to inject the resin during the initial part of the curve where resin viscosity is low and is

only increasing slowly. As discussed in section 2:9, the rate at which the fibres are impregnated has an important effect on air entrapment.

2:10:2 Processing Temperature

Figure 2:46 shows the effect that the processing temperature has on the rate of reaction and the increase in viscosity. It clearly shows that relatively small changes in temperature have large effects on the viscosity of the sample and hence the mould and resin temperatures are critical when designing the process.
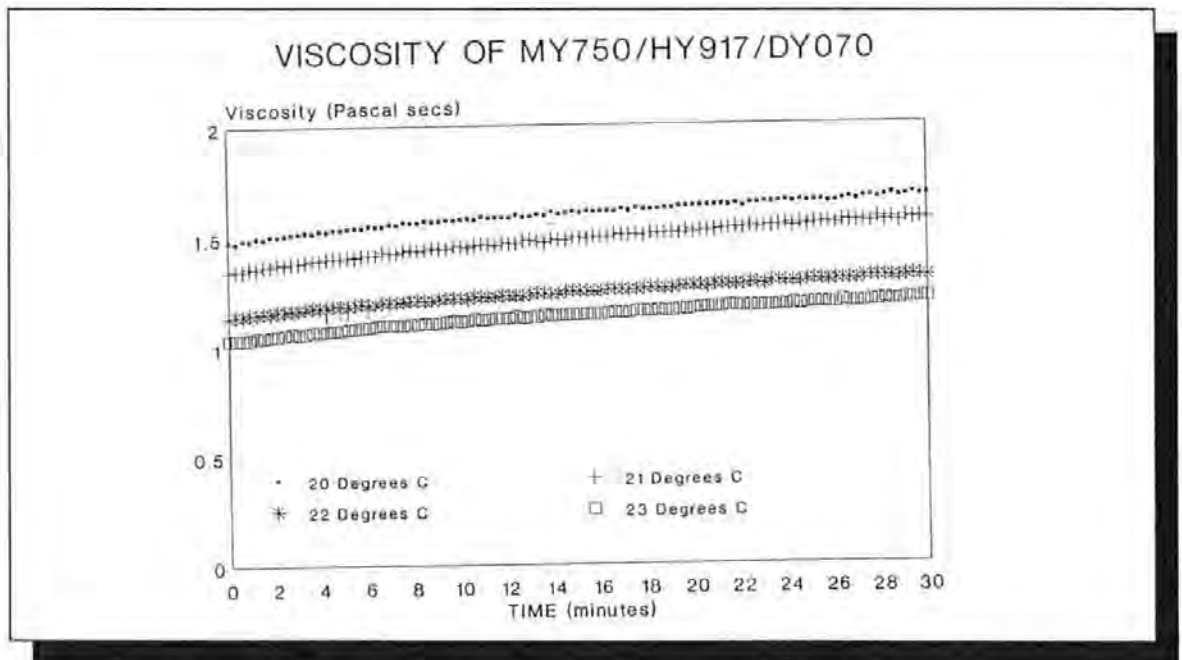
Figure 2:46 The Effect of Processing Temperature on the Cure Rate of the

MY750 Epoxy Resin System

Some resins such as Ciba-Geigy Epoxy MY750 shown in Figure 2:47 require elevated temperatures to aid the curing which initially reduce the viscosity of the resin and improves its impregnation properties. Temperature is not required for most common polyester resins as the rate of reaction is relatively high compared to epoxies. The increase of temperature into a process

95

increases the production rate but adds to the costs so this is a consideration when planning production.

2:10:3 Mixture Constituent Ratio

This is quoted in suppliers data and usually consists of several variations depending upon the curing time required for a specific moulding. Resins are either two or three part depending upon whether they are pre-accelerated. By varying the catalyst ratio, the reaction rate is varied. Once again it can be seen that using the MY750 epoxy resin, figure 2:47 shows this cure variation and also shows the cure time variation for differing temperatures.
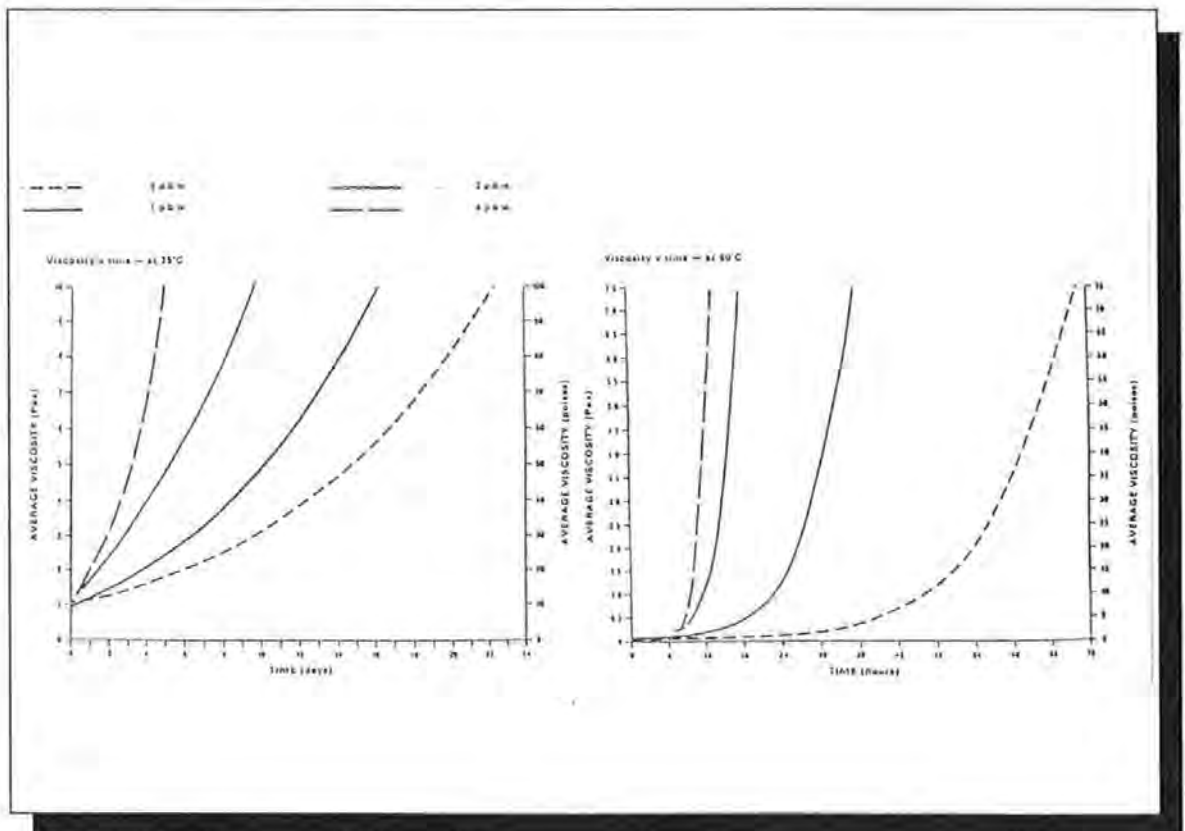
Figure 2:47 The Effect of Accelerator Content on the Curing Rate of

MY750 Epoxy Resin at Two Temperatures

2:10:4 Model Resins for Permeability Measurement

During the review of permeability measurement in chapter 2:6:4, a number

of fluids were used instead of resins as the injection fluid. These included

glycerol, silicone oil, corn oil and water. There were several reasons behind

the use of these fluids:

i) the fluids exhibited constant time-dependent viscosity values

ii) in the case of glycerol, the values were of similar magnitude to typical

injection resins (~ 1000-1500cP)

ii) the fluids all possess different viscosity values within this range to enable

a comparison of permeability values with different fluids to be made

iii) the fluids are considerably cheaper than resins

iv) the moulds used for the visualisation tests required no mould releasing

which reduced the preparation time of the experiment.

However, there were drawbacks of using the fluids:

i) the injection did not produce a cured plate for mechanical and

microstructural examination

ii) the use of a constant viscosity fluid did not accurately portray RTM as

usually, the resin was increasing in viscosity during the injection.

The use of a model resin depends upon the requirements of the test

i.e. qualitative or quantitative. Unfortunately, the variation of viscosity from

sample to sample of resin contributes to large scatter when measuring

permeability, thus justifying the use of model resins.

CHAPTER 3

PERMEABILITY MEASUREMENT

3:1 Introduction

This chapter deals with the development of flow visualisation moulds to enable

monitoring of the fluid flow front progressions and subsequent calculation of

permeability values for specific fibre lay-ups based on Darcy's law. Initially it

was decided to undertake a series of preliminary, fact-finding tests for the

following reasons

> i) to obtain an understanding of the variables associated with the filling

> process

> ii) to observe flow characteristics produced by different reinforcement

> styles

> iii) by using Darcy's Law, to gain an understanding of the orders of

> magnitude of permeability values to be expected

3:1:2 Darcy's Law and Assumptions for Testing

The theory used in this permeability testing was based on the radial Darcy's

Law (equation 2:34), and therefore, the variables present in this equation, i.e.

fluid viscosity, flow distance, pressure drop and flow time require monitoring.

Darcy's law assumes that the porous medium is a homogeneous material.

Fibrous reinforcements are assumed to be macroscopically homogeneous but

microscopically inhomogeneous.

The fluid used in the first set of tests was a non-curing 'model' resin called glycerol. This was used for the reasons explained in Chapter 2:10:4.

These preliminary results were all obtained at ambient temperature and so it was assumed that the glycerol had a constant viscosity.

The pressure drop was assumed to be equal to the difference between the vacuum pressure at the flow front and the atmospheric pressure above the glycerol beaker with no pressure losses in the tube connecting the mould to the glycerol beaker. Any losses in the tubes were accounted for by using equal lengths of tube, and were therefore consistent in each test.

3:1:3 Flow Test Apparatus and Experimental Procedure - 1

The mould used for the first set of visualisation tests is shown in Figure 3:1. It consisted of a square, aluminium base plate, 20mm thick into which was milled a 3mm cavity. The inlet and outlet ports were positioned on two opposite edges as shown. The flange around the perimeter of the cavity contained holes to enable the base to be bolted to the top plate. The top plate was manufactured from 15mm thick perspex for visualisation purposes. Separating the top and base plates was a rubber gasket which provided a seal for the vacuum.

The apparatus arrangement for the visualisation test is shown in Figure 3:2. The reinforcement was carefully marked out, cut and laid into the mould cavity to the required volume fraction determined by equation 3:1, the gasket coated
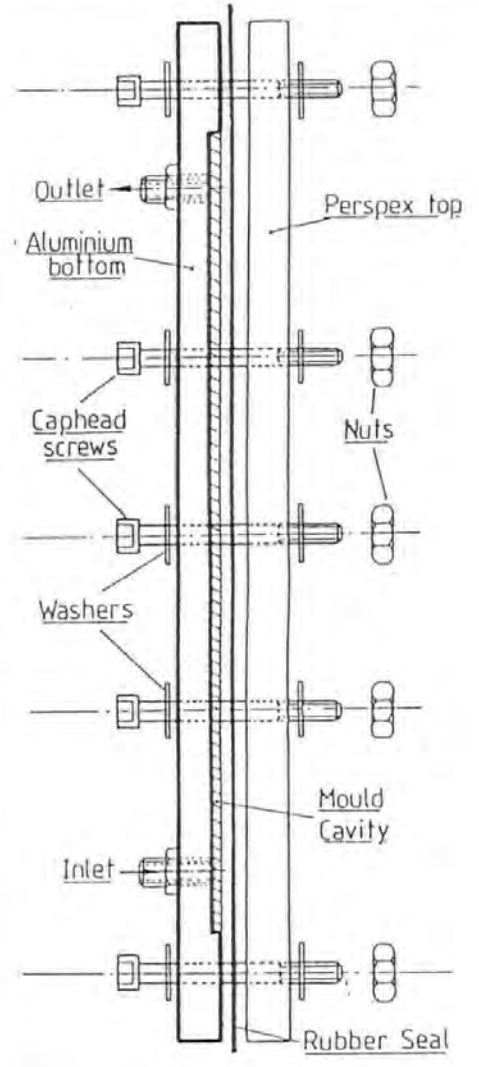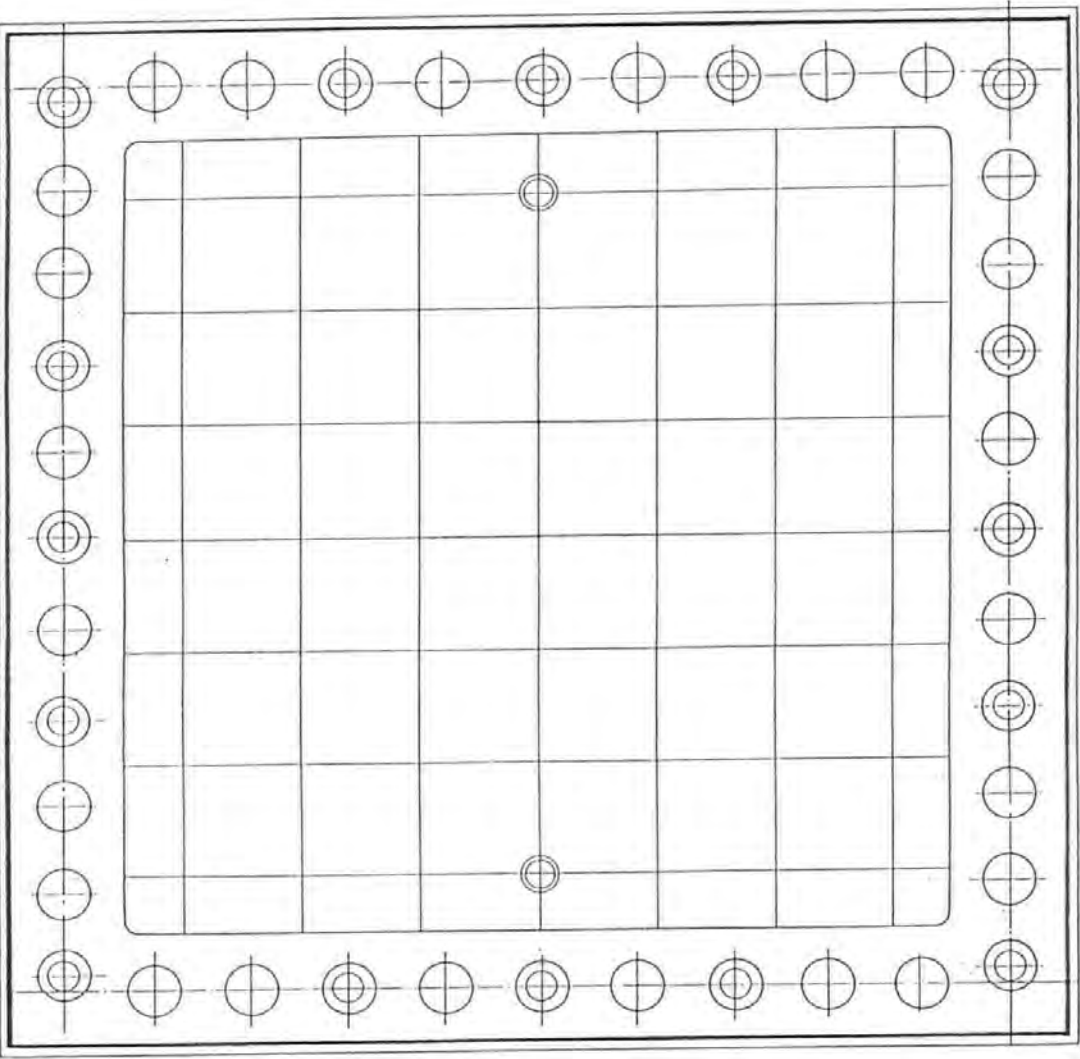
Figure 3:1 Aluminium / Perspex Flow Visualisation Mould

Outlet

Aluminium
bottom

Caphead
screws

Washers

Inlet

Perspex top

Nuts

Mould
Cavity

Rubber Seal

in silicone grease sealant to aid vacuum sealing and finally the top was laid and

bolted in place.

The lay-up was designed using the following formula, with the number of

layers rounded up to the nearest whole layer.

$$N = \frac{\rho.V_f.d}{A_w}$$ ---- Equation 3:1

where : N = the number of layers in the lay-up
V_f = the required volume fraction of the laminate
A_w = the areal weight of the reinforcement
ρ = the density of the reinforcement fibre
d = the thickness of the mould cavity

The mould was positioned vertically and held in position by two retort stands.

The inlet tube led to the beaker of glycerol which had been dyed purple to aid

the visualisation, while the exit tube led to the vacuum gauge and supply. The

test was commenced and timing started when the glycerol witnessed through

the fibres. At specific time intervals, the progression of the glycerol was

recorded on an acetate sheet placed on top of the mould. This procedure was

continued until the glycerol reached the outlet at which point the test was

terminated to prevent ingress of the glycerol into the vacuum supply

3:1:4 Test Reinforcements and Fluid

All the reinforcements were 'E' glass of density 2500 kg/m³ and the

configurations of the weaves are explained in more detail in Chapter 2:7. The

injection fluid used was glycerol supplied by BDH Chemicals and added to this

was a purple potassium permaganate dye. Table 3:1 shows the details of the

Labels in figure: To Vacuum, Retort Stand, Outlet, Fibre, Flow Front, Inlet, Aluminium mould 285mm square with perspex lid, Retort Stand, Beaker of Glycerol
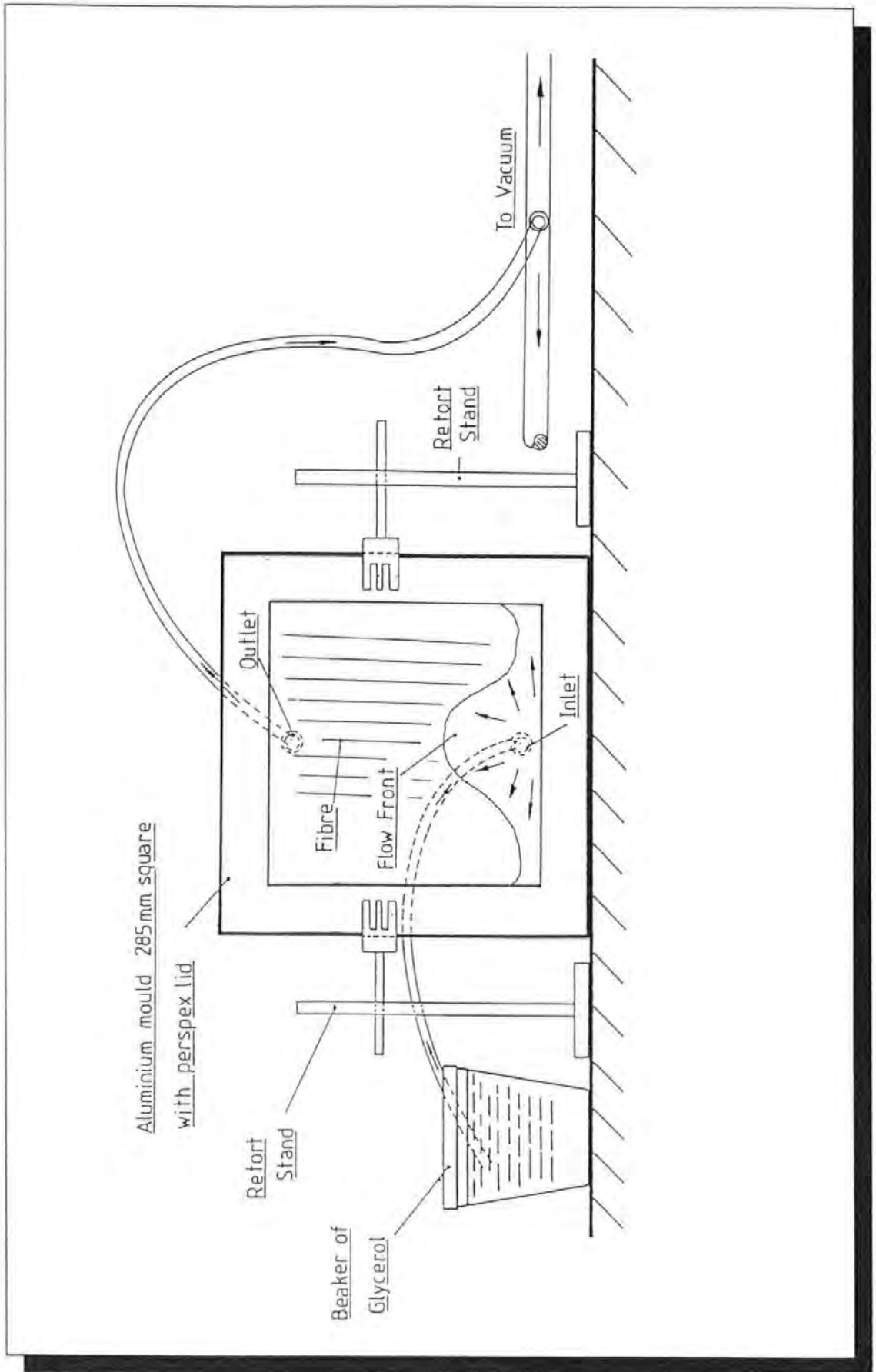
Figure 3:2. Experimental Set-up of Flow Visualisation Test using Vacuum Impregnation

102

reinforcements and the flow testing schedule. The complete set of flow

progressions are shown in Appendix 1:1.

Test Reference No.	Reinforcement Style	Orientation (degrees)	Areal Weight (g/m^2)	Number of Layers	TargetVolume Fraction (%)
VAC PW0-90-1	Plain Weave	0, 90°	210	22	50
VAC PW+/-45-1		+/-45°	450	10	50
VAC PW+/-45-2		+/-45°	900	5	50
VAC PW+/-45-3	Plain Woven (washed)	+/-45°	900	5	50
VAC TWILL-1	Twill (2x2) Weave	0, 90°	290	19	50
VAC U-D0-1	Uni-Directional	0°	250	19	50
VAC U-D0-2		0°	250	19	50
VAC U-D0-3		0°	250	19	50
VAC U-D+45-1		45°	250	19	50
VAC U-D-45-1		-45°	250	19	50

Table 3:1 Schedule of the Preliminary Flow Visualisation Tests

3:1:5 Data Processing

The flow front progressions were then analysed to determine reinforcement

permeabilities. This entailed measuring the incremental flow areas throughout

the progression using a planimeter, an instrument used for determining areas of

complex perimeter shapes. Figure 3:3 shows the planimeter in use, it works on

a system of two wheels, one measuring 'x' movement and one 'y' movement.

This movement is transmitted to a calibrated area measuring scale. The

incremental flow distance was analysed for several flow paths in differing

areas of the flow front to determine the permeability variation across the

mould. These flow paths are shown in the frontal progressions in Appendix

1:1:1. The incremental flow distances together with the viscosity, pressure

drop and incremental flow time were then put into a spreadsheet and using
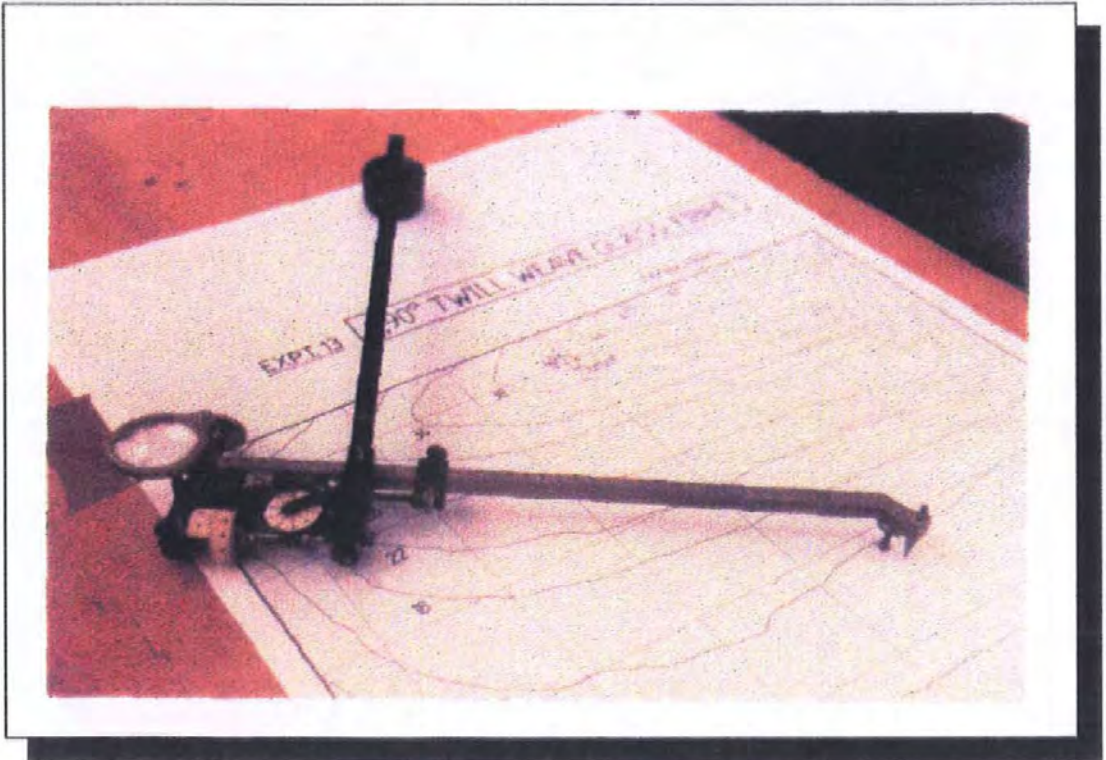
Figure 3:3 Measurement of Flow Areas using the Planimeter
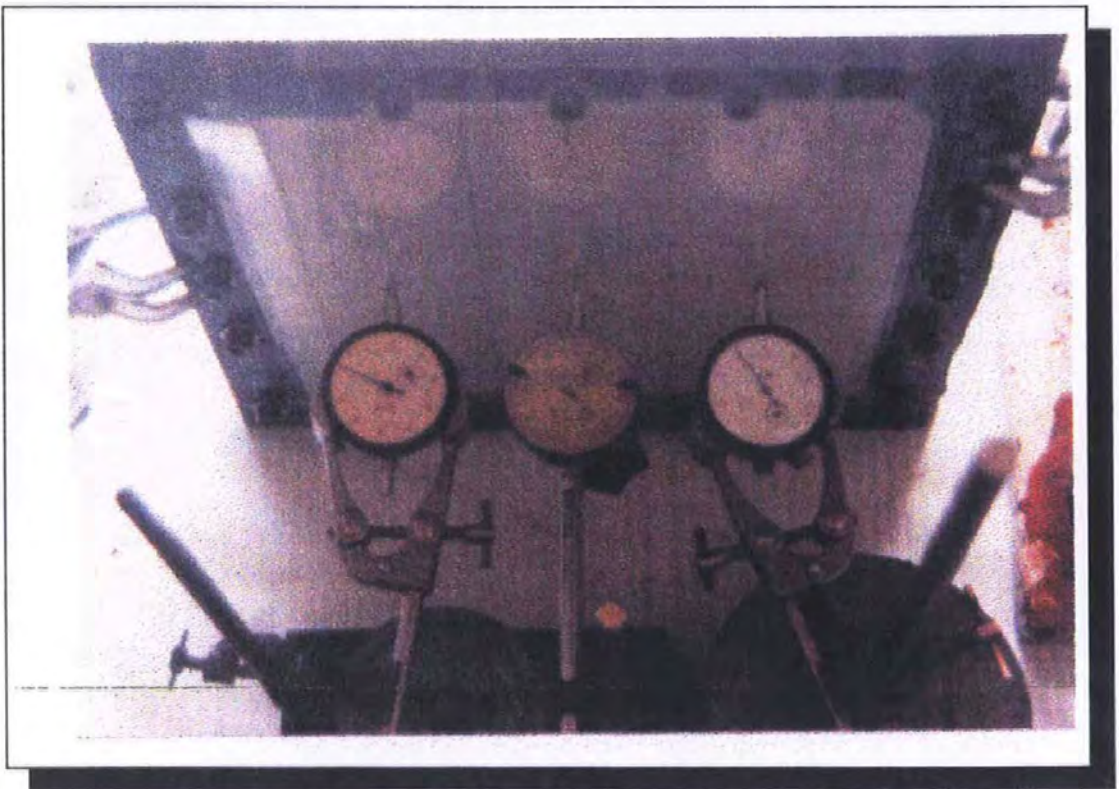
Figure 3:4 Dial Test Indicators Measuring Mould Deflection

equation 2:34, a series of incremental permeability values were obtained. Any unduly large values present during the transient flow at the beginning of the tests were removed and the remaining values averaged. The average incremental permeability values determined for the specific flow paths are shown in the results section 4:1.

3:1:6 Observations and Criticisms

The first and most important thing to notice is that the radial Darcy equation is not relevant after the resin comes into contact with the side walls. This is the point at which the radial flow ceases and different boundary conditions are introduced. Therefore the permeability values displayed in Tables 4:1:1 - 4:1:4 should be used only as a guide to the relative flow rates between different tests. However, the flow fronts developed in the tests showed several interesting features. These flow phenomena are discussed in detail in a paper by Griffin et al. [91] in Appendix 7. The most obvious deviation from uniform flow was seen around the edge of the mould where the glycerol raced ahead of the main flow front and reaches the outlet before 100% impregnation of the fibre pack has been achieved. The cause of this was the inability to maintain fibre integrity at the cut edge with the result being the creation of an edge gap. 'Edge effects' were evident to varying degrees in all the tests. In some tests it was only apparent on one side due to the fibres butting up against one side of the mould leaving a large gap on the opposite edge. Edge effects were apparent in the permeability values as there was a larger permeability in the edge region.

At high volume fractions, edge effects can be a problem because the fluid encounters more flow resistance and takes preferential, least resistance routes through to the outlets, but they can also be useful in promoting resin flow in areas of high volume fraction by the use of a channel designed in the mould.

In uni-directional reinforcements, there may be a non-uniform distribution of fibres due to the method by which they have been restrained (either chemically bound or woven with a small weft yarn). This particular uni-directional fabric has been bound chemically and there is an irregular or heterogeneous flow front. This is caused when the fluid again takes the easy path along the channels between the tows and a 'fingering' effect is produced in the flow front. This is the type of flow where several mechanisms of impregnation exist as discussed in Chapter 1. The main wetting front is behind the fingers where the tows are wetted out. The same fabric oriented at 45° to the inlet /outlet axis shows a marked difference in flow parallel to the fibres (axial) and flow across the fibres (transverse). This characteristic is known as anisotropy and is a result of an imbalance in the direction of the fibres.

There was large variation in the fill-times for the tests which may be attributed to a number of factors.

> i) differing ambient temperatures affected the viscosity of the fluid in the process

> ii) the vacuum pressure differed in several of the tests due to leaks in the sealing.

An important consideration with this mould was the deflection of the perspex top produced by the vacuum pressure. This was measured by the positioning of three Dial Test Indicators (DTI) across the mould face as shown in Figure 3:4. The maximum deflection encountered was 0.7mm at the centre which corresponds to 23% of the mould cavity depth and significantly increases the volume fraction in the central regions. This makes impregnation of this region more difficult and preferential flow takes place in the outer regions.

The problem of edge effects was addressed briefly in a trial injection under a vacuum bag. The set-up shown in Figure 3:5 involved the use of vacuum pressure to impregnate the reinforcement contained in the vacuum bag. The edges of the reinforcement were restrained by the vacuum bag and therefore there was no gap at the edges and hence negligible edge effects. Appendix 1:2 shows the progression of these tests with plain weave and also the problems that vacuum leakage cause to the flow. The permeability values are shown in results section 4:1:4 and it will be noticed that the permeability values at the edge are similar to those in the central regions. Injection VAC BAG PW-2 highlighted these problems where the loss of vacuum reintroduced the edge effects and a fold in the vacuum bag provided an easy path for the fluid. It was decided to abandon this technique in favour of the double-sided rigid mould.

3:2:1 Improvements to the Test Procedure

Figure 3:6 shows a new visualisation rig taking into account the observations and criticisms in the previous section. The mould is a 12mm thick mild steel

Figure 3:5 Resin Impregnation under a Vacuum Bag
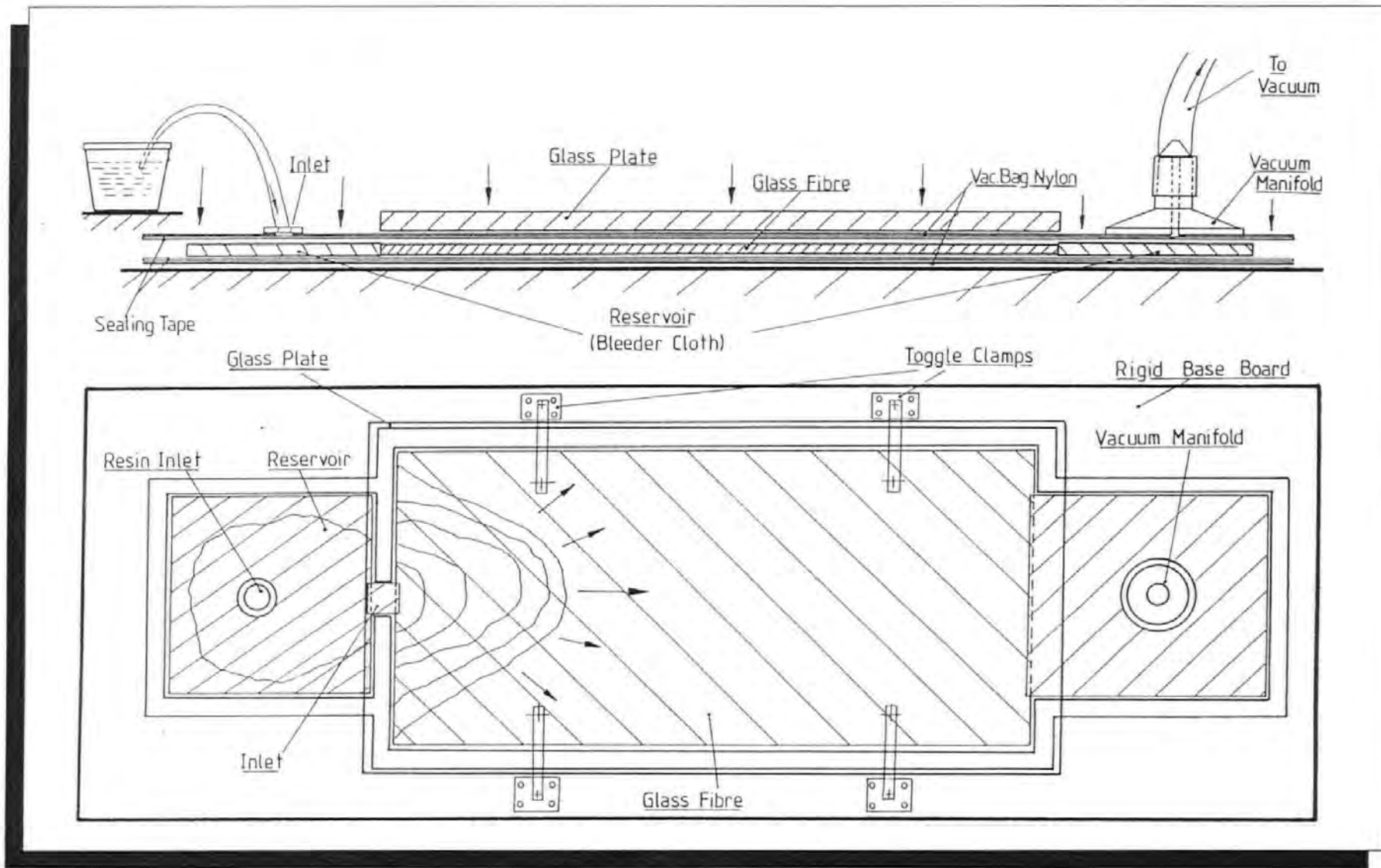
Figure 3:6 Steel/Glass Radial Flow Visualisation Mould
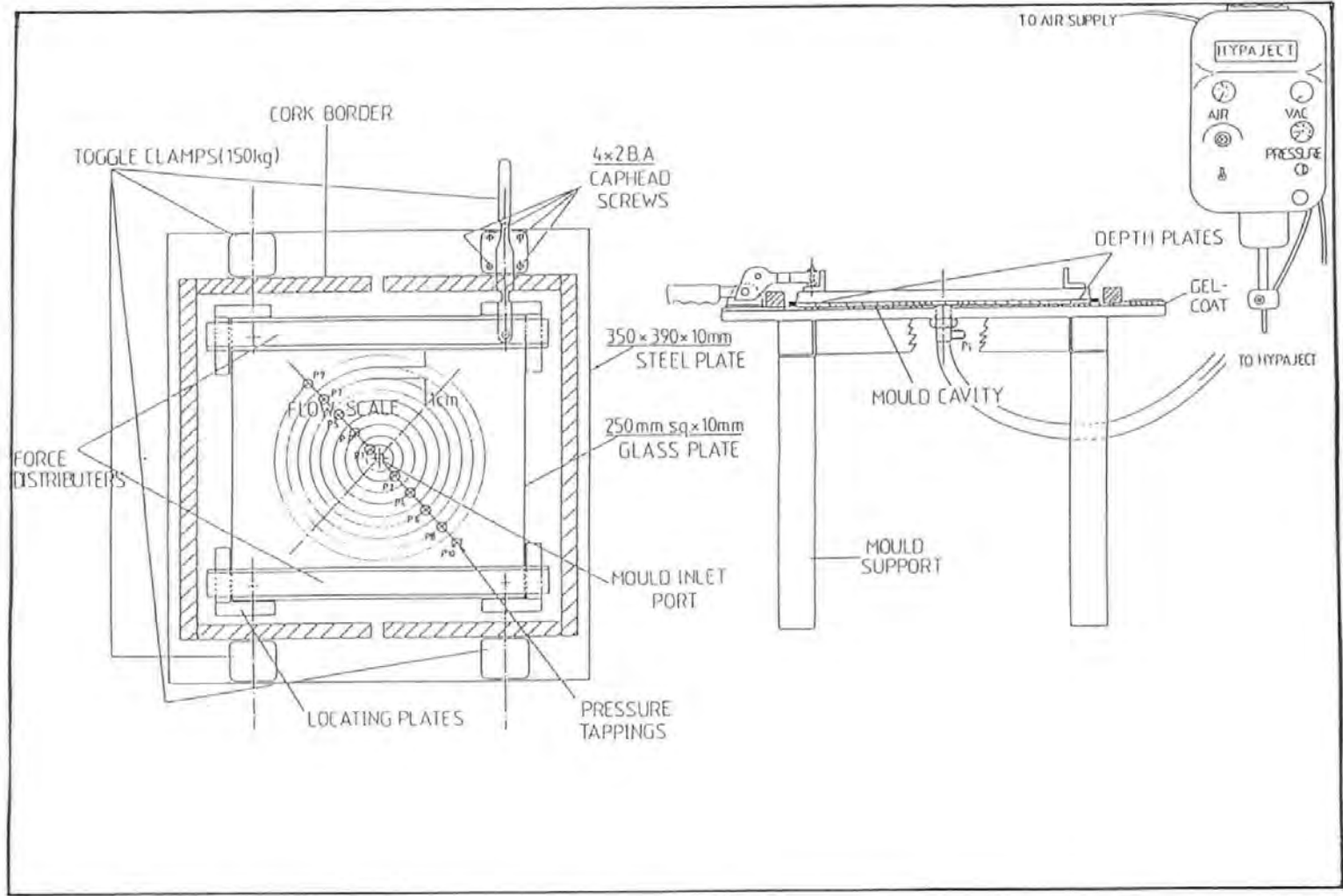
plate, 350mm square with a 2mm gelcoat bonded to it. The gelcoat was ground flat with various grades of wet and dry grinding paper. The major difference in this rig was that the mould was used for the injection of fluids under positive pressure rather than vacuum. This provided scope for pressures greater than 1bar to be used if required. The mould used radial injection from a central port which avoided the problem of edge effects. The depth of the mould cavity may be varied with the use of different depth plates. There was no seal and therefore the fibre pack was open to the atmosphere. Positioned either side of the inlet port were measurement ports to which pressure transducers (RS 0-15 psi Piezo Resistive) were attatched. Three thermocouple leads were positioned in the mould base plate. The mould top was a piece of float glass 10mm thick, 350mm square. The glass plate was positioned on top of the fibre pack and held in place by four toggle clamps and two force-distributing angle sections. The toggle clamps were more efficient than the caphead bolts as they released more easily. The set-up was postioned on a stand to enable easy access to the inlet port. The injection equipment,supplied by Plastech T.T. of Gunnislake, Cornwall consisted of a 3 litre steel cylinder with both vacuum and pressure injection capabilities. The maximum injection pressure available was 6 bar and the injection/vacuum was controlled by a valve positioned on the outlet tube of the cylinder. The cylinder also had the capabilities for solvent cleaning with a port at the head of the cylinder to allow a spray of acetone to

wash down the inside of the cylinder to dissolve unused resin which was then flushed out.

3:2:2 Reinforcements / Resin Tested

The fabrics used in this set of tests were as follows

i) Plain Woven 'E' Glass of 345g/m² areal weight

ii) Plain Woven 'E' Glass of 220 g/m² areal weight

A set of tests were undertaken to determine the repeatability of the injection. The tests were then continued to determine the effect of the following factors on permeability

i) laminate thickness

ii) volume fraction

iii) areal weight

The injection fluid used was the MY750 Epoxy resin system consisting of MY750 Resin / HY917 Hardener / DY070 Catalyst manufactured by Ciba-Geigy, see data sheet [92].

3:2:3 Data Collection

The procedure for data collection was improved by the use of a video camera and recorder to record the injection. An acetate sheet with a radial scale was placed on the top plate to enable the progression to be replotted as accurately as possible. The temperature of the mould was monitored throughout the injection and this temperature was used in the fluid viscosity testing. Viscosity tests were carried out after the injection at the measured mould temperature,

initially with a U-tube viscometer and latterly with a P-C controlled cone and plate viscometer. These tests are now discussed in more detail

3:2:4 Viscosity Test Procedure

Measured permeabilty value depended to a large extent upon the accuracy with which the viscosity was known, so viscosity measurements were conducted under strict conditions. These were carried out separately to the permeability tests and it was therefore required to obtain as much information regarding the state of the resin during the permeability test as possible. Therefore the following two temperatures were measured during the test:

i) the resin temperature

ii) the mould temperature

The ambient temperature was also measured but it was not believed that this would cause significant changes to the resin or mould temperatures during the test.

The viscosity tests undertaken during this research were done by two methods:

i) U-Tube Viscometer

ii) Cone and Plate Rheometer

3:2:5 U-Tube Viscometer

This method of viscosity determination was carried out in accordance with B.S. 188 'Methods for the Determination of the Viscosity of Liquids'. The correct U-tube was selected and was secured in position in the water immersion heater bath. Using a pipette, the fluid, (in this case glycerol) was

carefully inserted into the tube to the required level. The level was allowed to settle and then sucked up to the starting position on the tube. The vacuum was released and the timer started to time the descent of the glycerol between the two marks indicated in Figure 3:7.
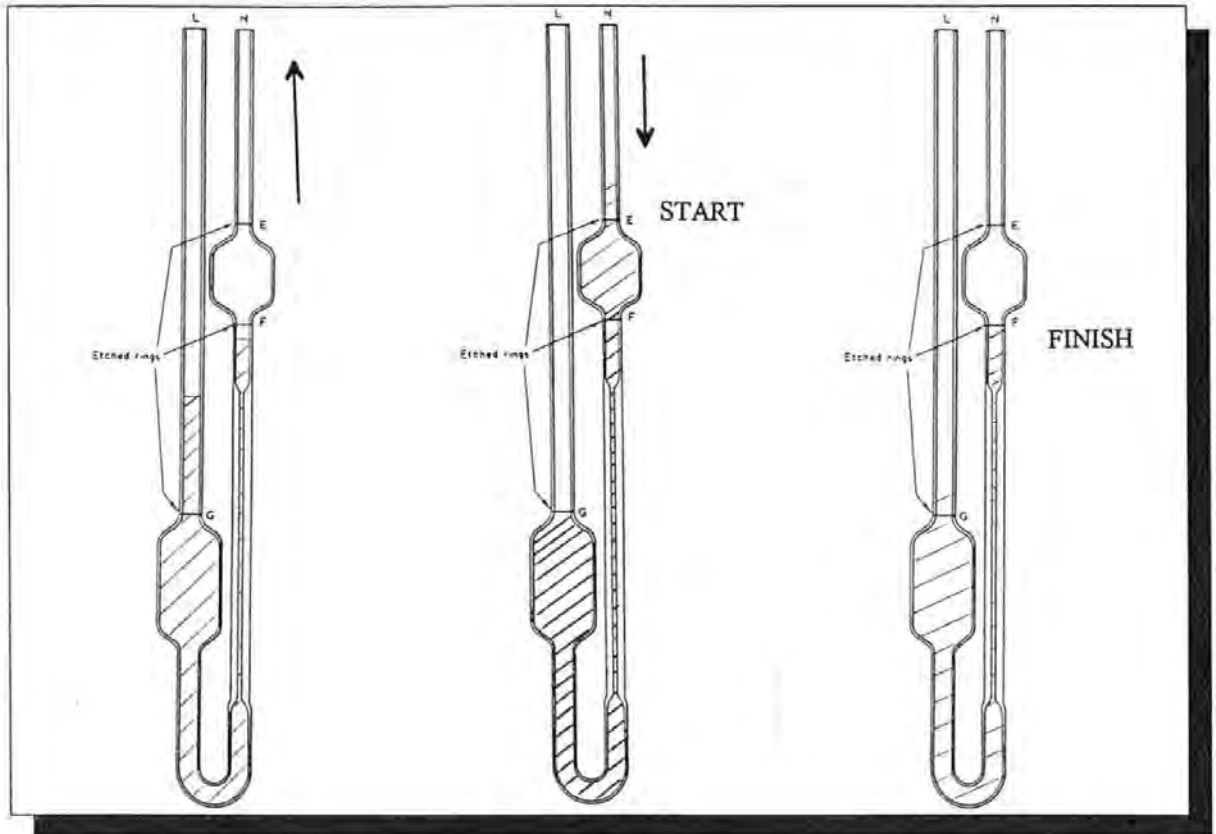
Figure 3:7. U-Tube Viscometer

Viscosity was determined as follows.

Kinematic Viscosity (v) = Flow time (s) x C - - - Equation 3:2

where

C = calibration constant for the specific U-tube.

Dynamic Viscosity (μ) = Kinematic Viscosity (v) x Fluid Density(ρ)

Using U-Tube 'G', with a calibration constant of 2.86, the glycerol timings

were taken at a temperature of 19.8°C for glycerol of 1.26 kg/m^3. Table 3:2

shows the calculated viscosities for three tests.

Flow Time (s)	Kinematic Viscosity (mm^2/s)	Dynamic Viscosity (Pa.sec)	(cP)
408	1170	1.47	1470
409	1170	1.47	1470
408	1170	1.47	1470

Table 3:2 U-Tube Viscosity Conversions

The average viscosity was found to be 1.47 Pa.s at 19.8°C and 1.18 Pa.s at

21.8°C. Then by the same method, the viscosity of Ciba-Geigy MY750 /

HY917 / DY070 epoxy resin was found to be 1.87 Pa.s. This resin was not

used at high temperature as recommendeded in its data sheet but was used in a

similar way to the glycerol, i.e. to observe flow characteristics. The resin

exhibited a 36% higher viscosity than glycerol at room temperature.

3:2:6 Problems with the U-Tube Viscometer

The resin wetted the glass tube which caused errors in the timing of the descent

of the fluid in the tube. There were no facilities to change the variables of the

test except the temperature, and hence varying the shear rate was not possible.

Obviously, the resin would have eventually gelled and care was taken not to

allow this to happen in the glass tube. To make the test more versatile, it was

decided to use a cone and plate rheometer controlled by a P.C. and the

'Carri-Med' package described in 3:2:7.

3:2:7 Cone and Plate Viscometer

The apparatus, a CSL100 controlled stress rheometer manufactured by Carri-Med is shown schematically in Figure 3:8:
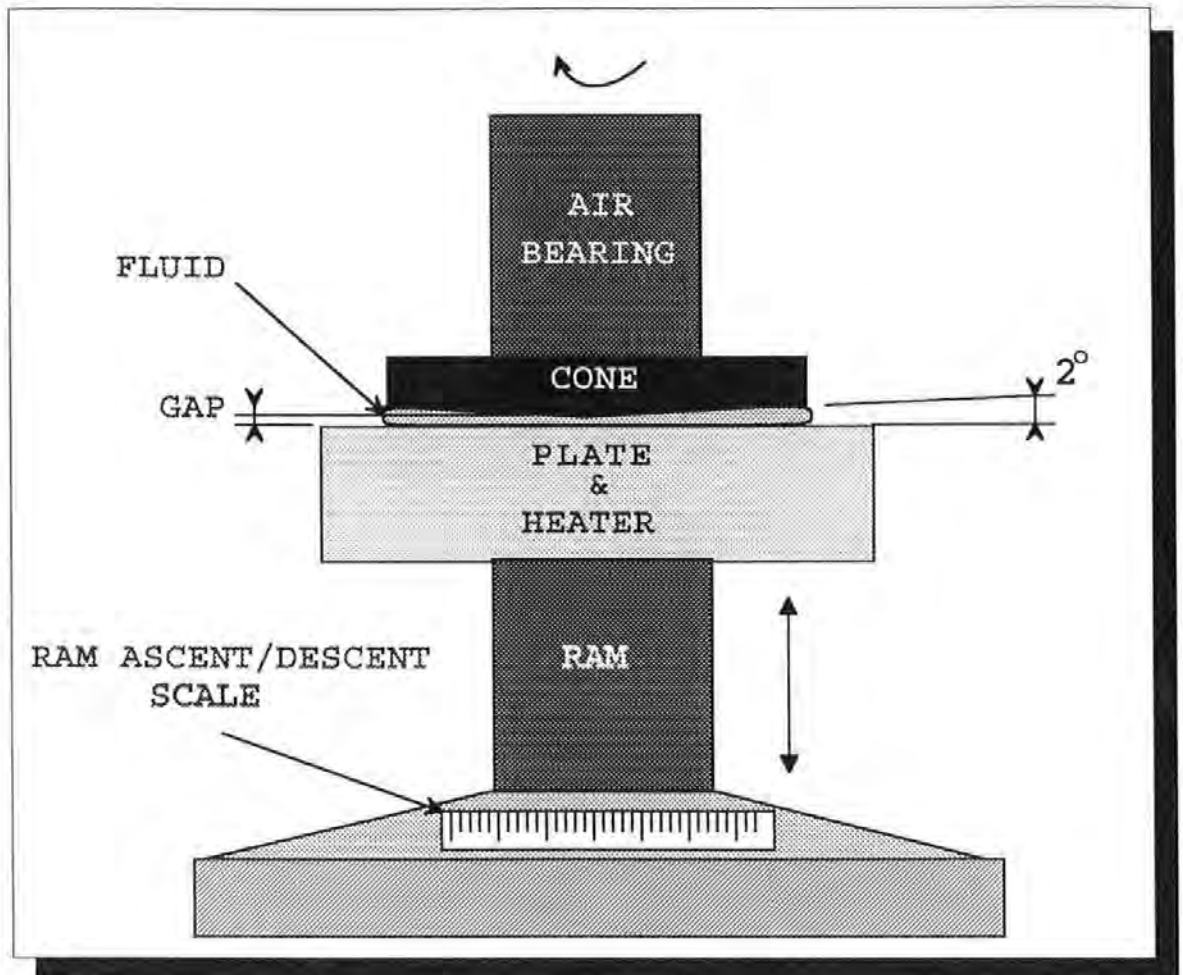
Figure 3:8 Cone and Plate Viscometer

The viscometer enabled different parameters (shear stress, shear rate) to be varied. The shear stress was set to level to simulate an approximate shear stress typical of RTM. The plate temperature was set to the resin temperature experienced during the permeability tests. The gap was set to 0.5mm using the dial scale on the base plate of the ram. The curing reaction in the resin commenced as soon as the constituents were mixed together and hence a similar mixing schedule to the permeability test was used. The test was started

at a similar time to the injection in the permeability test. The shear rate was monitored at a constant shear stress and a viscosity time plot obtained for each test. A comprehensive log of all the viscosity testing is in Appendix 2. This method was adopted as the standard viscosity determination test and was used in all the subsequent measurements. The preparation time was speeded up for the faster curing polyester resins. An advantage of using the cone and plate viscometer was that the viscosity could be monitored closely in order that the test be terminated when the gel commenced and the apparatus be cleaned off accordingly.

3:2:8 Fluid Pressure Measurement

In order to be able to analyse the fluid progression in greater detail, pressure readings at various points within the progression were required. The pressure gradient was also required in order to verify Darcy's Law i.e. that the flow velocity was proportional to the pressure gradient across the fluid. In the permeability tests undertaken, the pressure profile was not known but assumptions made were as follows:

i) the pressure at the inlet was equal to the injection pressure set on the gauge on the injection cylinder (no losses along the pipe between the mould and the cylinder)

ii) the pressure at the resin front was atmospheric if the mould was not sealed and therefore the pressure drop was simply the injection pressure minus the atmospheric pressure.

The permeability values calculated all used the total pressure difference between the front and the inlet.

To determine the pressure profile, some method of pressure measurement was required. It was decided to use pressure transducers placed at intervals across the mould . The specification of these transducers was as follows:

i) they should be easy to use

ii) owing to cost constraints, they should be reusable

iii) they should not degrade when in contact with resin

These specifications precluded the use of affordable transducers and hence it was decided not to use resin, but water-based glycerol as the injection fluid.

An RS 0-15 psi piezo-resistive transducer together with charge amplifier (the components and circuit of which are shown in Appendix 3) were selected for testing and this formed part of a B.Eng final year projects by Surphlis [93] and Mackenzie [94]. The first step was to realise the effectiveness of pressure measurement and after successful tests, further transducers were introduced to the mould to monitor the whole frontal progression. A problem encountered during measurement was the pressure limit on the transducer of 1 bar.

3:2:9 Calibration of the Pressure Transducer

The procedure for this was to use a precalibrated pressure gauge to apply specific pressures to the diaphragm located in the body of the transducer and record the voltage output (imbalance) in the circuit. The pressure was incremented upwards and downwards to observe any hysteresis losses. The voltage output was plotted against the gauge pressure to obtain the calibration

117

plot. The transducers were located in the positions indicated on the mould

diagrams in Figures 3:6 and 3:13. They were affixed to the mould by the

method shown in Figure 3:9.
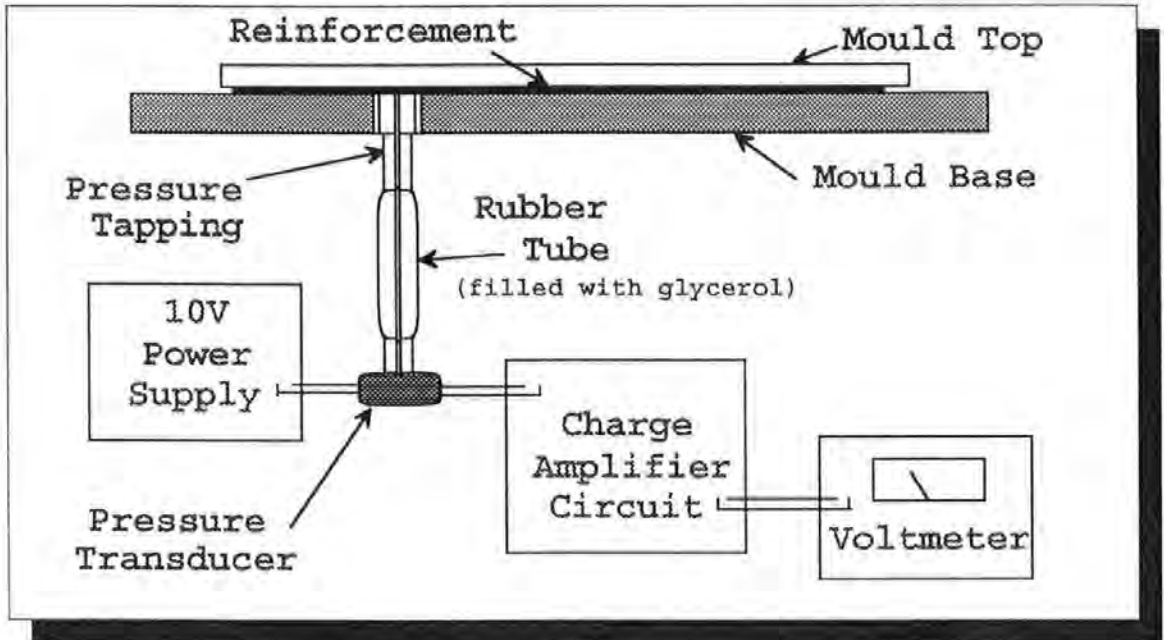
Figure 3:9. Apparatus for the Fluid Pressure Measurement

The initial project involved the measurement of the inlet pressure to work out

the losses along the inlet pipe and also to observe any fluctuations apparent in

the injection pressure. The transducer was placed on a T-junction standard 1/4"

BSP brass pipe fitting as close to the mould inlet as possible and the voltage

imbalance monitored as the test proceeded. Figure 3:10 shows the variability of

the inlet pressure for six tests with a set value of 0.8 bar.

The second project involved determining the pressure profile across the fluid

progression and used three transducers placed at specific ports. These port

locations changed for each test but all had a refererence inlet pressure.

To enable an estimation of the profile to be made, a plot of the pressure against port position was made by taking data from separate experiments at specific ports. The results of this are shown in Figures 3:11 & 3:12 .
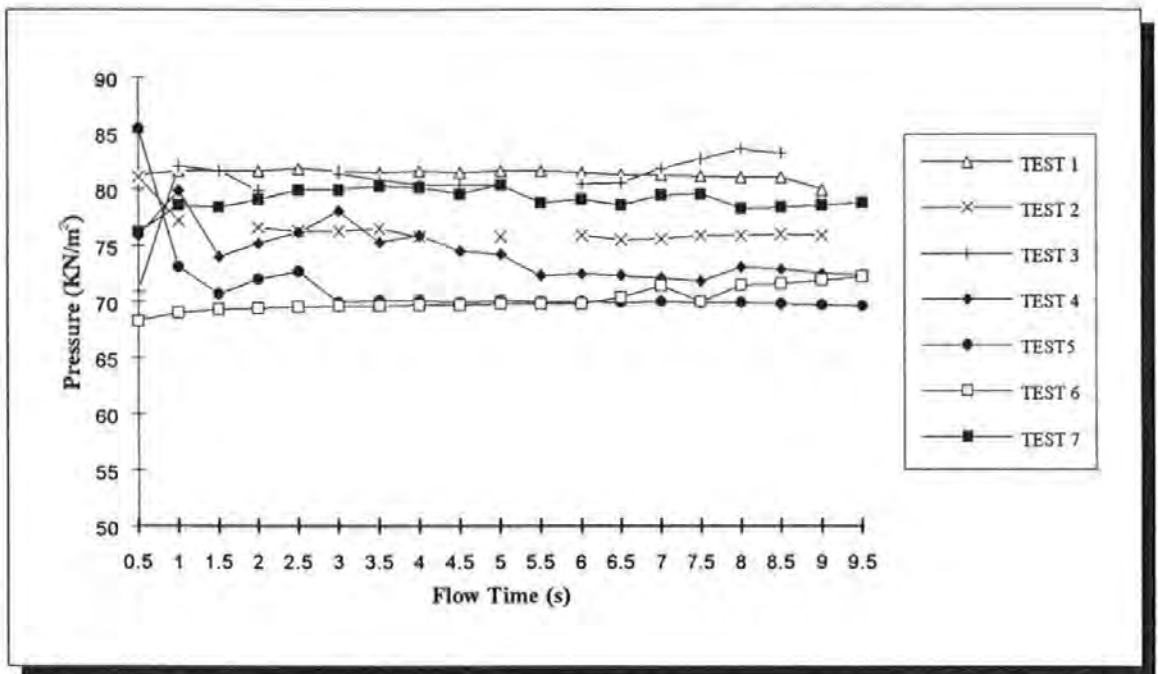
Figure 3:10 Fluctuation of the Inlet Pressure During an Injection
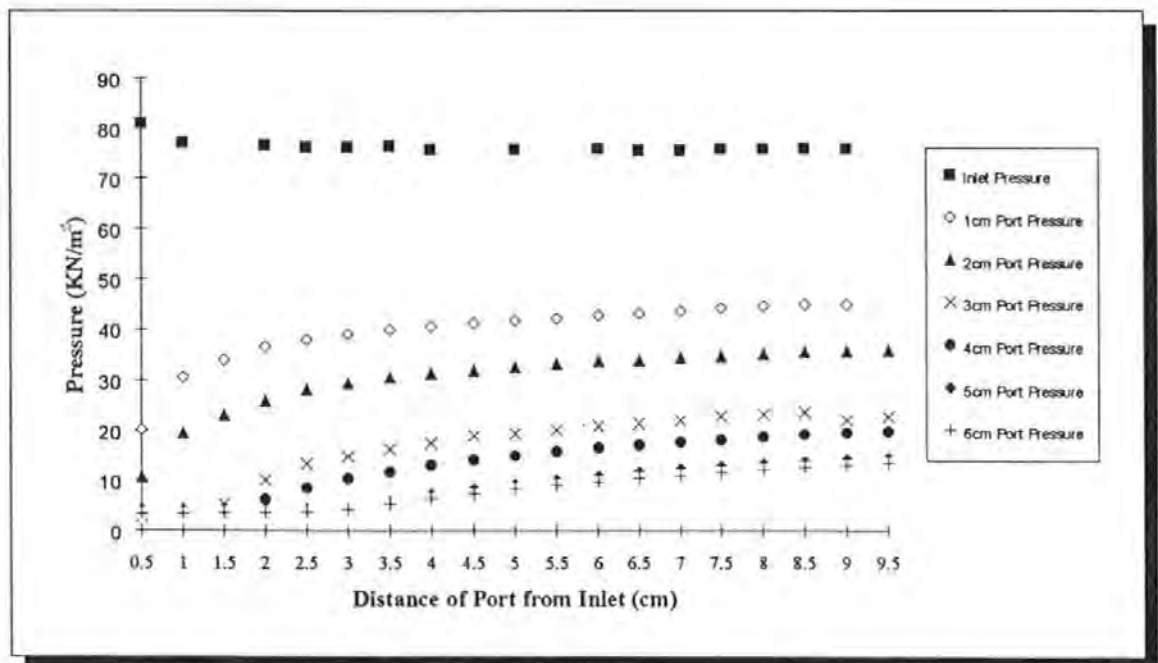
Figure 3:11 Pressure Rise at Specific Points in the Mould During the

Injection
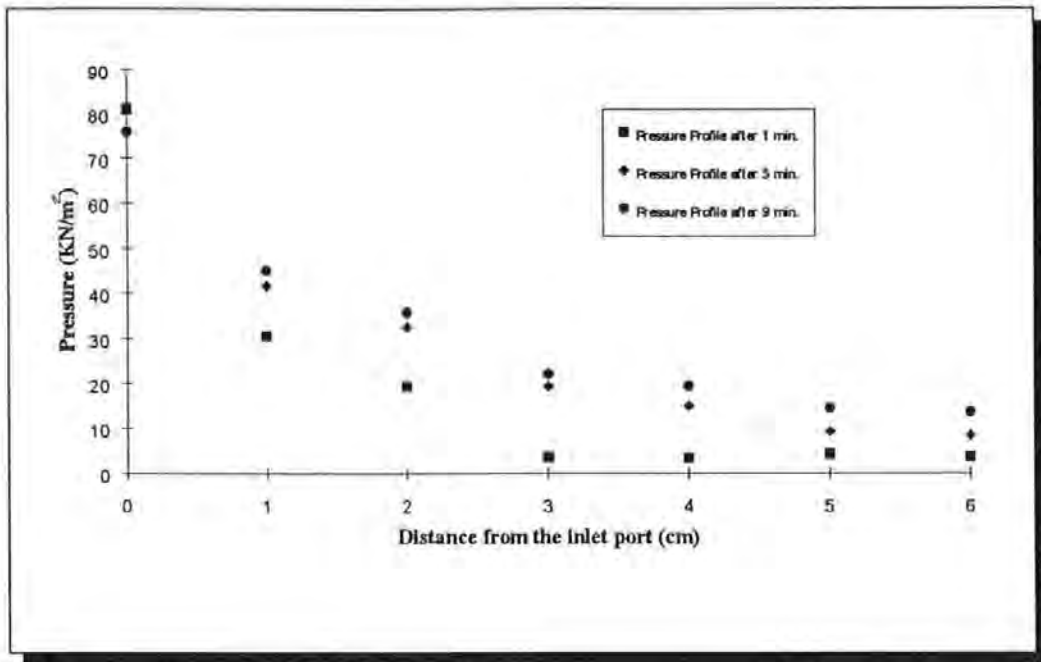
Figure 3:12. Pressure Profiles at Specific Times During the Injection

3:2:10 Determination of Permeability

Permeability calculation was based on the radial version of Darcy's Law

(equation 2:34). The viscosity tests which were conducted at the same ambient

temperature as the injection provided an independent set of values which took

into account the curing of the resin and consequent rise in viscosity. To obtain

the incremental flow radii, the video was replayed and the resin progression

replotted by freeze-framing the video at specific intervals. The flow areas were

measured with the planimeter in the same way as before. The areas were

converted into average flow radii by assuming the flow to be isotropic

(circular) and along with the pressure drop, viscosity values, flow interval

times and the inlet radius were programmed into a spreadsheet

(Microsoft Excel 5) to calculate the incremental permeability values. These

values were amended and an average permeability value determined which

120

was compared to the average permeability value for the whole injection i.e. the last incremental permeability. The complete set of flow front progressions for this series of tests is to be found in Appendix A1:2.

3:2:11 Observations and Possible Improvements

Observations made in this set of injections were that the initial percolation of the resin through the fibre pack to the top face proved to be very inconsistent. Some injections showed a large initial flow, some very little and some with two separate witness points i.e. the initial flow is three-dimensional rather than two-dimensional as assumed in Darcy theory. This effect is addressed in the next section. The mould deflection, determined by a similar method as before was found to be greatly reduced but for a mould depth of 2.12mm, there was still a deflection of 0.2mm (i.e. 9.4%) at the centre.

There was a problem of inconsistency in the viscosity tests being carried out using different samples of resin albeit with a similar time and temperature schedule as the injection. The homogeneity of the mixing was not guaranteed although care was taken to mix each sample well. The resin used in these injections was a high temperature cure epoxy which required heat to cure. In this set of tests, due to the absence of mould heating facilities, the resin was not cured. To enable samples for mechanical testing and plate thickness investigations to be moulded, there was a requirement for a heating system for the mould or the use of ambient temperature curing resins. The latter is adopted in the next schedule of permeability testing.

3:3 Adaption of Further Improvements.

The modified mould shown in Figure 3:13 was manufactured from a laminate

of glass and polyester resin enclosed by a rigid frame and includes several

improvements

i) the inclusion of a heater mat embedded in the mould base for high

temperature injections

ii) the addition of a rigid frame to be clamped to the mould top to prevent

mould deflection.

The toggle clamps were removed in favour of six G-clamps positioned around

the perimeter of the mould. Thermocouples were moulded into the base to

enable temperature monitoring to take place during the injection. The mould

also had the capability to be coupled to a vacuum supply if required.

3:3:1 New Reinforcement to be Tested

The new mould was used to test a set of development fabrics woven by Carr

Reinforcements Limited of Stockport, Cheshire. The fabric was a 2x2 twill

woven carbon, woven from Grafil 34-700 standard modulus in 6k tows. The

full specification of the fibres is seen in Table 3:3.

Fibre Type	Tensile Strength (GPa)	Modulus (GPa)	Density (g/cm³)	Elongation (%)	Filament Diameter (μm)
34-700-6000	4.5	234	1.8	1.9	6.9

Table 3:3 Carbon Fibre Specification

The new fabric was similar in form to 'Injectex' in that it included a bound or

twisted tow in the weft direction. This bound tow was woven in differing

proportions according the weave designation. Figure 3:14 shows the

Figure 3:13 Construction of Composite/Glass Radial Flow Visualisation Mould

123

Fabric Designation	38166	DWO 156	DWO 151	DWO 150	DWO 149	DWO 148	DWO 127	DWO 126
Tow Arrangement								
Ratio of Bound : Conventional Tows	N/A	1 : 7	1 : 6	1 : 5	1 : 4	1 : 3	1 : 2	1 : 1
Distance between Neighbouring Bound Tows	N/A	17mm	15mm	13mm	11mm	9mm	7mm	5mm
Areal Weight (g/m²)	380	380	381	380	385	384	388	384

Figure 3:14 Flow Enhancing, Carbon Twill Weave Specification

conventional twill and introduces the development fabric range. A limited

supply was provided by Carr Reinforcements for flow testing to determine the

flow enhancement produced by the twisted tows and for further microstructural

investigations.

The tests conducted on these fabrics used a nominal constant volume fraction

laminate which was made up of 4 layers. The slight variation in areal weight of

the fabrics required depth plates of slightly varying thicknesses to maintain a

50% volume fraction. The bound tow was orientated in the weft direction only

which meant that the flow enhancement was only in this particular direction.

To produce isotropic flow, the lay-up required balancing which was achieved

by laying the plies in a 0-90-90-0 orientation with respect to the bound tow. To

measure the degree of anisotropy produced in the flow by the bound tows,

some tests were undertaken on unbalanced laminates such as 0-90-0-0 and

0-0-0-0 orientation with respect to the bound tows. The first set of tests

undertaken measured the change in permeability produced by the flow

enhancing tows and used glycerol or 'Glycerin' supplied by Boots the Chemist.

There then followed a sequence of tests (see Tables 3:4 and 3:5) using

different polyester resins in order not only to produce plates for microstructural

analysis but also to investigate the effect of different fluids on the permeability

value.

3:3:2 Changes in the Permeability Measurement Procedure

After consulting the literature regarding the testing of laminates, it became apparent that similar problems of the initial three-dimensional flow had been experienced by other researchers. Montgomery et al [48] investigated the idea of cutting a circular hole above the inlet in order to reduce the variability of the initial contact of resin and fibre and also to initiate two dimensional flow. A 14mm diameter hole was punched through the whole laminate on a wooden board to reduce the problem of misalignment and the laminate positioned with the hole over the inlet on the base of the mould. The mould was then assembled with the frame being placed on the glass plate and then clamped at the corners using G-clamps. Table 3:4 shows the tests conducted on balanced (0-90-90-0), isotropic lay-ups, while Table 3:5 shows the schedule of testing conducted on anisotropic lay-ups.

A similar testing method was adopted for the lay-ups with an injection pressure of 0.85 bar with no vacuum. The progressions were videoed from above the mould and replayed to enable plotting. This procedure was thought to be one source of errors and therefore for one injection, three separate progressions were recorded and an error band obtained. This is discussed in the conclusion of Chapter 4. The planimeter was again employed to determine not only the incremental flow areas but also the average incremental flow radius. Viscosity values were obtained from the cone and plate viscometer in the same way as in section 3:2:7. The initial flow radius from (equation 2:34) was altered to the

radius of the hole cut in the laminate and as before , this information was introduced into a Microsoft Excel spreadsheet in order to determine the incremental permeabilities. These results are shown graphically in chapter 4:3

Fabric Designation	Ratio of Bound : Conventional Tows	Areal Weight (g/m²)	Cavity Thickness (mm)	Test Number	Injection Fluid
38166	Conventional 2x2 Twill Weave	380	1.69	Base Twill-1	Boots Glycerol
				Base Twill-2	Boots Glycerol
				Base Twill-3	Boots Glycerol
DWO 126	1:1	381	1.69	DWO126-1	Scott Bader 2-414 (Resin'E')
				DWO126-2	Scott Bader 2-414 (Resin'E')
				DWO126-3	Scott Bader 2-414 (Resin'E')
				DWO126-5	Boots Glycerol
				DWO126-7	BDH Glycerol
				DWO126-8	Boots Glycerol
				DWO126-9	Boots Glycerol
DWO 127	1:2	382	1.70	DWO 127-1	BDH Glycerol
				DWO 127-2	BDH Glycerol
DWO 148	1:3	384	1.71	DWO148-1	Scott Bader 2-414 (Resin'E')
				DWO148-3	Scott Bader 2-414 (Resin'E')
				DWO148-4	Scott Bader 471 (Resin'A')
				DWO148-6	Boots Glycerol
				DWO148-7	Boots Glycerol
				DWO148-8	Boots Glycerol
DWO 149	1:4	385	1.71	DWO 149-1	Boots Glycerol
				DWO 149-2	Boots Glycerol
				DWO 149-3	Boots Glycerol
DWO 150	1:5	380	1.69	DWO 150-1	Boots Glycerol
				DWO 150-2	Boots Glycerol
				DWO 150-3	Boots Glycerol
DWO 151	1:6	381	1.69	DWO 151-1	Boots Glycerol
				DWO 151-2	Boots Glycerol
				DWO 151-3	Boots Glycerol
DWO 156	1:7	380	1.69	DWO 156-1	Boots Glycerol
				DWO 156-2	Boots Glycerol
				DWO 156-3	Boots Glycerol

Table 3:4. Permeability Testing Schedule for Flow Enhancing Fabrics

Fabric Designation	Ratio of Bound : Conventional Tows	Areal Weight (g/m²)	Lay-up Orientation (wrt Bound Tow)	Cavity Thickness (mm)	Test Number	Injection Fluid
38166	N/A	380	N/A	1.69	38166-1	Scott Bader 2-414 (Resin'E')
DWO126	1:1	381	0-0-0-0	1.69	DWO126-4	Jotun Norpol 42-10 Polyester + MEKP Catalyst
			0-0-0-0		DWO126-6	Boots Glycerol
DWO148	1:3	384	0-90-0-0	1.71	DWO148-2	Scott Bader 2-414 (Resin'E')
			0-0-0-0		DWO148-5	Scott Bader 471 (Resin'A')
DWO 149	1:4	385	0-0-0-0	1.71	DWO149-4	Jotun Norpol 42-10 Polyester + AAP Catalyst
DWO 150	1:5	380	0-0-0-0	1.69	DWO150-4	Jotun Norpol 42-10 Polyester + MEKP Catalyst
DWO 151	1:6	381	0-0-0-0	1.69	DWO151-4	Jotun Norpol 42-10 Polyester + AAP Catalyst
DWO 156	1:7	380	0-0-0-0	1.69	DWO156-4	Jotun Norpol 42-10 Polyester + AAP Catalyst

Table 3:5. Permeability Testing Schedule for Unbalanced, Anisotropic Lay-ups.

3:4 Flow Monitoring Procedure Modifications

This section describes a new method of collecting the flow radius data, on the

Brite-Euram RTM development program at the University of Plymouth.

Figure 3:15 shows the arrangement of the permeability measurement facilities

while Figure 3:16 shows the heater mat and porting arrangements. It involved

the use of a frame grabbing camera placed above the mould, much the same as

the video camera, except that it was programmed to take and store images at

set intervals. After the injection was finished, these frames were analysed by

means of grey level detection, the wetted region being a different shade to the

unwetted region. Comparison of the wetted regions with an unwetted

calibration image yielded flow radii. The calibration image dictated the centre
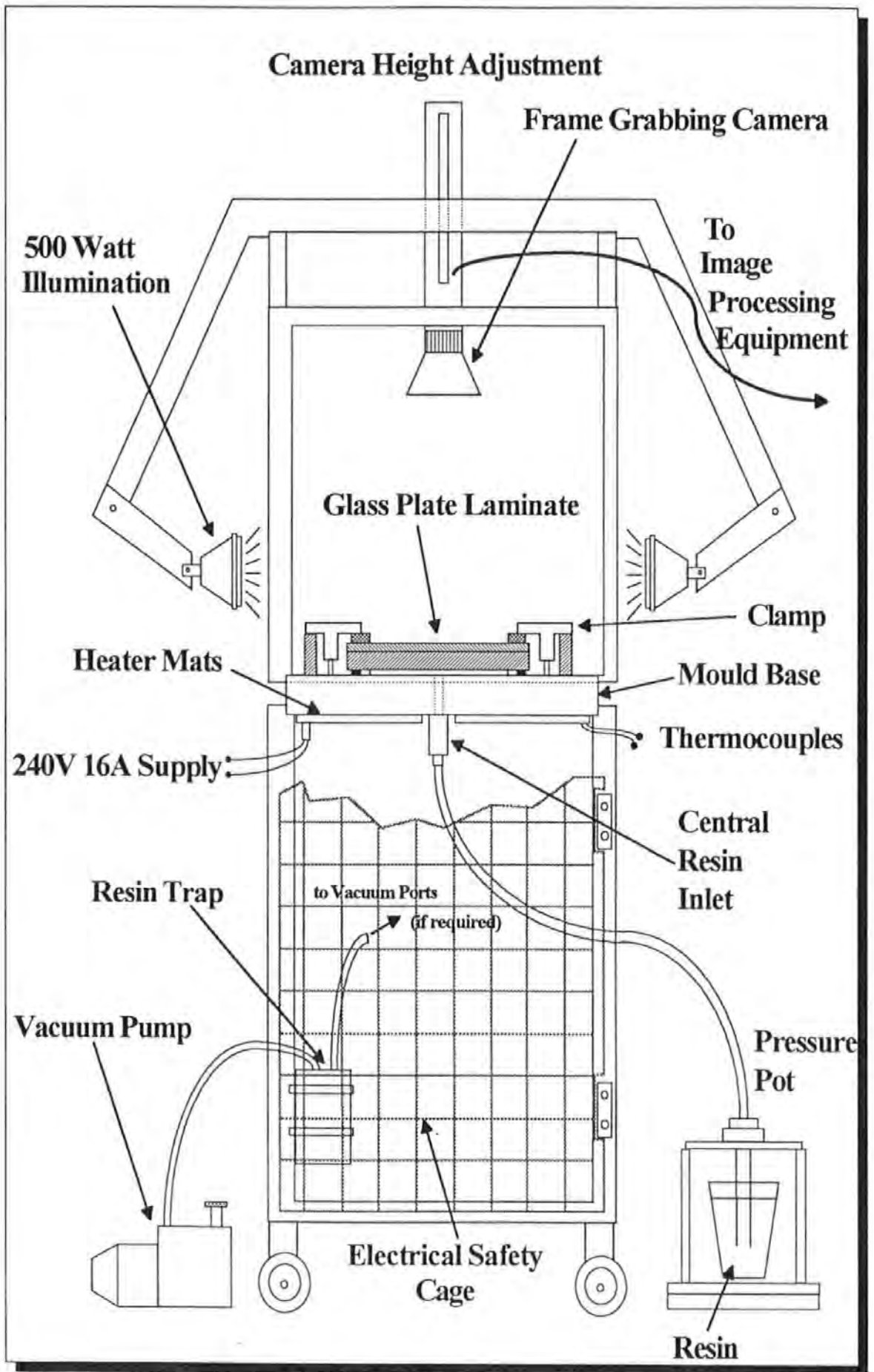
Figure 3:15 Brite-Euram Permeability Measurement Apparatus
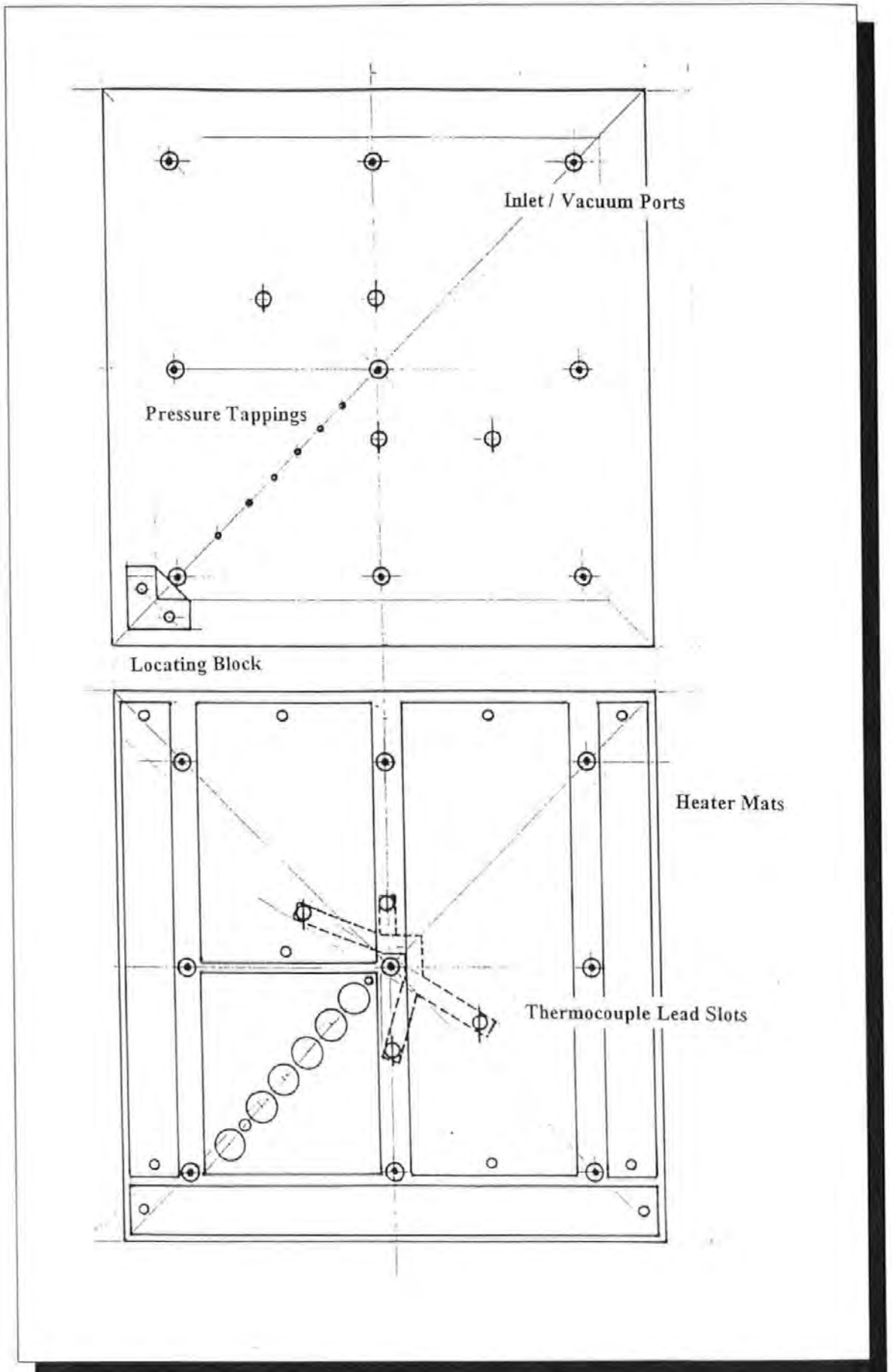
Figure 3:16 Porting and Heater Mat Arrangements on the Brite-Euram Permeability Mould

of the injection and also the 'x' and 'y' measured distances . The flow radii were measured at 15° intervals around the front which were stored on disk and imported onto a spreadsheet to determine the permeabilities. This was much more efficient than the planimeter at producing flow radii although it was susceptible to slight changes in the grey threshold level. This caused problems when different lighting conditions prevailed owing to a failure in the illumination system or when carbon reinforcements were used producing weave patterns on the glass plate. Smears on the glass caused by mould release also caused problems as they too produced different grey levels which affected the flow radii determination and therefore great care was taken to ensure the glass was clean before assembling the mould.

3:4:1 Verification of Permeability Testing

This set of tests is used to check the permeability values obtained from the previous section. Table 3:6 shows the testing schedule for these tests.

Fabric	Test Number	Nominal Volume Fraction (%)	Lay-up Orientation (wrt twisted tow)	Resin System
2x2 Twill	VTWILL - 1	53	N/A	Jotun Norpol 42-10
DWO 156 (1:7)	V156 - 1	53	0-90-90-0	Jotun Norpol 42-10
DWO 150 (1:5)	V150 - 1	53	0-90-90-0	Jotun Norpol 42-10
DWO 148 (1:3)	V148 - 1	53	0-90-90-0	Jotun Norpol 42-10
DWO 126 (1:1)	V126 - 1	53	0-90-90-0	Jotun Norpol 42-10

Table 3:6 Schedule for the Permeability Verification Tests

These series of tests were undertaken on 5 selected fabrics with an increment of 1,3,5 and 7 conventional tows per twisted tow. The tests were conducted at ambient temperature at an injection pressure of 1 bar and a mould depth of 1.59mm.

3:4:2 Data Processing

The flow radii data were imported into a spreadsheet and in a similar method as before, the incremental permeability values determined. The results of these permeability tests are shown in chapter 4:4. The plates produced by the permeability tests were sectioned, measured and mounted to provide data for mould deflection and samples for image analysis which is discussed in chapters 5 and 6.

CHAPTER 4

PERMEABILITY TEST RESULTS

This chapter presents the results of all the permeability tests undertaken using the four experimental procedures described in Chapter 3. The results are presented in both tabular and graphical form to enable comparison of the values. The plots of the flow progressions for all of the permeability tests are presented in Appendix 1.

4:1 Preliminary Flow Test Results

This section reports the results of the tests described in Chapter 3:1:3 involving the impregnation of various 'E' glass reinforcements using vacuum pressure only. It is important to realise that the permeability values are not strictly correct. This was due to the radial Darcy's law (equation 2:34) being inapplicable after the glycerol meets the side walls of the mould. At this point the boundary conditions change as the radius of the flow front at the wall is constant. Therefore, the relative magnitude of the permeability values should only be used as a comparison between different fibre lay-ups.

4:1:1 Plain Weave

Table 4:1 lists a sequence of average incremental permeability values for each test using a plain weave fibre bed with a nominal 50 % volume fraction. The sequence of flow path identities (A-G) give a representation of the variation of permeability across the flow front for each.particular test. Reference to

Appendix 1:1 will show the exact position of these flow paths. These permeability values are then plotted on a histogram shown in Figure 4:1 and show graphically the range of values across the front.

4:1:2 Twill Weave

Table 4:2 shows the range of values obtained for a fibre bed nominally containing 50% by volume of a 2x2 twill woven glass reinforcement. The flow paths are again plotted on a histogram shown in Figure 4:1 to enable comparison with the plain woven fabric.

4:1:3 Uni-Directional Fabric

This set of tests exhibit the flow characteristics of various orientations of uni-directional glass fibre with a nominal 50% volume fraction. The permeability values are shown in table 4:3 and plotted on a histogram in Figure 4:2. A graph showing the respective permeabilities of the central region of flow is shown in Figure 4:3 for all the laminates tested in the rigid mould.

4:1:4 Resin Injection under a Vacuum Bag

As a variation to the rigid mould method, the vacuum bag injection described in section 3:1:6 was used to rid the problem of edge effects. However, although the volume fraction was not accurately controllable, the permeability values were of similar magnitude as will be observed in Table 4:4. Unfortunately, problems with wrinkles producing preferential flow channels and vacuum loss were apparent in experiment 'VACBAG PW-2' as seen in Appendix 1:1 and

Test Reference No.	Reinforcement Style	Orientation (degrees)	Areal Weight (g/m²)	Vacuum Pressure (bar)	Average Permeability of Specific Resin Paths (darcies)						
					A	B	C	D	E	F	G
VAC PW0-90-1	Plain Weave	0, 90°	210	0.54	41	31	26	32	40		
VAC PW+/-45-1		+/-45°	450	0.56	5	18	29	37	35	19	5
VAC PW+/-45-2		+/-45°	900	0.59	20	28	33	39	41	14	6
VAC PW+/-45-3	Plain Woven (washed)	+/-45°	900	0.56	49	92	106	99	45		

Table 4:1 Permeability Values obtained for Plain Weave using Vacuum Assisted Impregnation in a Rigid Mould

Test Reference No.	Reinforcement Style	Orientation (degrees)	Areal Weight (g/m²)	Vacuum Pressure (bar)	Average Permeability of Specific Resin Paths (darcies)				
					A	B	C	D	E
VAC TWILL-1	Twill (2x2) Weave	0, 90°	290	0.92	56	52	45	45	46

Table 4:2 Permeability Values obtained for 2x2 Twill Weave for Vacuum Impregnation

Test Reference No.	Reinforcement Style	Orientation (degrees)	Areal Weight (g/m²)	Vacuum Pressure (bar)	Average Permeability of Specific Resin Paths (darcies)							
					A	B	C	D	E	F	G	H
VAC U-D0-1		0°	250	0.92	40	57	57	55				
VAC U-D0-2	Uni-Directional	0°	250	0.85	2	28	36	38	3	2		
VAC U-D0-3		0°	250	0.87	5	67	75	7				
VAC U-D+45-1		45°	250	0.91	65	124	137	121				
VAC U-D-45-1		-45°	250	0.85	14	12	29	25	28	13	45	10

Table 4:3 Permeability Values obtained for Uni-Directional Reinforcement for Vacuum Impregnation

Test Reference No.	Reinforcement Style	Orientation (degrees)	Areal Weight (g/m²)	Vacuum Pressure (bar)	Average Permeability of Specific Resin Paths (darcies)				
					A	B	C	D	E
VAC BAG PW -1	Plain Weave	0, 90°	210	0.71	1	6	20	7	1
VAC BAG PW -3	Plain Weave	0,90°	210	0.73	1	20	23	5	1

Table 4:4 Permeability Values obtained for Plain Weave using Vacuum Assisted Impregnation in a Vacuum Bag
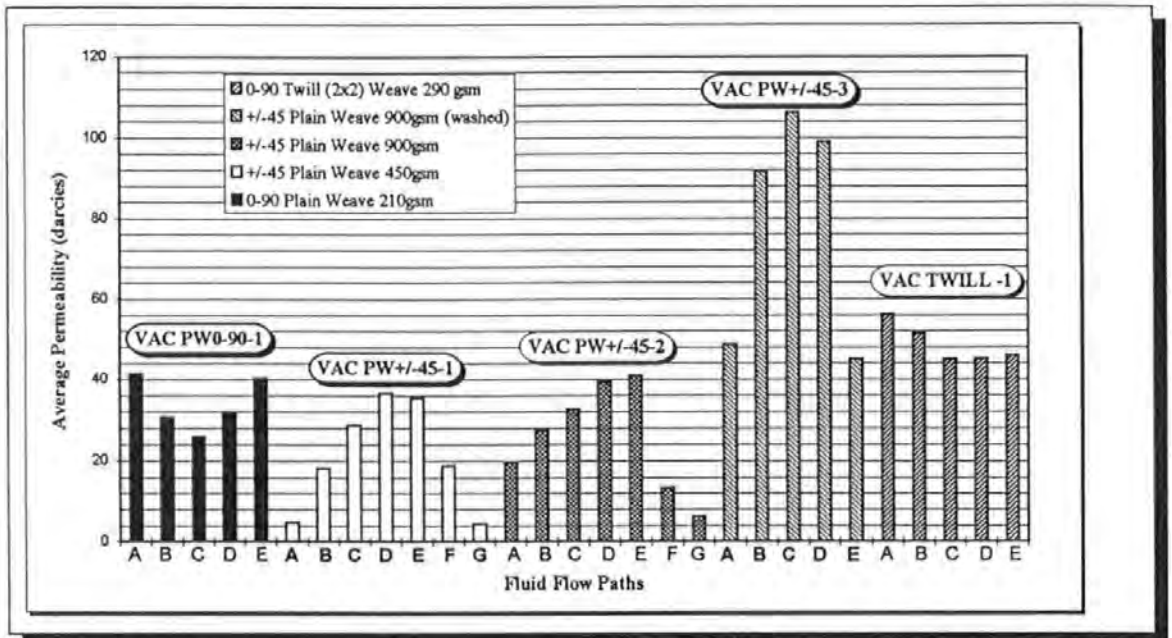
Figure 4:1 Permeability Variation across Flow Fronts for Plain and Twill Weaves during Vacuum Impregnation
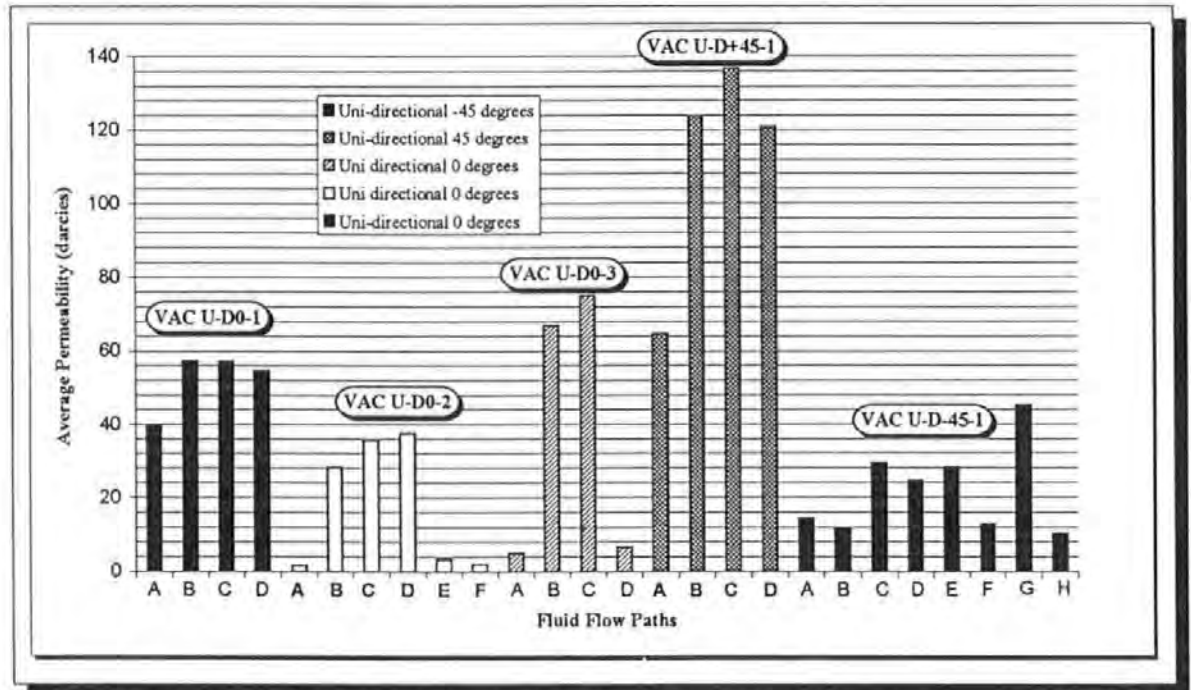
Figure 4:2 Permeability Variations in Various Orientations of Unidirectional Reinforcement during Vacuum Impregnation
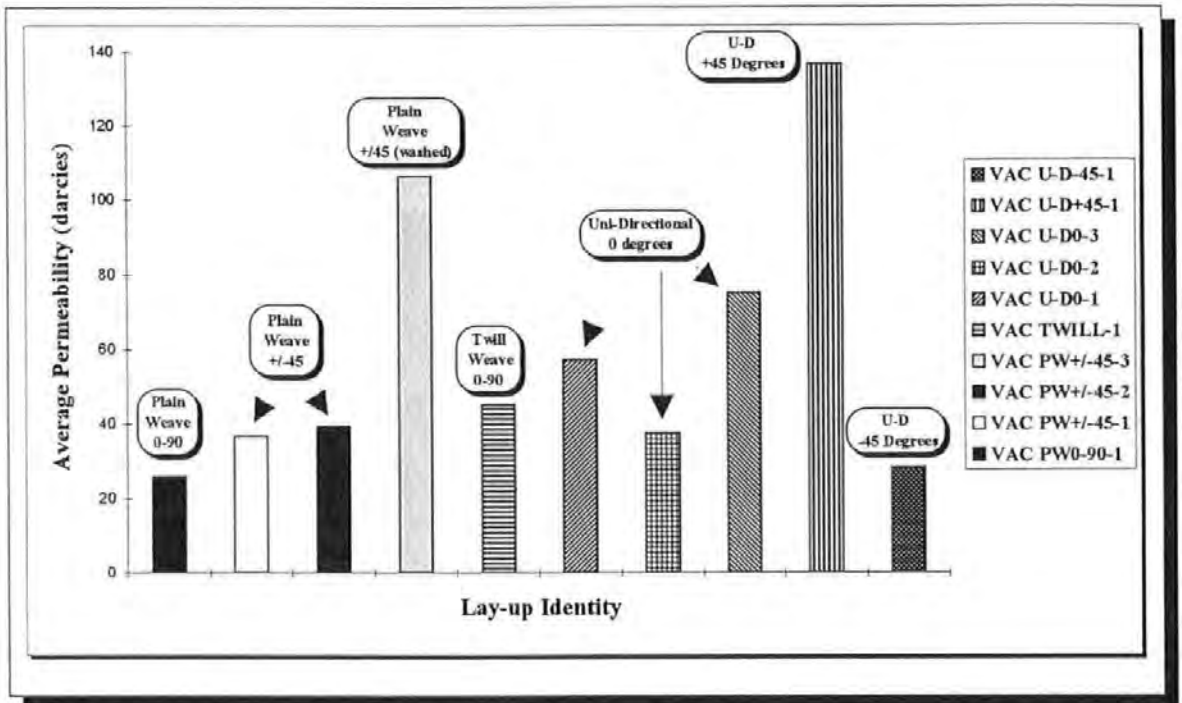
Figure 4:3 Comparison of Permeabilities of the Central Region of the Flow Fronts
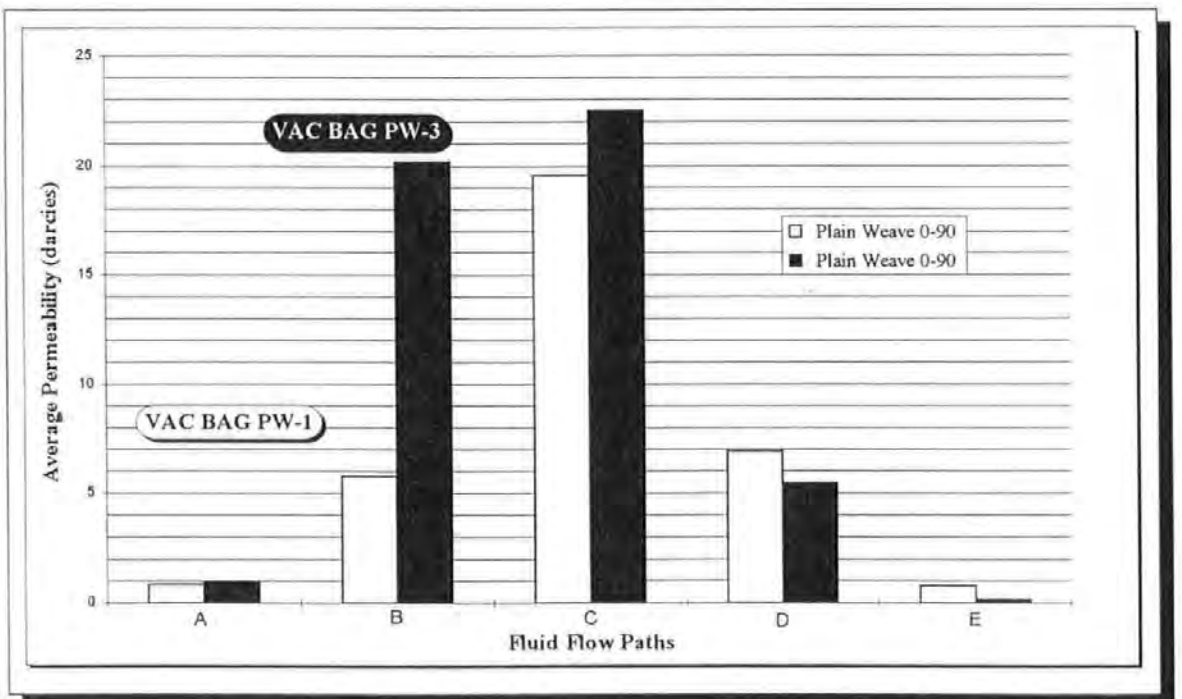
Figure 4:4 Permeability Variation of Plain Weave using Impregnation under a Vacuum Bag

138

this technique was abandoned in favour of a rigid mould. The permeability range across the bag is presented graphically in Figure 4:4.

4:2 Permeability Test Results with Modified Mould and Procedure

These were undertaken on a mould with a central injection port to produce radial flow. The modified mould and procedure are described in detail in Chapter 3:2. The radial flow was designed to avoid edge effects. A series of tests were undertaken to observe the variation in permeability due to changes in the following parameters

i) cavity thickness (three different thicknesses)

ii) areal weight (two different areal weights)

iii) volume fraction (two different volume fractions)

4:2:1 Changing Laminate Thickness

Table 4:5 forms the basis for comparison of all the testing i.e. the parameters are changed with respect to the first set of tests. As will be noticed, two separate permeability values are quoted

i) Cumulative Permeability - this is the average permeability of the progression and is determined, (in isotropic flow) by using the maximum flow radius with respect to the central port as shown in equation 4:1

$$ K_{cum} = \frac{\varepsilon.\mu}{P_o.T_{max}} \left[\cdot \left(\frac{r_o^2}{4} \right) + \frac{R_{max}^2}{4} \left(2 \ln \left(\frac{R_{max}}{r_o} \right) - 1 \right) \right] - - - - \text{Equation 4:1} $$

where : T_{max} = the time for the flow to reach the maximum flow radius R_{max}

It is susceptible to the inconsistent initial flow problem and may produce a larger range of values than incremental permeability.

ii) Incremental Permeability - is an average of all the individual permeabilities calculated at the flow front isochrones plotted.

$$K_{\text{average incremental}} = \Sigma \cdot \frac{K}{n} \text{ - - - - Equation 4:2}$$

where K = the incremental permeability for between each isochrone

n = the number of isochrones

To enable a more meaningful value to be produced, unusually large and small values of K (~ +/- 15% above or below the average) have been ignored. Table 4:5 has also been produced to give an idea of the repeatability of the test and both the error range and standard deviation have been quoted to show the degree of scatter.

4:2:2 Changing the Cavity Thickness, Volume Fraction & Areal Weight

Table 4:6 shows the effect of changing the laminate thickness, areal weight and the volume fraction. As before, both cumulative and incremental permeabilities are determined together with the ranges and standard deviations. Figures 4:7 and 4:8 compare the results graphically showing the experimental scatter encountered as well as the difference in permeability produced by altering the process conditions. It is observed from Figure 4:7 there are several values of permeability which are either unusually high or low, proving that permeability values are difficult to reproduce accurately. Finally in this set of tests, Figure 4:9 shows a plot of the variation in permeability for all five process conditions. The reduction in volume fraction is the only test to show significant increases in permeability.

EXPERIMENT NUMBER	CUMULATIVE PERMEABILITY (darcies)	INCREMENTAL PERMEABILITY (darcies)
Plain Weave 1-1	307	235
Plain Weave 1-2	279	253
Plain Weave 1-4	266	260
Plain Weave 1-5	267	263
Plain Weave 1-6	253	240
Plain Weave 1-7	251	229
Plain Weave 1-8	384*	262
Plain Weave 1-9	271	229
Plain Weave 1-10	217	177
Plain Weave 1-11	235	215
Plain Weave 1-12	314	282
Plain Weave 1-13	361*	356*
Plain Weave 1-14	229	213
Plain Weave 1-15	211	150*
Plain Weave 1-16	354*	288
Plain Weave 1-17	185*	176*
Plain Weave 1-18	321	353*
Plain Weave 1-19	229	211
Average Permeability	274	244
Range	+40% -33%	+46% -39%
Standard Deviation	54	53
Omitting the large and small values (outside the range of +/- 60 darcies from the average) indicated by the asterisk from the following values were obtained		
Average Permeability	261	240
Range	+23% -19%	+20% -27%
Standard Deviation	34	29

Table 4:5 Permeability Values for Plain Woven 'E' Glass

Omission of the large and small values from Table 4:5 shows the effect that these values have on the average permeability and particularly the standard deviation which reduces by approximately 40%. As there appears to be no obviuos reason why these results should be so, it is recommended that the average permeability and standard deviation from the 18 tests be used.

141

Volume Fraction (%)	Injection Pressure (bar)	Cavity Thickness (mm)	Number of Layers	Areal Weight (g/m³)	Cumulative Permeability (darcies)	Incremental Permeability (darcies)
52	0.85	**4.24**	16	345	157	134
52	0.85	**4.24**	16	345	168	152
52	0.85	**4.24**	16	345	217	203
				Average Permeability	180	163
				Range	+20% -13%	+25% -18%
				Standard Deviation	26	29
CHANGE IN MOULD CAVITY DEPTH						
52	0.85	**6.36**	24	345	193	179
52	0.85	**6.36**	24	345	243	191
52	0.85	**6.36**	24	345	223	181
				Average Permeability	220	184
				Range	+11% -12%	+4% -3%
				Standard Deviation	21	5
CHANGE IN FABRIC AREAL WEIGHT						
52	0.85	2.12	15	**220**	231	241
52	0.85	2.12	15	**220**	245	222
52	0.85	2.12	15	**220**	337	271
				Average Permeability	271	245
				Range	+24% -15%	+11% -9%
				Standard Deviation	47	20
CHANGE IN FIBRE VOLUME FRACTION						
39	0.85	2	6	345	1104	886
39	0.85	2	6	345	2888*	2031*
39	0.85	2	6	345	1162	1007
39	0.85	2	6	345	1127	876
				Average Permeability	1570	1200
				Range	+84% -30%	+69% -27%
				Standard Deviation	761	482
Omitting the large value indicated by the asterisk from the calculations the following values were obtained						
				Average Permeability	1131	923
				Range	+3% -2%	+9% -5%
				Standard Deviation	24	59

Table 4:6. Permeability Values for Various Process Changes
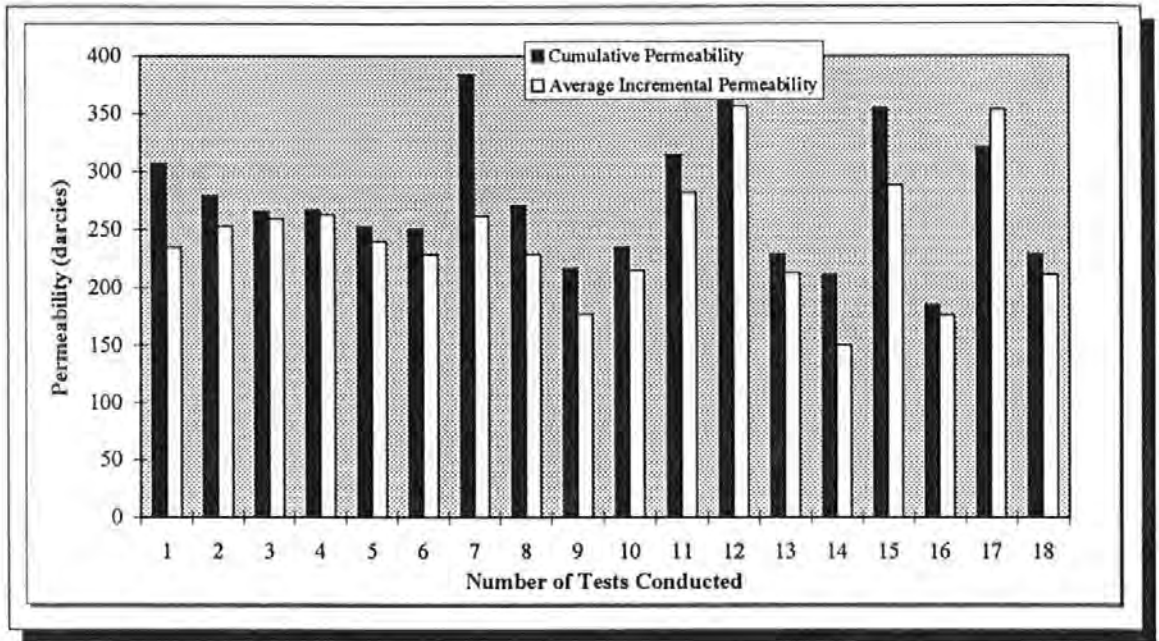
Figure 4:7 Scatter of Permeability Values Associated with a Nominally Similar Test
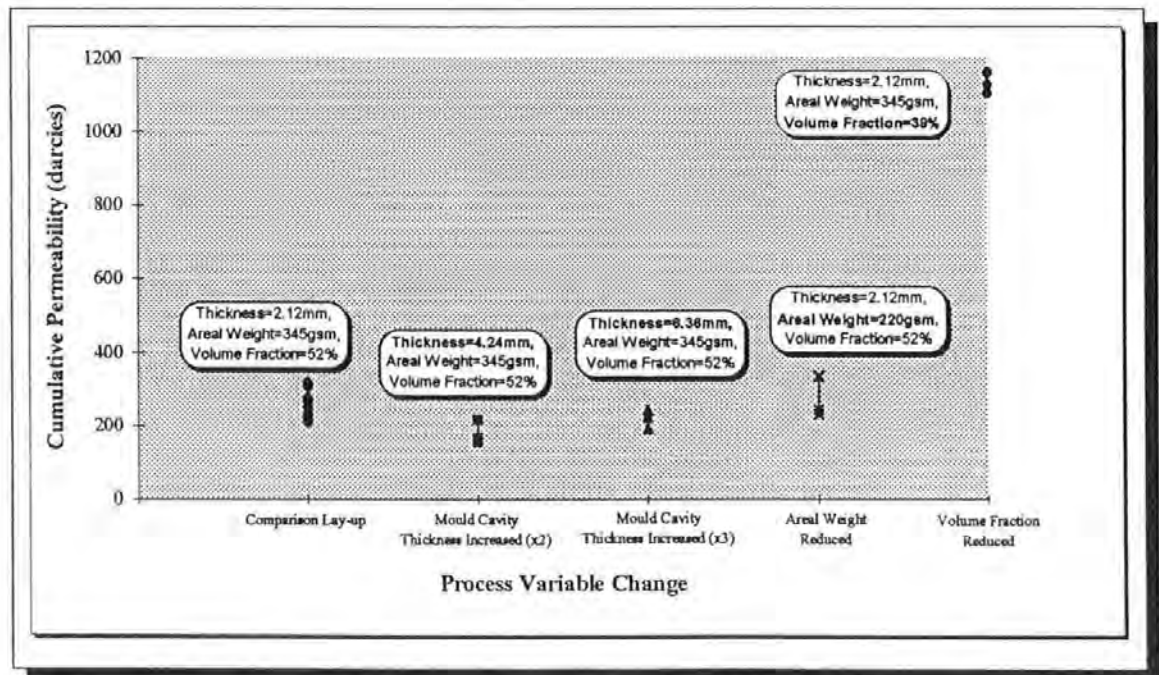
Figure 4:8 Scatter of Permeability values Associated with the Respective Change in Process Variables
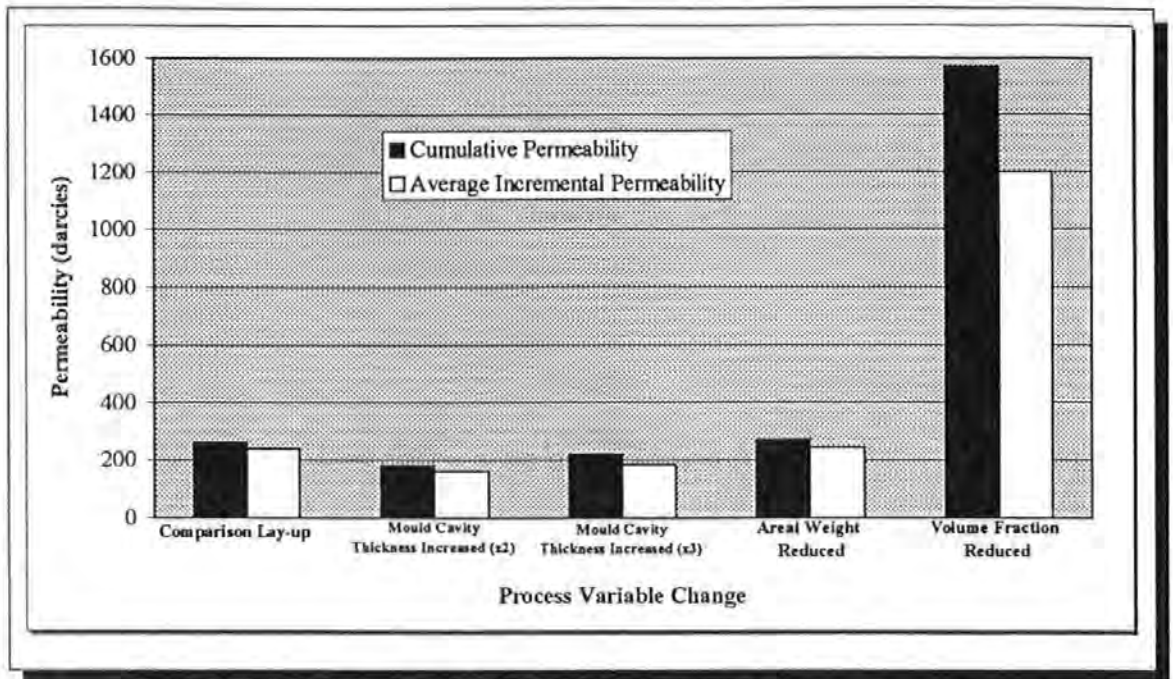
*Figure 4:9 Variation of Cumulative and Average Incremental
Permeabilities for Various Process Variable Changes*

4:3 Second Modification of Test Rig and Procedure

After observing the scatter produced in the results in 4:2, another set of tests

were designed using another mould test rig. This rig and the modified

procedure are described in Section 3:3. The fibre reinforcement used in these

tests was a 2x2 carbon twill with the addition of varying percentages of bound

weft tows as described in Section 3:3:1.

4:3:1 Isotropic Lay-up Tests

Tests in this category used 4 layers oriented at 0-90-90-0 degrees with respect

to the bound tow direction (weft). The seven flow enhancing fabrics together

with a base twill of similar areal weight were tested with a range of fluids and

resins. The plots of the flow progressions will be found in Appendix 1:3. This

was to observe if a change of fluid affected the permeability values. Tables

4:7a - 4:7d show the results of the tests and as before an error range and

Fabric Designation	Ratio of Bound :Conventional WarpTows	Test Number	Injection Fluid	Cumulative Permeability (darcies)	Average Incremental Permeability (darcies)
DWO 38166	Conventional Twill Weave	Base Twill - 1	Boots Glycerol	20	27
		Base Twill - 2	Boots Glycerol	16	22
		Base Twill - 3	Boots Glycerol	25	28
		Average Permeability (darcies)		20	26
		Error Range		+ 23% -21%	+9% -14%
		Standard Deviation		3.7	2.6
DWO 126	1:1	DWO126 -1	Scott Bader 2-414(Resin 'E')	1467	1713
		DWO126 -2	Scott Bader 2-414(Resin 'E')	888	1010
		DWO126 -3	Scott Bader 2-414(Resin 'E')	1030	1143
		DWO126 -5	Boots Glycerol	212	189
		DWO126 -7	BDH Glycerol	75	82
		DWO126 -8	Boots Glycerol	130	127
		DWO126 -9	Boots Glycerol	153	156
		Average Permeability for Resin E (darcies)		1128	1289
		Error Range		+30% -21%	+33% -22%
		Standard Deviation		246.4	304.9
		Average Permeability for Boots Glycerol (darcies)		165	157
		Error Range		+28% -21%	+20% -19%
		Standard Deviation		34.4	25.1

Table 4:7a Isotropic Permeabilities for Twill and Flow Enhancing Fabric DWO 126

Fabric Designation	Ratio of Bound :Conventional WarpTows	Test Number	Injection Fluid	Cumulative Permeability (darcies)	Average Incremental Permeability (darcies)
DWO127	1:2	DWO127 -1	BDH Glycerol	385	402
		DWO127 -2	BDH Glycerol	399	425
		Average Permeability (darcies)		392	414
		Error Range		+/- 2%	+/- 3%
		Standard Deviation		7	11.5
DWO148	1:3	DWO148 -1	Scott Bader 2-414 (Resin 'E')	1819	2036
		DWO148 -3	Scott Bader 2-414 (Resin 'E')	1461	1992
		DWO148 -4	Scott Bader 471 (Resin 'A')	2565	3258
		DWO148 -6	Boots Glycerol	191	174
		DWO148 -7	Boots Glycerol	212	200
		DWO148 -8	Boots Glycerol	260	247
		Average Permeability for Resin E (darcies)		1640	2014
		Error Range		+/- 11%	+/- 1%
		Standard Deviation		179	22
		Average Permeability for Boots Glycerol (darcies)		221	207
		Error Range		+18% -14%	+19% -16%
		Standard Deviation		28.9	30.2

Table 4:7b Isotropic Permeabilities for Flow Enhancing Fabrics DWO 127 and DWO 148

Fabric Designation	Ratio of Bound :Conventional WarpTows	Test Number	Injection Fluid	Cumulative Permeability (darcies)	Average Incremental Permeability (darcies)
DWO149	1:4	DWO149 -1	Boots Glycerol	184	186
		DWO149- 2	Boots Glycerol	192	209
		DWO149- 3	Boots Glycerol	206	201
		Average Permeability (darcies)		194	199
		Error Range		+6% -5%	+5% -6%
		Standard Deviation		9.1	9.5
DWO150	1:5	DWO150- 1	Boots Glycerol	158	172
		DWO150- 2	Boots Glycerol	164	169
		DWO150- 3	Boots Glycerol	202	199
		Average Permeability (darcies)		175	180
		Error Range		+16% -10%	+11% -6%
		Standard Deviation		19.5	13.5

Table 4:7c . Isotropic Permeabilities for Flow Enhancing Fabrics DWO 149 and DWO 150

Fabric Designation	Ratio of Bound :Conventional WarpTows	Test Number	Injection Fluid	Cumulative Permeability (darcies)	Average Incremental Permeability (darcies)
DWO151	1:6	DWO151- 1	Boots Glycerol	150	162
		DWO151- 2	Boots Glycerol	158	162
		DWO151- 3	Boots Glycerol	201	181
		Average Permeability (darcies)		170	168
		Error Range		+18% -12%	+7% -3%
		Standard Deviation		22.4	8.9
DWO156	1:7	DWO 156- 1	Boots Glycerol	156	161
		DWO156- 2	Boots Glycerol	125	125
		DWO156- 3	Boots Glycerol	160	164
		Average Permeability (darcies)		147	150
		Error Range		+9% -15%	+9% -17%
		Standard Deviation		15.6	17.7

Table 4:7d. Isotropic Permeabilities for Flow Enhancing Fabrics DWO 151 and DWO 156
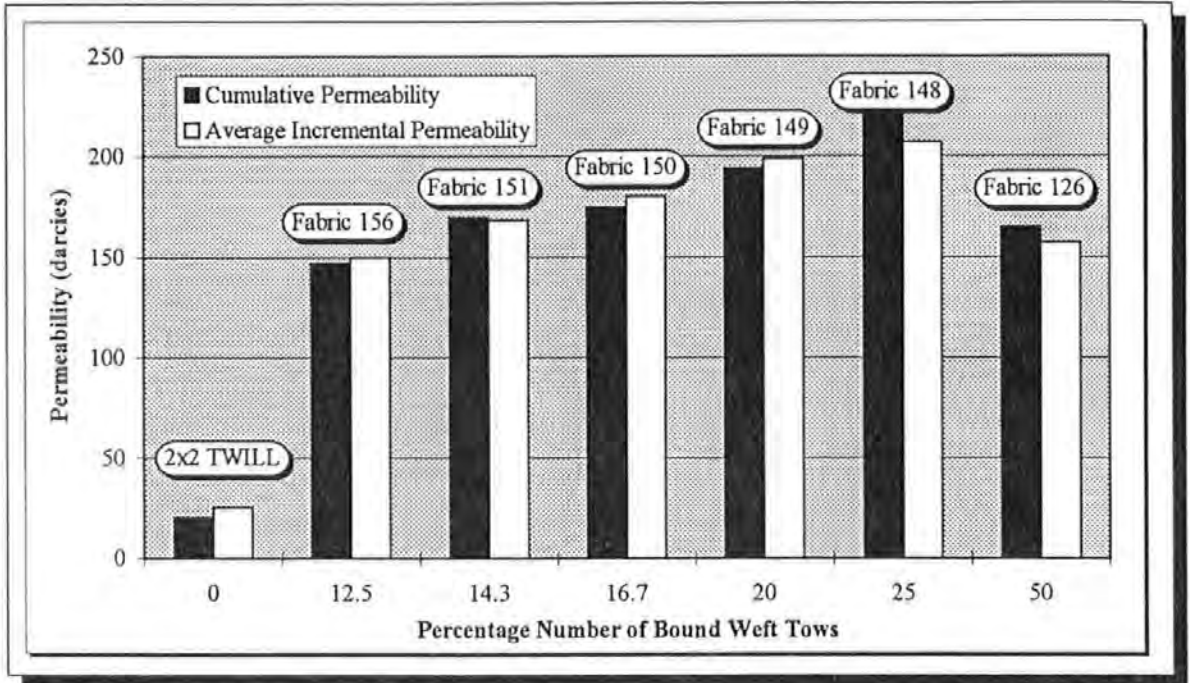
Figure 4:10 Cumulative and Average Incremental Permeabilities Associated with the Flow Enhancing Fabrics
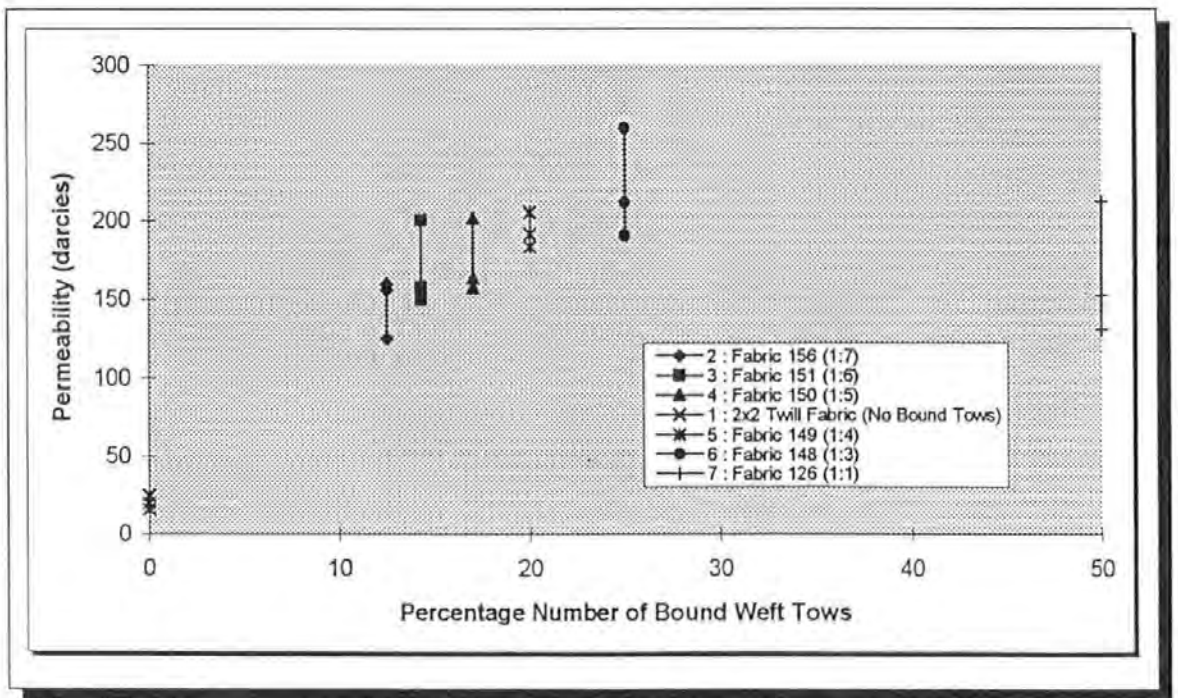
Figure 4:11 Scatter of Permeability Values Associated with the Flow Enhancing Fabrics

standard deviation of values is shown. Figure 4:10 shows the comparison of the average incremental permeabilities calculated for each of the fabrics using Boots Glycerol as the injection fluid, while Figure 4:11 shows the scatter encountered. A plot of the permeability with respect to the injection fluid is shown in Figure 4:12.
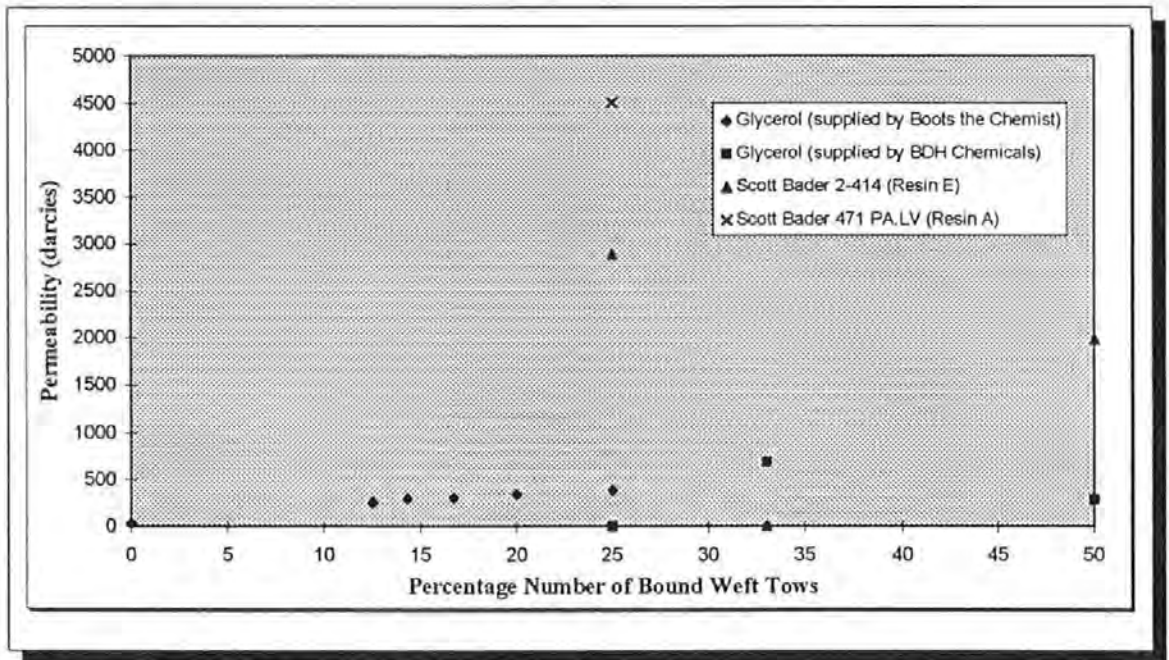
Figure 4:12 Variation in Average Permeability caused by the use of Different Fluids and Resins

4:3:2 Anisotropic Tests

In this test, the bound tows were all oriented in the same direction so that the flow enhancement was in one direction only and produced an anisotropic (elliptical) flow. Four different polyester resins were used to mould plates for use in the image analysis investigation described in Chapters 5 and 6. The major and minor permeabilities (equations 2:42, 2:43) were determined for each case together with the anisotropy index, the ratio of the major and minor permeabilities. Table 4:8 shows results of the tests conducted on this lay-up.

Fabric Designation	Ratio of Bound: Conventional Warp Tows	Areal Weight (g/m²)	Test Number	Injection Fluid	Cumulative Permeability (darcies)		Anisotropy Index γ (A/B)	Average Incremental Permeability (darcies)		Anisotropy Index γ (C/D)
					Major Axis(A)	Minor Axis(B)		Major Axis(C)	Minor Axis(D)	
DWO126	1:1	381	DWO126- 4	Jotun Norpol 42-10 Polyester +MEKP	5948	852	7.0	6118	904	6.8
			DWO126- 6	Boots Glycerol	341	140	2.4	345	131	2.6
DWO148	1:3	384	DWO148- 2	Scott Bader 2-414 PA LV(Resin 'E') +MEKP	4265	1385	3.1	5023	1718	2.9
			DWO148- 5	Scott Bader 471 (Resin 'A') +MEKP	14041	1403	8.2	13032	1403	9.3
DWO149	1:4	385	DWO149- 4	Jotun Norpol 42-10 Polyester +AAP	2155	165	13.1	3202	209	15.3
DWO150	1:5	380	DWO150- 4	Jotun Norpol 42-10 Polyester +MEKP	13697	1424	9.6	12056	1388	8.7
DWO151	1:6	381	DWO151- 4	Jotun Norpol 42-10 Polyester +AAP	5361	461	11.6	6078	584	10.4
DWO156	1:7	380	DWO156- 4	Jotun Norpol 42-10 Polyester +AAP	2155	186	11.6	2268	175	13

Table 4:8 Anisotropic Permeabilities of Flow Enhancing Fabrics

4:4 Brite Euram Flow Rig Tests

The final permeability measurement was a series of tests to verify the work in

4:3. This time it was conducted on a mould constructed for the Brite-Euram

BE5477 RTM Research Program. This mould and modified data collection

procedure are described in Chapter 3:4.

The tests were all carried out on the isotropic (balanced) lay-up with the same

resin (Jotun Norpol 42-10) to verify the tests conducted with glycerol. Table

4:9 shows the permeability values and Figure 4:13 shows a plot of the

incremental permeabilities at specific isochrones. The problem of mould

deflection caused by the increasing number of bound tows is shown in Figure

4:14 where the permeability and average volume fractions are compared for the

injections.

Fabric	Nominal Volume Fraction (%)	Actual Average Volume Fraction (%)	Average Incremental Permeability (darcies)
Twill	53	51	154
DWO 156	53	49	1423
DWO 150	53	48	2204
DWO 148	53	46	2513
DWO 126	53	46	3968

Table 4:9 Permeability Verification Test Results

4:4:1 Comparison of the Permeability Values using Glycerol and Resin

As will be observed, the permeability values using the two fluids show an

increase with the introduction of the bound tows. The values using the two

fluids are however widely different which confirms the results shown in Figure

4:12.
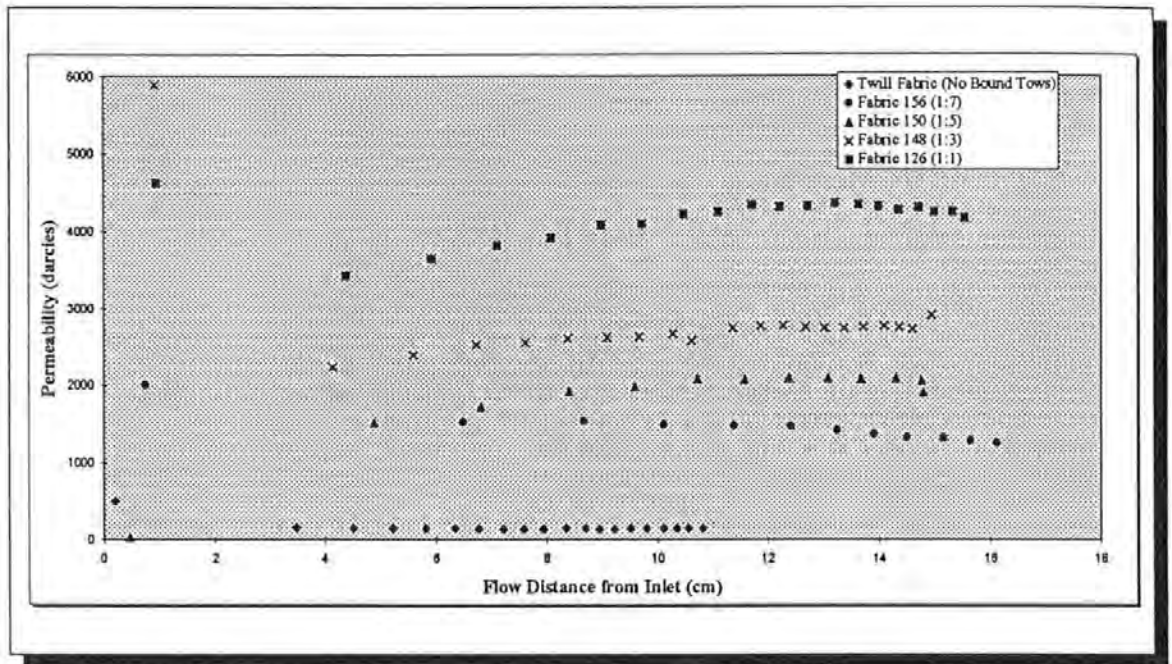
Figure 4:13 Incremental Permeability Variation with respect to the Inlet Port
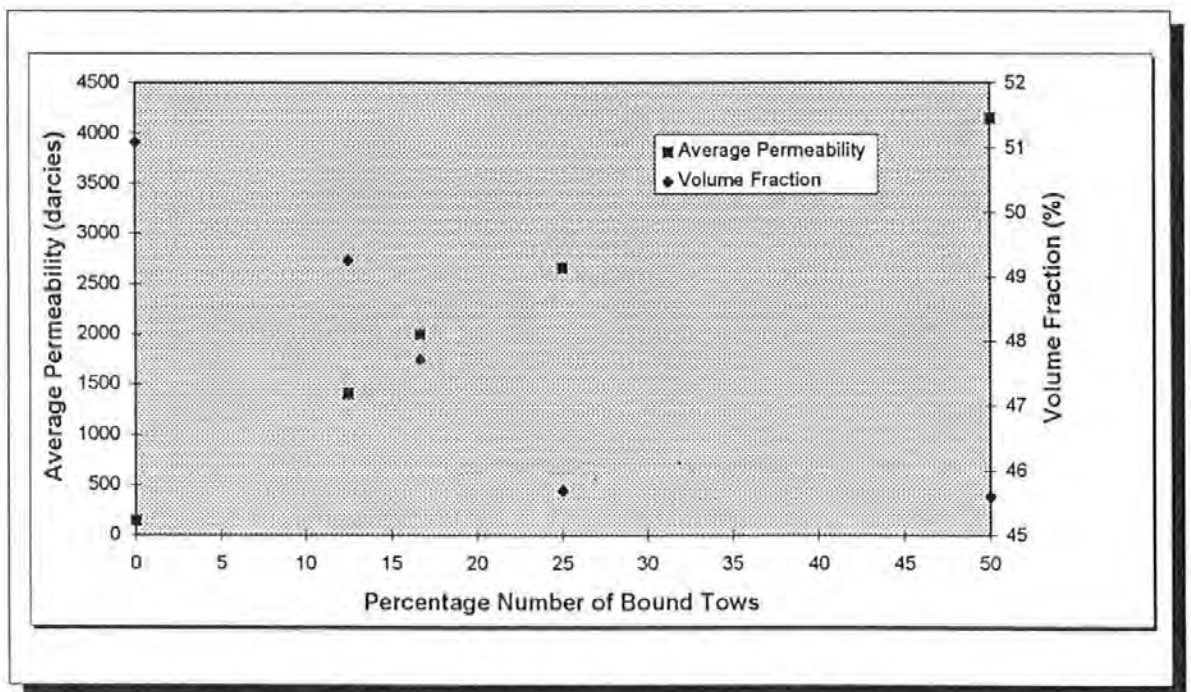
Figure 4:14 Permeability and Actual Volume FractionVariation with Respect to the number of Twisted Tows

These results show how important the fluid is when undertaking permeability tests. The simulations available rely on consistent viscosity and permeability figures for their accuracy. This would suggest that experiments undertaken to determine permeability values should use the actual resin for which the simulation is being designed rather than model resins such as oils and glycerol. The model resins may be used as a comparison of the flow properties of fabrics rather than to determine permeabilities.

4:5 Precision of the Measured and Calculated Values

This section deals with how precisely each of the variables used in the determination of the lay-up permeability were measured and hence estimates the accuracy of the permeability values obtained.

4:5:1 Flow Distance (in-situ recording of the flow front on an acetate)

The problem with this method was that while the position of the flow front was being recorded, the front was in motion and hence at the end of each 'isochrone' the front was in a different position than at the commencement of recording. The flow in the initial part of the injection is faster and therefore a larger error will be observed.

4:5:2 Flow Radius (reproduction from video)

This method solved the above problem because it was possible to freeze-frame the video recording at fixed time intervals and record the front position. The interpretation of the frontal position was open to error and so two separate recordings were made of the same test and the areas compared in Table 4:10.

Time Increment (s)	Measured Area (Recording 1) (mm²)	Measured Area (Recording 2) (mm²)	Difference (%)
30	38.8	34.7	10.6
60	72.3	67.9	6.1
90	100.2	98.9	1.3
120	126.8	123.6	2.5
150	154.6	154	0
180	178.3	181.5	-1.8
210	203.5	203.5	0
240	227	227.5	0.2
270	252.5	249	1.4

Table 4:10 Variation of Measured Area from Video Reproduction

The average measurement difference was 2.7 % which after neglecting the two large differences reduced to 1 %. This was repeated on a separate test and the average difference was found to be 2.9 % which reduced to 1.7 % after neglecting the initial large differences.

4:5:3 Measuring using the Planimeter

This instrument was calibrated using a piece of graph paper over an area of 100cm². The area was measured 7 times and the accuracy calculated, the results of which are shown in Table 4:11.

Measurement Number	1	2	3	4	5	6	7
Area Measured (cm²)	102.3	104	.104.2	102	103.3	102	102.3
Average Area Measured = 102.97 cm²							

Table 4:11 Precision Measurements of the Planimeter

It can therefore be seen that the planimeter measures with an accuracy of around +3% which varies between 2% and 4% .

4:5:4 Setting the Injection Pressure

The injection pressure was supplied by a main which was susceptible to pressure fluctuations when other machinery was engaged. Therefore it was important to know the variation of the set pressure on the regulator. The pressure transducer situated on a T-junction just prior to the inlet position was monitored for a set pressure of 0.8 bar for 11 tests and the average pressure over the injections is shown in Table 4:12. Fluctuations in pressure may have been caused by the uncontrollable constriction of flow by the stacking or nesting of the fibre pack

Test Number	Average Pressure (bar)	Difference from set value (0.8 bar)(%)
1	0.8	1.8
2	0.8	-4.5
3	0.8	1.8
4	0.7	-5.7
5	0.7	-8.8
6	0.7	-9.9
7	0.8	-0.8
8	0.7	-5.6
9	0.7	-7
10	0.8	-4.5
11	0.8	-3.6

Table 4:12 Variation of Set Injection Pressure during Permeability Tests

The average difference was found to be 5.9 % which reduced to 4.7 % when the larger differences were neglected.

4:5:5 Resin Viscosity

The viscosity figures used in the calculation of the fabric permeability were all obtained by interpolating between temperatures from a family of viscosity - time curves. It was required to know how consistent these figures were.

156

Therefore a set of consistency tests were undertaken by reproducing a viscosity test for different samples in the same time period and with the same mixing procedure.

The tests were undertaken on the MY 750 / HY917 / DY 070 resin system and involved three different samples being mixed and prepared in approximately 5 minutes and a 30 minute test being undertaken at 20°C. The resin is cross-linking and increasing in viscosity and Table 4:13 shows the values obtained at the start and finish of the tests and percentage differences between them

Test Number	Start Viscosity (Pa.s)	End Viscosity (Pa.s)	Percentage Difference
1	1.6	2.1	29.7
2	1.5	1.9	24.4
3	1.5	1.8	20.1
Average	1.6	1.9	24.9
Range	+4.2% - 2.24%	+8.27% - 6.01%	

Table 4:13 Viscosity Consistency of 3 Samples of Similar Resin

4:6 Conclusions regarding Permeability Measurement

After conducting the error analysis it was important to determine the overall accuracy of the permeability values. This was obtained from the cumulative experimental error from all the variables measured from equation 2:34. Listed below are the relevant variables with their respective errors:

Resin Viscosity : 8%
Injection Pressure : 6%
Flow Radius : 2.6%
Flow Time : 1%

The flow radius error varied at different times in the injection and therefore this produced a variation in the overall permeability error as shown in Table 4:14.

157

R (cm)	$\left[\left(\frac{r_o^2}{4}\right) + \frac{R^2}{4}\left(2\ln\frac{R}{r_o} - 1\right)\right]$	ΔR %	$\Delta\left[\left(\frac{r_o^2}{4}\right) + \frac{R^2}{4}\left(2\ln\frac{R}{r_o} - 1\right)\right]$	Error %
2	1.22	3	1.35	9
4	10.07	2	10.63	5.3
6	29.79	1	30.57	2.55
8	62.08	0.5	62.86	2.38
10	107.96	0.2	108.62	0.06
12	168.72	0.2	169.54	0.05

Table 4:14 Actual Error in the Flow Radius Term

Therefore accumulating the errors into equation 2:34, the error in the

permeability is seen in Table 4:15.

$\mu.\epsilon/P_o.t$ (%)	ΔR (%)	ΔK (%)
15	9	24
15	5.3	20.3
15	2.55	17.55
15	2.38	17.38
15	0.06	15.06
15	0.05	15.05

Table 4:15 Cumulative Permeability Error during an Injection

The permeability values are seen to vary from between 15% and 24%. The

larger errors are apparent during the initial transient part of the injection when

the flow rates are faster. It can be seen that the major contributors to the errors

are from the viscosity and pressure measurements. Therefore in future

permeability testing it is important that the measurement of these parameters is

carefully monitored . Mould bow will also affect these figures as the porosity

will vary from the centre towards the edge of the mould cavity. Therefore the

visualisation moulds used for permeability testing need redesigning with

stiffening grids over the glass to prevent bow.

CHAPTER 5

MICROSTRUCTURAL EXAMINATION
&
IMAGE ANALYSIS

5:1 Introduction and Objectives

Chapter 5 describes the development of the technique by which the

flow-enhancing reinforcements, described in Chapter 3:3, may be categorised

according to their flow channel geometries, particularly their respective flow

channel areas and perimeters. A series of specimens was prepared from the

moulded plates produced from the permeability tests described in Chapters 3:3

and 3:4. A detailed investigation into the flow channels produced in the

reinforcements by the spiral bound tows was carried out to determine the effect

on the permeability and the flow channel geometries. This investigation was

accomplished using the Q570 Image Analyser at the University of Plymouth.

5:2 Preparation of Microstructural Samples

The anisotropic plates (described in Chapter 3:3) were marked out

perpendicular to the flow enhancing tow and cut using a diamond circular saw

at 20, 40 & 60 mm intervals from the inlet centre position. These samples were

labelled before being cut according to the diagrams in Appendix 4:1, an

example of which is shown in Figure 5:1. It was decided that the samples

should be no less than 25mm wide in order to provide enough specimen to

include a unit cell for each of the laminates. The unit cell was based upon the

distance between repeat unit bound tows in an arbitrary layer as shown in

Figure 5:2.
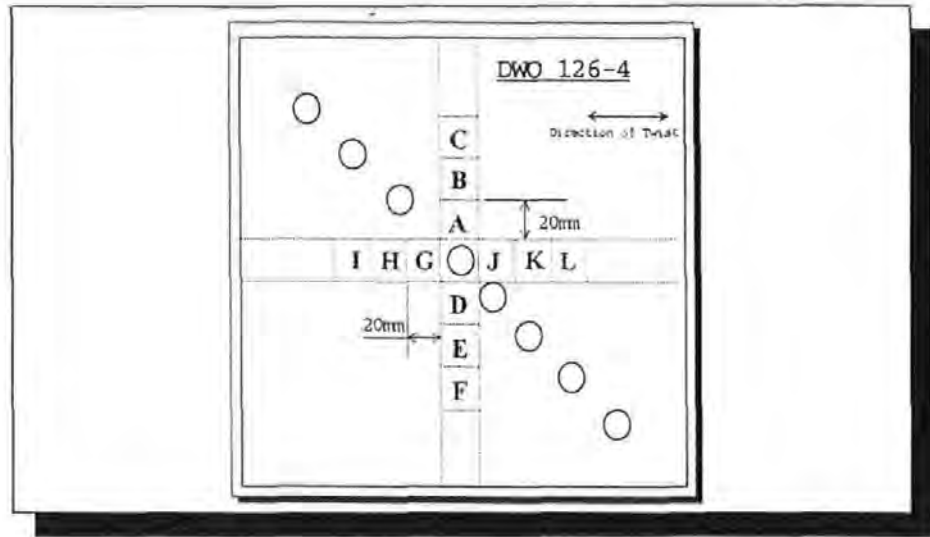
Figure 5:1 Specimen Locations from Permeability Test DWO126-4
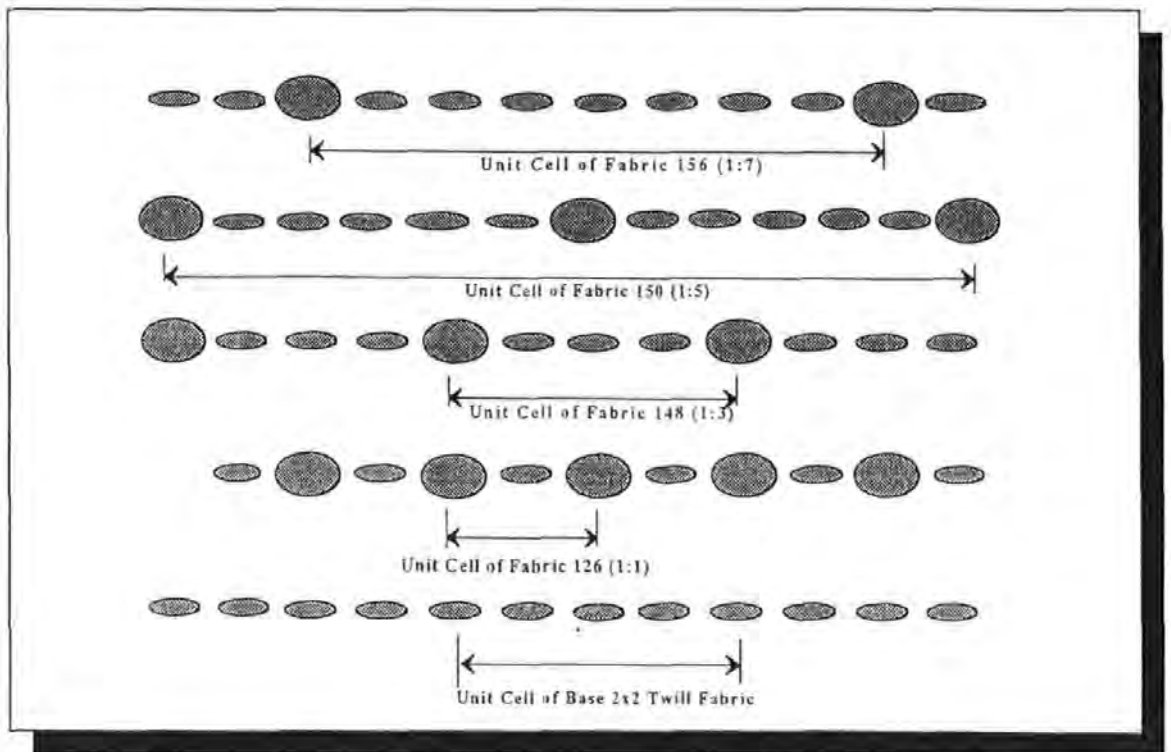
Figure 5:2 Unit Cells of the Flow Enhancing Fabrics

The sections were then placed in a specimen mould and mounted using a

polyester casting resin. After curing the samples were demoulded and prepared

for microstructural examination. The relevant face was ground flat using the

following grades of wet and dry grinding paper ; 320, 400, 800 & 1200. Special care was taken to cleanse the specimen face in a vibrating water bath between grades to rid the face of larger particles which may have caused scratches. When the face appeared flat, it was polished using an automatic polishing machine with descending grades of diamond paste. Starting with 14 micron paste, the face was then polished with 6 micron, 1 micron and finally with 0.25 micron paste until scratches were not detectable on an optical microscope. All the samples were prepared in the same way and were then ready for image analysis.

5:3 Image Analysis - Introduction

Before describing the application of image analysis to this work, the general principles of the technique are described

5:3:1 Stages of Image Analysis

The principal stages of image analysis may be considered as

i) Image Capture

ii) Image Enhancement (Segmentation)

iii) Object Detection

iv) Measurement

v) Analysis

These stages form the backbone of the flow diagram shown in Figure 5:3 and are now discussed in greater detail.

Figure 5:3 Flow Diagram of an Image Analysis Operation [95]

5:3:1:1 Image Capture

This involves the conversion of the image into an electronic signal suitable for

digital processing and storage. The image is a 2-dimensional distribution of

visible electromagnetic radiation (light). Images may be typically captured by

video-cameras but several other methods are available for capture. In general

terms it is the task of the image capturing process to quantify the image in both

space and tone. Spatially, the image is usually divided into a square or

rectangular grid of picture elements known as pixels. Tonally, the image is detected between 0 and 256 (2^8) intensity levels, known as 'grey levels'.

5:3:1:2 Image Enhancement

This involves several processes designed to improve the quality of the captured image and distinguish regions of interest. For example, an image of fibre ends in a laminate may include the following

- small areas (holes) in the region of interest due to fibre breakage during polishing which do not reflect light

- regions in which two separate areas merge and produce erroneous measurements.

- regions which may be out of focus

- regions of interest which cannot to be measured due to them extending beyond the bounds of the image frame.

Some of the above will be demonstrated later in the chapter.

A possible solution to these problems is now discussed. Segmentation describes the act of separating regions of interest from the background. It may be necessary to consider the regions of interest individually.

There are three main methods of segmentation:

i) Thresholding

ii) Edge Finding

iii) Region Growing

Thresholding involves altering the grey level to an appropriate value to cover the region of interest. The threshold level may vary from sample to sample due

to the varying strength of artificial light. Edge finding techniques pick out regions with a high rate of change of grey level on the grounds that they are likely to indicate edges of objects or at least regions of interest. 'Region Growing' makes use of information regarding neighbouring pixels to group them together if they are similar or establish a boundary if they are sufficiently dissimilar.

The result of the enhancement will be a binary image in which each pixel may have one of two states, classified as either 'regions of interest' or 'background'.

5:1:1:3 Object Detection, Measurement and Analysis

This is where the regions of interest are detected. It is a data reduction step which produces a compact list of co-ordinates for each pixel within a region of interest. Features regarding the regions of interest which require measurement are inserted into a QBasic program which controls the image analysis sequence. These measurements are then printed and saved to disc for further analysis.

5:4 The Q570 Image Analyser

There are several companies which manufacture image processing and analysis equipment but the largest is Leica-Cambridge of Cambridge, UK.

At present there are four systems available, all offering different facilities.

The system based in the Department of Biological Sciences at the University of Plymouth is the Quantimet Q570. This system sees extensive work in a number of areas of research, some of which are now described. Flook et al.[96] used

image analysis to determine the spatial distribution of several hundred fragments and lethality due to penetration in a series of thin witness plates due to a mock attack. The plates (of which a typical one is shown in Figure 5:4), were photographed and the negatives analysed with the result that the holes of specific size were measured to a fixed accuracy according to their areas and position with respect to a datum .
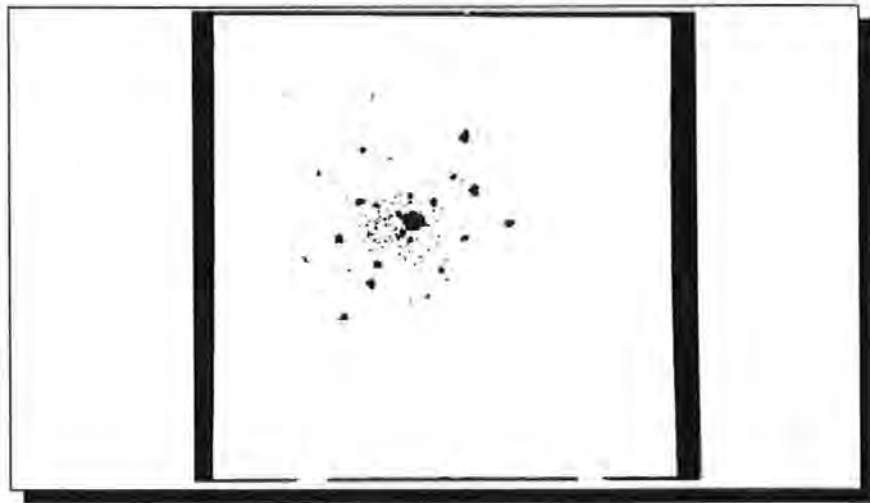
Figure 5:4 A Typical Witness Plate showing Fragment Size and Distribution

Wright et al. [97] at the University of Plymouth have used the Q570 system to detect damage to fish livers from pollution, notably cadmium. This involved the analysis of the livers of the dab fish which when exposed to cadmium, changed colour (grey level) due the increased density of liver cell cytoplasm corresponding to the liver cell number increasing and the cell size decreasing as shown in Figure 5:5. By measuring the cell size and the grey level, the presence of pollutants were confirmed.
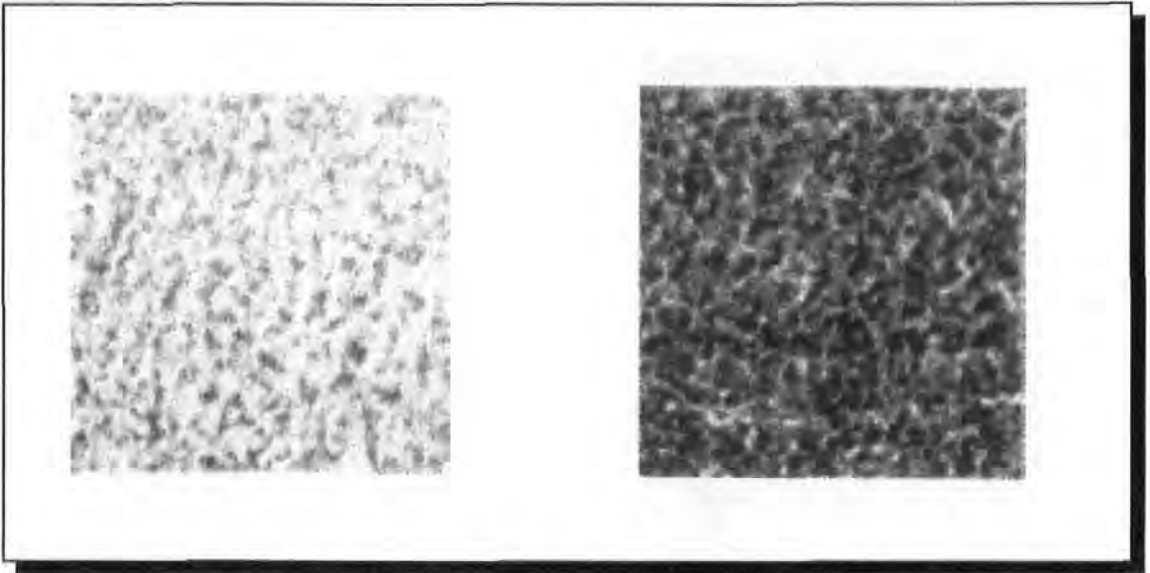
Figure 5:5 Two Sections of Dab Fish Liver showing (left) unpolluted and (right) polluted livers

A topic closer to this research was conducted by Russell et al. [98] and involved the measurement of pores in sandstone, a particulate porous medium with pores of irregular size. Images of the sandstone structure were imported from an SEM into the image analyser, and by superimposing a binary mask or transparent grid over the images, the area fraction of the pores was determined. Shadowing was a problem and this was addressed by taking three images with the different orientations of the electron beam and superimposing the three images on top of one another.

These examples illustrate only a very small percentage of the capabilities of image analysis but involve facilities which are used in the analysis of flow channels.

Plate 5:1 Micrograph of 2x2 Base Twill Laminate (4 layers)
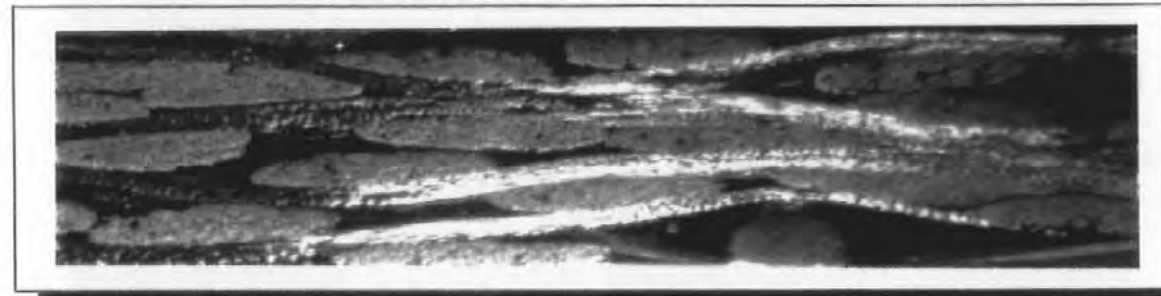
Plate 5:2 Micrograph of Fabric 156 Twill Laminate (1:7 ratio of bound to conventional tows)
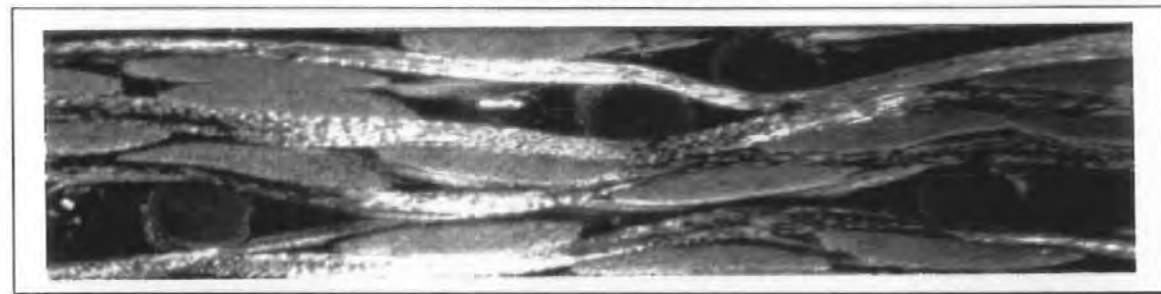
Plate 5:3 Micrograph of Fabric 150 Laminate (1:5 ratio of bound to conventional tows)
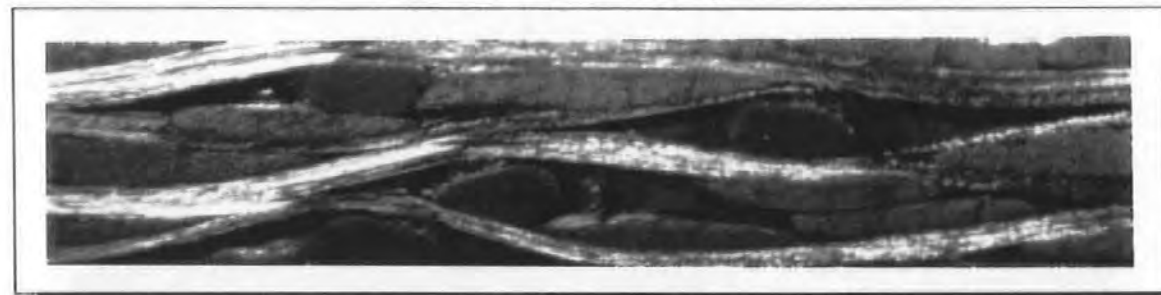
Plate 5:4 Micrograph of Fabric 148 Laminate (1:3 ratio of bound to conventional tows)
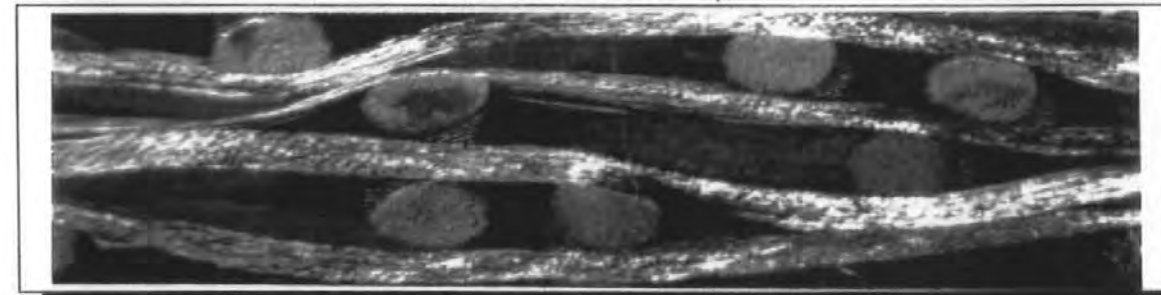
Plate 5:5 Micrograph of Fabric 126 Laminate (1:1 ratio of bound to conventional tows)

5:5 Application of Image Analysis to the Measurement of Flow Channels

This section describes the method by which data regarding the size, shape and

perimeter were obtained from the Q570 Image Analysis System. Figure 5:6

shows a schematic diagram of the arrangement of the image analysis system.
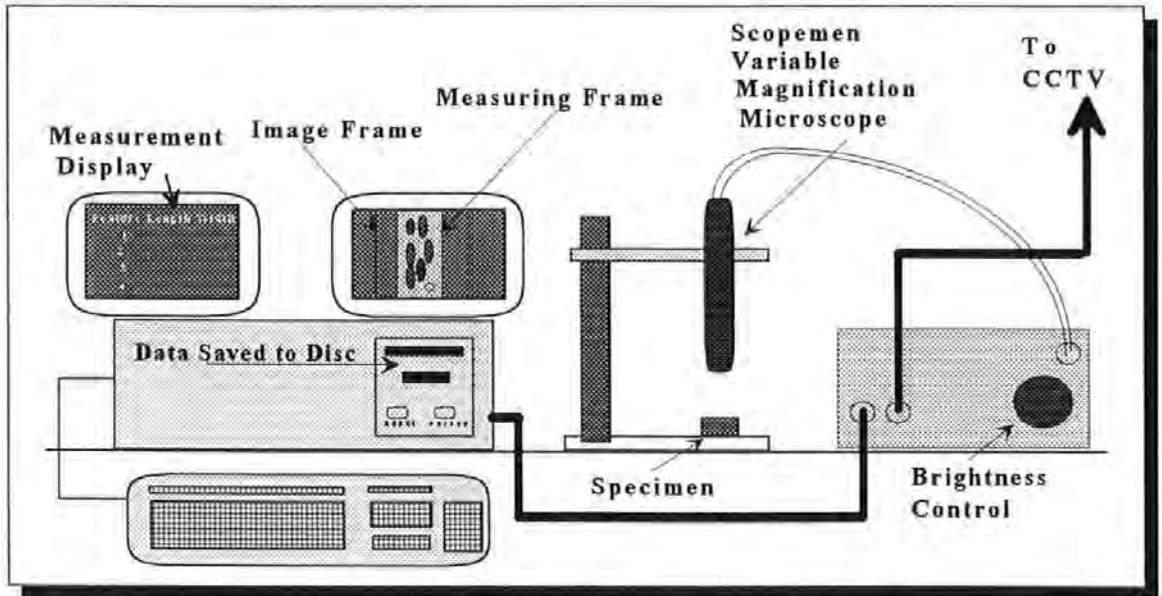
Figure 5:6 Schematic Diagram of the Image Analysis Arrangement

The following microscopes were used for the analysis

i) Microvision MV2100 Scopeman Single Lens Variable Low Magnification

ii) Carl Zeiss Optical Fixed High Magnification

The former was used to investigate the flow channel sizes and tow

arrangements within the laminate, while the latter was used to investigate the

volume fraction within the tows as well as the fibre packing arrangement. Five

separate laminates were used from the permeability tests described in Chapter

3:3. These were all based on the 2 x 2 twill carbon weave, the details of which

are listed in Table 5:1. Examples of laminates for the five reinforcements

investigated are shown in Plates 5:1 to 5:5.

LAMINATE IDENTIFICATION	RATIO OF BOUND TOWS : CONVENTIONAL TOWS	AREAL WEIGHT (g/m^2)
38166	conventional twill (no bound tows)	380
DWO 156	1:7	384
DWO 150	1:5	381
DWO 148	1:3	380
DWO 126	1:1	382

Table 5:1 Image Analysis Sample Specification

5:6 Calibration of the Image Analyser

When using the Carl Zeiss microscope, the fixed values of magnification

provided by the lenses linked in with an automatic calibration procedure

provided by the Quantimet. However, with the Scopeman microscope, owing

to the variable magnification involved, a separate calibration was required for

each magnification. This was achieved by the use of a graduated calibration

slide and the calibration frame on the image analyser which was focused and

set to a specific size on the calibration slide. This was essential to provide

accurate results for each image measured. Whenever the magnification was

altered, recalibration was undertaken.

5:7 Detection and Measurement of Large Flow Areas

The first set of analysis involved the detection and measurement of the flow

channels caused by the spiral bound tows. Typical sections of the five

laminates investigated are shown in Plates 5:1 to 5:5. This was undertaken

using the Scopeman Optical Microscope linked to the image analyser. A

Q-Basic program "Resinlow", shown in Appendix 5:1, was designed and

written to measure the following parameters of the detected flow areas:

i) the 'x' position of the detected area

ii) the 'y' position of the detected area

iii) the area of the detected area

iv) the perimeter of the detected area

v) the centre of gravity of the detected area

The detection of the specimen area was accomplished by running the program 'Resinlow' which initially detected a grey binary image of the laminate, examples of which are shown in Figure 5:7. The image frame measured 512 x 512 pixels and was fixed whereas the measuring frame was a variable rectangle according to the size of the specimen. By distinguishing the different levels of grey obtained on the image by use of the variable contrast control, the matrix areas, which were darker than the fibres, could be separated. The contrast used 256 grey levels, black being at grey level 0 and white at 255. The contrast threshold was altered manually to produce the best reproduction of the flow channels within the laminate. The program then proceeded to analyse the areas of interest for the parameters set in the program. Several problems were encountered during the detection.

Initially, the whole image was measured and it was found that the very small inter-fibre matrix areas within tows as well as variations in light reflection were detected as shown in Figure 5:8. These areas were of a different scale to the areas produced by the spiral bound tows and to make the analysis more efficient were neglected. To solve this problem an image enhancement program was introduced to filter out these very small areas. This was done by
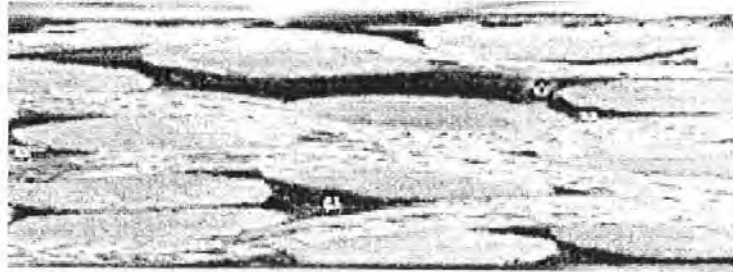
Grey Binary Image of the Twill Laminate
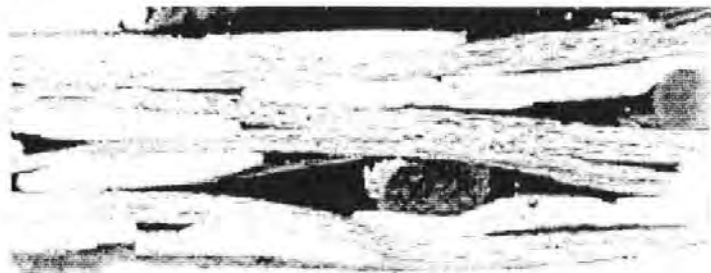
Grey Binary Image of the Fabric 156 Laminate

Grey Binary Image of the Fabric 150 Laminate
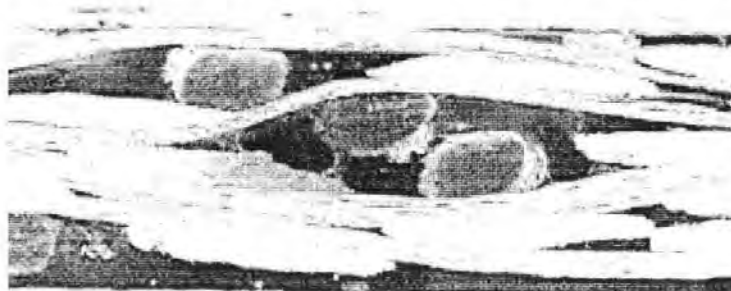
Grey Binary Image of the Fabric 148 Laminate

Grey Binary Image of the Fabric 126 Laminate

Figure 5:7 Typical Grey Binary Images of Five Laminates
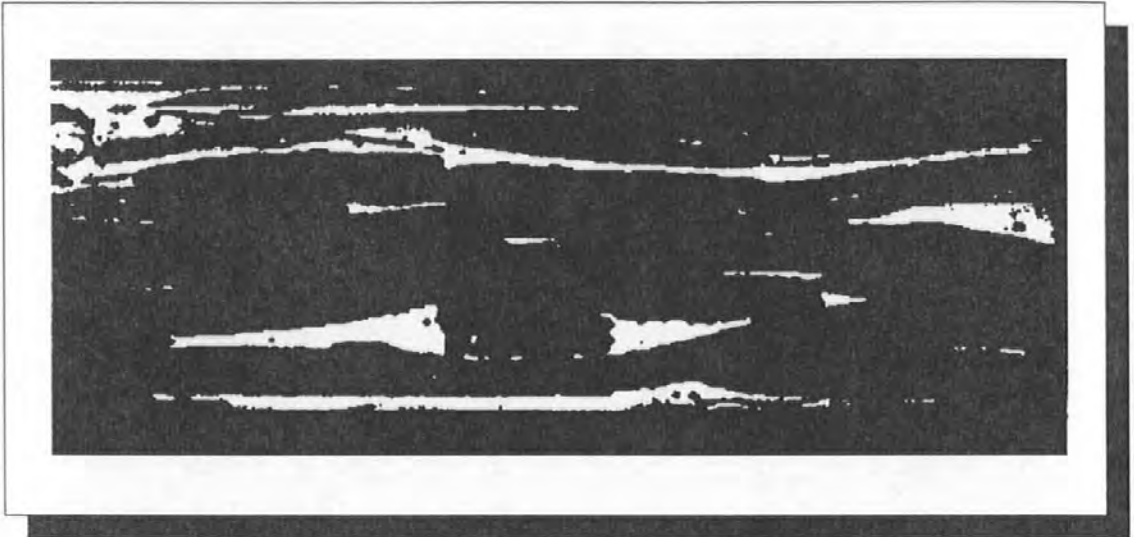
Figure 5:8 Detection of Flow Channels at Fixed Grey Level
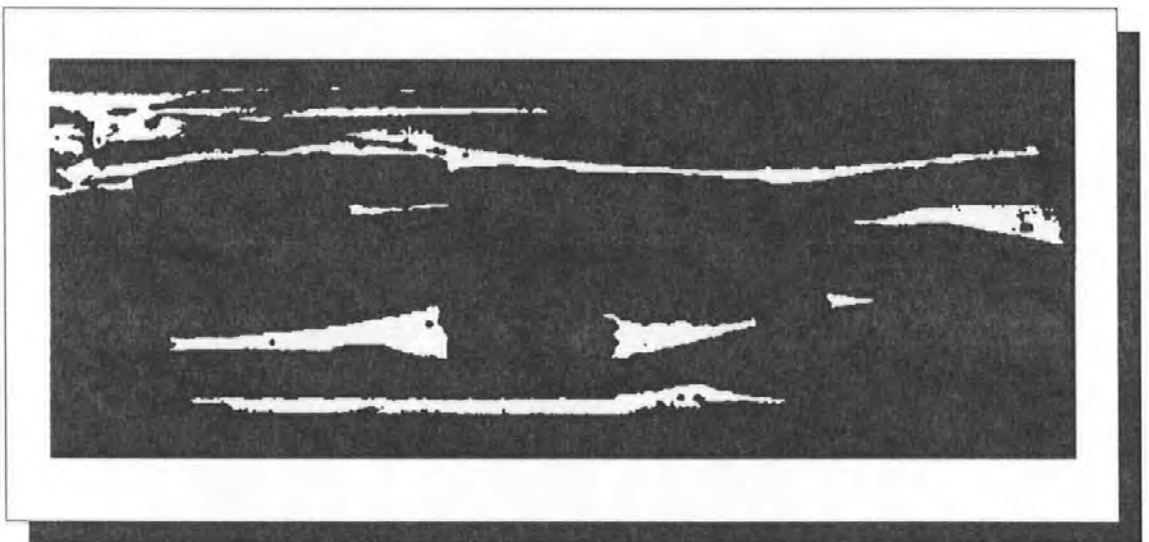
Figure 5:9 Filtering Out the Small Areas
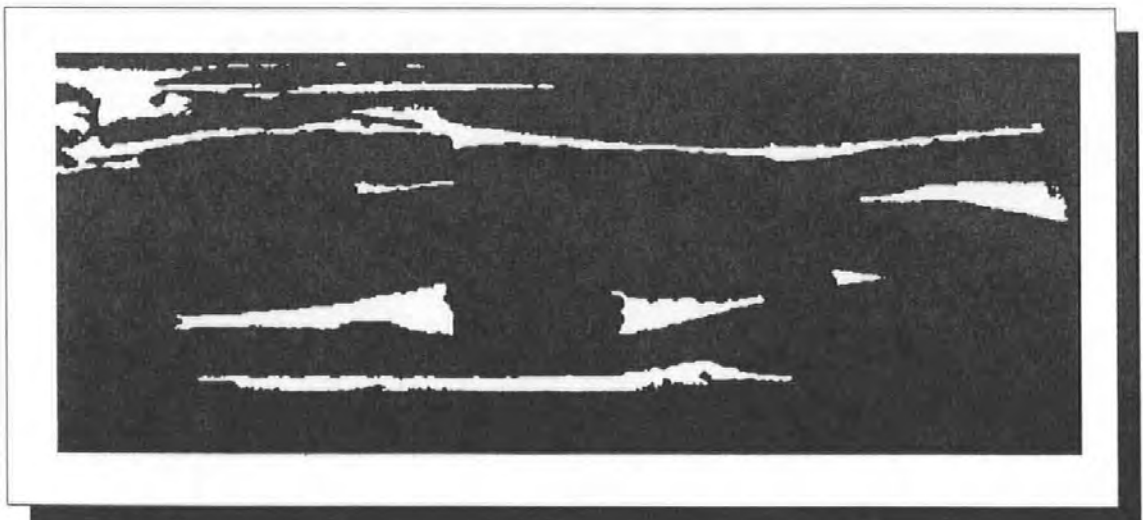
Figure 5:10 Filling in the Holes in the Detection

introducing a size threshold into the program whereby any areas below a specified size were excluded as shown in Figure 5:9. Also, due to imperfections such as a small percentage of voids and inclusions from the polishing process which had a differing grey level in the laminate, holes appeared in some of the detected areas which were filled by means of image enhancement. The results of this enhancement can be seen in Figure 5:10. Several long areas were apparent in a number of the laminates as shown in Figure 5:8 (this section is at 90° to the image on the image analyser monitor) which posed problems for the measurement process. This was due to the point which governed the measurement of the area, known as the XFCP point, being outside the measurement frame. Figure 5:11 shows the result - all areas in contact with the left side of the frame in Figure 5:10 have been excluded. To counter this problem, a segmenting procedure was introduced whereby the long areas were divided into smaller areas at points where the width of the area of interest was below a specified pixel value as shown in Figure 5:12. The result of this image enhancement is seen in Figure 5:13, and as will be appreciated the segmentation produces a more appropriate detection of the flow channels than the unsegmented detection. This turned out to be the standard method for each image measurement, with the contrast threshold level varying for each laminate due to slight matrix colour differences, but the magnification remaining constant. The size of the specimen compared to the measurement frame meant that several images were required to analyse the whole of the
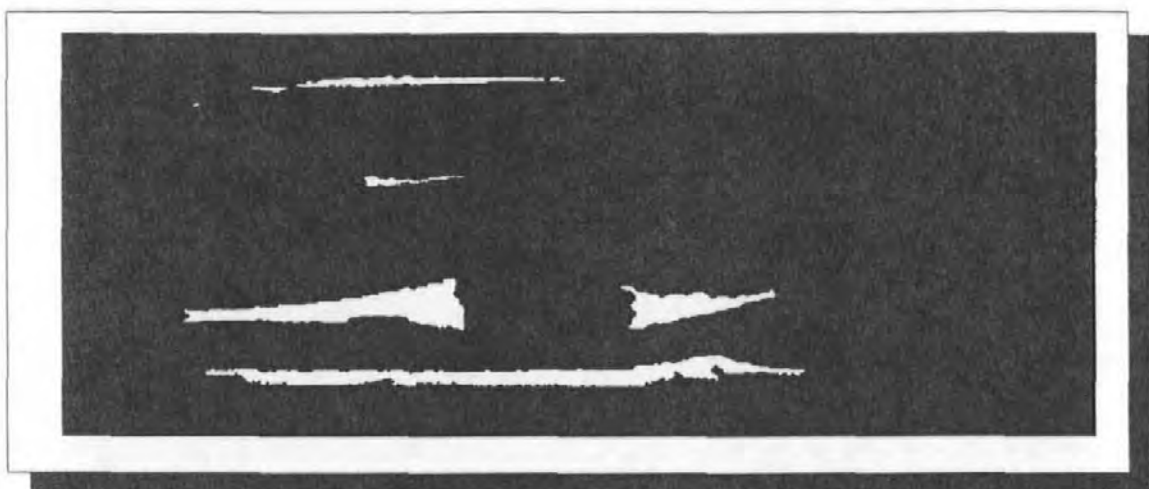
Figure 5:11 Actual Detected Regions Measured before Segmentation
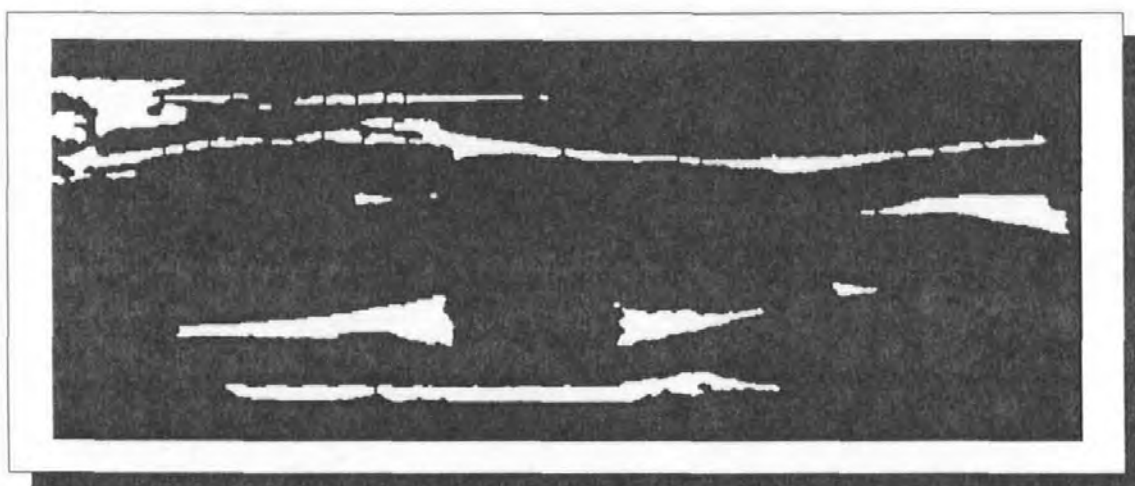
Figure 5:12 Segmenting the Detection
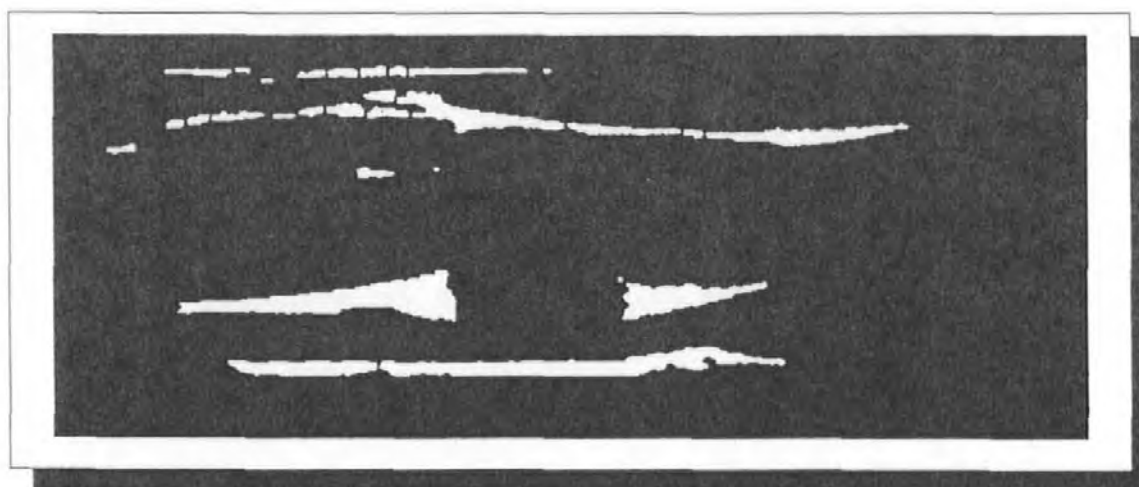
Figure 5:13 Actual Detected Area Measured after Segmentation

specimen. Each of the specimens were analysed individually and the results saved on disc. The flow areas detected along with their respective perimeters were manipulated, totalled and compared on the Microsoft Excel spreadsheet, the results of which are shown in Chapter 6.

5:8 Fixed Specimen Area Image Analysis

The first set of measurements undertaken used a fixed area for investigation. This was to provide an adequate representation of the laminates being investigated. The analysis was accomplished by taking three adjacent images of equal size and area and summing the results. As there was a slight difference in the thickness of each specimen, the measurement frame dimensions were changed accordingly although no change was made to the area. The results of this set of tests is shown in Chapter 6:2.

5:9 Unit Cell Image Analysis

After analysing the data for a fixed area, it was decided that a different approach was required due to results being affected by random groupings of spiral bound tows or conventional tows. This new approach adopted the unit cell technique whereby repeat units of the fabrics (as shown in figure 5:2) were measured. This meant that several frames were required for the large unit cell of Fabric 156 (1:7) and only two for the base twill and Fabric 126 (1:1). The results of the unit cell analysis are shown in Chapter 6:3

5:10 Unit Cell in the Thickness Direction

After considering the results of the unit cell analysis, it was decided to undergo some more testing in order to produce a better representation of the flow areas detected together with their perimeters. This was due to the fact that the transverse tows in the layers were staggered as shown in Figure 5:14 and as a consequence were evident to varying degrees in the cross section. It was therefore decided to investigate the unit cell in the thickness direction through the width of a fibre tow.
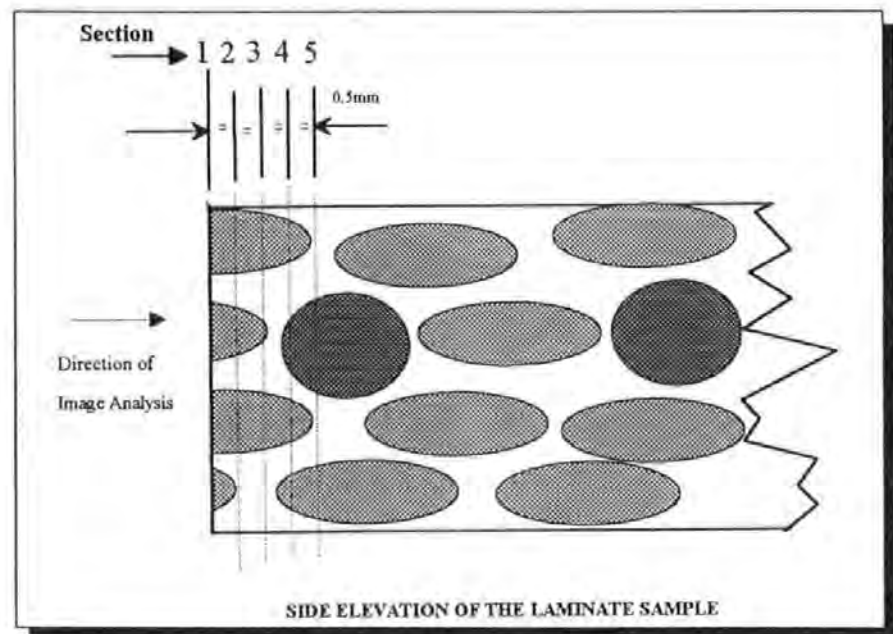
Figure 5:14 Staggering Effect of the Transverse Tows in the Laminates

The samples were carefully ground on a polishing table using 1200 grade 'wet and dry' grinding paper and polished in four 0.5mm increments into the thickness controlled by a micrometer. There then followed a similar image analysis sequence for each section. This provided data to compare flow channel areas and perimeters for each fabric, taking into account the

staggering of the tows in the thickness direction. These analyses are presented in Chapter 6:4.

5:11 Unit Cell Image Analysis of Balanced Isotropic Plates

The permeability tests undertaken on the Brite-Euram apparatus (figure 3:15) used quasi-isotropic lay-ups. This section is designed to investigate the detected areas of these isotropic plates where there are only half the twisted tows in any one direction compared to the anisotropic plates. The plates were all manufactured with the same resin (Jotun-Norpol Polyester 42-10). The plates were marked and cut to produce sections at 40mm from the inlet centre in both the 0° and 90° directions. The location of the specimens in the plates will be found in Appendix 4:2, one of which is shown in Figure 5:15.
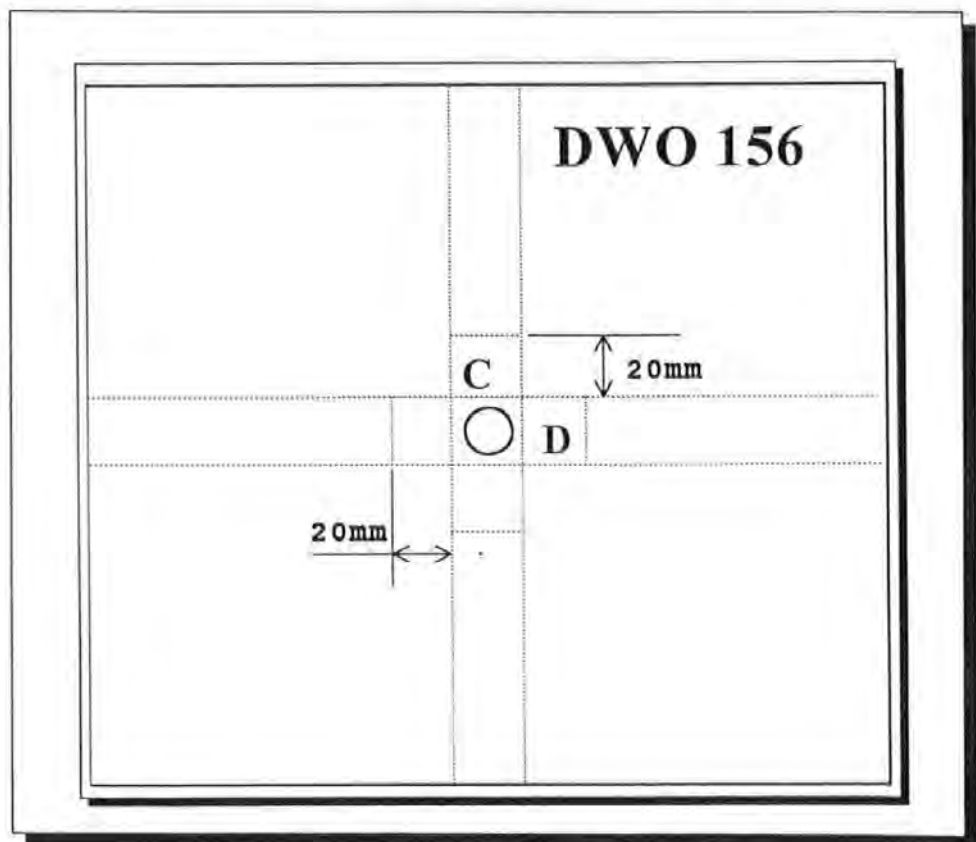
Figure 5:15 Specimen Location from Isotropic Plate DWO 156

The '0' direction was defined as the direction of the spiral bound tow on the outer layer of the plate and is also referred to as the weft direction. The '90' direction is defined as the direction of the conventional tows and is also termed the warp direction. These two directions were measured and compared for each laminate by the unit cell method to determine if the flow channel areas were evident in similar proportions. The results of the area and perimeter comparisons are shown in Chapter 6:5.

5:12 Measurement of Tow Volume Fractions

The second set of measurements required was that of the volume fraction of fibres within the two distinctive types of tows. This was performed using the Carl Zeiss microscope with fixed magnifications. This method has been used previously by Guild et al. [99] to measure conventional tow volume fractions and fibre distribution. The calibration procedure was completed automatically with the respect to the magnification being used. The fibre distribution analysis was undertaken using the Voronoi Cell method as reported by

Vrettos et al. [100 & 101] whereby the neighbouring fibre centres were joined together and the perpendicular bisectors were drawn to produce cells around the fibres. This method is shown sequencially in Figure 5:16 .

Program "Zone1" in Appendix 5 shows the QBasic procedure for detecting the Voronoi cells. Figure 5:17 shows a binary image of a small area of a conventional tow with a segmented image to separate out merged fibres into single entities. Figure 5:18 shows a different segmented area followed by the

178

constructed Voronoi cells or 'zones of influence'. These cell areas were then measured in a similar way to the flow channel areas to produce an array of cell sizes, positional co-ordinates and hence the fibre distribution. The area of fibres detected was compared to the total sample area considered to provide the volume fraction of fibres with in the two distinct tows. The results of the analysis are shown in Table 5:2. This work is discussed further in a paper by Griffin et al. [102] in Appendix 7.

Tow Type	Number of Fibres	Volume Fraction (%)
Conventional	525	39.9
Spiral Bound	745	56.6

Table 5:2 Volume Fractions of Conventional and Bound Tows

Construction procedure of the Voronoi-Delaunay tessellation (a) location of 'centres' (b) perpendicular bisectors of lines connecting the 'centres' (c) Voronoi polygons

Cross-section of the spatial configuration. Cyclic boundary conditions are imposed

Voronoi network.
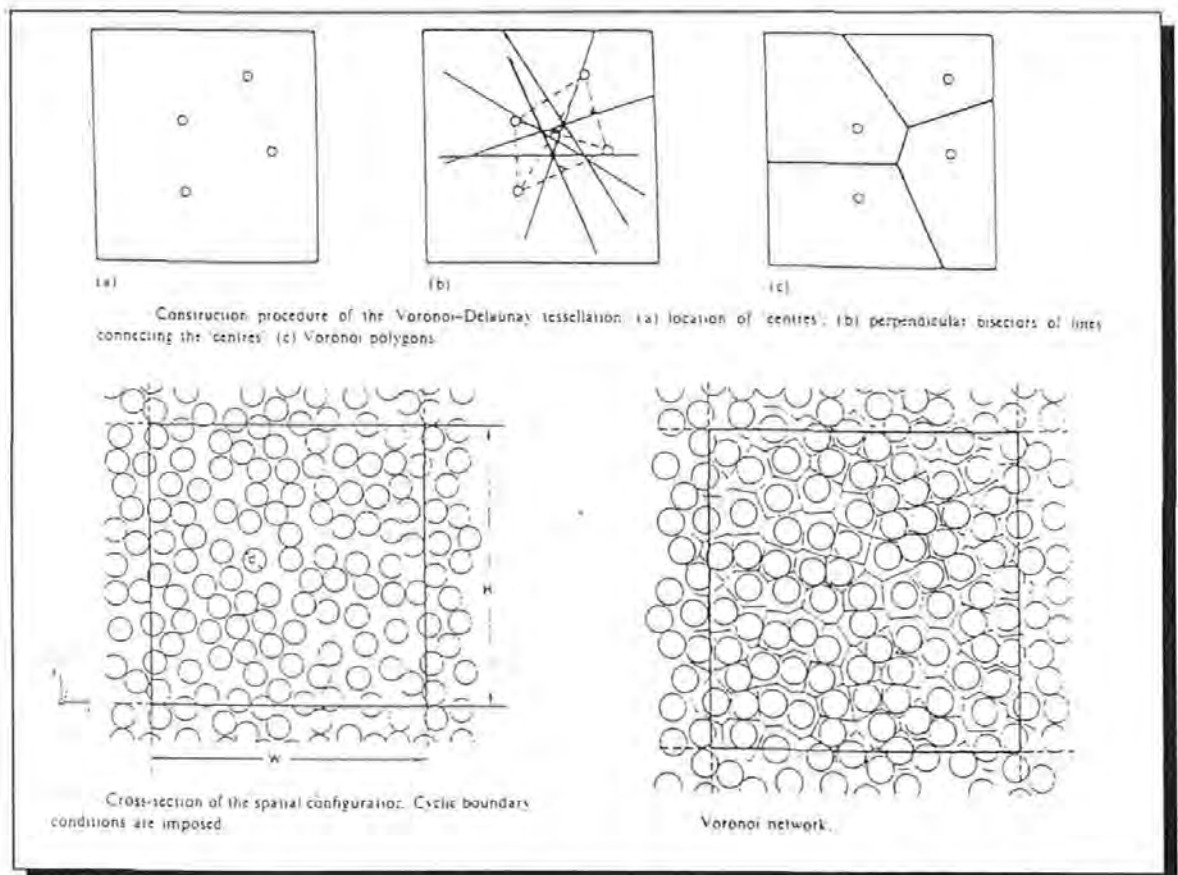
Figure 5:16 Sequential Construction of Voronoi Cells around Fibres
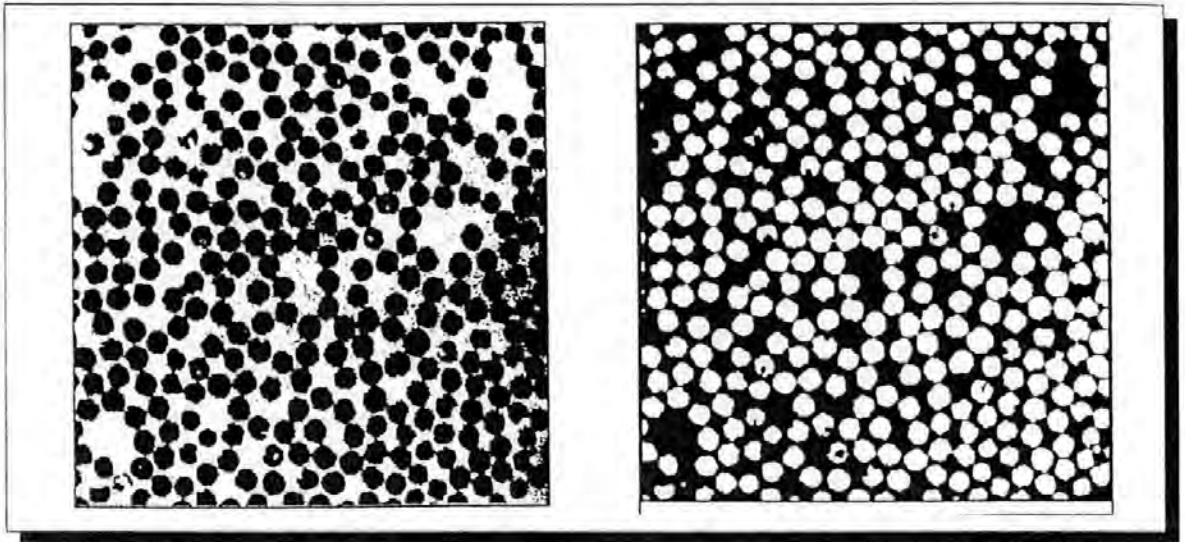
Figure 5:17 Detection and Segmentation of a Conventional Tow
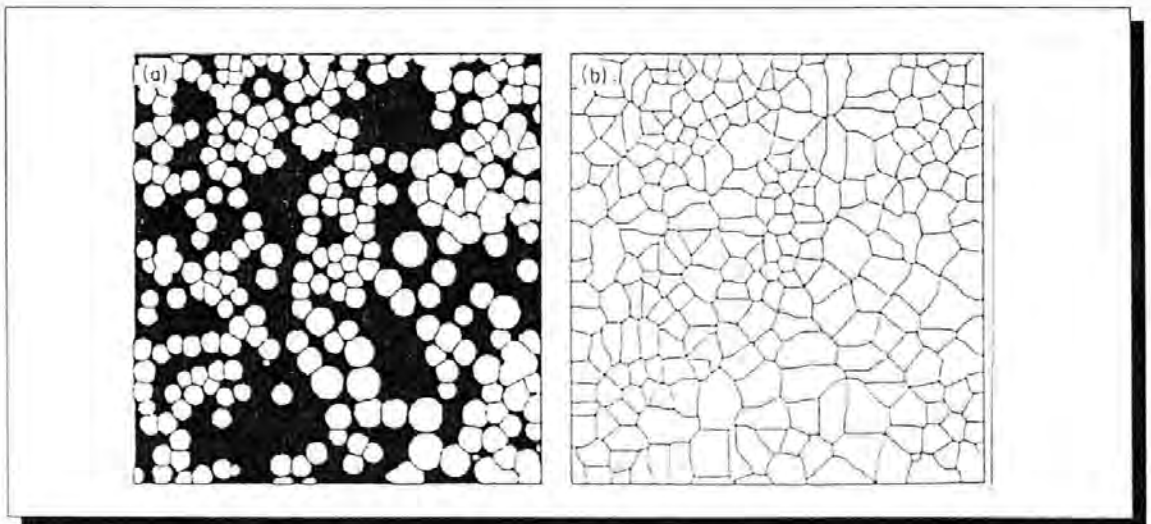
Figure 5:18 (a) Segmented Region and (b) Voronoi Cells

5:13 Image Analysis conclusions

This chapter has described a detailed analysis of the flow channels in a

laminate produced by the inclusion of spiral bound tows into the reinforcement.

It has dealt with both isotropic and anisotropic laminates and has considered a

3-dimensional effect produced by the staggering of the transverse tows. The

results produced by the analysis are now presented in Chapter 6 with

conclusions regarding the use of image analysis for such an application.

CHAPTER 6

IMAGE ANALYSIS RESULTS

This chapter presents the results of the image analysis described in Chapter 5. The main areas of interest were the size and geometry of the large flow channel areas produced by the flow enhancing, spiral bound tows in five anisotropic and isotropic lay-ups.

6:1 Preliminary Flow Channel Investigation

Initially, a set of image analyses were conducted not only to measure the flow areas but also to provide a learning exercise for the user. The method of measurement of the flow channel geometry is described in detail in Chapter 5:7. This set of results was obtained from the anisotropic plates moulded, as described in Chapter 3:3. The specimens analysed were taken at 60mm from the inlet port in the '0' direction (perpendicular to the spiral bound tows).

6:2 Fixed Sample Area Investigation

The specimen area analysed for each fabric was fixed as specified in Chapter 5:8. The results of the image analysis were imported into Microsoft Excel 5.0 from where they were processed. Figure 6:1 shows the cumulative range of sorted flow areas detected, the vast majority of which were less than $0.1mm^2$ area. Figure 6:2 displays the result of segregating these areas into bins and plotting them on a histogram. The size of the bins was decided by considering the range of the flow areas detected and using a suitable increment. As expected, Figure 6:2 shows that Fabric 126 exhibits a greater frequency of the

larger flow channels due to the increase in the number of twisted tows, whereas twill weave has a larger percentage of smaller flow channels. This is consistent with the permeability results shown in Chapter 4:3 and 4:4.
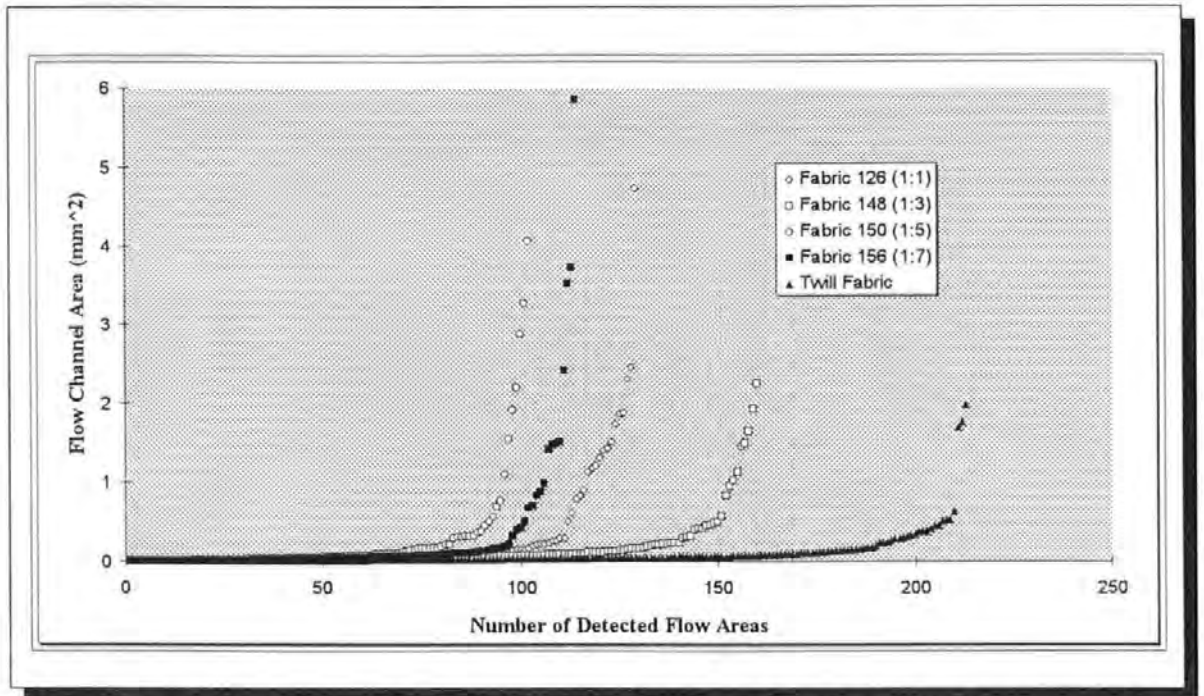
Figure 6:1 Cumulative Flow Channel Area Size Distribution in the Five Laminates
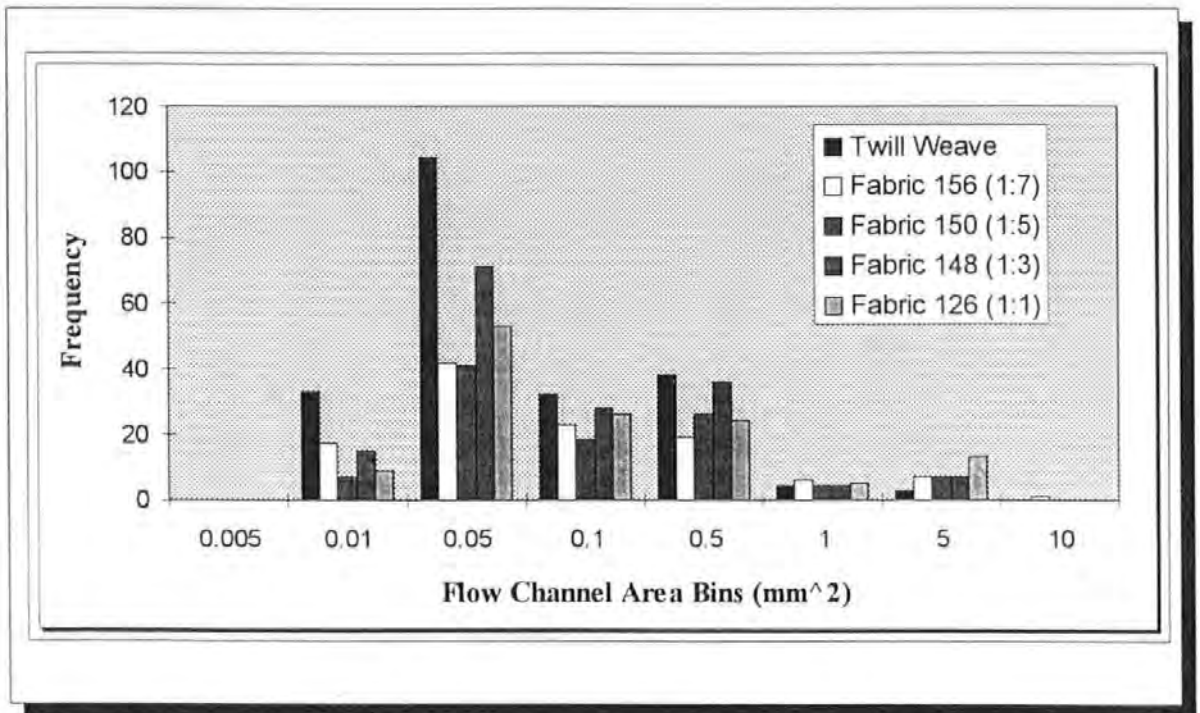
Figure 6:2 Segregation of Larger Flow Areas

Figures 6:3 & 6:4 combine the three image sections tested and show the total

flow areas and their respective perimeters for each fabric laminate. It is

observed that the flow areas and their perimeters do not correlate directly with

the increase in spiral bound tows and it was therefore decided to modify the

testing procedure and to conduct further tests.
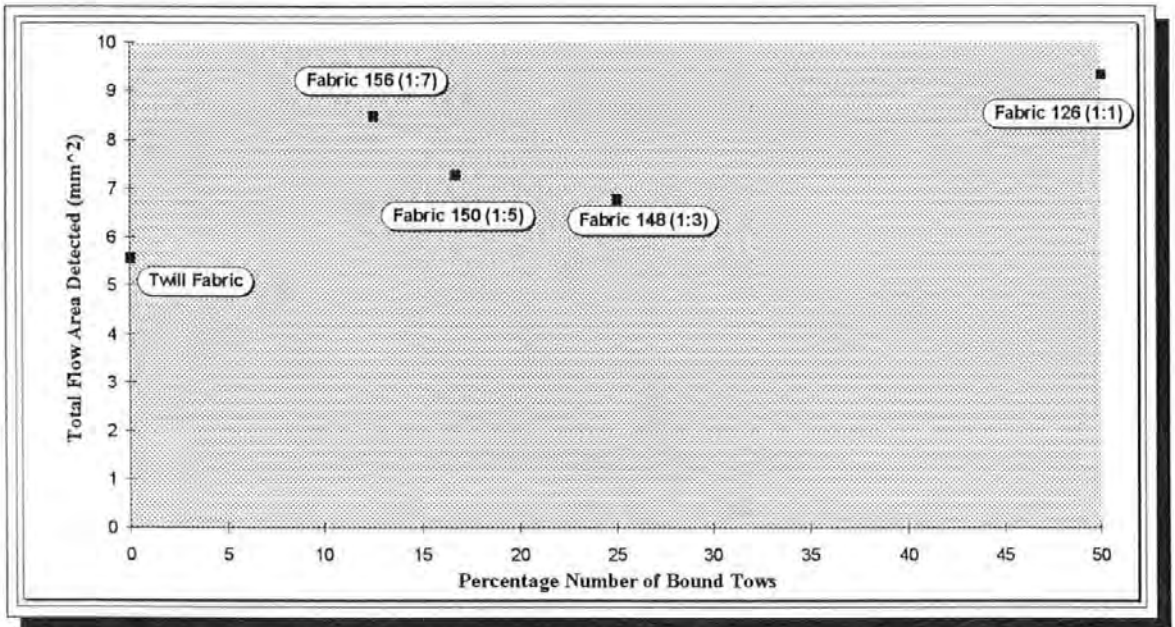
Figure 6:3 Total Flow Channel Areas Detected
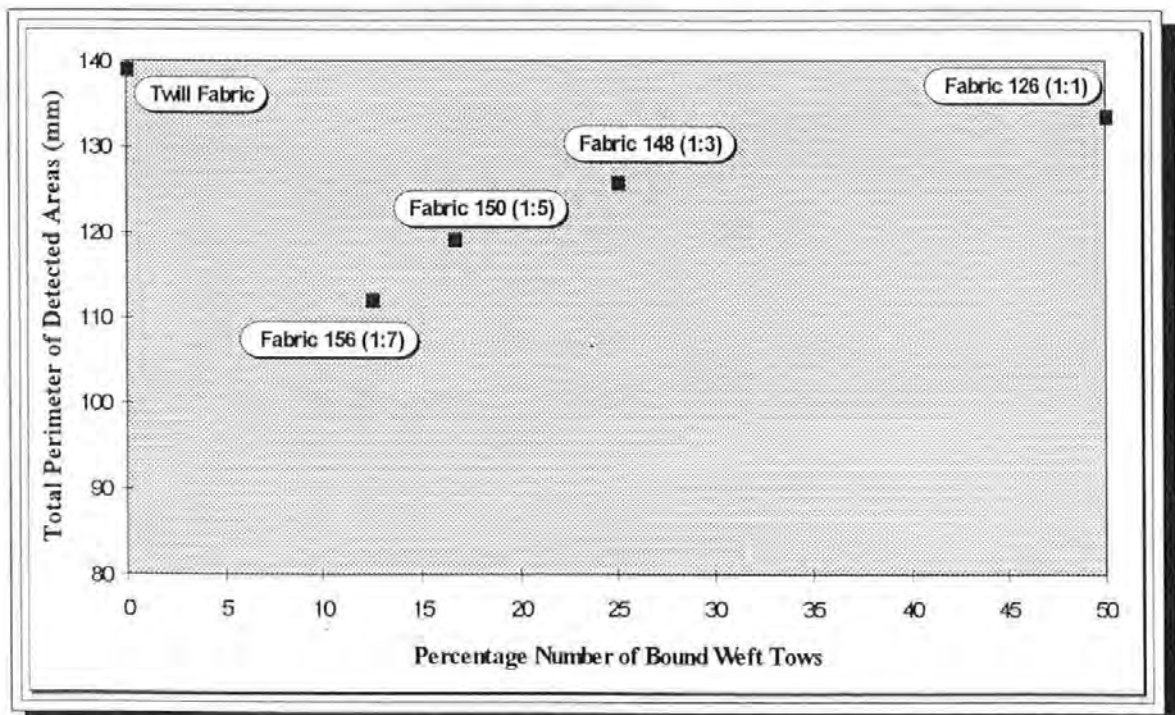
Figure 6:4 Total Perimeters of the Flow Channel Areas

183

6:3 Unit Cell Area Method

As will be observed, the expected increase in total flow area and perimeter for an increase in spiral bound tows was not evident, although the general trend was upwards. This was thought to be due to the analysis of an arbitrary area in the section, even though the specimen area was fixed. Therefore a modification was made to the analysis procedure to counter this problem. The new area of detection was based on the unit cell of any particular layer of fabric in the laminate, i.e. the distance between repeat units as shown in Figure 5:2. The results of the modification of the procedure are seen in Figures 6:5 to 6:7. The distribution of the detected areas above $0.01mm^2$ is shown in Figure 6:5. To enable a clearer distribution to be observed, the values less than $0.01mm^2$ have been omitted and the remaining values sorted in descending order. As with the fixed area method, it was apparent that there was a greater number of larger areas in fabric 126 with the largest number of spiral bound tows. This is highlighted better in Figure 6:6 which shows all the flow channel areas divided into specific size bins as before. Plotting of the total areas and perimeters of the flow channels allowed a comparison of the five laminates and this is shown in Figure 6:7. Again the sequence shows a general upward trend in the areas and perimeters detected but several fabrics (notably Fabric 156 with 12.5% spiral bound tows)) show unexpectedly large increases in detected areas and perimeters. Therefore a slightly different method of measurement was adopted.
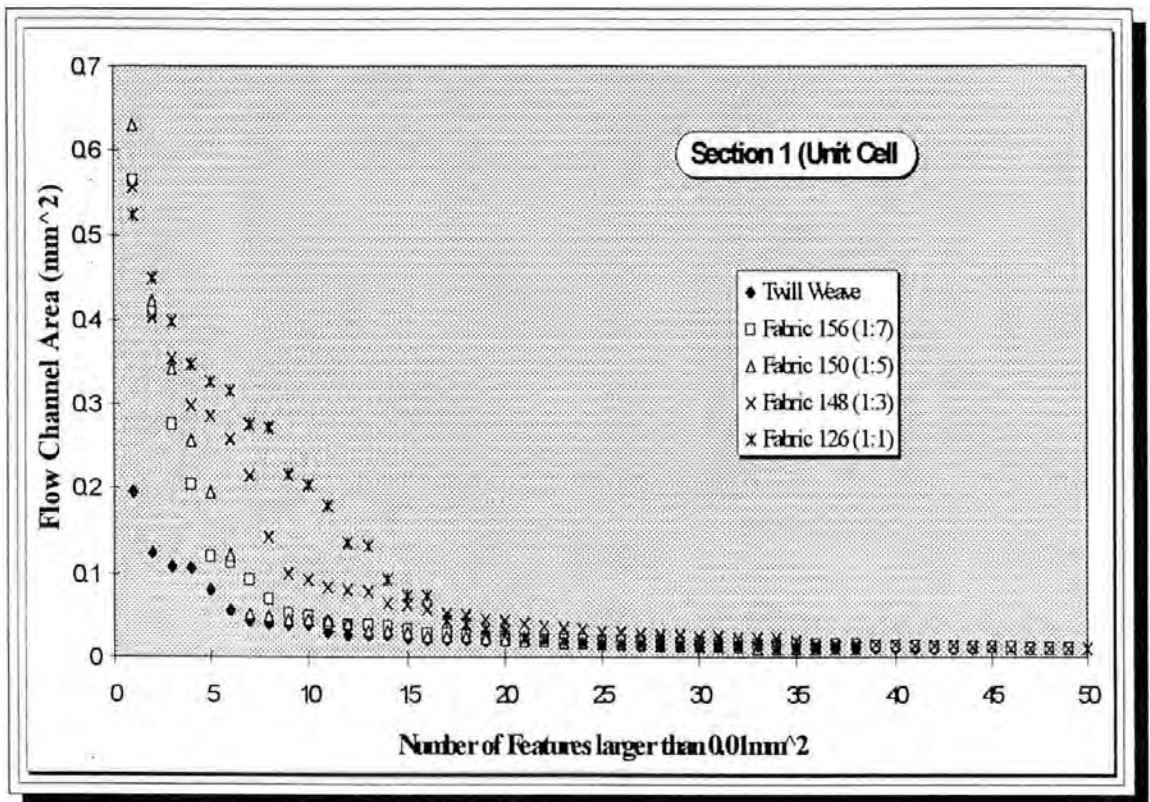
*Figure 6:5 Distribution of the Flow Channel Sizes larger than 0.01mm² in a
Unit Cell Specimen Area for the Five Laminates*
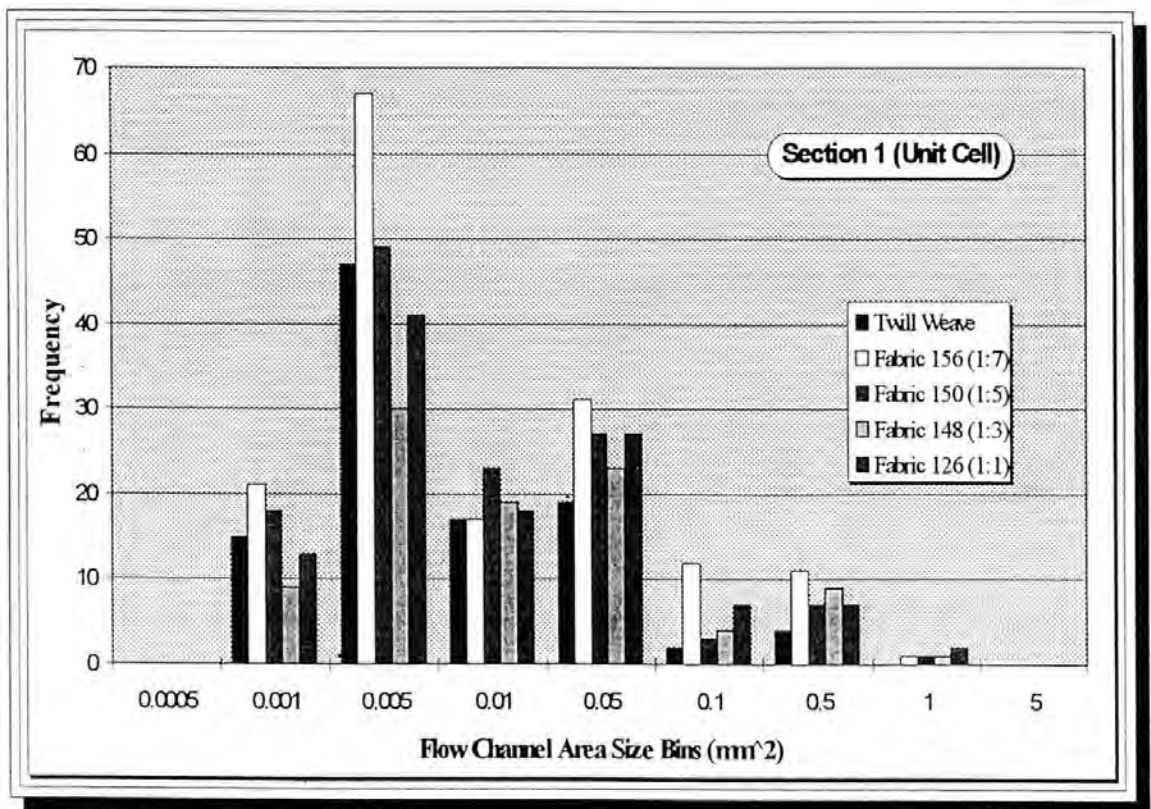
*Figure 6:6 Histogram of the Flow Channel Area Frequency Distribution
for Flow Channels detected by the Unit Cell Method*
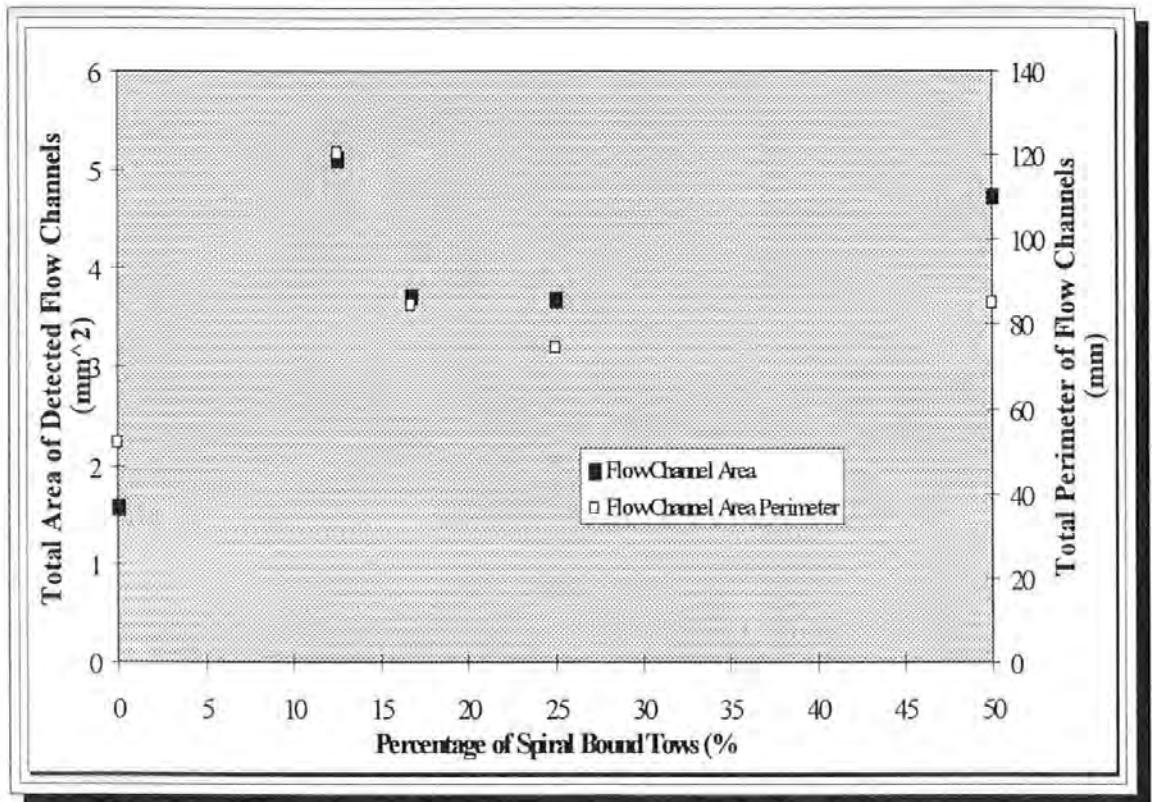
Figure 6:7 Comparison of the Total Areas and the Respective Perimeters of the Laminates using the Unit Cell Method

6:4 Fixed Specimen Area in the Thickness Direction

On further consideration of the laminates, it was realised that the transverse

tows appeared to varying degrees on the laminate face depending upon their

position within the laminate. This was due to the staggering of the tows

produced in the laying-up procedure. Owing to the elliptical section of the tow,

varying proportions were visible at arbitrary positions which affected the area

of the flow channels detected. Therefore by taking several detections into

consideration, it was expected that an average figure would be more

appropriate than just a single detection. Figure 5:14 shows the staggering of the

tows in the thickness direction of the specimen. Figure 5:14 also illustrates the

method by which the staggering was accounted for. Each of the specimen were

ground down 0.5mm using 1200 grade grinding paper on a rotating plate,

repolished and reanalysed four times. This provided five sets of data which were imported into a spreadsheet. Figures 6:8a-d show the distribution of the flow channel sizes which are larger than 0.01mm^2 using the fixed specimen area method for the four new specimen faces. These again show that Fabric 126 has a greater proportion of large flow channels as do the histograms of the flow channel area bins of the four new sections shown in Figures 6:9a-d. After importing all the data for the totalled areas and perimeters for each fabric and each section an average value was obtained for each of the laminates. Tables 6:1 and 6:2 show the total areas and perimeters of the flow channels detected for the five sections investigated.

FABRIC	SECTION 1	SECTION 2	SECTION 3	SECTION 4	SECTION 5	AVERAGE
Twill	2.0	0.0	1.2	2.5	1.3	1.5
156 (1:7)	3.0	1.9	1.8	1.6	2.2	2.1
150 (1:5)	3.0	2.1	3.0	3.5	1.9	2.7
148 (1:3)	4.2	5.0	3.9	4.0	3.0	4.0
126 (1:1)	4.8	5.4	5.4	5.7	6.2	5.5

Table 6:1 Sum of the Flow Areas (mm^2) for each Section

FABRIC	SECTION 1	SECTION 2	SECTION 3	SECTION 4	SECTION 5	AVERAGE
Twill	86.7	19.5	57.2	79.4	46.6	57.9
156 (1:7)	81.2	54.2	47.6	48.0	59.0	58.0
150 (1:5)	69.8	52.5	79.4	89.3	58.2	69.8
148 (1:3)	94.4	107.6	87.1	94.1	64.8	89.6
126 (1:1)	93.3	95.6	108.4	113.8	107.9	103.8

Table 6:2 Sum of the Perimeters (mm) of the Detected Areas for each Section

Figure 6:10 shows the total flow channel areas for the five sections together with the average of the five sections. Figure 6:11 shows the respective perimeters of the flow channels for the five sections, again including the
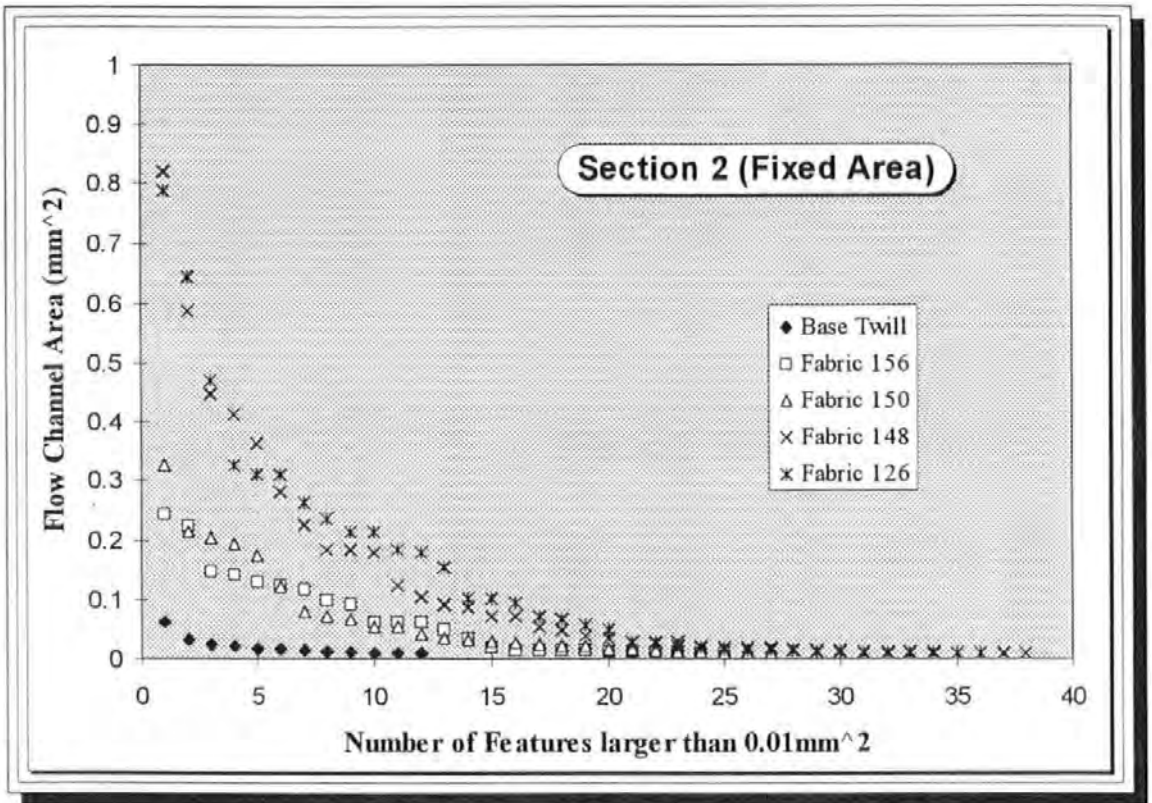
Figure 6:8a Distribution of Flow Channel Sizes larger than 0.01mm² in a Fixed Specimen Area from Section 2 (in descending order)
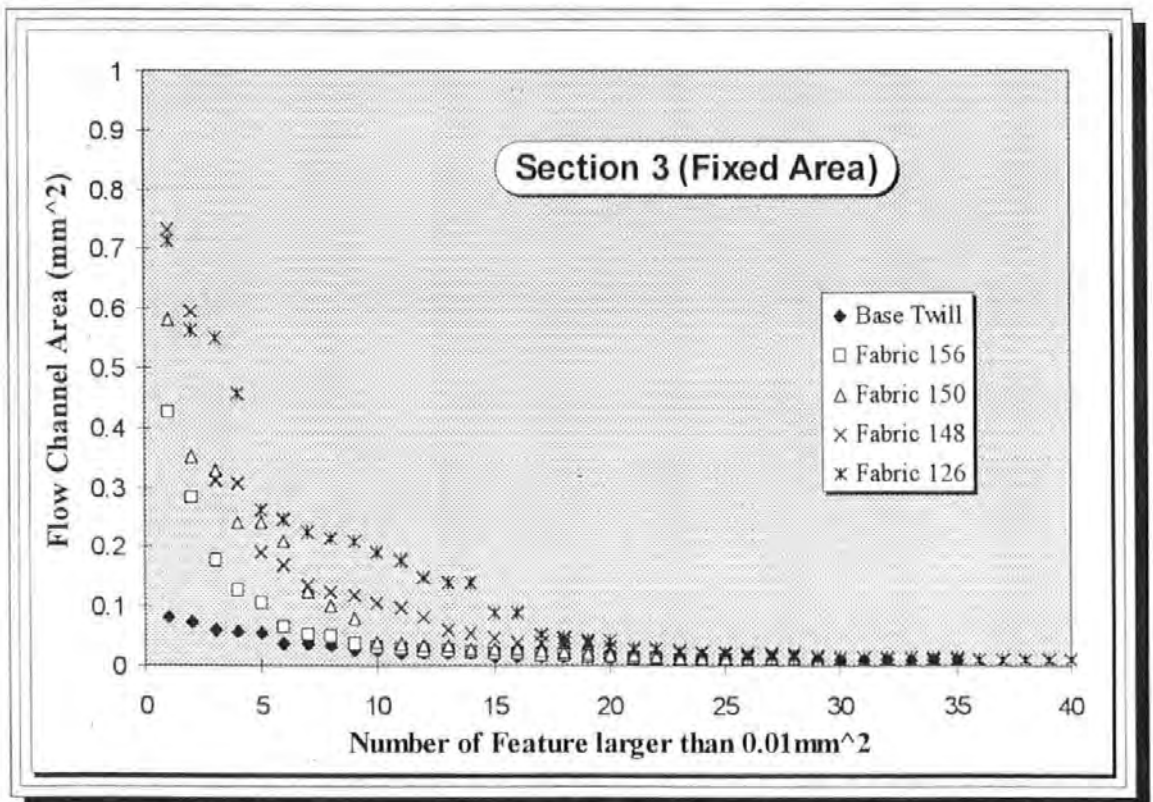
Figure 6:8b Distribution of Flow Channel Sizes larger than 0.01mm² in a Fixed Specimen Area from Section 3 (in descending order)
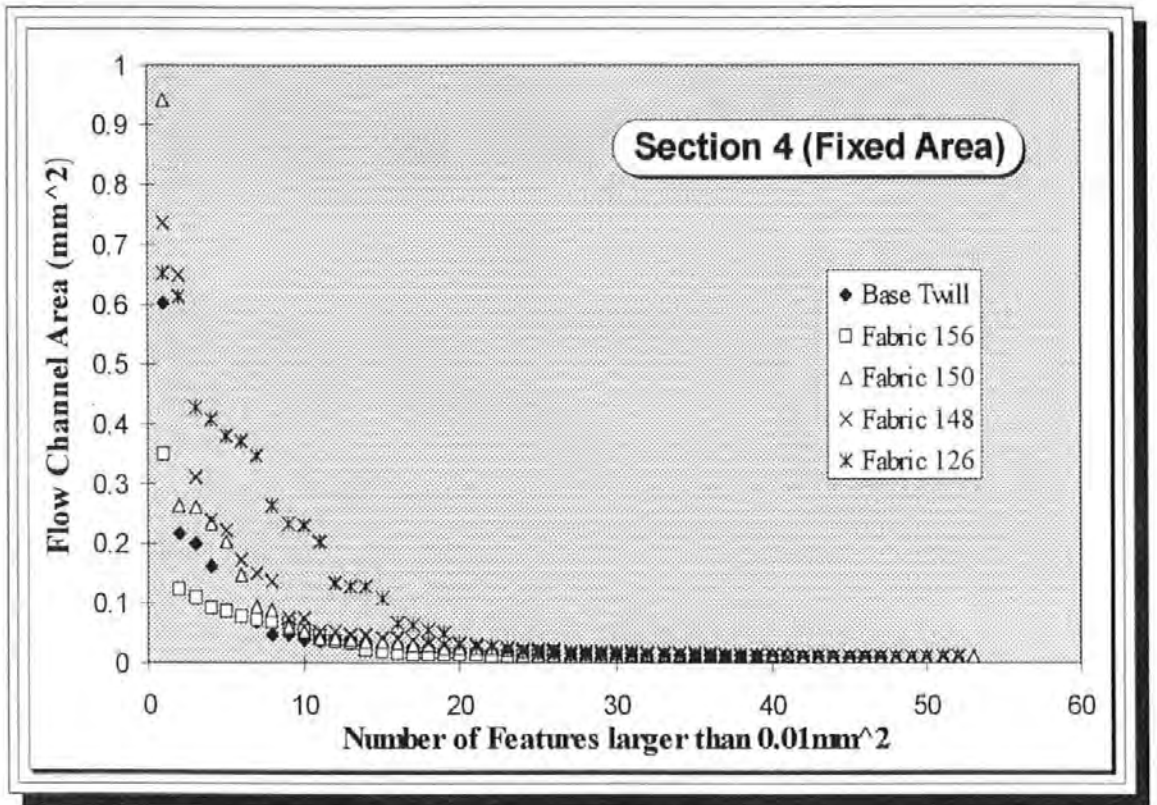
Figure 6:8c Distribution of Flow Channel Sizes larger than 0.01mm² in a Fixed Specimen Area from Section 4 (in descending order)
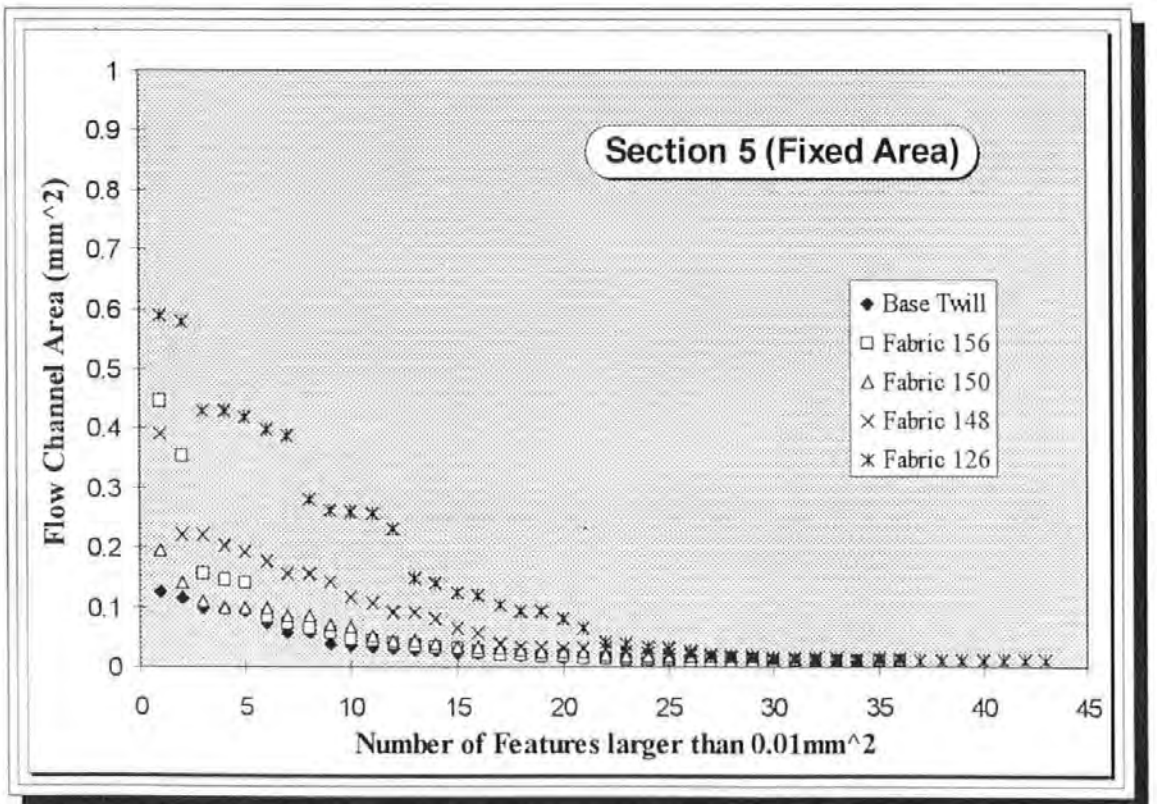
Figure 6:8d Distribution of Flow Channel Sizes larger than 0.01mm² in a Fixed Specimen Area from Section 5 (in descending order)
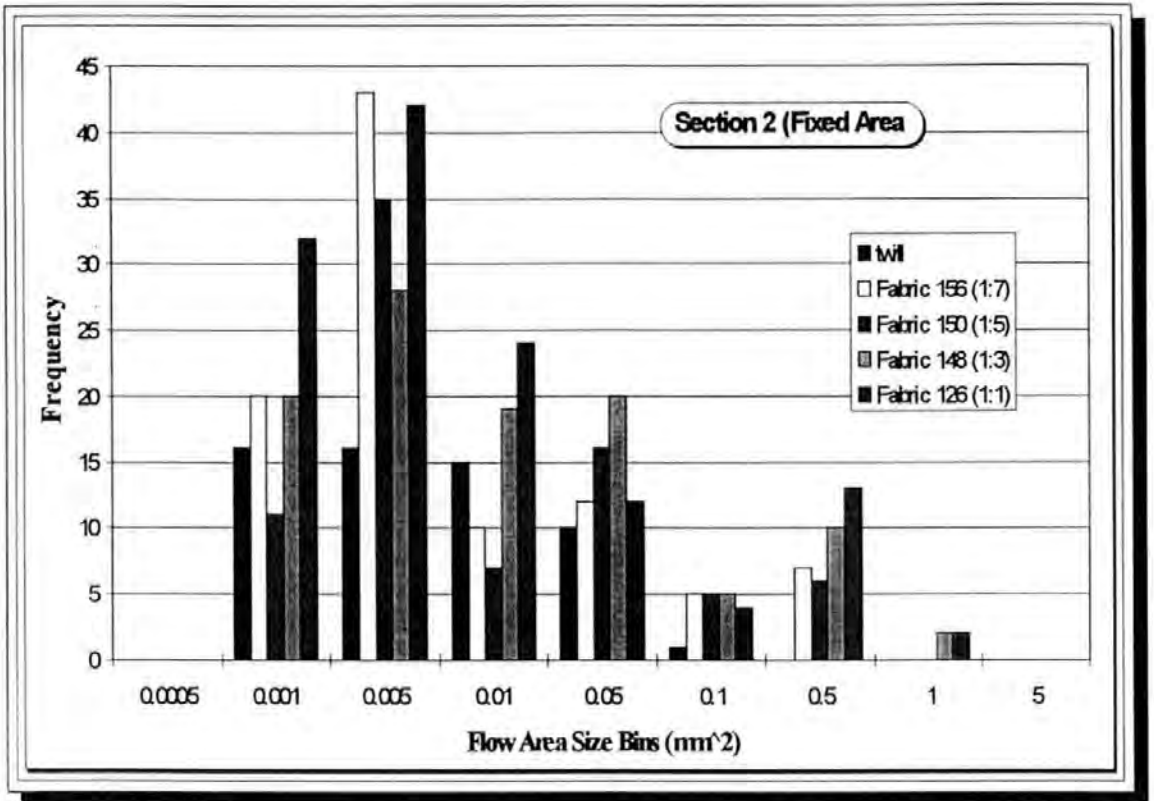
Figure 6:9a Histogram of the Flow Channel Area Frequency Distribution from Section 2
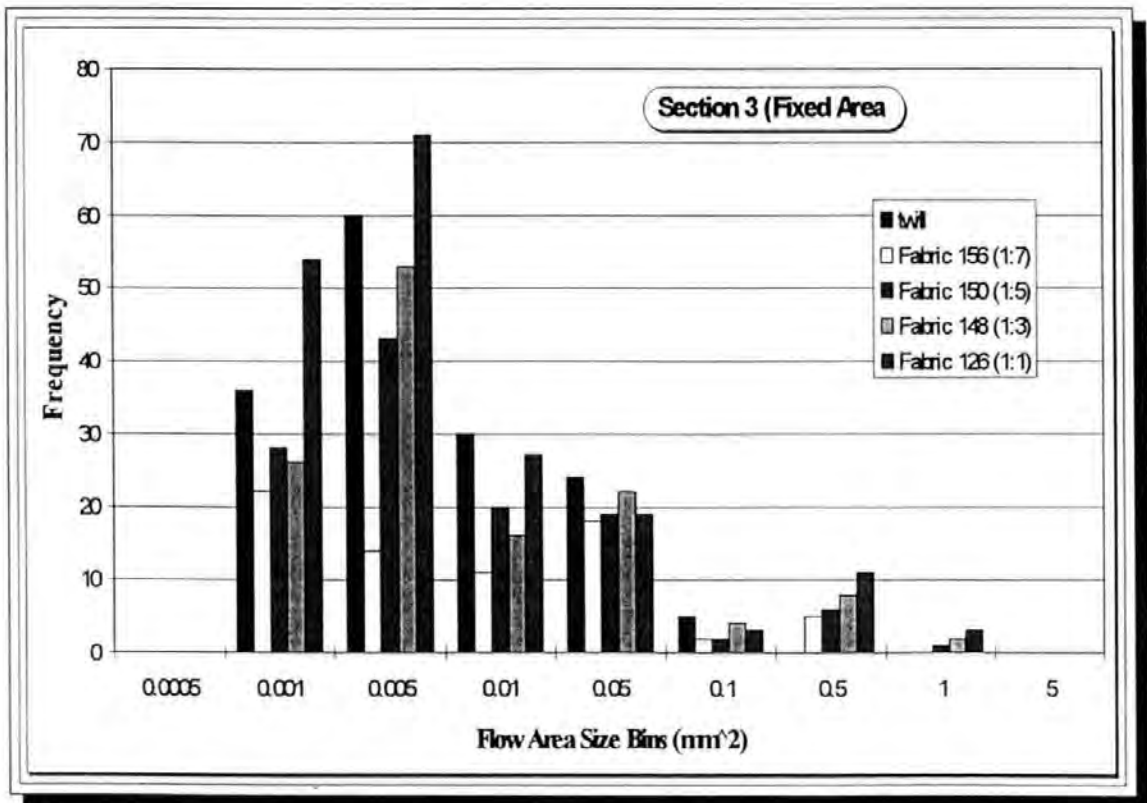
Figure 6:9b Histogram of the Flow Channel Area Frequency Distribution from Section 3
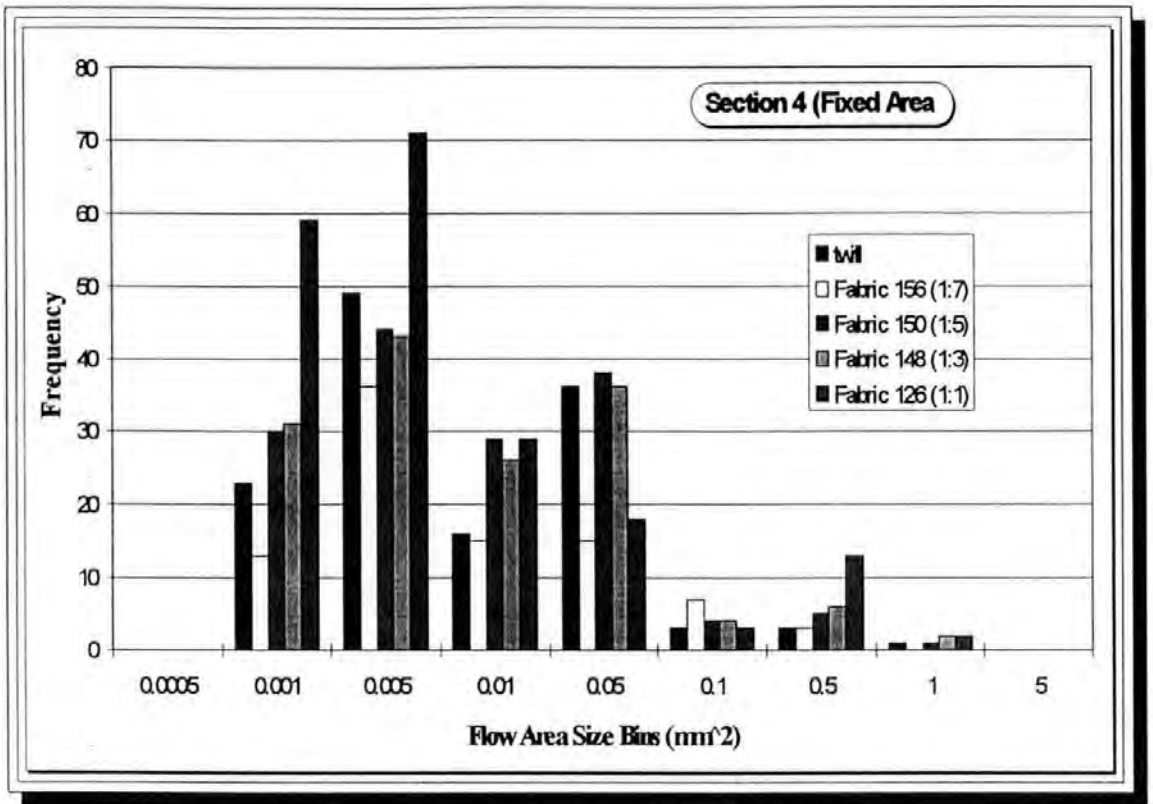
Figure 6:9c Histogram of the Flow Channel Area Frequency Distribution from Section 4
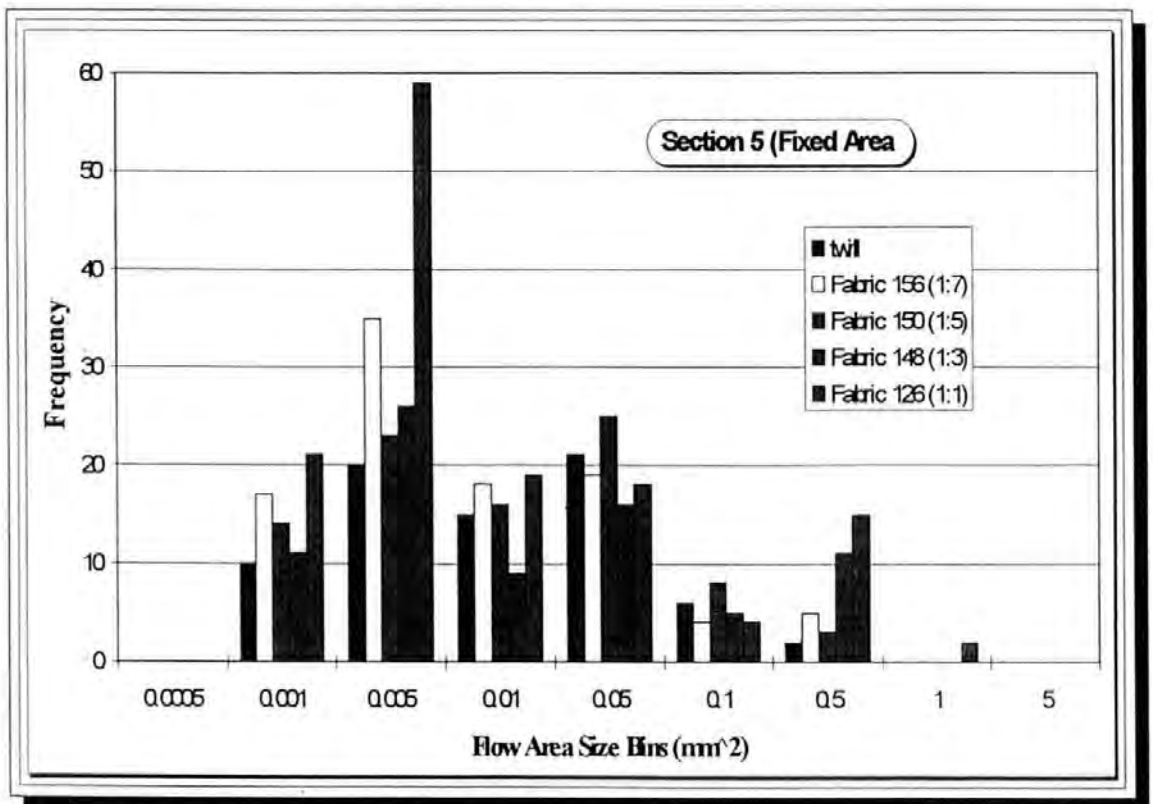
Figure 6:9d Histogram of the Flow Channel Area Frequency Distribution from Section 5
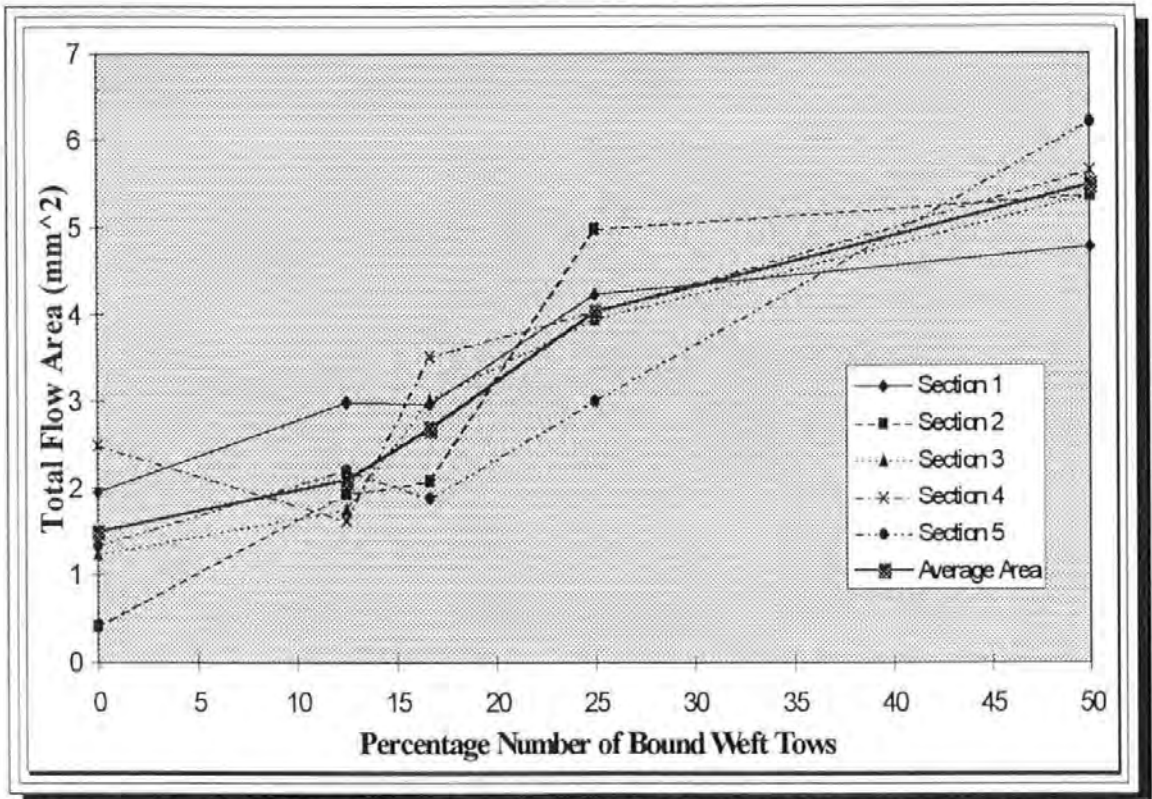
Figure 6:10 Flow Channel Area with respect to the Five Laminates obtained by Averaging the Results of Five Sections using a Fixed Area.
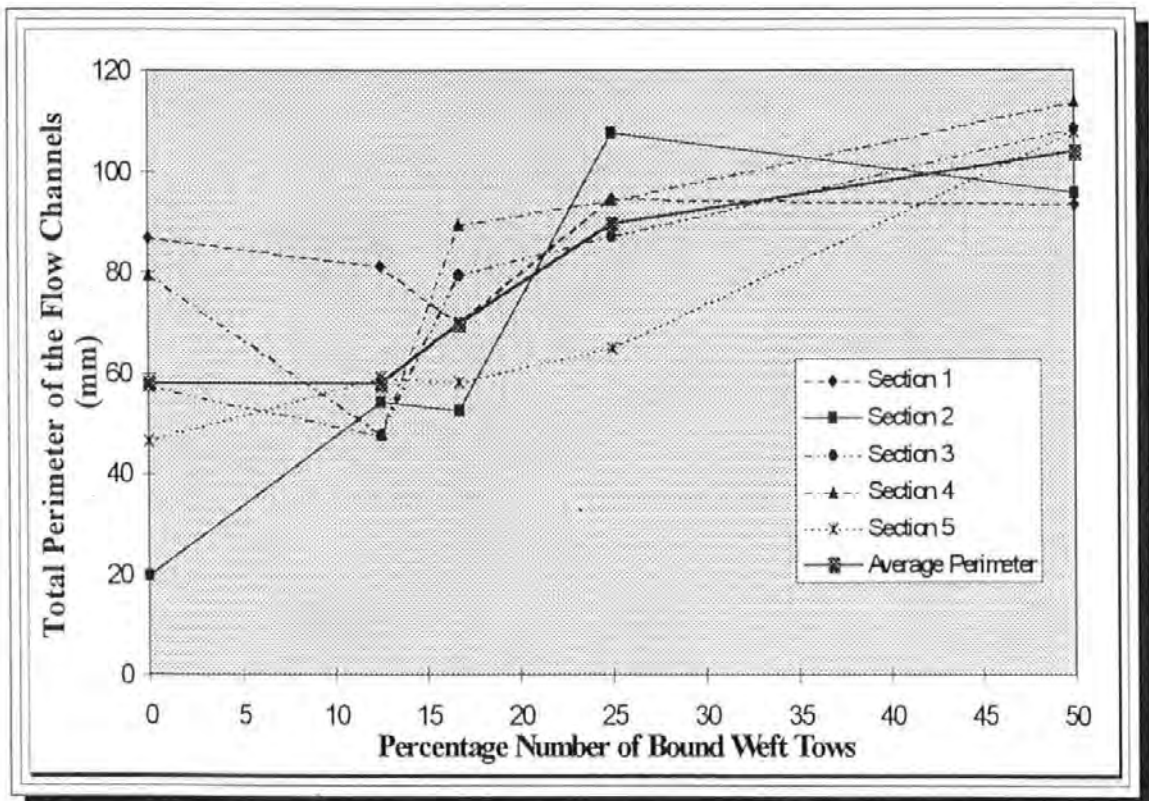
Figure 6:11 Flow Channel Perimeters with respect to the Five Laminates obtained by Averaging the Results of Five Sections using a Fixed Area

average of the five sections investigated. As will be observed, there is increase

in detected flow area with an increase in the number of spiral bound tows

which correlates with the permeability results in Chapter 3:3. The five section

method is now applied using the unit cell procedure.

6:5 Unit Cell in the Thickness Direction

This section investigates the five sections analysed previously using the unit

cell method. Figures 6:12a-d show the distribution of the flow channel sizes

for the four new sections which differ from those the fixed area method. This is

also true of the histograms of the four sections shown in Figures 6:13a-d which

once again show expected greater number of larger flow areas in fabric 126.

As the unit cells are of different size, the flow areas detected required

normalisation. Therefore, the unit cell areas were noted from the image

analyser during the investigation and were consistent for each fabric. The

difference between fabrics 156 and 150 was due to the difference in thickness

of the specimens. Table 6:3 shows the unit cell areas used

Fabric	Unit Cell Area (mm^2)
Twill	15.2
156 (1:7)	18.6
150 (1:5)	16.7
148 (1:3)	23.3
126 (1:1)	31.0

Table 6:3 Unit Cell Areas for Flow Enhancing Fabrics

Table 6:4 shows the detected areas and their respective perimeters within the

unit cells for the five sections considered.
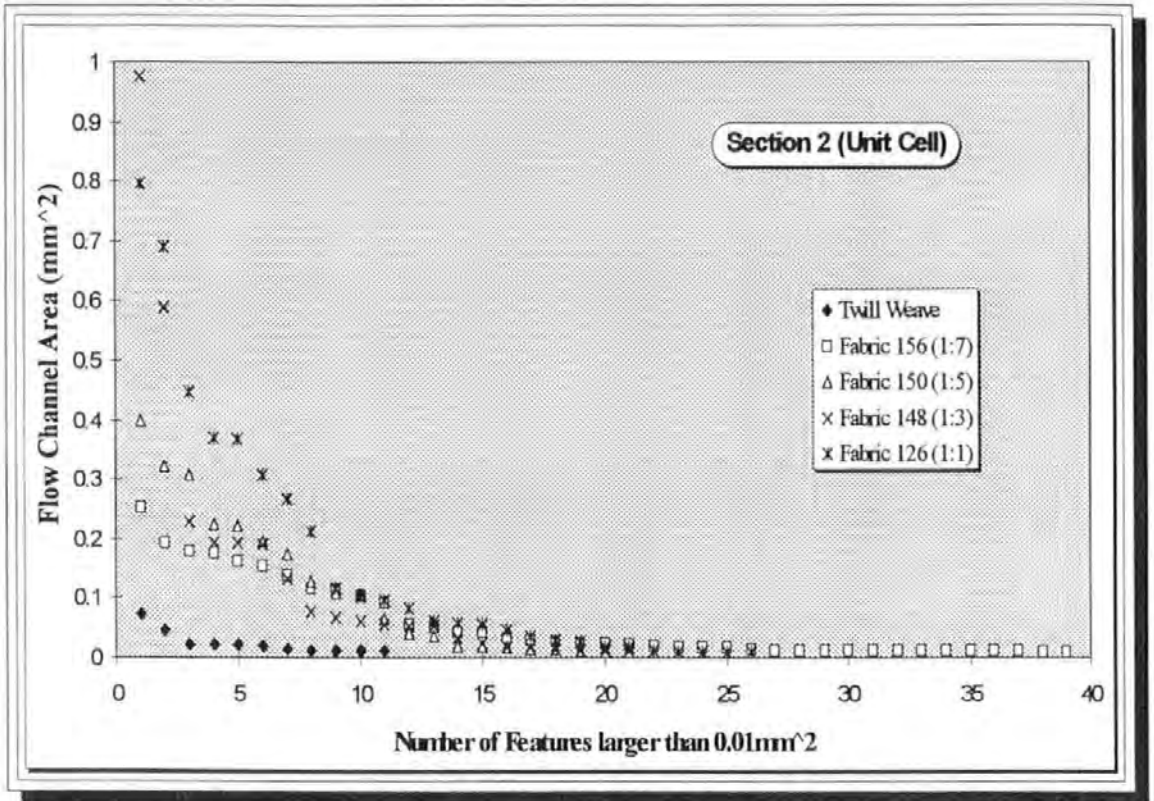
*Figure 6:12a Distribution of Flow Channel Sizes larger than 0.01mm² in a
Unit Cell of Specimen Area from Section 2 (in descending order)*
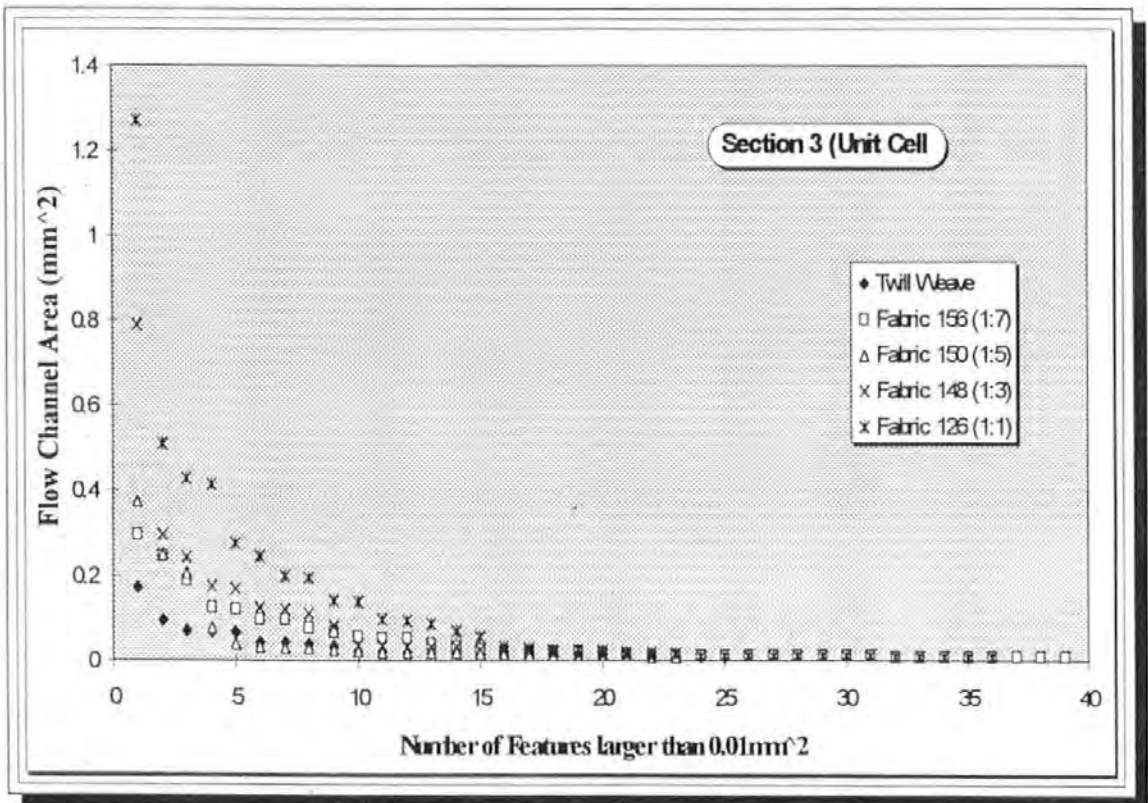
*Figure 6:12b Distribution of Flow Channel Sizes larger than 0.01mm² in a
Unit Cell of Specimen Area from Section 3 (in descending order)*
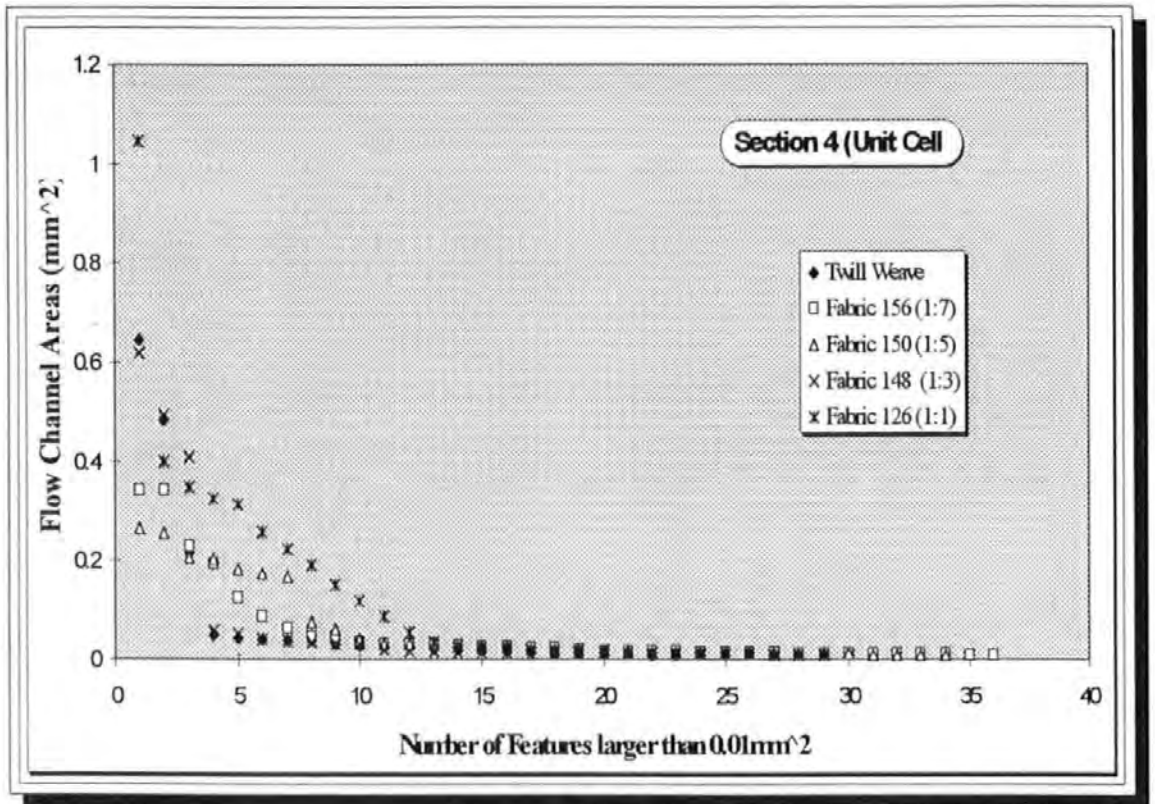
Figure 6:12c Distribution of Flow Channel Sizes larger than 0.01mm² in a Unit Cell of Specimen Area from Section 4 (in descending order)
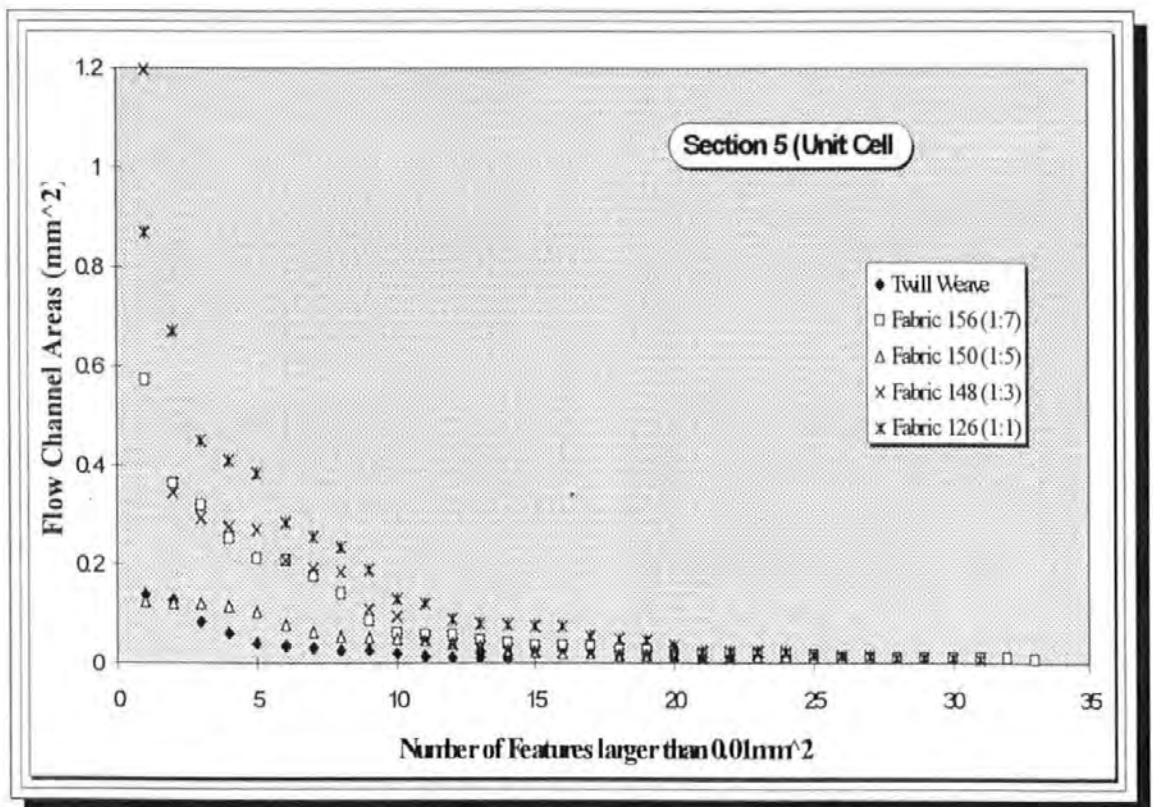
Figure 6:12d Distribution of Flow Channel Sizes larger than 0.01mm² in a Unit Cell of Specimen Area from Section 5 (in descending order)
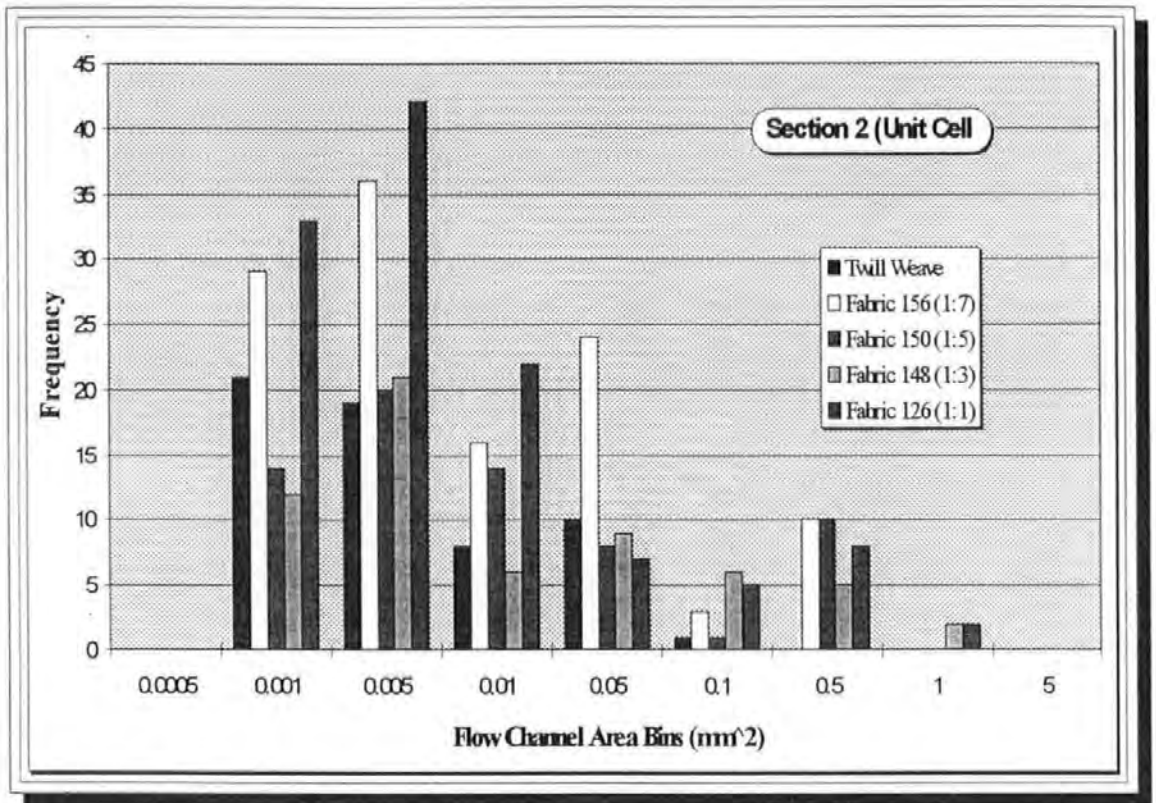
Figure 6:13a Histogram of the Flow Channel Area Frequency Distribution in a Unit Cell Area from Section 2
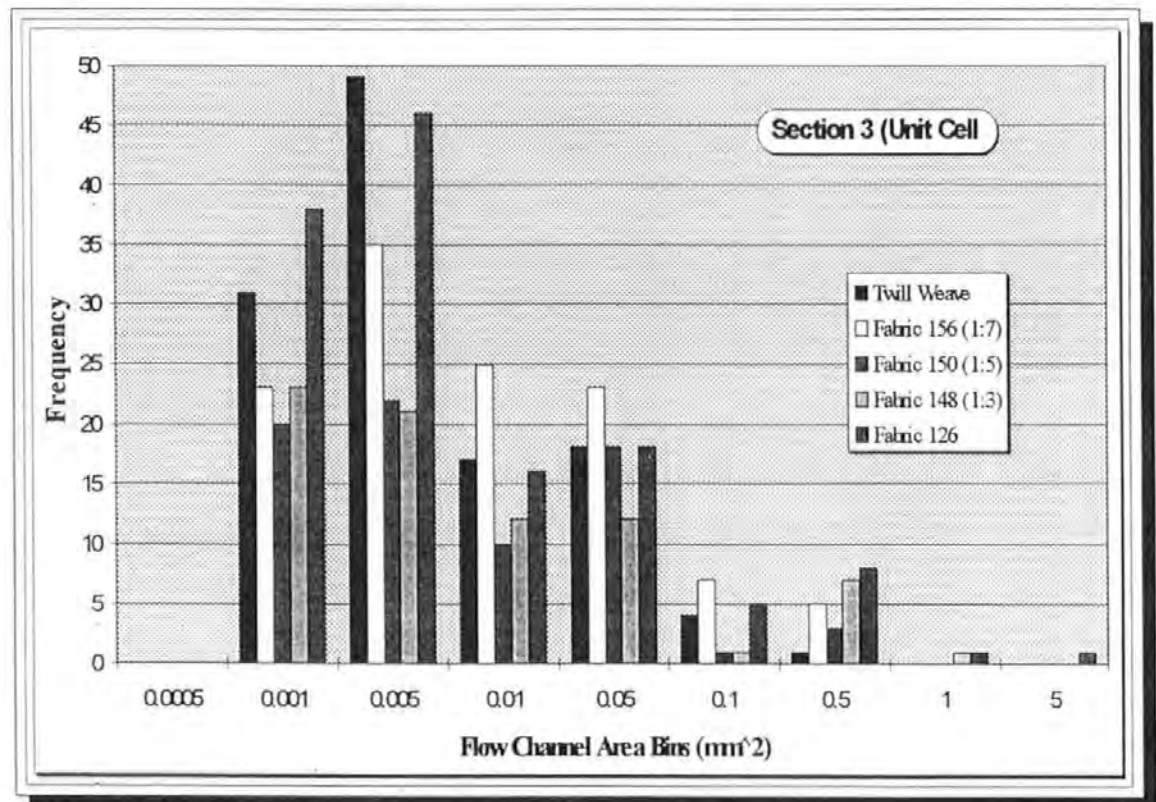
Figure 6:13b Histogram of the Flow Channel Area Frequency Distribution in a Unit Cell Area from Section 3
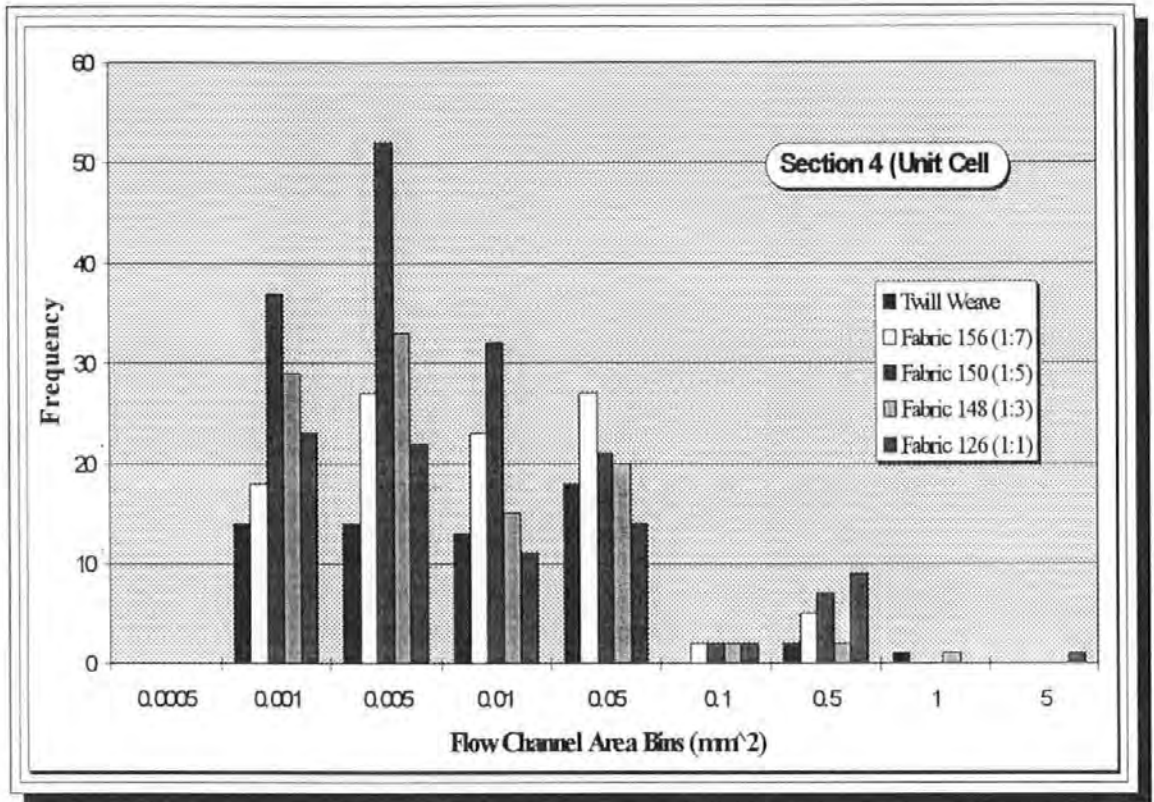
Figure 6:13c Histogram of the Flow Channel Area Frequency Distribution in a Unit Cell Area from Section 4
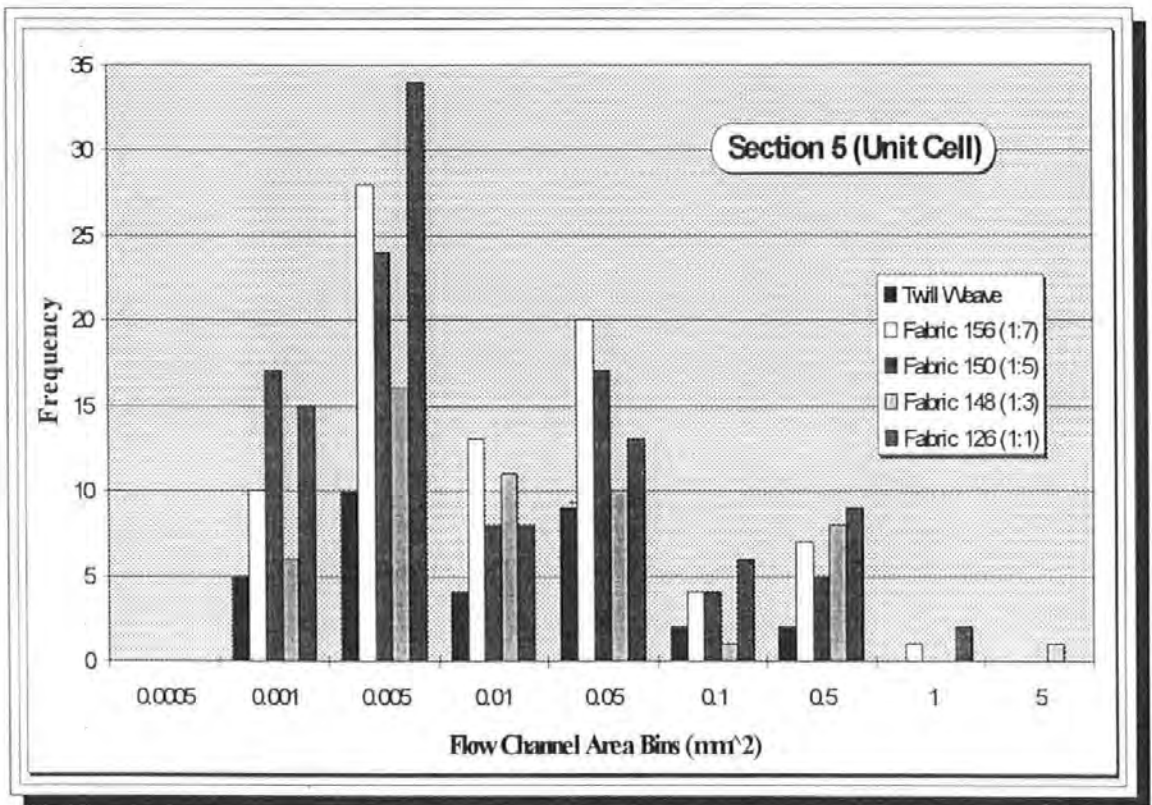
Figure 6:13d Histogram of the Flow Channel Area Frequency Distribution in a Unit Cell Area from Section 5

Section	TWILL		156.0		150.0		148.0		126.0	
	Area mm²	Perimeter mm	Area	Perimeter	Area	Perimeter	Area	Perimeter	Area	Perimeter
1.0	1.6	52.1	5.1	120.7	3.7	84.7	3.7	74.6	4.7	85.2
2.0	0.4	19.8	2.5	68.3	2.6	52.1	3.1	58.6	4.5	82.7
3.0	1.2	48.7	2.2	66.5	1.4	41.6	2.6	56.1	4.8	91.6
4.0	2.0	50.0	2.2	59.0	2.5	75.3	2.2	55.2	4.0	66.6
5.0	0.7	22.3	3.1	72.0	1.4	45.4	3.6	56.4	4.4	85.8

Table 6:4 Flow Channel Area and Perimeters Measured from the Unit Cells

After normalising this data by dividing the detected areas by the unit cell areas, the five sections were plotted in Figure 6:14 and averaged to show the relationship between normalised flow channel area and percentage number of spiral bound weft tows. The perimeters of the flow channels in the unit cell areas were summed for each of the sections. Due to the perimeter of the unit cells not being available, the total perimeters were divided by the unit cell area and plotted against the percentage number of bound tows as shown in Figure 6:15. In both figures, there is an increase in normalised flow area and perimeter correlating with an increase in the number of spiral bound tows, although fabric 148 (16.7% spiral bound weft tows) does not show as large an increase in detected flow area.

Both the fixed area and unit cell area methods appear to provide evidence that the large flow channels detected are indeed produced by the introduction and subsequent increase in spiral bound tows. The relationship between detected flow channels and permeability for the flow enhancing fabrics is discussed in Chapter 6:7.
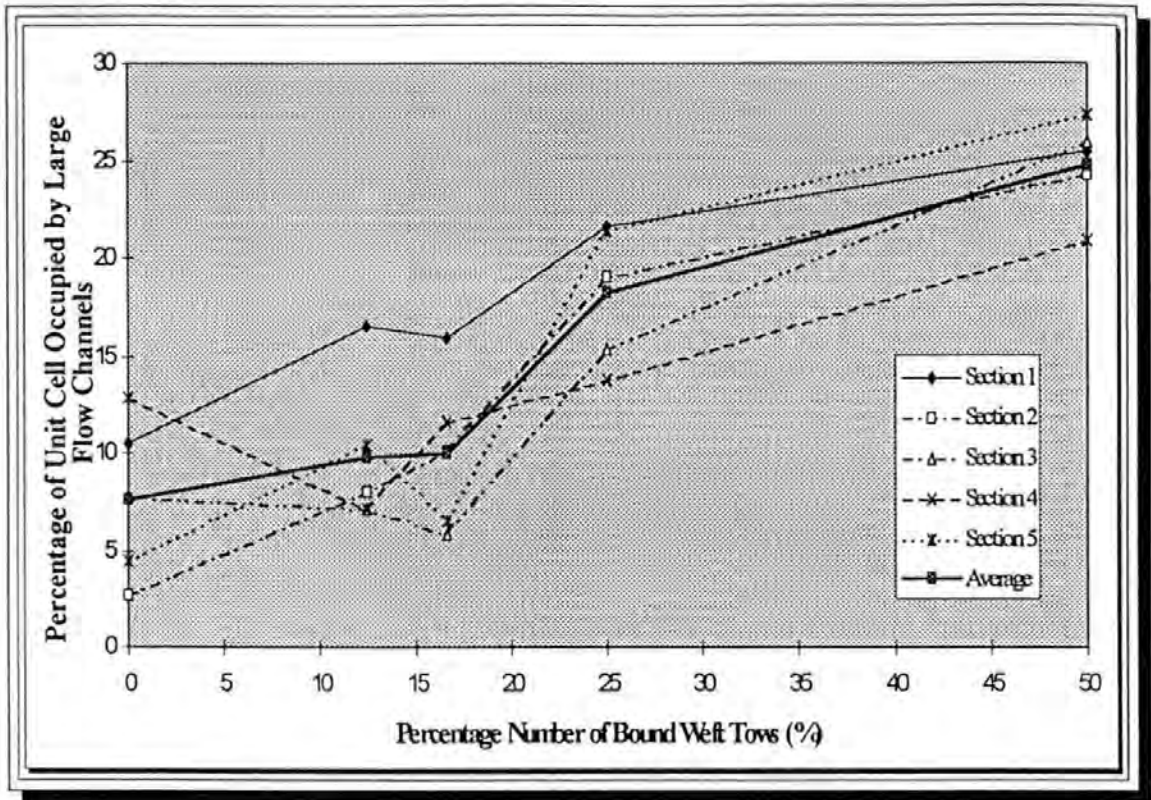
Figure 6:14 Total Detected Flow Areas and Average Detected Area per Unit Cell for the Five Sections of each Fabric Laminate
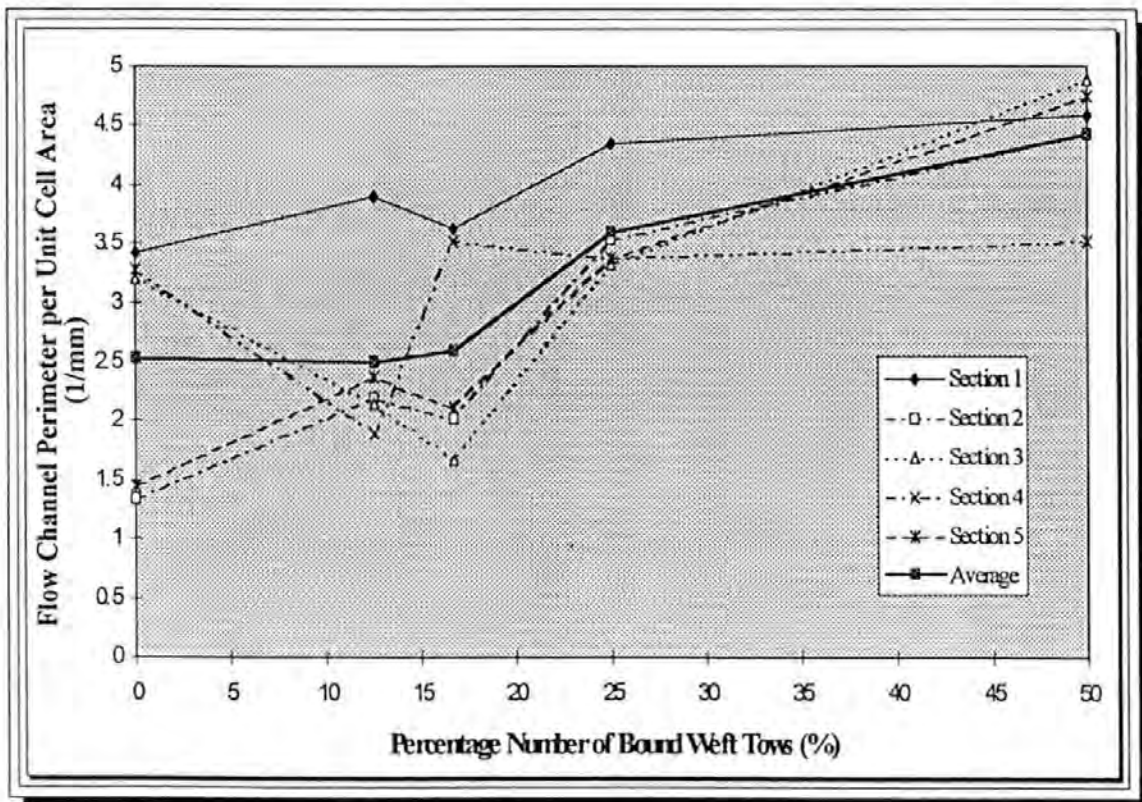
Figure 6:15 Total Flow Channel Perimeters and Average Flow Channel Perimeters per Unit Cell Area for the Five Sections of Each Laminate

6:6 Image Analysis of the Balanced Isotropic Plates

After undertaking the investigation using anisotropic plates (lay-up 0-0-0-0), it

was decided that tests were also required on isotropic lay-ups (0-90-90-0).

Therefore the plates moulded in Chapter 3:4 in the Brite-Euram mould (figure

3:14) were sectioned and polished at 40mm from the inlet in both the '0' an '90'

directions. These specimens were then analysed using the unit cell method

only. The measurements taken were imported into a spreadsheet from where

the total areas and perimeters in the 0 and 90 directions were summed,

normalised and plotted to compare both directions as shown in Figures 6:16

and 6:17. As will be observed in Figure 6:16, the percentage detected area is

approximately half of the detected areas from the anisotropic plates which

would be expected as there were only half the number of spiral bound tows. As

with the anisotropic analysis, an upward trend in detected area with increasing

tows is observed with only fabric 148 not showing an increase in detected area

for this particular section. The method of averaging five sections was expected

to produce an increasing percentage of flow channels per unit for increase in

bound tows as it did in the anisotropic analysis.

6:7 Comparison of the Fixed Area and Unit Cells Detections with Permeability

After completing the programs of permeability measurement and image

analysis of the flow enhancing fabrics, a comparison was made of both the

fixed area and unit cell average detected areas with the permeability results

reported in Chapter 4:4. Figure 6:18 shows the relationship of the permeability
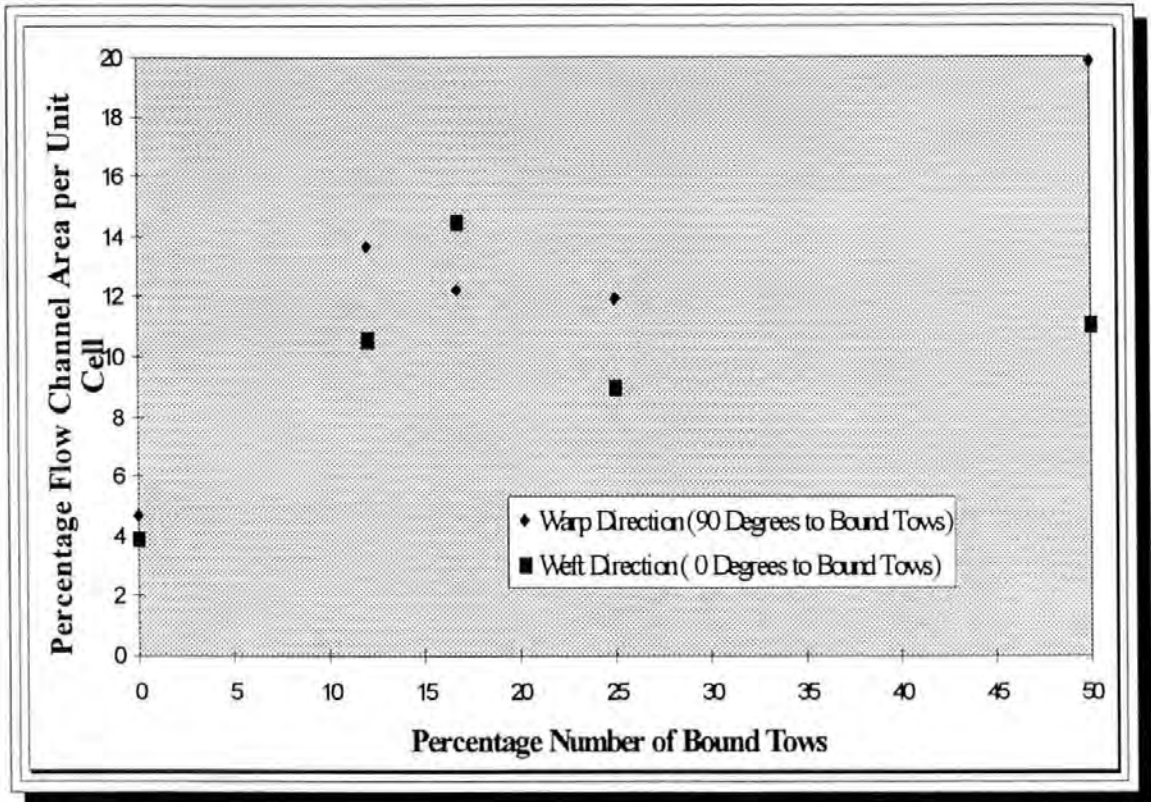
Figure 6:16 Percentage of Unit Cell Occupied by Detected Flow Channels in the Isotropic Laminates
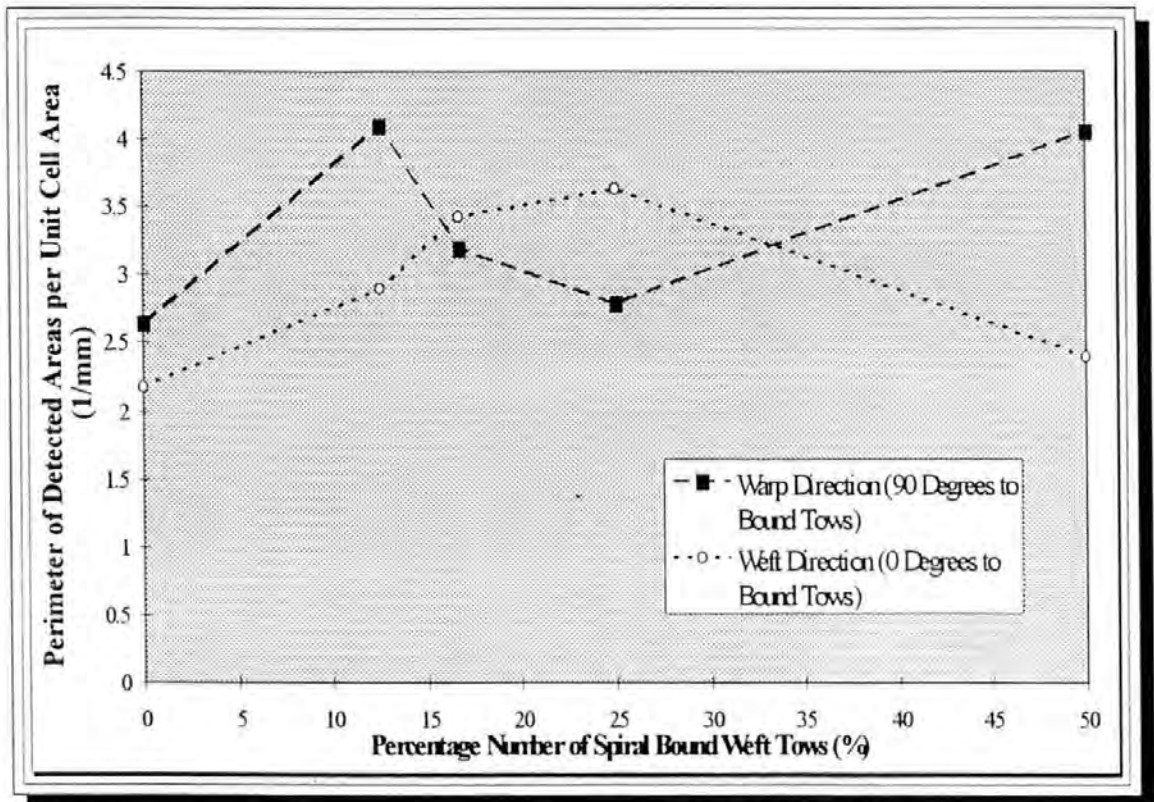
Figure 6:17 Perimeter of Detected Flow Areas per Unit Cell Area for the Five Isotropic Lay-ups
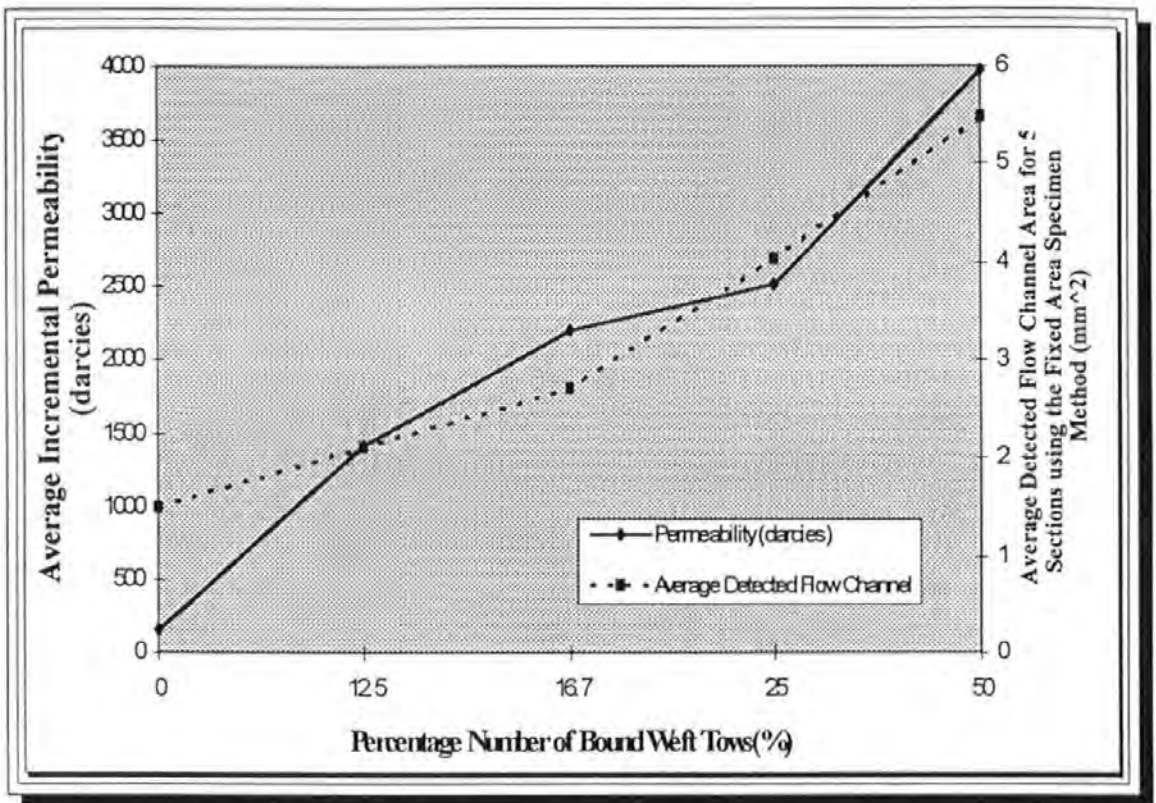
Figure 6:18 Comparison between the Measured Permeabilities and the Average Detected Flow Areas for the Fixed Area Method
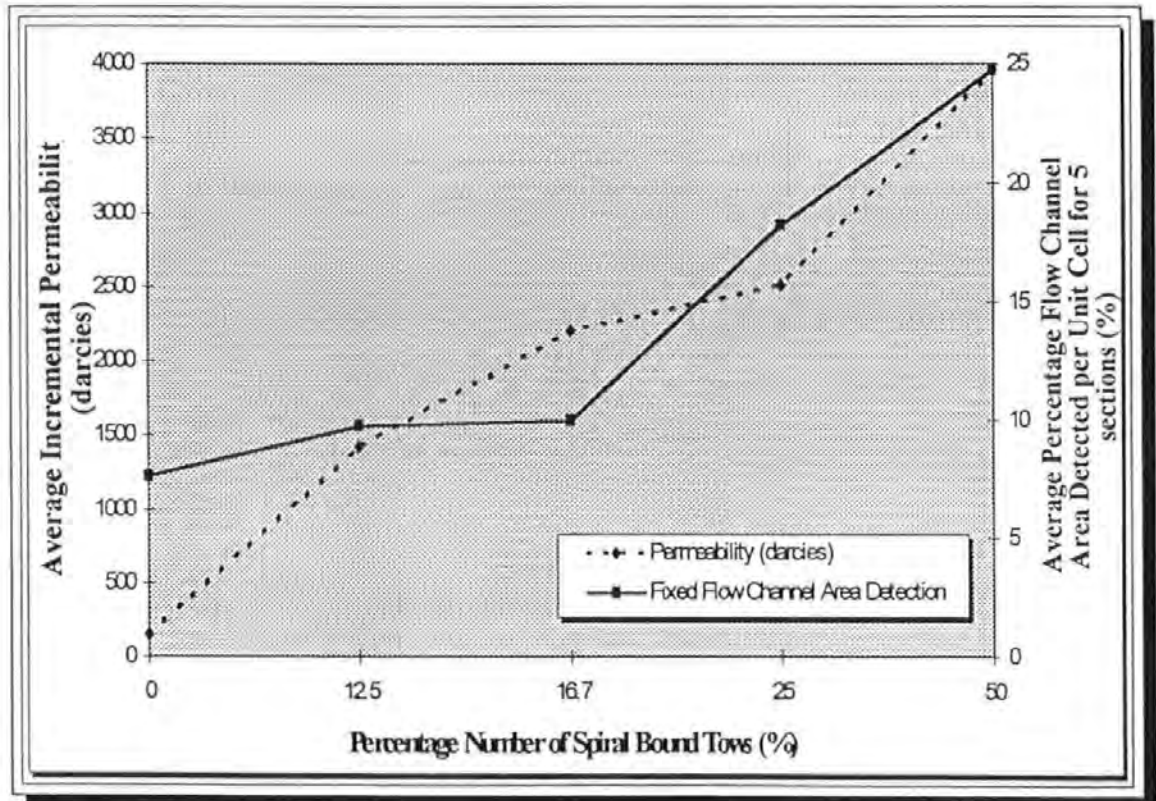
Figure 6:19 Comparison of the Measured Permeabilities with the Normalised Flow Channel Areas obtained by the Unit Cell Method for the Five Fabrics

and average detected flow areas using the fixed area method while figure 6:19 shows the relationship using the unit cell method. Both methods show good correlation with permeability with the expected increase in detected area with the inclusion of more spiral bound tows. As will be seen, there are certain fabrics which show smaller or larger changes in detected flow area than expected and this was thought to be due to a number of phenomena encountered in the image analysis. This is now discussed further.

6:8 Precision of Image Analysis Procedure

During the detection and measurement of the large flow channel areas in the laminate sections, a number of factors were observed which affected the final measurement of the detected regions. There now follows a qualitative breakdown of these factors and a quantitative precision analysis is made where possible.

6:8:1 Grey Levels

Whilst analysing the flow channel areas, the grey level selection, which was at the user's discretion, was observed to vary from section to section, sometimes quite markedly. This was due to the difference in intensity of the reflected light from the microscope from section to section. It was also noted that small differences (+/-1) in grey level would produce different detected areas. Therefore, for a given specimen section of fixed measurement frame area, the grey level was varied by increments of 1 from a set value. Table 6:5 shows the

results of these measurements and quantifies the percentage difference and the percentage range of the detected areas.

Grey Level	Total Area Detected (mm²)	Variation
132.0	1.2	Level 132-136 12.7% Difference
133.0	1.2	
134.0	1.3	
135.0	1.3	Level 132-133 2.7% Difference
136.0	1.4	

Table 6:5 Effect of Small Grey Level Threshold Changes on Total Detected Area for a Given Specimen Area

6:8:2 Imperfections in the Laminate

Whilst undergoing the image analysis, it became obvious that the detected areas were being affected to some degree by small voids within the resin areas and also minor scratches left from the polishing process. The image enhancement provided a means of filling in some of these small areas but scratches presented a problem. The light reflection from the scratches was at a different intensity and therefore on detection separated larger regions into two or more areas, thus invalidating the measurement. This was not a common problem but emphasised the need for good quality polishing. The colour difference in the polyester resins in some of the specimen was believed to be the reason behind large differences in grey level required for some detections. This thought was not supported in the final set of image analyses conducted on the isotropic lay-ups (0-90-90-0) due to the fact that all the specimen were moulded using Jotun Norpol 42-10 polyester resin and still, large grey level variation was apparent. This light variation was therefore accepted as being an

uncontrollable variable and therefore great care was taken in setting the most appropriate grey level for feature detection.

6:8:3 'X' FCP Positioning

As explained in Section 5:3 , the 'XFCP' point is located on the lowest 'x' co-ordinate of a detected area. If, therefore, the region of interest protrudes outside the boundary of the measurement frame, the region is ignored during measurement. Therefore, a segmentation procedure was implemented which divided the large regions into smaller regions to enable measurement to take place as shown in Figure 5:12. This also invalidated some results as the size of the detected region was the object of part of the analysis. To cater for this problem, several frames were varied in length within the sampling area to suit the flow channels being measured.

6:8:4 Plate Thickness Variation

As discussed in Chapter 4:4, there was evidence of mould deflection during the permeability measurements with a consequent thickness variation of the plates. The thickness of each plate was not constant and therefore the area of investigation varied. The volume fraction of the plates varied between 42.45% for fabric 126 up to 46.17% for fabric 150. This was believed to be due to different mould closure forces being required for each of the laminates because of the inclusion of varying percentages of spiral bound tows. The geometry of the bound tow (~ circular) was designed not to crush significantly under mould clamping pressure, thus producing adjacent large flow channels. Therefore, to

produce a constant volume fraction, greater clamping pressure was required. As the percentage of bound tows increased, so did the deflection of the mould as shown in Figure 4:14.

6:8:5 Tow Misalignment

Misalignment of tows was a result of storage and handling of the reinforcements. The scale of the microstructural measurements exaggerates the problem, as very small misalignments of the transverse tows were noticeable . The problem of misalignment was catered for in the image analysis by taking five sections and averaging the results. The misalignment of the tows may possibly be reduced by preforming and minimum handling although small misalignments are common in many reinforcements.

6:8:6 Measuring Frame Size

During the measurement of the unit cell, the problem of thickness variation was met. This meant that the width of the frame size for each section measured required a modification. Therefore small differences in measuring frame area and unit cell area were evident. The normalising procedure with the unit cells eradicated this problem.

CHAPTER 7

MODELLING OF THE FLOW ENHANCING FABRICS

7:1 Modes of Flow within the Fibre Bed

After conducting the image analysis on the fibre laminates, it was decided to model these flow enhancing fabrics according to the categories of flow domains which existed in the cross section. Summarising the cross sections of the laminates, it was observed that the flow required to fill all the 'space' in the fibre pack could be divided into the following categories according to the fibre distribution and orientation,

i) Enlarged Flow Channels caused by the addition of Spiral Bound Tows

ii) Axial Capillary Flow along both the conventional and bound tows

iii) Transverse Flow through the tows.

7:2 Modelling the Flow

The purpose of this section is to describe the derivation of equations to model the categories of flow described above. The approach was to determine the proportion of each type of flow evident in a given unit cell section and using the rule of mixtures, produce a total flow model. Therefore by considering a simplified version of the flow enhancing fabrics as shown in Figure 7:1, a derivation of an equation to calculate the proportions of each type of flow is now presented.

The measurements of tow and inter tow dimensions were taken by averaging

actual measurements taken from the laminate micrographs.
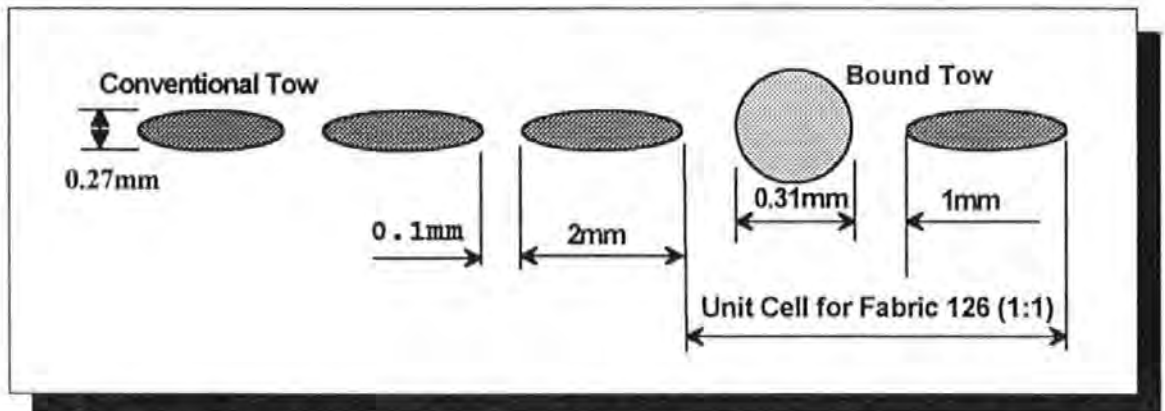
Figure 7:1 Schematic Diagram of the Flow Enhancing Weaves with Dimensions

Figures such as 7:1 are used as the basis for determining the percentage of each

type of flow area within the laminate.

7:2:1 Assumptions

To determine the proportion of each category of flow region required certain

assumptions to be made

i) the conventional tows were all of similar geometry, assumed to be elliptical

with dimensions as in Figure 7:1.

ii) the spiral bound tows were also of similar geometry, assumed to be circular

with dimensions also in Figure 7:1

iii) the thickness of the ply was constant and was the height of two

conventional tows (1 axial and 1 transverse) i.e. 0.27mm x 2 = 0.54mm

iv) all the equations were derived for one ply only with the number of

conventional tows varying for each fabric.

208

7:2:2 Percentage Axial Flow Area

To enable the proportion of axial flow to be determined for each of the fabrics, the volume of axial tows per unit area was first determined. This was ascertained by summing the areas of the axial tows, both conventional ($\pi.a.b$) and bound ($\pi.r^2$), and dividing it by the length of the unit cell (sum of the lengths of the tows plus the inter-tow gaps). This at first appears to be area per unit length but as the length of the cell was constant, the length cancels out. The number of conventional tows increases by one for each fabric and therefore 'n' increments by one in equation 7:1. The average volume of the axial tows per unit area was given by :

$$V_{AXIAL} = \frac{n.\pi.a.b + \pi.r^2}{2.a.n + s(n-1) + 2s' + 2} \quad - - - - - \text{Equation 7:1}$$

where:

n = number of conventional tows per unit cell
a = half the length of the major axis of the conventional tow = 1mm
b = half the length of the minor axis of the conventional tow = 0.135mm
s = distance between conventional tows = 0.1mm
s' = distance between conventional tow and bound tow = 1mm
r = radius of bound tows (assumed to be circular) = 0.155mm

Substituting these values into equation 7:1, for n = 1 to 7 to simulate the fabrics, Table 7:1 is obtained.

Fabric	n	Volume per Unit Area of Axial Flow Area (mm)
DWO 126 (1:1)	1	0.12
DWO 148 (1:3)	3	0.16
DWO 149 (1:4)	4	0.17
DWO 150 (1:5)	5	0.17
DWO 151 (1:6)	6	0.18
DWO 156 (1:7)	7	0.18

Table 7:1 Volume of Axial Flow with the Individual Unit Cells

The base twill weave is not included in table 7:1 because equation 7:1 requires a slight modification due to there being no bound tows. Equation 7:2 shows the volume of axial tows per unit area in twill weave:

$$V_{AXIAL} = \frac{2.\pi.a.b}{4.a + 2s} \quad \text{------ Equation 7:2}$$

Fabric	n	Volume per Unit Area of Axial Flow Area (mm)
Base Twill	0	0.2

Table 7:2 Volume per Unit Area in Base Twill Ply

7:2:3 Percentage Transverse Flow

As there were no spiral bound tows in the transverse direction for anisotropic (0_4) lay-up, the unit cell was a constant size for all the fabrics. The transverse unit cell consisted of one conventional tow (area 'πab' and length '2a') together with one inter-tow space (length 's') . Therefore in one ply, the volume of transverse flow area per unit area of fabric is given by the Equation 7:3

$$V_{TRANSVERSE} = \frac{\pi.a.b}{2.a + s} \quad \text{------- Equation 7:3}$$

Substituting the relevant dimensions from figure 7:1 into equation 7:3, the volume of transverse tows per unit area is:

$$V_{TRANSVERSE} = 0.1944$$

This is assumed to be constant for all the fabrics.

7:2:4 Percentage Space (Large Flow Channels)

This section determines the proportion of the ply occupied by 'space available for flow' (except intra-tow space). The thickness of the ply was assumed to be double the thickness of a conventional tow (0.54mm).

Therefore by subtracting the volume per unit area of both the axial and transverse flow areas, the volume per unit area of 'space' was determined i.e.

$$V_{SPACE} = V_{TOTAL} - V_{AXIAL} - V_{TRANSVERSE} \quad \text{- - - - Equation 7:4}$$

The results of this are shown in table 7:3.

Fabric	n	Space (Large Flow Channels) mm
DWO 126	1	0.23
DWO 148	3	0.19
DWO 149	4	0.18
DWO 150	5	0.17
DWO 151	6	0.17
DWO 156	7	0.17
Base Twill	all conventional	0.14

Table 7:3 Volume of the Large Flow Channels per unit Area

The proportions of the different flow areas were then determined and are presented in Table 7:4 and illustrated in Figure 7:2

Fabric	n	% Axial Flow Area	% Transverse Flow Area	% Large Flow Area
DWO 126	1	21.46	36	42.54
DWO 148	3	29.32	36	34.69
DWO 149	4	30.91	36	33.09
DWO 150	5	32	36	32
DWO 151	6	32.76	36	31.24
DWO 156	7	33.48	36	30.52
Base Twill	0	37.4	36	26.6

Table 7:4 Percentage of Different Flow Areas Apparent in Each Fabric

The proportions of each of the categories of flow apparent in the single ply were then ready to be used in the cumulative flow model. However, before the cumulative flow could be determined for each of the fabrics, suitable equations were required to model the flow in each of the three flow areas.
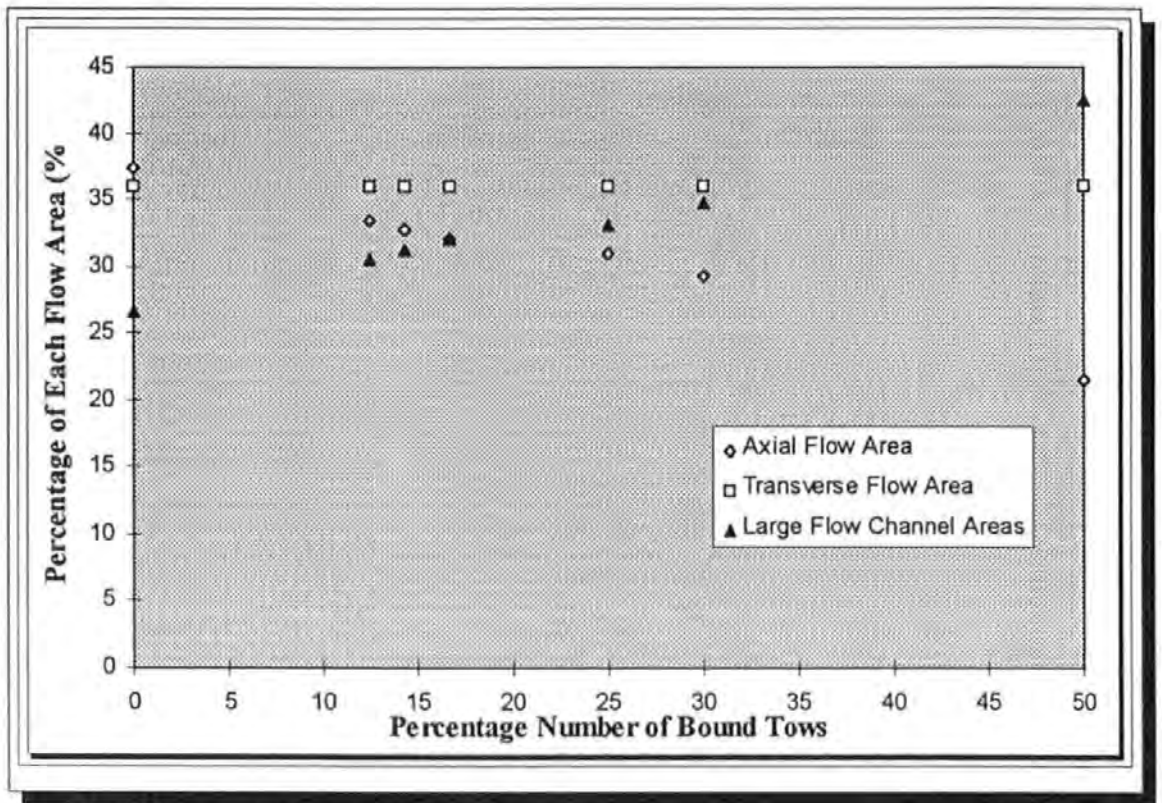
Figure 7:2 Variation in the Percentage of each Flow Mode

7:3 Modelling the Cumulative Flow

It was thought that the total flow could be predicted by the combination of the three flow models, having determined a suitable equation for each. Several equations have already been reviewed regarding axial and transverse flow in chapter 2:8 and these are repeated below:

7:3:1 Axial Permeability Equations

$$K_A = \frac{D^2}{32}\left[4 - V_f - \frac{1}{V_f}(3 + 2\ln(V_f))\right] \quad \text{- - - - - - Equation 7:5 (Happel)}$$

$$K_A = \frac{D^2 V_f}{128\pi}\left[\left(\frac{2\pi}{V_f}\right)^{\frac{1}{2}} - \left(\frac{\pi(1+\sqrt{2})}{2}\right)^{\frac{1}{2}}\right]^4 \quad \text{- - - -Equation 7:6 (Cogswell)}$$

212

$$K_A = D^2 \frac{\pi\sqrt{3}}{480} \frac{(1-V_f)}{V_f}$$ ------ Equation 7:7 (Wheeler)

$$K_A = \frac{8R^2}{c}\left(\frac{(1-V_f)^3}{V_f^2}\right)$$ -------- Equation 7:8 (Gebart)

7:3:2 Transverse Permeability Equations

$$K_T = -\frac{D^2}{32.V_f}\cdot\left[\ln(V_f) + \left(\frac{1-V_f^2}{1+V_f^2}\right)\right]$$ -------- Equation 7:9 (Happel)

$$K_T = \frac{\left[\left[\left(\frac{\pi}{V_f}\right)^{\frac{1}{2}} - \left(\frac{\pi\left(1+\sqrt{2}\right)}{2}\right)^{\frac{1}{2}}\right]^3\right]}{\left[48\left[0.58\left[\left(\frac{\pi}{V_f}\right)^{\frac{1}{2}} - \left(\frac{\pi\left(1+\sqrt{2}\right)}{2}\right)^{\frac{1}{2}}\right]\right]\left(\frac{\pi}{2\left(1+\sqrt{2}\right)}\right)^{\frac{1}{2}}\right]}$$ -Equation 7:10 (Cogswell)

$$K_T = D^2 \frac{\left[\left(\frac{2\pi}{V_f\sqrt{3}}\right)^{\frac{1}{2}} - 2\right]}{48\left(\frac{\pi\sqrt{3}}{2.V_f}\right)^{\frac{1}{2}}}$$ --------- Equation 7:11 (Wheeler)

$$K_T = c\left(\sqrt{\frac{V_{f.max}-1}{V_f}}\right)^{\frac{5}{2}}.R^2$$ ------- Equation 7:12 (Gebart)

7:4 Application to the Flow Enhancing Fabrics

The equations listed above were then individually applied to each of the fabrics to determine the permeability value for each category of flow areas. An example is presented for each flow category.

7:4:1 Transverse Permeability

According to equation 7:12, and using the volume fractions determined from the image analysis, the transverse permeability is given by

$$K_T = c \left(\sqrt{\frac{V_{f.max} - 1}{V_f}} \right)^{\frac{5}{2}} . R^2$$

where: $c = \dfrac{16}{9\pi\sqrt{6}}$ *for hexagonal packing*

$V_{f(max)} = 0.91$ *for maximum packing*

$R = Fibre\ Radius\ (\mu m) = 3.45\ x10^{-6}m$

$V_f =$ *the volume fraction within the tows* = 57% =0.57 *(from 5:12)*

Therefore, the transverse permeability equates to the following

$$K_T = 6.9\ X\ 10^{-14}\ m^2 = 0.07\ darcies$$

This is assumed to be constant for the set of fabrics under investigation

7:4:2 Axial Permeability

Using Equation 7:8 and once again using the volume fractions from the image analysis, the axial permeability is given by:

$$K_A = \frac{8R^2}{c} \left(\frac{(1 - V_f)^3}{V_f^2} \right)$$

where c= 53 (used by Gebart to model the flow channel shape)
The axial permeability equates to the following
$$K_A = 3.2\ X\ 10^{-13}\ m^2 = 0.32\ darcies$$

This figure was then multiplied by the appropriate axial flow area apparent in each of the fabrics and the values substituted into the rule of mixtures, equation 7:13.

7:4:3 Large Flow Channel Permeability

Several assumptions are made in the following calculation and these are listed.

i) the fibre tows are solid i.e. there is no cross-flow between channels and tows

ii) to simplify the calculation, the tows are assumed to be circular with an average radius of 0.15mm (the radius of a circle with a similar cross sectional area to an elliptical tow).

The laminate is, in effect, being analysed macroscopically, where the whole tow is now assumed to behave as if it were a single fibre. Therefore using equation 7:8 again, it is possible to work out the permeability of the large flow channels. Using a volume fraction of 50% i.e. (the areas of the tows in a unit cell divided by the total area of the cell) and c = 53 as before, the permeability equates to the following:

$$K_{LFC} = 1.84 \times 10^{-9} \ m^2 = 1840 \ \text{darcies}$$

7:5 Total Permeability

The section presented to the flowing resin consists of a proportion of each of the types of flow which were determined earlier in this chapter. By taking Fabric 126 with the 1:1 ratio of conventional and bound tows as an example, the total permeability is determined using a rule of mixtures of permeability, equation 7:13,

$$K_{TOTAL} = x.K_{AXIAL} + y.K_{TRANSVERSE} + z.K_{L.F.C.} \qquad \text{- - - Equation 7:13}$$

where :

x, y and z are the respective proportions of each flow area apparent in the laminate (table 7:4).

Substituting the appropriate values into equation 7:13 gives

$$K_T = 0.215 [3.2 \times 10^{-13}] + 0.36 [7.0 \times 10^{-14}] + 0.425 [1.84 \times 10^{-9}]$$

$$K_{TOTAL} = 7.70 \times 10^{-10} \text{ m}^2 = 780 \text{ darcies}$$

By altering the unit cell to cater for the increase in conventional tows (see figure 7:1), the total permeability of all the fabrics was determined by summing the three respective permeabilities as shown. Figures 7:3 and 7:4 show the respective contributions of the flow area permeabilities towards the total permeability. Figure 7:5 then illustrates the total permeability with respect to the number of spiral bound tows. It is clear that the dominant permeability is the one associated with the large flow channels while the transverse and axial permeabilities are three orders of magnitude smaller. Nevertheless these contribute significantly to the wet-out of the reinforcement and ultimately the strength of the component.
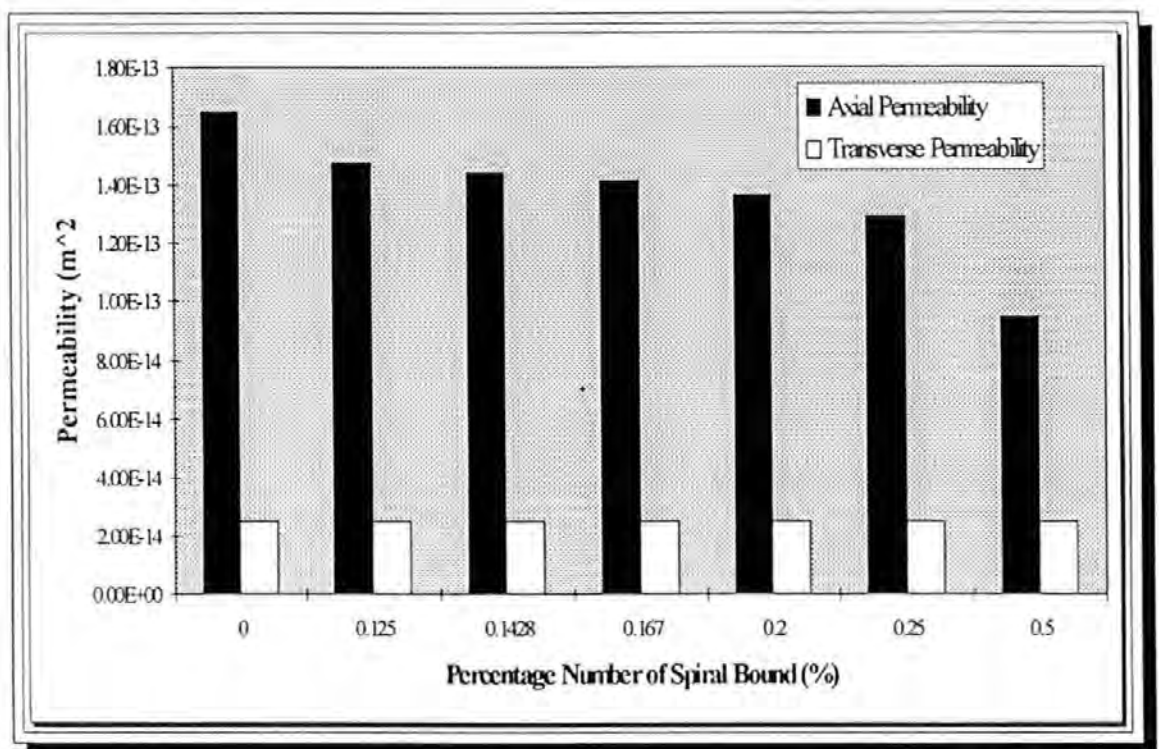
Figure 7:3 Axial and Transverse Permeability in Each of the Fabrics
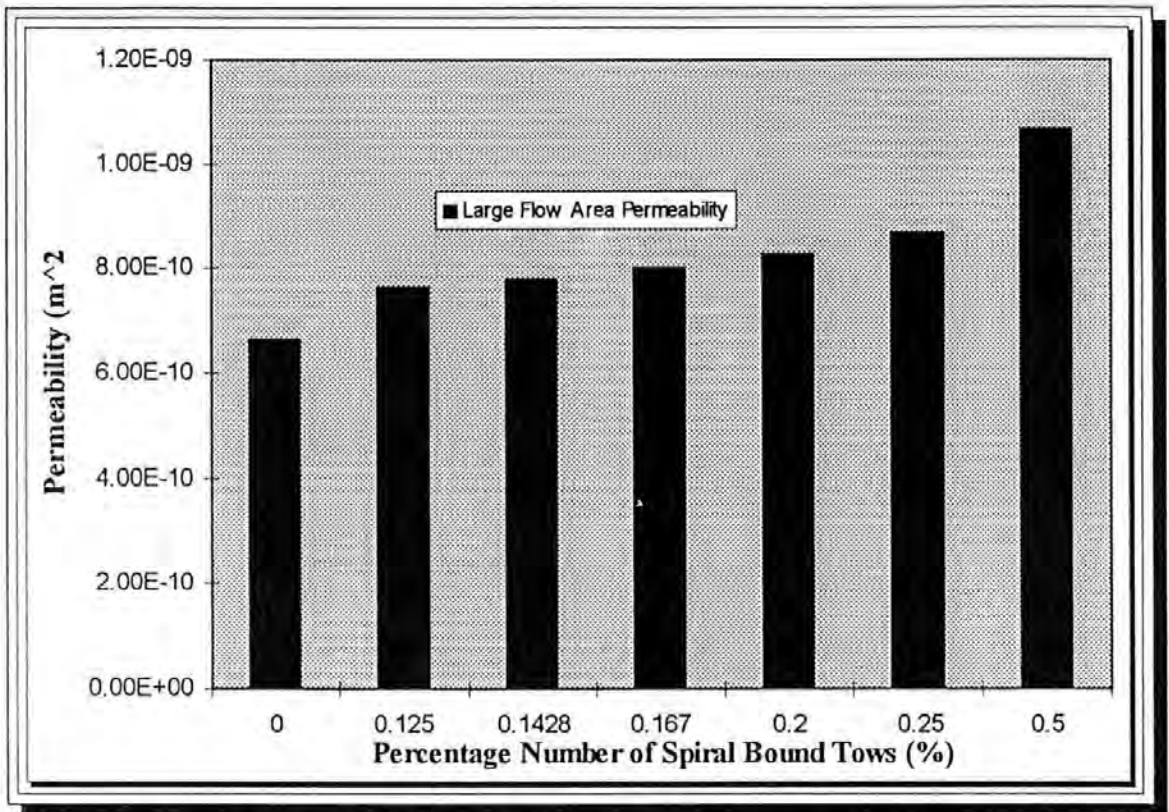
Figure 7:4 Large Flow Channel Permeability Variation with an Increase in Spiral Bound Tows
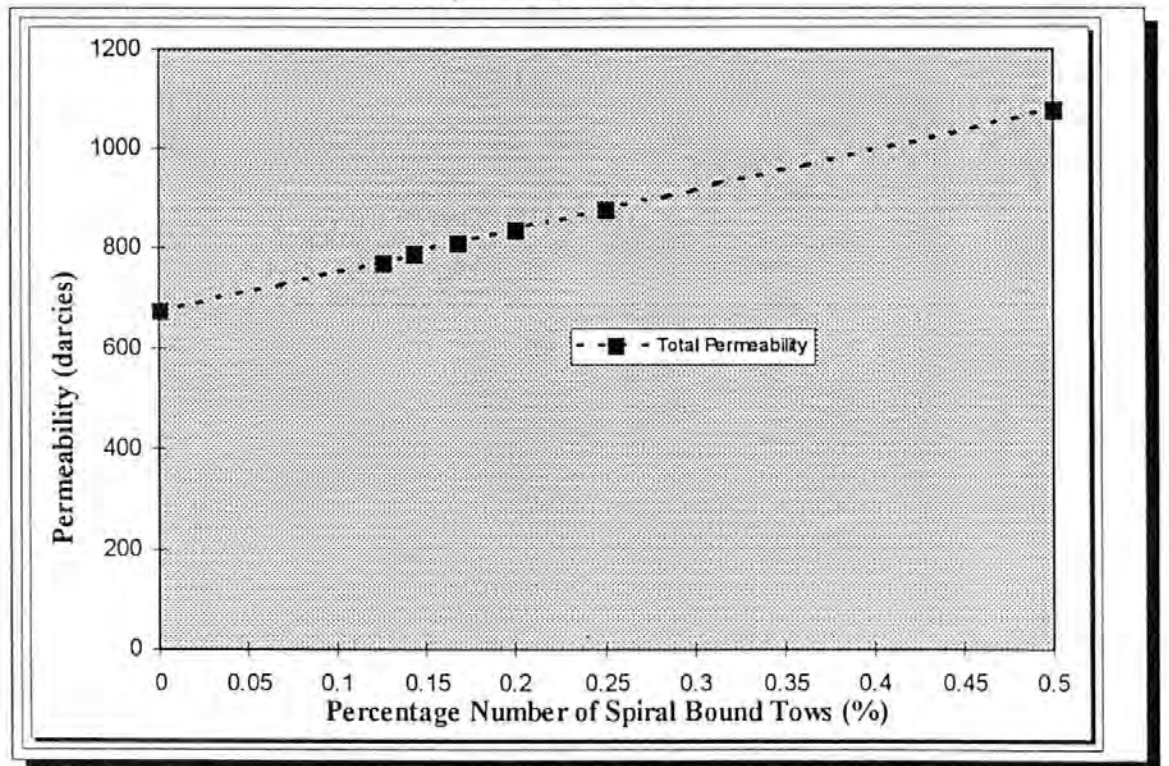
Figure 7:5 Variation of the Total Permeability with an Increase in Spiral Bound Tows

It was decided to use the equations developed by the other authors in 7:3:1

and 7:3:2 in a similar manner to compare the respective models, together with

the permeability results from Chapter 3:3 and these are illustrated in Figure 7:6.

The large flow channel permeabilities were determined in a similar fashion for

all of the models by assuming the fibre tows to be solid and hexagonally

arranged.
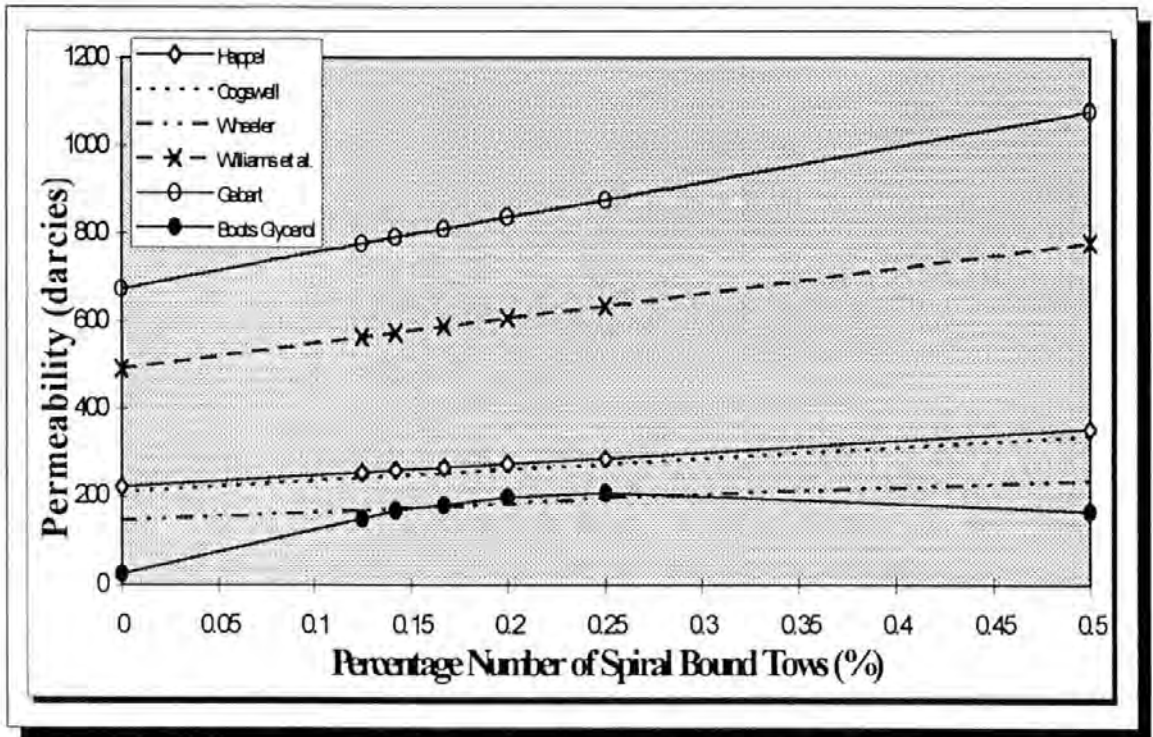
Figure 7:6 Comparison of Permeability Models and Experimental Results
for the Flow Enhancing Fabrics

The values of permeability determined using the Happel, Cogswell and

Wheeler models all show good agreement with the experimental permeability

results obtained using glycerol. Although not shown in figure 7:6, the

permeability figures using Jotun Norpol 42-10 polyester show agreement with

the Gebart model although the higher permeabilities were affected by mould

deflection and the consequent reduction in volume fraction.

In summary, the models derived from the rule of mixtures appear to show good

agreement with permeability values based on using the radial Darcy equation.

The models presented in this chapter are not dependent on RTM process variables such as injection pressure and fluid viscosity. From experience gained in the measurement of permeability, the fluid viscosity particularly proved difficult to measure accurately and appeared to be dependent upon several variables. Therefore, the methodology presented in this chapter provides a way of determining the true permeability of a fabric by using the proportions of each of the flow mechanisms.

CHAPTER 8
DISCUSSION, CONCLUSIONS
and
FUTURE DEVELOPMENT

When designing an RTM process for a component, the knowledge of the flow properties through the reinforcement has been shown to be critical. Therefore, an accurate permeability measurement for the reinforcement is an essential parameter for RTM production planning, simulation and optimisation.

The permeability of a fabric is very difficult or impossible to determine analytically and therefore experimental or semi-empirical techniques have been used extensively to measure its value. The measurement of permeability as reviewed has been shown to be susceptible to inconsistency. Several factors have been shown to affect the measured permeability and these are now discussed.

8:1 Resin Viscosity

The calculated value of permeability depends on the accurate measurement of viscosity. As the viscosity was determined from a separate sample of resin from the one used in the permeability test (see Chapter 4:5:5), inaccuracies were expected from a lack of consistent mixing producing local inhomogeneities in individual resin samples. This inhomogeneity in mixing, particularly for a polyester resin with a faster cure rate than a typical epoxy

such as Ciba Geigy LY 556, would cause a difference in cure reaction rate thus affecting the measured viscosity value.

An idea was suggested by McLeish [103] that the topological nature of thermoplastic polymer chains entangling in a random manner, may affect the resultant flow properties. An example of this phenomenon is seen with low and high density polyethylene (LDPE & HDPE) which exhibit different molecular weights. The HDPE consists of linear branching from the monomer (base molecule) whereas the LDPE has randomly positioned branches from the monomer. Tests have shown that by tuning the molecular weights of HDPE and LDPE polymers to produce identical viscosities, the resultant flow properties are very different. HDPE produces a converging flow pattern akin to Newtonian fluids whereas LDPE sets up vortices within the flow. This is believed to be caused by the difference in the molecular topologies. Work on molecular topology has so far concentrated on thermoplastics. The monomers of thermoplastics exhibit lengths of a few angstroms whereas the lengths of several thermoplastic chains have been up to a micron in length which in a typical reinforcement used in RTM is of the order of the inter fibre spaces in a single tow. The difference with thermosets is that the chains are being formed and crosslinked by chemical reaction during the injection. Since, during the injection the resin should exhibit as low a viscosity as possible, the chain size would not adversely affect the impregnation.

8:2 Glycerol Viscosity

After undertaking the permeability tests with the two glycerols (supplied by Boots and BDH Chemicals), it was observed in that both samples exhibited quite different viscosity values (Appendix 2). Shankar et al [104] have discussed the atmospheric water absorption properties of glycerol, it was likely that the viscosity of both samples may have been affected by the hygroscopic effect. As a consequence, the calculated permeability would have been affected due to the glycerol reducing in viscosity. This shows the merits of measuring the viscosity of the fluid for each permeability test. Concluding, the use of glycerol for permeability measurement is not recommended, although it is useful for understanding qualitative flow phenomena.

8:3 Permeability Tests using Different Injection Fluids

The permeability tests conducted on the flow enhancing fabrics (Chapter 3:3) exhibited a marked difference in values produced for specific lay-ups using different injection fluids. Initially, it was thought that the viscosity values of the fluids were contributing to this large difference and therefore the separate injections were analysed with respect to their flow rates thus removing the viscosity dependency. Appendix 6 shows the individual flow rates for all the injections with respect to the injection fluids. These flow rates support the permeability values in that the larger flow rates were associated with the higher permeability values. Further support of this variation was provided by Steenkamer et al. [105] who tested two specific reinforcements using a range

of oils (corn and silicone) and polyester resins and obtained a variation for each fluid. It has been found that with different resins that the measured permeability varies. It is therefore recommended that permeability values which are used for simulation purposes are determined using a similar resin to the actual component mould being simulated.

8:4 Fabric Layer Nesting

The woven fabrics for which permeability was measured consisted of tows ranging from 2000 (2k) to 6000 (6k) filaments. As a result of handling, some of the tows are likely to become misaligned during lay-up and therefore did not lie in phase (i.e. tows in layers lying in the valleys of adjacent layers) with neighbouring layers. Upon closure of the mould, small localised areas of high and low volume fraction would be produced above or below the nominal design volume fraction. As a result, the impregnation would be affected by varying resistance to flow encountered within the fibre pack. This effect was thought to be present in most of the fibre lay-ups tested. It may average out over the mould but initially has a large effect on the flow.

8:5 Mould Compression and Deflection

The compression force required to close the mould produced mould deflection, resulting in a lower volume fraction than intended in the central regions of the mould. As observed in Chapter 4:4, the mould deflection rose with an increase in the number of spiral bound tows included in the fabric. This was thought to be due to the resistance of the twisted tows to crushing under the compressive

load because of the spiral binding. As a result, the permeabilities were affected as the average volume fractions of the moulded plates differed from the nominal design volume fraction. Pearce et al.[106] showed that the compression force required to close the mould reduced quite considerably by clamping, opening and reclamping the fibre pack due to the relaxation of the fibres.This strategy is recommended for permeability measurement and also manufacturing to reduce mould deflection.

8:6 Process Flow Phenomena

During the impregnation of the fibre pack, it was noticed that the initial percolation of the fluid into the reinforcement affected the final value of permeability obtained. This initial flow was thought to be affected by the distribution of the fibres directly above the inlet port. For instance, if there was a local region of lower volume fraction above the inlet, the impregnating fluid would initially flow at a faster rate than if a higher volume fraction. This initial variation in flow is shown well in Appendix 1:2. Although in manufacturing it would not be appropriate, the initial variation was reduced by the introduction of a punched hole in the fibre pack above the inlet.

After discussing the problems of the lack of repeatability with permeability measurement, it is recommended that the measurement technique be standardised. Therefore, at present, for two-dimensional flow only, two methods of measurement are proposed.

i) Linear Flow Front
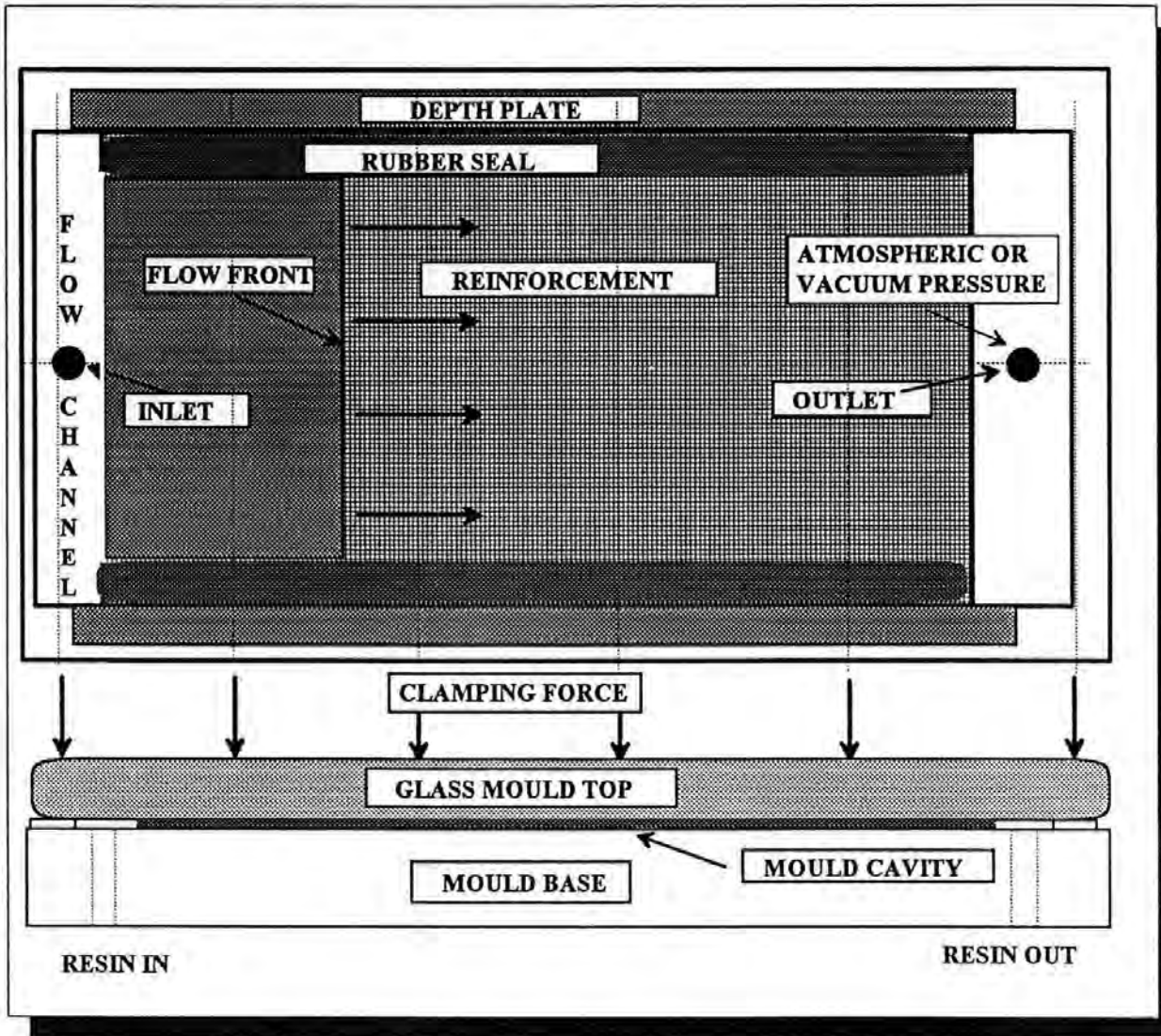
Figure 8:1 Schematic Diagram of Proposed Linear Flow Permeameter

This method uses a two port mould arrangement as shown schematically in Figure 8:1. The resin is introduced at constant pressure into the mould where a flow channel distributes the resin to produce the linear flow front. To reduce edge effects, the fibres are laid between two rubber strips, which compress and seal the side of the fibre pack when the mould is closed.

ii) Radial Flow Front

This method uses a single central injection port with a cavity similar to Figure 3:13 in Chapter 3. The reinforcement is laid on the mould between the depth

plates which dictate the thickness of the cavity and hence the volume fraction of the laminate. The glass is then clamped to the depth plates. As discussed, the actual volume fraction of fibres being impregnated is difficult to measure where mould bow occurs. Therefore, a solution to the problem of mould bow is required in the mould design stage. A steel frame may be used with care as the compression loads on the glass may cause catastrophic fracture.
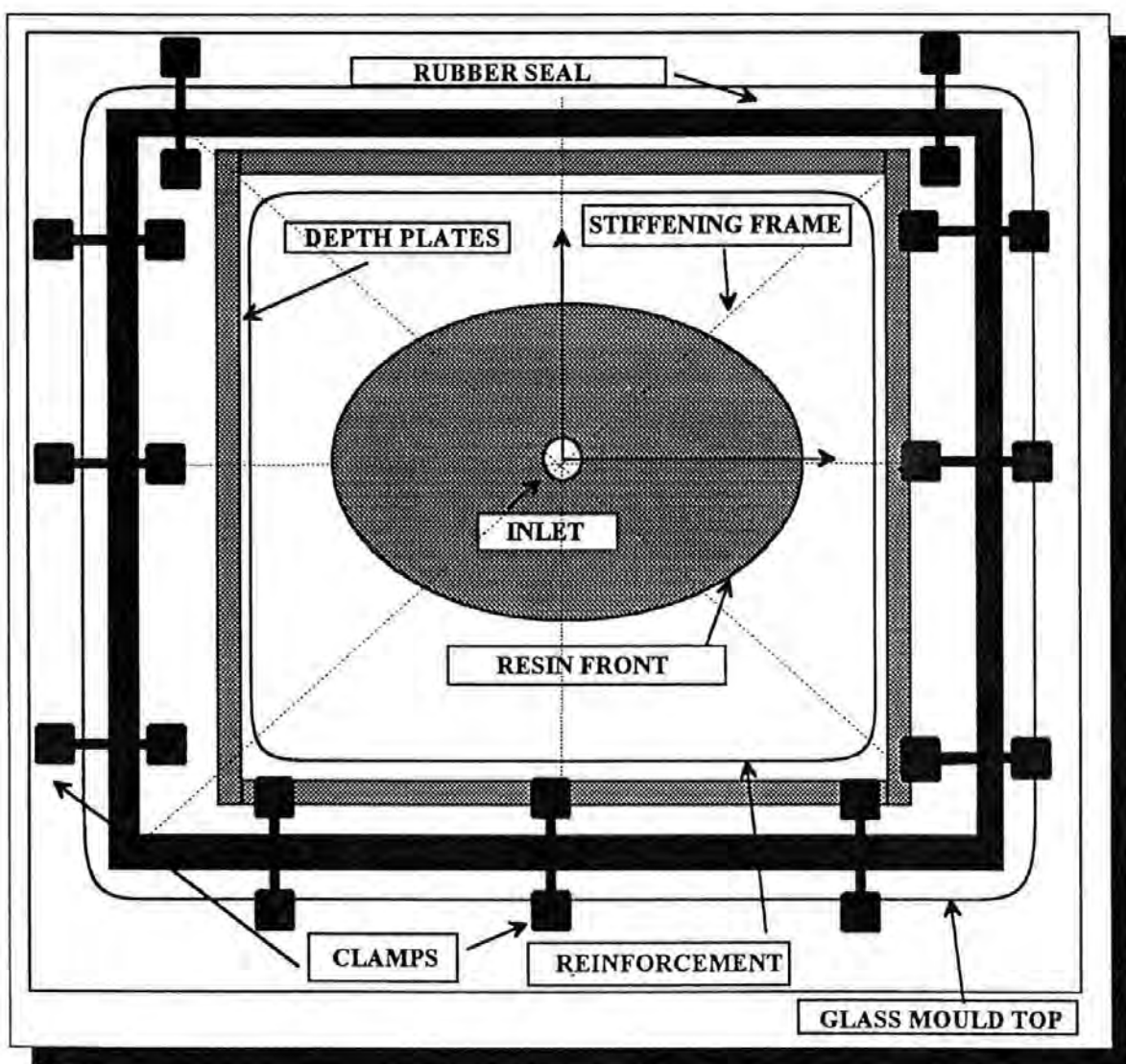
Figure 8:2 Schematic Diagram of Radial Flow Permeameter

8:7 Image Analysis

The results of the investigations of the flow channels in the laminates by image analysis displayed good correlation with the corresponding permeability values

obtained. Both the fixed area and unit cell methods of investigation showed an increase in the flow area detected with an increase in the number of spiral bound tows. The unit cell method is more versatile due to the fact that it considers a specific amount of tows according to the weave rather than considering a random fixed area of investigation. The fixed area investigation would be a suitable method for standard weaves with uniform size and frequency of tows with no bound tows as the unit cell does not vary. In conclusion, image analysis may be used in conjunction with the permeability tests to optimise the flow properties of reinforcements and preforms.

8:8 Mechanical Properties

A very important aspect of the work, hitherto unconsidered is the effect on the mechanical properties caused by the inclusion of bound tows. Basford et al. [107] reported a decrease in both compression and inter-laminar shear (ILSS) as the number of bound tows increased as shown in Figure 8:3.
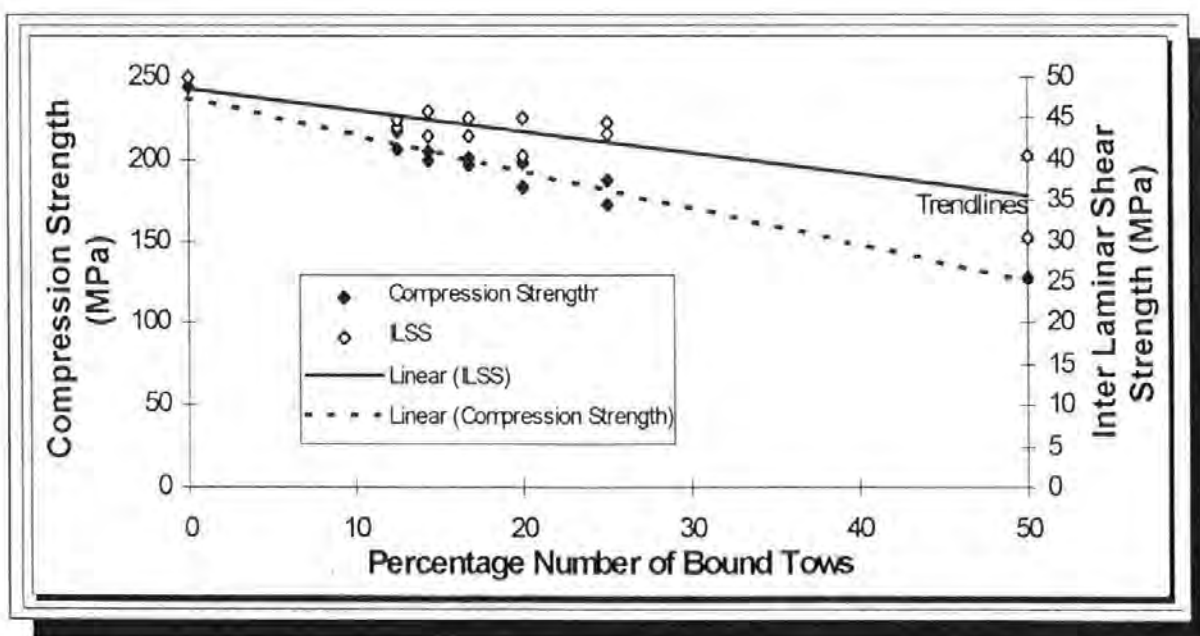
Figure 8:3 Compression and Inter-Laminar Shear Strengths of the Laminates

Compression tests were undertaken in accordance with CRAG method 418 on an Instron 1175 Universal Testing Machine (S/N H0525) calibrated to BS1610:1985 Grade 1 while the ILSS tests were carried out in accordance with CRAG method 100. Results which are discussed in Appendix 7 showed for example, that with the minimum amount of spiral bound tows, the compression strength reduced from 245kPa for twill fabric to 218kPa for Fabric 156 (1:7 ratio of bound to conventional tows) and the corresponding inter-laminar shear strength reduced from 49.9MPa to 44MPa. Therefore, the improvement in processing characteristics produced by the inclusion of spiral bound tows is compromised by the reduction in mechanical properties. Further modifications to the reinforcement are therefore required to optimise the mechanical properties as well as improving the processability of the fabrics.

8:9 Conclusions

. The importance of representing the permeability of a fabric reinforcement accurately has been shown. The RTM simulations discussed and developed in references [108-115] all rely heavily on accurate permeability measurements in order to predict the passage of resin through a fibre pack. All the simulations showed deviation from the actual injection due to inaccurate permeability data. The permeability tests conducted in future require a simultaneous viscosity test with the same resin sample at a fixed temperature similar to the mould temperature. Although this is more time-consuming, it alleviates the variation in viscosity detected from sample to sample. In order to simulate the process

accurately, resins are required for permeability tests rather than resin models such as glycerol due to the fact that large differences in permeability are obtained for different fluids on similar fibre packs.

8:10 Future Development

The image analysis technique has been shown to distinguish slight differences in reinforcement construction according to their respective flow channel areas. To further this work and to test the versatility and sensitivity of the technique, it would be interesting to investigate the following topics to determine if the method would

i) distinguish between different weaves with a similar tow size

(i.e. plain / twill)

ii) distinguish between a specific weave with different tow sizes

(3k, 6k, 10k)

With regard to the flow enhancing fabrics, a number of research programs are ongoing at the University of Plymouth based on the work in this thesis into optimising the flow properties of reinforcements without reducing the mechanical properties. A new fabric is being woven with a mixture of tow sizes with smaller bound tows replacing the larger bound tows previously. This is expected to produce more smaller flow channels, thus not compromising the mechanical properties. A paper in preparation by Guild et al [116] introduces the proposed modifications to the reinforcements.

References

1. R.A.Higgins " The Properties of Engineering Materials"
    Published by Hodder and Stoughton. London 1977 pp 296-301

2. L.Mir, E.Leblond, H.Auduc, G.Bazerque "RTM-A Process for
    Aircraft Structural Composite Parts" Proceedings of the 15th
    International Conference of SAMPE,Toulouse, June 8-10 1994
    pp171-180

3. J.M.Berthier, J.Saporito "Development of Organic Matrix Composites
    in Helicopters" Proceedings of the 15th International Conference of
    SAMPE, Toulouse, June 8-10 1994. pp213-220

4. W.D.Bascom "Structure of Silane Adhesion Promoter Films on Glass
    and Metal Surfaces" Macromolecules Volume 5 1972. p.792

5. D.Hull "An Introduction to Composite Materials"
    Cambridge University Press, Cambridge 1981

6. N.C.W.Judd, W.W.Wright "Which Resin for Reinforced Plastics"
    Reinforced Plastics Vol.22 Feb 1978 pp39-

7. J.M.Guillemot "Composite Materials for New Generation Railways"
    Proceedings of the 15th International Conference of SAMPE, Toulouse,
    June 8-10 1994. pp255-262

8. M.Cleon "Feasibility of a Rail Car Structure in Composites for Trains
    of the Future operating at >350 kmh" Proceedings of the 15th
    International Conference of SAMPE,Toulouse,June 8-10 1994
    pp 235-254

9. K.B.Spaulding   "Fibre Glass Boats in Naval Service"
    U.S. Naval Engineers Journal. Vol.78 April 1966. pp 333-340

10. T.M.Gotch   "Developments and Potential of Vacuum Impregnation
    Techniques for GRP Manufacture"
    12th BPF Reinforced Plastics Congress Nov.25-27. 1980 pp25-34

11. M.Sudol "RTM Volume Production for Automotive Composites" BPF
    Composites '94 Congress. Nov. 22-23rd Nov 1994 Paper 7

12. A.T.Echermeyer, R.F.Pinzelli, K.B.Raybould, N.Skomedal
    "Advanced Composite Hull Structures for High Speed Craft"
    Proceedings of the 15th International Conference of SAMPE, Toulouse,
    June 8-10 1994. pp299-318

13. R.J.Bland, A.R.Harper, S.M.Grove "RTM Automation - The
    Building Blocks" Proceedings 50th Annual Technical Conference.
    SPI Composite Institute, Cincinatti, Jan 1995

14. H.G.P.Darcy "Les Fontaines Publiques de la Ville de Dijon"
    Published in 1856 in Paris. Edited by Victor Dalmont

15. A.J.E.J.Dupuit "Etudes theoriques et pratiques sur le
    mouvement des eaux" 2nd Edition, Dunod, Paris 1863.

16. P.C.Carman   "Flow of Gases through Porous Media"
    Butterworth Scientific Publications. London 1956

17. **M.Muskat** "Flow of Homogeneous Fluids through Porous Media"
McGraw Hill, New York 1937

18. **W.E.Johnson, R.V. Hughes** "Directional Permeability Measurements
and their significance" Bull.Miner.Ind.Exp.Sta.
Vol.52. No.180. 1948 pp 54

19. **B.T.Astrom, R.B.Pipes, S.G.Advani** "On Flow through Aligned Fibre
Beds and its Application to Composites Processing"
Journal of Composite Materials Vol.26, No.9. 1992 pp 1351-1373

20. **R.B.Pipes** "Anisotropic Viscosities of an Oriented Fibre Composite
with a Power-Law Matrix"
Journal of Composite Materials Vol.26,No.10 1992 pp1536-1552

21. **J.E.Drummond, M.I.Tahir** "Laminar Viscous Flow through Regular
Arrays of Parallel Solid Cylinders"
Int.J.Multiphase Flow Vol.10. No.5 1984 pp515-540

22. **E.M.Sparrow, A.L.Loeffler** "Longitudinal Laminar Flow between
Cylinders Arranged in a Regular Array"
Trans. Amer. Inst. Chem. Engrs. Vol.5 No.3 1959 pp 325-330

23. **C.S.Slichter** 19th Annual Report Part 2
U.S. Geology Survey, 1899 pp.295

24. **F.C.Blake** "The Resistance of Packing to Fluid Flow"
Transactions of the Institution of Chemical Engineers
1922 , No.14 pp 415- 421

25. **T.E.Stanton, J.R.Pannell**
Coll.Research National Physical Laboratory, London, 1914

26. **L.Schiller** "Uber den Stromungswiderstand von Rohren Verschiedenen
Querschmitts und Rauhigkeitsgrades" Z. Angew. Math. Mech. 1923.
Vol.3 No.2 pp 2-13

27. **J.Kozeny** "The Capillary Action of Water in Soil" Sitzungsberichte
Akademie Wissenschaft Wien Math-Naturw 1927 Vol..136 pp 271-306

28. **R.R.Sullivan** "Further Study of the Flow of Air through Porous Media"
Journal of Applied Physics 1941 Vol.12 pp 503-508

29. **F.E.Bartell, H.J.Osterhoff** Journal of Physical Chemistry. 1928
Vol. 32 pp 1553

30. **P.C.Carman** "Fluid Flow through Granular Beds"
Transactions of the Institution of Chemical Engineers (London) 1937
Volume 15, pp150-166

31. **H.E.Rose** "An Investigation into the Laws of Flow of Fluids through
Beds of Granular Materials" Applied Mechanics Vol 153
1945 pp 145-162

32. **F.A.L.Dullien** "Single Phase Flow through Porous Media and Pore
Structure" The Chemical Engineering Journal 1975 Volume 10 pp1-34

33. **E.J.Carter, A.W.Fell, J.Summerscales** "The Permeability of
Reinforcement Fabrics Part 1: A Simplified Model for the Derivation of
the Permeability Tensor of an Anisotropic Fibre Bed"
Composites Manufacturing 1995 Volume 6 No.3/4 pp 228-234

34. **B.R.Gebart** "Permeability of Unidirectional Reinforcements for RTM" Journal of Composite Materials, 1992, Vol 26, No.8, pp 1100-1133

35. **H.Schlichting** "Boundary Layer Theory" 7th Edition. McGraw Hill New York 1979

36. **J.G.Williams, C.E.M.Morris, B.C.Ennis** "Liquid Flow through Aligned Fibre Beds" Polymer Engineering and Science 1974. Volume 14. Part 6. pp 413-419

37. **R.G.Latini** "Measurement of Directional Permeabilities" M.S. Thesis. Dept of Chemical Engineering and Metallurgy. Syracuse University. 1967

38. **G.H.Fancher, J.A.Lewis, K.B.Barnes** "Some Physical Characteristics of Oil Sands" Bull.Miner.Ind.Exp.Sta. Volume 12. 1933

39. **W.E.Johnson, R.V. Hughes** "Directional Permeability Measurements and their significance" Bull.Miner.Ind.Exp.Sta. Vol.52. No.180. 1948 pp 49-50

40. **D.Fontugne** "Permeability Measurement in Anisotropic Media" M.S. Thesis. Dept of Chemical Engineering and Metallurgy. Syracuse University. 1969

41. **K.N.Kendall** "Mould Design for High Volume Resin Transfer Moulding"Ph.D Thesis, University of Nottingham 1991

42. **K.van Harten** "Production by Resin Transfer Moulding" W.E.G.E.M.T. 18th Graduate School 22-26th March 1993 pp106-111

43. **A.S.Verheus, J.H.A.Peeters** "The Role of Reinforcement Permeability in Resin Transfer Moulding" Composites Manufacturing March 1993 Volume 4 Part 1, pp 33-38

44. **L.Trevino, K.Rupel, W.B.Young, M.J.Liou, L.J.Lee** "Analysis of Resin Injection Moulding in Moulds with preplaced Fibre Mats i)Permeability and Compressibility Measurements" Polymer Composites Feb 1991 Vol.12 No.1 pp 20-29

45. **M.J.Perry, T.J.Wang, Y.Ma, L.J.Lee** "Resin Transfer Moulding of Epoxy / Graphite Composites" 24th International SAMPE Technical Conference. Toronto Oct 20-22 1992

46. **K.J.Ahn, J.C.Seferis, J.C.Berg** "Simultaneous Measurements of Permeability and Capillary Pressure of Thermosetting Matrices in Woven Fabric Reinforcements" Polymer Composites June 1991. Vol 12. No. 3

47. **K.L.Adams, L.Rebenfeld** "In-Plane Flow of Fluids in Fabrics:Structure/ Flow Characterisation" Textile Research Journal 1987. Vol 57. pp647-654

48. **S.M.Montgomery, K.L.Adams, L.Rebenfeld** "Directional In-Plane Permeabilities of Geotextiles" Geotextiles and Geomembranes 1988 Vol.7, pp 275 -292

49. **S.M.Montgomery, B.Miller, L.Rebenfeld**
"Spatial Distribution of Local Permeabilities in Fibrous Networks"
Textile Research Journal, March 1992. Vol.62 No.3. pp 151-161

50. **B.R.Gebart, L.A.Strombeck, C.Y.Lundemo**
"Permeability of Reinforcenment Materials for RTM"
6th Annual Meeting Polymer Processing Society, Nice, France
Apr 17-20 1990

51. **Unifilo U-750 Data Sheet for Preforming**
published by Vetrotex International, St.Gobain 1987

52. **A.S.Verheus** "The Role of Reinforcement Permeability in Resin
Transfer Moulding" TNO Plastics and Rubber Institute
(same as reference 43)

53. **J.P.Fannucci, Y.R.Kim, C.Koppernaes, S.C.Nolet**
"Product and Process Development of 1000 foot Underwater Towed
Cable System" American Composites Technology Inc.1991 pp 243-261

54. **K.van Harten** "Production by Resin Transfer Moulding"
W.E.G.E.M.T. 18th Graduate School 22-26th March 1993 pp 96-103

55. **G.Q.Martin, J.S.Son** "Fluid Mechanics of Mold Filling for Fibre
Reinforced Plastics" Advanced Composites:The Latest Developments
Nov 1986, pp 149-157

56. **J.M.Thirion, H.Girardy, U.Waldwogel** "New Developments in Resin
Transfer Moulding of High Performance Composite Parts"
Composites, Paris 1988, Volume 28, No.3, pp 81-84

57. **R.C.Lam, J.L.Kardos** "The Flow of Resin through Aligned and
Cross-plied fibre beds during Processing of Composites"
Polymer Material Science Engineering 1988 Vol.59, pp 1190-1195

58. **T.G.Gutowski, Z.Cai, S.Bauer, D.Boucher, J.Kingery, S.Wineman**
"Consolidation Experiments for Laminate Composites"
Journal of Composite Materials Vol.21 July 1987 pp650-669

59. **L.Skartsis, B.Khomami, J.L.Kardos** "Resin Flow through Fibre Beds
during Composite Manufacturing Processes. Part II: Numerical and
Experimental Studies of Newtonian Flow through Ideal and Actual Fibre
Beds" Polymer Engineering and Science"
Feb 1992 Vol.32 No.4 pp 231-239

60. **K.L.Hatch** "Textile Science" West Publishing Company 1993

61. **F.K.Ko** "Advanced Textile Structural Composites"
Advanced Topics in Materials Science and Engineering
Plenum Press, New York 1993

62. **A.Newton, C.Georgallides, M.P.Ansell** "A Geometrical Model for
a 2 Layer Woven Composite-Reinforcement Fabric "
Microscopy of Materials II,
University Museum, Oxford 11-13 Apr 1994

63. **N.A.Shibata, A.Nishimum, T.Norita**
SAMPE Quarterly July 1976 Vol.25

64. **ASTM Standard D4032-82 (07:01)** "Test Method for Stiffness of Fabrics by the Circular Bend Procedure" 1982

65. **BS 3356 (1990)** "Method for the Determination of the Bending Length and Flexural Rigidity of Fabrics"

66. **BS 5058 (1986)** "Method for the Assessmant of the Drape of Fabrics"

67. **S.M.Grove, A.J.Lewis** "Resin Transfer Moulding of Ballistic GFRP Panels" Confidential Report for the DRA, University of Plymouth 1993.

68. **W.Rose, P.A.Witherspoon** "Trapping Oil in a Pore Doublet" Producers Monthly Dec 1956, Vol 20 pp 32-37

69. **F.A.L.Dullien** "Characterisation of Porous Media - Pore Level" Transport in Porous Media 1991 Vol.6, pp 581-606

70. **A.B.Wheeler** "Modelling the Flow of Fibre Reinforced Materials" Ph.D Thesis. University College of Wales, Aberystwyth 1991

71. **J.Happel** "Viscous Flow Relative to Arrays of Cylinders" Transactions of the American Institute of Chemical Engineers Vol.5, No.2 1959. pp174-177

72. **F.N.Cogswell** "Percolation Through and Along Fibrous Beds" ICI New Science Group Paper 52/86, 1986

73. **B.Astrom, R.B.Pipes, S.G.Advani** "On Flow through Aligned Fibre Beds and its Application to Composite Processing" Journal of Composite Materials, Vol.26, No.9. 1992. pp 1351 - 1373

74. **R.R.Sullivan** "Specific Surface Measurements on Compact Bundles of Parallel Fibres" Journal of Applied Physics Vol.13 Nov 1942 pp725-730

75. **S.L.Anderson, F.L.Warburton** "The Porous Plug and Fibre Diameter Measurement Effect of Fibre Orientation and Use of Plugs of Randomised Fibres" Journal of the Textile Institute Transactions 1949 Part 40 pp T749-T758

76. **M.M.Roy, R.R.Mukherjee,M.K.Sen** "The Air Flow Method of Measuring the Specific Surface of Jute" Journal of the Textile Institute Transactions 1950 Part 41 pp T249-T254

77. **J.Summerscales** "A Model for the Effect of Fibre Clustering on the Flow Rate in Resin Transfer Moulding" Composites Manufacturing, Vol.4 No.1 1993 pp 27-31

78. **A.G.Gibson J.-A.Manson** "Impregnation Technology for Thermoplastic Matrix Composites Composites Manufacturing Vol.3 Pt.4 1992 pp 223-233

79. **R.Dave** "A Unified Approach to Modelling Resin Flow During Composite Processing" Journal of Composite Materials, Jan 1990, Vol.24. pp 22-41

80. **J.C.Melrose, C.F.Brander** The Journal of Canadian Petroleum Technology Vol.13 No.54 1974

81. **M.Connor, S.Toll, J.A-E Manson** "On Surface Energy Effects in Composite Impregnation and Consolidation" Conference of Flow Processes in Composite Materials, July 7-9th 1994 Composites Manufacturing. 1995 Volume 6 No.3/4 pp 289-295

82. **R.S.Parnas, F.R.Phelan Jr**
    "The Effect of Heterogeneous Porous Media on Mold Filling in RTM"
    SAMPE Quarterley Vol.22 No.2 January 1991   pp53-60

83. **T.Al-Fariss, K.L.Pinder** "Flow through Porous Media of a
    Shear-Thinning Liquid with Yield Stress" The Canadian Journal of
    Chemical Engineering, June 1987. Vol.65

84. **E.H.Wissler** "Viscoelastic Effects in the Flow of Non-Newtonian
    Fluids through a Porous Medium" Industrial Chemical Engineering
    Fundamentals Vol.10. No.3 1971 pp 411-417

85. **M.B.Roller** "Rheology of Curing Thermosets- A Review" Polymer
    Engineering and Science" March 1986 Vol.26. No.6, pp 432- 440

86. **M.B.Roller** "Characterisation of the Time-Temperature Behaviour of
    Curing B-staged Epoxy Resin" Polymer Engineering and Science,
    June 1975, Vol.15, No.6. pp 406-414

87. **R.Gauvin, M.Chibani, P.Lafontaine** "The Modelling of Pressure
    Distribution in Resin Transfer Moulding" Journal of Reinforced Plastics
    and Composites Vol.6 Oct 1987 pp 367-377

88. **N.Epstein,** "On Tortuosity and the Tortuosity Factor in Flow and
    Diffusion through Porous Media" Chemical Engineering Science 1989,
    Vol.44 No.3 pp779-779

89. **C.D.Rudd** "Preform Processing for High Volume Resin Transfer
    Moulding" Ph.D Thesis University of Nottingham Sept 1989

90. **M.R.Groleau and M.T.Bishop** "Modelling of Viscosity Profiles and a
    Novel Method for Evaluation of Resin Transfer Moulding Processability
    for Thermoset Resins" 24th International SAMPE Technical Conference
    Toronto Oct 20-22 1992

91. **P.R.Griffin, A.J.Lewis, S.M.Grove, D.Short**
    "Flow Visualisation in Resin Transfer Moulding" 3rd International
    Proceedings of the Conference of Flow Processes in Composite
    Materials, University College Galway. July 7-9th 1994

92. **Araldite MY 750 Data Sheet**, Ciba Geigy Instruction Sheet C.35b
    (Resin now renumbered LY556 but still uses HY917 Hardener and
    DY070 Accelerator)

93. **D.R.Surphlis** "An Experimental Analysis of the Pressures Induced
    within a Mould during Resin Transfer Moulding (RTM)"
    B.Eng(Hons) Final Year Project,SMMME, University of Plymouth.1991

94. **P.G.MacKenzie** "An Experimental Analysis of Pressure within a Mould
    during Resin Transfer Moulding" B.Eng(Hons) Final Year Project,
    SMMME, University of Plymouth.1992

95. **Image Analysis - Principles and Practice**, A Technical Handbook
    published by Joyce Loebl. Gateshead 1985. ISBN 0951070800

96. **A.Flook, S.Brown** "Automatic Witness Plate Analysis"
    Quantimet New Review No.8 pp 6-7 Oct 93

97. **D.Wright** "Detection of Pollution Damage to Fish Livers"
    Quantimet News Review No7 pp10-11 Jan 93

98. **P.Russell, D.Wright, A.K.Moss** "The Measurement of Pores in an Irregular Surface" Quantimet News Review No.8 pp 4-5 Oct 93

99 **F.J.Guild, J.Summerscales** "Microstructural Image Analysis applied to Fibre Composite Materials : A Review"
Composites Vol.24 No.5 1993. pp 383-393

100. **N.A.Vrettos, H.Imakoma, M.Okazaki**
"Characterisation of Porous Media by means of the Voronoi-Delaunay Tessellation" Chemical Engineering Processes 1989 Vol.25 pp35-45

101. **N.A.Vrettos, H.Imakoma, M.Okazaki**
"Transport Properties of Porous Media for the Microgeometry of a 3-D Voronoi Network"
Chemical Engineering Processes 1989 Vol.26 pp 237-246

102. **P.R.Griffin, S.M.Grove, J.Summerscales, F.J.Guild, P.Russell, E.Taylor, D.Short** "The Effect of Reinforcement Architecture on the Long Range Flow in Fibrous Reinforcments"
Conference of Flow Processes in Composite Materials, July 7-9th 1994
Composites Manufacturing, 1995 Volume 6 Parts 3&4, pp 231-235

103. **T.McLeish** "On the Trail of Topological Fluids"
Physics World Volume 8. No.3 March 1995 pp32-37

104. **P.N.Shankar, M.Kumar** "Experimental Determination of the Kinematic Viscosity of Glycerol Water Mixtures"
Proc.Roy. Soc. London. 8th March 1994 A444 (1922) pp 573-582

105. **D.A.Steenkamer, D.J.Wilkins, V.M.Karbhari** "Influence of Test Fluid on Fabric Permeability Measurements and Implications for Processing of Liquid Moulded Composites" Journal of Materials Science Letters, 1st July 1993 Volume 12 No.13 pp 971-973

106. **N.R.L.Pearce, J.Summerscales**
"The Compressibility of a Reinforcement Fabric"
Composites Manufacturing Vol.6 No.1 1995 pp15-21

107. **D.M.Basford, P.R.Griffin, S.M.Grove, J.Summerscales**
"The Relationship between Mechanical Performance and Microstructure in Composites Fabricated with Flow Enhancing Fabrics"
Composites Vol. 25 No.9, Sept 1995 pp 675-679

108. **F.Trochu, R.Gauvin** "Limitations of a Boundary Fitted Finite Difference Method for the Simulation of the Resin Transfer Moulding Process" Journal of Reinforced Plastics and Composites
Vol.11 July 1992 pp 772-786

109. **R.Gauvin, F.Trochu, J.-F.Boudreault, P.Carreau**
"Finite Element Simulation of the Resin Transfer Moulding Process"
Proceedings of the 6th European Conference of Composite Materials
Bordeaux, France 20-24 Sept 1993 pp 57-62

110. **M.V.Bruschke, S.G.Advani**
"RTM:Filling Simulation of Complex Three Dimensional Shell-Like Structures"
SAMPE Quarterly Vol.23 No.1 Oct 1991 pp 2-11

111. **S.Li, R.Gauvin**
"Numerical Analysis of the Resin Flow in Resin Transfer Moulding"
Journal of Reinforced Plastics and Composites
Vol.10 May 1991 pp 314-327

112. **F.Trochu, R.Gauvin, D.-M.Gao**
"Numerical Analysis of the Resin Transfer Moulding Process by the
Finite Element Method"
Advances in Polymer Technology Vol.12 No.4 1993 pp 329-342

113. **Z.Cai** "Simplified Mould Filling Simulation in
Resin Transfer Moulding" Journal of Composite Materials"
Vol.26 No.17 1992 pp 2606-2630

114. **R.Gauvin, F.Trochu, S.Li**
"Numerical and Experimental Analysis of the Resin Flow in Resin
Transfer Moulding"
International Conference on Automated Composites. Oct 1991

115. **S.G.Advani, M.V.Bruschke, R.S.Parnas**
"Resin Transfer Moulding Phenomena in Polymeric Composites"
Flow and Rheology in Polymer Composites Manufacturing
(edited by S.G.Advani) Ch.12 pp 465-515 1994 Elsevier Science

116 **F.J.Guild, N.R.L.Pearce, P.R.Griffin, J.Summerscales**
"Optimisation of Reinforcement Fabrics for the Resin Transfer Moulding
of High Fibre Volume Fraction Composites"
proposed paper for ECCM 7, London, May 1996

APPENDIX 1

Glycerol and Resin Front Progressions during the Permeability Measurement Testing

A1:1 Vacuum Impregnation using Glycerol

    A1:1:1 Vacuum Impregnation of Various Reinforcements in a Rigid Mould

    A1:1:2 Vacuum Impregnation of Plain Weave Lay-ups under a Vacuum Bag

A1:2 Injection of MY750 Resin System into Various Plain Weave Lay-ups

    A1:2:1 Vol. Fraction =52%, Areal Wt.=345g/m^2,Thickness=2.12mm

    A1:2:2 Vol. Fraction =52%, Areal Wt.=345g/m^2,**Thickness=4.24mm**

    A1:2:3 Vol. Fraction =52%, Areal Wt.=345g/m^2,**Thickness=6.36mm**

    A1:2:4 Vol. Fraction =52%, Areal **Wt.=220g/m^2**,Thickness=2.12mm

    A1:2:5 **Vol. Fraction =39%, Areal** Wt.=345g/m^2,Thickness=2.12mm

A1:3 Glycerol and Resin Progression through Flow Enhancing Weaves

    A1:3:1   Base Twill

    A1:3:2   DWO 126 (1:1)

    A1:3:3   DWO 148 (1:3)

    A1:3:4   DWO 149 (1:4)

    A1:3:5   DWO 150 (1:5)

    A1:3:6   DWO 151 (1:6)

    A1:3:7   DWO 156 (1:7)

APPENDIX 1:1:1

INJECTION : VAC PW0-90 -1

0,90° PLAIN WOVEN GLASS FIBRE
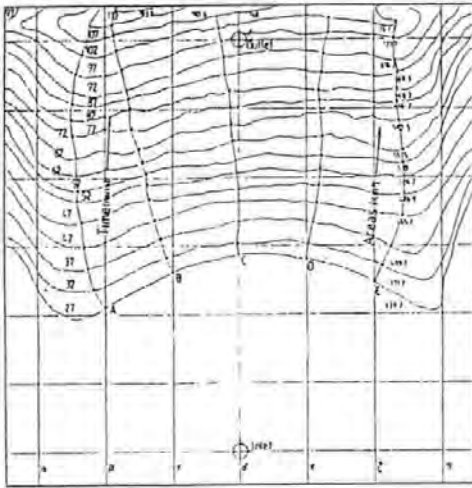
INJECTION : VAC PW+/-45 -1

±45°PLAIN WOVEN GLASS FIBRE
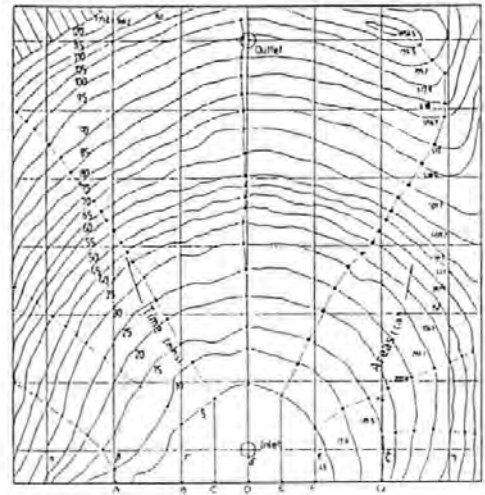
INJECTION : VAC PW+/-45 -2

±45° PLAIN WOVEN GLASS FIBRE
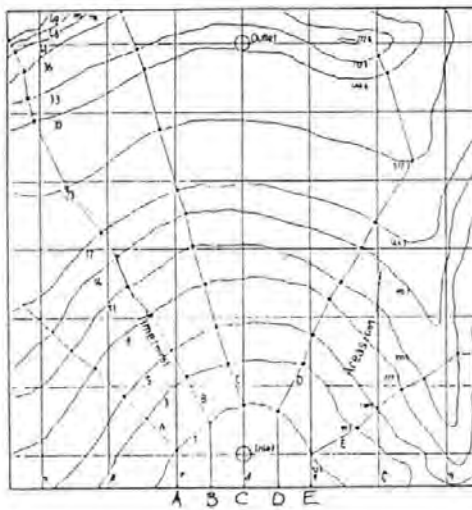
INJECTION : VAC PW+/-45 -3

±45°PLAIN WOVEN GLASS FIBRE
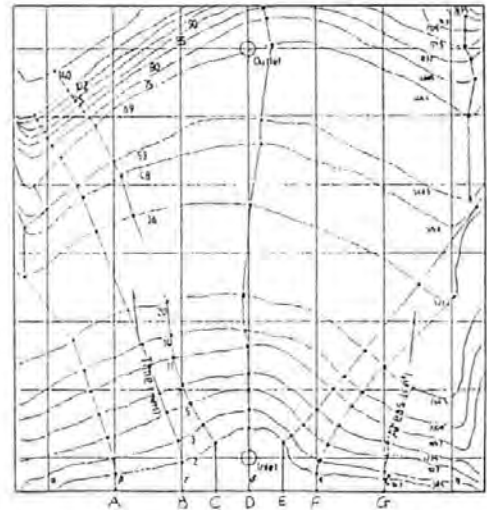
APPENDIX 1:1:1

INJECTION : VAC U-D0 - 1

0° UNI-DIRECTIONAL GLASS FIBRE
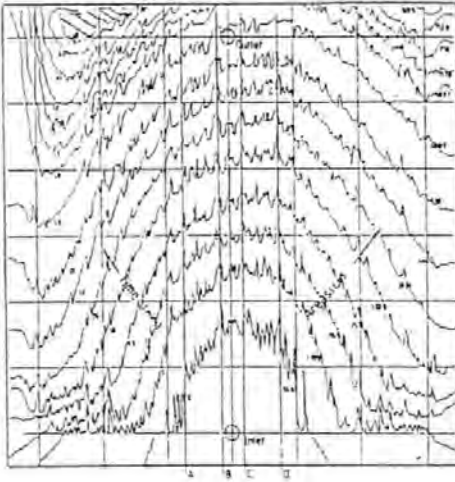
INJECTION : VAC U-D0 - 2

0° UNI-DIRECTIONAL GLASS FIBRE
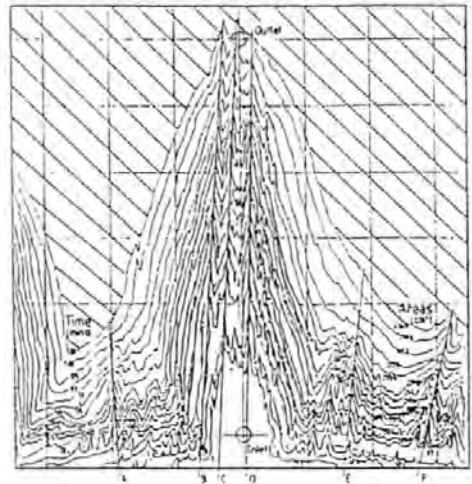
INJECTION : VAC U-D0 - 3

45° UNI-DIRECTIONAL GLASS FIBRE

INJECTION : VAC U-D+45 - 1

0° UNI-DIRECTIONAL GLASS FIBRE

APPENDIX 1:1:1

A1 : 3
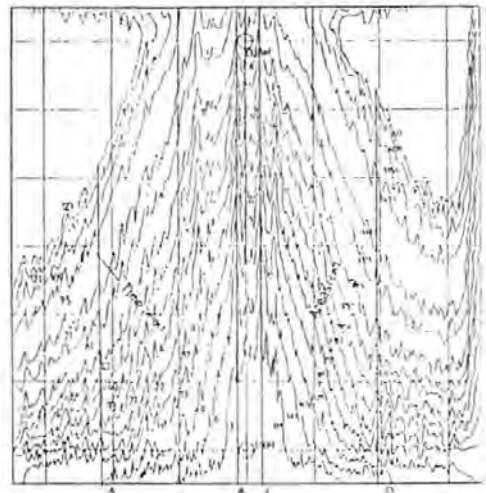
INJECTION : VAC U-D-45 - 1

45° UNI-DIRECTIONAL GLASS FIBRE
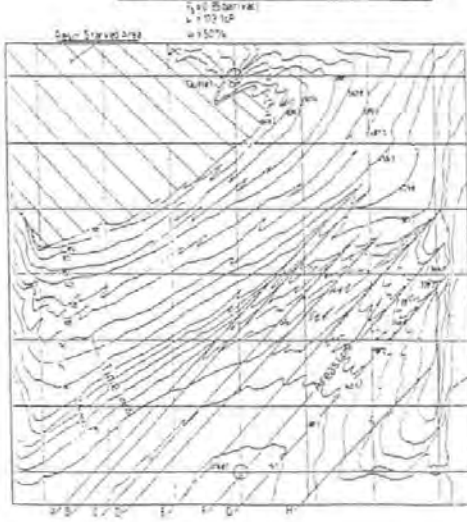
INJECTION : VAC TWILL -1

0,90° TWILL WEAVE GLASS FIBRE
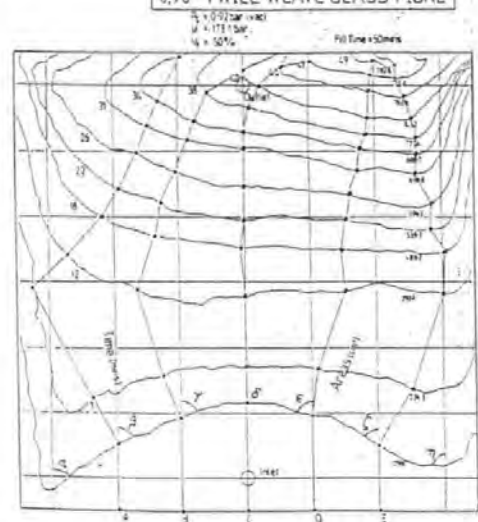
APPENDIX 1:1:2

INJECTION : VAC BAG PW-1

0,90° GLASS FIBRE 210g/m²
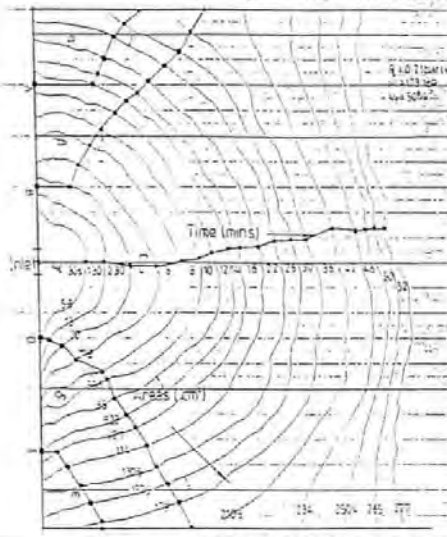
INJECTION : VAC BAG PW-2

0,90° Glass, VACUUM BAG METHOD
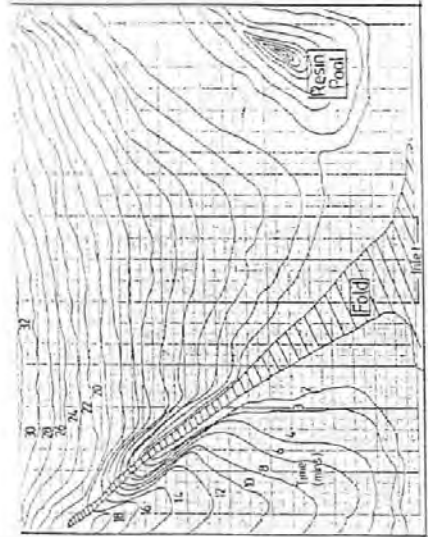
INJECTION : VAC BAG PW- 3

0,90° Glass VACUUM BAG METHOD
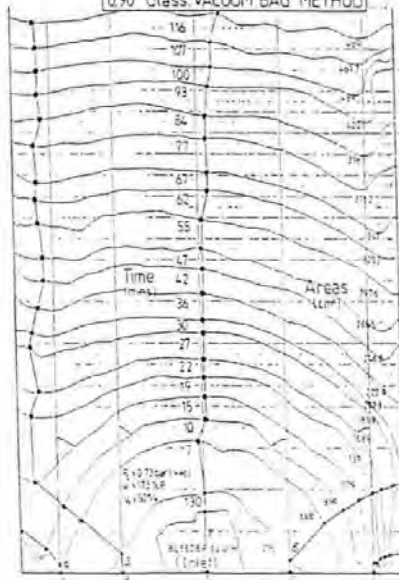
APPENDIX 1:2:1

INJECTION : Plain Weave 1-1
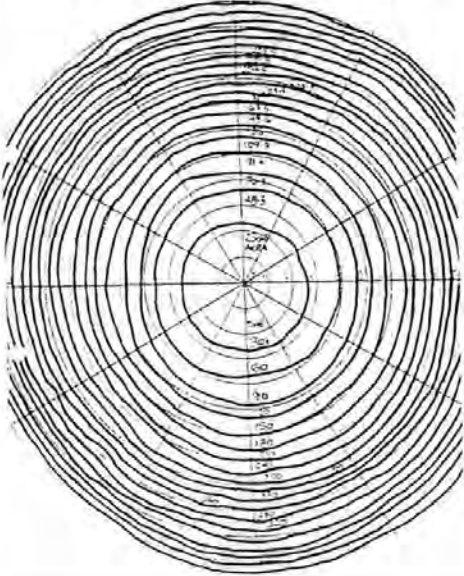
INJECTION : Plain Weave 1-2
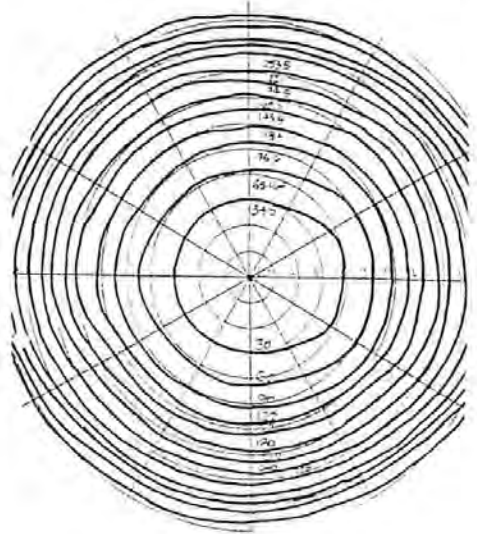
INJECTION : Plain Weave 1-4
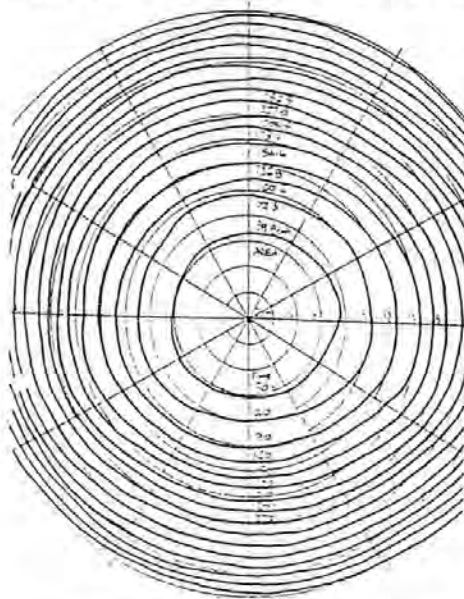
INJECTION : Plain Weave 1-5
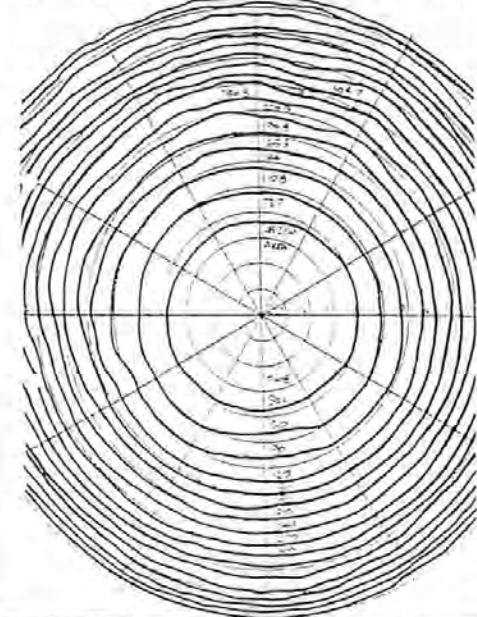
APPENDIX 1:2:1

INJECTION : Plain Weave 1-6
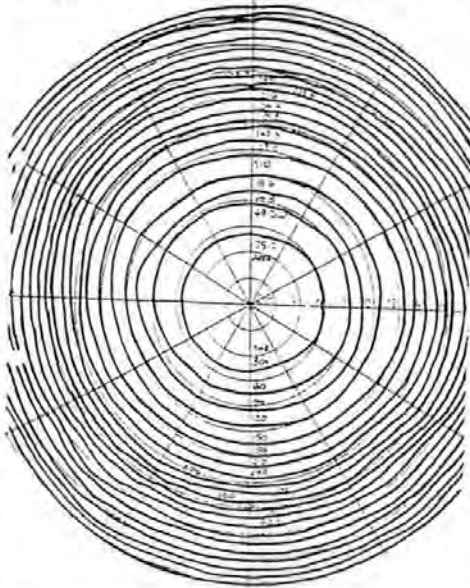
INJECTION : Plain Weave 1-7
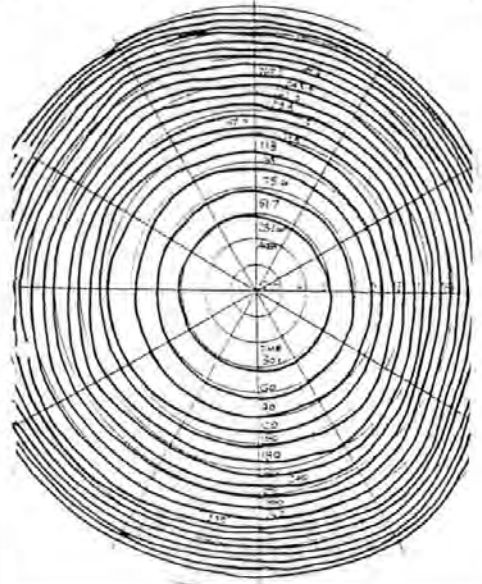
INJECTION : Plain Weave 1-8
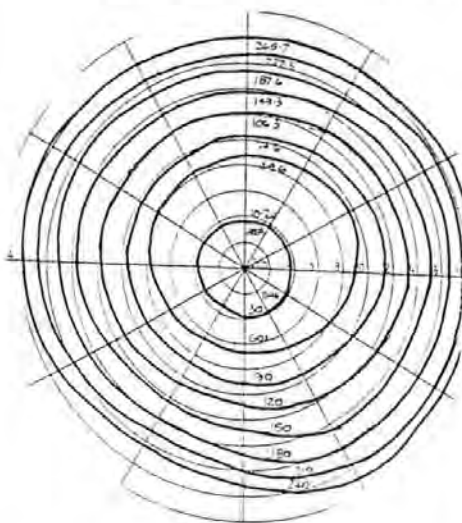
INJECTION : Plain Weave 1-9
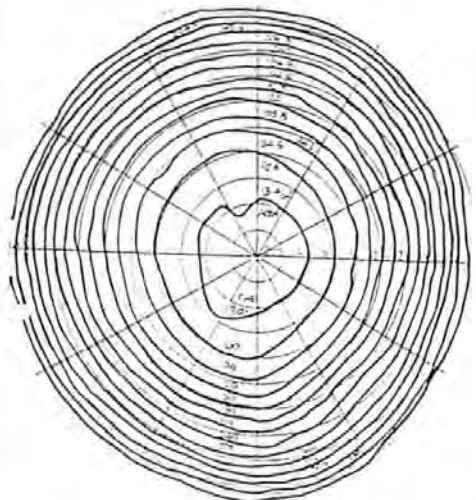
APPENDIX 1:2:1

INJECTION : Plain Weave 1-10
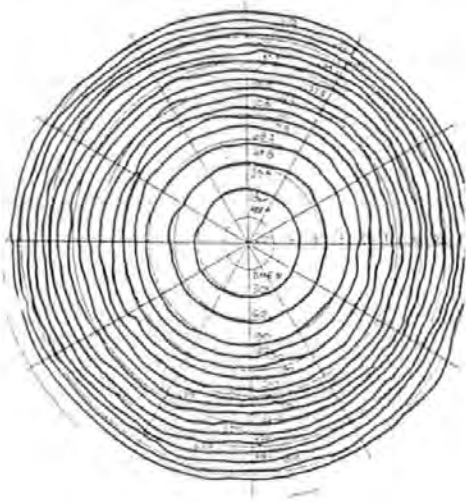
INJECTION : Plain Weave 1-11
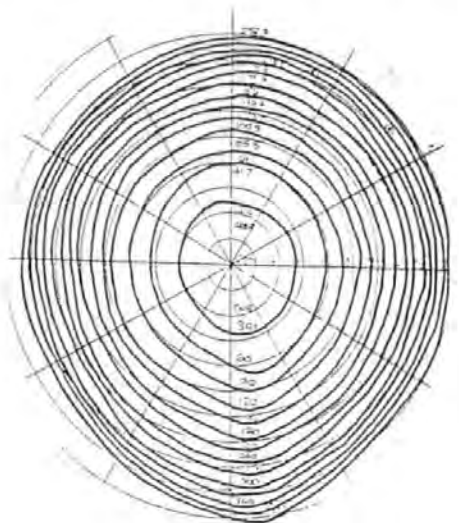
INJECTION : Plain Weave 1-12
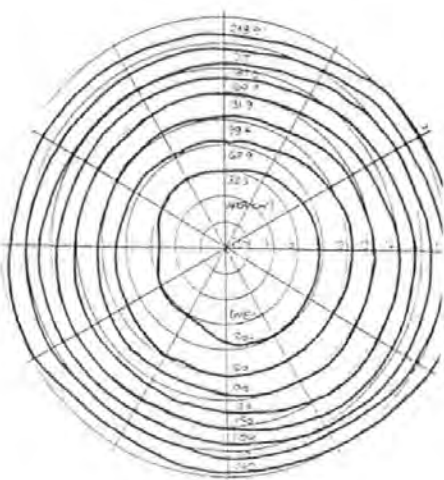
INJECTION : Plain Weave 1-13

APPENDIX 1:2:1

INJECTION : Plain Weave 1-14

INJECTION : Plain Weave 1-15

INJECTION : Plain Weave 1-16

INJECTION : Plain Weave 1-17
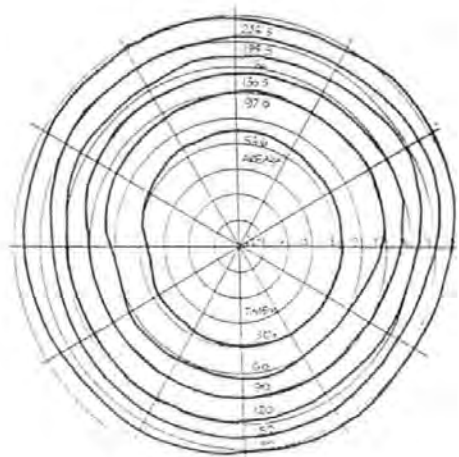
APPENDIX 1:2:1

INJECTION : Plain Weave 1-18
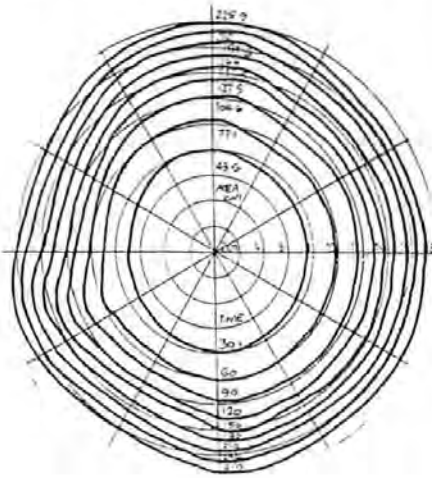
INJECTION : Plain Weave 1-19
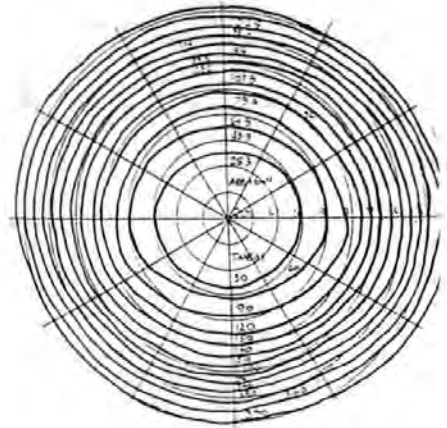
APPENDIX 1:2:2

INJECTION : Plain Weave 2T-1
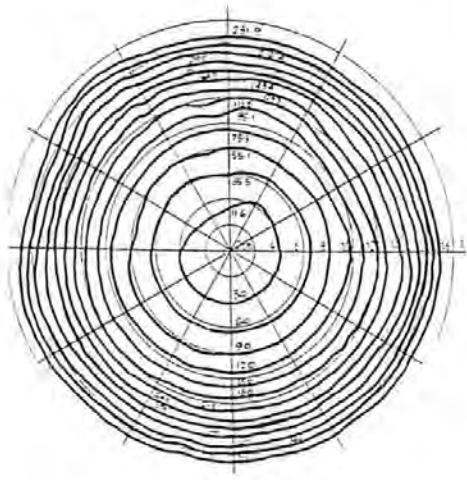
INJECTION : Plain Weave 2T-2
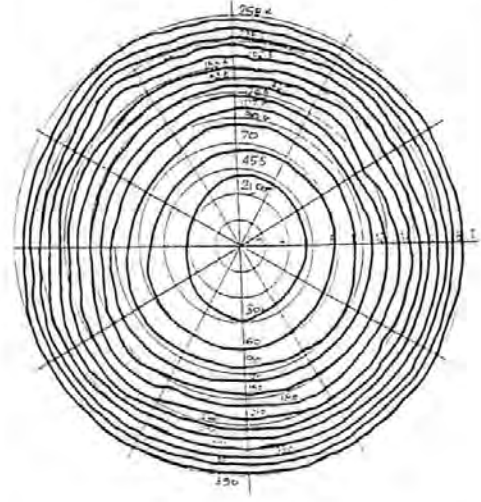
INJECTION : Plain Weave 2T-3
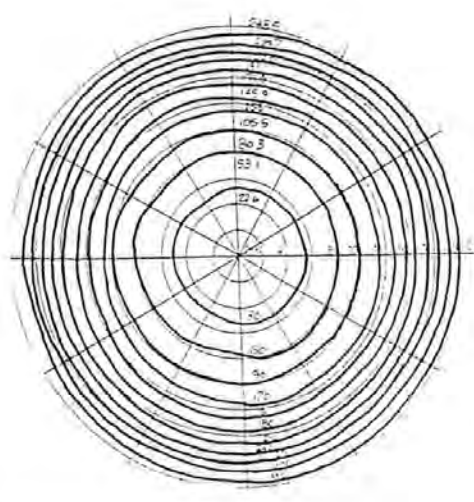
APPENDIX 1:2:3

INJECTION : Plain Weave 3T-1
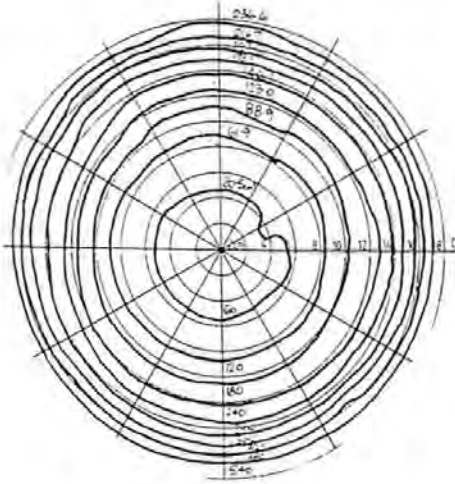
INJECTION : Plain Weave 3T-2
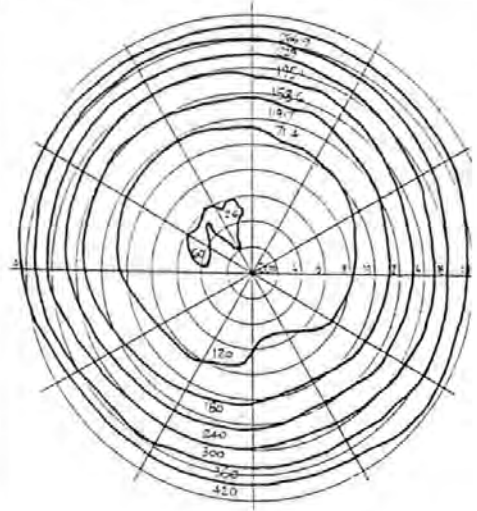
INJECTION : Plain Weave 3T-3
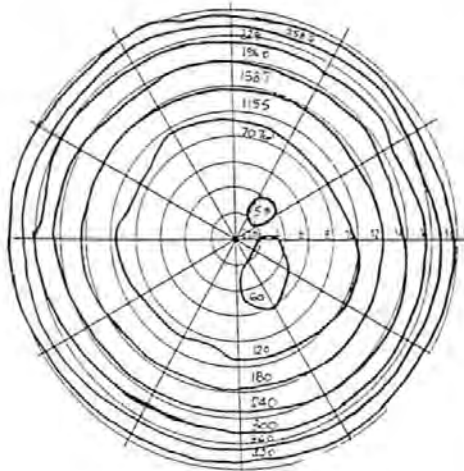
APPENDIX 1:2:4

INJECTION : Plain Weave A-1
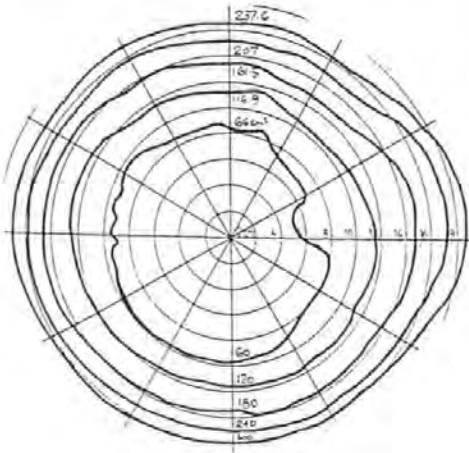
INJECTION : Plain Weave A-2
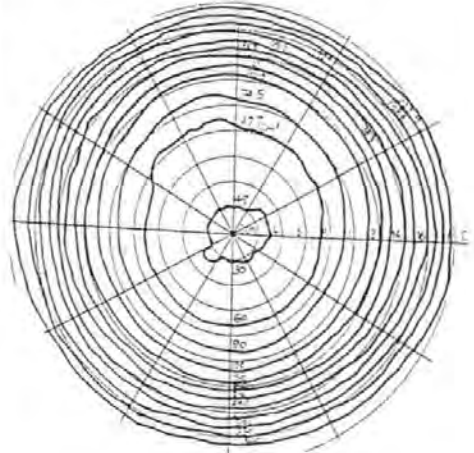
INJECTION : Plain Weave A-3
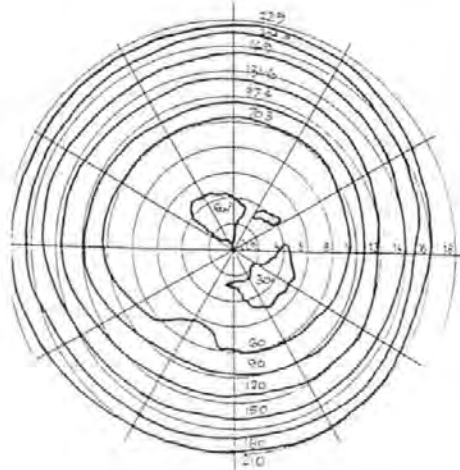
APPENDIX 1:2:5

INJECTION : Plain Weave V-1
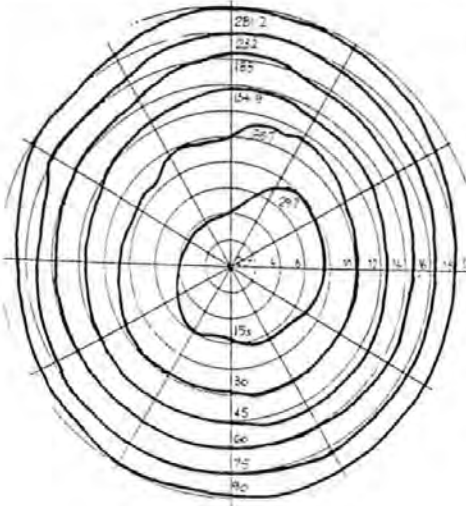
INJECTION : Plain Weave V-2
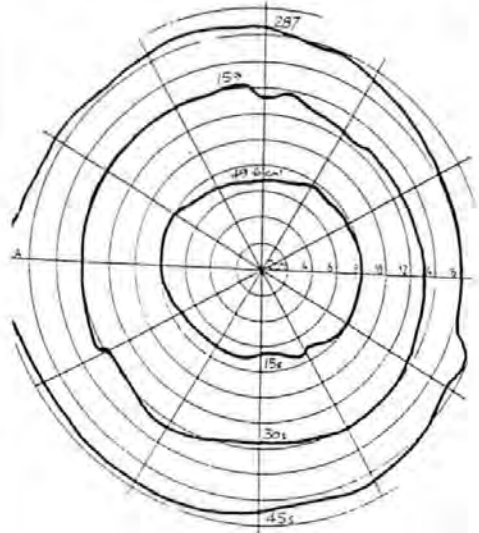
INJECTION : Plain Weave V-3
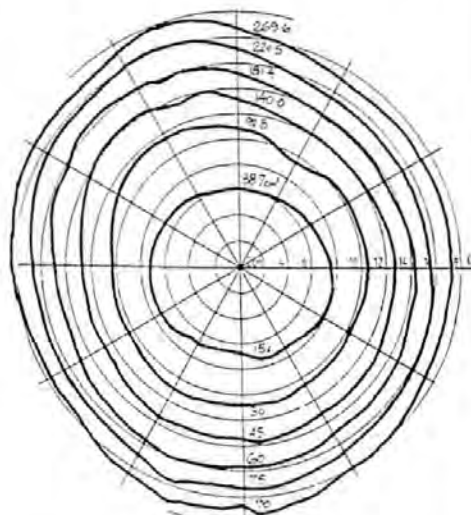
INJECTION : Plain Weave V-4

APPENDIX 1:3:1

INJECTION : DWO 38166 - 1

INJECTION : DWO 38166 - 2

INJECTION : DWO 38166 - 3

APPENDIX 1:3:2

INJECTION : DWO 126 - 1

INJECTION : DWO 126 - 2

INJECTION : DWO 126 - 3

INJECTION : DWO126 - 4
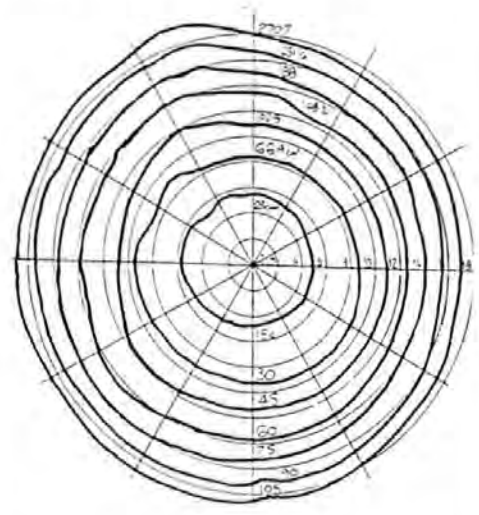
APPENDIX 1:3:2
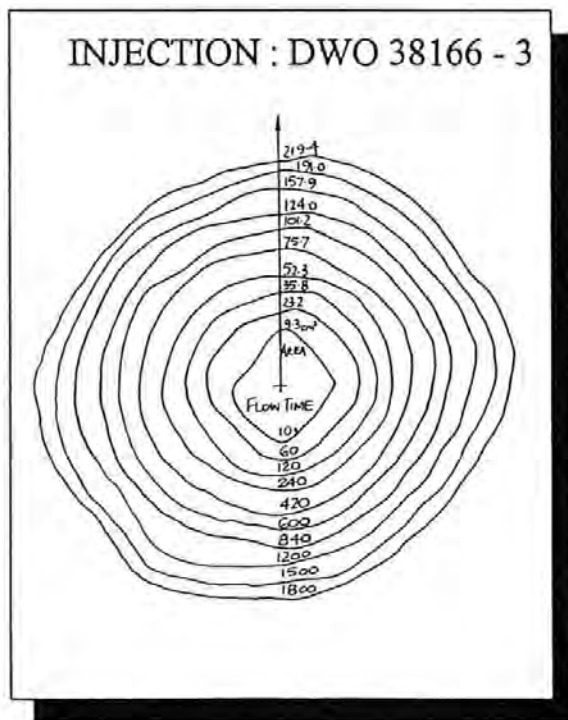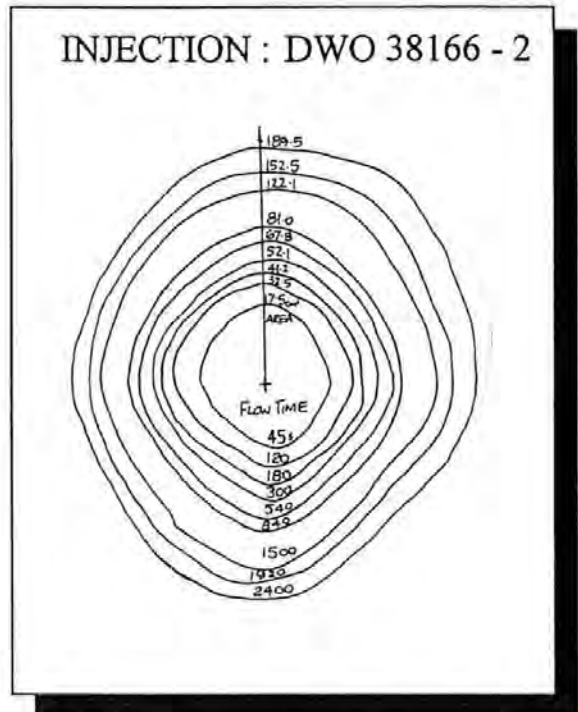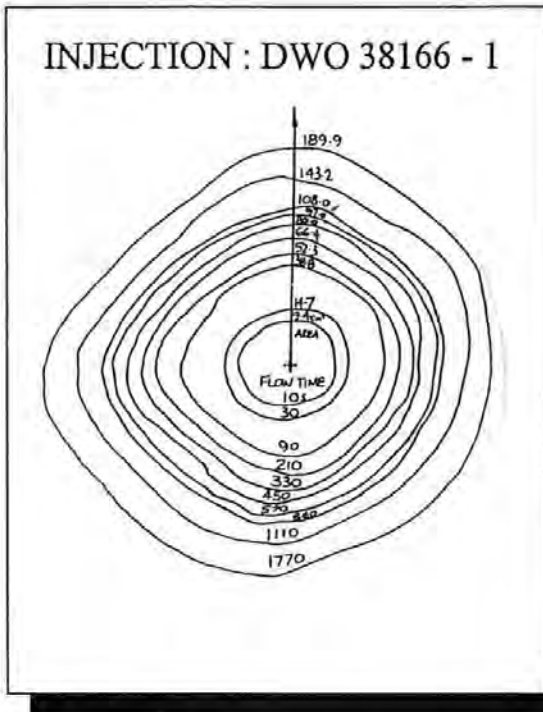
INJECTION : DWO 126 - 5
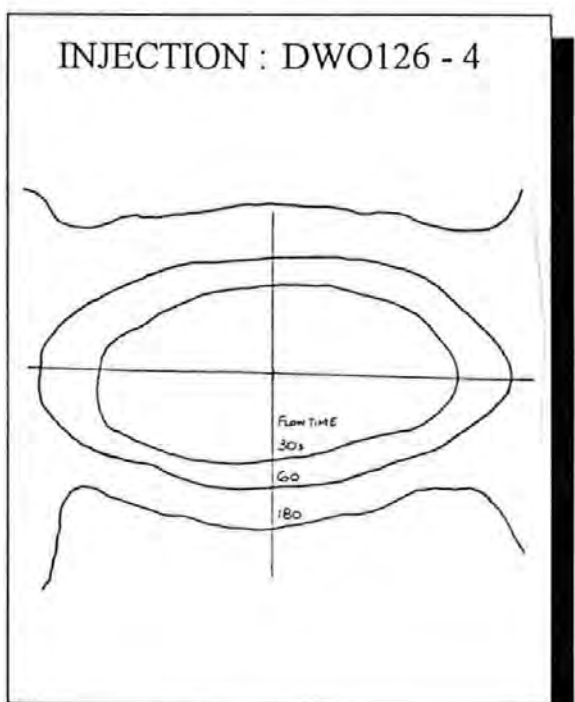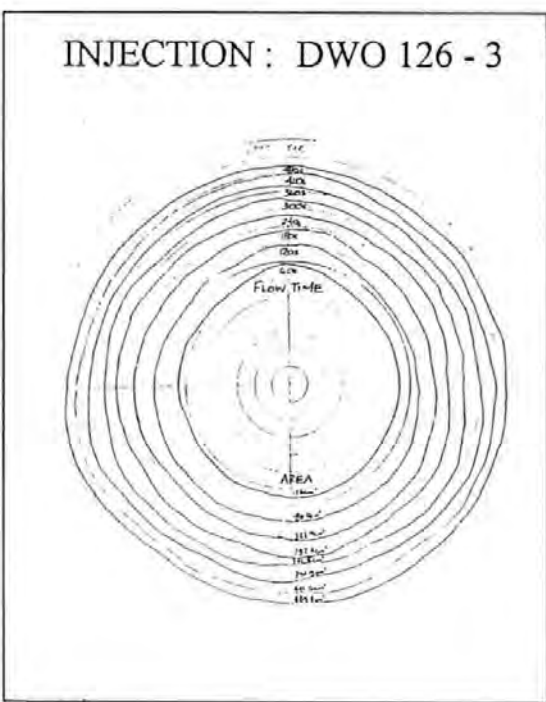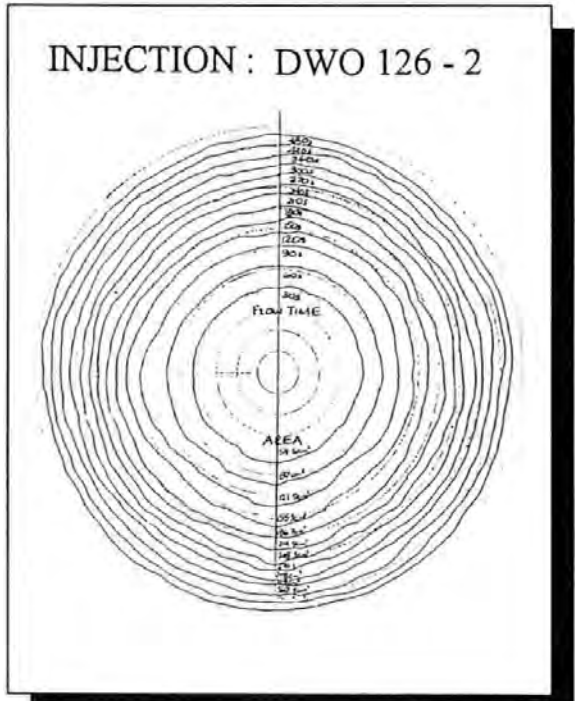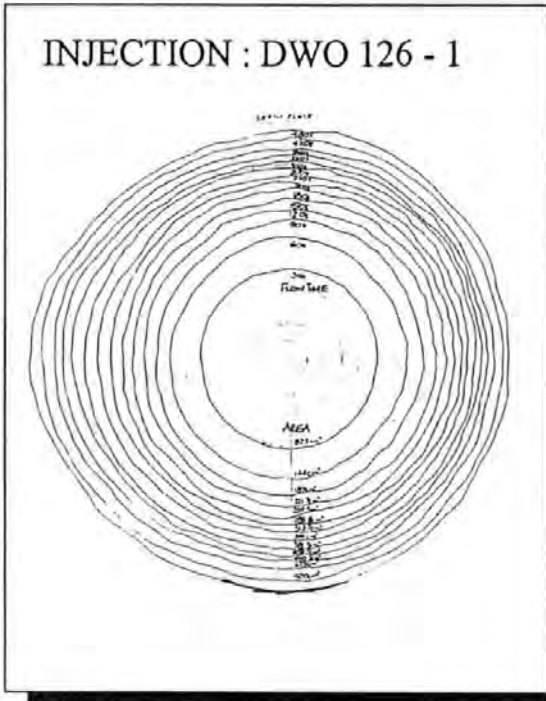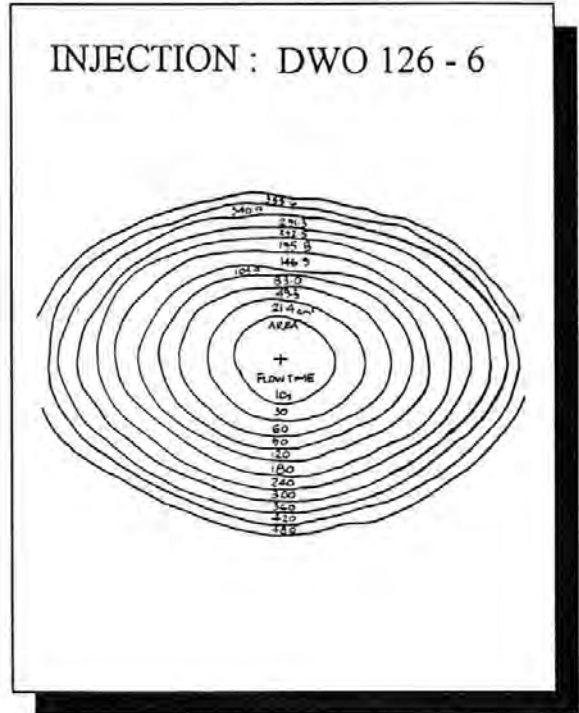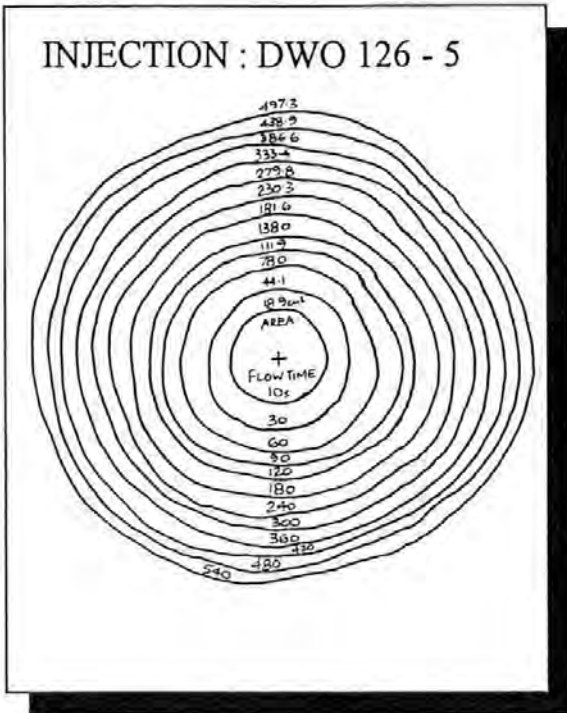
INJECTION : DWO 126 - 6

INJECTION : DWO 126 - 7

Progression recorded

o n

Frame Grabbing Camera

INJECTION : DWO126 - 8
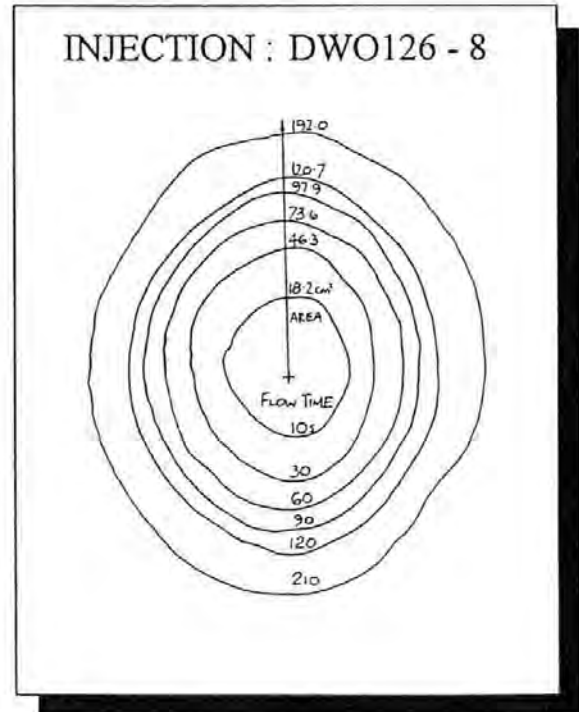
APPENDIX 1:3:2
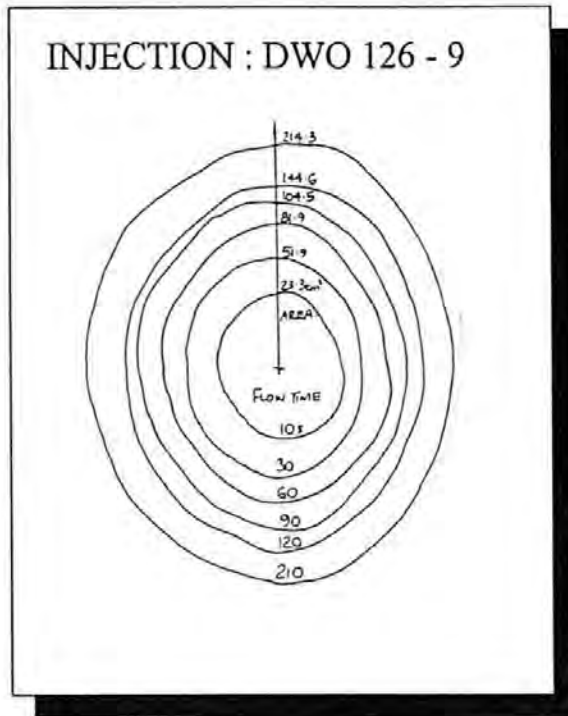
INJECTION : DWO 126 - 9

APPENDIX 1:3:3

INJECTION : DWO 148 - 1

INJECTION : DWO 148 - 2

2x2 CARBON TWILL
ANISOTROPIC LAY-UP 0-90-0-0
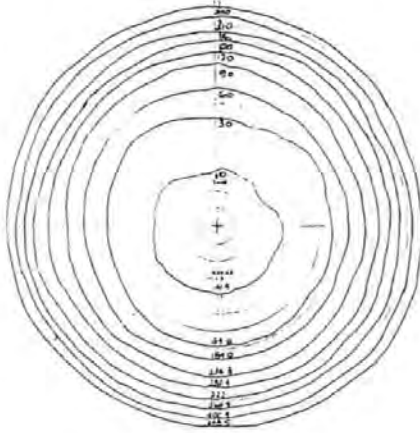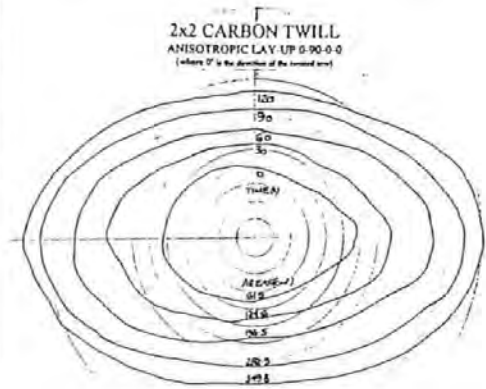
INJECTION : DWO 148 - 3

INJECTION : DWO148 - 4

2x2 CARBON TWILL
ISOTROPIC LAY-UP 0-90-90-0

A1 : 18

APPENDIX 1:3:3

INJECTION : DWO 148 - 5

2x2 CARBON TWILL
ANISOTROPIC LAY-UP 0-0-0-0

INJECTION : DWO 148 - 6
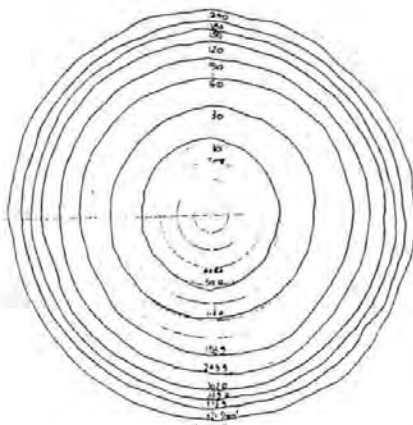
INJECTION : DWO 148 - 7
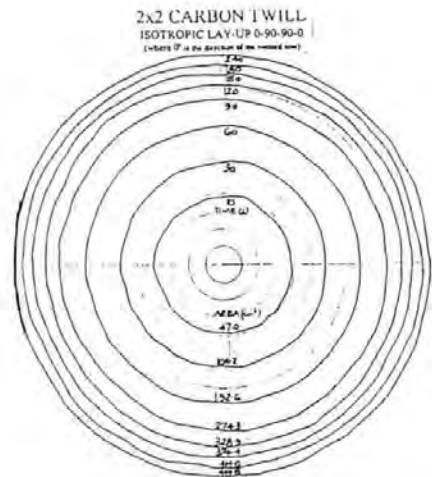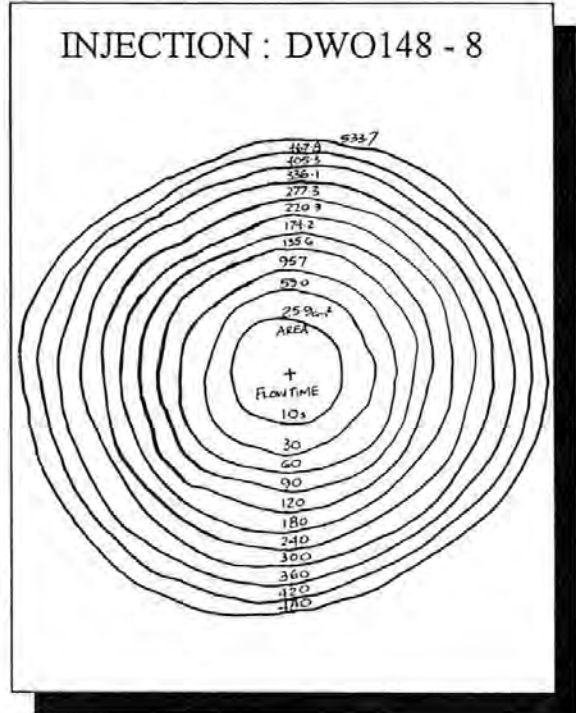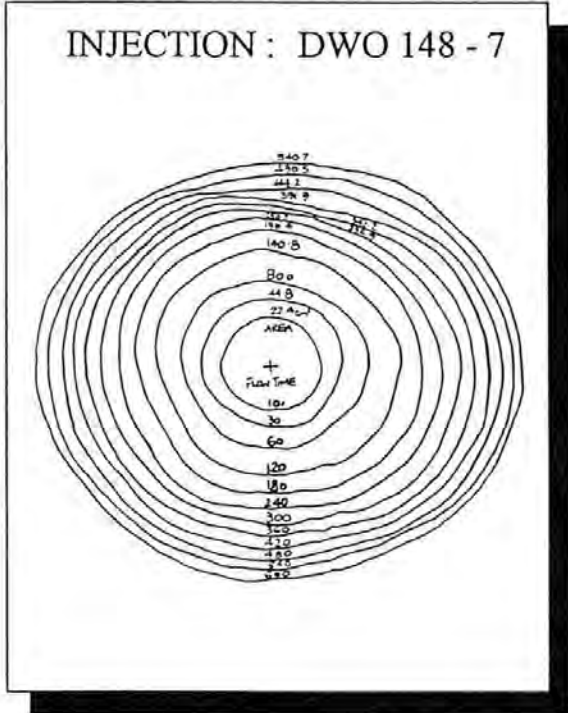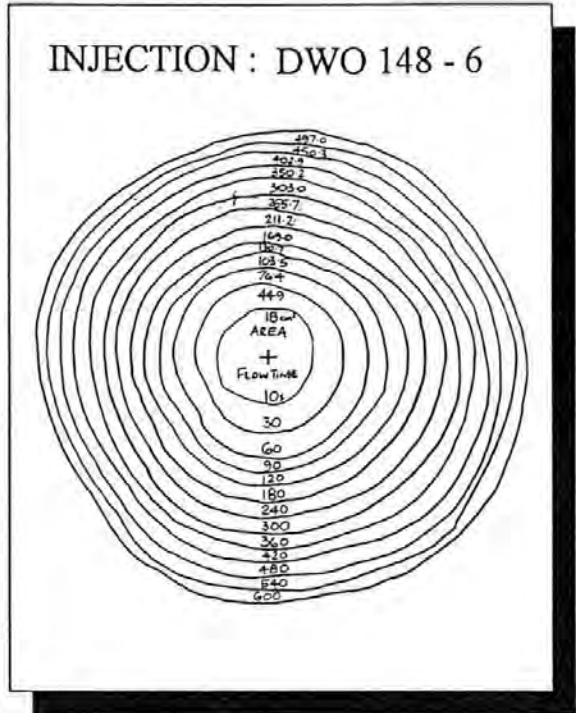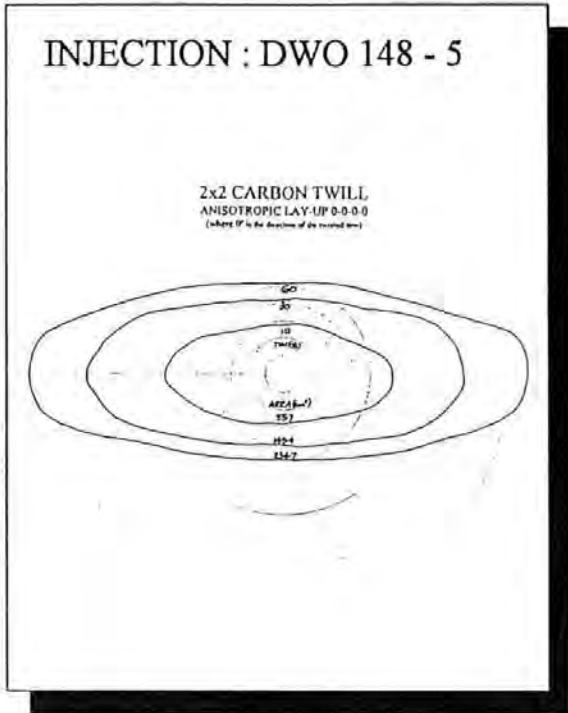
INJECTION : DWO148 - 8

APPENDIX 1:3:4

INJECTION : DWO 149 - 1
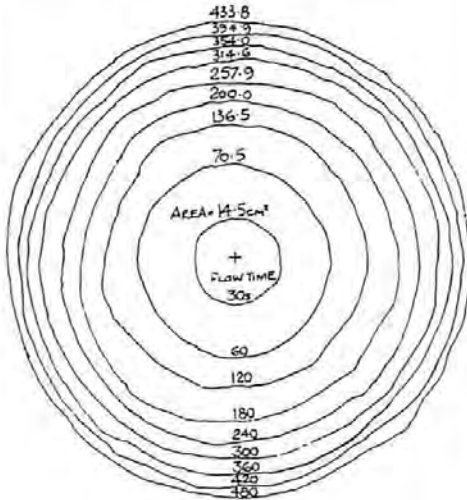
INJECTION : DWO 149 - 2
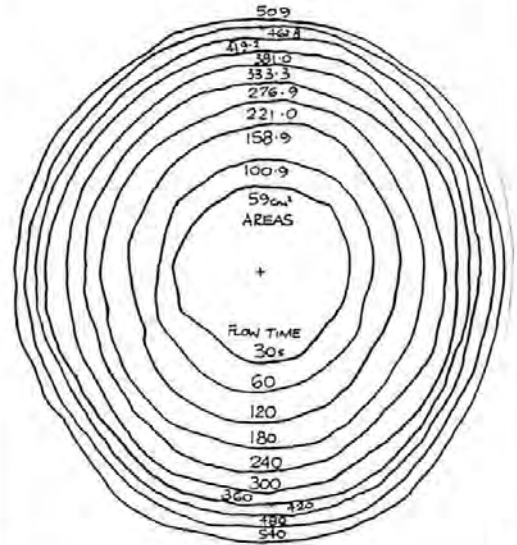
INJECTION : DWO 149 - 3
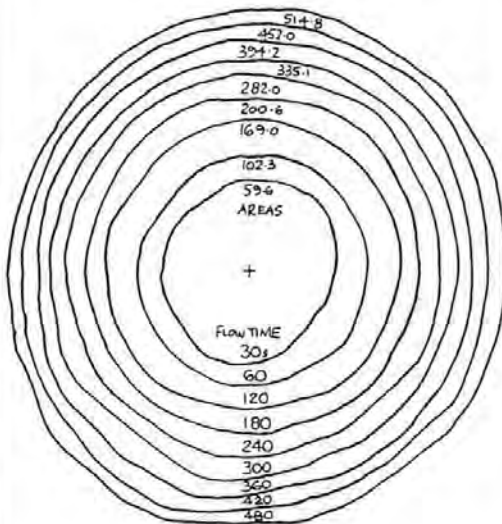
INJECTION : DWO149 - 4

APPENDIX 1:3:5

INJECTION : DWO 150 - 1

471·1
433·8
388·2
337·5
287·0
233·6
186·5
129·7
88·0
48·0
AREAS

+

FLOW TIME
30s
60
120
180
240
300
360
420
480
540

INJECTION : DWO 150 - 2

531·4
475
575   336·5
275·0
236·3
194·9
141·6
87·8
44·5cm²
AREAS

+

FLOW TIME
30s
60
120
180
240
300
360
420
480
540
660

INJECTION : DWO 150 - 3

447·8
386·2
330·1
288·3
243·5
205·4
163·5
119·4
82·0
48·0cm²
AREAS

+

FLOW TIME
30s
60
120
180
240
300
360
480
540
660

INJECTION : DWO150 - 4

INLET

FLOW TIME
30s
50s
120s

APPENDIX 1:3:6

INJECTION : DWO 151 - 1
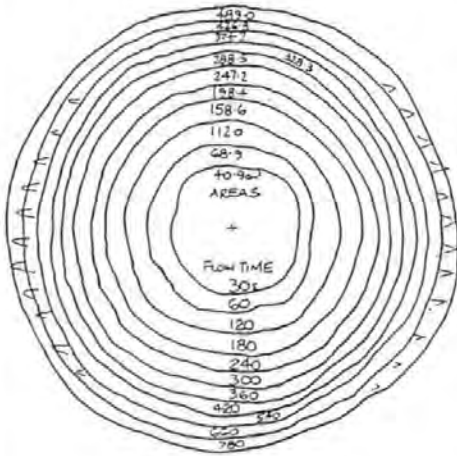
INJECTION : DWO 151 - 2
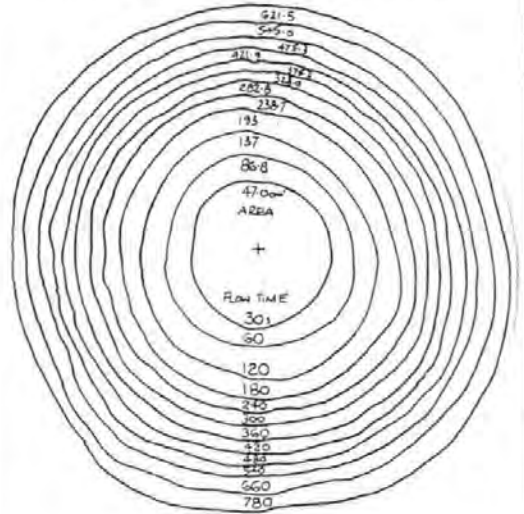
INJECTION : DWO 151 - 3
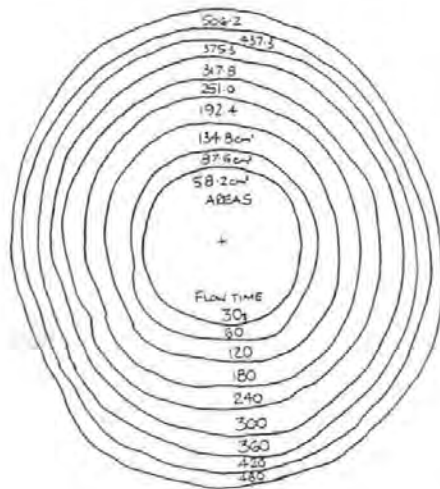
INJECTION : DWO151 - 4
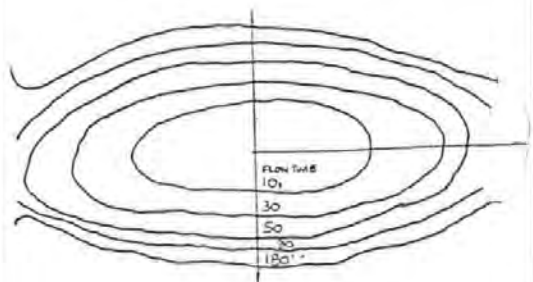
APPENDIX 1:3:7

INJECTION : DWO 156 - 1
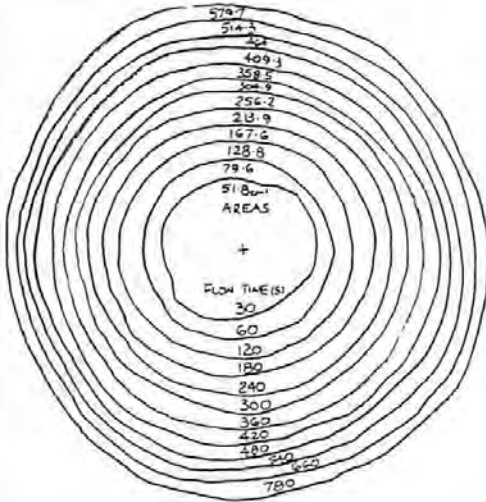
INJECTION : DWO 156 - 2
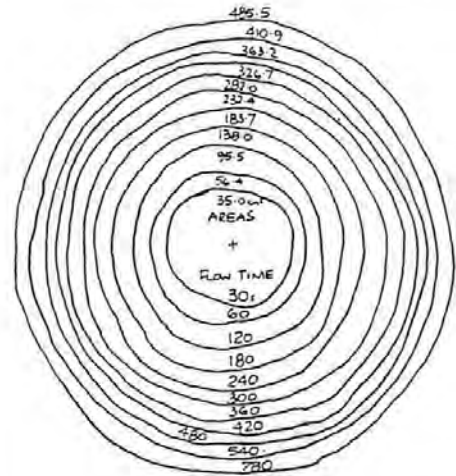
INJECTION : DWO 156 - 3
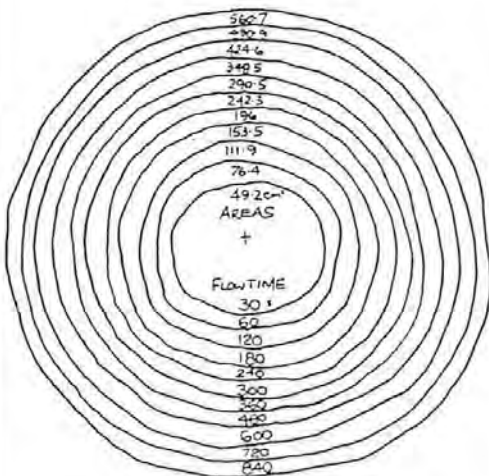
INJECTION : DWO156 - 4
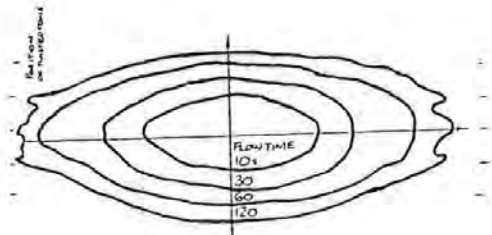
APPENDIX 2
Viscosity Data

A2:1 Glycerol supplied by Boots

    2:1:1 Boots Glycerol 18°C Test 1
    2:1:2 Boots Glycerol 20°C Test 1
    2:1:3 Boots Glycerol 22°C Test 1
    2:1:4 Boots Glycerol 24°C Test 1

A2:2 Glycerol supplied by BDH Chemicals

    2:2:1 BDH Glycerol 10-60°C Test 1

A2:3 MY 750/ HY 917/ DY 070 Ciba Geigy Epoxy System

    2:3:1 MY750   20°C Test 1
    2:3:2 MY750   20°C Test 2
    2:3:3 MY750   21°C Test 1
    2:3:4 MY750   22°C Test 1
    2:3:5 MY750   23°C Test 1

A2:4 Scott Bader Crystic 2-414 PA Polyester Resin 'E'

    2:4:1 Resin 'E'   16°C Test 1
    2:4:2 Resin 'E'   16°C Test 2
    2:4:3 Resin 'E'   18°C Test 1
    2:4:4 Resin 'E'   20°C Test 1
    2:4:5 Resin 'E'   22°C Test 1
    2:4:6 Resin 'E'   24°C Test 1
    2:4:7 Resin 'E'   24°C Test 2

A2:5 Scott Bader Crystic 471 PA LV Polyester Resin 'A'

    2:5:1 Resin 'A'   18°C Test 1
    2:5:2 Resin 'A'   20°C Test 1
    2:5:3 Resin 'A'   22°C Test 1

A2:6 Jotun Norpol 42-10 Polyester +2% Cobalt Acc.+1% MEKP Catalyst

    2:6:1 JNM 42-10 18°C Test 1
    2:6:2 JNM 42-10 20°C Test 1
    2:6:3 JNM 42-10 22°C Test 1

A2:7 Jotun Norpol 42-10 Polyester +2% Cobalt Acc.+1% AAP Catalyst

    2:7:1 JNA 42-10 16°C Test 1
    2:7:2 JNA 42-10 18°C Test 1
    2:7:3 JNA 42-10 20°C Test 1
    2:7:4 JNA 42-10 16°C Test 2
    2:7:5 JNA 42-10 18°C Test 2

Viscosity Test : BOOTS GLYCEROL 18-1

Resin : Glycerol (supplied by Boots)
Shear Stress = 500 dyne/cm²
Test Temperature = 18°C (+/-0.1°C)

Test Time (s)	Shear Rate (1/s)	Dynamic Viscosity (Poise)	Test Time (s)	Shear Rate (1/s)	Dynamic Viscosity (Poise)
1.000	43.290	11.550	63.000	43.170	11.580
3.000	43.000	11.630	65.000	43.320	11.540
5.000	43.440	11.510	67.000	43.240	11.560
7.000	42.980	11.630	69.000	43.250	11.560
9.000	43.470	11.500	71.000	43.330	11.540
11.000	43.090	11.600	73.000	43.120	11.590
13.000	43.390	11.520	75.000	43.410	11.520
15.000	43.070	11.610	77.000	43.150	11.590
17.000	43.090	11.600	79.000	43.520	11.490
19.000	43.500	11.490	81.000	42.990	11.630
21.000	42.960	11.640	83.000	43.510	11.490
23.000	43.400	11.520	85.000	43.120	11.590
25.000	43.060	11.610	87.000	43.230	11.570
27.000	43.210	11.570	89.000	43.440	11.510
29.000	43.400	11.520	91.000	43.080	11.610
31.000	43.020	11.620	93.000	43.560	11.480
33.000	43.480	11.500	95.000	43.060	11.610
35.000	43.040	11.620	97.000	43.210	11.570
37.000	43.490	11.500	99.000	43.420	11.520
39.000	43.000	11.630	101.000	43.120	11.590
41.000	43.370	11.530	103.000	43.490	11.500
43.000	43.170	11.580	105.000	43.000	11.630
45.000	43.060	11.610	107.000	43.430	11.510
47.000	43.480	11.500	109.000	43.090	11.600
49.000	43.000	11.630	111.000	43.490	11.500
51.000	43.460	11.500	113.000	43.150	11.590
53.000	43.180	11.580	115.000	43.110	11.600
55.000	43.330	11.540	117.000	43.570	11.480
57.000	43.190	11.580	119.000	43.070	11.610
59.000	43.250	11.560			
61.000	43.360	11.530			

Viscosity Test : BOOTS GLYCEROL 20-1

Resin : Glycerol (supplied by Boots)
Shear Stress = 500 dyne/cm²
Test Temperature = 20°C (+/-0.1°C)

Test Time (s)	Shear Rate (1/s)	Dynamic Viscosity (Poise)	Test Time (s)	Shear Rate (1/s)	Dynamic Viscosity (Poise)
1.000	51.810	9.650	61.000	52.270	9.567
3.000	52.080	9.600	63.000	51.790	9.654
5.000	51.970	9.620	65.000	52.190	9.580
7.000	52.220	9.575	67.000	52.040	9.609
9.000	52.250	9.569	69.000	52.080	9.600
11.000	52.130	9.592	71.000	52.310	9.559
13.000	52.050	9.610	73.000	52.140	9.590
15.000	52.110	9.596	75.000	51.970	9.620
17.000	52.020	9.612	77.000	52.170	9.583
19.000	52.340	9.553	79.000	51.890	9.635
21.000	52.170	9.583	81.000	52.370	9.548
23.000	51.900	9.633	83.000	52.240	9.572
25.000	52.170	9.584	85.000	51.930	9.629
27.000	52.300	9.560	87.000	52.070	9.603
29.000	51.790	9.654	89.000	52.170	9.584
31.000	52.350	9.551	91.000	51.970	9.620
33.000	52.080	9.600	93.000	52.250	9.570
35.000	51.930	9.628	95.000	52.250	9.570
37.000	52.260	9.568	97.000	51.990	9.617
39.000	51.970	9.620	99.000	52.050	9.605
41.000	52.320	9.557	101.000	52.120	9.593
43.000	52.200	9.578	103.000	52.080	9.601
45.000	52.050	9.605	105.000	52.320	9.557
47.000	52.120	9.593	107.000	51.870	9.639
49.000	52.310	9.559	109.000	52.420	9.538
51.000	51.800	9.652	111.000	52.130	9.592
53.000	52.360	9.549	113.000	51.970	9.621
55.000	52.250	9.570	115.000	52.230	9.574
57.000	51.890	9.635	117.000	52.100	9.597
59.000	52.370	9.547	119.000	52.090	9.599

Viscosity Test : BOOTS GLYCEROL 22-1

Resin : Glycerol (supplied by Boots)
Shear Stress = 500 dyne/cm^2
Test Temperature = 22°C (+/-0.1°C)

Test Time (s)	Shear Rate (1/s)	Dynamic Viscosity (Poise)	Test Time (s)	Shear Rate (1/s)	Dynamic Viscosity (Poise)
1.000	62.180	8.041	61.000	62.690	7.976
3.000	62.400	8.013	63.000	62.300	8.026
5.000	62.240	8.033	65.000	62.500	8.000
7.000	62.510	7.999	67.000	62.460	8.005
9.000	62.210	8.038	69.000	62.260	8.030
11.000	62.510	7.999	71.000	62.490	8.001
13.000	62.220	8.036	73.000	62.210	8.037
15.000	62.710	7.973	75.000	62.530	7.997
17.000	62.090	8.053	77.000	62.280	8.028
19.000	62.640	7.982	79.000	62.620	7.985
21.000	62.260	8.031	81.000	62.220	8.036
23.000	62.620	7.984	83.000	62.510	7.998
25.000	62.310	8.025	85.000	62.450	8.007
27.000	62.710	7.973	87.000	62.160	8.044
29.000	62.190	8.040	89.000	62.500	8.000
31.000	62.700	7.974	91.000	62.180	8.041
33.000	62.410	8.012	93.000	62.400	8.013
35.000	62.270	8.029	95.000	62.210	8.038
37.000	62.530	7.997	97.000	62.530	7.997
39.000	62.150	8.045	99.000	62.170	8.042
41.000	62.480	8.003	101.000	62.510	7.999
43.000	62.220	8.036	103.000	62.510	7.998
45.000	62.570	7.991	105.000	62.130	8.048
47.000	62.120	8.049	107.000	62.490	8.001
49.000	62.690	7.976	109.000	62.420	8.010
51.000	62.230	8.034	111.000	62.120	8.049
53.000	62.670	7.978	113.000	62.610	7.986
55.000	62.380	8.016	115.000	62.410	8.012
57.000	62.680	7.978	117.000	62.220	8.036
59.000	62.290	8.027	119.000	62.460	8.005

Viscosity Test : BOOTS GLYCEROL 24-1

Resin : Glycerol (supplied by Boots)
Shear Stress = 500 dyne/cm^2
Test Temperature = 24°C (+/-0.1°C)

Test Time (s)	Shear Rate (1/s)	Dynamic Viscosity (Poise)	Test Time (s)	Shear Rate (1/s)	Dynamic Viscosity (Poise)
1.000	74.460	6.715	61.000	74.270	6.733
3.000	74.360	6.724	63.000	74.320	6.727
5.000	74.060	6.751	65.000	74.560	6.706
7.000	74.360	6.724	67.000	73.900	6.766
9.000	74.600	6.702	69.000	74.130	6.745
11.000	74.410	6.719	71.000	74.470	6.714
13.000	74.080	6.750	73.000	74.250	6.734
15.000	74.290	6.730	75.000	73.940	6.762
17.000	74.600	6.702	77.000	74.330	6.726
19.000	74.530	6.708	79.000	74.350	6.725
21.000	74.000	6.757	81.000	74.100	6.748
23.000	74.430	6.718	83.000	73.940	6.762
25.000	74.420	6.719	85.000	74.270	6.733
27.000	74.600	6.703	87.000	74.530	6.708
29.000	74.000	6.757	89.000	73.700	6.784
31.000	74.220	6.736	91.000	74.220	6.736
33.000	74.620	6.701	93.000	74.240	6.735
35.000	74.530	6.708	95.000	74.660	6.697
37.000	74.050	6.752	97.000	73.840	6.771
39.000	74.210	6.738	99.000	74.130	6.745
41.000	74.510	6.710	101.000	74.370	6.723
43.000	74.480	6.713	103.000	74.400	6.720
45.000	73.930	6.763	105.000	73.940	6.762
47.000	74.410	6.720	107.000	74.110	6.747
49.000	74.480	6.713	109.000	74.380	6.722
51.000	73.930	6.763	111.000	74.130	6.745
53.000	74.120	6.746	113.000	73.870	6.769
55.000	74.240	6.735	115.000	74.330	6.726
57.000	74.600	6.702	117.000	74.420	6.719
59.000	73.740	6.780	119.000	73.960	6.760

Viscosity Test BDH Glycerol -1

Fluid : Glycerol (supplied by BDH Chemicals)
Shear Stress = 500 dyne/cm^2

Test Time (s)	Temperature (°C)	Shear Rate (1/s)	Dynamic Viscosity (Poise)
36.000	10.000	12.220	6.510
72.000	10.500	12.850	6.194
108.000	10.900	13.410	5.933
144.000	11.500	14.090	5.649
180.000	12.000	14.680	5.422
216.000	12.500	15.390	5.170
252.000	13.000	15.960	4.985
288.000	13.500	16.890	4.711
324.000	14.000	17.560	4.531
360.000	14.500	18.240	4.363
396.000	15.000	19.200	4.146
432.000	15.500	19.980	3.982
468.000	16.000	20.780	3.829
504.000	16.700	21.960	3.624
540.000	17.200	22.840	3.484
576.000	17.600	23.580	3.374
612.000	18.100	24.660	3.227
648.000	18.700	25.740	3.092
684.000	19.100	26.620	2.990
720.000	19.500	27.460	2.898
756.000	20.100	28.780	2.765
792.000	20.500	29.780	2.673
828.000	21.100	31.040	2.564
864.000	21.500	32.310	2.463
900.000	22.100	33.460	2.378
936.000	22.600	34.670	2.295
972.000	23.100	36.050	2.208
1008.000	23.700	37.510	2.121
1044.000	24.100	38.600	2.062
1080.000	24.600	40.000	1.989
1116.000	25.200	41.790	1.904
1152.000	25.700	43.420	1.833
1188.000	26.200	44.920	1.772
1224.000	26.800	46.600	1.708
1260.000	27.100	48.000	1.658
1296.000	27.600	49.600	1.604
1332.000	28.100	51.280	1.552
1368.000	28.800	53.370	1.491
1404.000	29.100	54.520	1.460
1440.000	29.600	56.670	1.404
1476.000	30.300	58.880	1.352
1512.000	30.700	60.340	1.319
1548.000	31.200	62.370	1.276
1584.000	31.600	64.320	1.237
1620.000	32.200	66.460	1.197
1656.000	32.600	68.300	1.165
1692.000	33.200	70.640	1.126
1728.000	33.700	73.060	1.089

Viscosity Test BDH Glycerol -1 continued

Test Time (s)	Temperature (°C)	Shear Rate (1/s)	Dynamic Viscosity (Poise)
1764.000	34.200	74.840	1.063
1800.000	34.700	77.400	1.028
1836.000	35.300	80.330	0.991
1872.000	35.700	82.470	0.965
1908.000	36.200	84.750	0.939
1944.000	36.800	87.430	0.910
1980.000	37.300	89.640	0.888
2016.000	37.800	92.970	0.856
2052.000	38.300	95.340	0.835
2088.000	38.900	98.590	0.807
2124.000	39.400	101.500	0.784
2160.000	39.800	104.000	0.765
2196.000	40.300	106.400	0.748
2232.000	40.700	109.100	0.730
2268.000	41.300	112.600	0.707
2304.000	41.900	115.700	0.688
2340.000	42.300	118.300	0.673
2376.000	42.800	121.900	0.653
2412.000	43.200	123.700	0.643
2448.000	43.900	128.300	0.620
2484.000	44.200	130.400	0.610
2520.000	44.800	135.000	0.589
2556.000	45.400	138.500	0.575
2592.000	45.900	142.100	0.560
2628.000	46.400	145.900	0.546
2664.000	46.900	148.600	0.535
2700.000	47.300	152.200	0.523
2736.000	47.800	155.500	0.512
2772.000	48.300	159.400	0.499
2808.000	48.800	163.000	0.488
2844.000	49.400	167.500	0.475
2880.000	49.800	170.700	0.466
2916.000	50.300	174.400	0.456
2952.000	50.800	178.600	0.446
2988.000	51.400	182.400	0.436
3024.000	51.900	187.100	0.425
3060.000	52.400	190.600	0.417
3096.000	53.000	195.500	0.407
3132.000	53.500	199.400	0.399
3168.000	53.800	202.800	0.392
3204.000	54.500	207.900	0.383
3240.000	54.800	211.600	0.376
3276.000	55.400	217.400	0.366
3312.000	56.100	222.700	0.357
3348.000	56.300	225.300	0.353
3384.000	56.900	230.400	0.346
3420.000	57.500	236.200	0.337
3456.000	57.900	239.700	0.332
3492.000	58.400	244.300	0.326
3528.000	58.900	249.300	0.319
3564.000	59.500	254.400	0.313
3600.000	60.100	259.400	0.307

Viscosity Test : MY750/20 -1

Resin :Ciba Geigy MY750 Epoxy System
Resin Constituents : MY750 Base Resin : 45% HY917 Hardener : 0.03% DY070 Catalyst
0.2g of Scott Bader Black Pigment added to aid Visualisation
Shear Stress : 500 dyne/cm²
Test Temperature : 20°C (+/-0.1°C)

Flow Time (s)	Shear Rate (1/s)	Dynamic Viscosity (Poise)
18.000	181.000	1.648
72.000	178.900	1.668
126.000	175.200	1.704
180.000	174.700	1.708
234.000	174.000	1.715
288.000	173.400	1.721
342.000	172.500	1.730
396.000	170.900	1.747
450.000	169.000	1.766
504.000	167.700	1.780
558.000	170.400	1.751
612.000	168.300	1.773
666.000	166.500	1.792
720.000	167.000	1.787
774.000	166.100	1.796
828.000	164.700	1.812
882.000	165.100	1.807
936.000	165.100	1.807
990.000	163.900	1.820
1044.000	164.400	1.815
1098.000	162.200	1.840
1152.000	163.800	1.821
1206.000	162.300	1.839
1260.000	160.700	1.857
1314.000	162.000	1.842
1368.000	160.400	1.860
1422.000	158.400	1.883
1476.000	160.400	1.860
1530.000	158.900	1.878
1584.000	159.600	1.869
1638.000	157.400	1.896
1692.000	158.000	1.889
1746.000	157.300	1.897
1800.000	156.600	1.906

Viscosity Test : MY750/20 -2

Resin :Ciba Geigy MY750 Epoxy System
Resin Constituents : MY750 Base Resin : 45% HY917 Hardener : 0.03% DY070 Catalyst
No pigment added
Shear Stress : 500 dyne/cm²
Test Temperature : 20°C (+/-0.1°C)

Test Time (s)	Shear Rate (1/s)	Dynamic Viscosity (Poise)
18.000	201.400	1.482
72.000	201.000	1.485
126.000	198.000	1.507
180.000	197.100	1.514
234.000	196.400	1.519
288.000	194.500	1.534
342.000	193.600	1.541
396.000	192.900	1.547
450.000	192.000	1.554
504.000	191.100	1.562
558.000	190.000	1.570
612.000	189.300	1.576
666.000	187.700	1.590
720.000	188.200	1.585
774.000	188.200	1.585
828.000	187.600	1.590
882.000	186.300	1.602
936.000	185.200	1.611
990.000	185.200	1.611
1044.000	185.400	1.609
1098.000	184.500	1.617
1152.000	184.100	1.621
1206.000	183.000	1.631
1260.000	182.600	1.634
1314.000	182.100	1.639
1368.000	181.600	1.643
1422.000	181.200	1.647
1476.000	180.400	1.654
1530.000	180.500	1.653
1584.000	180.100	1.657
1638.000	179.100	1.666
1692.000	178.700	1.670
1746.000	178.200	1.674
1800.000	177.800	1.678

Viscosity Test : MY750/21 -1

Resin :Ciba Geigy MY750 Epoxy System
Resin Constituents : MY750 Base Resin : 45% HY917 Hardener : 0.03% DY070 Catalyst
No pigment added
Shear Stress : 500 dyne/cm^2
Test Temperature : 21°C (+/-0.1°C)

Test Time (s)	Shear Rate (1/s)	Dynamic Viscosity (Poise)
18.000	222.200	1.343
72.000	219.300	1.360
126.000	218.100	1.368
180.000	216.300	1.380
234.000	213.900	1.395
288.000	212.800	1.402
342.000	212.500	1.404
396.000	210.700	1.416
450.000	209.600	1.424
504.000	208.000	1.435
558.000	207.000	1.441
612.000	205.200	1.454
666.000	203.900	1.464
720.000	203.200	1.469
774.000	202.200	1.476
828.000	203.100	1.469
882.000	201.900	1.478
936.000	201.100	1.484
990.000	199.800	1.493
1044.000	198.700	1.501
1098.000	197.400	1.512
1152.000	197.300	1.513
1206.000	197.500	1.511
1260.000	196.100	1.522
1314.000	194.500	1.534
1368.000	195.200	1.529
1422.000	193.900	1.539
1476.000	192.600	1.550
1530.000	192.800	1.547
1584.000	191.000	1.562
1638.000	190.800	1.564
1692.000	191.600	1.558
1746.000	189.300	1.576
1800.000	190.100	1.570

Viscosity Test : MY750/22 -1

Resin :Ciba Geigy MY750 Epoxy System
Resin Constituents : MY750 Base Resin : 45% HY917 Hardener : 0.03% DY070 Catalyst
No pigment added
Shear Stress : 500 dyne/cm^2
Test Temperature : 22°C (+/-0.1°C)

Test Time (s)	Shear Rate (1/s)	Dynamic Viscosity (Poise)
18.000	272.900	1.093
72.000	269.300	1.108
126.000	267.700	1.114
180.000	265.900	1.122
234.000	263.600	1.132
288.000	263.500	1.132
342.000	259.200	1.151
396.000	258.900	1.152
450.000	257.400	1.159
504.000	257.900	1.157
558.000	256.300	1.164
612.000	254.200	1.174
666.000	253.200	1.179
720.000	251.900	1.185
774.000	252.000	1.184
828.000	251.800	1.185
882.000	250.300	1.192
936.000	248.600	1.200
990.000	249.200	1.198
1044.000	248.100	1.203
1098.000	245.900	1.213
1152.000	244.700	1.220
1206.000	243.500	1.226
1260.000	243.100	1.228
1314.000	241.900	1.233
1368.000	242.000	1.233
1422.000	241.200	1.237
1476.000	239.900	1.244
1530.000	239.900	1.244
1584.000	240.200	1.242
1638.000	238.500	1.251
1692.000	236.900	1.259
1746.000	236.300	1.263
1800.000	236.000	1.265

Viscosity Test : MY750/23 -1

Resin :Ciba Geigy MY750 Epoxy System
Resin Constituents : MY750 Base Resin : 45% HY917 Hardener : 0.03% DY070 Catalyst
No pigment added
Shear Stress : 500 dyne/cm²
Test Temperature : 23°C (+/-0.1°C)

Test Time (s)	Shear Rate (1/s)	Dynamic Viscosity (Poise)
18.000	289.400	1.031
72.000	288.100	1.036
126.000	284.500	1.049
180.000	281.000	1.062
234.000	279.600	1.067
288.000	278.900	1.070
342.000	276.000	1.081
396.000	273.300	1.092
450.000	272.600	1.094
504.000	272.200	1.100
558.000	270.400	1.103
612.000	269.300	1.108
666.000	268.000	1.113
720.000	266.400	1.120
774.000	266.100	1.121
828.000	262.700	1.136
882.000	263.100	1.134
936.000	262.400	1.137
990.000	261.500	1.141
1044.000	260.500	1.146
1098.000	259.900	1.148
1152.000	259.100	1.152
1206.000	257.000	1.161
1260.000	255.700	1.167
1314.000	255.200	1.169
1368.000	255.600	1.167
1422.000	254.100	1.174
1476.000	254.000	1.175
1530.000	252.200	1.183
1584.000	250.500	1.191
1638.000	251.700	1.186
1692.000	248.500	1.201
1746.000	247.900	1.204
1800.000	247.300	1.207

Viscosity Test : RESIN E 16-1

Resin : Scott Bader Crystic 2-414 PA (Resin E)
Constituent Ratios - Resin 'E' : 1% Methyl Ethyl Ketone Peroxide (MEKP) Catalyst
Shear Stress = 300 dyne/cm²
Test Temperature = 16°C (+/-0.1°C)
Mixing and Preparation Time = 4.5 minutes

Test Time (s)	Shear Rate (1/s)	Dynamic Viscosity (Poise)	Test Time (s)	Shear Rate (1/s)	Dynamic Viscosity (Poise)
4.500	51.040	5.880	463.500	52.290	5.740
18.000	51.590	5.815	477.000	52.250	5.742
31.500	51.710	5.802	490.500	52.220	5.745
45.000	51.800	5.791	504.000	52.120	5.756
58.500	51.690	5.804	517.500	51.980	5.771
72.000	51.800	5.791	531.000	51.790	5.793
85.500	51.940	5.775	544.500	51.730	5.800
99.000	52.040	5.765	558.000	51.700	5.803
112.500	52.100	5.758	571.500	51.840	5.787
126.000	52.330	5.732	585.000	52.180	5.749
139.500	52.310	5.735	598.500	52.260	5.740
153.000	52.230	5.744	612.000	52.210	5.746
166.500	52.270	5.739	625.500	52.230	5.744
180.000	52.190	5.748	639.000	52.130	5.754
193.500	52.020	5.767	652.500	52.130	5.755
207.000	52.040	5.765	666.000	51.940	5.775
220.500	52.080	5.760	679.500	51.850	5.786
234.000	52.060	5.762	693.000	51.820	5.789
247.500	52.070	5.761	706.500	51.810	5.790
261.000	52.080	5.760	720.000	51.800	5.791
274.500	52.030	5.766	733.500	51.820	5.790
288.000	52.300	5.736	747.000	51.890	5.781
301.500	52.530	5.711	760.500	51.840	5.787
315.000	52.650	5.698	774.000	51.790	5.793
328.500	52.560	5.707	787.500	51.660	5.807
342.000	52.500	5.714	801.000	51.590	5.815
355.500	52.480	5.716	814.500	51.630	5.811
369.000	52.350	5.731	828.000	51.580	5.816
382.500	52.220	5.745	841.500	51.610	5.813
396.000	52.210	5.746	855.000	51.660	5.808
409.500	52.250	5.742	868.500	51.570	5.817
423.000	52.210	5.746	882.000	51.610	5.813
436.500	52.250	5.742	895.500	51.440	5.832
450.000	52.200	5.747			

Viscosity Test : RESIN E 16-2

Resin : Scott Bader Crystic 2-414 PA (Resin E)
Constituent Ratios - Resin 'E' : 1% Methyl Ethyl Ketone Peroxide (MEKP) Catalyst
Shear Stress = 300 dyne/cm^2
Test Temperature = 16°C (+/-0.1°C)
Mixing and Preparation Time = 4.5 minutes

Test Time (s)	Shear Rate (1/s)	Dynamic Viscosity (Poise)	Test Time (s)	Shear Rate (1/s)	Dynamic Viscosity (Poise)
4.500	49.650	6.042	463.500	52.180	5.749
18.000	50.530	5.937	477.000	52.390	5.726
31.500	51.240	5.855	490.500	52.590	5.705
45.000	51.720	5.801	504.000	52.160	5.751
58.500	51.780	5.794	517.500	52.340	5.732
72.000	52.250	5.741	531.000	52.370	5.728
85.500	52.060	5.763	544.500	52.150	5.753
99.000	52.410	5.724	558.000	52.310	5.735
112.500	52.190	5.748	571.500	51.820	5.789
126.000	52.620	5.702	585.000	52.100	5.758
139.500	52.290	5.737	598.500	52.210	5.746
153.000	52.620	5.701	612.000	51.850	5.786
166.500	52.730	5.689	625.500	51.980	5.771
180.000	52.610	5.702	639.000	51.590	5.815
193.500	52.860	5.676	652.500	51.820	5.789
207.000	52.530	5.711	666.000	51.950	5.775
220.500	52.850	5.677	679.500	51.620	5.811
234.000	52.450	5.719	693.000	51.820	5.789
247.500	52.760	5.686	706.500	51.350	5.842
261.000	52.800	5.682	720.000	51.590	5.815
274.500	52.630	5.701	733.500	51.510	5.824
288.000	52.830	5.678	747.000	51.340	5.844
301.500	52.570	5.707	760.500	51.420	5.835
315.000	52.890	5.673	774.000	51.090	5.872
328.500	52.500	5.714	787.500	51.290	5.849
342.000	52.700	5.693	801.000	51.410	5.835
355.500	52.820	5.680	814.500	51.100	5.871
369.000	52.480	5.716	828.000	51.270	5.852
382.500	52.660	5.697	841.500	50.840	5.901
396.000	52.360	5.730	855.000	51.130	5.867
409.500	52.570	5.707	868.500	50.600	5.928
423.000	52.760	5.686	882.000	50.870	5.898
436.500	52.310	5.735	895.500	50.830	5.902
450.000	52.570	5.707			

Viscosity Test : RESIN E 18-1

Resin : Scott Bader Crystic 2-414 PA (Resin E)
Constituent Ratios - Resin 'E' : 1% Methyl Ethyl Ketone Peroxide (MEKP) Catalyst
Shear Stress = 300 dyne/cm^2
Test Temperature = 18°C (+/-0.1°C)
Mixing and Preparation Time = 4.5 minutes

Test Time (s)	Shear Rate (1/s)	Dynamic Viscosity (Poise)	Test Time (s)	Shear Rate (1/s)	Dynamic Viscosity (Poise)
4.500	59.520	5.041	463.500	60.940	4.923
18.000	60.280	4.977	477.000	61.140	4.907
31.500	60.430	4.964	490.500	60.920	4.924
45.000	60.950	4.922	504.000	60.540	4.955
58.500	60.850	4.930	517.500	60.790	4.935
72.000	61.370	4.888	531.000	60.530	4.956
85.500	61.240	4.899	544.500	60.750	4.938
99.000	61.590	4.871	558.000	60.370	4.969
112.500	61.380	4.888	571.500	60.720	4.941
126.000	61.710	4.861	585.000	60.360	4.970
139.500	61.440	4.883	598.500	60.540	4.955
153.000	61.730	4.860	612.000	60.310	4.974
166.500	61.590	4.871	625.500	60.480	4.961
180.000	61.810	4.854	639.000	60.180	4.985
193.500	61.690	4.863	652.500	60.370	4.969
207.000	61.930	4.844	666.000	60.060	4.995
220.500	61.690	4.863	679.500	60.210	4.982
234.000	61.910	4.846	693.000	59.870	5.010
247.500	61.680	4.864	706.500	59.660	5.029
261.000	61.730	4.860	720.000	59.760	5.020
274.500	61.620	4.868	733.500	59.580	5.036
288.000	61.570	4.873	747.000	59.760	5.020
301.500	61.660	4.865	760.500	59.440	5.047
315.000	61.760	4.858	774.000	59.660	5.029
328.500	61.450	4.882	787.500	59.480	5.044
342.000	61.670	4.865	801.000	59.590	5.035
355.500	61.490	4.879	814.500	59.280	5.060
369.000	61.640	4.867	828.000	58.920	5.092
382.500	61.380	4.888	841.500	59.140	5.072
396.000	61.420	4.884	855.000	58.770	5.105
409.500	61.200	4.902	868.500	58.950	5.089
423.000	61.370	4.889	882.000	58.690	5.112
436.500	61.120	4.908	895.500	58.770	5.105
450.000	61.330	4.892			

Viscosity Test : RESIN E 20-1

Resin : Scott Bader Crystic 2-414 PA (Resin E)
Constituent Ratios - Resin 'E' : 1% Methyl Ethyl Ketone Peroxide (MEKP) Catalyst
Shear Stress = 240 dyne/cm^2
Test Temperature = 20°C (+/-0.1°C)
Mixing and Preparation Time = 4.5 minutes

Test Time (s)	Shear Rate (1/s)	Dynamic Viscosity (Poise)	Test Time (s)	Shear Rate (1/s)	Dynamic Viscosity (Poise)
4.500	50.100	4.790	463.500	52.350	4.584
18.000	50.960	4.710	477.000	52.020	4.614
31.500	51.370	4.672	490.500	52.300	4.589
45.000	51.880	4.626	504.000	52.020	4.614
58.500	51.900	4.624	517.500	52.130	4.604
72.000	52.370	4.583	531.000	51.860	4.628
85.500	52.260	4.592	544.500	52.100	4.607
99.000	52.570	4.566	558.000	51.790	4.634
112.500	52.510	4.570	571.500	52.060	4.610
126.000	52.690	4.555	585.000	51.700	4.643
139.500	52.530	4.568	598.500	51.960	4.619
153.000	52.820	4.544	612.000	51.610	4.650
166.500	52.740	4.551	625.500	51.800	4.633
180.000	52.950	4.533	639.000	51.520	4.658
193.500	52.740	4.551	652.500	51.640	4.647
207.000	52.940	4.533	666.000	51.390	4.670
220.500	52.750	4.550	679.500	51.570	4.653
234.000	52.960	4.532	693.000	51.280	4.680
247.500	52.810	4.544	706.500	51.500	4.660
261.000	53.020	4.526	720.000	51.210	4.687
274.500	52.820	4.544	733.500	51.450	4.664
288.000	52.880	4.539	747.000	51.110	4.696
301.500	52.670	4.557	760.500	51.280	4.680
315.000	52.860	4.541	774.000	51.060	4.700
328.500	52.630	4.560	787.500	51.160	4.691
342.000	52.780	4.547	801.000	51.010	4.705
355.500	52.660	4.557	814.500	51.120	4.695
369.000	52.760	4.549	828.000	50.870	4.718
382.500	52.560	4.566	841.500	51.030	4.703
396.000	52.580	4.565	855.000	50.790	4.725
409.500	52.480	4.573	868.500	50.420	4.760
423.000	52.140	4.603	882.000	50.600	4.743
436.500	52.450	4.576	895.500	50.370	4.765
450.000	52.130	4.604			

Viscosity Test : RESIN E 22-1

Resin : Scott Bader Crystic 2-414 PA (Resin E)
Constituent Ratios - Resin 'E' : 1% Methyl Ethyl Ketone Peroxide (MEKP) Catalyst
Shear Stress = 220 dyne/cm^2
Test Temperature = 22°C (+/-0.1°C)
Mixing and Preparation Time = 4.5 minutes

Test Time (s)	Shear Rate (1/s)	Dynamic Viscosity (Poise)	Test Time (s)	Shear Rate (1/s)	Dynamic Viscosity (Poise)
4.500	50.080	4.393	463.500	52.370	4.201
18.000	51.310	4.288	477.000	52.370	4.201
31.500	51.760	4.251	490.500	52.490	4.191
45.000	52.060	4.226	504.000	52.450	4.194
58.500	52.240	4.211	517.500	52.310	4.205
72.000	52.470	4.193	531.000	52.220	4.213
85.500	52.700	4.174	544.500	51.970	4.233
99.000	52.960	4.154	558.000	51.900	4.239
112.500	52.920	4.157	571.500	51.860	4.243
126.000	52.930	4.157	585.000	51.740	4.252
139.500	52.910	4.158	598.500	51.650	4.259
153.000	52.950	4.155	612.000	51.570	4.266
166.500	52.940	4.156	625.500	51.460	4.275
180.000	52.990	4.152	639.000	51.470	4.274
193.500	53.010	4.150	652.500	51.320	4.287
207.000	53.190	4.136	666.000	51.410	4.280
220.500	53.380	4.122	679.500	51.400	4.280
234.000	53.250	4.132	693.000	51.240	4.294
247.500	53.240	4.132	706.500	51.230	4.294
261.000	53.120	4.142	720.000	51.040	4.311
274.500	53.060	4.146	733.500	50.960	4.317
288.000	53.040	4.148	747.000	50.820	4.329
301.500	52.990	4.152	760.500	50.760	4.334
315.000	53.000	4.151	774.000	50.560	4.351
328.500	52.980	4.153	787.500	50.490	4.357
342.000	53.110	4.142	801.000	50.530	4.354
355.500	53.180	4.137	814.500	50.480	4.359
369.000	53.040	4.147	828.000	50.360	4.369
382.500	52.930	4.156	841.500	50.260	4.377
396.000	52.840	4.164	855.000	50.080	4.393
409.500	52.670	4.177	868.500	49.930	4.406
423.000	52.680	4.176	882.000	49.860	4.413
436.500	52.550	4.186	895.500	49.760	4.422
450.000	52.430	4.196			

Viscosity Test : RESIN E 24-1

Resin : Scott Bader Crystic 2-414 PA (Resin E)
Constituent Ratios - Resin 'E' : 1% Methyl Ethyl Ketone Peroxide (MEKP) Catalyst
Shear Stress = 200 dyne/cm²
Test Temperature = 24°C (+/-0.1°C)
Mixing and Preparation Time = 4.5 minutes

Test Time (s)	Shear Rate (1/s)	Dynamic Viscosity (Poise)	Test Time (s)	Shear Rate (1/s)	Dynamic Viscosity (Poise)
4.500	48.800	4.098	463.500	51.480	3.885
18.000	50.440	3.965	477.000	51.400	3.891
31.500	51.060	3.917	490.500	51.370	3.894
45.000	51.310	3.898	504.000	50.990	3.923
58.500	51.530	3.881	517.500	51.040	3.919
72.000	51.850	3.857	531.000	50.990	3.922
85.500	52.070	3.841	544.500	50.980	3.923
99.000	52.170	3.834	558.000	50.600	3.952
112.500	52.070	3.841	571.500	50.710	3.944
126.000	52.360	3.820	585.000	50.560	3.956
139.500	52.350	3.821	598.500	50.410	3.967
153.000	52.180	3.833	612.000	50.350	3.972
166.500	52.460	3.813	625.500	50.220	3.983
180.000	52.430	3.815	639.000	50.120	3.990
193.500	52.250	3.828	652.500	50.070	3.995
207.000	52.240	3.828	666.000	49.950	4.004
220.500	52.430	3.815	679.500	49.720	4.023
234.000	52.230	3.830	693.000	49.600	4.033
247.500	52.350	3.821	706.500	49.500	4.041
261.000	52.330	3.822	720.000	49.360	4.052
274.500	52.240	3.828	733.500	49.060	4.076
288.000	52.240	3.829	747.000	49.030	4.079
301.500	52.170	3.834	760.500	49.000	4.081
315.000	52.180	3.833	774.000	48.700	4.107
328.500	52.040	3.843	787.500	48.580	4.117
342.000	52.130	3.836	801.000	48.560	4.118
355.500	51.960	3.849	814.500	48.410	4.131
369.000	51.790	3.862	828.000	48.060	4.162
382.500	51.910	3.853	841.500	47.950	4.171
396.000	51.870	3.856	855.000	47.800	4.184
409.500	51.700	3.868	868.500	47.710	4.192
423.000	51.680	3.870	882.000	47.370	4.222
436.500	51.650	3.872	895.500	47.340	4.225
450.000	51.560	3.879			

Viscosity Test : RESIN E 24-2

Resin : Scott Bader Crystic 2-414 PA (Resin E)
Constituent Ratios - Resin 'E' : 1% Methyl Ethyl Ketone Peroxide (MEKP) Catalyst
Shear Stress = 200 dyne/cm^2
Test Temperature = 24°C (+/-0.1°C)
Mixing and Preparation Time = 12 minutes

Test Time (s)	Shear Rate (1/s)	Dynamic Viscosity (Poise)	Test Time (s)	Shear Rate (1/s)	Dynamic Viscosity (Poise)
4.500	56.050	3.568	463.500	58.730	3.405
18.000	57.370	3.486	477.000	58.680	3.408
31.500	58.400	3.425	490.500	58.760	3.404
45.000	58.780	3.402	504.000	58.610	3.413
58.500	59.000	3.390	517.500	58.410	3.424
72.000	59.520	3.360	531.000	58.380	3.426
85.500	59.610	3.355	544.500	58.370	3.426
99.000	59.850	3.341	558.000	58.240	3.434
112.500	59.940	3.336	571.500	58.080	3.443
126.000	60.040	3.331	585.000	57.910	3.453
139.500	59.940	3.337	598.500	58.000	3.448
153.000	60.080	3.329	612.000	57.840	3.458
166.500	59.910	3.338	625.500	57.690	3.467
180.000	60.010	3.333	639.000	57.500	3.478
193.500	60.060	3.330	652.500	57.490	3.479
207.000	60.240	3.320	666.000	57.430	3.483
220.500	60.010	3.333	679.500	57.360	3.487
234.000	60.010	3.333	693.000	57.140	3.500
247.500	60.010	3.333	706.500	56.930	3.513
261.000	60.150	3.325	720.000	57.040	3.507
274.500	59.940	3.337	733.500	56.910	3.514
288.000	60.000	3.333	747.000	56.750	3.524
301.500	59.630	3.354	760.500	56.520	3.538
315.000	59.830	3.343	774.000	56.540	3.537
328.500	59.730	3.348	787.500	56.510	3.539
342.000	59.650	3.353	801.000	56.380	3.547
355.500	59.280	3.374	814.500	56.040	3.569
369.000	59.380	3.368	828.000	56.150	3.562
382.500	59.400	3.367	841.500	56.030	3.570
396.000	59.310	3.372	855.000	55.940	3.575
409.500	58.990	3.390	868.500	55.850	3.581
423.000	59.100	3.384	882.000	55.590	3.598
436.500	58.990	3.390	895.500	55.490	3.604
450.000	58.910	3.395			

Viscosity Test : RESIN A 18-1

Resin : Scott Bader Crystic 471 PA LV (Resin A)
Constituent Ratios - Resin 'A' : 1% MEKP Catalyst
Shear Stress = 238 dyne/cm^2
Test Temperature = 18°C (+/-0.1°C)
Mixing and Preparation Time = 4.5 minutes

Test Time (s)	Shear Rate (1/s)	Dynamic Viscosity (Poise)	Test Time (s)	Shear Rate (1/s)	Dynamic Viscosity (Poise)
4.500	29.330	8.115	463.500	26.580	8.954
31.500	29.430	8.086	486.000	26.320	9.042
36.000	29.570	8.048	490.500	26.150	9.102
45.000	29.590	8.042	504.000	25.920	9.182
54.000	29.740	8.004	517.500	25.610	9.293
58.500	29.600	8.040	531.000	25.340	9.391
63.000	29.630	8.031	544.500	24.910	9.553
72.000	29.640	8.031	558.000	24.510	9.709
94.500	29.610	8.039	571.500	24.110	9.869
117.000	29.490	8.071	585.000	23.610	10.080
148.500	29.520	8.063	598.500	23.020	10.340
157.500	29.470	8.075	612.000	22.410	10.620
162.000	29.370	8.104	625.500	21.850	10.890
180.000	29.350	8.108	639.000	21.070	11.300
202.500	29.240	8.141	652.500	20.370	11.680
211.500	29.220	8.145	670.500	19.200	12.400
225.000	29.150	8.166	684.000	18.190	13.080
229.500	29.070	8.188	697.500	17.230	13.810
261.000	29.000	8.207	711.000	16.130	14.760
265.500	28.890	8.238	724.500	15.520	15.330
279.000	28.840	8.253	738.000	14.420	16.510
283.500	28.930	8.227	751.500	13.320	17.860
306.000	28.790	8.265	765.000	12.300	19.340
319.500	28.750	8.279	778.500	11.260	21.130
328.500	28.700	8.293	792.000	10.250	23.230
351.000	27.900	8.531	801.000	9.652	24.660
355.500	27.790	8.565	814.500	8.709	27.330
373.500	27.600	8.624	828.000	7.796	30.530
382.500	27.550	8.637	841.500	6.891	34.540
396.000	27.350	8.703	855.000	5.960	39.930
414.000	27.210	8.746	868.500	5.038	47.240
423.000	27.120	8.774	882.000	3.970	59.960
436.500	26.900	8.846	900.000	2.380	100.000
459.000	26.740	8.899			

Viscosity Test : RESIN A 20-1

Resin : Scott Bader Crystic 471 PA LV (Resin A)
Constituent Ratios - Resin 'A' : 1% MEKP Catalyst
Shear Stress = 238 dyne/cm^2
Test Temperature = 20°C (+/-0.1°C)
Mixing and Preparation Time = 4.5 minutes

Test Time (s)	Shear Rate (1/s)	Dynamic Viscosity (Poise)	Test Time (s)	Shear Rate (1/s)	Dynamic Viscosity (Poise)
3.000	32.510	7.320	273.000	26.640	8.933
12.000	32.710	7.276	282.000	25.970	9.163
21.000	32.750	7.267	291.000	25.270	9.416
30.000	32.810	7.253	300.000	24.550	9.693
39.000	32.740	7.269	309.000	23.720	10.030
48.000	32.760	7.266	318.000	22.790	10.440
57.000	32.800	7.256	327.000	21.900	10.870
66.000	32.700	7.279	336.000	20.880	11.400
75.000	32.670	7.286	345.000	19.870	11.980
84.000	32.540	7.315	354.000	18.790	12.660
93.000	32.480	7.327	363.000	17.770	13.390
102.000	32.410	7.344	372.000	16.690	14.260
111.000	32.230	7.385	381.000	15.590	15.260
120.000	32.180	7.397	390.000	14.520	16.390
129.000	32.050	7.426	399.000	13.540	17.580
138.000	31.860	7.471	408.000	12.520	19.000
147.000	31.740	7.498	417.000	11.530	20.640
156.000	31.520	7.551	426.000	10.580	22.500
165.000	31.310	7.601	435.000	9.672	24.610
174.000	31.130	7.644	444.000	8.718	27.300
183.000	30.840	7.717	453.000	7.781	30.590
192.000	30.590	7.781	462.000	6.894	34.520
201.000	30.280	7.861	471.000	5.977	39.820
210.000	29.980	7.939	480.000	4.895	48.630
219.000	29.630	8.031	489.000	3.855	61.740
228.000	29.300	8.122	498.000	2.778	85.670
237.000	28.800	8.265	507.000	1.698	140.100
246.000	28.390	8.384	516.000	0.765	311.200
255.000	27.810	8.559	525.000	0.166	1433.000
264.000	27.250	8.735	534.000	0.020	11870.000

Viscosity Test : RESIN A 22-1

Resin : Scott Bader Crystic 471 PA LV (Resin A)
Constituent Ratios - Resin 'A' : 1% MEKP Catalyst
Shear Stress = 300 dyne/cm²
Test Temperature = 22°C (+/-0.1°C)
Mixing and Preparation Time = 4.5 minutes

Test Time (s)	Shear Rate (1/s)	Dynamic Viscosity (Poise)	Test Time (s)	Shear Rate (1/s)	Dynamic Viscosity (Poise)
2.400	48.360	6.203	247.200	45.150	6.644
9.600	48.940	6.130	254.400	44.860	6.687
16.800	49.180	6.100	261.600	44.520	6.738
24.000	49.000	6.122	268.800	44.110	6.801
31.200	49.140	6.105	276.000	43.550	6.889
38.400	49.260	6.090	283.200	42.810	7.008
45.600	49.380	6.075	290.400	42.360	7.082
52.800	49.440	6.067	297.600	41.830	7.172
60.000	49.530	6.057	304.800	41.150	7.291
67.200	49.260	6.090	312.000	40.480	7.411
74.400	49.250	6.091	319.200	39.370	7.621
81.600	49.280	6.088	326.400	38.640	7.764
88.800	49.340	6.080	333.600	37.910	7.915
96.000	49.300	6.085	340.800	36.890	8.131
103.200	48.990	6.124	348.000	35.950	8.345
110.400	48.960	6.127	355.200	34.730	8.638
117.600	48.950	6.129	362.400	33.720	8.897
124.800	48.930	6.132	369.600	32.620	9.197
132.000	48.880	6.137	376.800	31.440	9.543
139.200	48.500	6.185	384.000	30.220	9.928
146.400	48.490	6.187	391.200	28.950	10.360
153.600	48.420	6.196	398.400	27.540	10.890
160.800	48.320	6.209	405.600	26.310	11.400
168.000	48.260	6.217	412.800	25.140	11.930
175.200	48.200	6.225	420.000	23.860	12.570
182.400	47.700	6.289	427.200	22.620	13.260
189.600	47.550	6.309	434.400	21.290	14.090
196.800	47.360	6.334	441.600	20.120	14.910
204.000	47.230	6.352	448.800	18.940	15.840
211.200	47.000	6.383	456.000	17.790	16.870
218.400	46.500	6.451	463.200	16.600	18.070
225.600	46.350	6.472	470.400	15.360	19.530
232.800	46.090	6.509	477.600	14.290	20.990
240.000	45.800	6.550			

Viscosity Test : JOTNORM 18

Resin : Jotun Norpol 42-10 Polyester
Constituent Ratios -
JN 42-10 : 2% Cobalt Accelerator : 1% Methyl Ethyl Ketone Peroxide (MEKP) Catalyst
Shear Stress = 120 dyne/cm²
Test Temperature = 18°C (+/-0.1°C)
Mixing and Preparation Time = 12 minutes

Test Time (s)	Shear Rate (1/s)	Dynamic Viscosity (Poise)	Test Time (s)	Shear Rate (1/s)	Dynamic Viscosity (Poise)
3.600	41.960	2.860	144.000	39.960	3.003
7.200	41.790	2.871	147.600	39.630	3.028
10.800	41.580	2.886	151.200	39.630	3.028
14.400	41.520	2.890	154.800	39.690	3.023
18.000	41.400	2.899	158.400	39.920	3.006
21.600	41.510	2.891	162.000	39.780	3.017
25.200	41.680	2.879	165.600	39.500	3.038
28.800	41.630	2.883	169.200	39.430	3.043
32.400	41.440	2.896	172.800	39.380	3.047
36.000	41.340	2.902	176.400	39.390	3.046
39.600	41.320	2.904	180.000	39.360	3.049
43.200	41.280	2.907	183.600	39.200	3.061
46.800	41.180	2.914	187.200	39.310	3.053
50.400	41.100	2.919	190.800	39.270	3.056
54.000	41.100	2.920	194.400	39.160	3.064
57.600	41.170	2.915	198.000	38.990	3.078
61.200	41.110	2.919	201.600	38.860	3.088
64.800	41.130	2.917	205.200	38.860	3.088
68.400	40.990	2.928	208.800	38.830	3.091
72.000	40.730	2.946	212.400	38.800	3.092
75.600	40.670	2.951	216.000	38.800	3.093
79.200	40.650	2.952	219.600	38.720	3.099
82.800	40.930	2.932	223.200	38.790	3.094
86.400	40.770	2.943	226.800	38.750	3.097
90.000	40.820	2.939	230.400	38.450	3.121
93.600	40.570	2.958	234.000	38.410	3.124
97.200	40.640	2.953	237.600	38.320	3.131
100.800	40.390	2.971	241.200	38.290	3.134
104.400	40.440	2.967	244.800	38.250	3.137
108.000	40.520	2.961	248.400	38.210	3.141
111.600	40.290	2.979	252.000	38.190	3.142
115.200	40.390	2.971	255.600	38.320	3.131
118.800	40.240	2.982	259.200	38.160	3.145
122.400	40.370	2.973	262.800	37.910	3.166
126.000	40.290	2.979	266.400	37.840	3.171
129.600	40.130	2.990	270.000	37.880	3.168
133.200	40.030	2.998	273.600	37.760	3.178
136.800	39.950	3.004	277.200	37.540	3.197
140.400	40.040	2.997	Continued over the page >		

Viscosity Test : JOTNORM 18
continued

Test Time (s)	Shear Rate (1/s)	Dynamic Viscosity (Poise)	Test Time (s)	Shear Rate (1/s)	Dynamic Viscosity (Poise)
280.800	37.640	3.188	435.600	34.500	3.479
284.400	37.770	3.177	439.200	34.530	3.475
288.000	37.650	3.187	442.800	34.410	3.488
291.600	37.380	3.210	446.400	34.160	3.513
295.200	37.250	3.222	450.000	34.000	3.529
298.800	37.290	3.218	453.600	33.970	3.533
302.400	37.230	3.224	457.200	33.730	3.558
306.000	37.130	3.232	460.800	33.860	3.544
309.600	37.170	3.228	464.400	33.910	3.539
313.200	37.270	3.220	468.000	33.610	3.570
316.800	37.020	3.241	471.600	33.630	3.569
320.400	36.780	3.262	475.200	33.560	3.576
324.000	36.690	3.271	478.800	33.260	3.608
327.600	36.770	3.264	482.400	33.280	3.606
331.200	36.830	3.258	486.000	33.090	3.626
334.800	36.680	3.271	489.600	32.990	3.638
338.400	36.620	3.277	493.200	33.110	3.624
342.000	36.550	3.283	496.800	33.010	3.635
345.600	36.370	3.300	500.400	32.760	3.663
349.200	36.240	3.311	504.000	32.710	3.668
352.800	36.220	3.314	507.600	32.620	3.679
356.400	36.310	3.305	511.200	32.400	3.703
360.000	36.140	3.321	514.800	32.350	3.710
363.600	35.970	3.336	518.400	32.270	3.718
367.200	36.090	3.325	522.000	32.160	3.732
370.800	35.830	3.349	525.600	32.220	3.724
374.400	35.690	3.362	529.200	32.160	3.731
378.000	35.730	3.359	532.800	31.880	3.764
381.600	35.790	3.352	536.400	31.860	3.766
385.200	35.560	3.374	540.000	31.560	3.803
388.800	35.470	3.383	543.600	31.490	3.810
392.400	35.510	3.379	547.200	31.460	3.815
396.000	35.320	3.398	550.800	31.360	3.826
399.600	35.150	3.414	554.400	31.370	3.825
403.200	35.320	3.398	558.000	31.360	3.827
406.800	35.260	3.403	561.600	30.980	3.874
410.400	34.980	3.430	565.200	31.000	3.871
414.000	35.040	3.425	568.800	30.720	3.906
417.600	34.930	3.436	572.400	30.610	3.920
421.200	34.680	3.460	576.000	30.660	3.914
424.800	34.620	3.466	579.600	30.550	3.928
428.400	34.600	3.468	583.200	30.460	3.939
432.000	34.570	3.471	586.800	30.340	3.955

Viscosity Test : JOTNORM 18

continued

Test Time (s)	Shear Rate (1/s)	Dynamic Viscosity (Poise)	Test Time (s)	Shear Rate (1/s)	Dynamic Viscosity (Poise)
590.400	30.100	3.987	655.200	27.960	4.291
594.000	29.970	4.004	658.800	27.710	4.330
597.600	29.740	4.035	662.400	27.530	4.360
601.200	29.850	4.021	666.000	27.330	4.390
604.800	29.670	4.045	669.600	27.410	4.379
608.400	29.630	4.051	673.200	27.100	4.427
612.000	29.450	4.075	676.800	27.040	4.438
615.600	29.290	4.097	680.400	26.780	4.481
619.200	29.290	4.097	684.000	26.660	4.501
622.800	28.900	4.152	687.600	26.600	4.512
626.400	28.940	4.147	691.200	26.530	4.523
630.000	28.860	4.158	694.800	26.410	4.543
633.600	28.640	4.190	698.400	26.160	4.587
637.200	28.510	4.209	702.000	26.030	4.611
640.800	28.240	4.249	705.600	25.720	4.665
644.400	28.250	4.248	709.200	25.710	4.668
648.000	28.120	4.268	712.800	25.540	4.699
651.600	28.100	4.271	716.400	25.480	4.709

Viscosity Test : JOTNORM 20

Resin : Jotun Norpol 42-10 Polyester
Constituent Ratios -
JN 42-10 : 2% Cobalt Accelerator : 1% Methyl Ethyl Ketone Peroxide (MEKP) Catalyst
Shear Stress = 120 dyne/cm²
Test Temperature = 20°C (+/-0.1°C)
Mixing and Preparation Time = 12 minutes

Test Time (s)	Shear Rate (1/s)	Dynamic Viscosity (Poise)	Test Time (s)	Shear Rate (1/s)	Dynamic Viscosity (Poise)
3.600	46.830	2.563	136.800	44.280	2.710
7.200	46.530	2.579	140.400	43.900	2.733
10.800	46.720	2.568	144.000	44.130	2.719
14.400	46.380	2.587	147.600	43.660	2.748
18.000	46.540	2.579	151.200	43.950	2.730
21.600	46.320	2.591	154.800	43.570	2.754
25.200	46.340	2.590	158.400	43.480	2.760
28.800	46.550	2.578	162.000	43.600	2.752
32.400	46.260	2.594	165.600	43.350	2.768
36.000	46.370	2.588	169.200	43.480	2.760
39.600	45.940	2.612	172.800	43.190	2.778
43.200	46.220	2.596	176.400	43.250	2.774
46.800	45.840	2.618	180.000	42.960	2.793
50.400	45.830	2.618	183.600	42.860	2.800
54.000	45.860	2.617	187.200	43.010	2.790
57.600	45.660	2.628	190.800	42.620	2.815
61.200	45.760	2.622	194.400	42.850	2.801
64.800	45.400	2.643	198.000	42.540	2.821
68.400	45.630	2.630	201.600	42.680	2.812
72.000	45.300	2.649	205.200	42.270	2.839
75.600	45.550	2.634	208.800	42.320	2.835
79.200	45.350	2.646	212.400	42.310	2.836
82.800	45.250	2.652	216.000	42.130	2.848
86.400	45.450	2.640	219.600	42.270	2.839
90.000	44.940	2.670	223.200	41.890	2.865
93.600	45.040	2.665	226.800	42.090	2.851
97.200	44.720	2.684	230.400	41.510	2.891
100.800	44.870	2.674	234.000	41.640	2.882
104.400	44.780	2.680	237.600	41.760	2.874
108.000	44.720	2.683	241.200	41.490	2.893
111.600	44.900	2.673	244.800	41.580	2.886
115.200	44.520	2.696	248.400	41.270	2.908
118.800	44.660	2.687	252.000	41.160	2.916
122.400	44.230	2.713	255.600	40.880	2.935
126.000	44.240	2.712	259.200	40.940	2.931
129.600	44.180	2.716	262.800	41.130	2.918
133.200	44.130	2.719	Continued over the page		

Viscosity Test : JOTNORM 20

continued

Test Time (s)	Shear Rate (1/s)	Dynamic Viscosity (Poise)	Test Time (s)	Shear Rate (1/s)	Dynamic Viscosity (Poise)
266.400	40.770	2.943	406.800	36.100	3.324
270.000	40.760	2.944	410.400	35.940	3.339
273.600	40.400	2.971	414.000	35.680	3.364
277.200	40.480	2.964	417.600	35.810	3.351
280.800	40.310	2.977	421.200	35.470	3.383
284.400	40.300	2.978	424.800	35.290	3.401
288.000	40.000	3.000	428.400	34.980	3.430
291.600	39.960	3.003	432.000	34.990	3.429
295.200	39.820	3.013	435.600	34.740	3.454
298.800	39.840	3.012	439.200	34.650	3.464
302.400	39.880	3.009	442.800	34.710	3.457
306.000	39.500	3.038	446.400	34.290	3.499
309.600	39.500	3.038	450.000	34.270	3.502
313.200	39.210	3.061	453.600	34.070	3.522
316.800	39.390	3.046	457.200	33.990	3.530
320.400	39.020	3.075	460.800	33.610	3.571
324.000	38.910	3.084	464.400	33.750	3.556
327.600	38.920	3.083	468.000	33.350	3.598
331.200	38.660	3.104	471.600	33.240	3.610
334.800	38.920	3.083	475.200	33.230	3.612
338.400	38.470	3.120	478.800	32.940	3.643
342.000	38.360	3.128	482.400	32.820	3.657
345.600	38.060	3.153	486.000	32.560	3.685
349.200	38.310	3.132	489.600	32.400	3.704
352.800	38.130	3.147	493.200	32.000	3.750
356.400	37.790	3.175	496.800	32.140	3.734
360.000	37.880	3.167	500.400	31.800	3.773
363.600	37.620	3.190	504.000	31.640	3.792
367.200	37.630	3.189	507.600	31.610	3.796
370.800	37.090	3.235	511.200	31.120	3.856
374.400	37.230	3.223	514.800	31.160	3.851
378.000	37.350	3.213	518.400	30.880	3.886
381.600	37.090	3.235	522.000	30.770	3.900
385.200	36.890	3.253	525.600	30.470	3.938
388.800	36.590	3.280	529.200	30.290	3.962
392.400	36.780	3.263	532.800	30.320	3.958
396.000	36.330	3.303	536.400	29.990	4.001
399.600	36.310	3.305	540.000	29.780	4.030
403.200	36.130	3.321	Continued over the page >		

Viscosity Test : JOTNORM 20

continued

Test Time (s)	Shear Rate (1/s)	Dynamic Viscosity (Poise)	Test Time (s)	Shear Rate (1/s)	Dynamic Viscosity (Poise)
543.600	29.520	4.065	633.600	23.850	5.032
547.200	29.360	4.087	637.200	23.810	5.040
550.800	28.950	4.145	640.800	23.420	5.123
554.400	29.040	4.132	644.400	23.280	5.156
558.000	28.730	4.177	648.000	23.070	5.202
561.600	28.520	4.208	651.600	22.820	5.259
565.200	28.370	4.229	655.200	22.570	5.316
568.800	28.140	4.265	658.800	22.180	5.409
572.400	27.880	4.304	662.400	22.030	5.448
576.000	27.510	4.362	666.000	21.590	5.557
579.600	27.520	4.360	669.600	21.550	5.568
583.200	27.190	4.414	673.200	21.270	5.643
586.800	27.140	4.422	676.800	20.980	5.721
590.400	26.890	4.463	680.400	20.730	5.788
594.000	26.570	4.516	684.000	20.310	5.907
597.600	26.410	4.543	687.600	20.250	5.925
601.200	26.110	4.597	691.200	19.730	6.083
604.800	25.980	4.620	694.800	19.620	6.116
608.400	25.610	4.686	698.400	19.230	6.241
612.000	25.430	4.718	702.000	18.980	6.323
615.600	25.200	4.762	705.600	18.870	6.358
619.200	24.960	4.807	709.200	18.440	6.509
622.800	24.890	4.820	712.800	18.270	6.568
626.400	24.440	4.910	716.400	17.840	6.727
630.000	24.370	4.925	720.000	17.630	6.807

Viscosity Test : JOTNORM 22

Resin : Jotun Norpol 42-10 Polyester
Constituent Ratios -
JN 42-10 : 2% Cobalt Accelerator : 1% Methyl Ethyl Ketone Peroxide (MEKP) Catalyst
Shear Stress = 120 dyne/cm²
Test Temperature = 22°C (+/-0.1°C)
Mixing and Preparation Time = 12 minutes

Test Time (s)	Shear Rate (1/s)	Dynamic Viscosity (Poise)	Test Time (s)	Shear Rate (1/s)	Dynamic Viscosity (Poise)
3.600	46.300	2.592	136.800	42.990	2.791
7.200	46.240	2.595	140.400	42.810	2.803
10.800	46.220	2.596	144.000	42.700	2.810
14.400	46.200	2.597	147.600	42.660	2.813
18.000	46.210	2.597	151.200	42.660	2.813
21.600	46.160	2.600	154.800	42.540	2.821
25.200	45.890	2.615	158.400	42.430	2.828
28.800	45.750	2.623	162.000	42.290	2.838
32.400	45.760	2.622	165.600	41.900	2.864
36.000	45.700	2.626	169.200	41.920	2.863
39.600	45.470	2.639	172.800	41.990	2.858
43.200	45.410	2.643	176.400	41.820	2.870
46.800	45.410	2.642	180.000	41.810	2.870
50.400	45.330	2.647	183.600	41.610	2.884
54.000	44.970	2.668	187.200	41.550	2.888
57.600	45.020	2.666	190.800	41.220	2.911
61.200	45.050	2.663	194.400	41.210	2.912
64.800	45.010	2.666	198.000	41.090	2.920
68.400	44.910	2.672	201.600	41.040	2.924
72.000	44.940	2.670	205.200	40.840	2.938
75.600	44.700	2.685	208.800	40.720	2.947
79.200	44.600	2.690	212.400	40.730	2.947
82.800	44.200	2.715	216.000	40.690	2.949
86.400	44.240	2.712	219.600	40.260	2.980
90.000	44.230	2.713	223.200	40.090	2.993
93.600	44.230	2.713	226.800	40.000	3.000
97.200	44.190	2.715	230.400	40.020	2.998
100.800	44.070	2.723	234.000	39.950	3.004
104.400	44.130	2.719	237.600	39.850	3.011
108.000	43.870	2.735	241.200	39.630	3.028
111.600	43.410	2.764	244.800	39.570	3.032
115.200	43.500	2.758	248.400	39.220	3.060
118.800	43.490	2.759	252.000	39.200	3.061
122.400	43.420	2.764	255.600	39.120	3.067
126.000	43.420	2.764	259.200	38.980	3.079
129.600	43.300	2.771	262.800	38.840	3.090
133.200	43.170	2.780	266.400	38.830	3.090

Viscosity Test : JOTNORM 22

continued

Test Time (s)	Shear Rate (1/s)	Dynamic Viscosity (Poise)	Test Time (s)	Shear Rate (1/s)	Dynamic Viscosity (Poise)
270.000	38.660	3.104	406.800	32.160	3.732
273.600	38.160	3.145	410.400	31.860	3.766
277.200	38.180	3.143	414.000	31.640	3.792
280.800	38.110	3.149	417.600	31.450	3.816
284.400	37.990	3.158	421.200	31.170	3.850
288.000	37.820	3.173	424.800	31.130	3.855
291.600	37.670	3.186	428.400	30.770	3.901
295.200	37.530	3.197	432.000	30.750	3.902
298.800	37.470	3.203	435.600	30.470	3.938
302.400	37.050	3.238	439.200	30.010	3.999
306.000	36.990	3.244	442.800	29.930	4.010
309.600	36.870	3.254	446.400	29.620	4.051
313.200	36.730	3.267	450.000	29.500	4.068
316.800	36.610	3.278	453.600	29.300	4.096
320.400	36.430	3.294	457.200	29.010	4.137
324.000	36.420	3.295	460.800	28.930	4.148
327.600	36.300	3.306	464.400	28.560	4.202
331.200	35.750	3.357	468.000	28.180	4.259
334.800	35.770	3.354	471.600	27.960	4.292
338.400	35.610	3.370	475.200	27.800	4.317
342.000	35.440	3.386	478.800	27.620	4.345
345.600	35.270	3.402	482.400	27.350	4.387
349.200	35.180	3.411	486.000	27.190	4.414
352.800	35.100	3.419	489.600	26.840	4.472
356.400	34.540	3.474	493.200	26.720	4.491
360.000	34.460	3.482	496.800	26.170	4.585
363.600	34.390	3.490	500.400	26.090	4.599
367.200	34.050	3.525	504.000	25.730	4.664
370.800	34.050	3.524	507.600	25.580	4.692
374.400	33.910	3.539	511.200	25.260	4.751
378.000	33.620	3.570	514.800	25.080	4.784
381.600	33.580	3.574	518.400	24.760	4.847
385.200	33.140	3.621	522.000	24.490	4.899
388.800	32.920	3.645	525.600	24.060	4.987
392.400	32.830	3.656	529.200	23.970	5.007
396.000	32.700	3.670	532.800	23.530	5.100
399.600	32.430	3.701	536.400	23.450	5.117
403.200	32.350	3.710	Continued over the page >		

Viscosity Test : JOTNORM 22

continued

Test Time (s)	Shear Rate (1/s)	Dynamic Viscosity (Poise)	Test Time (s)	Shear Rate (1/s)	Dynamic Viscosity (Poise)
540.000	23.070	5.202	630.000	15.310	7.838
543.600	22.830	5.256	633.600	14.840	8.087
547.200	22.520	5.329	637.200	14.530	8.259
550.800	22.140	5.421	640.800	14.290	8.395
554.400	21.880	5.485	644.400	13.880	8.644
558.000	21.550	5.568	648.000	13.520	8.879
561.600	21.330	5.626	651.600	13.250	9.053
565.200	20.970	5.722	655.200	12.940	9.276
568.800	20.800	5.768	658.800	12.550	9.564
572.400	20.410	5.879	662.400	12.180	9.854
576.000	20.250	5.926	666.000	11.810	10.160
579.600	19.730	6.083	669.600	11.500	10.440
583.200	19.410	6.183	673.200	11.140	10.780
586.800	19.180	6.257	676.800	10.770	11.140
590.400	18.860	6.362	680.400	10.440	11.500
594.000	18.560	6.467	684.000	10.140	11.840
597.600	18.270	6.568	687.600	9.766	12.290
601.200	17.930	6.694	691.200	9.317	12.880
604.800	17.670	6.793	694.800	8.996	13.340
608.400	17.180	6.986	698.400	8.666	13.850
612.000	16.860	7.118	702.000	8.369	14.340
615.600	16.620	7.222	705.600	8.048	14.910
619.200	16.260	7.378	709.200	7.676	15.630
622.800	15.940	7.529	712.800	7.326	16.380
626.400	15.660	7.661	716.400	7.005	17.130

Viscosity Test : JOTNORA 16-1

Resin : Jotun Norpol 42-10 Polyester
Constituent Ratios -
JN 42-10 : 2% Cobalt Accelerator : 1% Acetyl Acetone Peroxide Catalyst
Shear Stress = 150 dyne /cm²
Test Temperature = 16 °C (+/-0.1°C)
Mixing and Preparation Time = 12 minutes

Test Time (s)	Shear Rate (1/s)	Dynamic Viscosity (Poise)	Test Time (s)	Shear Rate (1/s)	Dynamic Viscosity (Poise)
3.600	42.040	3.568	165.600	32.620	4.598
7.200	42.110	3.562	169.200	32.220	4.655
10.800	42.130	3.560	172.800	31.780	4.720
14.400	41.700	3.597	176.400	31.460	4.768
18.000	41.850	3.584	180.000	31.040	4.833
21.600	41.570	3.608	183.600	30.580	4.904
25.200	41.210	3.640	187.200	30.010	4.999
28.800	41.240	3.637	190.800	29.630	5.063
32.400	41.290	3.633	194.400	29.110	5.153
36.000	40.890	3.669	198.000	28.480	5.267
39.600	40.740	3.682	201.600	28.120	5.335
43.200	40.730	3.683	205.200	27.480	5.458
46.800	40.700	3.686	208.800	26.860	5.585
50.400	40.360	3.717	212.400	26.240	5.716
54.000	40.320	3.720	216.000	25.640	5.851
57.600	40.330	3.720	219.600	24.910	6.021
61.200	39.760	3.772	223.200	24.320	6.167
64.800	39.780	3.771	226.800	23.670	6.336
68.400	39.720	3.776	230.400	22.870	6.559
72.000	39.270	3.820	234.000	22.150	6.771
75.600	39.280	3.818	237.600	21.500	6.978
79.200	39.090	3.838	241.200	20.510	7.315
82.800	38.570	3.889	244.800	19.840	7.561
86.400	38.670	3.879	248.400	19.020	7.885
90.000	38.600	3.886	252.000	18.040	8.316
93.600	38.110	3.936	255.600	17.290	8.674
97.200	38.030	3.944	259.200	16.360	9.171
100.800	37.950	3.953	262.800	15.330	9.788
104.400	37.700	3.978	266.400	14.480	10.360
108.000	37.270	4.025	270.000	13.560	11.060
111.600	37.170	4.035	273.600	12.540	11.970
115.200	37.090	4.044	277.200	11.440	13.110
118.800	36.570	4.102	280.800	10.340	14.500
122.400	36.440	4.117	284.400	9.216	16.280
126.000	36.270	4.135	288.000	7.968	18.830
129.600	35.760	4.195	291.600	6.624	22.640
133.200	35.700	4.202	295.200	4.895	30.650
136.800	35.380	4.239	298.800	1.481	101.300
140.400	34.810	4.309	302.400	0.289	518.600
144.000	34.710	4.321	306.000	0.052	2910.000
147.600	34.400	4.360	309.600	0.017	8729.000
151.200	34.000	4.412	313.200	0.011	13090.000
154.800	33.700	4.451	316.800	5.73E-03	26190.000
158.400	33.290	4.505	320.400	5.73E-03	26190.000
162.000	32.970	4.550			
Continued in the next column					

Viscosity Test : JOTNORA 18-1

Resin : Jotun Norpol 42-10 Polyester
Constituent Ratios -
JN 42-10 : 2% Cobalt Accelerator : 1% Acetyl Acetone Peroxide (AAP)Catalyst
Shear Stress = 150 dyne/cm^2
Test Temperature = 18°C (+/-0.1°C)
Mixing and Preparation Time = 12 minutes

Test Time (s)	Shear Rate (1/s)	Dynamic Viscosity (Poise)	Test Time (s)	Shear Rate (1/s)	Dynamic Viscosity (Poise)
1.500	35.120	4.271	60.000	21.230	7.064
3.000	34.910	4.297	61.500	20.740	7.231
4.500	34.620	4.332	63.000	20.210	7.424
6.000	34.390	4.362	64.500	19.630	7.640
7.500	34.250	4.379	66.000	19.220	7.804
9.000	33.940	4.419	67.500	18.670	8.034
10.500	33.600	4.464	69.000	18.170	8.253
12.000	33.280	4.507	70.500	17.630	8.506
13.500	33.070	4.535	72.000	17.020	8.814
15.000	32.720	4.585	73.500	16.540	9.071
16.500	32.400	4.629	75.000	15.950	9.406
18.000	32.170	4.663	76.500	15.430	9.719
19.500	31.920	4.699	78.000	14.880	10.080
21.000	31.550	4.755	79.500	14.380	10.430
22.500	31.150	4.815	81.000	13.760	10.900
24.000	30.970	4.844	82.500	13.200	11.360
25.500	30.600	4.901	84.000	12.580	11.920
27.000	30.240	4.961	85.500	11.990	12.510
28.500	29.860	5.023	87.000	11.480	13.060
30.000	29.620	5.064	88.500	10.820	13.860
31.500	29.230	5.132	90.000	10.260	14.630
33.000	28.850	5.199	91.500	9.626	15.580
34.500	28.430	5.275	93.000	8.861	16.930
36.000	28.100	5.338	94.500	8.076	18.570
37.500	27.740	5.407	96.000	6.951	21.580
39.000	27.300	5.494	97.500	5.416	27.700
40.500	26.890	5.578	99.000	3.640	41.210
42.000	26.470	5.667	100.500	2.489	60.270
43.500	26.180	5.730	102.000	0.945	158.700
45.000	25.710	5.834	103.500	0.607	247.000
46.500	25.240	5.944	105.000	0.264	569.300
48.000	24.840	6.038	106.500	0.180	831.300
49.500	24.370	6.155	108.000	0.089	1689.000
51.000	24.000	6.251	109.500	0.066	2277.000
52.500	23.510	6.381	111.000	0.029	5237.000
54.000	23.010	6.520	112.500	0.026	5819.000
55.500	22.670	6.617	114.000	0.011	13090.000
57.000	22.200	6.758	115.500	8.59E-03	17460.000
58.500	21.780	6.887			
Continued in the next column					

Viscosity Test : JOTNORA 20
Resin : Jotun Norpol 42-10 Polyester
Constituent Ratios -
JN 42-10 : 2% Cobalt Accelerator : 1% AAP Catalyst
Shear Stress = 150 dyne/cm²
Test Temperature = 20°C (+/-0.1°C)
Mixing and Preparation Time = 5 minutes

Test Time (s)	Shear Rate (1/s)	Dynamic Viscosity (Poise)	Test Time (s)	Shear Rate (1/s)	Dynamic Viscosity (Poise)
3.000	66.130	2.268	114.000	63.140	2.376
6.000	66.100	2.269	117.000	63.010	2.381
9.000	66.040	2.271	120.000	62.960	2.382
12.000	65.780	2.280	123.000	62.660	2.394
15.000	65.720	2.283	126.000	62.740	2.391
18.000	65.710	2.283	129.000	62.430	2.403
21.000	65.790	2.280	132.000	62.480	2.401
24.000	65.690	2.283	135.000	62.270	2.409
27.000	65.830	2.279	138.000	62.170	2.413
30.000	65.760	2.281	141.000	61.960	2.421
33.000	65.590	2.287	144.000	61.750	2.429
36.000	65.250	2.299	147.000	61.780	2.428
39.000	65.340	2.296	150.000	61.460	2.441
42.000	65.270	2.298	153.000	61.490	2.439
45.000	65.010	2.307	156.000	61.230	2.450
48.000	65.060	2.306	159.000	61.220	2.450
51.000	65.010	2.307	162.000	61.070	2.456
54.000	64.820	2.314	165.000	60.840	2.465
57.000	64.910	2.311	168.000	60.930	2.462
60.000	64.880	2.312	171.000	60.600	2.475
63.000	64.900	2.311	174.000	60.660	2.473
66.000	64.650	2.320	177.000	60.390	2.484
69.000	64.470	2.327	180.000	60.370	2.485
72.000	64.490	2.326	183.000	60.110	2.496
75.000	64.390	2.330	186.000	60.000	2.500
78.000	64.080	2.341	189.000	59.830	2.507
81.000	64.120	2.339	192.000	59.530	2.520
84.000	63.960	2.345	195.000	59.500	2.521
87.000	63.920	2.347	198.000	59.170	2.535
90.000	63.610	2.358	201.000	59.040	2.541
93.000	63.790	2.351	204.000	58.840	2.549
96.000	63.860	2.349	207.000	58.490	2.565
99.000	63.620	2.358	210.000	58.470	2.565
102.000	63.360	2.368	213.000	58.020	2.585
105.000	63.600	2.358	216.000	58.080	2.583
108.000	63.310	2.369	219.000	57.750	2.597
111.000	63.380	2.367	Continued over the page		

Viscosity Test : JOTNORA 20

continued

Test Time (s)	Shear Rate (1/s)	Dynamic Viscosity (Poise)	Test Time (s)	Shear Rate (1/s)	Dynamic Viscosity (Poise)
222.000	57.540	2.607	333.000	43.820	3.423
225.000	57.390	2.613	336.000	43.090	3.481
228.000	57.070	2.629	339.000	42.630	3.519
231.000	57.020	2.631	342.000	41.890	3.581
234.000	56.650	2.648	345.000	40.960	3.662
237.000	56.510	2.654	348.000	40.260	3.726
240.000	56.270	2.666	351.000	39.430	3.804
243.000	55.980	2.680	354.000	38.540	3.892
246.000	55.910	2.683	357.000	37.710	3.978
249.000	55.470	2.704	360.000	36.700	4.087
252.000	55.360	2.709	363.000	35.780	4.193
255.000	55.010	2.727	366.000	34.760	4.316
258.000	54.840	2.735	369.000	33.710	4.449
261.000	54.350	2.760	372.000	32.760	4.579
264.000	53.970	2.779	375.000	31.420	4.774
267.000	53.800	2.788	378.000	30.490	4.920
270.000	53.340	2.812	381.000	29.080	5.159
273.000	53.090	2.826	384.000	28.080	5.342
276.000	52.850	2.838	387.000	26.620	5.634
279.000	52.580	2.853	390.000	25.440	5.897
282.000	52.160	2.876	393.000	24.050	6.237
285.000	51.740	2.899	396.000	22.740	6.597
288.000	51.330	2.923	399.000	21.290	7.047
291.000	51.000	2.941	402.000	19.880	7.546
294.000	50.600	2.964	405.000	18.330	8.182
297.000	50.210	2.987	408.000	16.740	8.959
300.000	49.760	3.014	411.000	14.840	10.110
303.000	49.510	3.030	414.000	12.960	11.580
306.000	48.780	3.075	417.000	11.440	13.110
309.000	48.320	3.104	420.000	9.672	15.510
312.000	47.950	3.129	423.000	7.968	18.830
315.000	47.430	3.162	426.000	5.857	25.610
318.000	46.920	3.197	429.000	1.965	76.350
321.000	46.110	3.253	432.000	0.610	245.900
324.000	45.750	3.279	435.000	0.241	623.500
327.000	45.090	3.327			
330.000	44.500	3.371			
Continued in the next column					

Viscosity Test : JOTNORA : 16-2

Resin : Jotun Norpol 42-10 Polyester
Constituent Ratios -
JN 42-10 : 2% Cobalt Accelerator : 1% AAP Catalyst
Shear Stress = 150 dyne/cm^2
Test Temperature = 16°C (+/-0.1°C)
Mixing and Preparation Time = 5 minutes

Test Time (s)	Shear Rate (1/s)	Dynamic Viscosity (Poise)	Test Time (s)	Shear Rate (1/s)	Dynamic Viscosity (Poise)
3.000	52.070	2.881	117.000	50.620	2.963
6.000	51.620	2.906	120.000	50.480	2.972
9.000	51.790	2.896	123.000	50.330	2.981
12.000	51.790	2.896	126.000	50.460	2.972
15.000	51.640	2.905	129.000	50.150	2.991
18.000	51.830	2.894	132.000	50.170	2.990
21.000	51.490	2.913	135.000	50.370	2.978
24.000	51.610	2.907	138.000	50.120	2.993
27.000	51.640	2.905	141.000	50.110	2.993
30.000	51.210	2.929	144.000	50.310	2.981
33.000	51.420	2.917	147.000	49.780	3.013
36.000	51.610	2.906	150.000	49.910	3.005
39.000	51.290	2.924	153.000	50.140	2.992
42.000	51.370	2.920	156.000	49.780	3.013
45.000	51.530	2.911	159.000	49.880	3.007
48.000	51.060	2.938	162.000	50.010	3.000
51.000	51.170	2.931	165.000	49.410	3.036
54.000	51.410	2.918	168.000	49.700	3.018
57.000	51.000	2.941	171.000	49.830	3.010
60.000	51.140	2.933	174.000	49.450	3.034
63.000	51.370	2.920	177.000	49.530	3.028
66.000	51.080	2.937	180.000	49.710	3.018
69.000	50.940	2.945	183.000	49.250	3.046
72.000	51.090	2.936	186.000	49.440	3.034
75.000	50.960	2.943	189.000	49.540	3.028
78.000	50.880	2.948	192.000	49.210	3.048
81.000	51.100	2.935	195.000	49.370	3.038
84.000	50.900	2.947	198.000	49.350	3.039
87.000	50.830	2.951	201.000	48.960	3.064
90.000	50.780	2.954	204.000	49.110	3.054
93.000	50.860	2.950	207.000	49.320	3.041
96.000	50.650	2.961	210.000	48.950	3.064
99.000	50.800	2.953	213.000	49.120	3.054
102.000	50.580	2.966	216.000	49.030	3.059
105.000	50.670	2.960	219.000	48.720	3.079
108.000	50.680	2.960	222.000	48.870	3.069
111.000	50.270	2.984	225.000	48.960	3.064
114.000	50.420	2.975	Continued over the page		
Continued in the next column					

A2 : 35

Viscosity Test : JOTNORA : 16-2

continued

Test Time (s)	Shear Rate (1/s)	Dynamic Viscosity (Poise)	Test Time (s)	Shear Rate (1/s)	Dynamic Viscosity (Poise)
228.000	48.630	3.085	342.000	45.760	3.278
231.000	48.600	3.086	345.000	45.700	3.282
234.000	48.690	3.080	348.000	45.410	3.304
237.000	48.360	3.101	351.000	45.490	3.297
240.000	48.630	3.085	354.000	45.500	3.297
243.000	48.460	3.095	357.000	44.980	3.334
246.000	48.210	3.111	360.000	45.140	3.323
249.000	48.300	3.105	363.000	45.140	3.323
252.000	48.140	3.116	366.000	44.710	3.355
255.000	48.060	3.121	369.000	44.810	3.347
258.000	48.170	3.114	372.000	44.730	3.353
261.000	47.860	3.134	375.000	44.450	3.375
264.000	47.790	3.139	378.000	44.550	3.367
267.000	47.920	3.130	381.000	44.090	3.402
270.000	47.810	3.137	384.000	44.030	3.407
273.000	47.680	3.146	387.000	44.170	3.396
276.000	47.710	3.144	390.000	43.840	3.422
279.000	47.270	3.173	393.000	43.610	3.440
282.000	47.420	3.163	396.000	43.710	3.432
285.000	47.600	3.151	399.000	43.370	3.459
288.000	47.100	3.184	402.000	43.320	3.463
291.000	47.130	3.183	405.000	43.280	3.466
294.000	47.240	3.175	408.000	42.890	3.497
297.000	46.920	3.197	411.000	42.930	3.494
300.000	47.060	3.188	414.000	42.890	3.497
303.000	47.210	3.177	417.000	42.420	3.536
306.000	46.540	3.223	420.000	42.570	3.524
309.000	46.860	3.201	423.000	42.380	3.540
312.000	46.850	3.202	426.000	41.960	3.575
315.000	46.470	3.228	429.000	41.990	3.573
318.000	46.520	3.224	432.000	41.950	3.576
321.000	46.370	3.235	435.000	41.460	3.618
324.000	46.250	3.244	438.000	41.450	3.619
327.000	46.380	3.234	441.000	41.170	3.643
330.000	46.090	3.255	444.000	40.950	3.663
333.000	45.920	3.267	447.000	40.900	3.668
336.000	46.000	3.261	450.000	40.450	3.708
339.000	45.740	3.280	453.000	40.410	3.712
Continued in the next column			Continued over the page >		

Viscosity Test : JOTNORA : 16-2

continued

Test Time (s)	Shear Rate (1/s)	Dynamic Viscosity (Poise)	Test Time (s)	Shear Rate (1/s)	Dynamic Viscosity (Poise)
456.000	40.310	3.721	531.000	32.810	4.571
459.000	39.930	3.756	534.000	32.450	4.623
462.000	39.720	3.776	537.000	31.890	4.704
465.000	39.700	3.778	540.000	31.420	4.774
468.000	39.230	3.823	543.000	30.880	4.858
471.000	39.090	3.838	546.000	30.380	4.937
474.000	39.080	3.839	549.000	30.080	4.986
477.000	38.580	3.888	552.000	29.240	5.130
480.000	38.360	3.910	555.000	28.950	5.182
483.000	38.210	3.926	558.000	28.410	5.279
486.000	37.920	3.955	561.000	27.700	5.415
489.000	37.660	3.983	564.000	27.190	5.516
492.000	37.270	4.025	567.000	26.630	5.633
495.000	37.000	4.054	570.000	25.890	5.793
498.000	36.750	4.082	573.000	25.230	5.944
501.000	36.260	4.137	576.000	24.700	6.074
504.000	36.090	4.157	579.000	23.880	6.282
507.000	35.890	4.180	582.000	23.280	6.444
510.000	35.260	4.254	585.000	22.380	6.702
513.000	35.090	4.275	588.000	21.670	6.920
516.000	34.840	4.305	591.000	21.070	7.120
519.000	34.230	4.382	594.000	20.080	7.471
522.000	34.130	4.395	597.000	19.300	7.773
525.000	33.590	4.465	600.000	18.680	8.030
528.000	33.090	4.533			

Viscosity Test : JOTNORA 18-2

Resin : Jotun Norpol 42-10 Polyester
Constituent Ratios -
JN 42-10 : 2% Cobalt Accelerator : 1% Acetyl Acetone Peroxide Catalyst
Shear Stress = 150 dyne/cm^2
Test Temperature = 18°C (+/-0.1°C)
Mixing and Preparation Time = 5 minutes

Test Time (s)	Shear Rate (1/s)	Dynamic Viscosity (Poise)	Test Time (s)	Shear Rate (1/s)	Dynamic Viscosity (Poise)
3.000	57.610	2.604	114.000	53.760	2.790
6.000	57.490	2.609	117.000	53.570	2.800
9.000	57.440	2.611	120.000	53.490	2.805
12.000	57.370	2.614	123.000	53.340	2.812
15.000	57.270	2.619	126.000	53.160	2.821
18.000	57.180	2.623	129.000	53.110	2.824
21.000	57.140	2.625	132.000	53.000	2.830
24.000	57.210	2.622	135.000	52.610	2.851
27.000	57.110	2.627	138.000	52.480	2.858
30.000	56.940	2.635	141.000	52.230	2.872
33.000	56.780	2.640	144.000	52.110	2.878
36.000	56.620	2.649	147.000	51.970	2.886
39.000	56.600	2.650	150.000	51.760	2.898
42.000	56.520	2.654	153.000	51.690	2.902
45.000	56.460	2.657	156.000	51.450	2.915
48.000	56.390	2.660	159.000	51.330	2.922
51.000	56.290	2.665	162.000	51.000	2.941
54.000	56.180	2.670	165.000	50.840	2.950
57.000	56.030	2.677	168.000	50.630	2.963
60.000	56.090	2.674	171.000	50.470	2.972
63.000	55.970	2.680	174.000	50.350	2.979
66.000	55.920	2.683	177.000	50.080	2.995
69.000	55.770	2.690	180.000	49.630	3.022
72.000	55.650	2.696	183.000	49.410	3.036
75.000	55.560	2.700	186.000	49.210	3.048
78.000	55.340	2.710	189.000	48.950	3.064
81.000	54.980	2.728	192.000	48.790	3.075
84.000	54.930	2.731	195.000	48.540	3.090
87.000	54.880	2.733	198.000	48.170	3.114
90.000	54.790	2.738	201.000	47.910	3.131
93.000	54.660	2.744	204.000	47.610	3.151
96.000	54.600	2.747	207.000	47.440	3.162
99.000	54.480	2.753	210.000	47.130	3.183
102.000	54.410	2.757	213.000	46.660	3.215
105.000	54.170	2.769	216.000	46.230	3.245
108.000	54.180	2.768	219.000	46.000	3.261
111.000	53.950	2.780	Continued over the page >		
Continued in the next column					

Viscosity Test : JOTNORA 18-2

continued

Test Time (s)	Shear Rate (1/s)	Dynamic Viscosity (Poise)	Test Time (s)	Shear Rate (1/s)	Dynamic Viscosity (Poise)
222.000	45.720	3.281	306.000	28.380	5.286
225.000	45.220	3.317	309.000	27.260	5.503
228.000	44.920	3.339	312.000	26.380	5.686
231.000	44.650	3.359	315.000	25.200	5.953
234.000	44.220	3.392	318.000	24.050	6.238
237.000	43.670	3.435	321.000	23.020	6.515
240.000	43.260	3.467	324.000	21.800	6.880
243.000	43.030	3.486	327.000	20.590	7.286
246.000	42.480	3.531	330.000	19.420	7.724
249.000	41.980	3.573	333.000	18.180	8.249
252.000	41.550	3.610	336.000	16.880	8.885
255.000	40.910	3.667	339.000	15.550	9.644
258.000	40.250	3.727	342.000	14.130	10.620
261.000	39.810	3.768	345.000	12.590	11.920
264.000	39.310	3.815	348.000	10.870	13.790
267.000	38.650	3.881	351.000	9.193	16.320
270.000	38.100	3.937	354.000	7.724	19.420
273.000	37.510	3.999	357.000	6.521	23.000
276.000	36.740	4.083	360.000	5.453	27.510
279.000	36.120	4.153	363.000	3.268	45.900
282.000	35.300	4.250	366.000	0.596	251.800
285.000	34.580	4.338	369.000	0.103	1455.000
288.000	33.860	4.430	372.000	0.034	4365.000
291.000	32.810	4.571	375.000	0.014	10470.000
294.000	32.020	4.684	378.000	5.73E-03	26190.000
297.000	31.140	4.816	381.000	2.86E-03	52370.000
300.000	30.260	4.958	384.000	2.86E-03	52370.000
303.000	29.300	5.120			

APPENDIX 3

Pressure Measurement Elements

I) Pressure Measurement Component List

II) Pressure Transducer Amplifier Circuit

Pressure Transducer Component List

The following table is a list of the components used for one pressure transducer circuit. All the components were ordered from the Radio Spares Catalogue.

Component Description	Quantity	RS Stock No.
0-15psi pressure gauge transducer	1	303-343
50V 0.1µF ceramic disc capacitor	2	124-178
12V to +/- 15V d.c to d.c. converter	1	592-515
1.26V precision voltage reference	1	283-564
UA741CP	1	305-311
CA3240E-1	2	308-641
63V 10µF electrolytic capacitor	3	105-060
100KΩ cermet trimmer resistor	2	187-258
10KΩ cermet trimmer resistor	4	187-220
10KΩ side adjusting resistor	1	186-621
37.4KΩ 55y precision resistor	1	167-276
10KΩ 55y precision resistor	1	166-728
1KΩ 55y precision resistor	3	165-769
200KΩ metal film resistor	2	164-564
4-way pcb mounted screw terminals	1	425-847
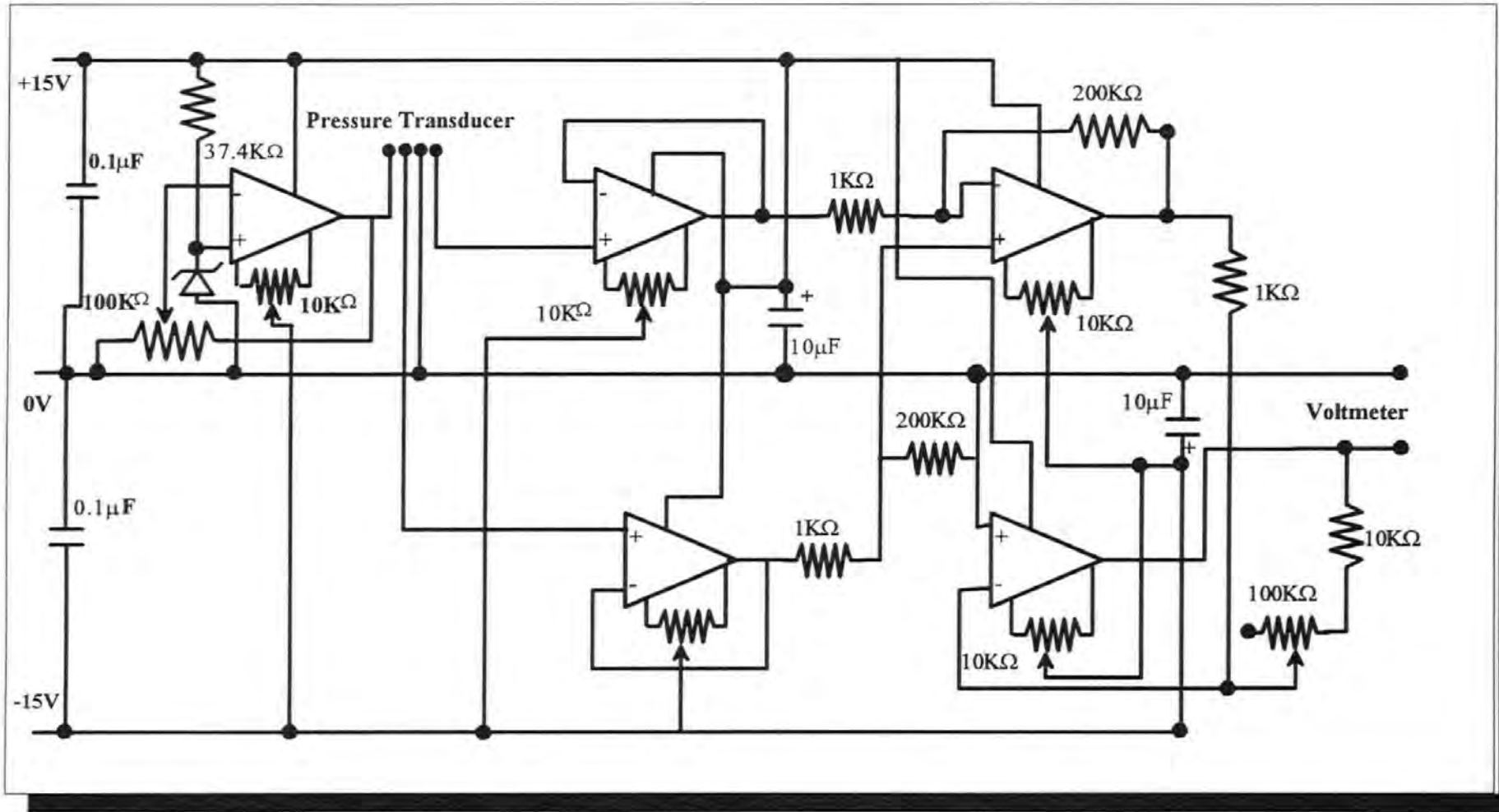
Pressure Transducer Amplifier Circuit Diagram

APPENDIX 4

Location of Microspecimen taken from the Moulded Plates and used in the Image Analysis

I) For Anisotropic Plates (0-0-0-0 lay-up wrt Bound Tows)

II) For Isotropic Plates (0-90-90-0 lay-up wrt Bound Tows)

Appendix 4:1

A4 : 1

DWO 149-4

A
E D C ○ F G H
B

20mm

20mm

Direction of Bound Tow

DWO 150-4

A
B
C
I H G ○ J K L
D
E
F

20mm

20mm

Direction of Bound Tow

DWO 151-4

A
B
G F E ○ H I J
C
D

20mm

20mm

Direction of Bound Tow

DWO 156-4

A
E D C ○ F G H
B

20mm

20mm

Direction of Bound Tow
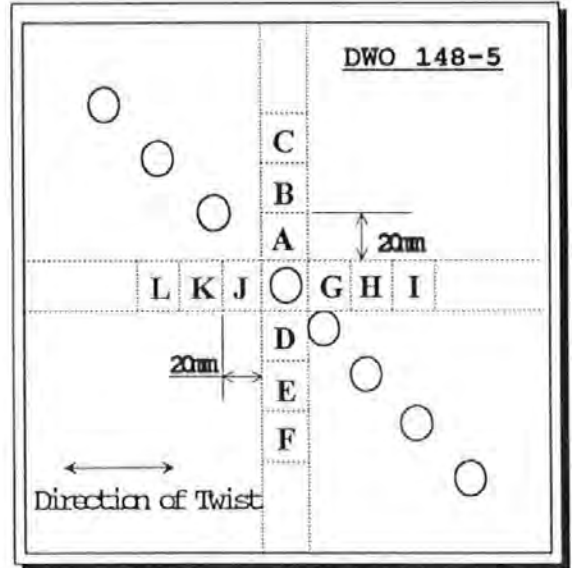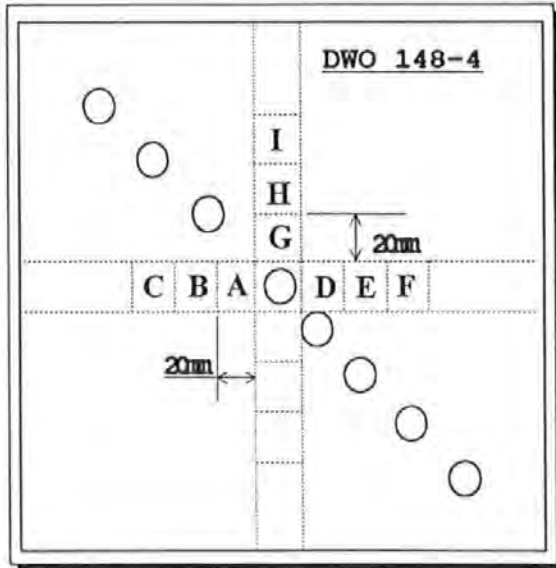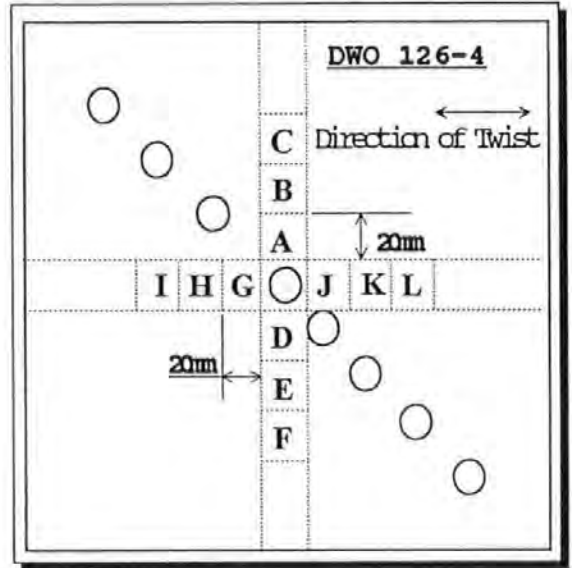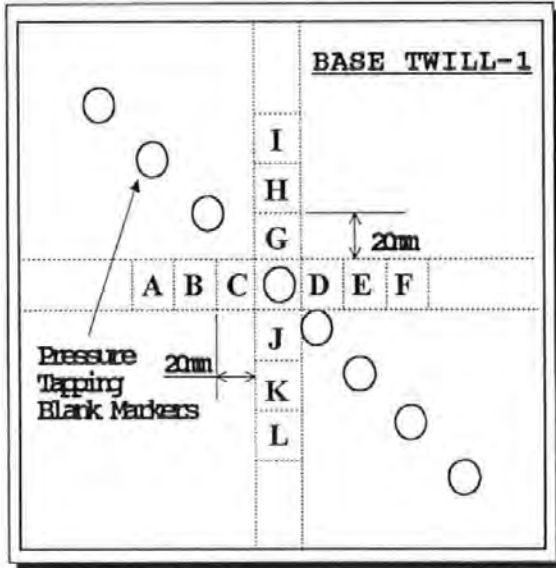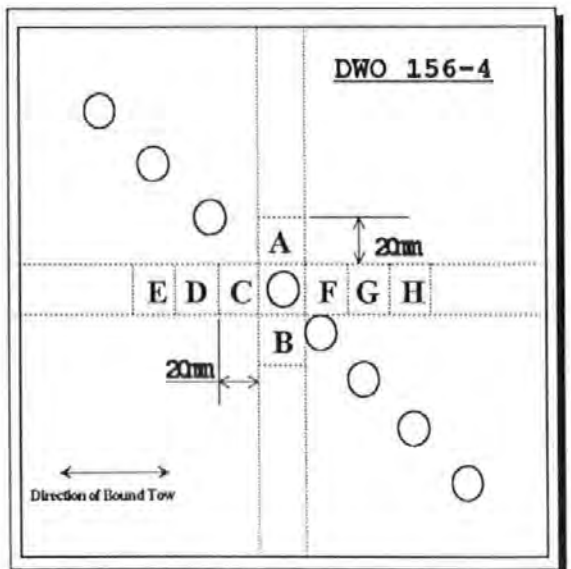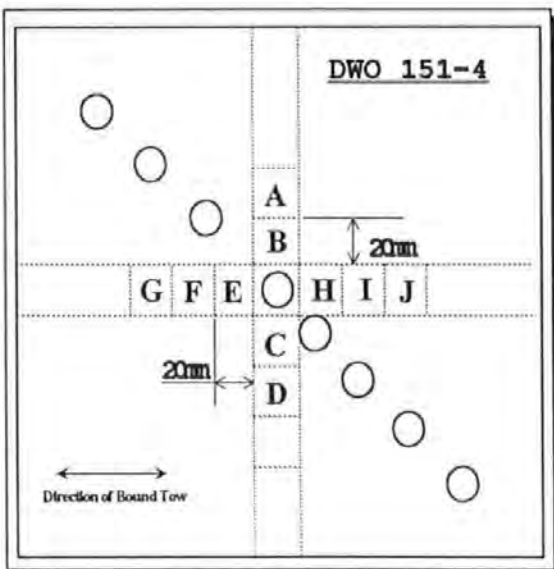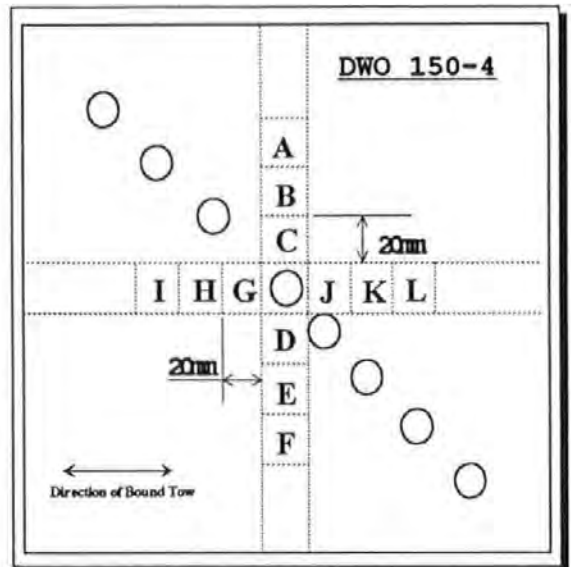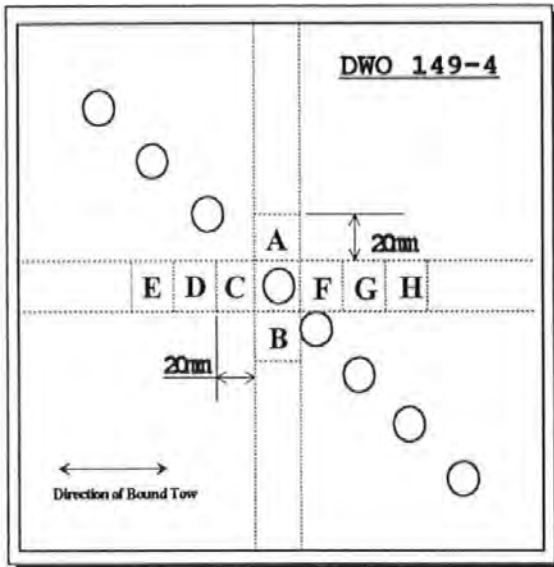
Appendix 4:2

Isotropic Plates

Plates in this appendix are layed up in a balanced isotropic pack i.e. (0-90-90-0) with respect to the Spiral Bound Tows

DWO 126

I   20mm

○ J

20mm

DWO 148

E   20mm

○ F

20mm
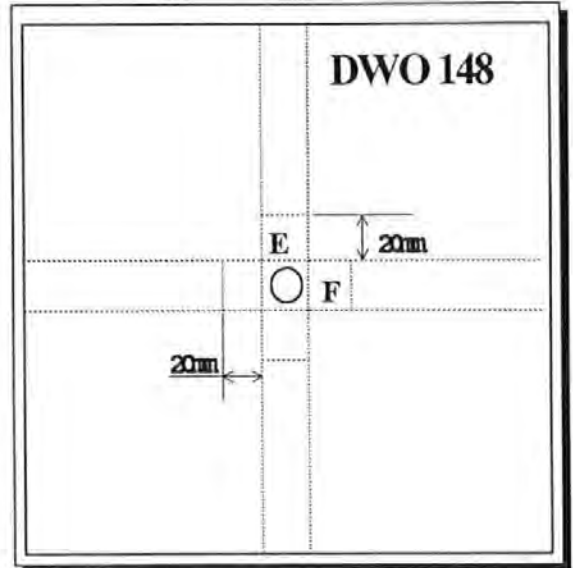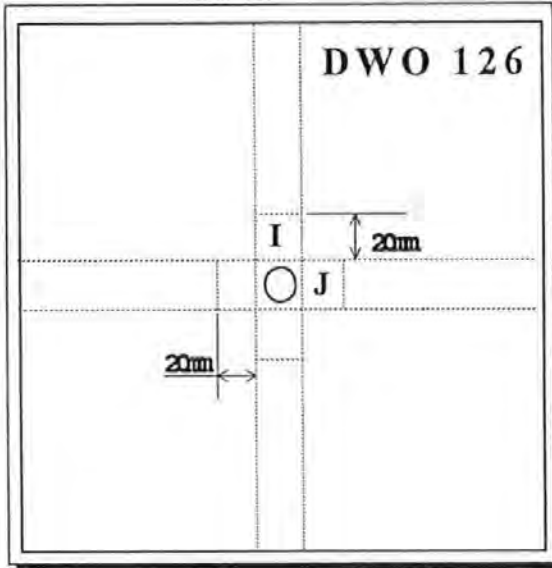
I & E - Warp Direction (Perpendicular to Bound Tows)
according to outer layer of laminate
J & F- Weft Direction (Parallel to Bound Tows)

DWO 150

G   20mm

○ H

20mm

DWO 156

C   20mm

○ D

20mm
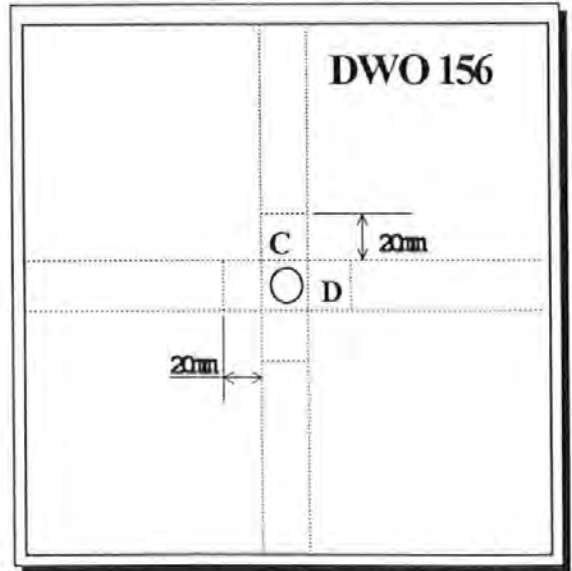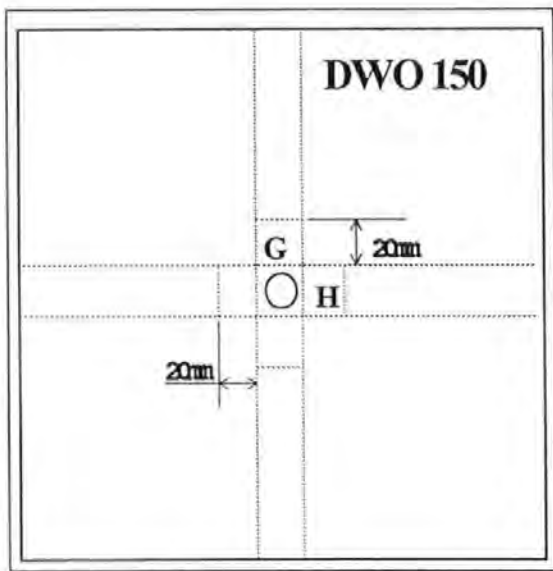
C & G - Warp Direction (Perpendicular to Bound Tows)
according to outer layer of laminate
D & H - Weft Direction (Parallel to Bound Tows)

A4 : 4

BASE TWILL

A

20mm

B

20mm
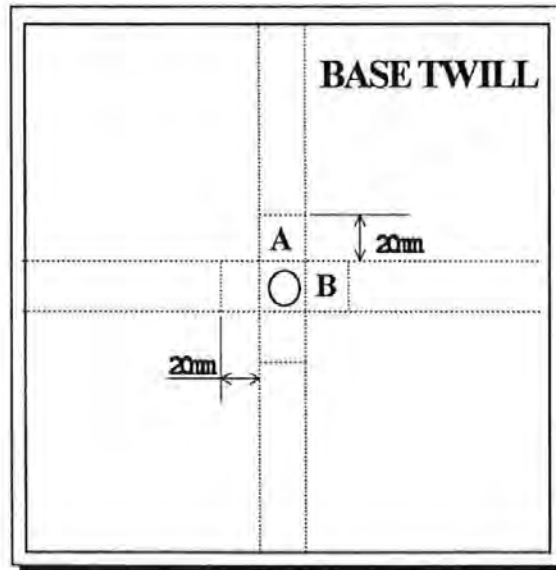
Warp and Weft layers in balanced 0-90-90-0 lay-up
A - Warp
B - Weft

APPENDIX 5

Image Analysis QuickBasic Programs

I) RESIN LOW :

Used to detect

Flow Channel Size and Geometry

II) ZONE1:

Used to determine the

Fibre Distribution within the Tows

PROGRAM : RESINLOW.QBA

1 rem for low magnification work looking at resin areas. The very small areas
                    are removed and the remaining areas measured.
2 rem after a segmentation the areas are measured again. This shows up thin
                    lines of resin.

10 qmenu 'image_setup'
20 mframe 74 143 197 353
21 iframe 76 0 193 512
50 qmenu 'acquire'
55 qmenu 'frames'
60 btoph 0 1 256 3 : sub8 0 1 5
70 wtoph 0 1 256 3 : add8 5 1 1
80 greydetect 0 56 126 4 1 0
85 pausetext 2"Check that resin areas are detected i.e. red"
90 qmenu 'detect'
95 pausetext 2""
100 binerode 1 2 0 2
110 build 1 2
120 fillholes 2 3
130 setftrpar "1,33,13,8,2,3,9,11"
140 ftrgrey 1 : measfeat 3 1 0 300000 : clraccept
150 acceptxfer 3 5 155 pausetext 2"Use print to save data to disc"
160 qmenu 'feature_results'
165 pausetext 2"Use print to save data to disc"
170 binsegment 3 4 256 1 1
175 pausetext 2""
180 setftrpar "1,29,28,4,2,3,5,13"
190 ftrgrey 1 : measfeat 4 1 0 300000 : clraccept
200 acceptxfer 4 6
205 pausetext 2"Use print to save data to disc"
210 qmenu 'feature_results'
220 end

PROGRAM : ZONE1.QBA

```
 5 REM TO MEASURE ZONES OF INFLUENE IN RESIN OF FIBRES
10 C=1
20 I$="1"
30 INPUT "WHICH SPEC NO.?  "N$
40 camera 1
50 scanner   38.24   8.30
60 setlamps  62.91 0
70 calibrate 2, 'i'
80 RIASETTINGS "CAL_VALUE" K
90 qmenu 'calibrate'
100 mframe 100 100 312 412
110 iframe 0 0 512 512
120 FOR I=1 TO 54
130 autofocus 20 2 5
140 multiacquire 5 0 4
150 greydetect 0 78 154 4 1 0
160 binsegment 1 2 256 1 0
170 binopen 2 3 256 3
180 skiz 3 5 0
190 rem 1area, 4width, 5height, 13perim, 29Y C OF G, 28X C OF G
200 setftrpar "1,4,5,13,29,28,2,3"
210 ftrgrey 0 : measfeat 5 1 4 300000 : clraccept
220 acceptxfer 5 6
230 OPEN#1 "c:/fel/"+N$+"Z"+I$+".PRN"
240 RFEATNUM N(1)
250 FOR F=0 TO N(1)-1
260 RFEATRES F 1 A(1)
270 RFEATRES F 4 B(1)
280 RFEATRES F 5 C(1)
290 RFEATRES F 13 D(1)
300 RFEATRES F 29 E(1)
310 RFEATRES F 28 F(1)
320 PRINT#1:K*K*A(1),K*B(1),K*C(1),K*D(1),E(1),F(1)
330 NEXT F
340 CLOSE#1
350 HISTOFEAT 0 0 1 0.000000 3173.388889 60 0
360 binx 3 5 10 1 0 0
370 setftrpar "1,4,5,13,29,28,2,3"
380 ftrgrey 0 : measfeat 10 1 4 300000 : clraccept
390 acceptxfer 10 1
400 OPEN#2 "c:/fel/"+N$+"F"+I$+".PRN"
```

```
410 RFEATNUM N(1)
420 FOR F=0 TO N(1)-1
430 RFEATRES F 1 A(1)
440 RFEATRES F 4 B(1)
450 RFEATRES F 5 C(1)
460 RFEATRES F 13 D(1)
470 RFEATRES F 29 E(1)
480 RFEATRES F 28 F(1)
490 PRINT#2:K*K*A(1),K*B(1),K*C(1),K*D(1),E(1),F(1)
500 NEXT F
510 CLOSE#2
520 HISTOFEAT 1 0 1 0.000000 952.016667 60 0
530 IF I=46 GOTO 580
540 STEPSTAGE 4
550 C=C+1
560 I$=STR$(C)
570 NEXT I
580 QUIC
590 END
```

APPENDIX 6

Flow Rates of Various Fluids and Resins into the Flow Enhancing Fabrics

Figure A6:1 Isotropic Flow through 2x2 Base Twill Fabric
(no bound tows)
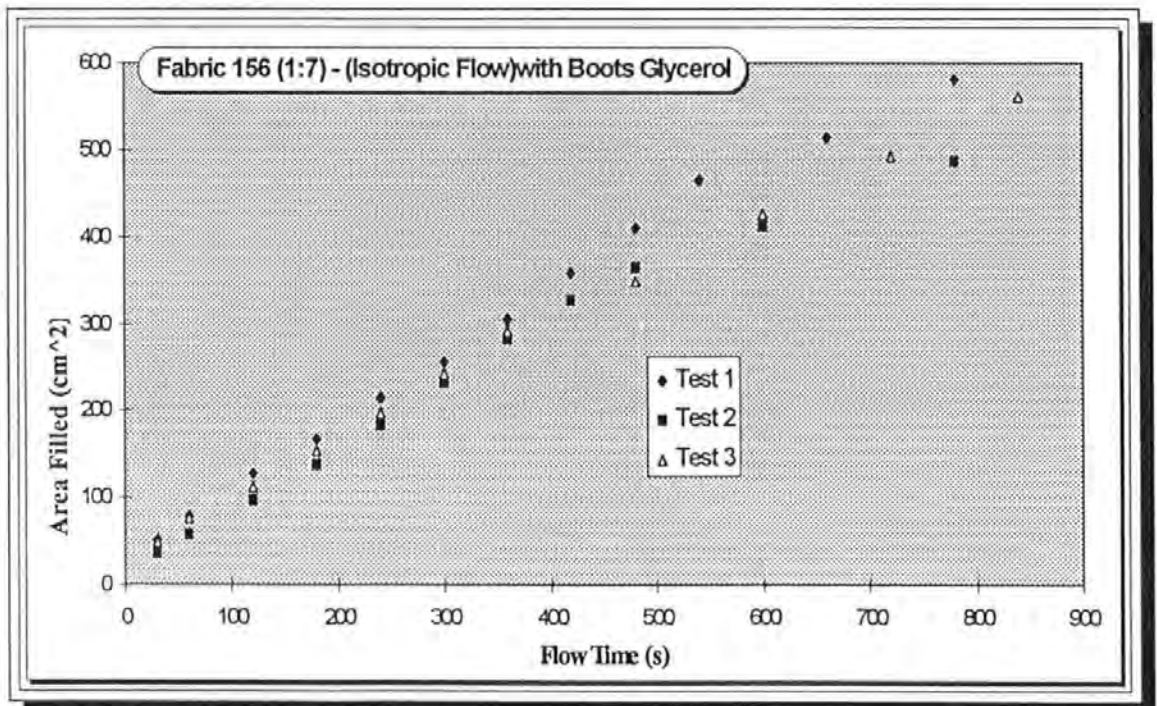
Figure A6:2 Isotropic Flow through Fabric DWO 156
(Ratio of 1:7 of Bound to Conventional Tows)
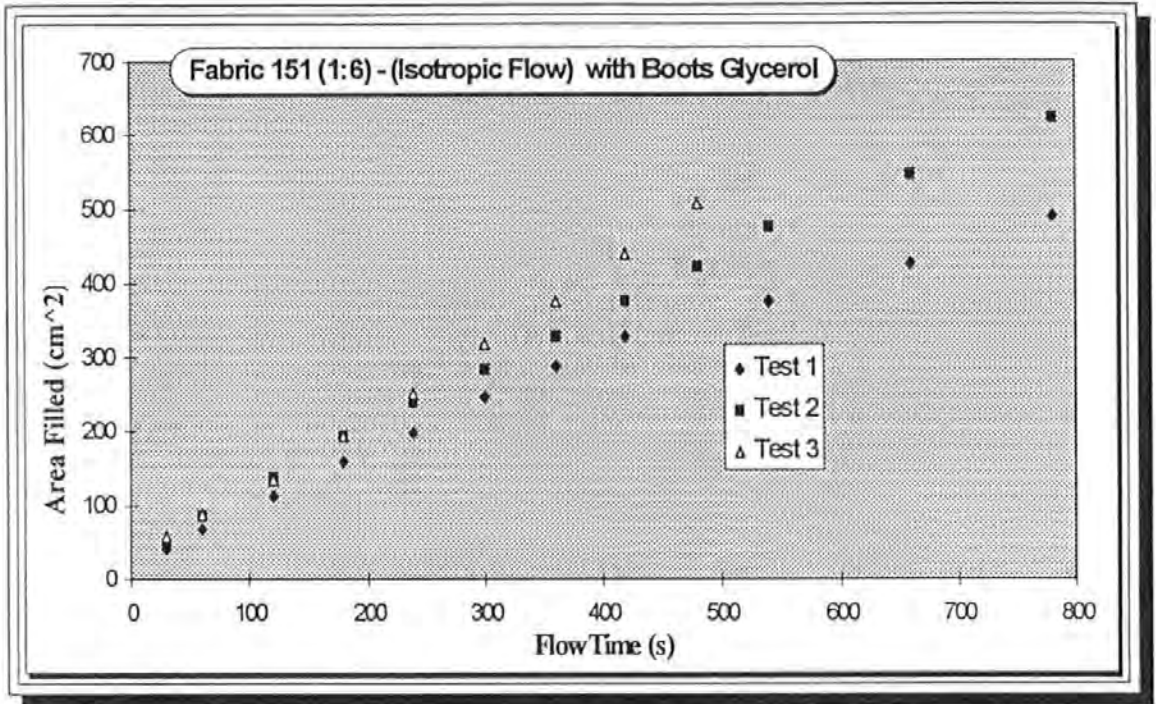
Figure A6:3 Isotropic Flow through Fabric DWO 151
*(Ratio 1:6 of Bound to Conventional Tows)*
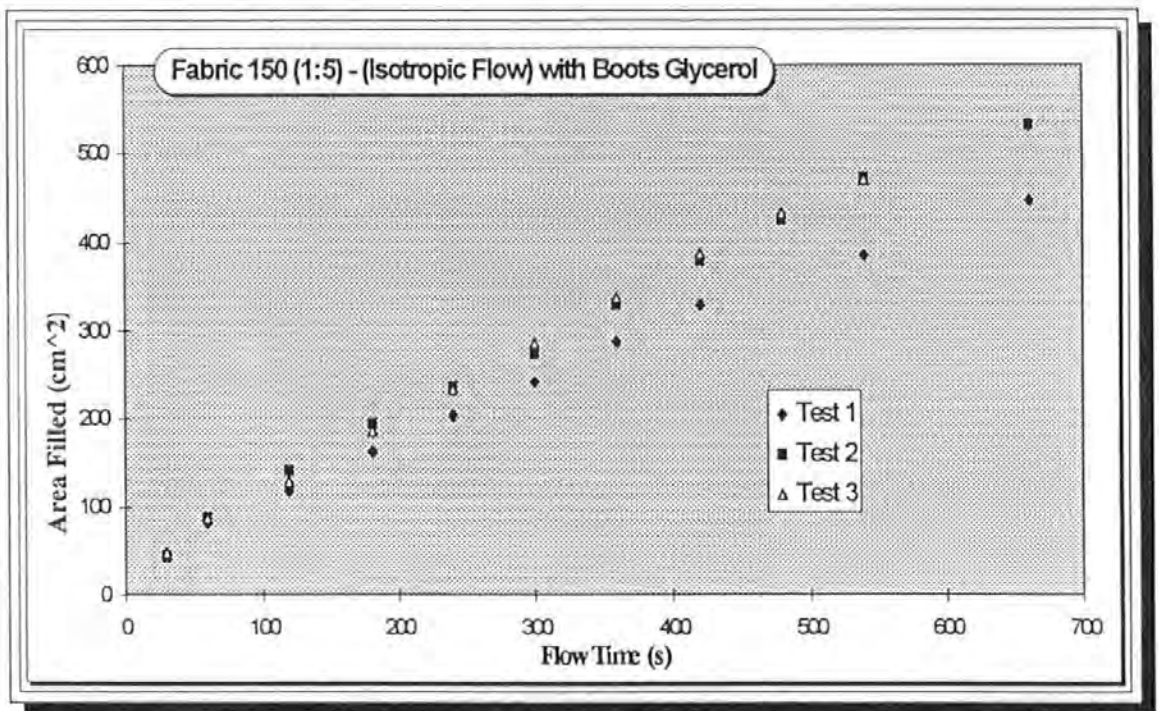
Figure A6:4 Isotropic Flow through Fabric DWO 150
(Ratio 1:5 of Bound to Conventional Tows)
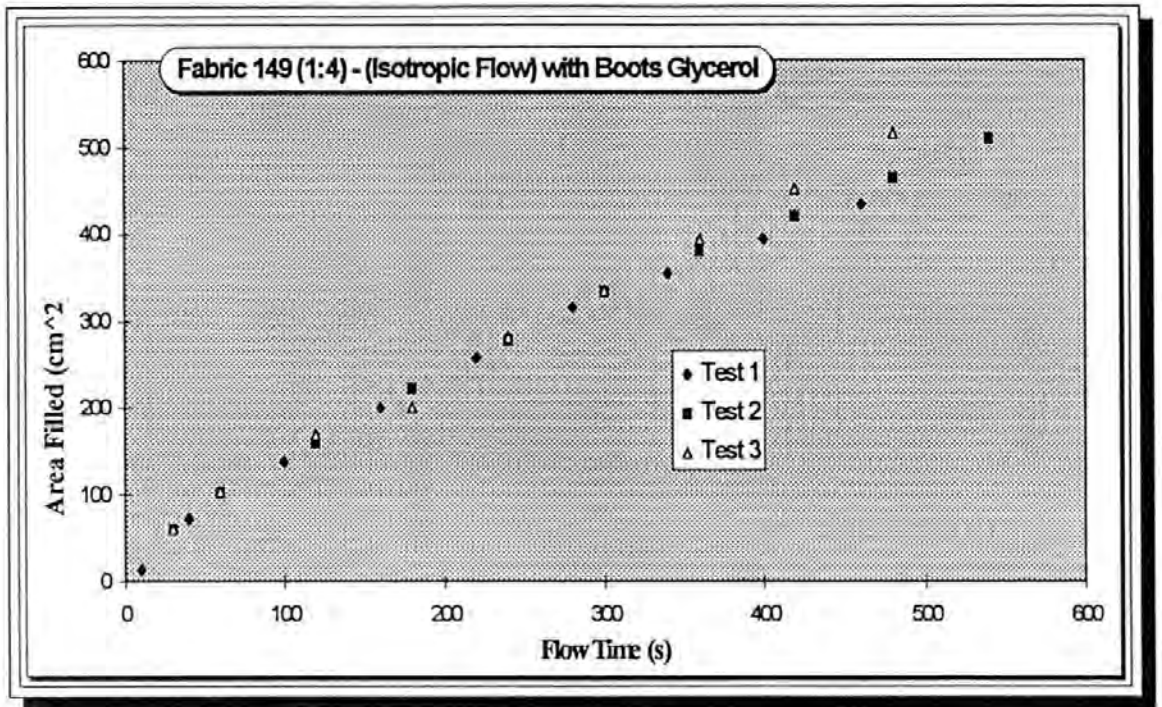
Figure A6:5 Isotropic Flow through Fabric DWO 149
(Ratio of 1:4 Bound to Conventional Tows)
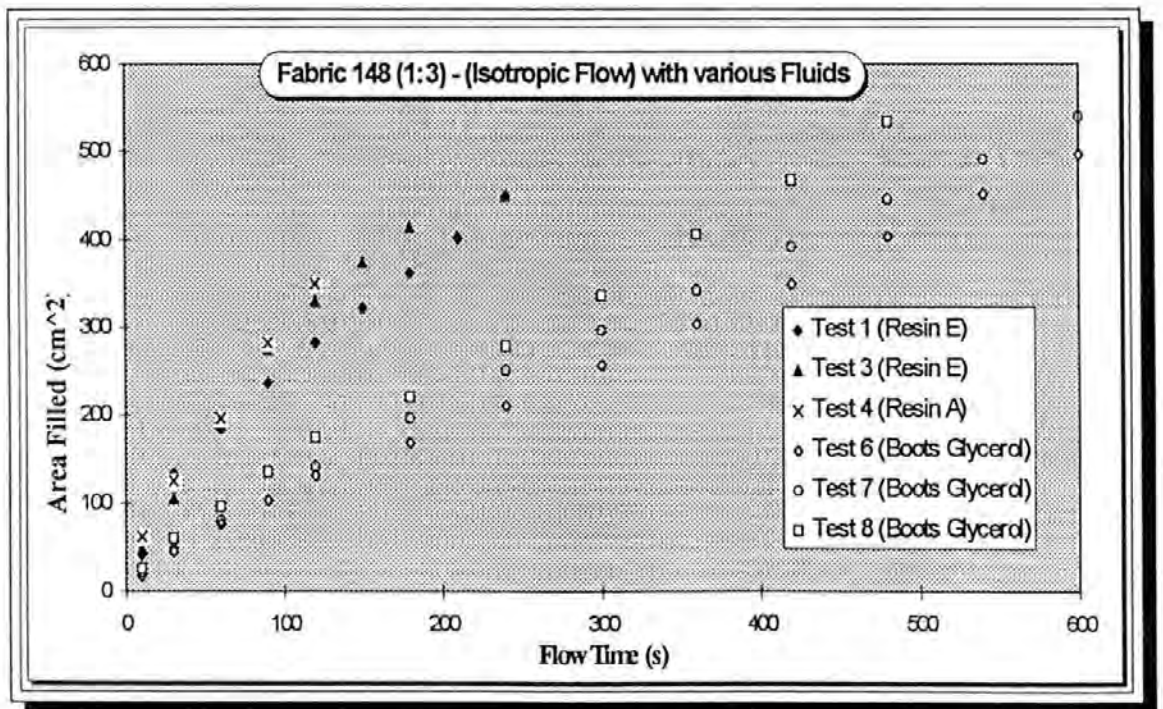
Figure A6:6 Isotropic Flow through Fabric DWO 148
(Ratio of 1:3 Bound to Conventional Tows)
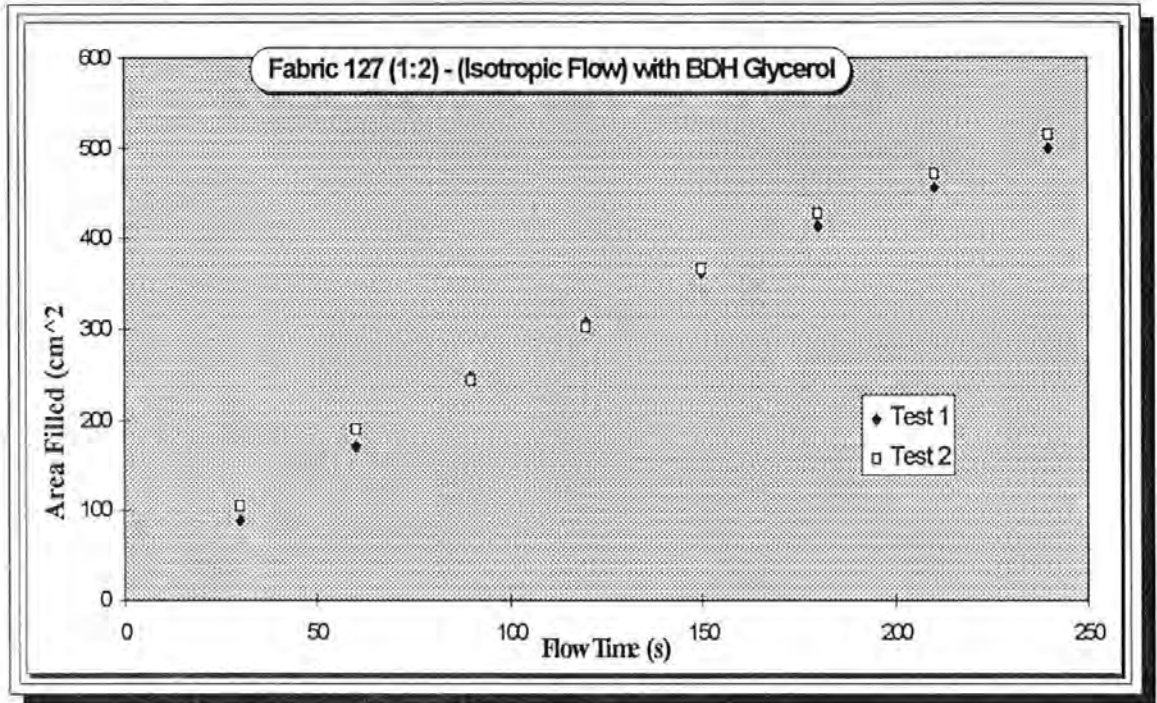
Figure A6:7 Isotropic Flow through Fabric DWO 127
(Ratio of 1:2 Bound to Conventional Tows)
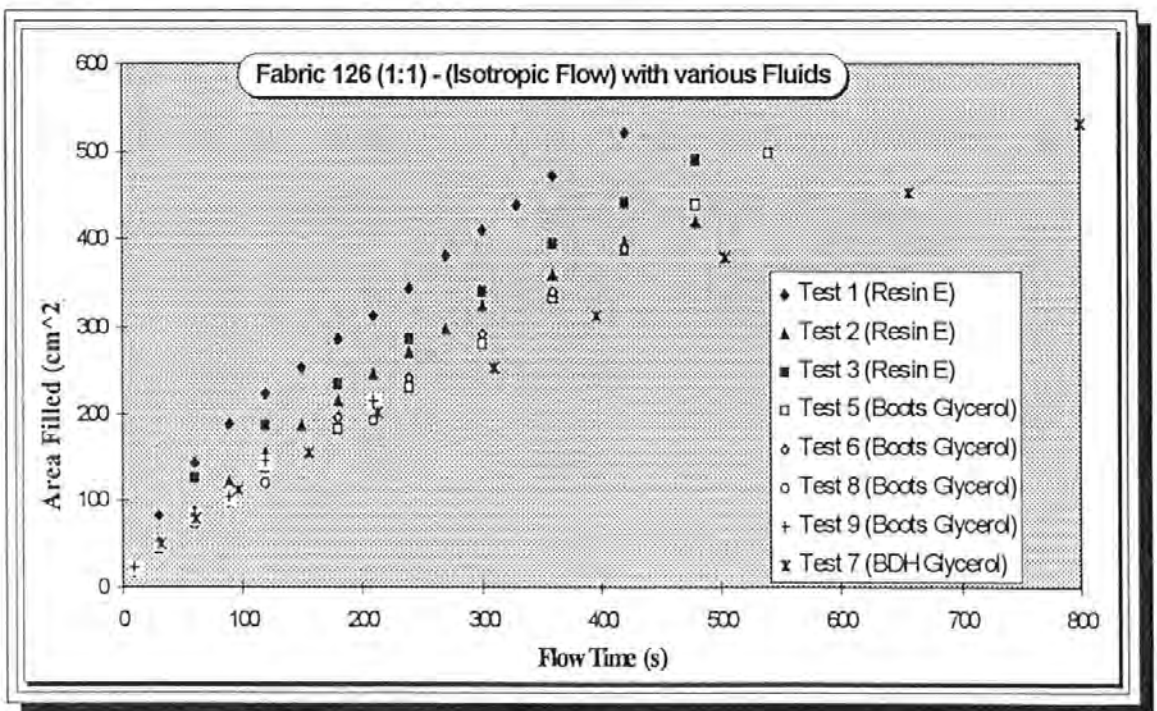
Figure A6:8 Isotropic Flow through Fabric DWO 126
(Ratio of 1:1 Bound to Conventional Tows)
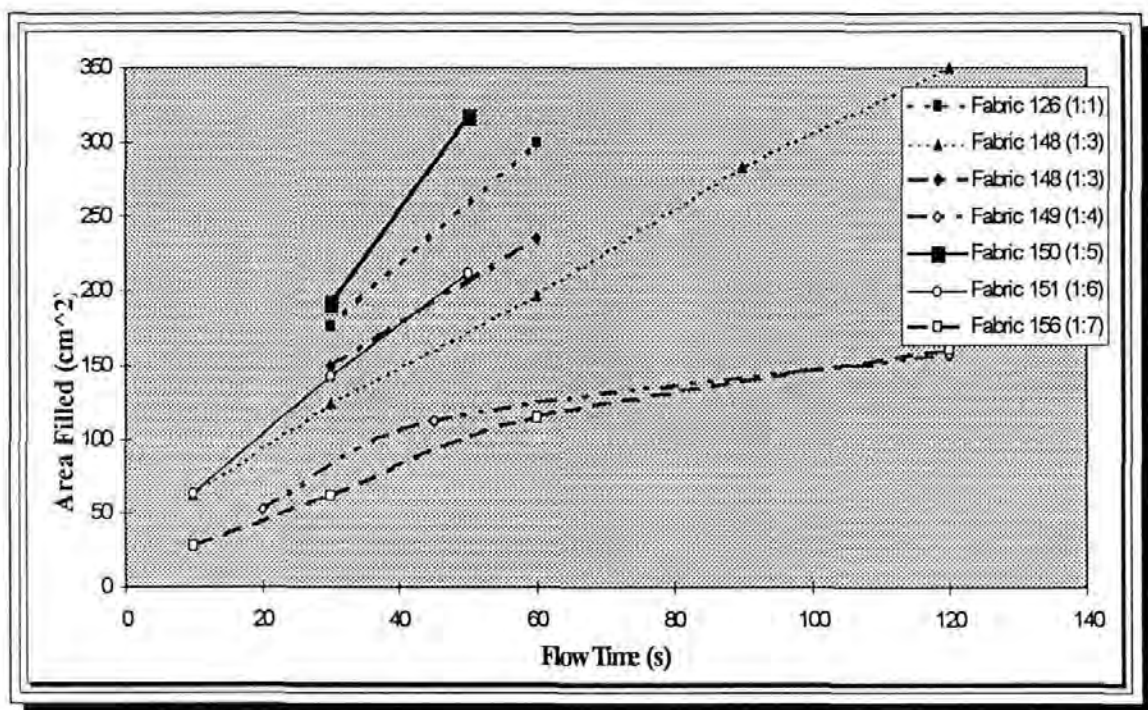
Figure A6:9 Anisotropic Flow through Flow Enhancing Fabrics

APPENDIX 7

Published Conference and Journal Papers

7:1). The Effect of Microstructure on Flow Promotion in Resin Transfer Moulding Reinforcement Fabrics
P.R.Griffin S.M.Grove F.J.Guild P.Russell J.Summerscales
Presented at Conference of Microscopy, Oxford, April 1994
Published in the Journal of Microscopy Vol 177 Pt.3
March 1995 pp 207-217

7:2). Flow Visualisation in Resin Transfer Moulding
P.R.Griffin S.M.Grove A.J.Lewis D.Short
Presented at 3rd International Conference of Flow Processes in
CompositeMaterials, University College Galway, July 7-9th 1994

7:3). The Effect of Reinforcement Architecture on the Long Range Flow in Fibrous Reinforcements
P.R.Griffin S.M.Grove J.Summerscales F.J.Guild D.Short P.Russell
E.Taylor
Presented at 3rd International Conference of Flow Processes in
CompositeMaterials, University College Galway, July 7-9th 1994
To be published in Composites Manufacturing Sept 1995 Vol 6, Pt.3

7:4). Quantitative Microstructural Examination of RTM Fabrics Designed to Enhance Flow
J.Summerscales P.R.Griffin S.M.Grove F.J.Guild
To be presented at the 8th International Conference on Composite
Structures, Paisley Nov 1995
To be published in Composite Structures 1995

7:5). The Relationship between Mechanical Performance and Microstructure in Composites Fabricated with Flow Enhancing Fabrics
D.M.Basford P.R.Griffin S.M.Grove J.Summerscales
Published in Composites Vol. 25

7:6). The Effect of Microstructure on Flow Promotion in RTM Reinforcement Fabrics
P.R.Griffin
Presented at the SAMPE Student Seminar, Toulouse, France June 1994

The effect of microstructure on flow promotion in resin transfer moulding reinforcement fabrics

P. R. GRIFFIN,* S. M. GROVE,* F. J. GUILD,† P. RUSSELL‡ & J. SUMMERSCALES*

*School of Manufacturing, Materials and Mechanical Engineering, University of Plymouth,
Plymouth, Devon PL4 8AA, U.K.

†Department of Materials Science and Engineering, University of Surrey, Guildford,
Surrey GU2 5XH, U.K.

‡Department of Biological Sciences, University of Plymouth, Plymouth, Devon PL4 8AA, U.K.

Summary

The resin transfer moulding (RTM) process is becoming
increasingly important for the manufacture of continuous
fibre-reinforced thermosetting resin matrix composites. The
RTM process is a closed mould technique which reduces
volatile emissions relative to traditional hand lay-up
methods. The fibres, generally as several layers of fabric,
are prepared as a preform and laid in the closed mould. The
resin is injected, at one or more points, and flows through
the mould to form the finished product. In the manufacture
of high-performance composite structures, the flow of resin
is constrained by the high volume fraction of reinforcement
fibres required to achieve the performance. Commercial
fabrics are becoming available which are woven with
specially designed mesoscale architecture to promote flow of
the resin. The flow rates in a series of such fabrics have been
studied. The microstructures of the resulting composites
have been examined using brightfield optical microscopy. A
Quantimet image analyser was used to quantify the
structures on both the mesoscale and the microscale. The
flow rate has been shown to be related to the presence of
both large and more modest sized pore space in the
reinforcement architecture.

Introduction

The use of resin transfer moulding (RTM) as a method of
manufacture of continuous fibre-reinforced plastics leads to
the production of consistent composite components at a
reasonable cost. This closed mould technique leads to
considerable reduction in volatile emissions relative to
traditional hand lay-up methods, yielding significant

improvements in health and environmental conditions.
The cost of the process is critically dependent on the mould
fill-time, which is directly related to the rate of resin flow
through the fibre preform. This long-range resin flow is
primarily flow through the pore space between the
reinforcement fibres; the process and the associated
governing equations have been described by Tucker &
Dessenberger (1994). Summerscales (1993) has presented
a model which predicts a significant increase in flow rate
with increasingly clustered fibres at a constant volume
fraction.

Commercial fabrics designed to promote faster processing
in RTM are becoming available. These commercial fabrics
exhibit feature variations in the mesoscale architecture of
the reinforcement; fibres are deliberately clustered into tows
leading to uneven distribution of pore space. The clustering
in the fabrics examined here is achieved by inclusion of a
varying proportion of twisted flow-enhancing warp threads.
However, the presence of uneven fibre distribution has been
predicted to lead to degradation of the mechanical
properties of continuous fibre-reinforced laminates (Guild
et al., 1989). These predictive results may be confirmed by
recent measurements of the mechanical properties of these
laminates which show reduction in longitudinal com-
pressive strength with increasing proportions of clustered
tows (Basford et al., 1995). Thus, the requirements for good
mechanical performance are in conflict with the require-
ments of large pore space for rapid manufacture using the
RTM method. The results described here are part of a wider
research programme which has the long-term aim of
resolving this manufacture–properties dilemma.

The flow rates of the resin front in RTM for the different
fabrics have been measured. The microstructures of the
laminates, on both the mesostructural and microstructural
scales, have been examined using a Quantimet 570 Image

207

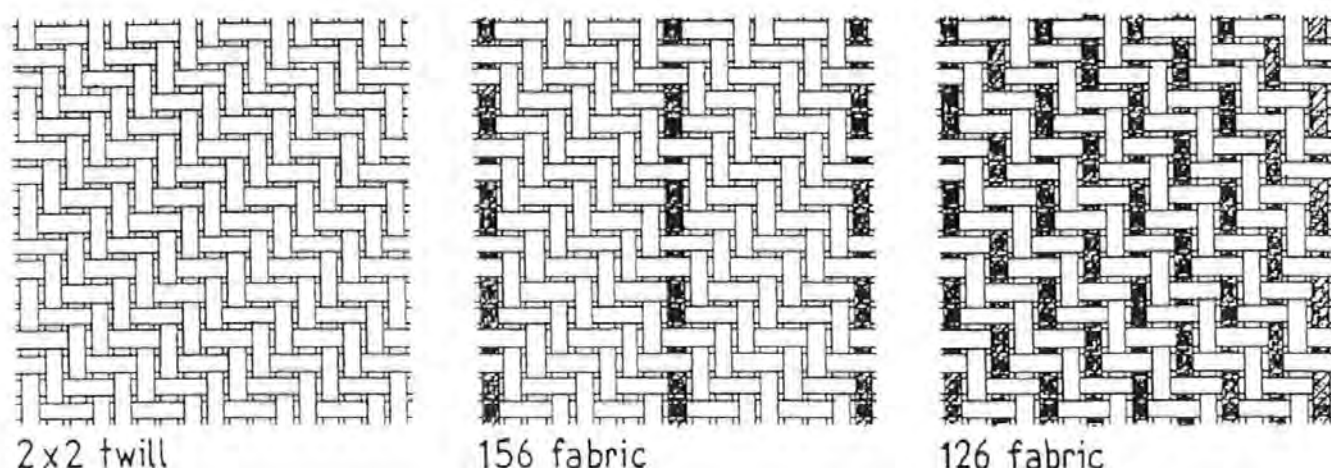2 x 2 twill   156 fabric   126 fabric

Fig. 1. Diagrams showing plan views of the three fabrics; the bound tows are shaded.

Analyser. The relationship between permeability and micro-structure has been explored.

Preparation of the laminates

The carbon-fibre reinforcement fabrics used in this study were developed by Carr Reinforcements Limited (Stockport, Cheshire, U.K.) with the specific aim of promoting resin flow by including a varying proportion of bound, twisted tows. All fabrics are 2 × 2 twill weaves (for a definition of textile terms see Tubbs & Daniels, 1991); the fibres in both warp and weft directions are tows containing 6000 fibres of standard-modulus high-strain carbon fibres (Grafil 34-700-6000) with a diameter of 6·9 μm (diameter from suppliers product specification). The twisted tows are bound with a low-melt-point thermoplastic filament with a diameter of around 100 μm. (The manufacturers do not disclose the precise material used.) Figure 1 shows diagrams of the three fabrics in plan view. The characterization of the materials in the three laminates included here is shown in Table 1.

Four layers of one type of fabric were laid up in a flat steel mould with parallel sides. The mould was 350 mm square and 1·7 mm deep. The mould was closed on its upper surface using a glass plate so that the resin flow could be observed. For safety, a Perspex sheet was placed over the glass sheet, and the mould was secured using G-clamps around the Perspex sheet and the bottom steel plate. A grid of black concentric circles on a clear acetate sheet was placed between the glass and Perspex sheets; this was centred on a fluid inlet port which was included at the centre of the lower face of the mould. A central hole, with a diameter of 14 mm, was punched in the centre of each fabric layer to encourage true two-dimensional flow.

The viscosities of the resins were measured at the time of the flow experiments (Table 1). The Scott Bader resin has significantly higher viscosity than the Jotun Polymer resin. This difference in viscosity must be taken into account when considering the measured flow rates for the twill and the laminates containing the twisted tows; Darcy's equation (Summerscales, 1993) predicts that the flow rate will be inversely proportional to the viscosity. The effect of the proportion of twisted tows can be considered without reference to the value of viscosity.

The inclusion of the bound flow-enhancing thread makes the fabrics anisotropic (see Fig. 1). The layer stacking sequence was $[0]_4$; thus, the Twill laminate is isotropic but laminates 126 and 156 are anisotropic. The resin was introduced through the central inlet port into the space punched into the reinforcement layers. The fluid pressure at the reservoir was 0·9 bar gauge pressure (i.e. 1·9 bar pressure absolute). The resin permeated radially outwards from the inlet port. As expected, the flow was circular for

Table 1. Constituent materials.

Designation	Fabric	% Bound tows	Resin	Viscosity (centipoise)
Twill	normal 2 × 2 twill weave	0	Scott Bader E	4600
156	one bound tow in each 8 tows	12·5	Jotun Polymer 4210	2600
126	one bound tow in each two tows	50	Jotun Polymer 4210	2600

FABRIC 156

Direction of Twisted Tow

FLOW TIME (seconds)

120
60
30
10
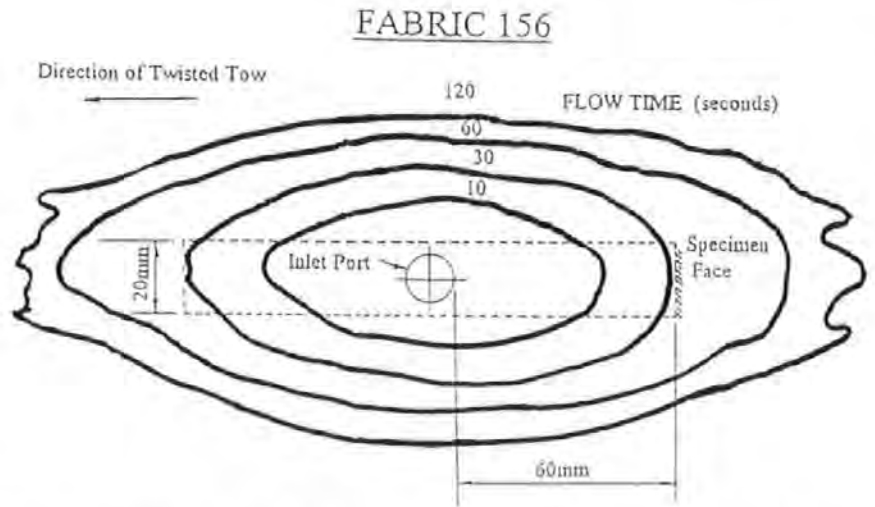
Inlet Port

Specimen Face

20mm

60mm

Fig. 2. Isochrones of resin flow for laminate 156, showing the location of micro-structural section.

the twill laminate but elliptical for the 126 and 156 laminates: higher flow rate was observed in the direction parallel to the twisted tows. The flow front position with respect to the grid was recorded using a video camera. The laminates were cured overnight at room temperature before removal from the mould. The finished thickness of the laminates was approximately 2 mm.

Measurement of flow-front velocity

Figure 2 shows typical isochrones for the anisotropic (elliptical) flow. As shown in Fig. 2, the sections for microstructural examination were cut 60 mm from the edge of the inlet hole, perpendicular to the twisted tows. The flow front velocities for this position for the three laminates were calculated from the isochrones; the values are shown in Table 2. These calculations are shown in more detail elsewhere (Griffin et al., 1995). It should be noted that these values of flow-front velocity are the values of average velocity between the inlet port and the point of sectioning; the velocity varied across the mould.

These results in Table 2 show that the resin flow is increased by the inclusion of the twisted tows and is increased with an increased proportion of twisted tows. The velocity for the Twill laminate should be compared with the values for the other laminates taking into account the

Table 2. Measured flow-front velocities.

Designation	Flow rate (mm/s)	'Normalized' flow rate (centipoise mm/s)
Twill	0·173	796
156	2·00	5200
126	3·07	7982

different viscosities of the resins. Since, as described above, the velocity is expected to be inversely proportional to the viscosity, 'normalized' results have been calculated from the product of the measured velocity and viscosity. These results are included in Table 2. These 'normalized' results indicate that the increase in flow-front velocity between the Twill and the laminates containing the twisted tows is not explained by the changing viscosity of the resin systems used. The differences in flow-front velocity for the three laminates must arise from differences in the reinforcement architecture.

Microstructural preparation

Sections were cut at the position shown in Fig. 2, 60 mm from the inlet position, perpendicular to the twisted tows. The size of the sections was typically 20 mm long and 2 mm deep, the thickness of the laminate. The sections were mounted in casting resin. The sections were polished using 'wet-and-dry' diamond papers of 200, 320, 400 and 600 grade in turn, until the surface appeared flat to the unaided eye. The sections were then polished using an automatic metallurgical polishing machine with diamond pastes and a specimen load of 1 kg. The sequence used was: 1 h at 14 μm; 1 h at 6 μm; 30 min at 1 μm; and a final short polish at 0·25 μm. The resulting sections were well polished for examination in reflected light. Contrast at low magnification between fibre tows and pore space was achieved since the carbon fibres reflect more light; the fibre tows appear lighter than the pore space. Similarly, at higher magnification, the individual bright fibres contrast with the darker surrounding resin.

Microstructural definition

Micrographs of the three laminates are shown in Fig. 3. The bright areas are tows parallel to the plane of the section.
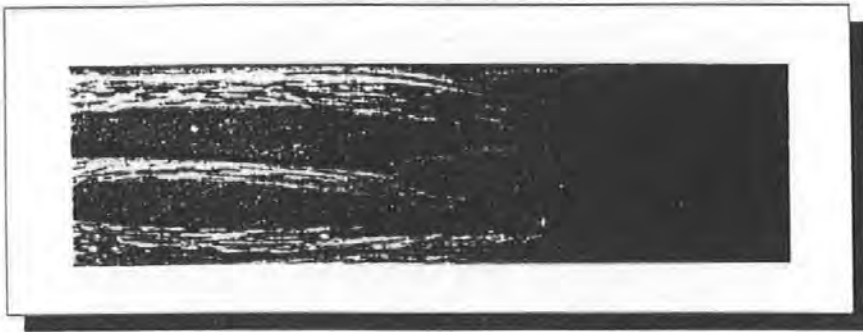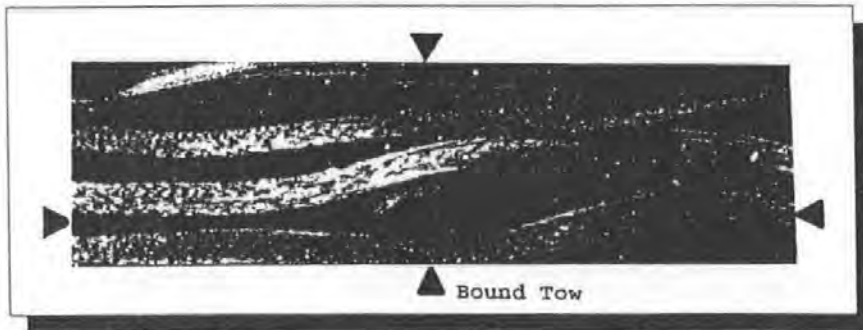
Micrograph of the Base Twill Laminate

Micrograph of the 126 Twill Laminate

Bound Tow

Micrograph of the 156 Twill Laminate

Fig. 3. Micrographs of sections through the laminates: twill weave (top: no bound tows), 126 fabric (middle: 50% bound tows) and 156 fabric (bottom: 12·5% bound tows). The one bound tow in the bottom micrograph is at the intersection of the lines between horizontal and vertical arrowheads.

Since the flow was perpendicular to the section, the effects of fibre architecture on flow must arise from tows perpendicular to the section. The individual tows perpendicular to the section are clearly distinguishable at this low magnification; the tows are brighter than the pore space. The two types of tow perpendicular to the section can be seen in the figure. The conventional tows are approximately elliptical due to the closing forces on the mould flattening the tow. The twisted tows are 'circular' before and after mould closure. A typical twisted tow is at the position marked by the intersection of the lines between the horizontal and vertical arrow heads. The continuous lines are the weft fibres running in the plane of the section. The

twisted tows keep the adjacent layers apart and create significant areas of additional pore space in regions immediately adjacent to their positions.

This description of the laminate structure suggests two distinct features of the microstructure which could be used for its definition. First, the presence of the twisted tows leads to pore space: the occurrence of this pore space can be described. Second, two distinct types of tows have been observed; the fibre arrangement within the two types of tow can be described. The laminates were examined using a Quantimet 570 Image Analyser using brightfield illumination in the microscope. The occurrence of pore space was measured at low magnification, when individual fibres were
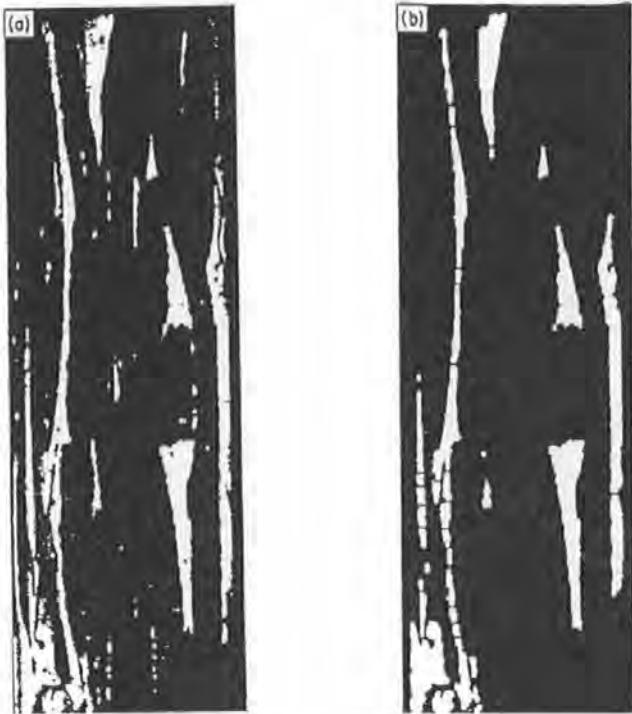
Fig. 4. Measurement of pore space; (a) binary image; (b) binary image after image enhancement.

not distinguished. The arrangement of fibres within the different types of tow was measured separately at higher magnification.

Microstructural measurements

Measurement of pore space

The magnification used for the pore space measurements was 0·0162–0·0178 mm/pixel. The measure frame size was 438 × 123 pixels. Three contiguous frames were analysed; for the 156 sample the total area analysed was 21·3 × 1·99 mm². The total area analysed was close to the total area of the section. Figure 4(a) is a binary image

showing bright areas of pore space; the pore space is defined but there are some small speckles which are not required for this analysis. There are some 'holes' within the detected pore space. Figure 4(b) shows the enhanced binary image, after image processing. The image is clarified by removal of the speckles and filling of the holes. The very long thin areas arising from the space between the conventional tows have been subdivided via 'segmentation' to prevent overlap across the guard frame. This subdivision does not occur for the wider pore space areas around the twisted tows.

The regions of pore space were detected as 'features' and the size and position of the features were recorded. The processes of image capture, image processing, measurement and section movement on the microscope stage were programmed using QBASIC, the command language of the Quantimet. The results were written onto a floppy disk; for each feature the parameters recorded were area, maximum width (horizontal feret), maximum height (vertical feret), perimeter and x- and y-centres of gravity. The results were subsequently analysed using a spreadsheet (LOTUS 1-2-3).

Measurement of fibre arrangement

The fibre arrangement within the two types of tow, conventional and twisted, was measured using an overall magnification of 0·619 μm/pixel. Results were obtained from one frame for each type of tow; the measurement frame size was 312 × 412 pixels. The fibre arrangement within these tows is entirely defined by sections perpendicular to the fibre direction, as used here. The arrangement of fibres can be described by the 'zone of influence' around each fibre. The zone of influence (or Voronoi cell) for a given fibre is the area of matrix closer to that fibre than any other. This method of description of fibre arrangement has previously been successfully used by Summerscales et al. (1993).

The Quantimet was programmed using QBASIC. The image was acquired and transformed with the 'sharpen' function which uses top-hat algorithms. The bright fibres
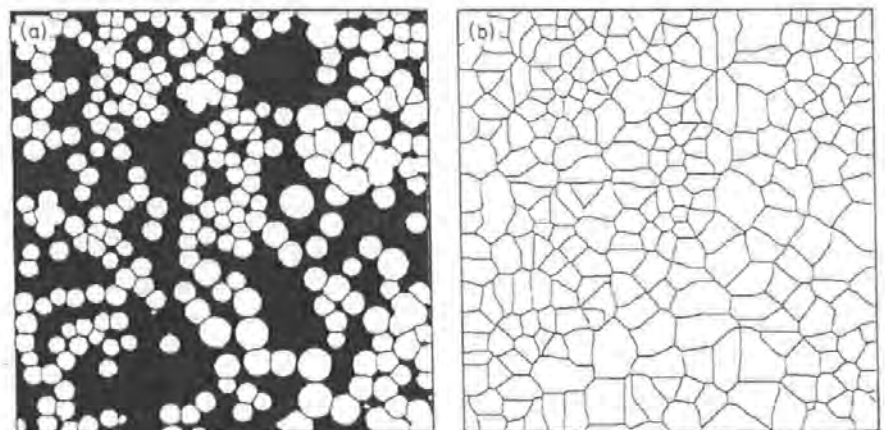

Fig. 5. Measurement of fibre arrangement:
(a) segmented image; (b) zones of influence.

were detected; clumps were separated using the 'segment' function. The zones of influence around each fibre were found and measured. The process is illustrated in Fig. 5. Figure 5(a) shows a detected, binary, image; the corresponding zones of influence, derived by the Quantimet, are shown in Fig. 5(b). The dimensions of the zones of influence were written to a floppy disk. The results were subsequently analysed using a spreadsheet (LOTUS 1-2-3).

Analysis

The data from the two methods of microstructural definition were both analysed using the spreadsheet. Initial com-

parisons can be made by summing the measurements. For the pore space measurements, the total area detected was found. This area denotes the area of pore space available for resin flow. For the fibre arrangement, the total number of zones was found; this number corresponds to the number of fibres within the measured area. Using the value for fibre diameter, the values of fibre volume fraction can be obtained.

The results were then analysed in more detail. The data were divided into bins from which histograms can be drawn. An alternative presentation of the data is a continuous plot showing the total number in a given range and all smaller ranges. Results from different
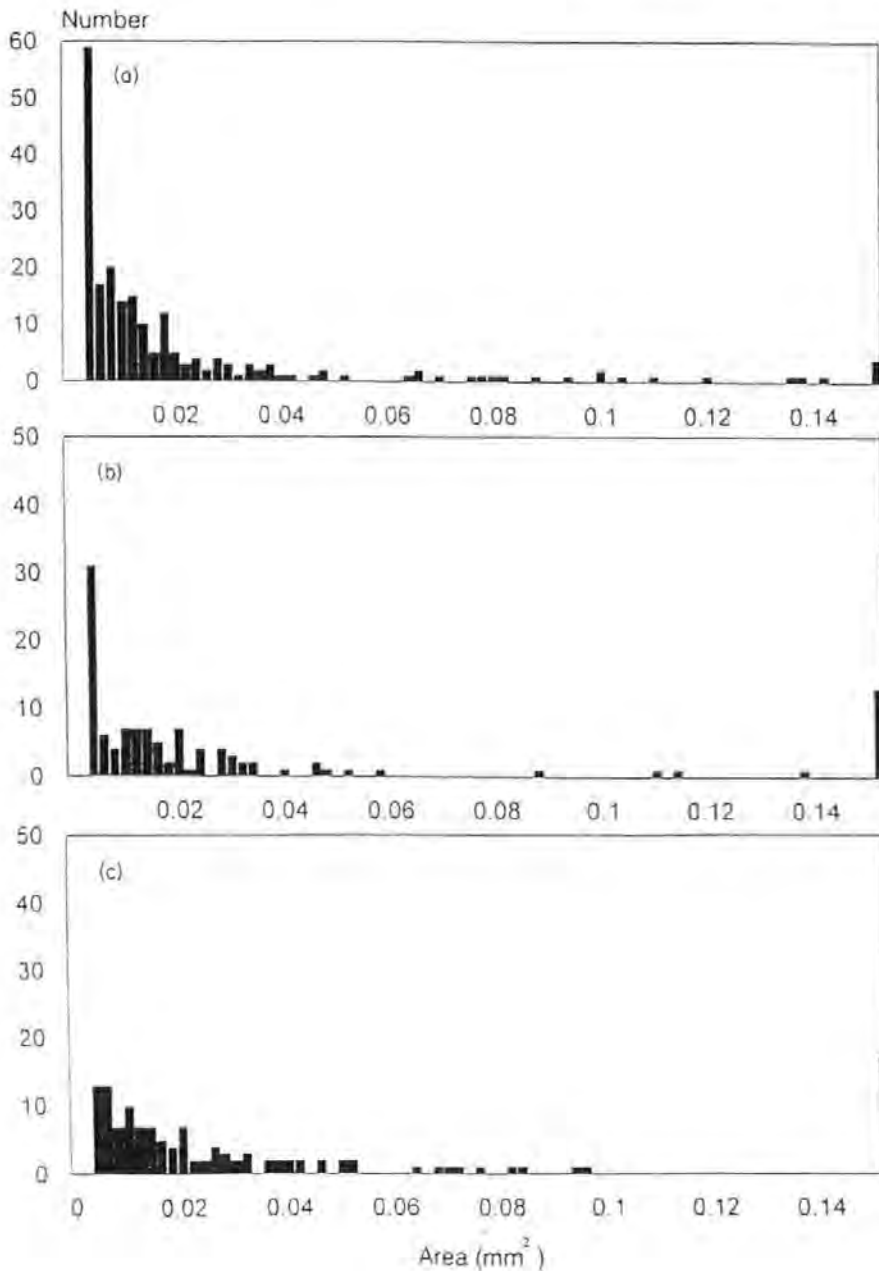
Fig. 6. Histograms of pore space area: (a) Twill laminate; (b) 156 laminate; (c) 126 laminate.

laminates are more easily compared using such continuous plots. Comparisons can be made if the total number is normalized: the y-axis range is 0 to 1. These are plots of the cumulative distribution function.

Results

Pore space

The total number of areas and the values of total area of pore space for the three laminates are shown in Table 3. The Twill laminate has the largest number of areas

Table 3. Measurement of pore space.

Laminate	Number of areas	Total area of pore space (mm²)
Twill	210	5·47
156	115	8·54
126	130	11·21

measured, but the smallest total area. As expected, the 126 laminate, with the highest proportion of twisted tows, has the highest total area of pore space.
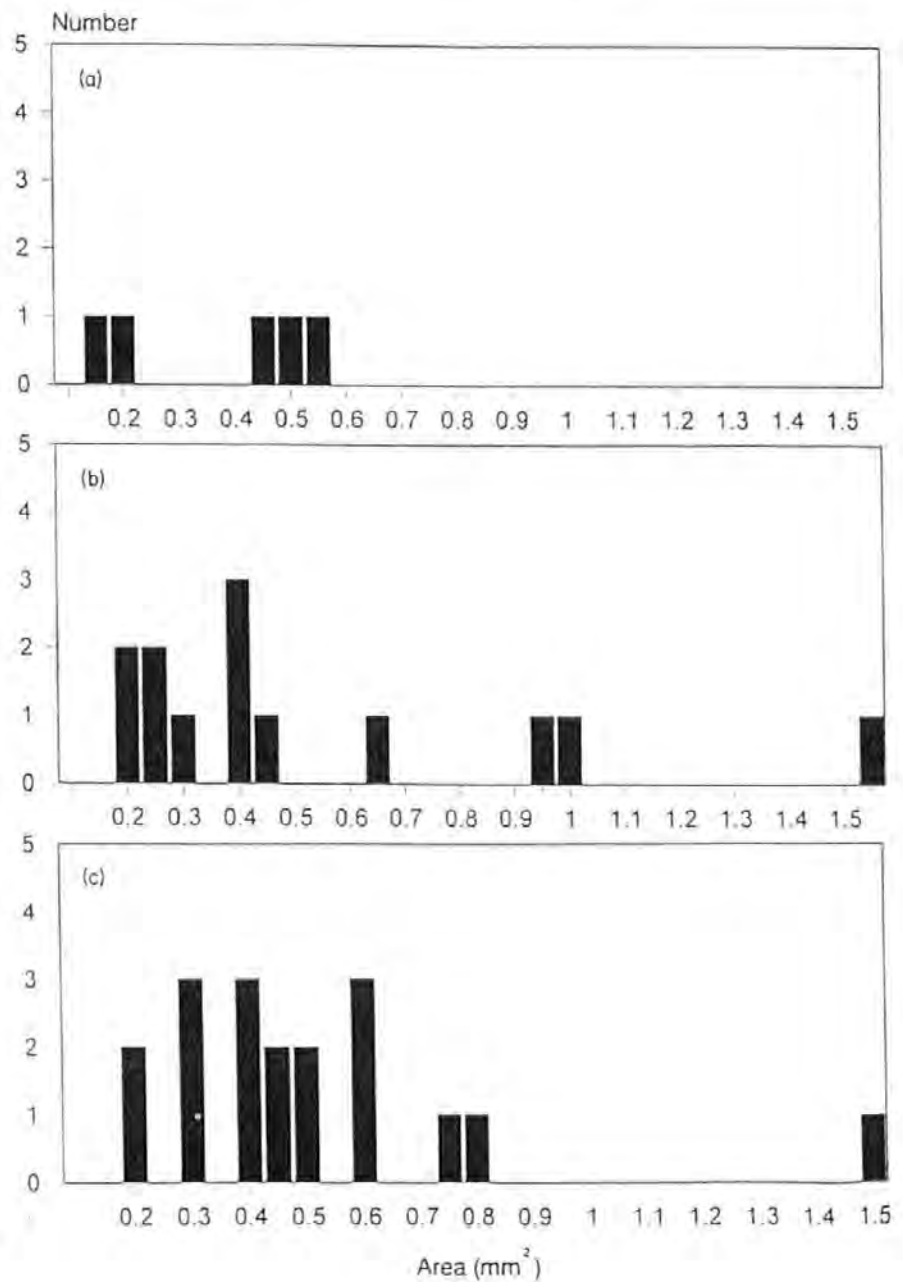
Fig. 7. Histograms of large pore space area: (a) Twill laminate; (b) 156 laminate; (c) 126 laminate.
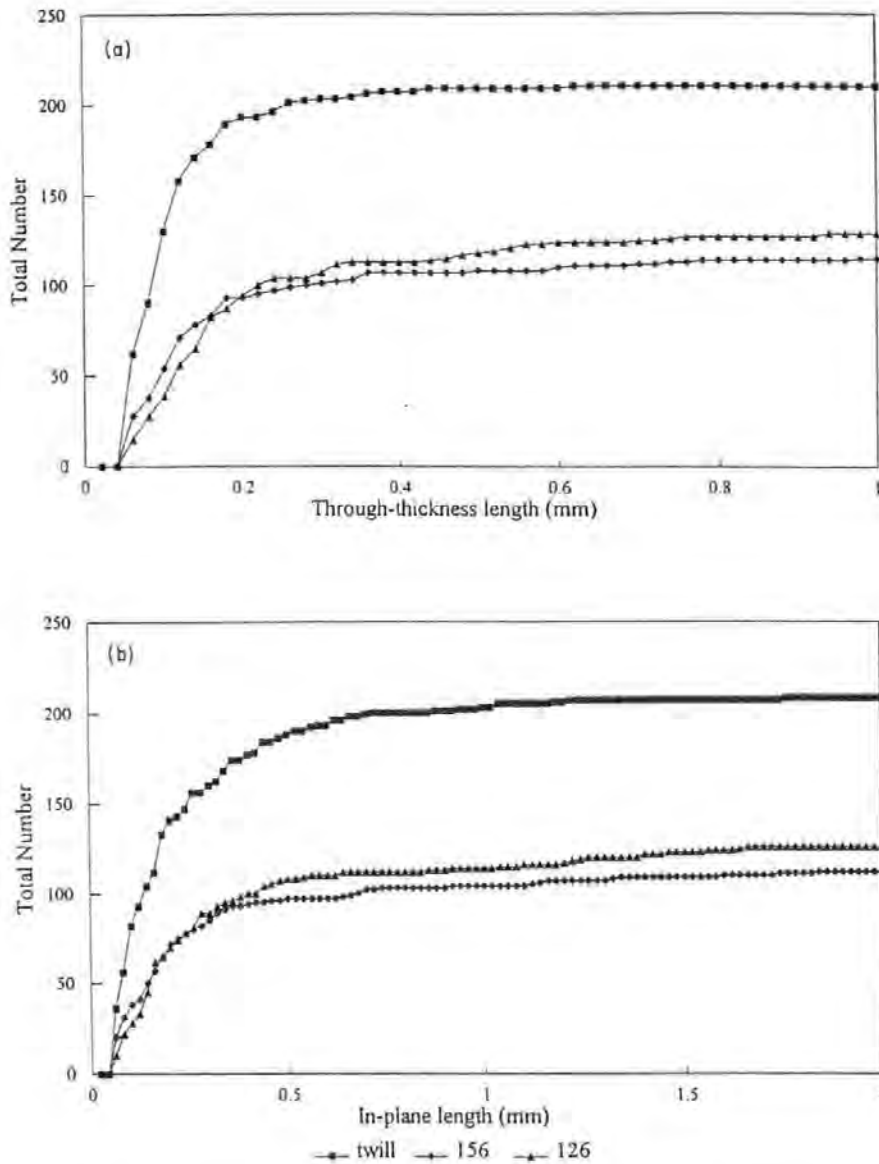
Fig. 8. Total numbers of specified pore space lengths in the Twill, 156 and 126 laminates: (a) through-thickness length; (b) in-plane length.

The histograms of zone area for the three laminates are shown in Fig. 6. The highest bin used is 0·15 mm². The final bin includes all areas greater than the size of the highest bin. The larger total number of areas measured for the Twill (Table 3) is clear from comparison of the histograms; the larger total number arises from larger numbers of small areas. Similarly, there is a higher number of very small areas for the 156 laminate, with the smaller proportion of twisted tows, than for the 126 laminate.

Histograms for the large areas, included in the highest bin in Fig. 6, are shown in Fig. 7. Comparing these histograms, it is clear that the introduction of the twisted tows allows more large areas to occur. The number and distribution of these large areas are not significantly changed by changing the frequency of the twisted tows (Fig. 7b,c). The effect of the twisted tows on the intermediate areas is not clear from comparison of these histograms.

The dimensions of the pore space were compared using cumulative plots. Figure 8 shows the plots of the total number. As expected from the overall laminate construction, the values of through-thickness length (Fig. 8a) are smaller that the values of in-plane length (Fig. 8b); the x-axes are different lengths for each direction. For both through-thickness and in-plane length, the ranking of the graphs for the very small lengths is the ranking expected from the number of twisted tows: increasing the number of twisted tows leads to a decrease in the number of small areas. The difference is clearer for the values of through-thickness length. However, for both directions, the plots for the 156 and 126 laminates cross since the 126 laminate had a higher overall number of zones (Table 3).
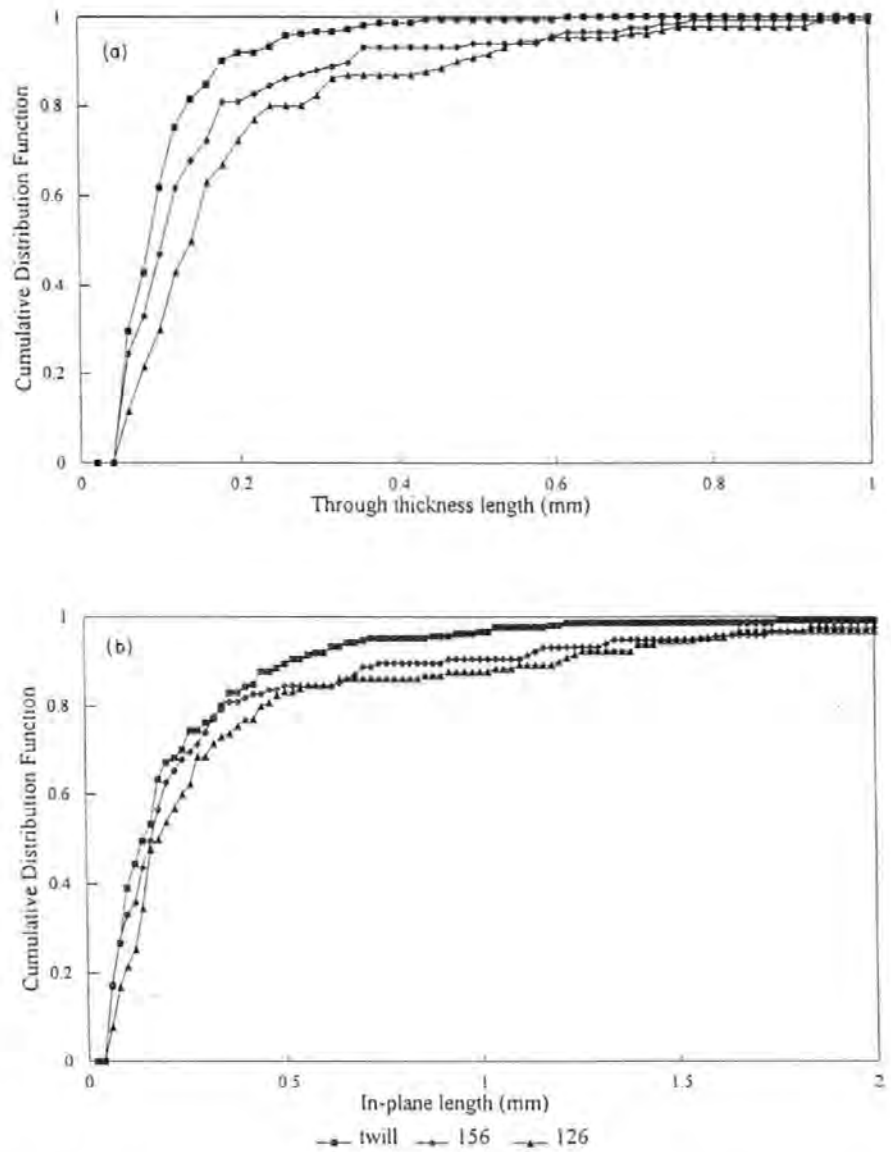
Fig. 9. Normalized distributions of pore space lengths in the Twill, 156 and 126 laminates: (a) through-thickness length; (b) in-plane length.

Figure 9 shows the plots where the total number has been normalized; the difference between the laminates is clarified by the normalization; the ranking remains unchanged throughout the range. The difference is clearer for the through-thickness length. Comparing the shapes of these cumulative distribution functions, it is clear that the introduction of twisted tows decreases the proportion of small pore areas, and therefore increases the proportion of larger pore areas. The effect is increased by increasing the proportion of twisted tows.

Fibre arrangement

The values of volume fraction occupied by the fibres within the two types of tow were calculated from the total numbers of zones recorded and the fibre diameter. The results are shown in Table 4. As expected from examination of the micrograph (Fig. 3) the volume fraction in the conventional tow is lower than the volume fraction within the twisted tow. The process of mould closure forces the conventional tow to the elliptical shape; this leads to spreading of the fibres and a corresponding decrease in volume fraction.

The fibre separation in the two directions was investigated in detail for the two types of tow. The results are shown in Fig. 10; these are continuous plots showing the

Table 4. Measurement of different tows.

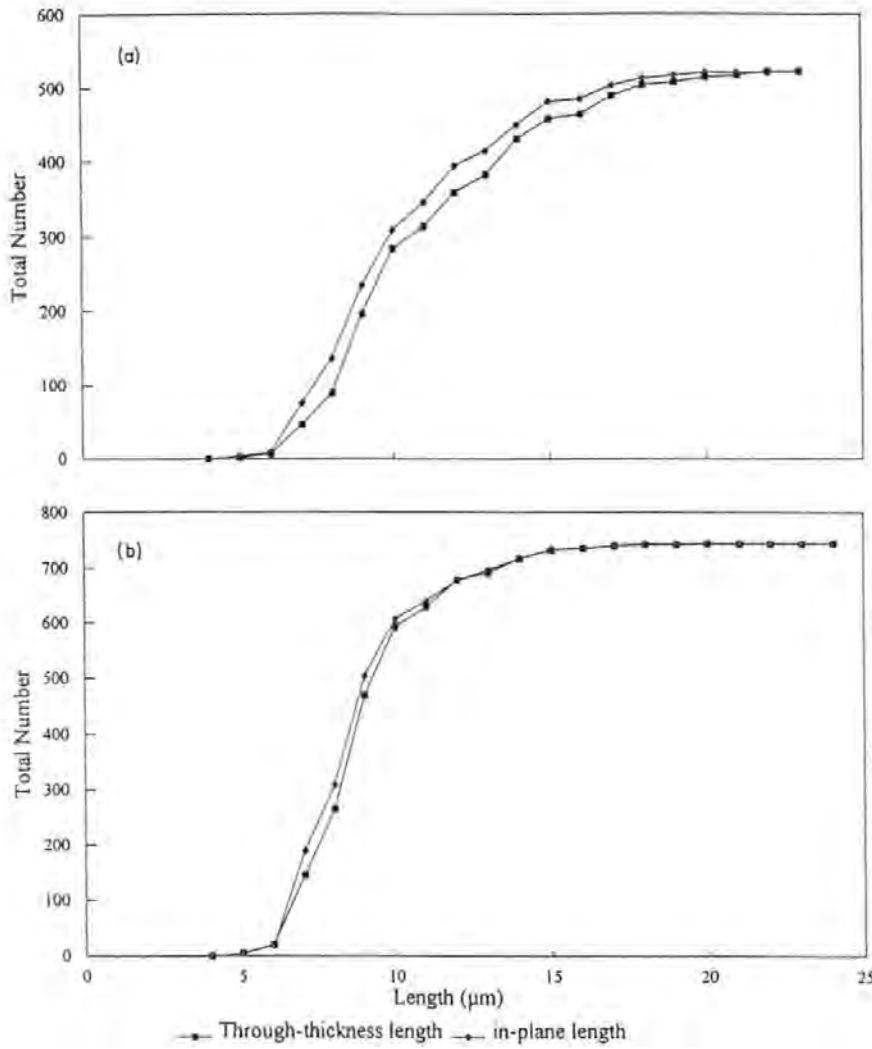|	Number of fibres	Volume fraction (%)
Conventional tow	525	39·9
Twisted tow	745	56·6

Fig. 10. Total numbers of specified lengths of zones of influence around fibres: (a) conventional tow; (b) twisted tow.

total number of zone lengths within a bin and all smaller bins. The results for the conventional tow (Fig. 10a) show different distributions of lengths for the in-plane and through-thickness directions. The through-thickness direction has a smaller proportion of small lengths, and thus a higher proportion of long lengths. The forces arising from the mould closure have lead to greater separation of the fibres in the through-thickness direction, parallel to the consolidation direction. The results for the twisted tow (Fig. 10b), which retains its original circular shape, shows no difference in values for the two directions. This is the expected result for fibre arrangement within a tow; Green & Guild (1991) have shown the fibre arrangement within a single tow to be close to the theoretical arrangement derived for a random distribution. Comparing Fig. 10(a) and (b), the forces arising from the mould closure have lead to a change in the shape of the distribution of zone lengths; the difference appears greater than that which would be

expected from the difference in volume fraction alone (Green & Guild, 1991). This observation is confirmed by comparing the mean interparticle distance for the two types of tow: for the conventional tow the mean value is $10 \cdot 88$ μm while for the twisted tow the value is $8 \cdot 83$ μm. Comparing these mean values with the expected mean values for the random distribution calculated by Davy & Guild (1988), it is clear that the measured mean value for the twisted tow is closer to the predicted value than the value for the conventional tow.

Discussion

The microstructure of the laminates has been defined by two different methods at two different scales. These measurements of microstructure can be compared with the resin flow-rate during the moulding process. The flow rate measurements (Table 2) have shown that the inclusion

of bound tows increases the flow rate; increasing the proportion of bound tows leads to further increase in the flow rate.

The measurements of pore space may be directly related to these observations. The inclusion of twisted tows leads to large pore space areas, which do not occur for the Twill. Although the Twill has a larger number of areas detected, the total area is smaller. The extra areas are all small, with areas smaller than about 0.016 mm^2. The difference between the 156 and 126 laminates, containing different proportions of bound tows, appears to arise from differences in the numbers of areas of intermediate size, with through-thickness lengths up to about 0.6 mm. No differences between the 126 and 156 laminates can be observed for the very large areas. The differences in the histograms and cumulative distribution functions between these laminates is small, but consistent. The difference is in agreement with the significant increase in flow rate for the 126 laminate. Thus, although the inclusion of very large pore space areas does increase the flow rate, significant increase may also arise from the inclusion of pore space of more modest size. This may be an important result for the design of successful RTM fabrics. The mechanical behaviour of the finished laminate may be more favourable if very large areas of pore space can be avoided.

The microstructural definition of the pore space may be related to the description of the fibre arrangement within the two types of tow. The forces arising from mould closure lead to dispersion of the unbound fibres and lower volume fraction. The through-thickness separation increases more than the in-plane separation. Thus, the twisted tows take up less space; more areas are available for pore space. Increasing the number of twisted tows would be expected to increase the total area of pore space; this is the result observed.

Concluding remarks

The effect of microstructure on flow promotion in RTM reinforcement fabrics has been investigated. The dependence of flow rate on the size of pore space has been demonstrated. The pore space measurements have been correlated with measurements of fibre arrangement within the tows. Flow rate has been shown to be dependent on both very large and more modest size areas of pore space. The commercial fabrics which are currently available introduce large resin-rich areas into the laminate. These areas may be implicated in premature failure. The study

reported here may assist in the design of fabrics which achieve a balance between more even fibre distribution for mechanical properties while still allowing easy resin flow in manufacture.

Acknowledgments

References

Basford, D.M., Griffin, P.R., Grove, S.M. & Summerscales, J. (1995) The relationship between mechanical performance and microstructure in composites fabricated with flow-enhancing fabrics. *Composites* (in press).

Davy, P.J. & Guild, F.J. (1988) The distribution of interparticle distance and its application in finite-element modelling of composite materials. *Proc. R. Soc. Lond.* A418, 95–112.

Green, D. & Guild, F.J. (1991) Quantitative microstructural analysis of a continuous fibre composite. *Composites*, 22, 239–242.

Griffin, P.R., Grove, S.M., Guild, F.J., Russell, P., Summerscales, J. & Taylor, E. (1994) The effect of reinforcement architecture on the long range flow in fibrous reinforcements. *Composites Manufacturing*, 6 (in press).

Guild, F.J., Davy, P.J. & Hogg, P.J. (1989) A model for unidirectional composites in longitudinal tension and compression. *Composites Sci. Technol.* 36, 7–26.

Summerscales, J. (1993) A model for the effect of fibre clustering on the flow rate in resin transfer moulding. *Composites Manufacturing*, 00, 427–431.

Summerscales, J., Green, D. & Guild, F.J. (1993) Effect of processing dwell-time on the microstructure of a fibre-reinforced composite. *J. Microsc.* 169, 173–182.

Tubbs, M. & Daniels, P. (eds) (1991) *Textile Terms and Definitions.* The Textile Institute, Manchester.

Tucker, C.L. & Dessenberger, R.B. (1994) Governing equations for flow and heat transfer in stationary fibre beds. *Flow and Rheology in Polymer Composites Manufacture* (ed. by S. G. Advani), pp. 257–323. Elsevier, Amsterdam.

FLOW VISUALISATION IN RESIN TRANSFER MOULDING

P.R. Griffin, S.M. Grove, A. Lewis and D. Short

ACMC, School of Manufacturing, Materials and Mechanical Engineering
University of Plymouth, U.K.

Abstract

This paper will present and discuss a range of flow characteristics which have been observed in different fibre configurations and under different operating conditions, in both vacuum-assisted and pressure RTM. It is concluded that flow is inhomogeneous at every scale. At the scale of the component, flow is affected by geometrical factors such as fabric cutting and lay-up which may result in 'easy paths' for the resin. At the scale of fibre tows or bundles, there may be movement either within or between layers resulting in local variations in permeability. At the scale of the individual filaments, there are competing processes of viscous and capillary flow which may affect microstructural composite properties if fibre wet out is incomplete.

Small variations of this nature may be beyond the control of normal manufacturing processes, and can have a large effect on the way in which the mould fills. However, this does not preclude the production of quality RTM parts if these variables are understood and taken into account at the process design stage.

INTRODUCTION

Resin Transfer Moulding is an increasingly common process for the manufacture of reinforced plastic components. A pre-catalysed thermosetting resin is injected at low pressures (up to 7 bar) into a closed mould containing dry reinforcement. Impregnation may be assisted or driven by evacuating the mould; the process is the sometimes known as VARI (Vacuum Assisted Resin Injection).

The process originated in the mid 1940's when the US Navy used it to fabricate patrol boats [1]. In the last 10 years, the process has become of considerable commercial interest in the composites industry, both for 'reinforced plastics' (using relatively low amounts of randomly oriented glass reinforcement and polyester resin) and 'advanced composites' (high volume fraction, oriented glass, carbon or aramid reinforcement and epoxy resin).
RTM requires a matched mould of adequate stiffness built to high tolerances. Careful attention has to be paid to sealing arrangements, particularly if vacuum is used. The process has therefore encouraged developments in tooling design and automation [2-4] which are crucial to its commercial success in the production of high performance, load bearing engineering components.

Of equal importance is the interaction between raw material selection, mechanical properties/part quality and process cycle times. Of particular interest is the permeability of the reinforcement (i.e. the ease with which the flowing resin is able to impregnate the fibres and

1

fill the mould). There is now a considerable literature on both empirical [5-7] and theoretical [8, 9] studies of permeability measurement, as well as numerical models of resin flow [10-13]. Resin and fabric suppliers are now marketing raw materials specifically designed for RTM [14].

In common with many other academic groups, we have measured the permeabilities of a range of different reinforcements. The experiments and some typical results are briefly described in this paper. The twin objectives of this work are to provide basic data which can be used in flow simulation models [15], and to attempt to correlate permeability with the detailed fibre 'architecture' (i.e. the microscopic details of fibre arrangement - filament diameter, tow size and orientation, weave style, etc.) [16, 17].

Almost all experimental work assumes that the flow of resin through a reinforcement can be described by Darcy's law [18] - this is a linear relationship in which flow velocity is proportional to pressure gradient and inversely proportional to fluid viscosity. The apparent permeability is essentially the constant of proportionality in the Darcy equation. As described below, permeability is measured by observing the progress of a resin of known viscosity (in a transparent mould) as it flows under a controlled pressure gradient.

Experience over several years with this type of experiment, plus prototype production of real components, has indicated that Darcy's law is only a crude approximation. Within a real fabric, there are local inhomogeneities; flow takes place on different scales, from the relatively large gaps between tows (of the order of a few mm) down to micron-sized spaces between individual filaments. Both capillary and viscous forces may be significant in determining the overall flow pattern [11]. Flow may be 3-dimensional, especially near inlet ports and in thick composites.

The second part of the paper offers a purely qualitative description of some of these 'departures' from predictable flow according to Darcy's law. Some of these variables could (at least in principle) be eliminated by careful experimental design, preparation and process control, but others are inherent in the nature of the process and need to be taken account of for successful component production by RTM.

EXPERIMENTAL MEASUREMENT OF PERMEABILITY

The 'permeability' of a porous medium refers to the ease with which a fluid passes through it. Darcy's original work [18] was based on the flow of domestic water through porous rock, and has been used widely since then to classify particulate media in the petroleum industry. Darcy has lent his name to a unit of permeability; 1 darcy is the permeability of a medium in which a fluid of dynamic viscosity 1 centipoise flows with a velocity 1 cm/s under a pressure gradient of 1 atmosphere/cm. In SI units, permeability is expressed as an area, and 1 darcy = $1.01325 \times 10^{12} \, m^2$.

As indicated above, measurement of permeability requires monitoring the rate of progress of a fluid (resin) as it impregnates the porous medium (reinforcement). Fig. 1 shows a schematic of the type of experiment used at the University of Plymouth, in which the mould comprises a steel base plate to which is clamped a glass or Perspex cover. Resin flow is recorded either manually by tracing successive positions of the flow front, or photographically. Permeability is

2

then deduced from the ratio of flow velocity to pressure gradient. Table 1 gives some typical values for measured permeability, obtained over a number of years on several different fabrics. As can be seen, there are considerable differences between different types of reinforcement, and permeability is very sensitive to volume fraction.

One result of this sensitivity is that repeatability between experiments is difficult to achieve, due to the natural variations in local volume fraction which occur in commercial fabrics and accidental fibre disturbance which may be introduced through handling. Typical experimental scatter is illustrated in Fig. 2.

SOME OBSERVATIONS OF RESIN FLOW

Easy Paths. In a closed mould, any gap between the edge of the reinforcement and the sides of the cavity will result in a high permeability 'easy path' for resin flow. The effect of this is seen in Figures 3 & 4,where the position of the resin front has been recorded at 5 min. intervals during injection of a solution of glycerol under vacuum only. The initially circular front becomes straighter as time progresses, but the shape is dominated by much faster flow around the edges. In extreme cases, fluid which has 'race-tracked' around the edge can reach the vent port in advance of the main flow front, and lead to large unfilled areas and/or resin wastage.

In an idealised, symmetric mould, edge effects would be reduced (and fill times decreased) by the simple expedient of injecting resin at the centre of the mould. However, practical tooling is rarely so straightforward, and edge effects have to be controlled by accurate cutting and/or preforming and placement of the reinforcement. Even accurately cut fabric may be relatively unconstrained at the mould edges, and suffer movement as the resin front advances, particularly if injection pressures are high. In 'leaky' moulds (working without vacuum) it may be possible to clamp the reinforcement through the seal. Alternatively, the mould tool could incorporate an edge feature near the seal locally to compress the fabric - this would ensure high volume fraction and low permeability at the mould edges, but the part may then require additional finishing after moulding.

A different approach is to use edge effects to advantage, by designing 'galleries' to assist rapid mould filling.

Fibre Orientation and Anisotropy. Many advanced reinforcement fabrics are anisotropic in terms of fibre orientation, and this will be reflected in the nature of resin flow - permeability parallel to unidirectional fibres may be of the order of 6 times higher than in the transverse direction. Figs. 5 and 6 illustrate these orientation effects. In Fig. 4, a plain weave fabric is aligned with warp and weft at $\pm 45°$ to the mould edges; the rates of flow are similar to those in Fig. 3, although edge effects are less pronounced. In Figures 5 & 6 a unidirectional fabric was aligned at 45° and 0° respectively. The combination of anisotropy and easy paths results in a very different pattern of mould filling such that the resin reaches the outlet long before all the reinforcement is impregnated.

It should be noted that flow-enhancing fabrics are highly anisotropic in permeability. One such fabric in undergoing evaluation at the University of Plymouth [16, 17]. Flow enhancement is achieved by spirally wrapping a thermoplastic fibre around a proportion of the warp tows.

3

This maintains a roughly circular cross section, even when the fabric is compressed, and ensures that a larger inter-tow gap is maintained. Fig. 7 shows experiments with these fabrics in which resin was injected at the centre of a flat plate. When an 'isotropic' lay up is used, a succession of circular flow fronts is produced; changing the orientation of individual plies introduces anisotropy of permeability, and the flow front becomes elliptical rather than circular. In these cases, a tensor description of permeability is required [19] and Darcy's law is modified appropriately. Just as mechanically anisotropic reinforcements enable the designer to tailor laminate stiffness and strength, so anisotropic permeability can be exploited for optimum RTM process design.

Fingering. Local inhomogeneities in fibre distribution result in regions of high and low permeability within the reinforcement. The resulting flow front is far from smooth, as seen in Figs. 5,6 & 7. In these illustrations the inhomogeneities may arise from 'natural' variations in fibre orientation or from disturbances introduced by handling. Under some circumstances, the flowing resin may displace fibres laterally, and we have observed that the degree of fingering increases with injection pressure.

Many fabrics are inherently inhomogeneous, comprising stitched or woven tows or bundles of fibres which may be several mm apart. Close inspection of the flow front during injection reveals different rates of flow *between* the tows compared to *within* the tows (Fig. 8). At low pressures, the capillary flow within tows can lead the viscous flow in the spaces between them; at high pressure the situation is reversed, and the observed flow front does not indicate the extent of the wetted-out fabric.

The interaction of these complex mechanisms has been demonstrated in the manufacture of a rectangular test panel from a quadriaxial (0°, ±45°, 90°) non-crimp fabric. This fabric has well defined gaps between the stitched tows in the 0° direction, but evenly spread unidirectional fibres in the other 3 layers. Permeability is thus highly anisotropic. In this experiment, half the required volume of epoxy resin was pigmented yellow and injected in the normal way; the injection was completed with a second batch of black-pigmented resin. The result in shown in Fig. 9, in which the lighter coloured resin appears to occupy the tows, while the second batch of dark resin remains in the tow spaces. It is believed that the first batch of resin will have rapidly filled the spaces between the 0° tows, then subsequently impregnated the tows themselves, leaving the spaces relatively clear once again for the second batch. Whatever the precise details of resin flow, it seems unlikely that a single value of permeability as derived from a Darcy flow experiment will provide an adequate characterisation of this fabric.

Three-Dimensional Flow. Most composite components comprise thin, shell laminates, in which the lateral dimensions are several orders of magnitude greater than their thickness. In this case, the problems of materials characterisation and flow simulation can be considered in two dimensions. A few components, such as panels for ballistic protection, are required to be of considerable thickness - at the University of Plymouth monolithic GRP test panels for such applications of up to 60 mm thickness have been manufactured from a range of non-crimp fabrics [20]. In the quadriaxial fabric referred to above, the continuous 90° fibre layers offer a high resistance to through-thickness flow (Fig. 10). In-plane flow is relatively rapid due to the inter-tow gaps in the 0° plies. It was found that injecting thick laminates from one face of the tool resulted in resin flowing laterally and around the edges of the reinforcement to reach the far side of the tool (a distance of the order of 1 m) before resin had penetrated vertically through the fabric (a distance of only 60 mm). Unwetted plies were therefore located within

4

the laminate typically a few mm from the back surface. Subsequent experiments on biaxial (0°/90°) non-crimp fabrics (in which both warp and weft fibres comprise stitched tows) have proved more successful, due to the higher through-thickness permeability.

DISCUSSION

In most experiments, the initial shape of the flow front reflects the geometry of the inlet. For example, an isolated port produces a circular flow front, while linear injection from the mould edge produces a straight line. During the first few cm of mould filling, the flow appears to be in transition, and Darcy's law is inapplicable.

At the highest level, flow is subsequently influenced primarily by fibre orientation and anisotropy, and this determines the overall way in which the mould is filled. Location of inlet and vent ports should take this into account to avoid wastage of resin. At a lower level (smaller scale), any 'fingering' due to fabric design or irregularities will be superimposed on this pattern. In extreme cases, resin may progress rapidly towards the outlet without fully wetting the fibre bundles. At the lowest (microstructural) level, capillary forces affect flow within fibre tows. The magnitude of capillary forces will depend on the packing of fibres within the tow, and this in turn could be affected by the overall fibre volume fraction and the pressure gradients in the resin. Local movement of fibre in response to excessive pressures has been observed both in discontinuous and continuous reinforcements. In the latter case, resulting regions of high volume fraction and hence low permeability will restrict resin flow.

CONCLUSIONS

Darcy's law has been widely used as a model of resin flow during RTM. However, a number of observed features have been described in this paper which illustrate that the interaction between a fluid and advanced fabrics containing aligned fibres is considerably more complex. While many of these effects may be difficult to quantify, it is suggested that the use of flow visualisation can give an important insight into the various flow mechanisms, their interactions and likely influence on mould filling. An appreciation of these aspects is crucial to the meaningful characterisation of the raw materials used in RTM, and hence to the success of flow prediction and efficient process design and control.

REFERENCES

1. K.B. Spaulding. Fiber Glass Boats in Naval Service. *U.S. Naval Engineers' Journal*, **78** (April 1966), pp. 333-340.
2. Proc. Conf. *Composites Tooling 3*, Amsterdam. Elsevier (1994).
3. A. Harper. RTM Hollow Mouldings: from Fiction to Fact. *Reinforced Plastics* (April 1994), pp. 34-37.
4. A. Harper. Automated Transfer Moulding - a Reality. Proc. Conf. AVK, Berlin, November, 1993.
5. K.L. Adams and L. Rebenfeld. In-Plane Flow of Fluids in Fabrics: Structure/Flow Characterisation. *Textile Research Journal*, **57** (1987), pp. 647-654.

5

6. A.S. Verheus and J. Peeters. The Role of Reinforcement Permeability in Resin Transfer Moulding. *Composites Manufacturing*, 4 (1993), pp.

7. K.N. Kendall, C.D. Rudd, M.J. Owen and V. Middleton. Characterisation of the Resin Transfer Moulding Process. *Ibid.*, 3 (1992), pp. 235-249.

8. J.G. Williams, C.E.M. Morris and B.C. Ennis. Liquid Flow through Aligned Fibre Beds. *Polymer Engineering and Science*, 14 (1974), pp. 413-419.

9. B.R. Gebart. Permeability of Uni-directional Reinforcements for RTM. *Journal of Composite Materials*, 26 (1992), pp. 1100-1134.

10. R. Gauvin, F. Trochu and S. Li. Numerical and Experimental Analysis of Resin Flow in RTM. Proc. *3rd International Conference on Automated Composites*, Den Haag. Plastics and Rubber Institute (October 1991).

11. R. Dave, J.L. Kardos and M.P. Dudokovic. A Model for Resin Flow during Composite Processing - part II. *Polymer Composites*, 8 (1987), pp. 123-132.

12. L. Skartsis, B. Khomami and J.L. Kardos. Resin Flow through Fibre Beds during Composite Manufacturing Processes - part II. *Polymer Engineering Science*, 32 (1992), pp. 231-239.

13. M.J. Owen, C.D. Rudd and K.N. Kendall. Modelling the RTM Process. Proc. *7th Annual ASM/ESD Advanced Composites Conf.*, Detroit (October 1991).

14. J.M. Thirion, H. Girardy and U. Waldvogel. New Developments in Resin Transfer Moulding of High Performance Composite Parts. *Composites* (Paris), 28 (1988), pp. 81-84.

15. F.N. Scott, A. Koorevaar. Computer Aided Engineering of the Resin Transfer Moulding Process. STEC European Space Agency March 1994

16. P.R. Griffin, S.M. Grove, F.J. Guild, P. Russell, D. Short, J. Summerscales and E. Taylor. The Effect of Microstructure on Flow Promotion in RTM Reinforcement Fabrics. *Journal of Microscopy* (in submission).

17. P.R. Griffin, S.M. Grove, F.J. Guild, P. Russell, D. Short, J. Summerscales and E. Taylor. The Effect of Reinforcement Architecture on the Long Range Flow in Fibrous Reinforcements. Proc. *3rd Interniational Conf. on Flow Processes in Composite Materials*, Galway (1994).

18. H.G.P Darcy. Les Fountaines Publiques de la Ville de Dijon. Victor Dalmont, Paris (1856).

19. E.J. Carter, A.W. Fell and J. Summerscales. The Permeability of Reinforcement Fabrics - part I: A simplified model for the derivation of the permeability tensor of an anisotropic fibre bed. *Composites Manufacturing* (in submission).

20. S.M. Grove and A. Lewis. Resin Transfer Moulding of Ballistic GFRP Panels. Final Report for Contract RARDE 1C/5039, DRA, Chertsey (1993).
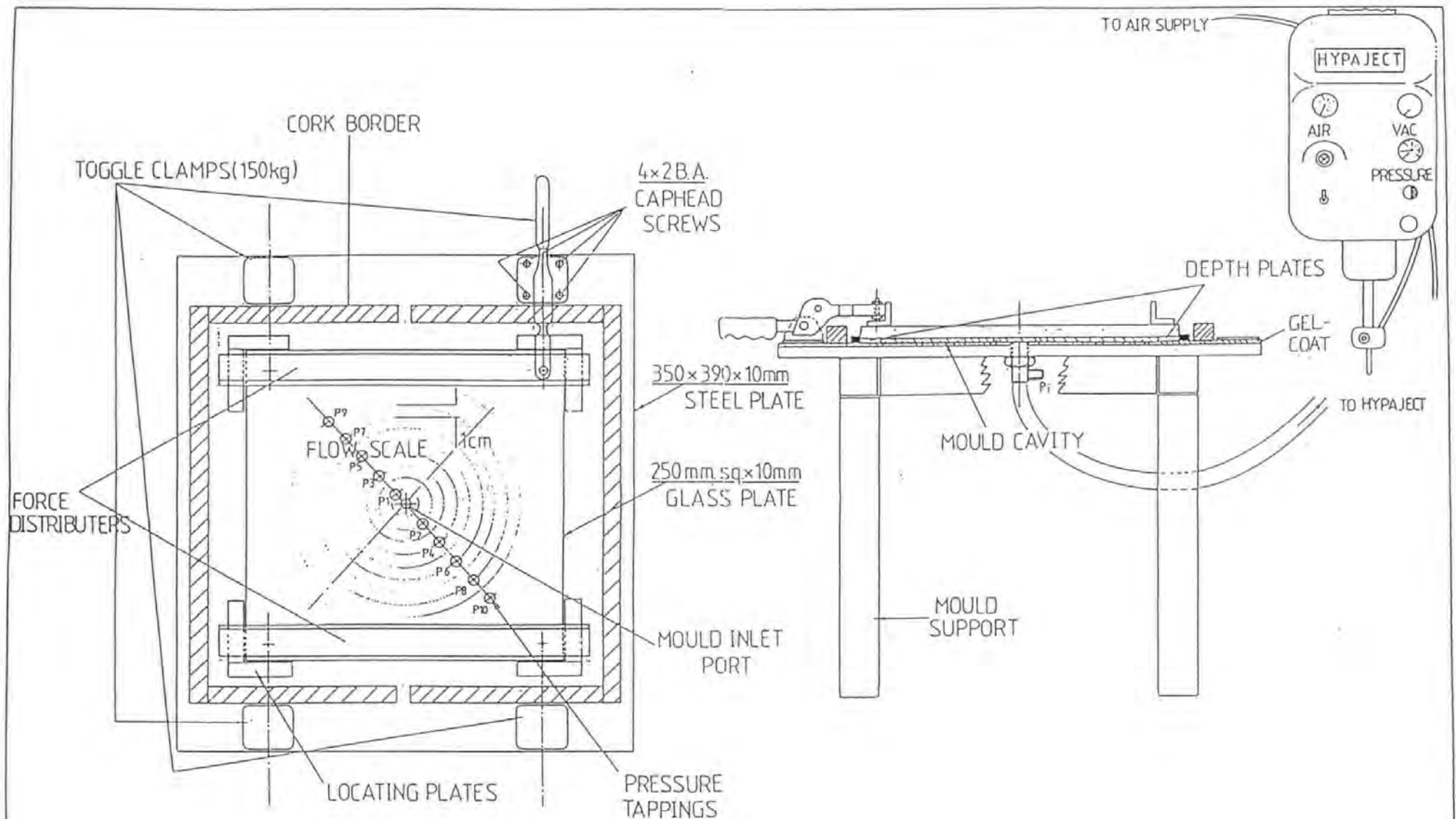
Figure 1. Permeability Test Apparatus

Reinforcement	Areal Weight (g/m²)	Volume Fraction (%)	Injection / Vacuum Pressure (bar)	Test Fluid	Permeability (darcies)
Plain Woven 'E' Glass	345	52	0.85	Ciba Geigy MY750 HY917 DY070	244.1
Plain Woven 'E' Glass	220	52	0.85	As Above	244.4
Plain Woven 'E' Glass	345	39	0.85	As Above	923.3
Twill Woven Carbon (2x2)	380	50	0.9	Boots Glycerol	22.9
Twill Woven Carbon with 1:7 Ratio of Bound Warp Tows	380	50	0.9	Boots Glycerol	149.3
As above with 1:6 Ratio of Bound Tows	380	50	0.9	Boots Glycerol	168
As above with 1:5 Ratio of Bound Tows	380	50	0.9	Boots Glycerol	180
As above with 1:4 Ratio of Bound Tows	380	50	0.9	Boots Glycerol	198
As above with 1:3 Ratio of Bound Tows	380	50	0.9	Boots Glycerol	207
As above with 1:2 Ratio of Bound Tows	380	50	0.9	BDH Glycerol	413
As above with 1:1 Ratio of Bound Tows	380	50	0.9	Boots Glycerol	208

Table 1. Typical Permeability Values worked out using Darcy's Law

Figure 2. Scatter Associated with a Typical Set of Permeability Tests

A7 : 20
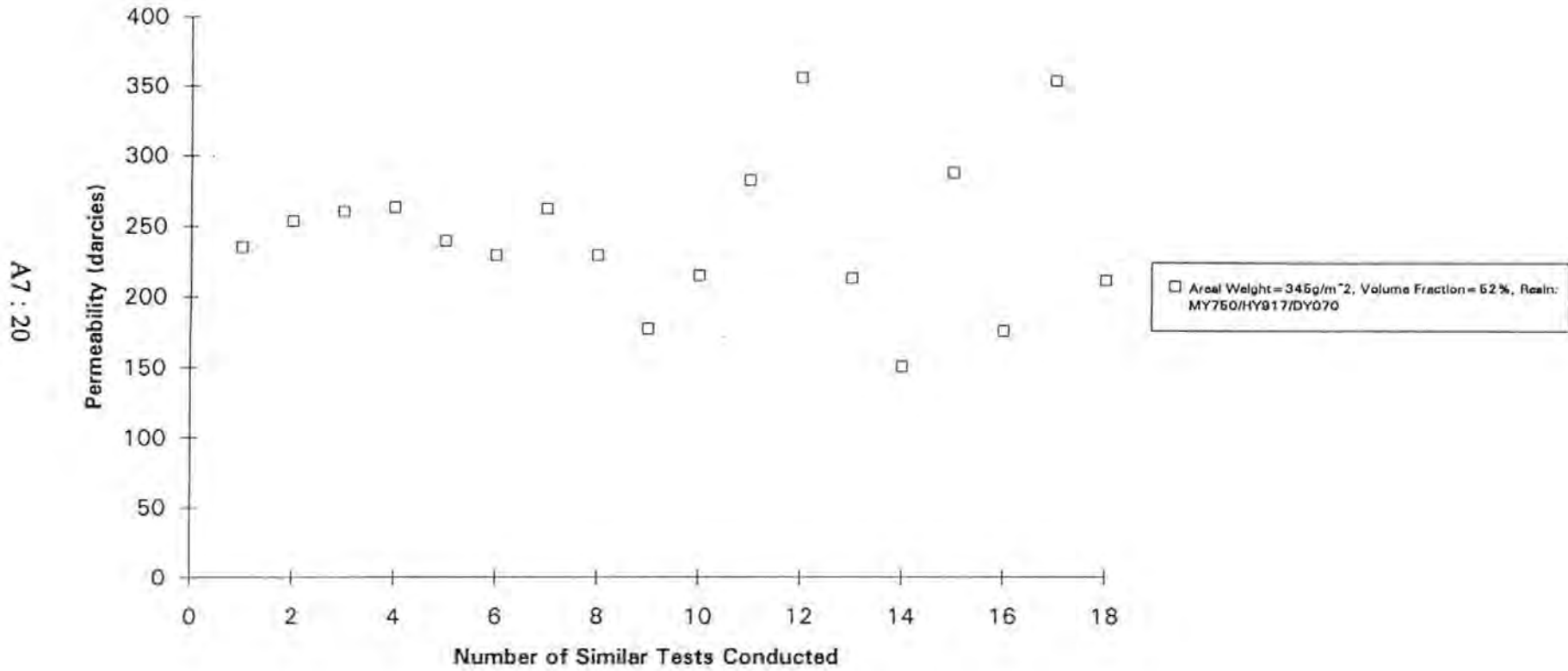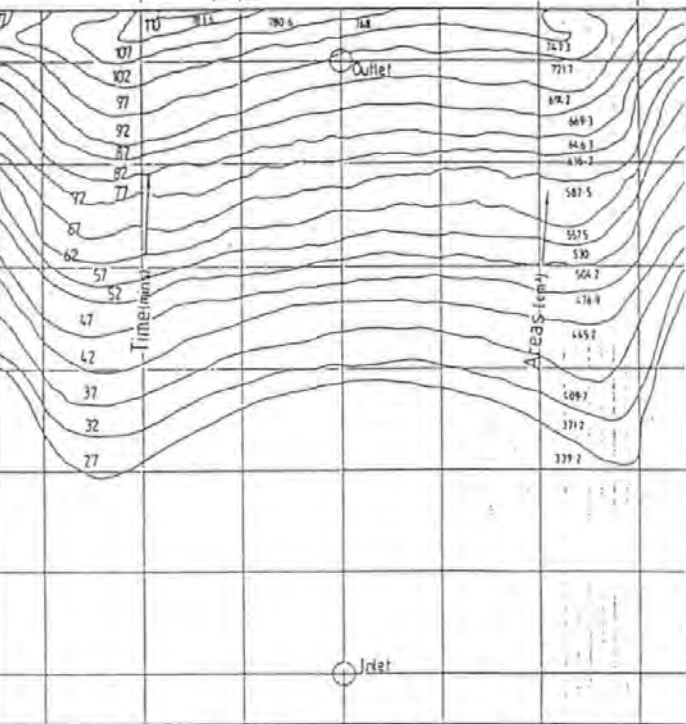
Figure 3. Example of the Problem of Easy Paths in a 0,90° Plain Woven Glass Laminate
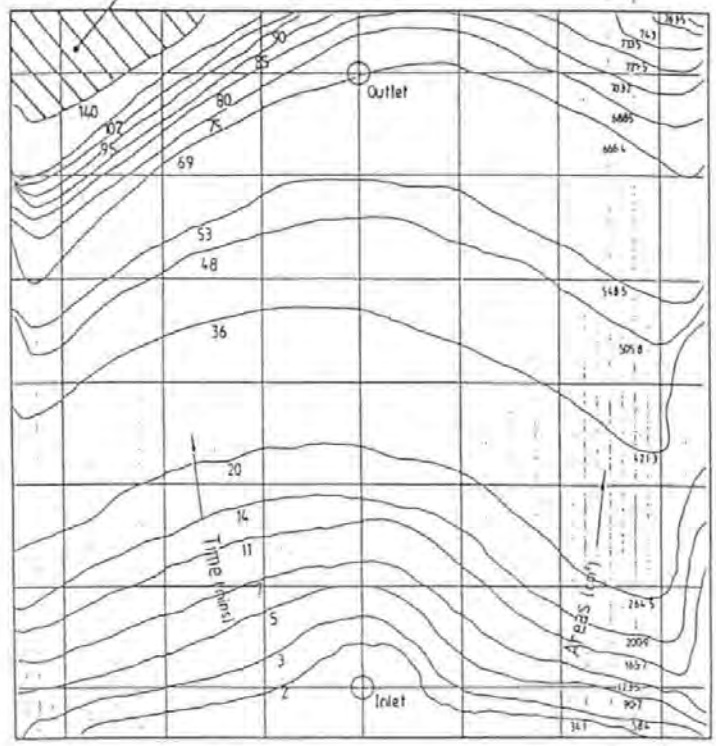
Figure 4. Example of the Resin Starved Area caused by Easy Paths in a ±45° Plain Woven Laminate
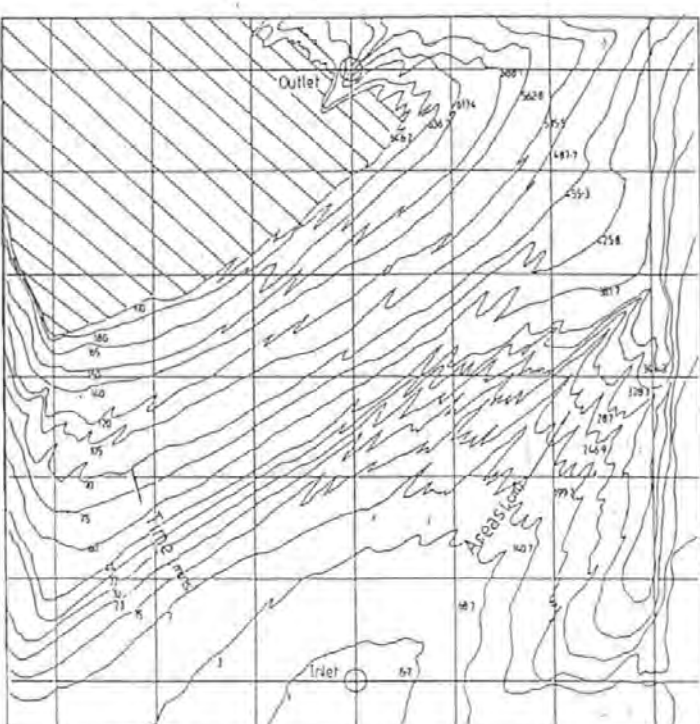
Figure 5. Illustration of the Fibre Orientation Effect in a 45° Uni-Directional Glass Laminate
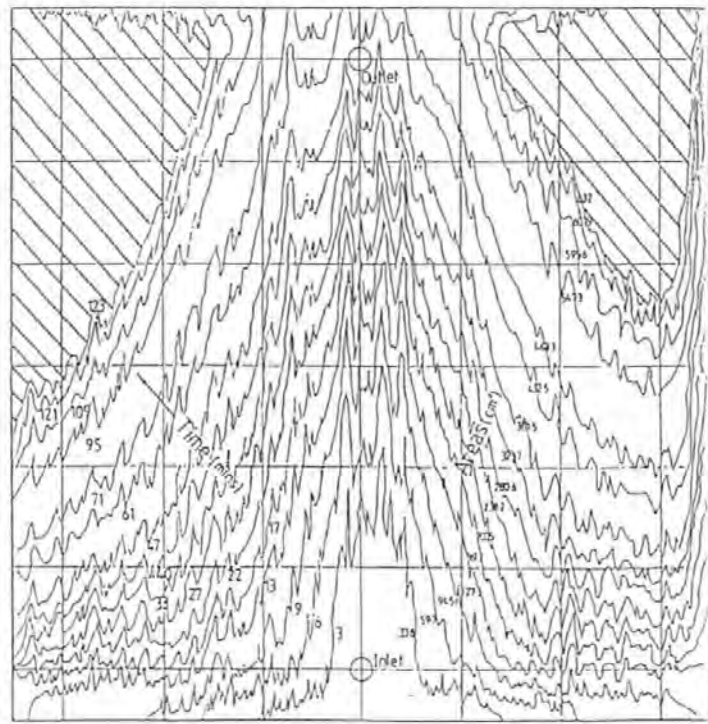
Figure 6. A Vacuum Impregnation of Uni-Directional Glass with Glycerol
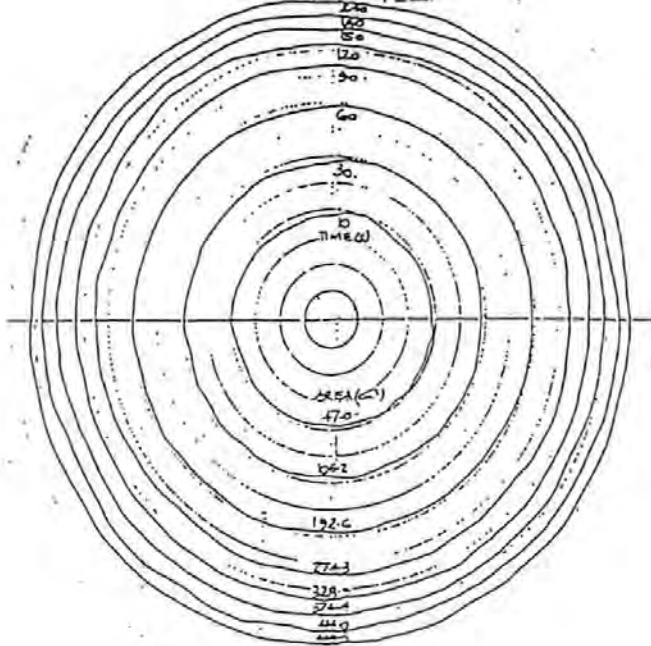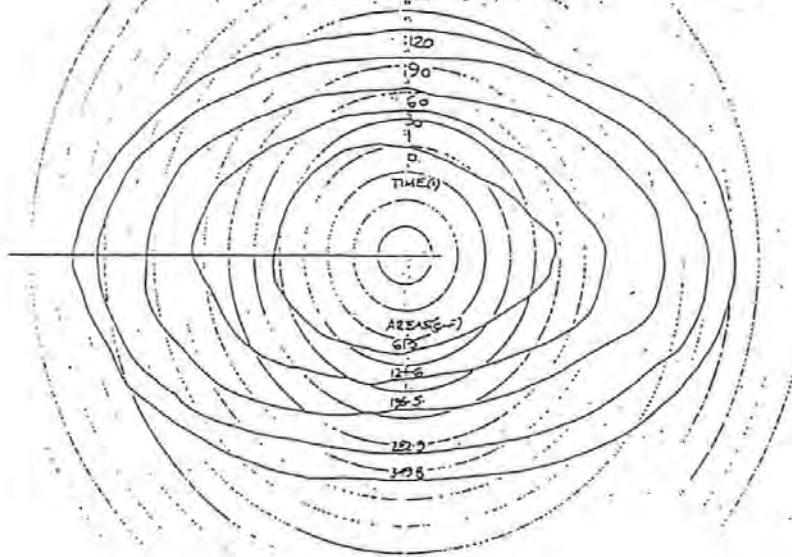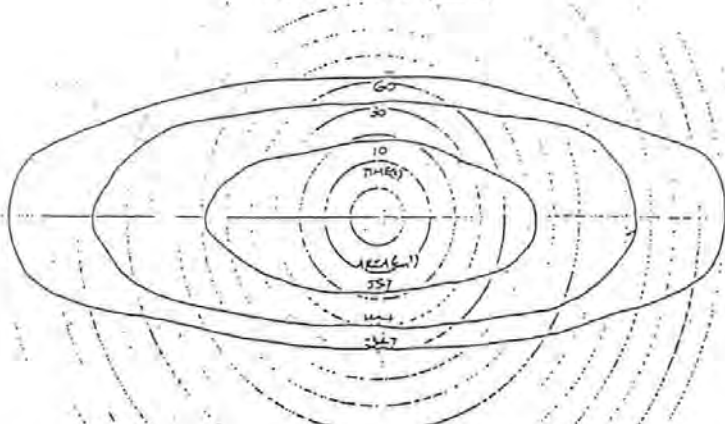
Figure 7. The Effects of Reinforcement Anisotropy on the Flow Front
Profile in a 0,90° Carbon Twill Fabric with a Flow Enhancing
Tow in the Warp Direction.   A7 : 22
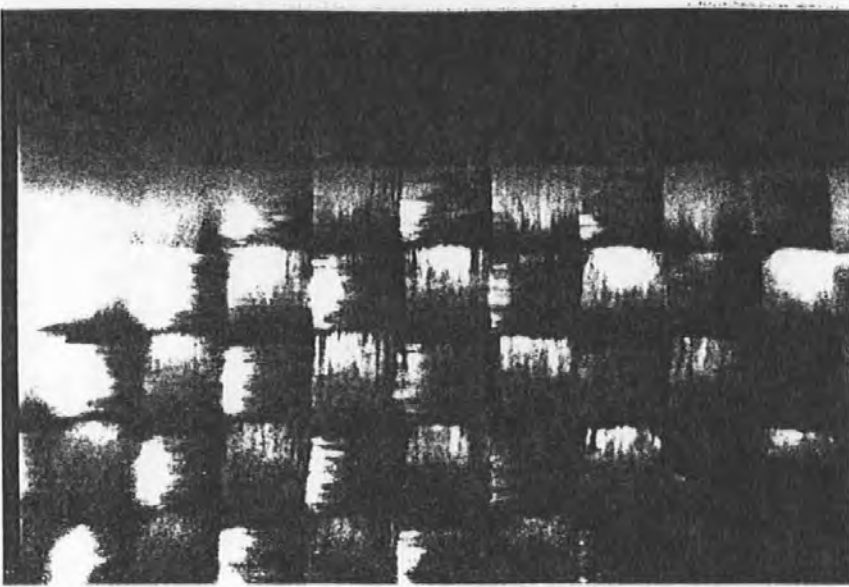
Figure 8. Three Macrophotographs at Varying Magnifications of the Edge of the Flow Front Showing Differing the Wet-out Rates of the tows and Inter-tow Spacings
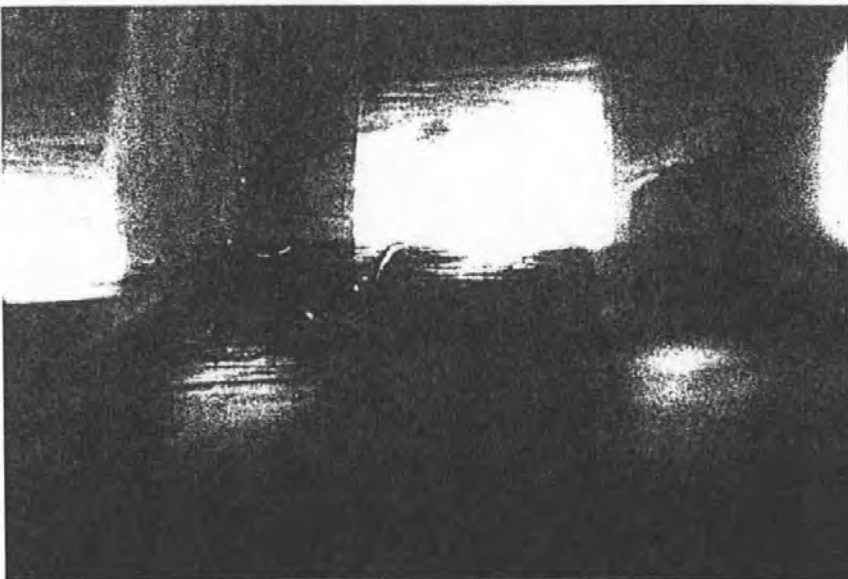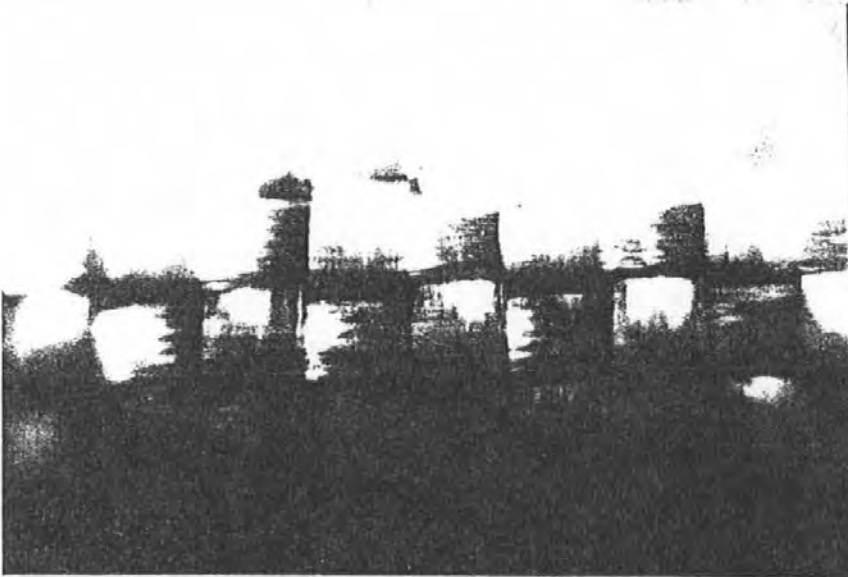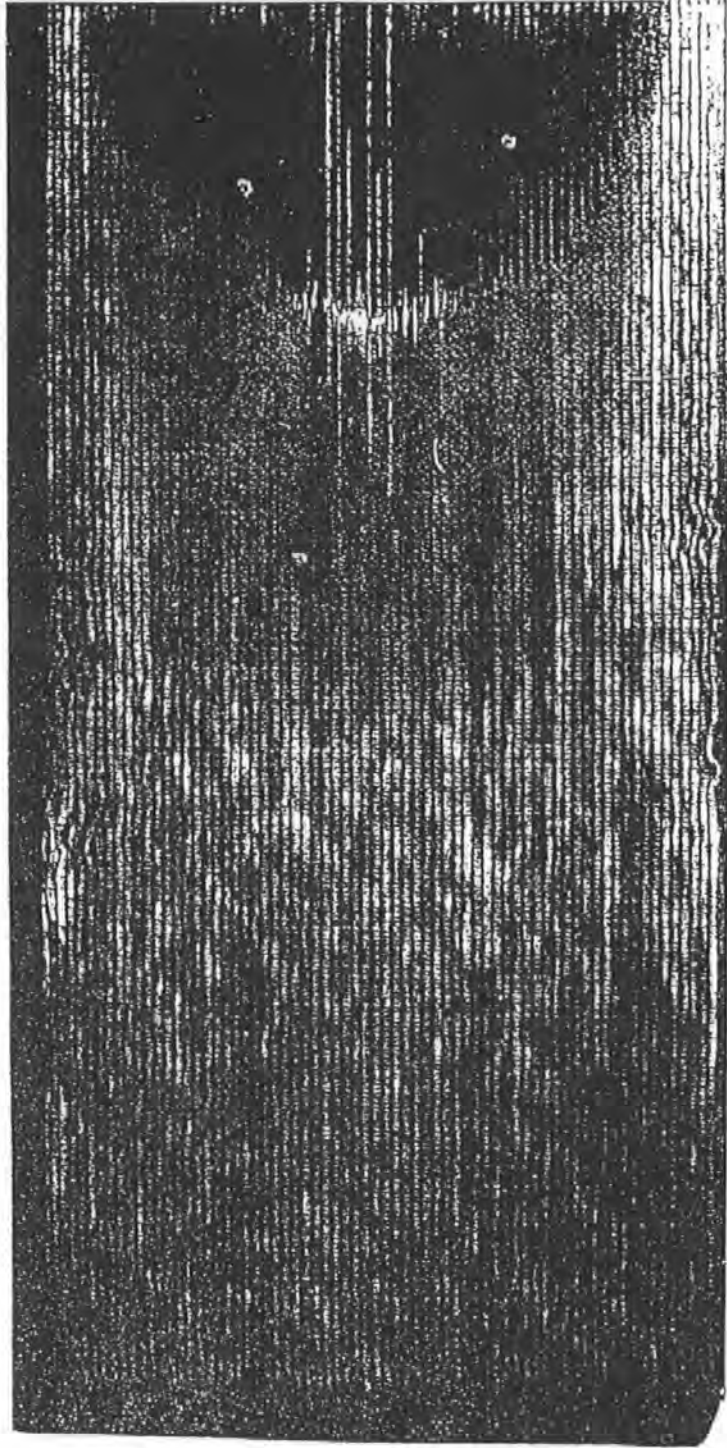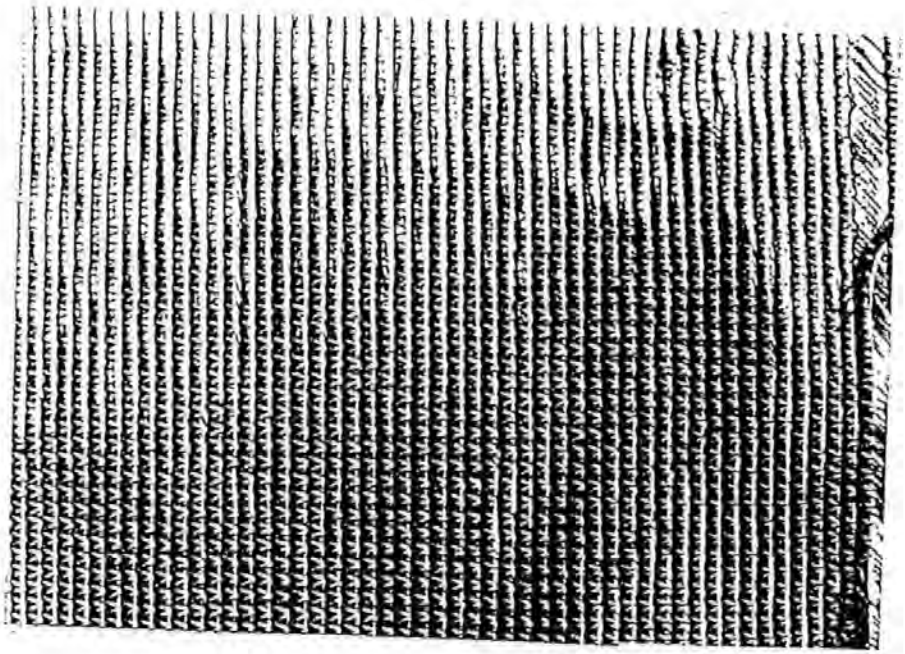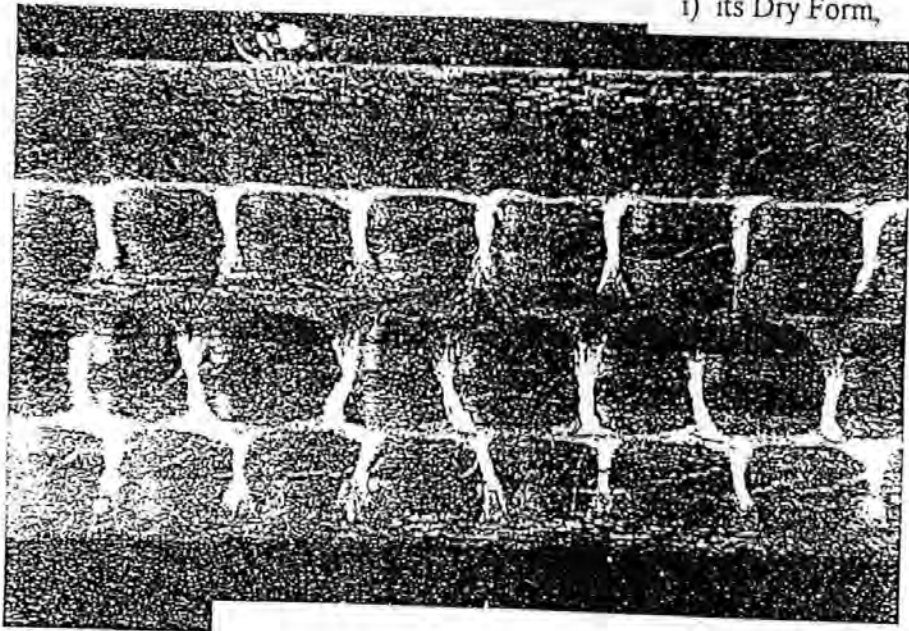
Figure 9. 'E' Glass / Epoxy Panel showing the Yellow (light) Fibre Tows
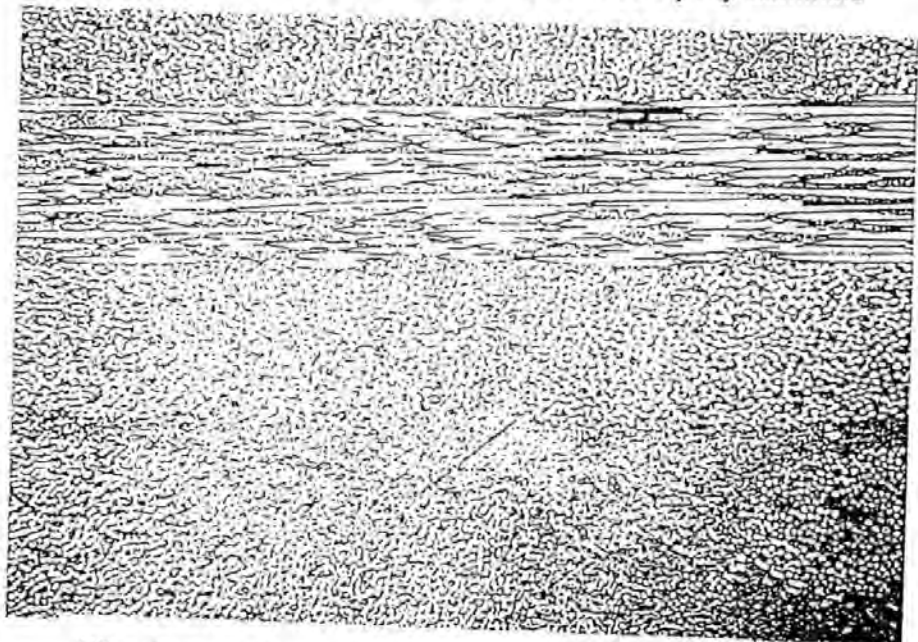and the Black Inter-Tow Flow Gaps

Figure 10. Quadraxial Stitched Fabric ('E' Glass) in

i) its Dry Form,

ii) a Microsection showing 4 layers in an Epoxy Laminate

iii) a Section of one layer illustrating a Deficiency
in Large Through-Thickness Flow Channels

A7 : 25

THE EFFECT OF REINFORCEMENT ARCHITECTURE ON THE LONG RANGE FLOW IN FIBROUS REINFORCEMENTS

P R Griffin (a); S M Grove (a); F J Guild (b); P Russell (c); D Short (a); J Summerscales (a); and E Taylor (d).

(a)   School of Manufacturing, Materials and Mechanical Engineering
        University of Plymouth, Plymouth, Devon PL4 8AA.

(b)   Department of Materials Science and Engineering
        University of Surrey, Guildford, Surrey, GU2 5XH.

(c)   Department of Biological Sciences
        University of Plymouth, Plymouth, Devon PL4 8AA.

(d)   Carr Reinforcements Limited
        Heapriding Business Park, Chestergate, Stockport, SK3 0BT.

Abstract

The resin transfer moulding process involves the long range flow of resin into a closed mould which is filled with dry fibre reinforcement. The rate of resin flow can be calculated using the Darcy and Kozeny-Carman equations. The flow rate is thus a function of the pressure drop across the fibre bed, the resin viscosity and the permeability of the fibre bed. The permeability constant is dependent on the fibre radius and the porosity of the bed.

A number of reinforcement fabrics are now available commercially which promote faster resin flow than that in equivalent fabrics of the same areal weight at the same fibre volume fraction. The Kozeny-Carman equation includes a parameter known as the mean hydraulic radius. If this parameter is varied by calculating a specific hydraulic radius, then the flow enhancement may be modelled. Calculations for model materials have been published and demonstrate that this approach predicts that significant changes in flow rate are possible.

The commercial fabrics do not have model structures, but feature variations in the mesoscale architecture of the reinforcement: fibres clustered into tows and uneven distribution of pore space. The paper will report on the correlation of quantitative image analysis of optical micrographs with the flow rates in a range of reinforcement fabrics.

Introduction

Resin transfer moulding (RTM) is a process for producing fibre-reinforced polymeric parts in final shape. A dry preform of reinforcement fibres is placed into a net-shape mould, which is closed before resin is injected into the mould to fill the spaces between the fibres. Once the resin has cured, the stiff solid composite component can be removed from the mould. Unlike all other composite manufacturing processes, RTM involves long-range flow of resin through the porespace between the reinforcement fibres. The process and the associated governing equations have been well described [1-3].

The one-dimensional flow of fluid through a porous bed was modelled by Darcy [4] in 1856. Darcy's law relates the linear flow rate, q, to a coefficient depending on the permeability, K, the pressure drop, ΔP, and the bed length, L, through the equation:

$$q = \frac{K.\Delta P}{L}$$

.... (1)

Kozeny [5] and Carman [6] considered the relationship between the volumetric flow rate of fluid, Q, and the porosity (fractional free volume in the bed), ε, and found it to be governed by the equation:

$$Q = \frac{A\varepsilon.m^2}{k\mu} . \frac{\Delta P}{L}$$

.... (2)

where A is the cross-sectional area of the bed, k is the Kozeny constant, m is the mean hydraulic radius of the bed, and μ is the dynamic viscosity of the fluid.

The concept of the hydraulic radius of the bed is attributed to Blake [7], and is defined as the cross-sectional area normal to the flow divided by the perimeter presented to the fluid. Williams et al [8] suggested that the mean hydraulic radius of a unidirectional fibre bed is given by Equation 5:

$$m = \frac{r}{2} . \frac{\varepsilon}{(1 - \varepsilon)} = \frac{rV_m}{2V_f}$$

.... (3)

where r is the fibre radius, V_m is the matrix volume fraction of the void-free composite and V_f is the fibre volume fraction. Hence:

$$\varepsilon = V_m = (1 - V_f)$$

.... (4)

The 1-D volumetric flow rate can be represented by Darcy's equation by including the cross sectional area normal to the flow on both sides of the equation, hence:

$$Q = q.A = KA . \frac{\Delta P}{L}$$

.... (5)

and substituting Equation 3 into Equation 2 gives:

$$Q = \frac{Ar^2}{4k\mu} . \frac{\varepsilon^3}{(1 - \varepsilon)^2} . \frac{\Delta P}{L}$$

.... (6)

Equating the right hand sides of Equations 5 and 6 gives:

$$K = \frac{r^2\varepsilon^3}{4k\mu(1 - \varepsilon)^2}$$

.... (7)

Thirion et al [9] have demonstrated that the linear flow rate through the same volume fraction of similar reinforcement fibres with different reinforcement architectures under identical flow conditions was more rapid in fabrics with clustered tows. Griffin [10] has conducted a comprehensive survey of international studies of the permeability of fibrous reinforcements and found that reported values for similar fabrics might vary by one or two orders of magnitude. Griffin and Grove [11] have reported that the rate of flow front advance increased with the proportion of spiral-bound tows at constant reinforcement volume fraction.

Clearly Equation 7 is only applicable to situations in which we might expect the fibres to be organised such that the **mean** hydraulic radius is an applicable concept. This situation is only likely to be relevant when the fibres are organised with uniform or truly random packing. The use of weaving techniques to produce commercially useful reinforcement will inevitably organise the reinforcement tows into clustered groups.

Summerscales has analysed situations with clustered fibres [12] and clustered layers [13] to determine the effect of variations in the reinforcement architecture on the flow rate. The predicted flow rate in a regular array of clustered fibres was significantly increased relative to a uniform distribution of individual fibres at the same volume fraction. Similarly, the flow rate is predicted to be higher in a small number of thick layers when compared to a large number of thin layers.

The materials analysed by Summerscales were idealised models. The evaluation of real materials will require the use of automated microstructural image analysis. The use of such techniques for fibre-reinforced composites has been reviewed by Guild and Summerscales [14].

Quantitative microscopy, using spatial statistics, is capable of revealing subtle relationships amongst the fibres in the composite. Summerscales et al [15] used the Voronoi half-interparticle distance to characterise the microstructure of carbon fibre-reinforced plastics processed by the vacuum-bag technique using different process dwell times.

Li et al [16] used automatic image analysis to quantitatively evaluate fibre distributions in cast continuous aligned aluminia fibre-reinforced aluminium alloy. Significant differences could not be detected between the fibre distributions of samples solidified under different conditions.

Everett and Chu [17] modelled the microstructural effects of non-uniform composite microstructures. Fibre positions and areas were determined from micrographs of Nicalon (SiC)/zirconia titanate ceramic by image analysis, or were generated by a computer program. Dirichlet cell tesselations, number of cell sides, cell volume fraction and nearest-neighbour distances were calculated. The flexural strength of the ceramic matrix composites which exhibited clustering was found to correlate with the maximum value of nearest-neighbour distance distribution skewness.

Experimental Techniques

Materials Used:

The carbon-fibre reinforcement fabrics in this study were developed by Carr Reinforcements with the specific aim of promoting resin flow. All fabrics were 2 x 2 twill weaves, with from 0-7 flow-enhancing warp threads to each normal warp tow. The materials used are summarised in Table 1.

TABLE 1: Materials used in the experimental study

REINFORCEMENT FABRICS		
Designation	Description	% Bound Tows
38166	normal 2 x 2 twill weave	0%
156	one bound tow in each eight tows	12.5%
150	one bound tow in each six tows	16.7%
148	one bound tow in each four tows	25%
126	one bound tow in each two tows	50%
FLUIDS		
Boots glycerol		
BDH glycerol		
Scott Bader unsaturated polyester resin A cured with MEKP		
Scott Bader unsaturated polyester resin E cured with MEKP		
Jotun Polymer unsaturated polyester resin 4210 cured with MEKP		
Jotun Polymer unsaturated polyester resin 4210 cured with AAP		

Permeability measurements and composite manufacture

Four layers of one type of fabric were laid up in a 350 mm square 1.7 mm deep parallel-sided flat mould. The fabrics are anisotropic due to the inclusion of the bound flow-enhancing warp thread. To measure the permeability in quasi-isotropic flow, the layer stacking sequence was $[0/90]_s$ and a fluid inlet port was included at the centre of the lower face of the mould. A central hole (diameter of 14 mm) was punched in the centre of each fabric layer to encourage true two-dimensional flow throughout the permeability experiment.

The flow fluid was introduced through the central inlet port into the space punched into the reinforcement layers. The fluid pressure at the reservoir was 0.9 bar gauge pressure (ie 1.9 bar pressure absolute). The fluid permeated radially outwards. The flow front isochrones were recorded at 30 second intervals during the early stages and one minute intervals in the later stages of each flow experiment. The permeability values were calculated using the radial form of Darcy's law. This approach is similar to that of Adams et al [18] and Hwang and Chang [19].

Further experiments were conducted using an anisotropic stacking sequence, $[0_2]_s$ under the same conditions as above.

The permeability results using Boots glycerol are shown in Figure 1. Since the experiments were performed, we have become aware of the high variability in the measured viscosity of glycerol [20]. All fabrics had similar areal weights (a range of 5g/m² for a nominal fabric weight of 382 g/m²). All experiments were conducted in the same mould, to the same nominal thickness, and hence at equivalent volume fractions. The permeability increased with the number of flow-enhancing tows. This result would not be predicted by Kozeny-Carman law as volume

fractions (porosities) were nominally identical and a _mean_ hydraulic radius is used in that equation (equation 2).

Figure 2 summarises the permeability results for the full range of fluids used (listed in Table 1). All experiments were conducted under identical conditions, except for the fluids and their viscosities, and hence it would not be expected that different permeabilities resulted. A similar problem has been reported by Steenkamer et al [21]. The explanation may be that the experimental configuration involves the wetting of fabric (unlike Darcy's original wetted flow experiment) and hence surface chemistry/physics may assume a significant importance. The flow regime could also involve extensional flow, rather than bulk flow, and the different performance of each flow fluid in this regime could be critical.

The procedure used follows that developed by Griffin [22-24]. The full mathematical derivation of the model has been reported by Carter et al [25]. A standard experimental apparatus and procedure have been proposed by Fell et al [26].

Microstructural Examination

Sections perpendicular to the flow-enhancing fibre direction were cut from the anisotropic plates at 20, 40 and 60 mm from the inlet position normal to the bound tow. The sections were mounted in casting resin. The sections were polished on 'wet-and-dry' diamond papers of 200, 320, 400 and 600 grade in turn, until the surface appeared flat to the unaided eye. The sections were then polished using an automatic metallurgical polishing machine with diamond pastes and a specimen load of 1 kg. The sequence used was: 1 h at 14 μm; 1 h at 6 μm; 30 min at 1 μm; and a final short polish at 0.25 μm.

The microstructure of a unidirectional continuous-fibre composite is entirely defined by sections perpendicular to the fibre direction, assuming that the fibres are perfectly straight and of constant cross-section along their length. The samples examined are reinforced with bidirectional (orthogonal) fabrics. The flow direction fibres appear as circles and the transverse fibres lie in the plane of the section. The sections were examined with a Quantimet 570 Automatic Image Analyser. The section was placed in bright-field illumination in the microscope. The overall magnification used was recorded for each individual frame, typically 0.0162-0.0178 mm/pixel.

The features of the Quantimet 570 used in this work will be briefly described. The maximum size of frame which can be examined is divided into a square grid of 512 x 512 square pixels. The contrast is divided into 256 grey levels; black is defined as grey level 0 and white is defined as grey level 255. The grey level of each pixel is recorded as an 8-bit digital word. Detection was carried out with respect to a single threshold. The threshold level and detection were set so that the carbon fibres appeared white with respect to the matrix. Figure 3 is a grey-level image of a typical section. The fibre bundles are darker than the flow space. Individual fibres are not detected at this magnification. The flow areas could thus be detected as features, and their centres of gravity, i.e., their x, y coordinates with respect to the frame, could be measured and recorded. The image-enhancement processing of the Quantimet is used to improve the image after converting the image to a binary form.

The microstructure of the laminate is variable due to its construction using carbon fibres in tows; measurements must be taken over an area which reflects the size of this variability. The total area analysed was a grid of 3 contiguous frames in the sample width, parallel to the weft direction. The measure frame used was 438 x 123 pixels: for sample 156 this corresponds to 21.3 mm wide by 1.99 mm high total area analysed.

js-galway

A7 : 30

The image shown in Figure 4 is a binary image; each pixel is defined as detected or not detected. The sophisticated image processing available on the Quantimet 570 arises from its large storage capacity. Such image enhancement was used here; the 'segment' process was used. This essentially consists of successive erosions and builds (dilations without remerge) of features, leading to their separation. Figure 5 shows the binary image of the same field after the image enhancement. The flow areas are now detected as separate features.

The process of image capture, image processing, measurement and movement of the stored image to prepare for the next frame was programmed using QBASIC, the command language of the Quantimet. The results were written onto a floppy disk; for each fibre-free zone, the parameters recorded were area, maximum feature height (vertical feret) and maximum feature width (horizontal feret), x- and y- centres of gravity and perimeter. The results were subsequently analysed using a spreadsheet (LOTUS 1-2-3).

The data was divided into bins from which histograms can be drawn. An alternative presentation of the data is a continuous plot showing the total number in a given range and all smaller ranges. Results from different laminates are more easily compared using such continuous plots. Comparisons can be made if the total number is normalised; the y-axis range is 0 to 1. These are plots of the cumulative distribution function.

Results and Discussion

The permeability of the reinforcement fabrics at constant (to within ± 2%) volume fraction increase with the proportion of (bound) flow-enhancing tows. The values are calculated from each of the flow front isochrones recorded using the radial form of Darcy's equation, and the values reported in Table 2 are the averages of at least ten values.

TABLE 2 : Permeability values determined with Boots glycerol

Fabric Number:	38166	156	150	148	126
Description:	Twill	12% bound	17% bound	25% bound	50% bound
Permeability: $(x\ 10^{-12}\ m^2)$	25.6	149	180	206	208

Tests were run on fabric 126 using a variety of flow fluids. The permeabilities calculated were dependent on the flow fluid (Table 3) which confirms the findings of Steenkamer et al [21].

TABLE 3: Variation of permeability with flow fluid for fabric 126

Flow Fluid:	BDH glycerol	Boots glycerol	Scott Bader Resin E
Mean permeability $(x\ 10^{-12}\ m^2)$	165	208	1288

It proved impractical to undertake the quantitative microscopy of samples manufactured with two of the fabrics (150 and 148), because the samples were damaged during preparation. The sum of the microstructure parameters measured are recorded in Table 4.

TABLE 4: Total areas and perimeters of voids determined by quantitative microscopy				
Fabric No.	Total no of areas	Total area (mm^2)	Total perimeter (mm)	Av perimeter area (mm)
126	130	11.21	146.4	1.126
156	115	8.54	112.4	0.977
Twill	210	5.47	139.6	0.655

The Blake-Kozeny-Carman (BKC) equation predicts that flow will be proportional to total area wetted per unit volume or to total perimeter wetted per unit area. The "areas" reported in Table 4 are the areas of the large pore space (voids in the unwetted reinforcement) and not the areas corresponding to the BKC equation. A threshold pore space area of ~5 pixels was set to eliminate the small pore spaces corresponding to close packing of the fibres as flow visualisation experiments [27] suggest that flow occurs in the macro-porosity of the reinforcement.

The perimeters recorded do correspond to those of the BKC equation. However, it is not yet practical to determine the effective penetration of the flow front into the tows during wetting, so a global perimeter has been determined from the large areas in isolation.

The parameters determined in Table 4 have been plotted as histograms. The results are reported in more detail elsewhere [28]. The middle-range flow areas are more abundant in fabric 126 (which has most flow enhancing tows) and least abundant in the twill fabric. The flow enhancing tow can therefore be seen to achieve the required effect by creating flow passages, which are predominantly in the range ~> 0.6 mm^2. These areas are of irregular shape and hence the ratio of perimeter to area is variable. The total perimeters in Table 4 do not correspond to the expectations of the BKC equation. The perimeters which correspond to the above middle-range flow areas are summarised in Table 5. The resolution of these perimeters is limited by the pixel size and by the diffuse edges of the large flow areas due to the separation of individual fibres along the tow edge. Further study of the perimeter as a factor determining the flow will require examination of this parameter over a range of magnifications.

TABLE 5: Sum of perimeters of large flow areas in millimetres. (number of areas considered)			
	Twill	156	126
Area >0.4mm^2	86.6 (47)	31.6 (34)	95.6 (41)
Area >0.6 mm^2	69.9 (32)	31.0 (23)	86.6 (30)
Area >0.8 mm^2	61.2 (24)	30.7 (18)	80.0 (25)
Area >1.0 mm^2	59.6 (23)	30.6 (17)	76.2 (22)

The histograms of zone area for the three laminates are shown in Figure 6. The highest bin used is 0.15 mm^2. The final bin includes all areas greater than the size of the highest bin. Histograms for these large areas are shown in Figure 7. The larger total number of areas measured for the twill (Table 4) is clear from the histogram; the larger total number arises from larger numbers of small areas. Comparing Figures 7a, b and c, it is clear that the introduction of the twisted tows allows more large areas to occur. The number and distribution of these large areas are not significantly changed by changing the frequency of the twisted tows (Figures 7b and c). The effect of the twisted tows on the intermediate areas is not clear from comparison of these histograms.

The dimensions of the fibre-free zones were compared using cumulative plots. Figure 8 shows the plots of the total number; Figure 9 shows the plots where the total number has been normalized. As expected from the overall laminate construction, the values of through-thickness length (Figures 8 and 9a) are smaller than the values of in-plane length (Figures 8 and 9b); the x-axes are different lengths for each direction. Considering first the plots of 'Total Number', Figure 8: the ranking of the graphs for very small lengths is the ranking expected from the number of twisted tows. Increasing the number of twisted tows leads to a decrease in the number of small zone lengths. The difference is clearer for the through-thickness length (Figure 8a). However, the plots for the 156 and 126 laminates cross since the 126 laminate had a higher overall number of zones (Table 4). The difference between the laminates is clarified by the normalisation (Figure 9). The ranking remains unchanged throughout the range. The 126 laminate has the lowest proportion of small dimensions, that is the highest proportion of long dimensions. The effect is most apparent in the through-thickness direction.

Summary

Permeability experiments have been conducted on a series of fabrics containing a variable number of flow enhancing tows. The permeability was found to be dependent on the flow fluid used, but values for a single fluid showed the expected increase in permeability with number of flow enhancing tows. Quantitative microscopy revealed that flow enhancement was accompanied by the presence of large flow areas adjacent to the "bound" tows and increased in line with the average perimeter of these areas.

js-galway

A7 : 33

References

1. K VAN HARTEN
    "Production by resin transfer moulding"
    Chapter 4 of RA Shenoi and J F Wellicome (editors):
    "Composite Materials in Maritime Structures", CUP, Cambridge, 1993, pp 86-126

2. C L TUCKER and R B DESSENBERGER
    "Governing Equations for Flow and Heat Transfer in Stationary Fibre Beds"
    Chapter 8 of SG Advani (editor):
    "Flow and Rheology in Polymer Composites Manufacturing", Elsevier, Amsterdam, 1994,
    pp 257-323

3. S G ADVANI and M V BRUSCHKE
    "Resin Transfer Moulding Phenomena in Polymeric Composites"
    Chapter 12 of S G Advani (editor):
    Ibid, pages 465-515

4. H P G DARCY
    "Les fontaines publiques de la ville de Dijon"
    Dalmont, Paris, 1856.

5. J KOZENY
    "Uber die Kapillare Leitung des Wassers in Boden""
    Sitzungsberichte Akademie der Wissenschaft Wien Math-naturw, 1927, 136 (Kl.abt.IIa),
    271-306.

6. P C CARMAN
    "Fluid flow through a granular bed"
    Transactions of the Institute of Chemical Engineers (London), 1937, 15, 150-166.

7. F C BLAKE
    "The resistance of packing to fluid flow"
    Transactions of the American Institute of Chemical Engineers, 1922, 14, 415-421.

8. J G WILLIAMS, CEM MORRIS and B C ENNIS
    "Liquid flow through aligned fibre beds"
    Polymer Engineering and Science, June 1974, 14(6), 413-419.

9. J M THIRION, H GIRARDY and U WALDVOGEL
    "New developments in resin transfer moulding of high-performance composite parts"
    Composites (Paris), 1988, 28(3), 81-84.

10. P R GRIFFIN
    "Reinforcement permeability values - a brief review"
    University of Plymouth report BE5477/UoP/BE/1.2/D/CC/1.0, December 1993

11. P R GRIFFIN and S M GROVE
    "Measurements of Permeability of Fibre Reinforcements: A Review"
    In preparation

12. J SUMMERSCALES
"A model for the effect of fibre clustering on the flow rate in resin transfer moulding"
Composites Manufacturing, 1993, 4(1), 27-31.

13. J SUMMERSCALES, E J CARTER and A W FELL
"A model for the effect of layer clustering and layer porosity on the flow rate in resin transfer moulding"
Composites Manufacturing, in submission.

14. F J GUILD and J SUMMERSCALES
"Microstructural image analysis applied to fibre composite materials"
Composites, 1993, 24(5), 383-394.

15. J SUMMERSCALES, D GREEN and F J GUILD
"Effect of processing dwell-time on the microstructure of a fibre reinforced composite"
Journal of Microscopy, February 1993, 169(2), 173-182.

16. Q F LI
"Quantitative evaluation of fibre distributions in a continuously reinforced aluminium alloy using automatic image analysis"
Materials Characterisation, 1992, 28(3), 189-203.

17. R K EVERETT and J H CHU
"Modelling of non-uniform composite microstructures"
Journal of Composite Materials, 1993, 27(11), 1128-1144.

18. K L ADAMS, W B RUSSEL and L REBENFELD
"Radial penetration of a viscous fluid into a planar anisotropic porous medium"
International Journal of Multiphase Flow, 1988, 14(2), 203-215.

19. A W CHAN and S HWANG
"Anisotropic in-plane permeability of fabric media"
Polymer Engineering and Science, 1991, 31(16), 1233-1239.

20. P N SHANKAR and M KUMAR
"Experimental determination of the kinematic viscosity of glycerol-water mixtures"
Proc Roy Soc London, 8 March 1994, A444(1922), 573-581

21. D A STEENKAMER, D J WILKINS and V M KARBHARI
"Influence of test fluid on fabric permeability measurements and implications for processing of liquid moulded composites"
Journal of Materials Science Letters, 1 July 1993, 12 (13), 971-973

22. P R GRIFFIN
"RTM flow visualisation and quantification"
BEng project report, Polytechnic South West, May 1990.

23. P R GRIFFIN
"Measurement of permeability of reinforcement fabrics to resin flow"
Advanced Composites Manufacturing Centre Report, February 1991.

24. P R GRIFFIN
"Simulation and Optimisation of the Resin Transfer Moulding Process"
MPhil/PhD Transfer Report, University of Plymouth, 1993

25. E J CARTER, A W FELL and J SUMMERSCALES
"The permeability of reinforcement fabrics, Part 1:
A simplified model for the derivation of the permeability tensor of an anisotropic fibre bed"
Composites Manufacturing, in submission.

26. A W FELL, E J CARTER and J SUMMERSCALES
"The permeability of reinforcement fabrics, Part 2:
A proposed standard experimental apparatus and procedure"
Composites Manufacturing, in preparation.

27. P R GRIFFIN, S M GROVE, A LEWIS and D SHORT
"Flow visualisation in resin transfer moulding"
This conference

28. P R GRIFFIN, S M GROVE, F J GUILD, P RUSSELL, D SHORT, J SUMMERSCALES
and E TAYLOR
"The Effect of Microstructure on Flow Promotion in RTM Reinforcement Fabrics"
Journal of Microscopy, in submission

Figure 1. Permeability of Glycerol (supplied by Boots) through a Range of Flow Enhancing Reinforcement Fabrics
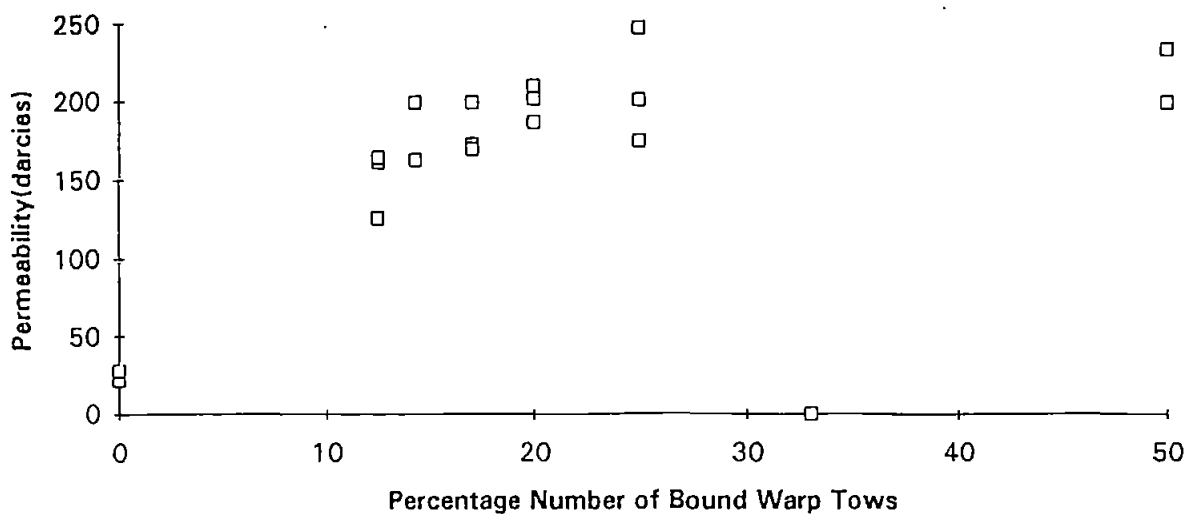
Figure 2. Permeability of a Range of Flow Enhancing Reinforcements to Various Test Fluids

O Glycerol (supplied by Boots)

△ Glycerol (supplied by BDH Chemicals)

◇ Scott-Bader Crystic 2-414 PA (Resin'E')

□ Scott-Bader Crystic 471PA LV (Resin'A')
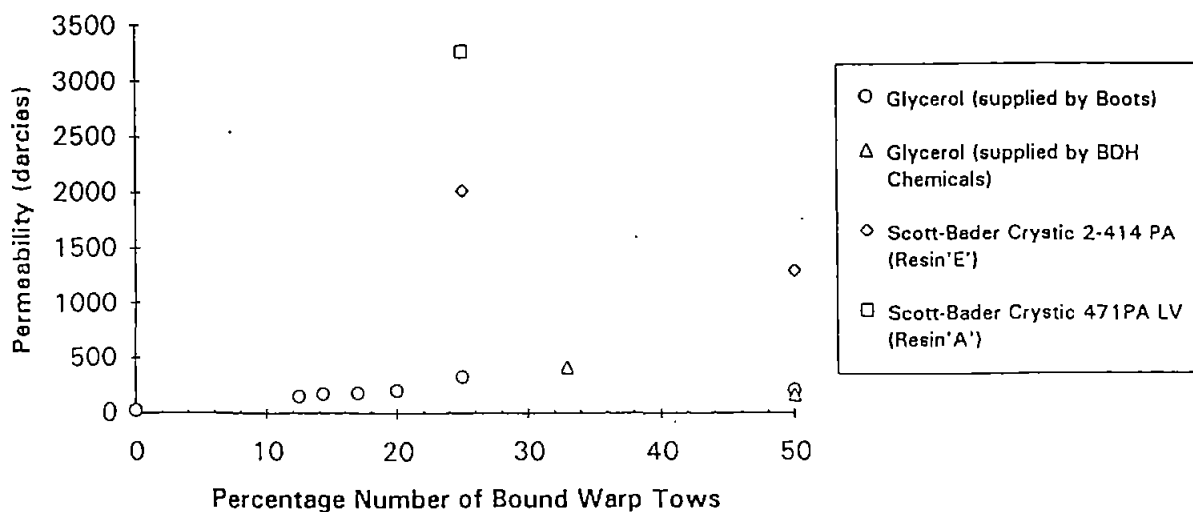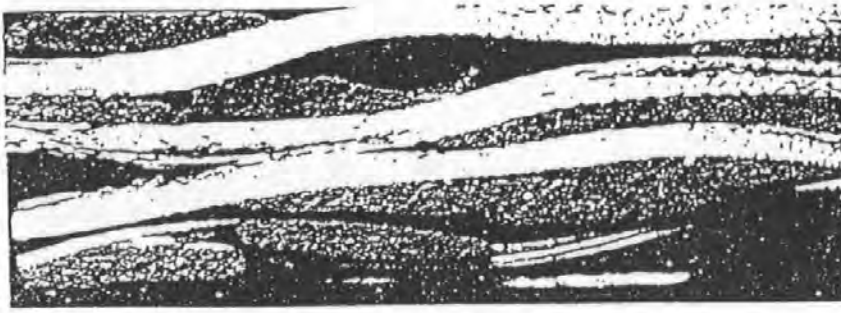
Figure 3. A Grey level Detection of a
Section of a Fabric 156 Laminate

Figure 4. A Binary Image of the Fabric
156 Laminate

Figure 5. The Section of 156 Fabric after
Image Enhancement
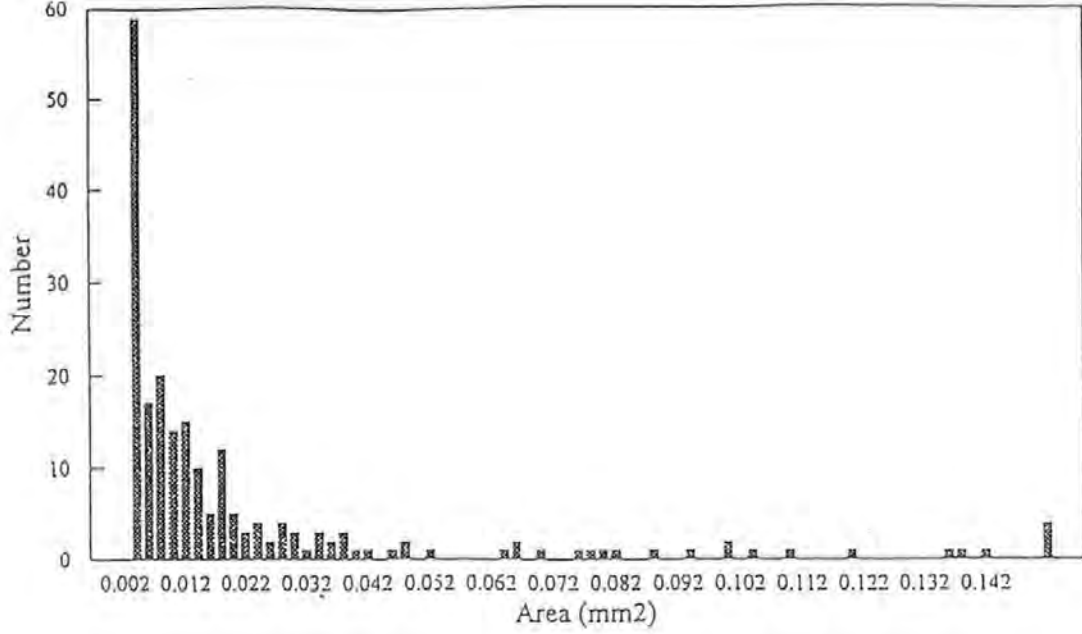
Figure 6a. Histogram of Zone Area in the Twill Laminate
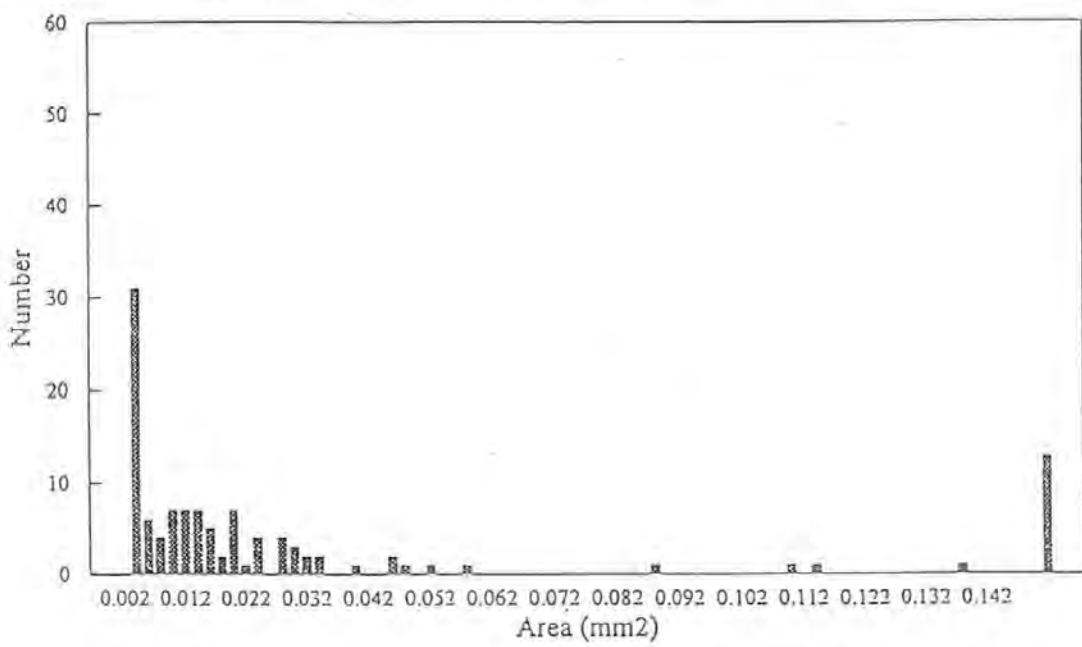
Figure 6b. Histogram of Zone Area in the 156 Laminate
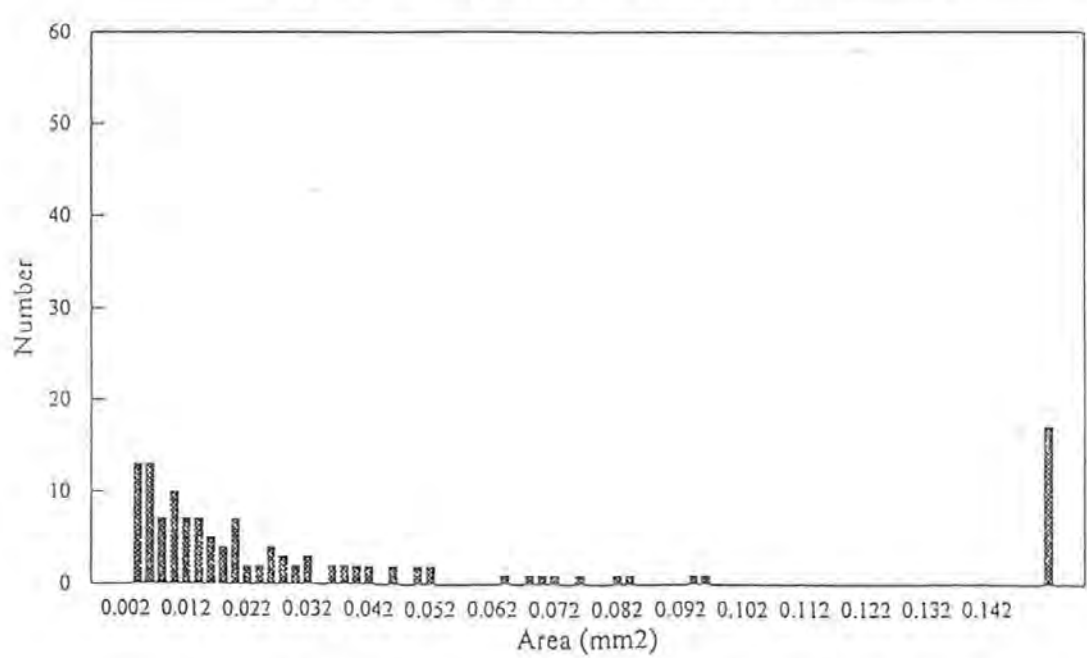
Figure 6c. Histogram of Zone Area in the 126 Laminate
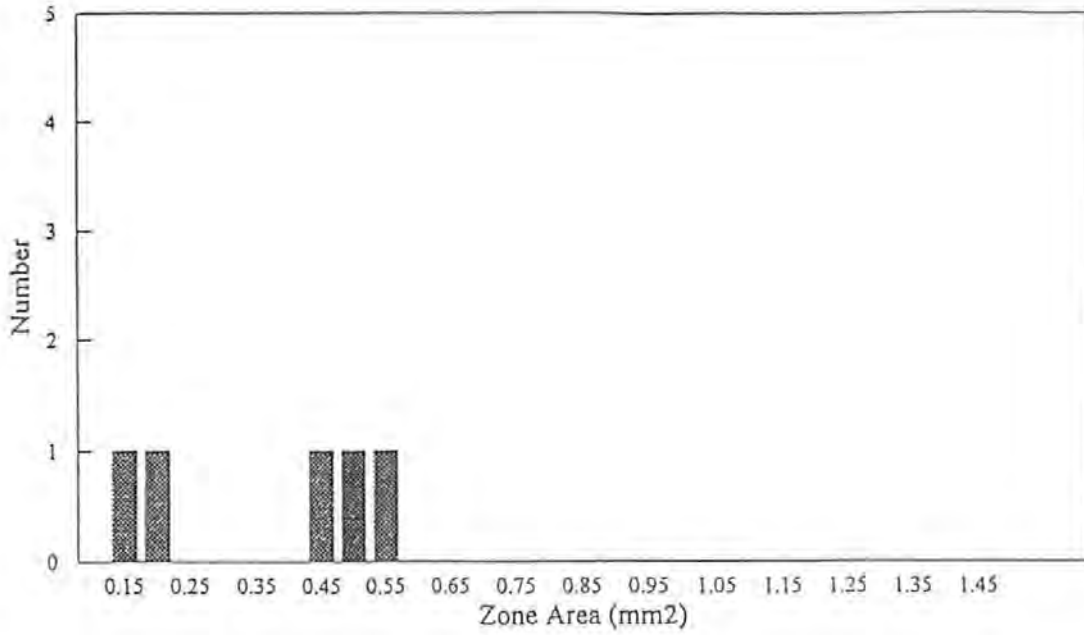
Figure 7a. Histogram of the Large Flow Areas in the Twill Laminate
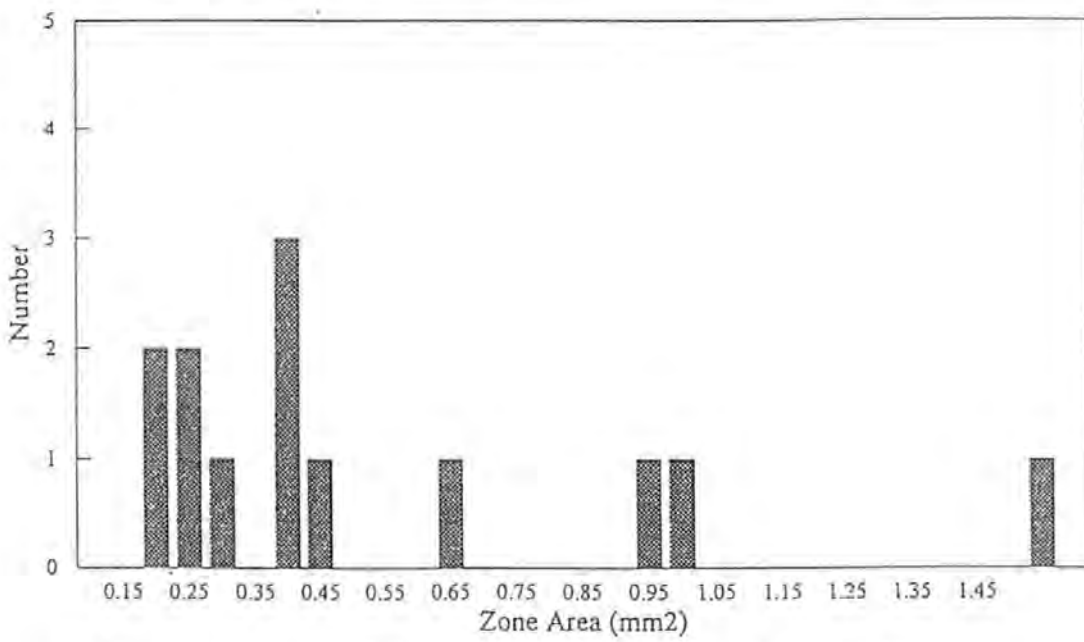
Figure 7b. Histogram of the Large Flow Areas in the 156 Laminate
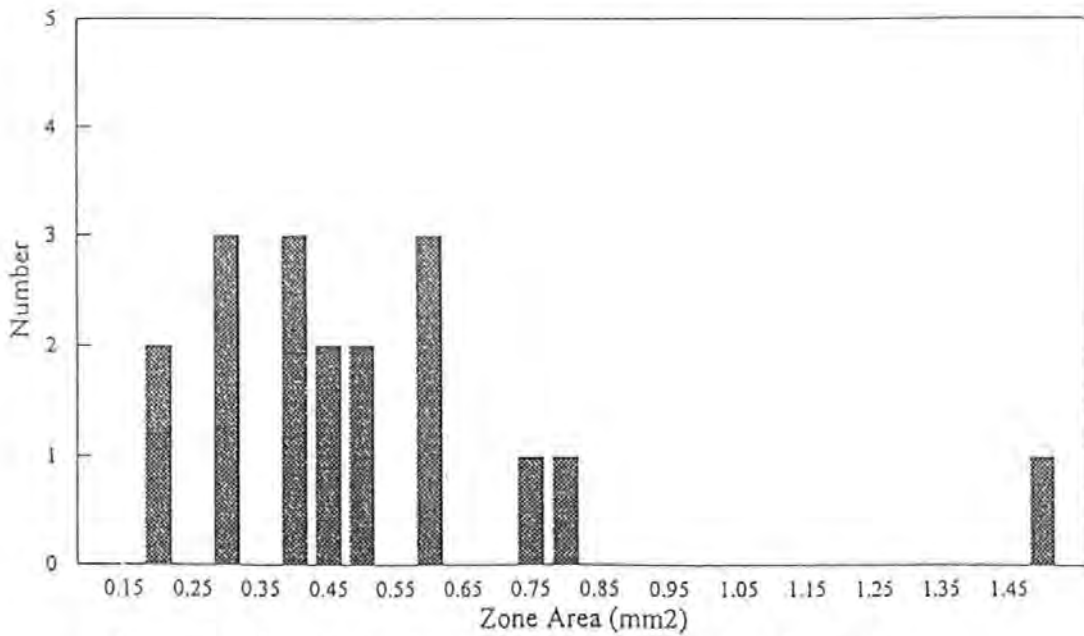
Figure 7c. Histogram of the Large Flow Areas in the 126 Laminate

A7 : 40
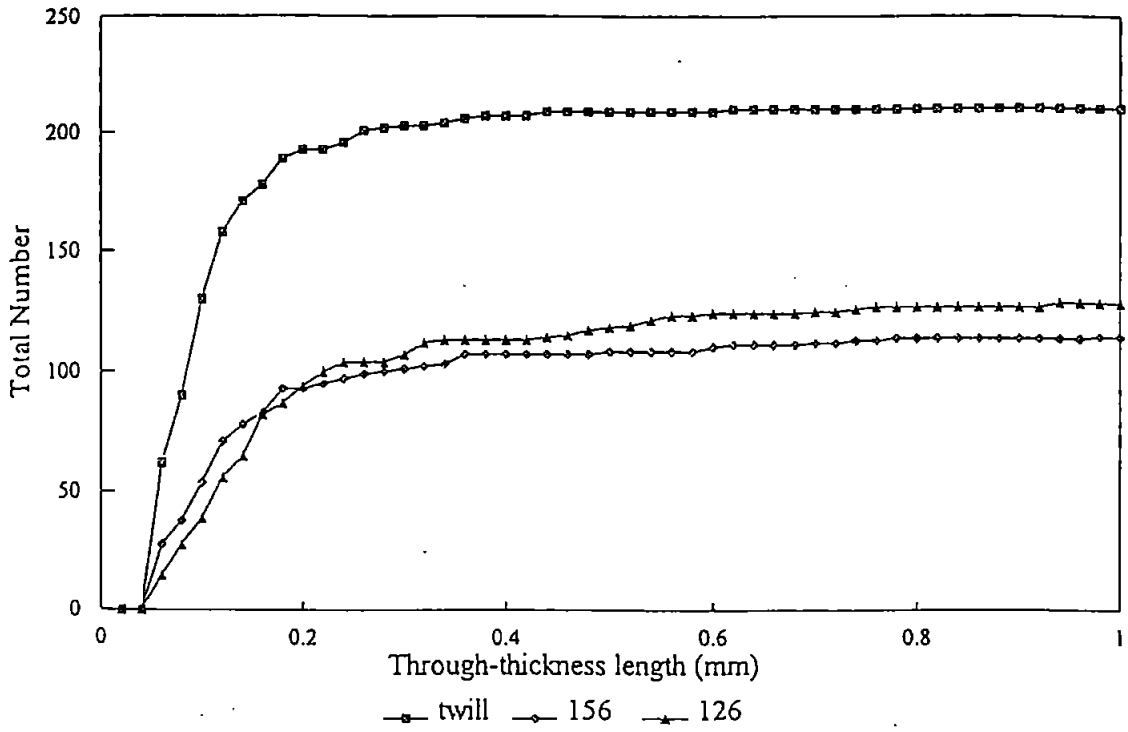
Figure 8a. Total Number of Specified Through-thickness lengths
in the Twill, 156 & 126 Fabric Laminates
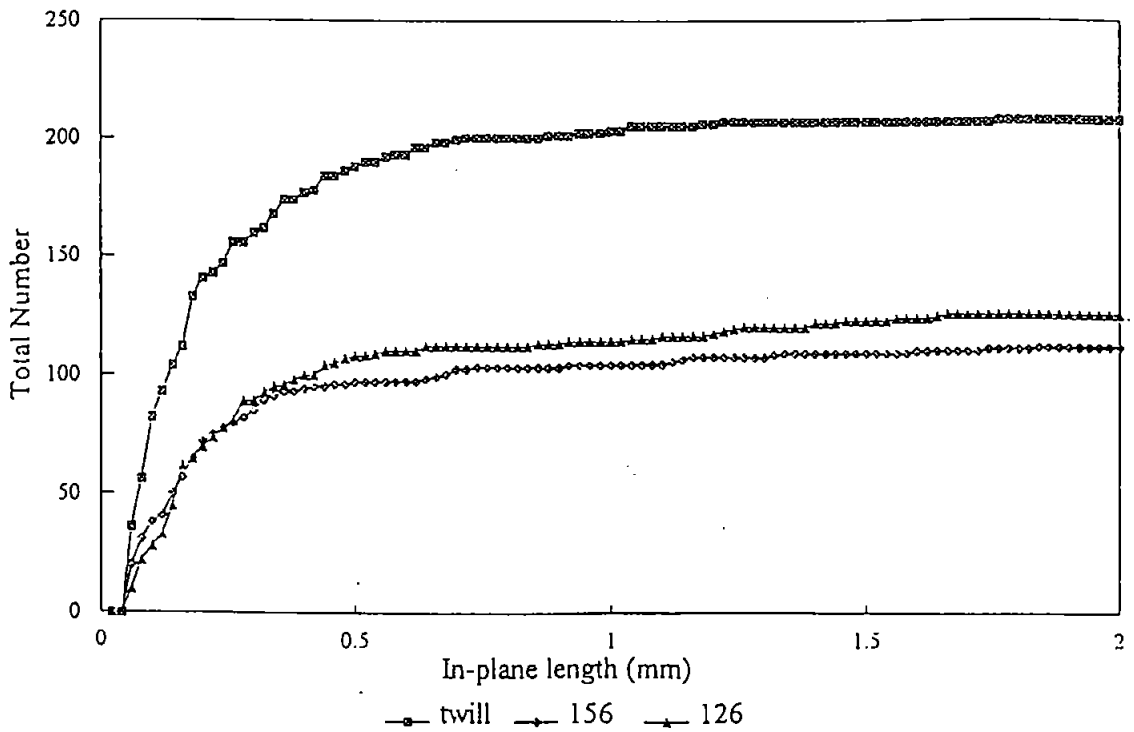
Figure 8b. Total Number of Specified In-plane lengths
in the Twill, 156 & 126 Fabric Laminates
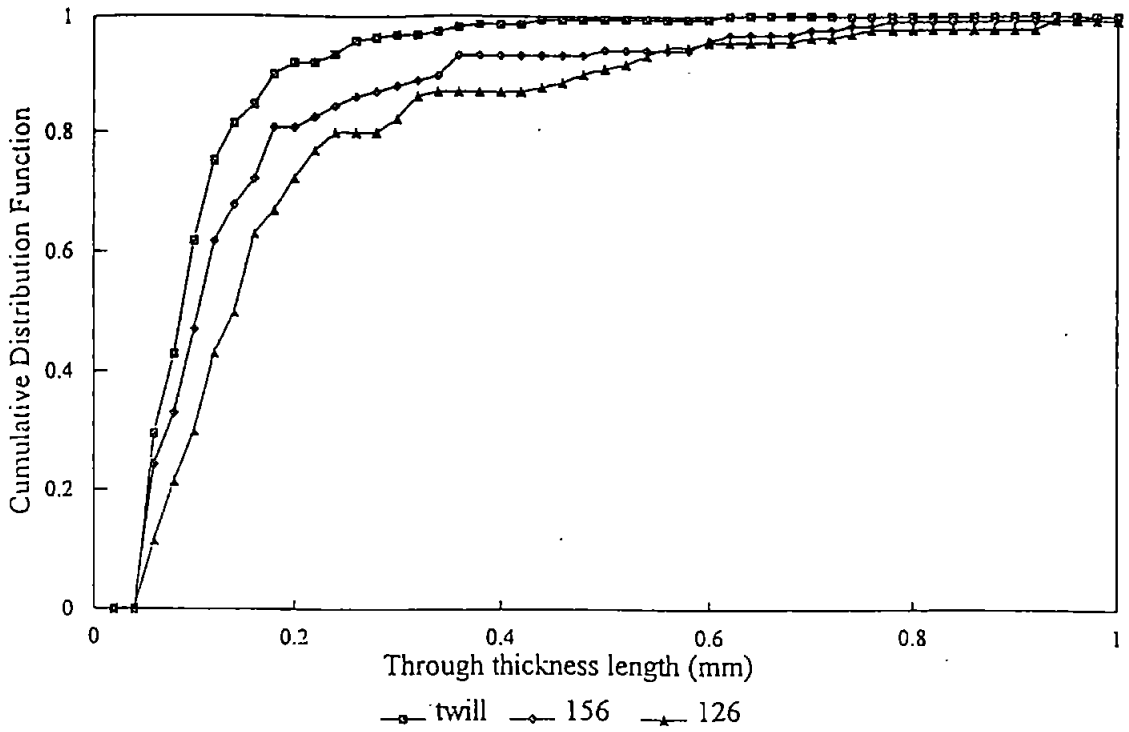
Figure 9a. Normalised Distribution of Through-Thickness lengths
in the Twill, 156 & 126 Fabric Laminates
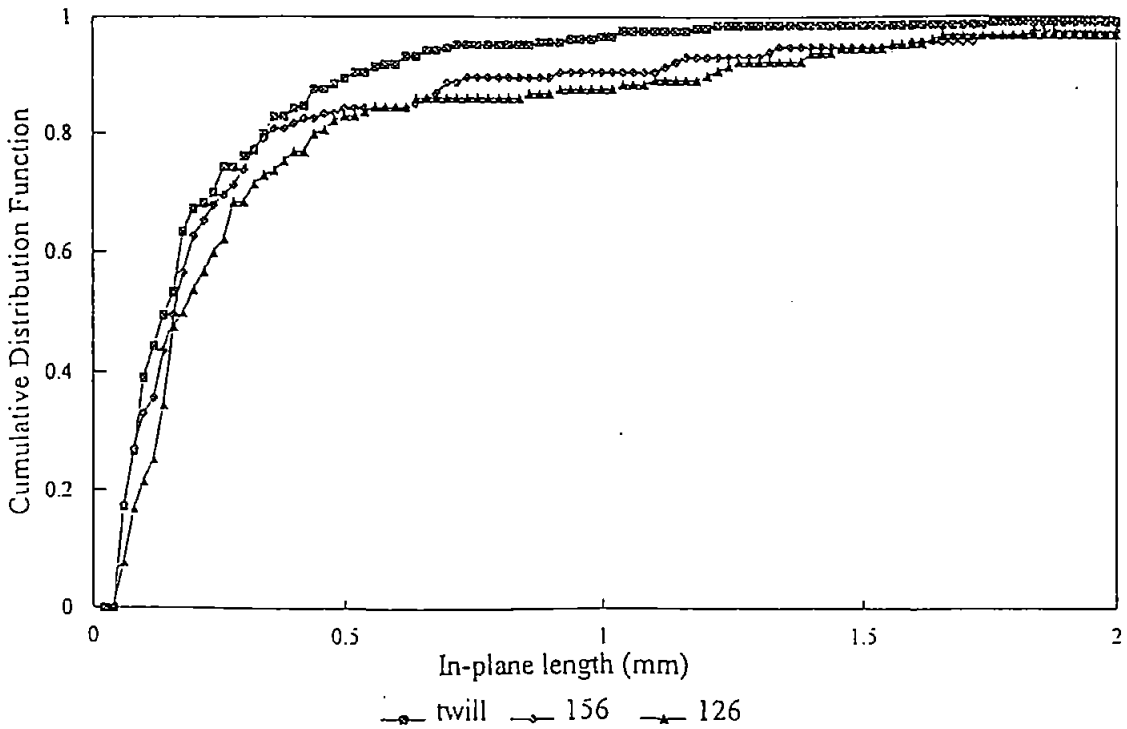
Figure 9b. Normalised Distribution of In-plane lengths
in the Twill, 156 & 126 Fabric Laminates

QUANTITATIVE MICROSTRUCTURAL EXAMINATION OF RTM FABRICS DESIGNED FOR ENHANCED FLOW

John Summerscales, P R Griffin, S M Grove and FJ Guild*
Advanced Composites Manufacturing Centre
School of Manufacturing, Materials and Mechanical Engineering
University of Plymouth
Plymouth
PL4 8AA
UK

*Department of Materials Science and Engineering
University of Surrey
Guildford
GU2 5XH

ABSTRACT

The resin transfer moulding (RTM) process involves the long-range flow of resin through a mould packed with dry reinforcement. The process can be considered as similar to the flow of fluids through porous media, and hence the situation can be modelled by the Darcy and Kozeny-Carman equations. The Kozeny-Carman equation predicts the effect of changes in the pore structure of the reinforcement on flow rate, through a parameter known as hydraulic radius, which is itself a function of the wetted surface in any given volume. Laminates have been manufactured, from fabrics which include flow-enhancing tows, in a transparent RTM mould. The cured laminates were sectioned for quantitative microscopy and image analysis. An analysis of the effect of substituting spiral-wound flow-enhancing tows for conventional tows in the reinforcement fabric is presented.

INTRODUCTION

The resin transfer moulding (RTM) process involves the long-range flow of resin through a closed mould packed with dry reinforcement. This situation can be compared to the flow of fluids through porous media in other engineering applications (e.g., groundwater in fractured rocks) and can be modelled by the appropriate equations.

Darcy [1] studied the water supply to the city of Dijon. He found that the linear flow rate, q, was proportional to the pressure drop, ΔP, over the bed length, L. The constant of proportionality for this empirically determined quantity is known as the permeability, K, and Darcy's equation is therefore:

$$q = K.\frac{\Delta P}{L} \qquad \dots\dots\dots [1]$$

Darcy's equation was first published in 1856. The volumetric flow rate, Q (= q.A) is given in equation 2, as modified to a more general form to allow for the viscosity of the fluid, μ:

$$Q = \frac{KA}{\mu} \bullet \frac{\Delta P}{L} \qquad \dots\dots\dots[2]$$

Darcy's law does not permit the calculation of changes in flow rate due to changes in the microstructural architecture of the reinforcement fibres. Permeability is an averaged macroscopic property of the medium, and does not describe microscopic inhomogeneities.

The work of Kozeny [2] and Carman [3] related flow rate to physically measurable characteristics of the porous medium. The volumetric flow rate of the fluid, Q, is given by the equation:

$$Q = \frac{\varepsilon A m^2}{k\mu} \cdot \frac{\Delta P}{L} \qquad \text{.......... [3]}$$

where: ε is the fractional free volume (porosity) of the bed [1-V_f]

$\quad$ A is the cross-sectional area of the bed

$\quad$ m is the mean hydraulic radius of the bed

$\quad$ k is the Kozeny constant

$\quad$ μ is the fluid viscosity

$\quad$ V_f is the volume fraction of fibre reinforcement

The mean hydraulic radius, m, of the porous medium is defined [4] as either the volume in which flow actually occurs, εV, divided by the surface area (S) presented to the fluid or the cross-sectional area normal to the flow divided by the circumference (C) presented to the fluid. In the former case, where m = $\varepsilon V/S$, Equation 3 becomes:

$$Q = \frac{\varepsilon^3 A V^2}{k\mu S^2} \bullet \frac{\Delta P}{L} \qquad \text{............[4]}$$

If a fluid is flowing under the same pressure gradient in a fixed volume of reinforcement, then A, ε, V, k, μ and $\Delta P/L$ are all constant. Thus, at constant fibre volume fraction:

$$Q \alpha \frac{1}{S^2} \text{ or } Q \alpha \frac{1}{C^2} \qquad \text{............ [5]}$$

The flow rate, and hence permeability, are simply inversely proportional to the square of the wetted surface area in a unit volume or to the square of the wetted perimeter in a unit area. Permeability can be shown to have the same dependence by equating the right hand sides of equations 2 and 4.

The use of resin transfer moulding (RTM) as a method of manufacture of continuous fibre reinforced composites leads to the production of consistent composite components at a reasonable cost. The cost of the process is critically dependent on the mould fill time, which is directly related to the rate of resin flow through the fibre preform. In the manufacture of high performance composite structures, the flow of resin is constrained by the high volume fraction of reinforcement fibres required to achieve the performance. This long-range resin flow is primarily flow through the pore space between the tows of reinforcement fibres. Summerscales [5] has presented a model which predicts a significant increase in flow rate with increasingly clustered fibres at a constant volume fraction.

Commercial fabrics, (e.g. 'Injectex' described by Thirion et al [6], designed to promote faster processing in RTM are becoming available. These commercial fabrics exhibit variations in the mescoscale architecture of the reinforcement leading to uneven distribution of pore space. However, the presence of uneven fibre distribution has been predicted to lead to degradation of the mechanical properties of continuous fibre reinforced laminates [7]. These predictive results may be confirmed by recent measurements of the mechanical properties of these laminates which show reduction in longitudinal compressive strength with increasing proportions of clustered tows [8]. Thus the requirements for good mechanical performance are in conflict with the requirements of large pore space for rapid manufacturing using the RTM method. The work described here seeks to correlate measurements of flow front velocity in RTM and measured microstructures of the finished laminates. The understanding of the microstructural parameters leading to enhanced flow may lead to resolution of this manufacture-properties dilemma.

EXPERIMENTAL DETAIL

The carbon-fibre reinforcement fabrics used in this study were developed by Carr Reinforcements Limited with the specific aim of promoting resin flow by including a varying proportion of bound, twisted tows in the weft direction. All fabrics are 2 x 2 twill weaves; the fibres in both warp and weft directions are tows containing 6000 fibres of standard modulus high strain carbon fibres (Grafil 34-700-6000) with a diameter of 6.9 μ m (from suppliers product specification). The twisted tows are bound with a low melt-point thermoplastic filament with a diameter of around 100 μm. (The manufacturers do not disclose the precise material used.) Figure 1 shows diagrams of three of the fabrics in plan view; varying proportions of the twisted tow are included.

TABLE 1: Materials used in the experimental study

REINFORCEMENT FABRICS		Proportion of Bound Tows	Distance Between Bound Tows
Designation	Description		
38166 (twill)	normal 2 x 2 twill weave	0%	n/a
156	one bound tow in each eight tows	12.5%	17 mm
150	one bound tow in each six tows	16.7%	13 mm
148	one bound tow in each four tows	25%	9 mm
126	one bound tow in each two tows	50%	5 mm
FLUIDS			
Boots glycerol			
BDH glycerol			
Scott Bader unsaturated polyester resin A cured with MEKP			
Scott Bader unsaturated polyester resin E cured with MEKP			
Jotun Polymer unsaturated polyester resin 4210 cured with MEKP			
Jotun Polymer unsaturated polyester resin 4210 cured with AAP			

Permeability measurements and composite manufacture

Four layers of one type of fabric were laid up in a 350 mm square 1.7 mm deep parallel-sided flat mould with a transparent upper face. The fabrics are anisotropic due to the inclusion of the bound flow-enhancing weft tow.

To measure the permeability in quasi-isotropic flow, the layer stacking sequence was $[0/90]_s$ and a fluid inlet port was included at the centre of the lower face of the mould. A central hole (diameter of 14 mm) was punched in the centre of each fabric layer to encourage true two-dimensional flow throughout the permeability experiment.

The flow fluid was introduced through the central inlet port into the space punched into the reinforcement layers. The fluid pressure at the reservoir was 0.9 bar gauge pressure (ie 1.9 bar pressure absolute). The fluid permeated radially outwards. The flow front isochrones were recorded using a video camera above the mould at 30 second intervals during the early stages and one minute intervals in the later stages of each flow experiment. The permeability values were calculated using the radial form of Darcy's equation. The approach is similar to that of Adams et al [9] and Chan and Hwang [10].

Further experiments were conducted using an anisotropic stacking sequence, $[0_2]_s$ under the same conditions as above.

The permeability results using Boots glycerol are shown in Figure 2. Since the experiments were performed, we have become aware of the high variability in the measured viscosity of glycerol [11]. All fabrics had similar areal weights (a range of $5g/m^2$ for a nominal fabric weight of 382 g/m^2). All experiments were conducted in the same mould, to the same nominal thickness, and hence at equivalent volume fractions. The permeability increased with the number of flow-enhancing tows. This result would not be predicted by the Kozeny-Carmen law as volume fractions (porosities) were nominally identical and a mean hydraulic radius is used in that equation (equation 2).

The full mathematical derivation of the model has been reported by Carter et al [12]. A standard experimental apparatus and procedure have been proposed by Fell et al [13].

Figure 3 summarises the permeability results for the full range of fluids used (listed in Table 1). All experiments were conducted under identical conditions, except for the fluids and their viscosities, and hence it would not be expected that different permeabilities resulted. A similar problem has been reported by Steenkamer et al [14]. The explanation may be that the experimental configuration involves the wetting of fabric (unlike Darcy's original wetted flow experiment) and hence surface chemistry/physics may assume a significant importance. The flow regime could also involve extensional flow, rather than bulk flow, and the different performance of each flow fluid in this regime could be critical.

Microstructural Examination

Sections perpendicular to the flow-enhancing fibre direction were cut from the anisotropic plates at 20 mm from the inlet position normal to the bound tow. The sections were mounted in casting resin. The sections were polished on 'wet-and-dry' diamond papers of 200, 320, 400 and 600 grade in turn, until the surface appeared flat to the unaided eye. The sections were then polished using an automatic metallurgical polishing machine with diamond pastes and a specimen load of 1 kg. The sequence used was: 1 h at 14 μm; 1 h at 6 μm; 30 min at 1 μm; and a final short polish at 0.25 μm. After each examination on the Quantimet, the sections were reground and repolished to expose the surface 0.5 mm behind the original. This was repeated to produce five different planes on each specimen.

Typical micrographs of three laminates are shown in Figure 4. The bright areas are tows parallel to the plane of the section. Since the flow was perpendicular to the section, the effects of fibre architecture on flow must arise from tows perpendicular to the section. Th e individual tows perpendicular to the section, are clearly distinguishable at this low magnification; the tows are brighter than the pore space. The two types of tow perpendicular to the section can be seen in the Figure. The conventional tows are approximately elliptic due to the closing forces on the mould flattening the tow. The twisted tows are "circular" before and after mould closure. A typical twisted tow is at the position marked by the intersection of the lines between the horizontal and vertical arrow heads. The continuous horizontal lines are the warp fibres running in the plane of the section. The twisted tows keep the adjacent layers apart and create significant areas of additional pore space in regions immediately adjacent to their positions.

The microstructure of a unidirectional continuous-fibre composite is entirely defined by sections perpendicular to the fibre direction, assuming that the fibres are perfectly straight and of constant cross-section along their length. The samples examined are reinforced with bidirectional (orthogonal) fabrics. The flow direction fibres appear as circles and the transverse fibres lie in the plane of the section.

The sections were examined with a Quantimet 570 Automatic Image Analyser. The section was placed in bright-field illumination in the microscope. The overall magnification used was recorded for each individual frame, typically 8.0μm/pixel. The features of the Quantimet 570 used in this work will be briefly described. The maximum size of frame which can be examined is divided into a square grid of 512 x 512 square pixels. The contrast is divided into 256 grey levels; black is defined as grey level 0 and white is defined as grey level 255. The grey level of each pixel is recorded as an 8-bit digital word. Detection was carried out with respect to a single threshold. The threshold level and detection were set so that the carbon fibres appeared white with respect to the matrix. Figure 5 is a grey-level image of a typical section. The fibre bundles are darker than the flow space. Individual fibres are not detected at this magnification. The flow areas could thus be detected as features, and their centres of gravity (their x, y coordinates) with respect to the frame, could be measured and recorded. The image-enhancement processing of the Quantimet is used to improve the image after converting the image to a binary form.

The microstructure of the laminate is variable due to its construction using carbon fibres in tows; measurements must be taken over an area which reflects the size of this variability. The total area analysed was the unit cell of the fabric, which occupied a maximum of 5 contiguous frames in the plane of the laminate parallel to the warp direction. The measure frame was adjusted to the thickness of the specimen and the width was compensated for the variation in thickness.

The image shown in Figure 6 is a binary image; each pixel is defined as detected or not detected. The sophisiticated image processing available on the Quantimet 570 arises from its large storage capacity. Such image enhancement was used here; the 'segment' process was used: this consists of successive erosions and builds (dilations without remerge) of features leading to their separation. Figure 7 shows the binary image of the same field after the image enhancement. The flow areas are now detected as separate features.

The process of image capture, image processing, measurement and sample movement by the stepping microscope stage to prepare for the next frame was programmed using QBASIC, the command language of the Quantimet. The results were written onto floppy disk; for each fibre-free zone, the parameters recorded were area, maximum feature height (vertical feret) and maximum feature width (horizontal feret), x- and y- centres of gravity and perimeter.

RESULTS AND DISCUSSION

The flow rate measurements show that the inclusion of bound tows increases the flow rate at constant fibre volume fraction. Increasing the proportion of bound tows leads to further increase in the flow rate.

The presence of the twisted tows leads to increased pore space. This pore space can be defined either by its area or perimeter. The laminates were examined using a Quantimet 570 Image Analyser using bright-field illumination in the microscope. The pore space was measured at low magnification, when individual fibres were not distinguished. The regions of pore space were detected as "features" and the size and position of the features were recorded.

The Quantimet data was imported into a spreadsheet (LOTUS 1-2-3 for Windows) and divided into bins from which histograms can be drawn. The results for each section from the five depths were combined. All results are normalised with respect to 1mm^2 area. The flow areas were characterised using perimeter and area. The data was analysed with respect to these two parameters. Table 2 shows the values of total perimeter and total area of flow regions for the five laminates.

Table 2 Values of Normalised Total Flow Perimeter and Total Flow Area

Laminates	Total Perimeter (mm)	Total Area (mm^2)	Permeability (darcies)
Twill	12.70	0.383	35.65
156	12.49	0.491	258.80
150	12.83	0.499	306.30
148	18.02	0.912	389.00
126	22.14	1.237	290.60

As expected, the total flow area increases with increasing frequency of bound tows. The results in Table 2 also show that the value of total perimeter increases with increasing frequency of bound tows. The increase in observed flow rate cannot be simply explained by these results. The flow rate increases sharply between the twill and 156 laminates; this difference is not described by the results in Table 2.

The results must be examined in more detail. The histograms of perimeter for the five laminates are shown in Figure 8. The Blake-Kozeny-Carman equation predicts that the flow rate will be inversely proportional to the square of the wetted surface area in a unit volume, or to the square of the wetted perimeter in a unit area.

The values of permeability and of perimeter in Table 2 are clearly not in line with the expections of the Blake-Kozeny-Carman equation, in that increasing permeability is associated with increasing perimeter. Griffin et al [15] have reported that the flow front shows differing wet-out rates in the tows and the inter-tow spacing. Close inspection revealed different rates of flow between the tows when compared to flow within the tows. It was believed that resin rapidly filled the spaces between the tows, then subsequently impregnated the tows themselves, leaving the inter-tow spaces clear for subsequent resin flow. Clearly the wet-out process is complex and the sampling of perimeter from single planes at the scale considered is inadequate to confirm or refute the Blake-Kozeny-Carman equation.

The advance of the flow front has been assumed to occur over the surface of the tow, without penetration of the interior of the tow. It is not currently possible to ascertain the full three-dimensional microscopic flow paths within the bulk of the reinforcement pack. It may eventually be possible to acquire this information through the use of computer micro-tomography (CMT) using radiographic or nuclear magnetic resonance techniques. However, a feature of current CMT systems is that the reconstruction algorithms assume that material exists throughout the entire circle of reconstruction. Data from a hollow object can then be reconstructed such that the apparent density on the inside edge falls off [16]. In an unwetted reinforcement stack, this density averaging at the air/fibre interface could easily mask the detail of the pore filling process. Kinney et al [17] have recently described a state-of-the-art synchrotron radiation CMT system with a smallest resolvable volume element (voxel) of 17 x 17 x 17 μm. This is clearly inadequate to follow the 3-D micro-flow between 7 μm fibres.

The histograms of the flow areas are shown in Figure 9. The bins are 0.005 mm^2 wide. The final bin includes all areas greater than 0.25 mm^2. Comparison of these histograms shows an increase in the number of large flow areas greater than 0.25 mm^2 with increasing frequency of bound tows; the values are shown in Table 3. However, this steady increase cannot be correlated with the change in flow rate. The number of flow areas of medium size, between 0.1 and 0.25 mm^2 are also shown in Table 3 and Figure 10. These values show a sharp increase between the twill and 156 laminates. This correlates with the shape of the change in flow rate.

Table 3 Values of Normalised Total Area in different ranges

Laminate	0.1 - 0.25 mm^2	greater than 0.25 mm^2
Twill	0.461	0.197
156	0.905	0.388
150	0.986	0.429
148	1.198	1.018
126	1.075	1.613

Results from the microstructural analyses show that, as expected, inclusion of the bound tows increases the total area of pore space. However, careful examination of the distributions of the size of pore space indicates that enhanced flow may arise primarily from the presence of many medium-sized areas rather than the presence of the large areas. This result could be most significant for good mechanical behaviour of the finished laminate. The Blake-Kozeny-Carman equation predicts that the flow rate will be dependent on the wetted surface area in a unit volume, or on the wetted perimeter in a unit area. The image processing capability of the Quantimet 570 permits the systematic analysis of the effective pore space by quantification of the features of the reinforcement architecture such as perimeter. It is thus practical to measure the effective perimeter in a complex real material such as the laminates of flow-enhancing fabrics. Examination of the values of the perimeter of the pore space reveals that the total perimeter is increased, not reduced, as expected, by the presence of the bound tows, although it is not simply related to the proportion of bound tows. This indicates that there may be a 'critical' value of perimeter below which the pore space is not filled via the primary flow. The correlation of flow rate and microstructural parameters could lead to improved understanding of the critical factors allowing enhanced flow, and ultimately lead to the design of fabrics which promote more rapid processing without seriously compromising the mechanical properties of the composite.

CONCLUSIONS

The permeability of laminates fabricated with flow-enhancing fabrics increases with the number of flow-enhancing tows present. However, the change from normal to enhanced fabric is far more effective than subsequent increases in the number of flow-enhancing tows. Quantitative microscopy of sections normal to the flow direction reveals that the flow-enhancing tows create significant pore spaces adjacent to their position. The inter-tow pore spaces have been quantified in terms of their perimeters and areas. The total perimeter of the pore space increases with the proportion of flow enhancing tows, as does the total area of pore space in the section. The sharp increase in the permeability of the reinforcement stack with the introduction of the first flow-enhancing tows is accompanied by a sharp increase in the flow areas in the range 0.10 - 0.25 mm^2.

ACKNOWLEDGEMENT
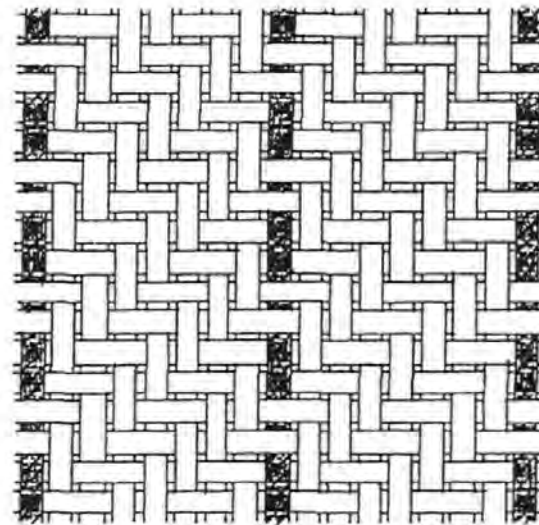
REFERENCES

1. H P G DARCY
    "Les fontaines publiques de la ville de Dijon"
    Dalmont, Paris, 1856.

2. J KOZENY
    "Uber die kapillare Leitung des Wassers in Boden"
    Sitzungsberichte Akademie der Wissenschaft Wien Math-naturw,
    1927, 136 (kl. Abt IIa), 271-306.

3. P C CARMAN
    "Fluid flow through a granular bed"
    Trans Inst. Chem. Engrs (London), 1937, 15, 150-166.

4. F C BLAKE
    "The resistance of packing to fluid flow".
    Trans. Amer. Inst. Chem. Engrs, 1922, 14, 415-421.

5. J SUMMERSCALES
    "A model for the effect of fibre clustering on the flow rate in resin transfer moulding"
    Composites Manufacturing, March 1993, 4 (1), 27-31.

6. J-M THIRION, H. GIRARDY and U WALDVOGEL
    "New developments in resin transfer moulding of high-performance composite parts"
    Composites (Paris), 1988, 28 (3), 81-84.

7. F J GUILD, P J DAVY and P J HOGG
    "A model for unidirectional composites in longitudinal tension and compression"
    Composites Science and Technology, 1989, 36(1), 7-26.

8. D M BASFORD, P R GRIFFIN, S M GROVE and J SUMMERSCALES
    "Research Report: The relationship between mechanical performance and microstructure in composites fabricated with flow enhancing fabrics".
    Composites, in submission.

9. K L ADAMS, W B RUSSEL and L REBENFELD
    "Radial penetration of a viscous fluid into a planar anisotropic porous medium"
    International Journal of Multiphase Flow, 1988, 14(2), 203-215

10. A W CHAN and S HWANG
    "Anisotropic in -plane permeability of fabric media"
    Polymer Engineering and Science, 1991, 31(16), 1233-1239

11. P N SHANKAR and M KUMAR
    "Experimental determination of the kinematic viscosity of glycerol-water mixtures"
    Proc. Roy. Soc. London, 8 March 1994, A444 (1922), 573-581

12. E J CARTER, A W FELL and J SUMMERSCALES
    "A simplified model to calculate the permeability tensor of an anisotropic bed".
    Composites Manufacturing, in submission.

13.   E J CARTER, A W FELL and J SUMMERSCALES
      "A proposed standard technique for the automated determination of the two-dimensional
      permeability tensor of a fabric reinforcement".
      4th Int. Conf. Automated Composites, Institute of Materials, Nottingham, September 1995,
      in preparation.

14.   D A STEENKAMER, D J WILKINS and V M KARBHARI
      "Influence of test fluid on fabric permeability measurements and implications for processing
      of liquid moulded composites".
      Journal of Materials Science Letters, 1 July 1993, 12(13), 971-973

15.   P R GRIFFIN, S M GROVE, A J LEWIS and D SHORT
      "Flow visualisation in resin transfer moulding"
      Preprints. 3rd. Int. Conf. Flow Processes in Composite Materials, Galway, July 1994,
      105-118.

16.   R H BOSSI, K D FRIDDELL and A R LOWREY
      "Chapter 4: Computed Tomography"
      In J Summerscales (ed): 'NDT of FRP Composites 2'
      Elsevier Applied Science Publishers, London, 1990, pp 201-252.

17.   J H KINNEY, D L HAUPT, M C NICHOLS, T M BREUNIG, G W MARSHALL and
      S J MARSHALL
      "The x-ray tomographic microscope: three dimensional perspectives of evolving
      microstructures".
      Nuclear Instruments and Methods in Physics Research, 1994, A347 (1-3), 480-486.

2 x 2 twill   156 fabric   126 fabric

Figure 1: Representative plan view of typical reinforcement fabrics

Summerscales et al (ICCS 8)

Figure 2. Measured Permeability of Flow-Enhancing Reinforcement Fabrics using Glycerol as the Flow Fluid
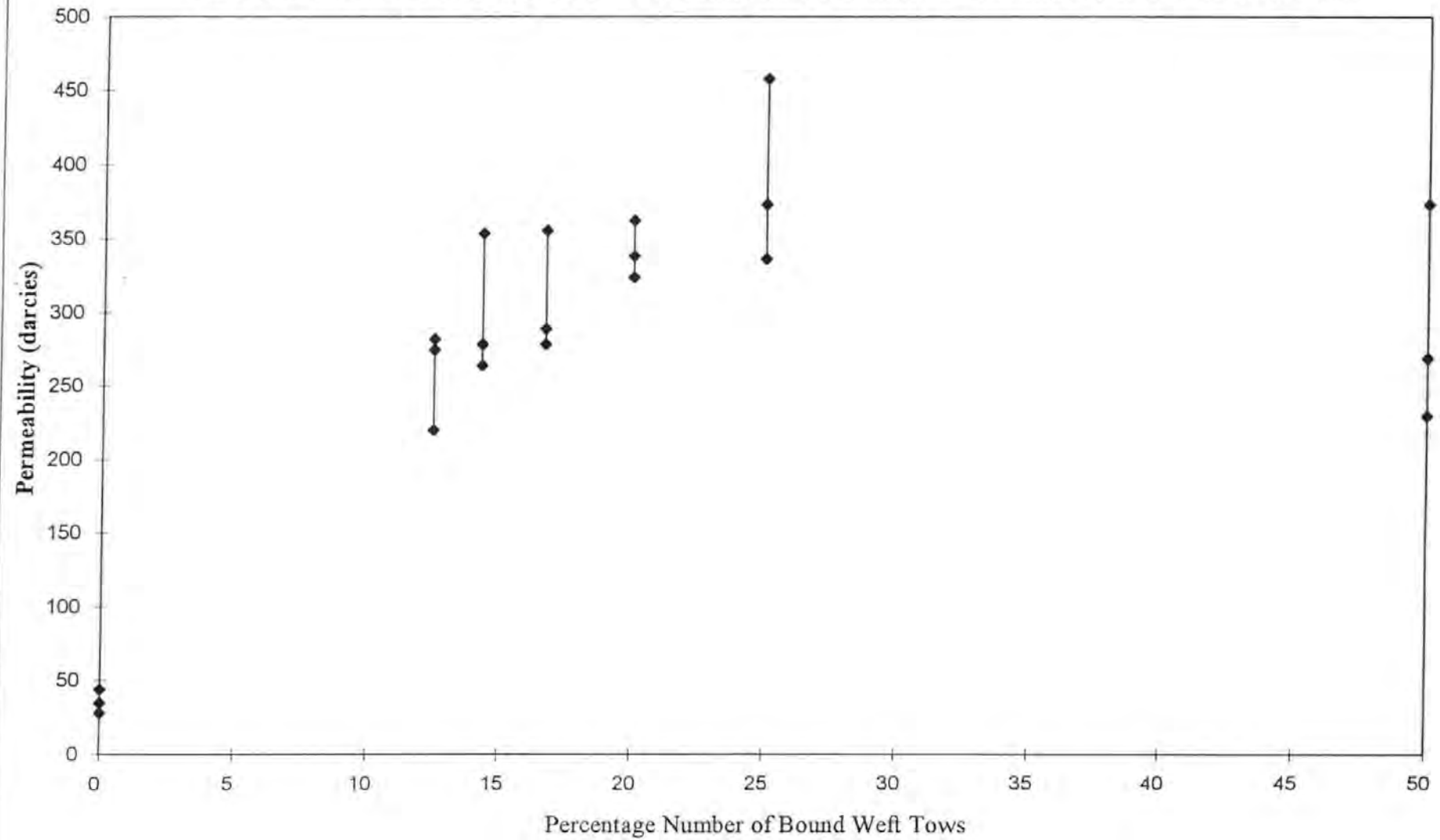
Figure 3. Measured Permeability of Flow Enhancing Reinforcement Fabrics using Various Test Fluids
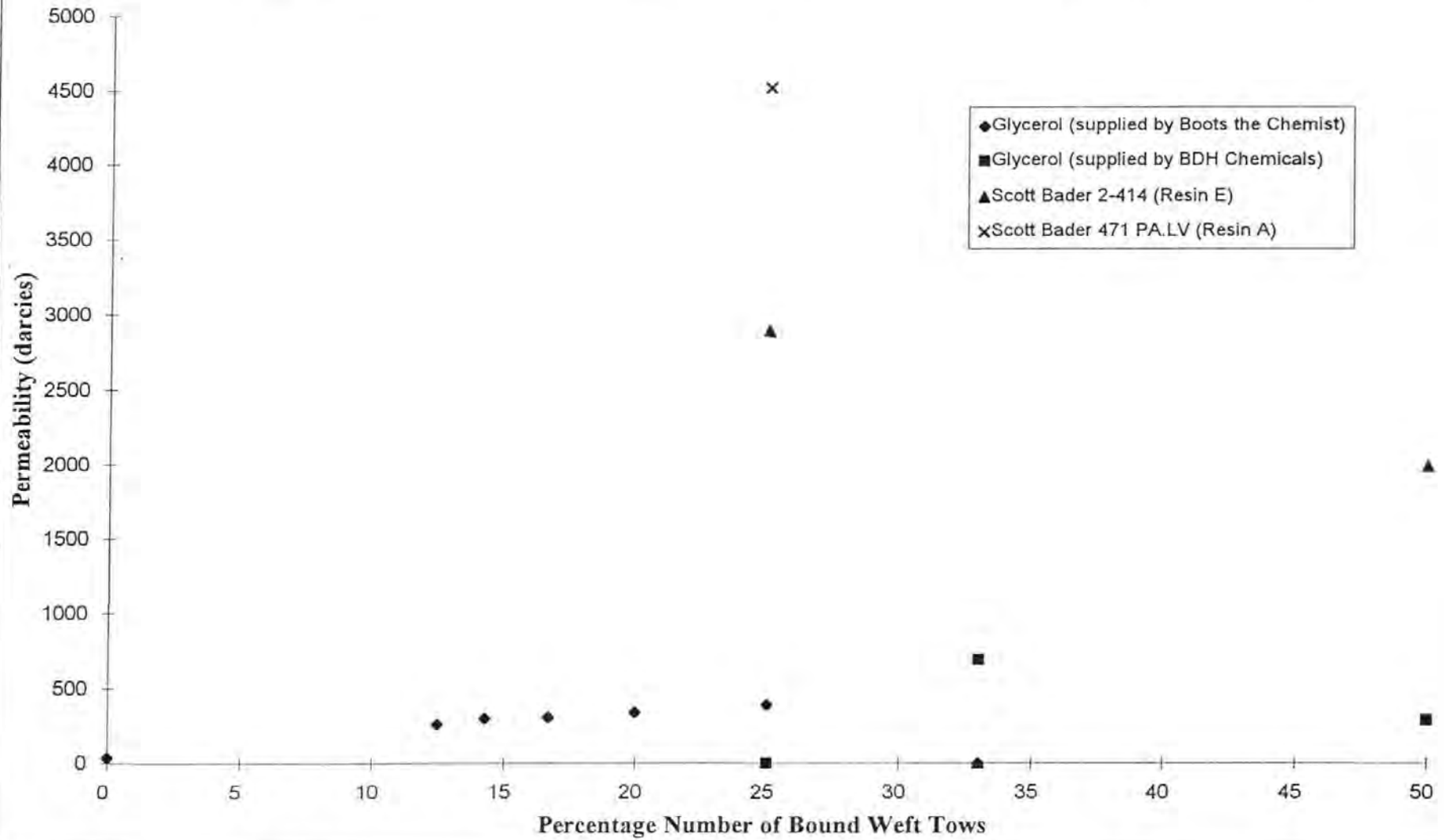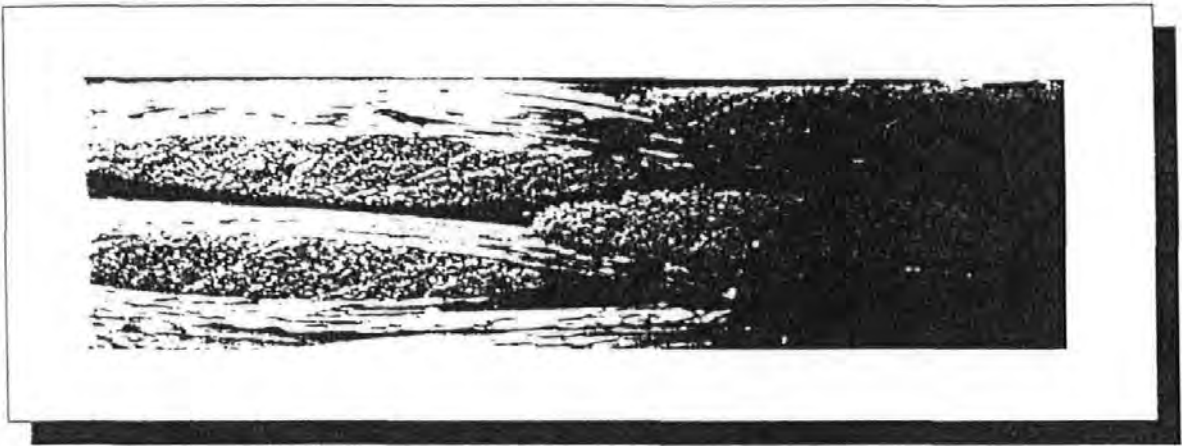
Micrograph of the Base Twill Laminate

Micrograph of the 126 Twill Laminate

▲ Bound Tow
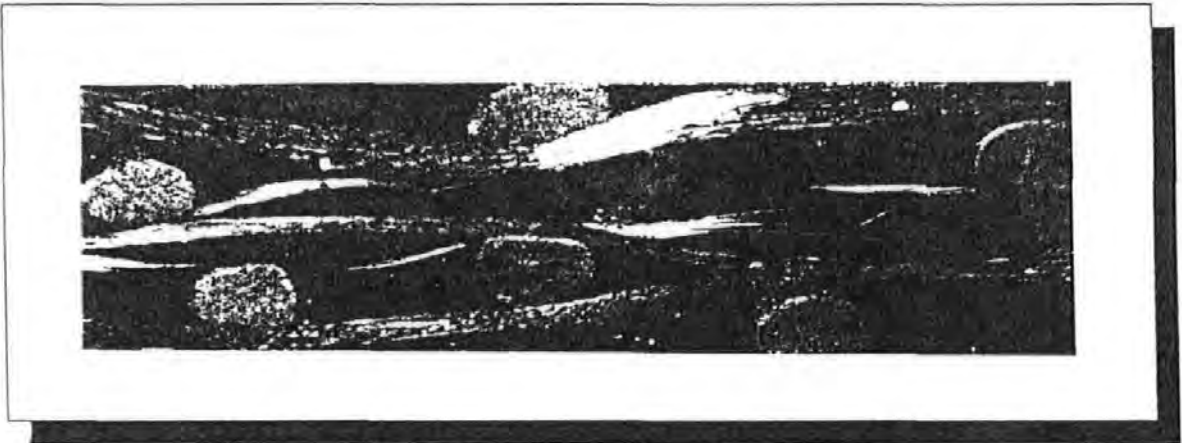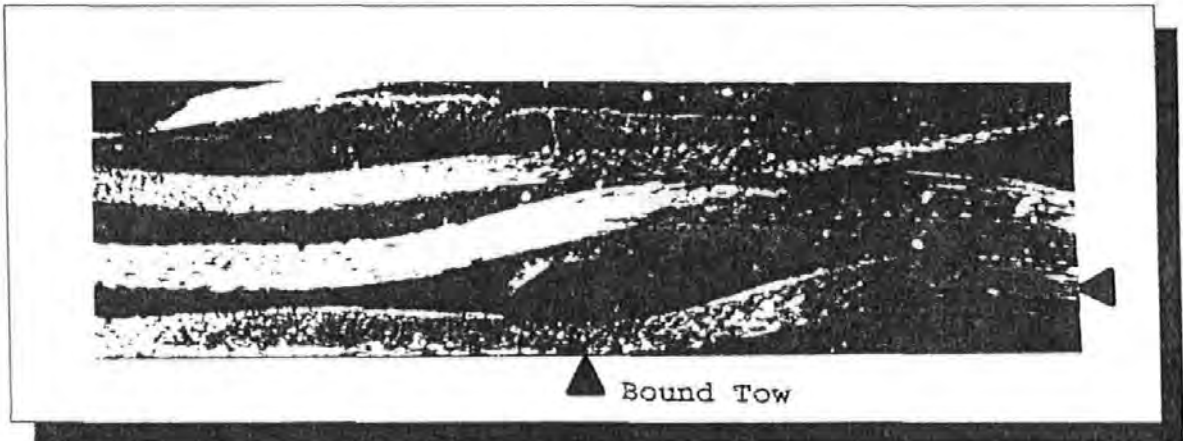
Micrograph of the 156 Twill Laminate

Figure 4: Typical microstructures of the various laminates.
Summerscales et al (ICCS 8)

A7 : 57

Figure 5 A Grey level Detection of a
Section of a Fabric 156 Laminate
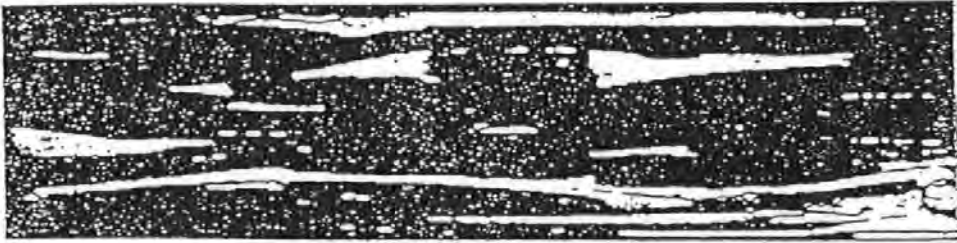
Figure 6 A Binary Image of the Fabric
156 Laminate

Figure 7 The Section of 156 Fabric after
Image Enhancement

Histogram of flow perimeters for twill

Histogram of perimeter for 156

Histogram of perimeters for 150

Histogram of perimeters for 148

Histogram of perimeters for 126

Summertesles et al (see b Figure 8a)   A7 : 59

Histogram of area for twill

Histogram of areas for 156

Histogram of areas for 150

Histogram of areas for 148

Histogram of areas for 126

A7 : 60

Summerfield et al (2005 Figure 7a)
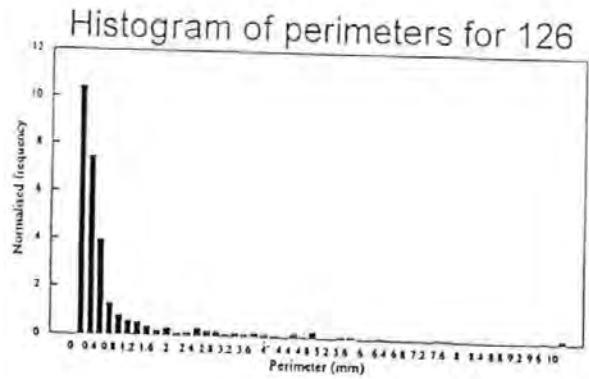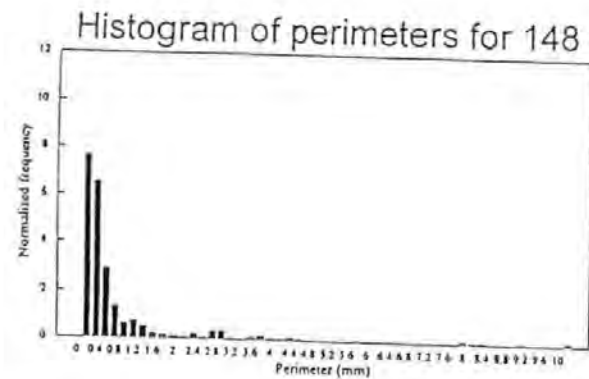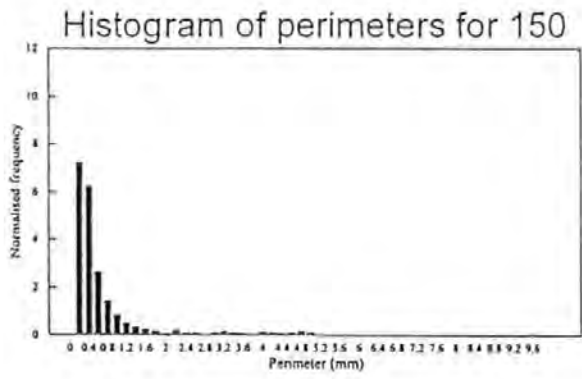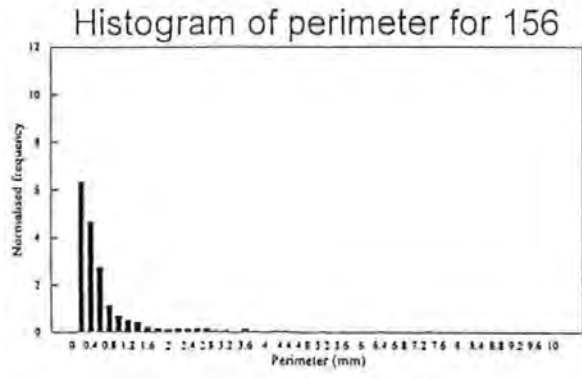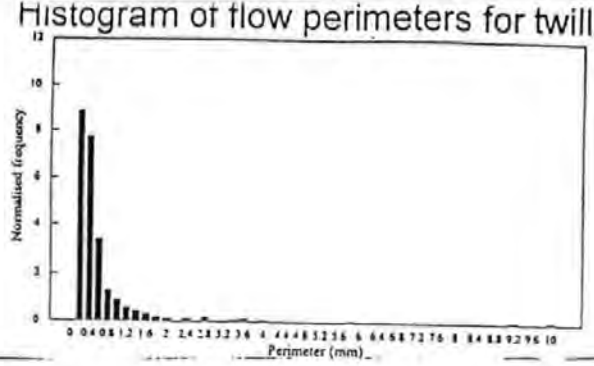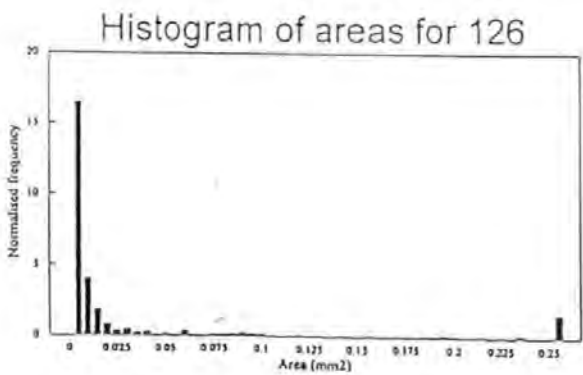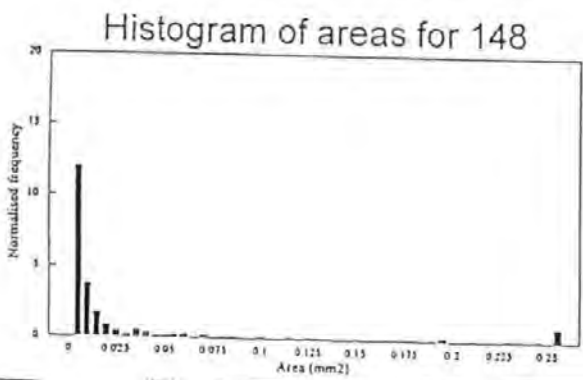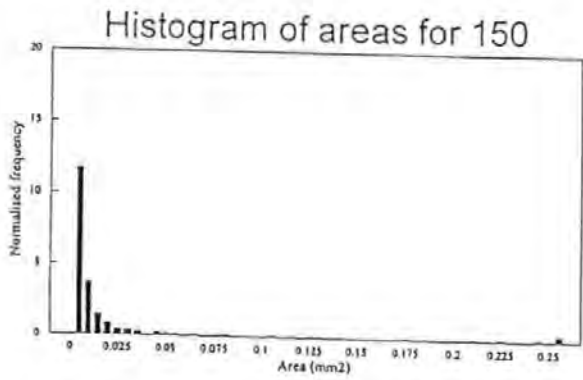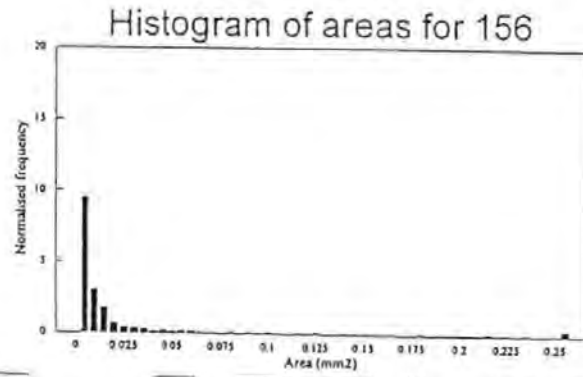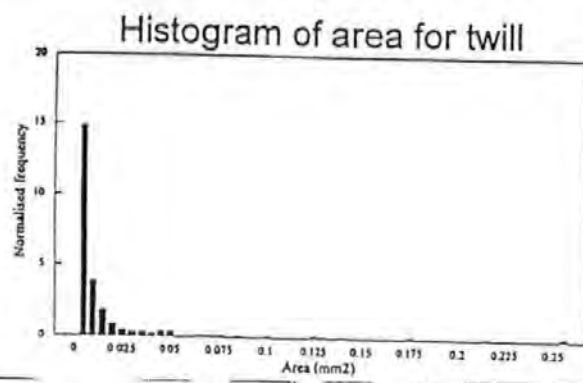
Figure 10. Variation of Medium Size Flow Areas and of Measured Permeability with Percentage of Bound Flow Enhancing Tows
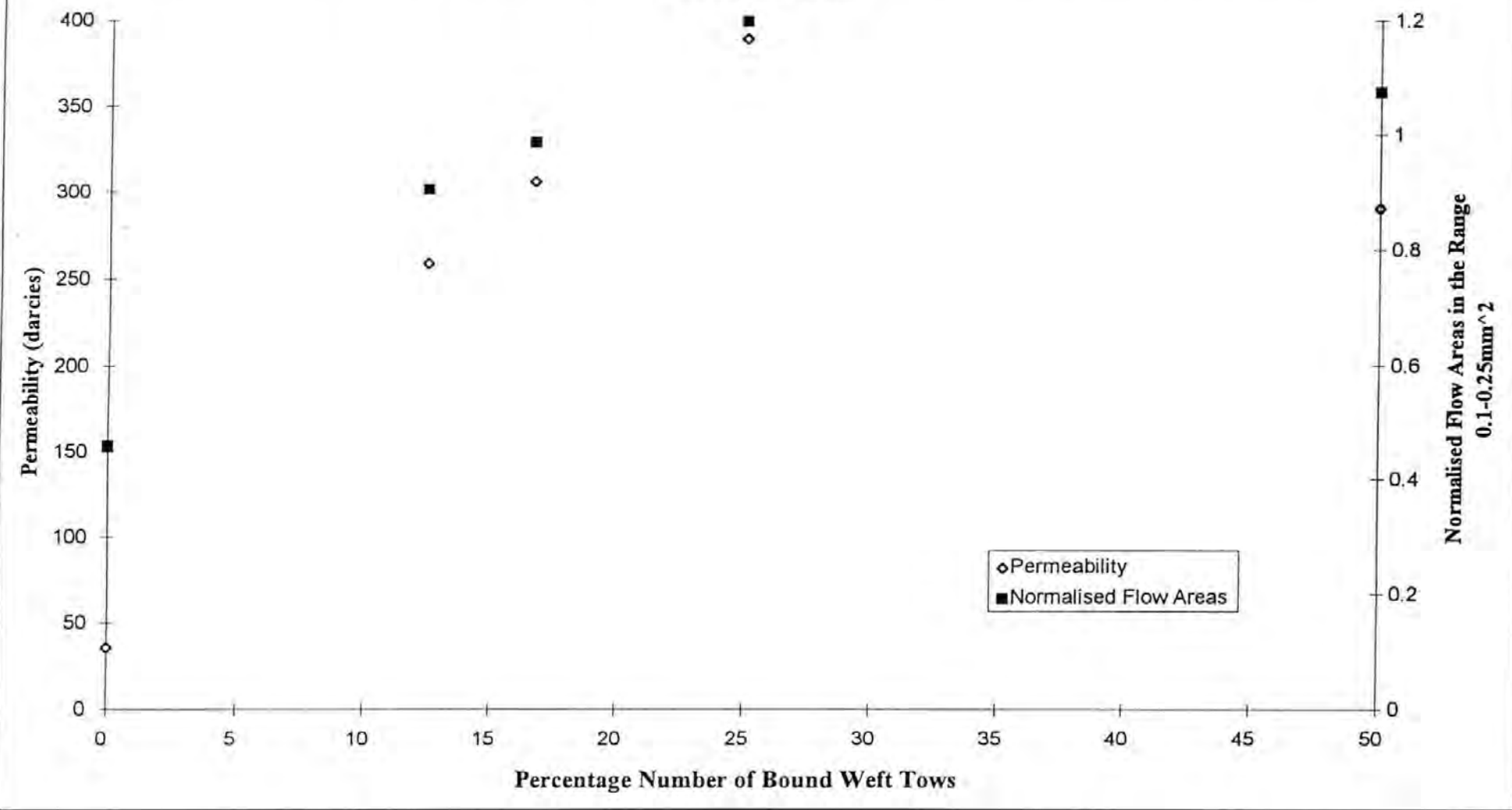
BUTTERWORTH
HEINEMANN

Relationship between mechanical performance and microstructure in composites fabricated with flow-enhancing fabrics

D.M. Basford, P.R. Griffin, S.M. Grove and J. Summerscales*
*School of Manufacturing, Materials and Mechanical Engineering, University of
Plymouth, Drake Circus, Plymouth, Devon PL4 8AA, UK*
(Received 8 September 1994; revised 6 March 1995)

The resin transfer moulding process involves the long-range flow of resin into a closed mould which is filled with dry reinforcement. High-performance composites require a high volume fraction of fibres, which results in low porosity of the fibre pack and therefore slow rates of mould filling. Commercial reinforcement fabrics are becoming available which promote faster resin flow than conventional fabrics, by engineering regions of large pore space into the reinforcement stack. However, theoretical models of the property–microstructure relationships have indicated that resin-rich areas (corresponding to filled large pore space) and fibre clustering will lead to degradation of the mechanical performance of the laminate. This report describes a series of compression and interlaminar shear tests on a range of twill-weave fabrics having 'flow-enhancing' tows substituted in the warp direction. The results provide some experimental support for existing theoretical models.

(KEYWORDS: resin transfer moulding; flow-enhancing fabrics; property–microstructure relationship)

INTRODUCTION

The resin transfer moulding (RTM) process is a route to the production of net-shape fibre-reinforced plastic parts. A dry preform is placed into the mould, which is closed before resin is injected to fill the pore space between the fibres. Once the resin has cured the component can be removed from the mould and is ready for use after a simple flash-removal operation.

High-performance composite structures (e.g. for aerospace, biomedical and defence applications) generally require a high volume fraction of fibres to achieve the required performance. It is inevitable that there will be a low volume fraction of pore space and therefore the reinforcement pack is likely to have a low permeability (high resistance to resin percolation) when used in RTM.

Summerscales[1] has analysed the flow rate parallel to the fibres in model arrays of unidirectional fibres with different degrees of clustering in the fibre reinforcement. On the basis of wetted perimeter per unit area, the flow rate through clustered fibres (with large areas of pore space) was predicted to increase significantly relative to a uniform distribution of individual fibres at the same volume fraction.

Commercial fabrics are available which utilize this phenomenon. Thirion *et al.*[2] have demonstrated that the linear flow rate in similar reinforcement fabrics at the same volume fraction under identical flow conditions but

with different reinforcement architectures was more rapid in the fabrics with clustered tows. Griffin *et al.*[3,4] have undertaken permeability measurements of twill-weave fabrics at constant areal weights where the conventional warp tows are systematically substituted by flow enhancing tows. The permeability was lowest in conventional twill fabrics and increased with the number of flow-enhancing tows present. This effect was related to the size of the pore space in the fabric structure using quantitative image analysis of optical micrographs. However, the enhancement of processing rates by fibre clustering may be offset by a deterioration of the mechanical properties with increasing departure from uniform fibre distribution.

The elastic properties of aligned continuous fibre composites have been analysed using several different theoretical approaches. Methods based on classical mechanics assume a uniform (hexagonal or square) fibre array. Different predictions were obtained for different fibre arrays. These approaches were summarised by Mansfield[5] who extended the analysis to take into account some randomness in fibre distribution. The predicted elastic properties were found to be highly dependent on variations in fibre distribution (resulting in localized areas containing no fibres). Guild and Ralph[6] measured lower values of specific damping capacity (indicative of greater stiffness) for unidirectional beams with a high proportion of resin-rich areas, compared with uniform materials. More recently, the finite element method has been used to predict the transverse stiffness

---

of unidirectional continuous fibre composites. Wisnom[7] assumed a regular array whilst Guild *et al.*[8] assumed that the fibres are randomly distributed. In both cases, the predictions of transverse modulus were found to be dependent on the fibre array: either on the type of packing[7] or the degree of randomness[8].

The finite element method has also been used to predict the dependence of fracture strength on fibre arrangement. Guild *et al.*[9] related failure in longitudinal compression to regions containing no fibres. Failure in longitudinal tension may also be related to fibre arrangement. Such dependence has been predicted by Zhang and Evans[10] using a micromechanical model for failure. Stress transfer around broken large diameter silicon carbide (SiC) fibres has been observed experimentally by Clarke and Bader[11]. Interaction between neighbouring SiC fibres was found to be negligible when the fibre separation was greater than about eight fibre diameters. The effects were considered on a statistical basis by Wolstenholme[12]. The strength of the model array was dependent on the arrangement of fibres. A similar dependence has been found by Sato *et al.*[13] for the fracture of carbon fibre-reinforced epoxy, where failure processes were observed *in-situ* and found to be dependent on neighbouring fibres. The importance of neighbouring fibres has also been demonstrated by Jones and Rock[14] for the process of stress corrosion cracking.

An effect of fibre distribution on longitudinal strength of polymer composites may arise from debond length. It is generally accepted that longer pull-out lengths are desirable as energy is absorbed both by the debonding process and the work done in friction during pull-out (see, for example, ref. 15). Longer debond lengths have been generally observed in fibre bundles[6]. The fracture

energy arising from fibre–matrix debonding and pull-out have recently been considered by Karbhari and Wilkins[16]. The analysis indicates that energy absorption may be increased if the fibres are arranged in bundles.

Stress concentrations in transverse loading have been investigated for metal matrix and polymer matrix unidirectional continuous fibre composites[7,8]. The analysis of Wisnom[7] takes into account the residual stresses arising from processing. For silicon carbide fibres in aluminium alloy matrix, the stress concentrations were found to be unaffected by fibre arrangement or fibre spacing. A similar result was found by Guild *et al.*[8] for glass fibres in polymer matrix. However, the analysis of high-strength carbon fibres, with a lower transverse modulus than the matrix material, showed a strong dependence of stress concentrations on fibre spacing. For this material, the transverse strength is expected to be highly dependent on fibre arrangement.

This report describes the experimental measurement of compression and apparent interlaminar strengths for a series of twill-weave carbon fibre composites with systematic substitution of spiral-bound 'flow-enhancing' tows in the warp direction of an otherwise conventional tow twill-weave cloth. The measurement of the permeability of these fabrics, using a two-dimensional radial flow method, has been reported elsewhere (*Figure 1*)[1].

EXPERIMENTAL

The carbon fibre fabrics used in this study were developed by Carr Reinforcements Limited (Stockport, UK) with the specific aim of promoting resin flow by including a varying proportion of spiral-bound twisted tows in the weft direction. All fabrics were 2 × 2 twill weaves
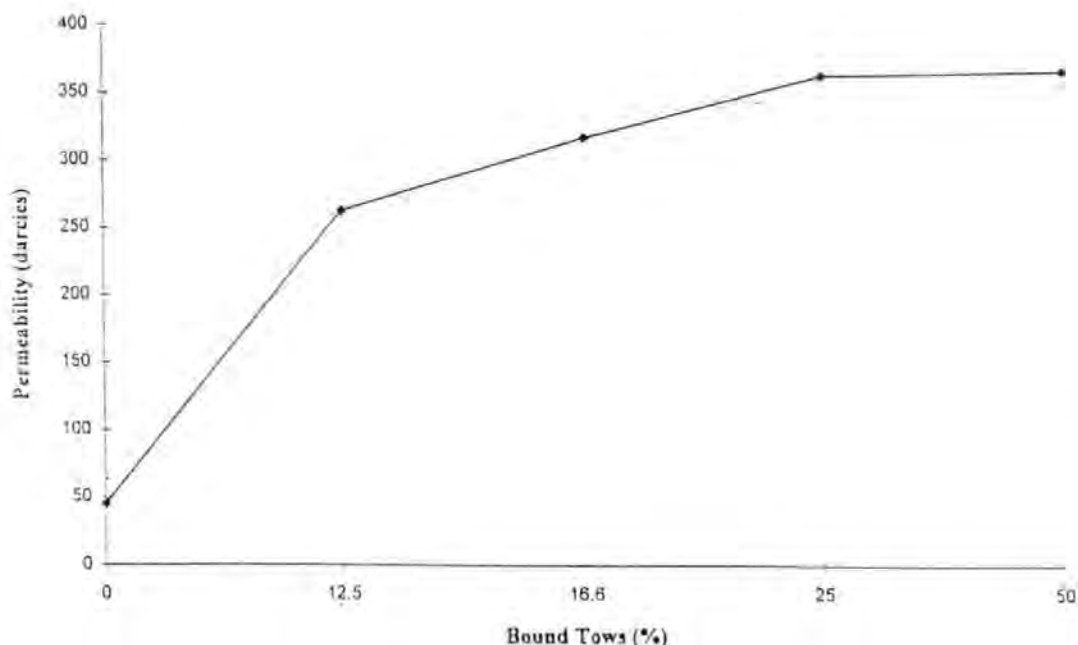

Figure 1 Variation of measured permeability (glycerol in two-dimensional radial flow) with the percentage of bound tows in the cross-ply laminate. Points indicated are each the mean of three values

2 x 2 twill   156 fabric   126 fabric

Figure 2 Representative diagrams of the plan view of the reinforcement fabrics. The twisted tows are indicated by shading

with an areal weight of 380 g m^{-2}. The fabrics in both warp and weft directions were 6 k tows of standard-modulus high-strain carbon fibres (Grafil 34-700-6000) with a diameter of 6.9 μm (manufacturer's product specification). The twisted tows were bound by a low melting point thermoplastic filament with a diameter of around 100 μm (the precise description is not available for commercial reasons). Representative diagrams of the fabrics are included in *Figure 2*, and the fabrics are defined in *Table 1*.

Cross-ply (0°/90°/90°/0°) laminates were manufactured in a 50 mm thick cast iron mould with a 10 mm thick plate glass top. The mould cavity dimensions were 200 × 200 × 2 mm, and resin was injected through a central injection port in the base of the mould. The resin system was Ciba–Geigy Araldite LY5052/HY1927 (100:38 parts by weight) with a viscosity of 1000 mPa s at 20°C. The part was allowed to cure for 18 h before demoulding, with a post-cure of 100°C for 4 h. Laminate thicknesses were measured to be 2.0 ± 0.02 mm; the nominal fibre volume fraction was 43.2%[17]. The cured plates were cut for micrographic examination and mechanical testing. Optical micrographs corresponding to the fabrics in *Figure 1* are shown in *Figure 3*. The tow dimensions are indicated in *Table 2*. These dimensions were measured on an Olympus CHC (S/N 264603) optical microscope with an *x–y* vernier stage (S/N 396835) and are mean values for three samples of each tow type per specimen for twill, 126, 148 and 156 fabrics. The difference in tow dimensions between the different fabrics measured was smaller than the estimated error (±50 μm) in the reading. The presence of the twisted tow leads to large resin-rich areas adjacent to the tow.

For mechanical testing, the directions were defined as '1' (twisted tows in the specimen surfaces parallel to the specimen axis) and '2' (twisted tows in the specimen surfaces normal to the specimen axis).

Micrograph of the Base Twill Laminate
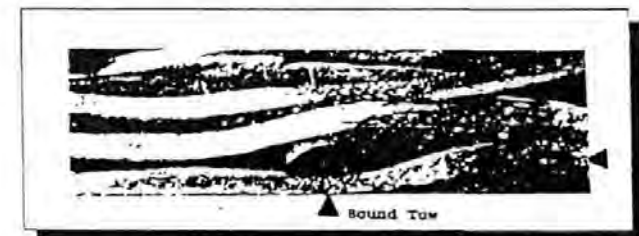

Micrograph of the 126 Twill Laminate

Micrograph of the 156 Twill Laminate

Figure 3 Representative micrographs of the reinforcement fabrics. A spiral-bound tow is located at the intersection of the horizontal and vertical lines from the arrowheads in the lowest panel. Approximate magnifications: twill, × 36, 126 laminate, × 16, 156 laminate, × 21

Compression tests were carried out in accordance with CRAG method 401[18] on an Instron 1175 universal testing machine (S/N H0525), calibrated to BS1610:1985 Grade 1, at a cross-head speed of 2 mm min^{-1}. Six

Table 1 Fabric definitions

Designation	Description	% Bound tows
38166	Normal twill weave	0
156	One bound tow per eight tows	12.5
151	One bound tow per seven tows	14.3
150	One bound tow per six tows	16.7
149	One bound tow per five tows	20
148	One bound tow per four tows	25
127(n/a)	One bound tow per three tows	33.3 (not available)
126	One bound tow per two tows	50

Table 2 Measured dimensions of the two tow types

	Horizontal (μm)	Vertical (μm)
Conventional	2050	250
Spiral-bound twisted tow	950	450

Table 3 Mean compression strengths

Designation	% Bound tows	Direction	Compression strength (MPa)	Standard deviation (MPa)
Twill	0	1	245	19
156	12.5	1	218	16
156	12.5	2	206	20
151	14.3	1	200	15
151	14.3	2	205	19
150	16.7	1	201	18
150	16.7	2	197	23
149	20	1	183	24
149	20	2	199	21
148	25	1	173	17
148	25	2	187	23
126	50	1	187	24
126	50	2	128	26
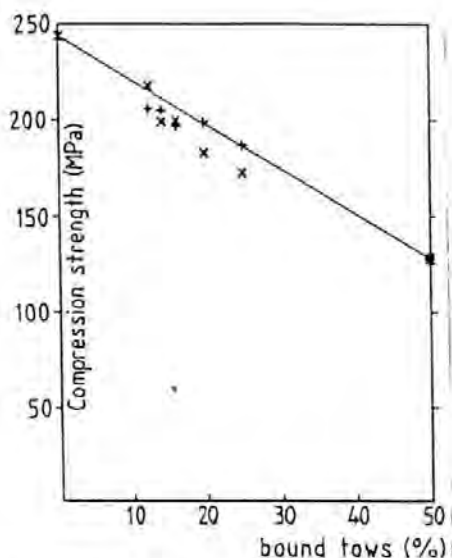
Figure 4 Variation of compression strength with the percentage of bound tows in the cross-ply laminate (×, surface layer bound tows parallel to loading axis. +, surface layer bound tows normal to loading axis). Points indicated are the mean of six values. The line joins the mean values at the two extreme percentages of bound tows

specimens of each type were tested and the results are shown in *Table 3* and *Figure 4*.

Interlaminar shear tests were carried out in accordance with CRAG method 100[19] on the Instron 1175 machine at a crosshead speed of 1 mm min^{-1}. Six specimens of each type were tested and the results are shown in *Table 4* and *Figure 5*.

DISCUSSION

The compression strength results in *Figure 4* show a reduction of strength values with increasing proportion of twisted tow. The difference between test directions was negligible in relation to the standard deviation on the results. Most of the fracture surfaces indicated a shear-mode failure, as predicted by Ewins and Ham[19]. The remaining six (of 78) specimens failed in pure compression. The exaggerated crimp of the twisted tow did not appear to induce buckling-mode failure. The standard deviation for the results increases with increasing proportion of twisted tows.

The apparent interlaminar shear strength (ILSS) results showed a slight reduction with increasing proportion of twisted tows, with the exception of fabric 126 which had a noticeable decrease in ILSS. The standard deviation again increased with increasing proportion of

Table 4 Mean interlaminar shear strengths (ILSS)

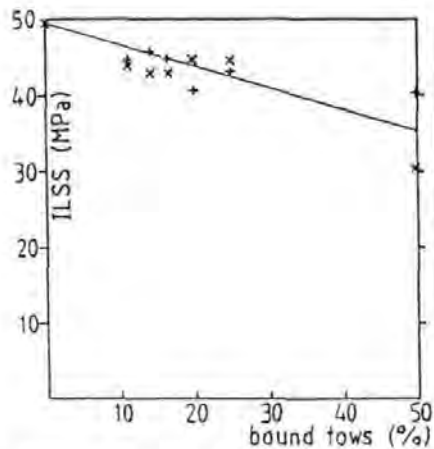| Designation	% Bound tows	Direction	ILSS (MPa)	Standard deviation (MPa)
Twill	0	1	49.9	2.6
156	12.5	1	44.0	1.5
156	12.5	2	44.8	2.5
151	14.3	1	43.0	2.7
151	14.3	2	45.8	3.8
150	16.7	1	43.0	2.4
150	16.7	2	45.0	1.3
149	20	1	45.0	5.2
149	20	2	40.6	4.2
148	25	1	44.6	4.0
148	25	2	43.2	3.1
126	50	1	30.5	5.0
126	50	2	40.4	3.7

Figure 5 Variation of apparent interlaminar shear strength with the percentage of bound tows in the cross-ply laminate (×, surface layer bound tows parallel to the loading axis; +, surface layer bound tows normal to the loading axis). Points indicated are the mean of six measurements. The line joins the mean values at the two extreme percentages of bound tows

twisted tows. The highest scatter (for fabric 126) corresponded to the lowest recorded ILSS values.

From optical micrographs of polished sections and examination of fracture surfaces it was not possible to discern any difference in the quality of impregnation of the two tow types.

It is not currently possible to separate the effects of the twist in the tow from the proportion and size of the resin-rich areas for the fabrics tested here. Further work on this problem is in progress. However, the results tend to confirm the suggestions in the literature that the mechanical properties decrease with increasing perturbation of the fabric structure. The permeability of these fabrics increases with increasing perturbation of the weave. There is obviously much further work to be done to optimize reinforcement fabrics to achieve a balance between the processing and property requirements.

SUMMARY

The mechanical properties of composite laminates fabricated with flow-enhancing tows in the reinforcement fabric have been measured. Both the compression and the apparent interlaminar shear strengths decrease with an increase in the proportion of flow-enhancing tows. The requirements of rapid processing and optimum mechanical properties are potentially in conflict, and further work is necessary to resolve this dilemma.

REFERENCES

1   Summerscales, J. *Composites Manufacturing* 1993, 4(1), 27
2   Thirion, J.M., Girardy, H. and Waldvogel, U. *Composites (Paris)* 1988, 28(3), 81
3   Griffin, P.R., Grove, S.M., Guild, F.J., Russell, P. and Summerscales, J. Paper presented at '2nd Int. Conf. on Microscopy of Composite Materials', Oxford, April 1994; *J. Microsc.* in press
4   Griffin, P.R., Grove, S.M., Guild, F.J., Russell, P., Short, D. Summerscales, J. and Taylor, E. Preprints 3rd Int. Conf. on Flow Process in Composite Materials', Galway, July 1994; *Composites Manufacturing* in press
5   Mansfield, E.H. *Technical Report RAE-TR-74-182*, Royal Aerospace Establishment, Farnborough, March 1975 [BR46834]
6   Guild, F.J. and Ralph, B. *J. Mater. Sci.* 1979, 14(11), 2555
7   Wisnom, M.R. *J. Compos. Mater.* 1990, 24(7), 707
8   Guild, F.J., Hogg, P.J. and Davy, P.J. in 'Proc 4th. Int. Conf. on Fibre-Reinforced Composites', Liverpool, March 1990, IMechE/PRI, Paper C400/022, pp. 89–99
9   Guild, F.J., Davy, P.J. and Hogg, P.J. *Compos. Sci. Technol.* 1989, 36(1), 7
10 Zhang, W.C. and Evans, K.E. in 'Proc 7th Int. Conf. on Composite Materials', Guangzhou, China, November 1989, Vol. 3, pp. 304–309.
11 Clarke, D.A. and Bader, M.G. in 'Proc. 7th. Int. Conf. on Composite Materials', Guangzhou, China, November 1989, Vol. 2, pp. 79–83
12 Wolstenholme, L.C. in 'Proc. 7th Int. Conf. Composite Materials', Guangzhou, China, November 1989, Vol. 2, pp. 84–89.
13 Sato, N., Kurauchi, T. and Kamigaito, O. *J. Mater. Sci.* 1986, 21 (3), 1005
14 Jones, F.R. and Rock, J.W. in 'Proc. 6th Int. Conf. on Fracture', New Delhi, 1984
15 Harris, B., Morley, J. and Phillips, D.C. *J. Mater. Sci.* 1975, 10(12), 2050
16 Karbhari, V.M. and Wilkins, D.J. *J. Mater. Sci.* 1991, 26(21), 5888
17 Sweet, A. *BEng 3 Project Report* School of Manufacturing, Materials & Mechanical Engineering, University of Plymouth, June 1994
18 Curtis, P.T. *Technical Report RAE-TR-88012*, Royal Aerospace Establishment, Farnborough, February 1988
19 Ewins, P.D. and Ham, A.C. *Technical Report RAE-TR-73057* Royal Aerospace Establishment, Farnborough, August 1973

Patrick Griffin
Advanced Composites Manufacturing Centre
University of Plymouth
England

Simulation and Design Optimisation for Resin Transfer Moulding

INTRODUCTION

Resin Transfer Moulding or RTM as it is more commonly known, is a manufacturing process for reinforced plastics. It involves the injection with pressure, vacuum or both of a thermosetting polymer resin into a bed of dry reinforcement laid up in a closed mould. It originates from the mid 1940's when it was used for the manufacture of US patrol boats but only relatively recently (1970's) has its potential been realised. The process has started to replace more traditional techniques such as hand lay-up mainly because of stricter regulations regarding the emission of styrene and also because the moulding produces two surface finishes rather than the one produced by hand lay-up. Fibre Reinforced Plastic (FRP) components are divided into two categories as seen below

i) Low Fibre Volume Fraction(<35%): Typical components in this category include gear box covers, freight container panels and car wings where an overall strength rather than specific strengths is required.
ii)High Fibre Volume Fraction(>35%): components such as helicopter rotor blades and impact panels need high strength and stiffness and are included in this category.

At present there is much research being undertaken to improve our knowledge of the process. Problems arise when the fibre volume fraction is increased due to requirements of the component. The flow of the resin becomes more dependent on the fibre characteristics i.e. orientation, bias and configuration (woven,stitched etc).

PROCESS MODELLING

It was realised that a model was required to describe the flow of resin through the fibre bed. Since a fibrous bed is a porous medium it was thought that an analogy could be made with Darcy's Law which described the flow of water through porous rock (a particulate media). The law was used extensively in the classification of sands and rock on the sea bed in the exploration of oil.

It states that the flow velocity of the fluid through the medium is proportional to the pressure gradient with which it is being driven.

$$u = -\frac{K}{\mu}.\Delta P$$

where

u = the flow velocity (cm/s)

K= the permeability of the medium (darcies)

μ = the dynamic viscosity of the fluid (cP)

ΔP = the pressure gradient across the fluid front (atm)

The constant of proportionality $\frac{K}{\mu}$ describes both the fluid and porous medium characteristics. This law has been applied extensively to model the RTM process with limited success. Figure 1 shows a set-up for a permeability test with a simultaneous viscosity test The test uses radial flow to rid the problem of edge effects produced by inaccurate cutting and laying in the mould. Figure 2 shows tests for a similar lay-up and process conditions and indicates the scatter associated with this type of test. Figure 3 shows that the permeability also varies with the test fluid used. The permeability tests also showed up some interesting flow features such as anisotropy (figure 4) which results from differing fibre bias in the 0,90 directions. There are two types of flow within the reinforcements, inter-tow flow and capillary flow into the tows and both seem to have their own particular infiltration rates (figure 5). Uni-directional fabrics have a uniquely shaped front in that the resin 'fingers' up between the tows

It was decided that to optimise the process, the flow properties for each individual reinforcement were required. A specially designed flow enhancing carbon twill weave was used as a basis for an investigation into some of the factors which may affect the permeability value of the fabric. A bound or twisted tow was woven at differing ratios in the warp direction of the fabric to introduce large flow channels into the fabric and improve flow through the weave. The reinforcements details are shown in table 1 below

Reinforcement Designation	Description	%Bound tows
DWO38166	conventional 2x2 twill weave	0%
DWO 156	one bound tow per 8 tows	12.5%
DWO151	one bound tow per 7 tows	14%
DWO150	one bound tow per 6 tows	16.7%
DWO149	one bound tow per 5 tows	20%
DWO148	one bound tow per 4 tows	25%
DWO127	one bound tow per 3 tows	33%
DWO126	one bound tow per 2 tows	50%

Table 1 Table of Reinforcements.

Permeability tests were undertaken on all these fabrics and figure 6 shows the values obtained and also the scatter. The next part of the investigation was to look at the flow channel geometry to determine if there was any relationship between the size and shape of the channels and the permeability. This was done by sectioning and polishing the plates used in the permeability tests and using an Image Analysis Technique determining the proportion and size of large flow channels. The Image Analyser measured values using greyscales which were adjustable and the image was enhanced to give the best results. Figure 7 shows a typical sequence of analysis. The flow areas were then divided into regions of a specific size range and a frequency histogram plotted. These results are shown in figure 8 and as can be seen there are more large flow areas in the fabric with the most bound tows and least in the conventional twill which agrees with the permeability values which state that the twill is the least permeable.

CONCLUSIONS

At present, only one set of data has been analysed so obviously more work is required to back-up these findings and this is being undertaken at present. There still remains a number of uncontrollable variables in the process, these tend to exist at the micro level, for instance inter-fibre distances, fibre sizing, fibre orientation due to handling damage.

Figure 1. Apparatus for a Permeability Test

400

2×15 2×20 40 40 25

1 ВАСОИЯТВИСТIOИ
2 NOULD BODY
3 GEL COAT
4 TOP FRAME
5 MARKING RINGS
6 U - CLAMP
7 CENTRAL INLET
8 RUBBER GASKET
9 FRAME OF MOULD BODY
10 OUTLET
11 TOP FRAME
12 RUBBER COAT STUCK ONTO FOR 11
13 PERSPEX PLATE (4 mm)
14 GLASS PLATE (10 mm)
15 SPACER
16 MOULD CAVITY

Gasket

○ Possible Inlets /
  Vacuum ports
⊘ Outlets
○ Ports for pressure transducers

+ Thermocouples
− Heater mat

Surface of the experimentation mould

1) Gel coat: high quality working surface
2) Very thin glass tissue to smoothen the lay-up
3) Two layers of medium weight carbon twill
4) One layer of light weight carbon twill
5) Thermocouples and filler paste
6) Thin E-glass to insulate the heater mat
7) Heater mat, leveled with filler paste
8) Stabilising composite tiles (mastercore)
9) One layer of light weight carbon twill
10) Two layers of medium weight carbon twill

not to scale

Figure 2. Scatter Associated with a Typical Set of Permeability Tests

Number of Similar Tests Conducted

□ Areal Weight = 346g/m^2, Volume Fraction = 62%, Resin: MY750/HY917/DY070
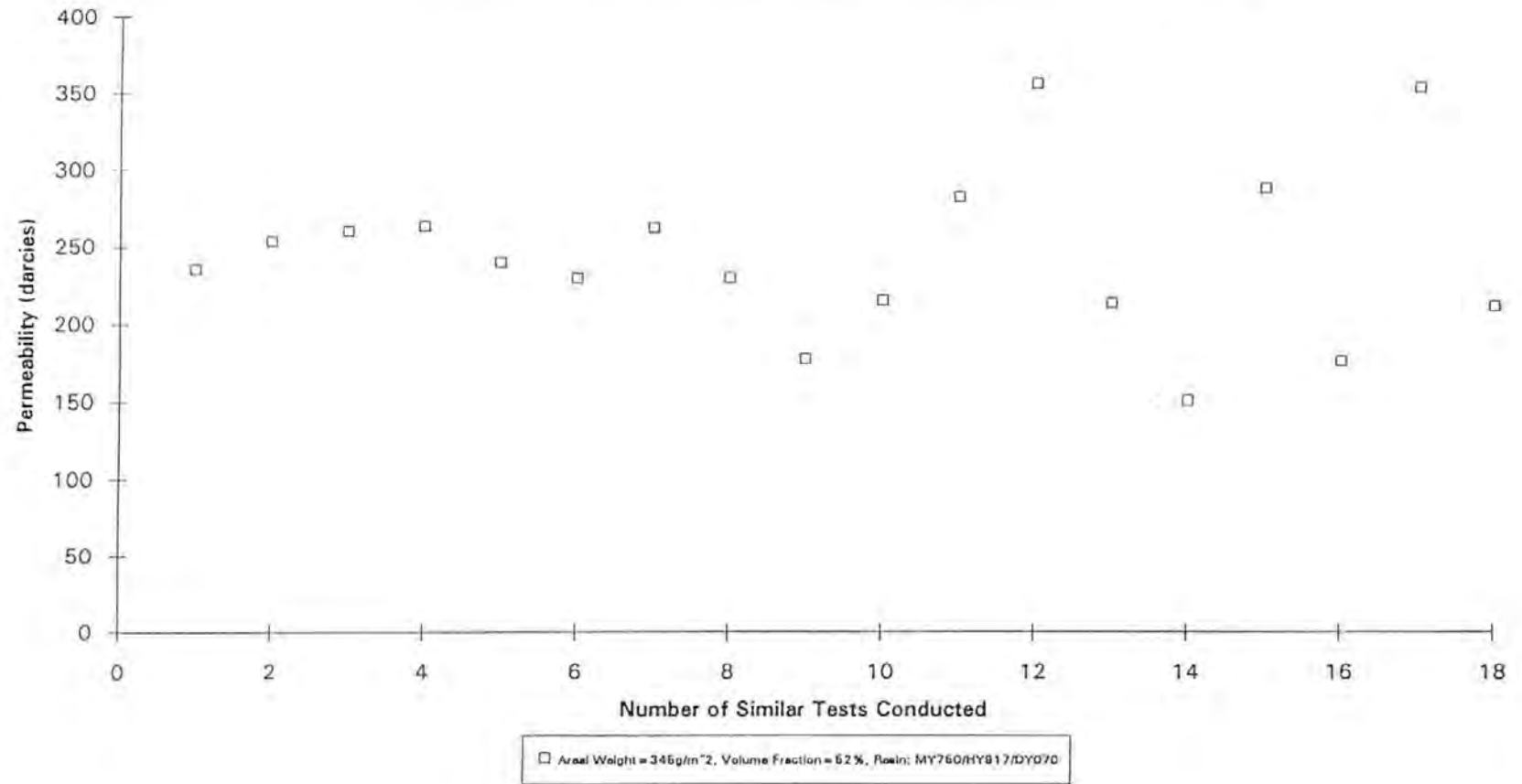
Figure 3. Permeability of a Range of Flow Enhancing Reinforcements to Various Test Fluids
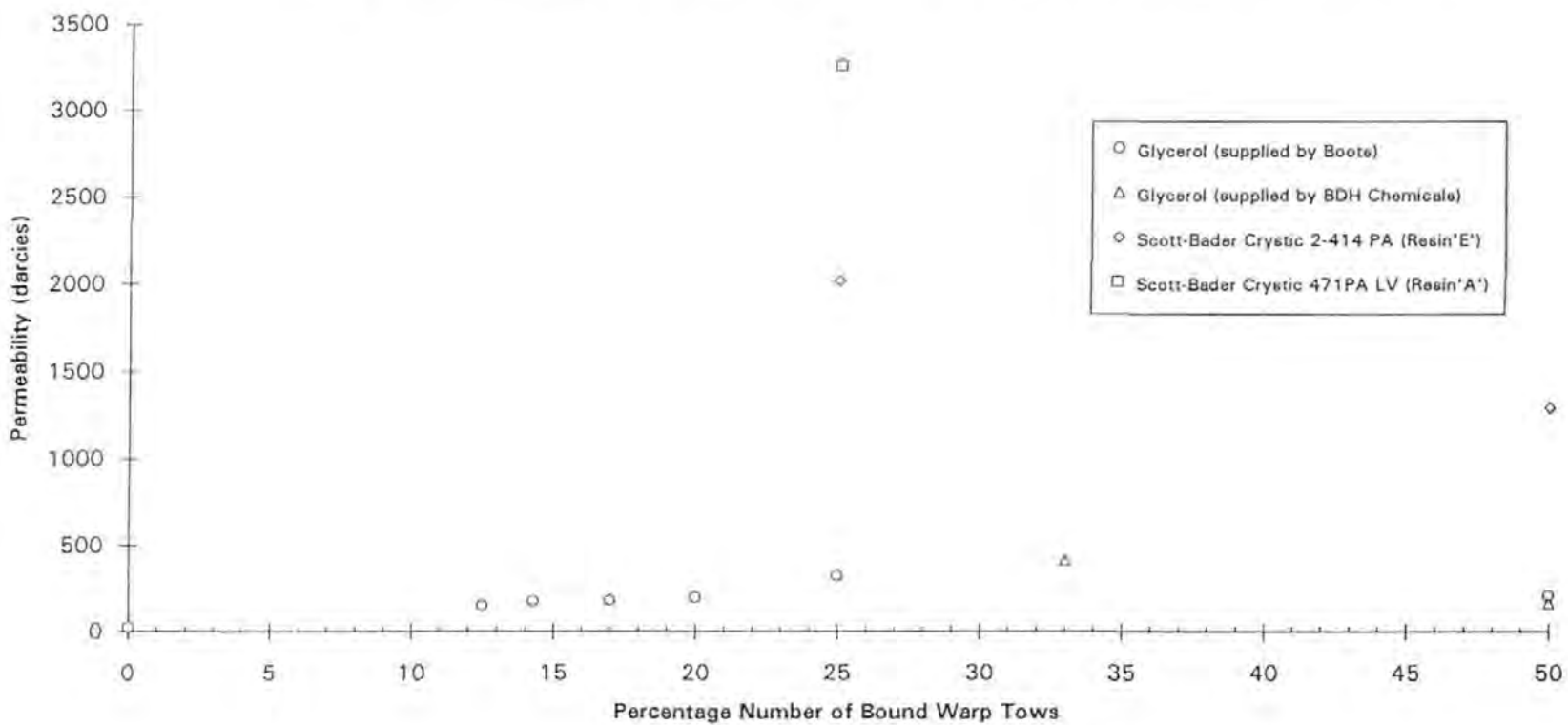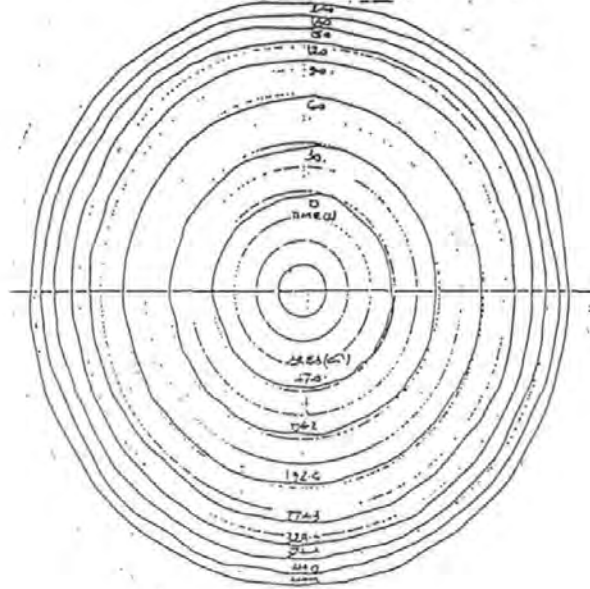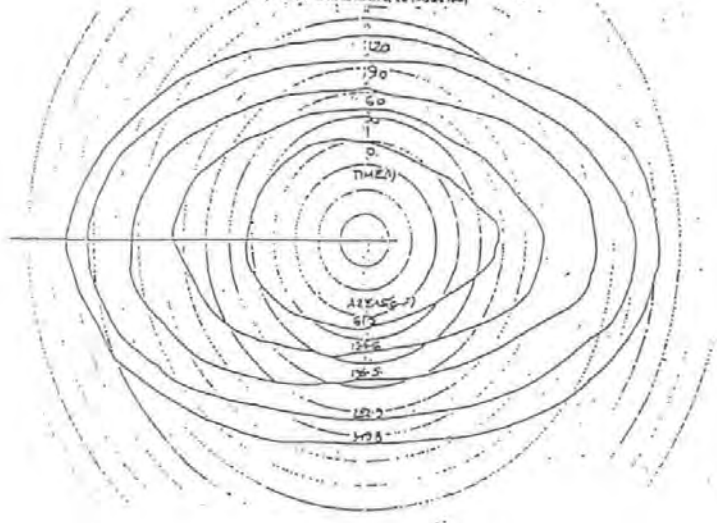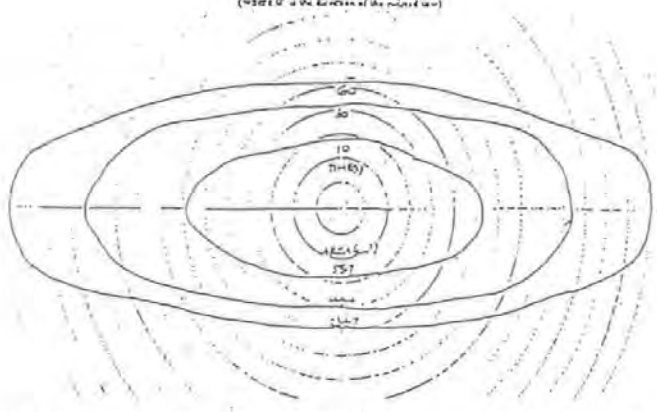
Figure 4. The Effects of Reinforcement Anisotropy on the Flow Front
Profile in a 0,90° Carbon Twill Fabric with a Flow Enhancing
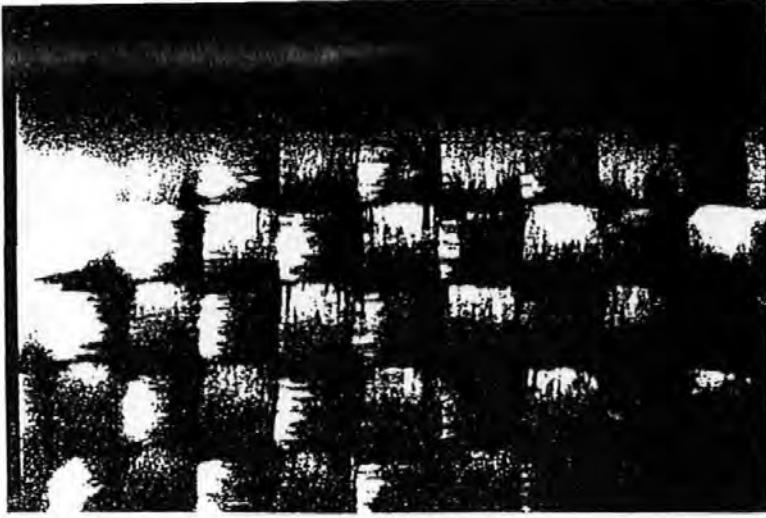Tow in the Warp Direction.

Figure 5. Three Macrophotographs at Varying Magnifications of the Edge of the Flow Front Showing Differing the Wet-out Rates of the tows and Inter-tow Spacings
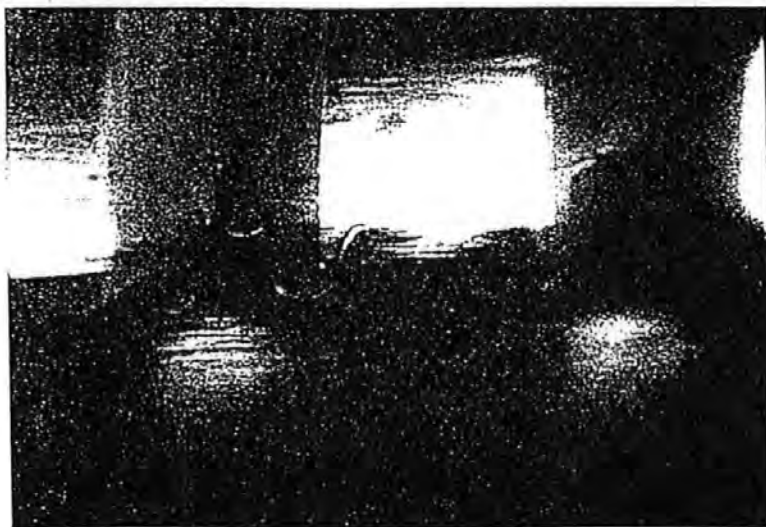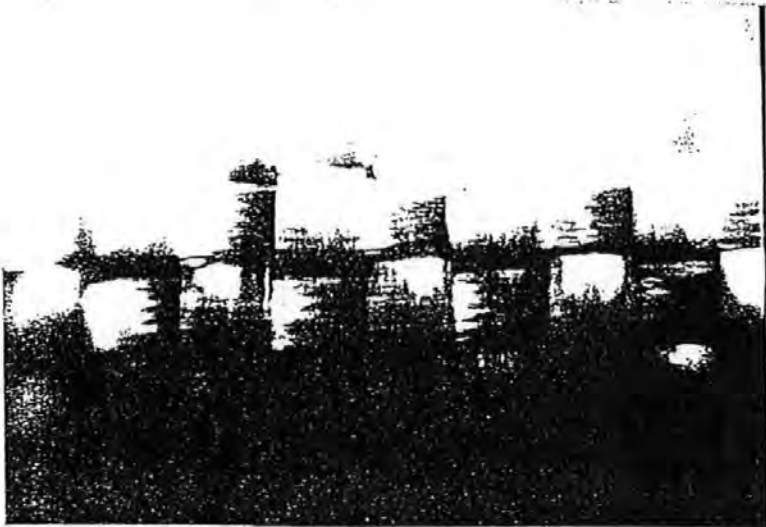
Figure 6. Permeability of Glycerol (supplied by Boots) through a Range of Flow Enhancing Reinforcement Fabrics
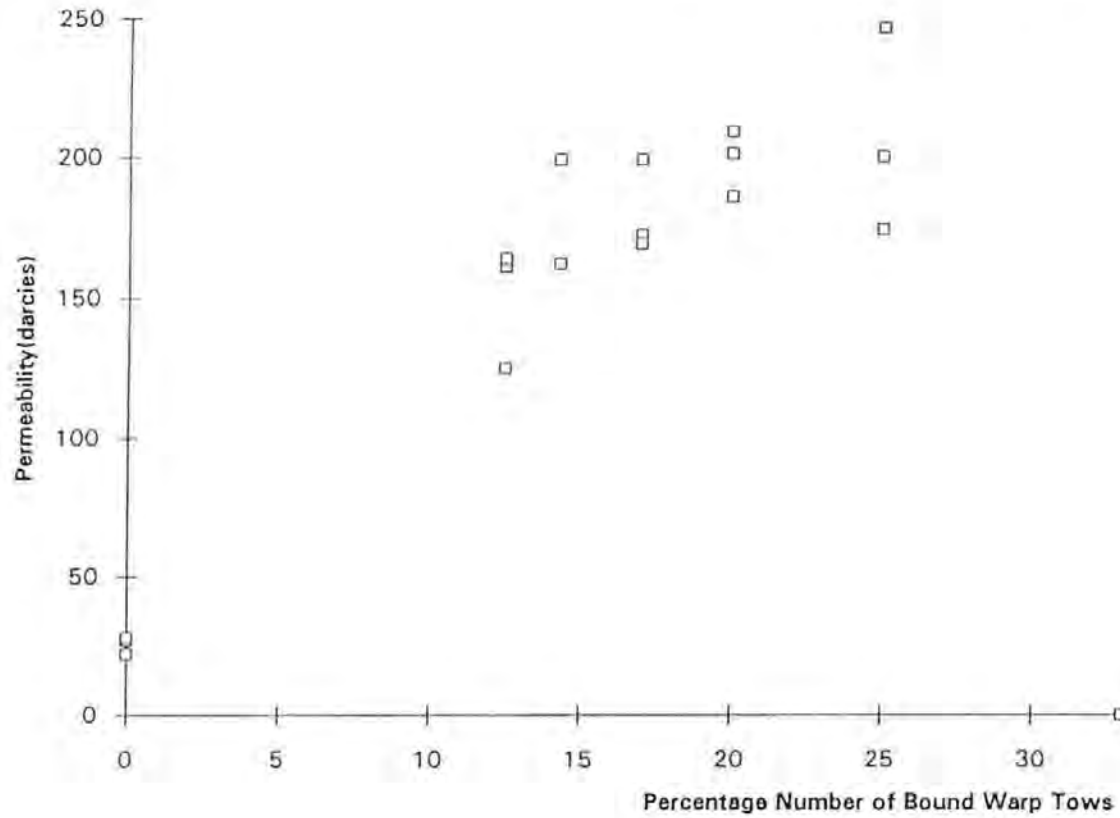
Figure 7. Sequence of Image Analysis

A Grey level Detection of a
Section of a Fabric 156 Laminate

A Binary Image of the Fabric
156 Laminate

The Section of 156 Fabric after
Image Enhancement
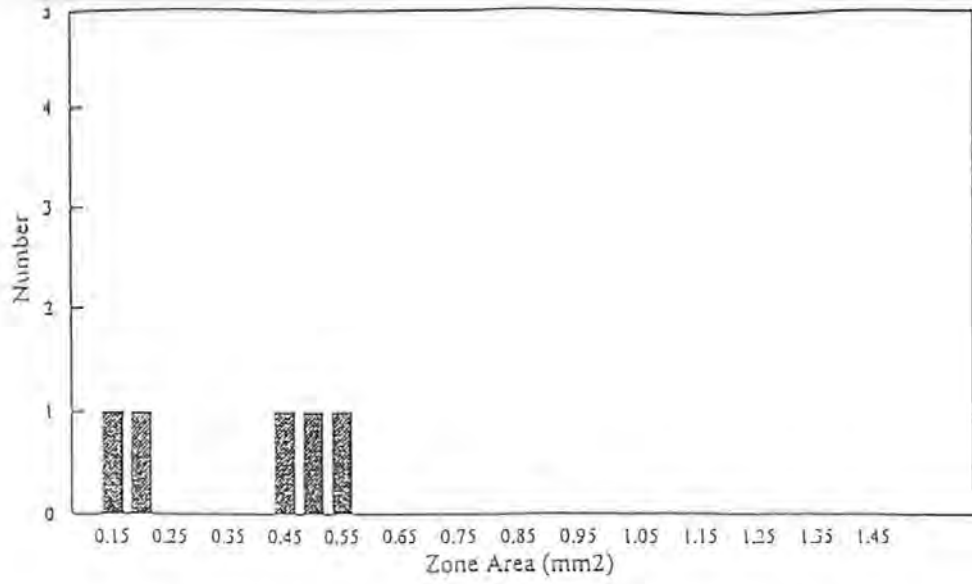
Advanced Composites
Manufacturing Centre

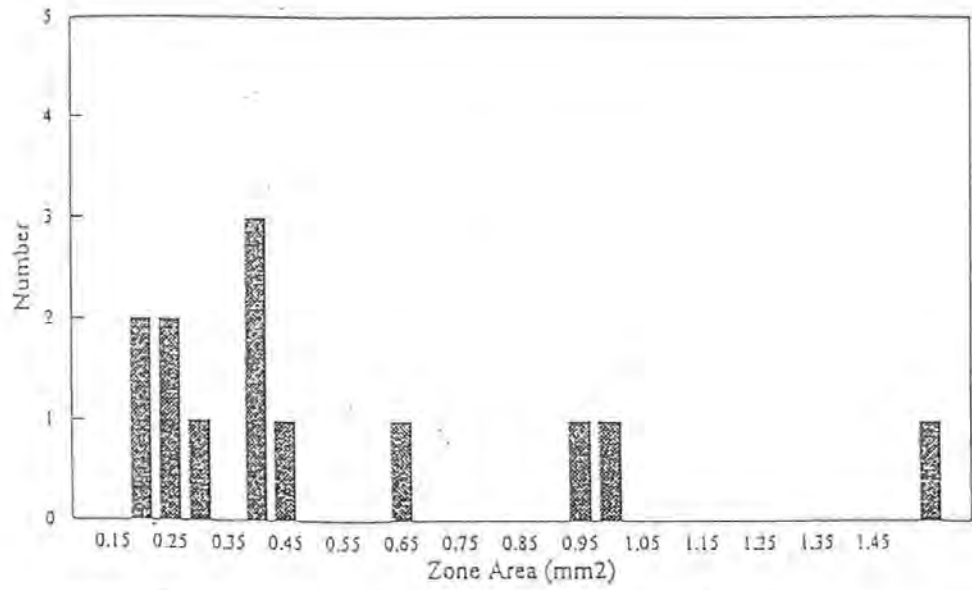Figure 8 a. Histogram of the Large Flow Areas in the Twill Laminate

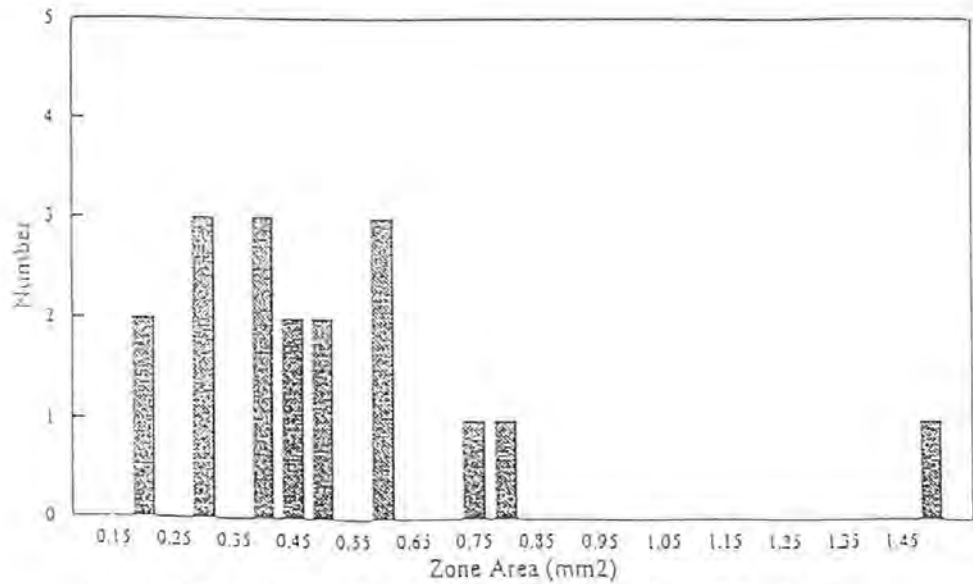Figure 8 b. Histogram of the Large Flow Areas in the 156 Laminate

Figure 8 c. Histogram of the Large Flow Areas in the 126 Laminate